DMPCO 2019

1st International Conference

DESIGN AND MANAGEMENT OF PORT, COASTAL AND OFFSHORE WORKS

Organised by:

Laboratory of Harbor Works

Laboratory for Floating Structures and Mooring Systems

Laboratory of Maritime Engineering and Maritime works

Hydraulic Engineering Laboratory

8-11 MAY 2019

Eugenides Foundation

Athens, Greece

PROCEEDINGS Volume II

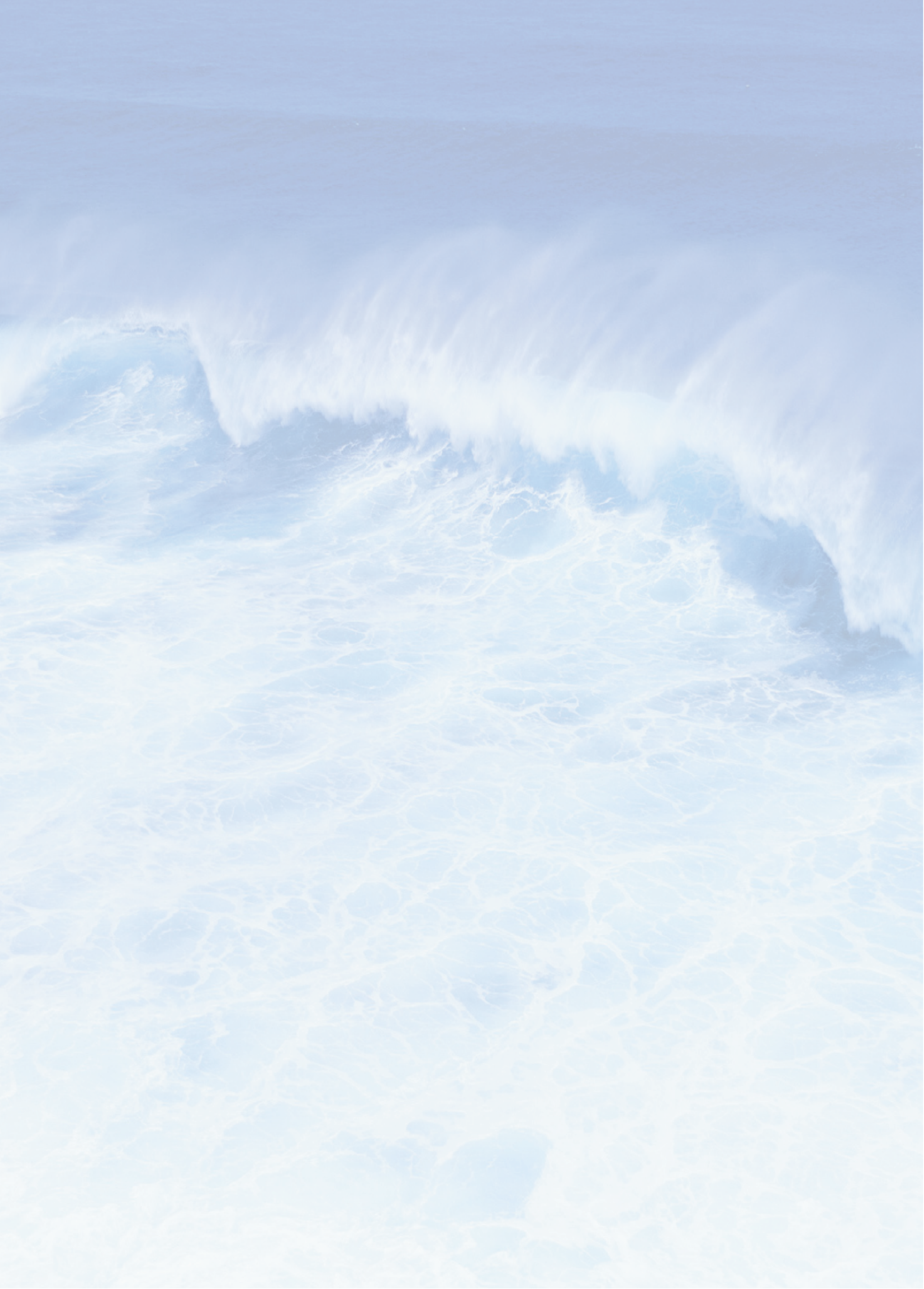

DMPCO 2019

1st International Conference DESIGN AND MANAGEMENT OF PORT, COASTAL AND OFFSHORE WORKS

8-11 May 2019 Eugenides Foundation, Athens, Greece

Proceeding of the International Conference
Design and Management of Port,
Coastal and Offshore Works DMPCO 2019

Published by
Laboratory of Harbor Works

Editor
V. K. Tsoukala

Technical Suport
M. Chondros
E. Belekou
C. Kouveli

Year of Publication: 2019

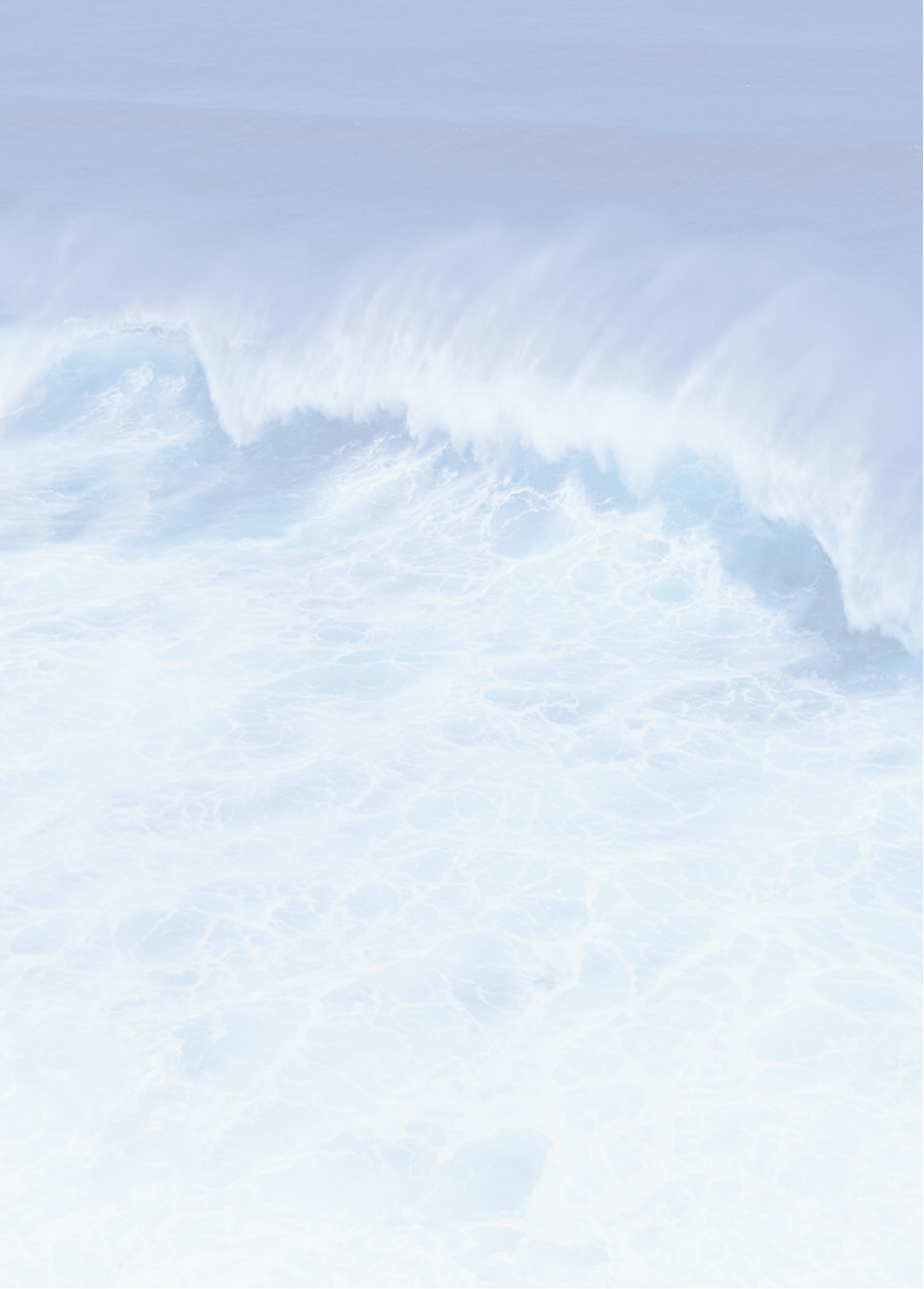

Preface

“Blue Growth” initiative drives the society to the new era. The future for making reach and maintain the consuming way of living for the European citizens belongs to the seas and the oceans. Marine environment with its vast unexploitable resources promises socio-economic development, but simultaneously requires to cope with new technological challenges that inevitably arise. Ports and coastal facilities are the necessary hubs for the transit of people, goods and equipment between civilizations. Over 90% of global trade is conducted on the world’s oceans. To ensure that “Blue Growth” and “Blue Economy” are kept safe, commercial operators are increasingly looking to a whole range of maritime technologies. In the same context, coastal infrastructures are expected to play a crucial role to secure undisturbed transportation and storage of goods before being distributed to land convey equipment. The new era requires that ports, coastal, nearshore and offshore infrastructures should be further developed and modernized to satisfy the increased demands. In the same time, they should follow modern rules and regulations, which are associated with safety, security, risks mitigation and environmental sustainability.

Marine and maritime sectors allow nations the opportunity to generate economic growth, enhance the security of supplies, resilience and foster competitiveness through technological innovation. There is only a single, but challenging, way to exploit the practically infinite sustainable resources of the marine environment. And that comes from continuous research and development (R&D) efforts, which will find practical and economically efficient ways to make rich out of the sea for the benefit of the society. R&D is the inevitable mechanism to conceive and implement ideas and to rein the harsh marine environment. The sea is open, provides a variety of opportunities, is unexplored economically, aside only from the traditional activities. On the other hand, it is not friendly. Sea have to be respected, but in the same time it has to allow employment of tasks of innovation. Innovation through R&D may generates opportunities using breakthrough technologies and developing state-of-the-art knowledge for a flourish future. The ultimate goal is to support visions for maintaining industrial leadership. With public support, the blue economy sector may be able to play a crucial role in the future. In fact, it is more that certain that the future for economic growth belongs to seaborne activities.

The **1st International Conference on the Design and Management of Port, Coastal and Offshore Works** has been particularly designed to address state-of-the-art topics, associated with “Blue Growth” and its pillars. The main goal, set by the organizers is to develop a forum for new ideas. Ambition of the organizing entities is to establish a long-lasting scientific environment, where novelty will prevail. Focus shall be given to the new generation and the ideas of the future. We sincerely hope that a new international scientific community will be generated by this effort, which aside from the pure scientific and engineering aspects, will address the most important for societal acceptance Science Practice Policy Interface. Our truthful aspiration is that DMPCO will stimulate discussions and intense scientific interactions between the participants about new trends and ideas in the design, construction, and operation of ports, coastal and offshore structures for the benefit of the engineering science and the society at large.

In terms of the core disciplines, the conference has been explicitly designed to update, to the major extend, the technical background of professionals involved in the production of port, coastal, and offshore projects, fostering the enhancement of the level of knowledge for engineers and scientists working in those subjects. Keynote speeches, special sessions and papers have been included in the program to address cutting-edge topics and state-of-the-art reviews in the current interdisciplinary professional environment that demands cooperation between specialties and acquaintance of the engineers with advanced techniques and good practices.

DMPCO 2019 International Conference which attracted 250 attendees from 8 Countries over the Europe discussing research and applications in port coastal and offshore engineering design and management.

The final program contained 103 presentations included submitted papers as well as, keynote invited speeches. In these 88 selected papers from the Scientific Committee are finally included. The papers have been listed within the ten main original conference topics, which included themes such as Sustainable Ports planning, construction and operation, design criteria guidelines and proposals for coastal structures adaptation in a changing climate, ecological issues monitoring and management under the framework and challenges of Marine Spatial Planning.

With the work of the secretariat, the Organizing, Scientific and External Advisory Committees, the persons who generously served as Chairmen of the technical sessions, the financial sponsors, this Conference has represented one of the premier technical meeting on Port, Coastal, and Offshore works. These e-proceedings amply reflect both the new scientific research results and the practical engineering achievements, fully in line with the concept of the DMPCO Conference.

This successful edition of e-proceedings gives more energy for organizing future DMPCO Conferences so that researchers and engineers from all countries will be able to participate in an exciting field with numerous intriguing problems to be solved.

See You in Thessaloniki in 2021.

On behalf of the DMPCO’s Organizing Committee

Vicky Tsoukala,
Assoc. Professor, NTUA

ORGANIZING COMMITTEE

Chairwoman

Tsoukala Vicky - Assoc. Professor of Laboratory of Harbor Works, NTUA

Members

Memos Constantinos - Professor Em., NTUA
Chondros Michalis - Dr. Civil Engineer, Research Assoc., NTUA
Malliouri Dimitra - Dr. Civil Engineer, Research Assoc., NTUA
Martzikos Nikolaos - Phd Student, NTUA
Repousis Elpidoforos - Phd Student, NTUA
Spyropoulos Kyriakos - MSc Civil Marine Engineer

Conference Secretariat

Mastroyianni Christina - Secretary of LHW, NTUA
Margaronis Panagiotis - Technical Assistant, NTUA
Belekou Eleni - Graduate Student, NTUA
Kouveli Kwnstantina - Graduate Student, NTUA

SCIENTIFIC COMMITTEE

Aggelidis D. - Professor Em., AUTH
Athanasoulis G. - Professor, NTUA
Chatjigeorgiou I. - Professor, NTUA
Chatzimpiros K. - Professor Em., NTUA
Chlomoudis K. - Professor, University of Pireus
Chondros M. - Dr. Civil Engineer, Research Assoc., NTUA
Coccosis Ch. - Professor, UTH
Dimakopoulos A. - Dr. Civil Engineer, HR Wallingford, UK
Dimas A. - Professor, University of Patras
Grigoropoulos G. - Professor, NTUA
Karambas Th. - Professor, AUTH
Karmpadakis I. - Research Assoc., Imperial College, UK
Katsardi V. - Assist. Professor, UTH
Klonaris G. - Dr. Civil Engineer, Research Assoc., NTUA
Kolokuthas G. - Dr. Civil Engineer, Flanders Hydraulics Research, Belgium
Koutitas Ch. - Professor Em., AUTH
Kupraios N. - Dr. Civil Engineer
Loizidou M. - Professor, NTUA
Loukogeorgaki E. - Assist. Professor, AUTH
Lyridis D. - Assoc. Professor, NTUA
Makris Ch. - Dr. Civil Engineer, Research Assoc., AUTH
Mavrakos S. - Professor, NTUA
Melissas D. - Professor, NTUA
Memos C. - Professor Em., NTUA
Metallinos A. - Dr. Civil Engineer, Research Assoc., NTUA
Mpardakis B. - Dr. Civil Engineer, President of HCCE
Pallis Ath. - Professor, University of the Aegean
Papadopoulou M. - Professor, NTUA
Prinos P. - Professor, AUTH
Soukissian Takvor - Dr. Naval Architecture and Marine Engineer, HCMR
Stamou A. - Professor, NTUA
Sylaios G. - Professor, DUT
Toumazis A. - Dr. Civil Engineer, University of Cyprus
Tsanis I. - Professor, University of Crete
Tsoukala V. - Assoc. Professor, NTUA
Vasilakis E. - Assist. Professor, UOA
Zacharias I. - Assoc. Professor, Univerity of Patrasor, Univerity of Patras

EXTERNAL ADVISORY COMMITTEE

Arcilla A. S. - Professor, Maritime Engineering Laboratory, UPC, Spain
Arena F. - Professor, University Mediterranea of Reggio Calabria, Italy
Benoit M. - Professor, IRPHE, France
Carevic D. - Professor, University of Zagreb, Croatia
Michailides C. - Professor, Cyprus University of Technology, Cyprus
Penchev V. - Professor, BDCA, Bulgary
Sannasiraj S. - Professor, Head, Department of Ocean Enginnering, IITM Chennai, India
Sundar V. - Professor Emeritus, IITM Chennai, India
Taveira Pinto F. - Professor, University of Porto, Portugal
Vicinanza D. - Professor, University Vanvitelli, Italy

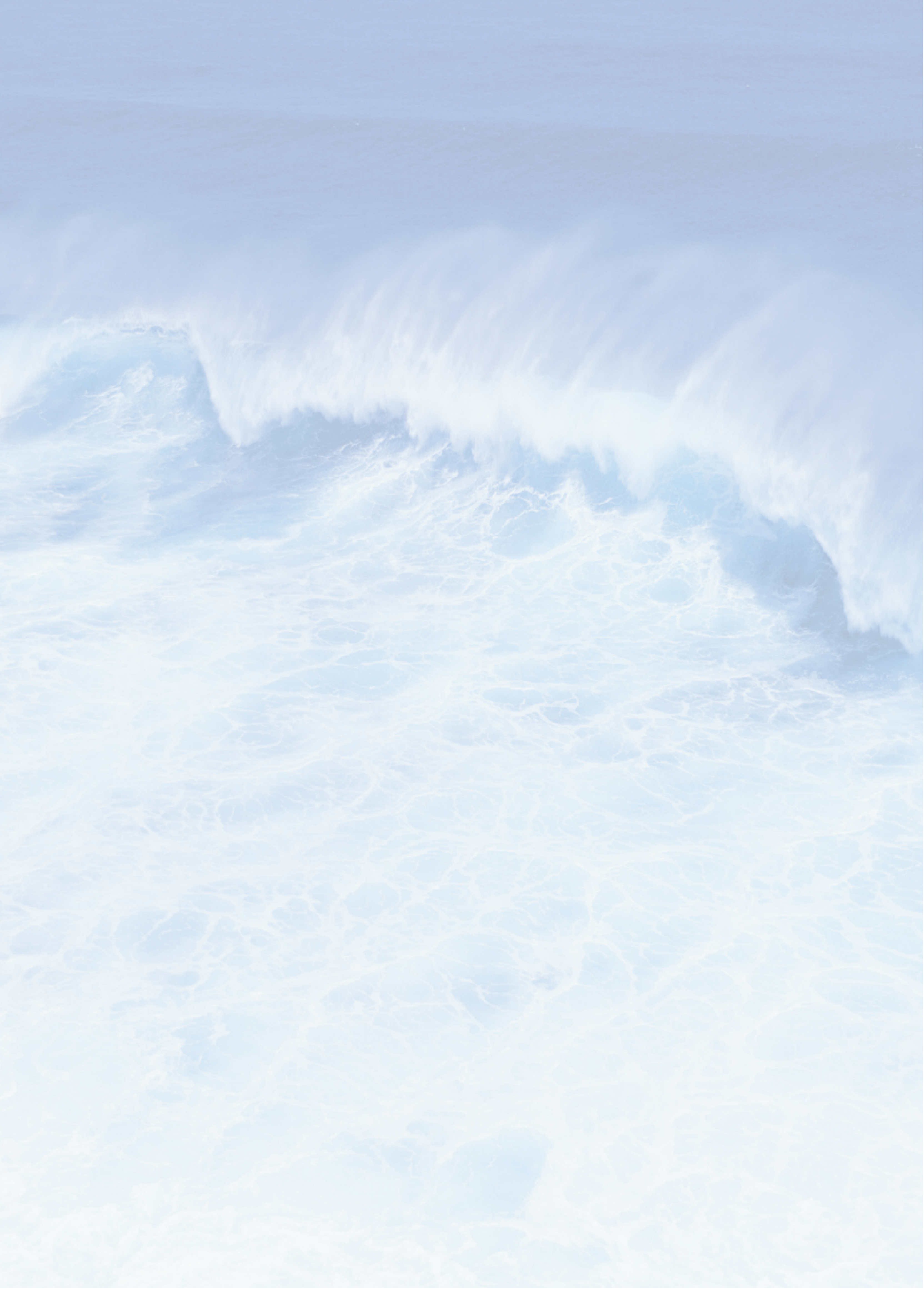

CONTENTS Volume I

CONTENTS Volume II

SESSION 4 INTEGRATED COASTAL ZONE MANAGEMENT (ICZM) - MARINE SPATIAL PLANNING (MSP)

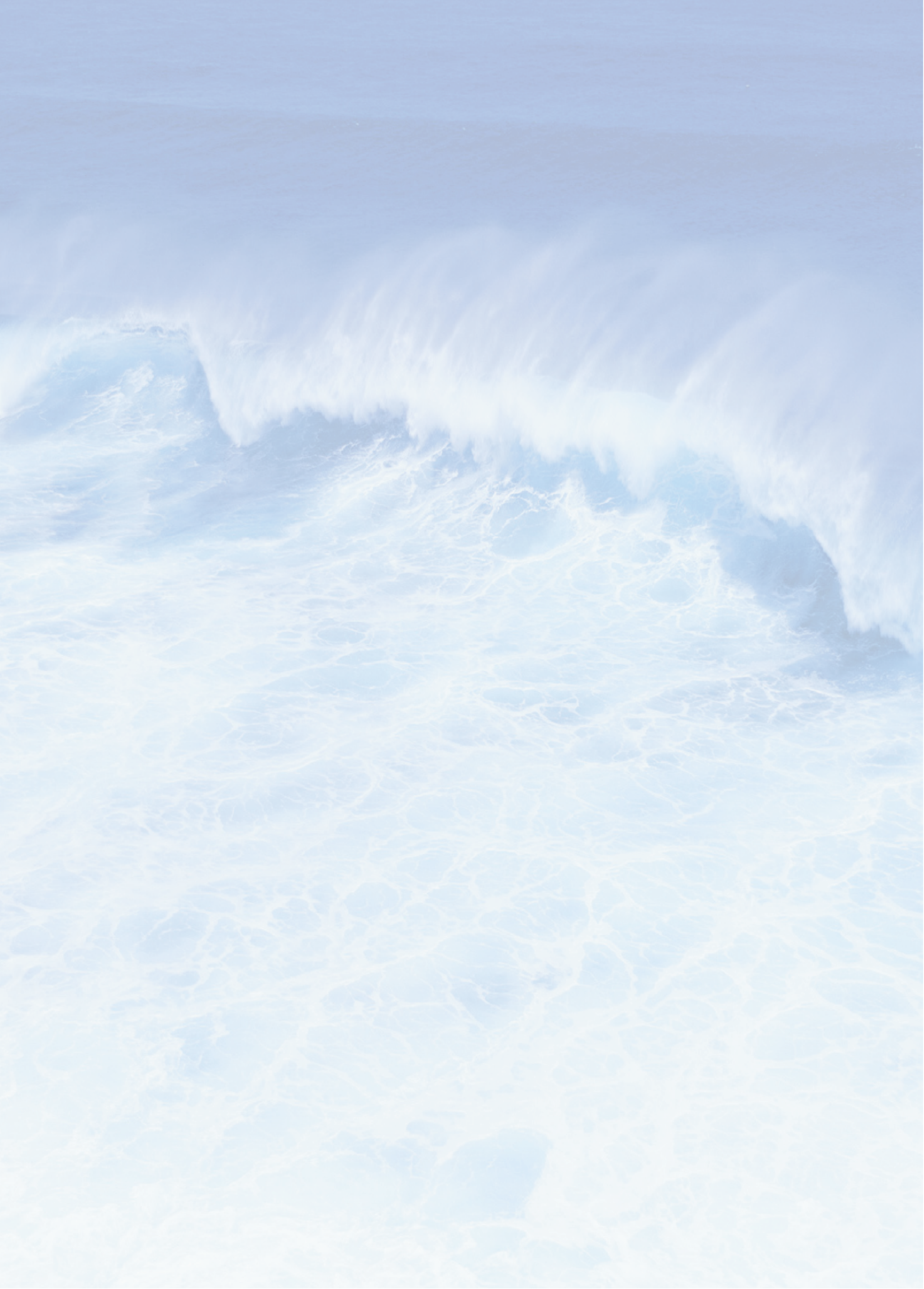

Sub session 4.1: Framework and Challenges

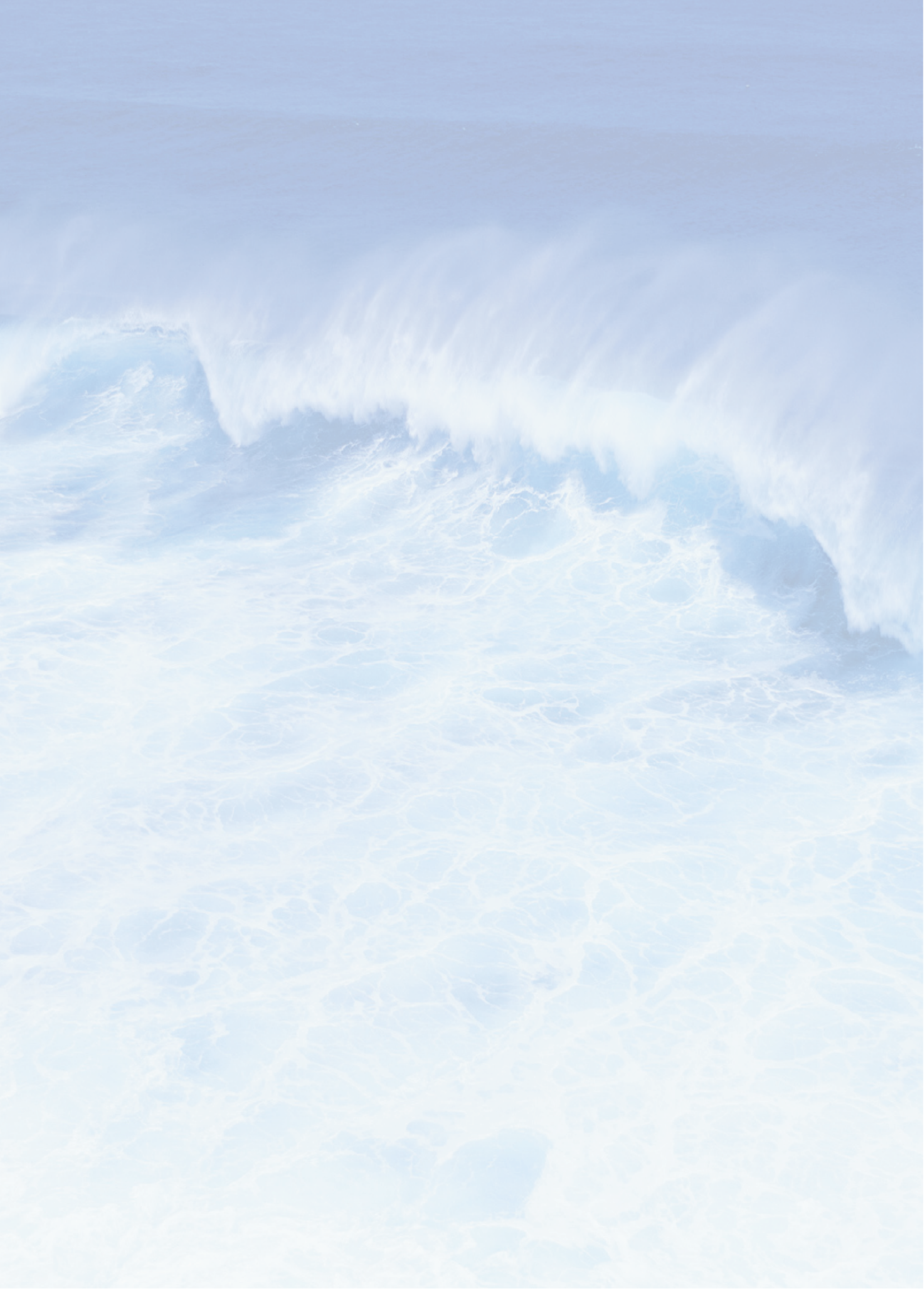

Πρώτες επισημάνσεις για θαλάσσιο χωροταξικό σχεδιασμό

Δ. Μέλισσας*

Σχολή Αρχιτεκτόνων Μηχανικών, ΕΜΠ
*Υπεύθυνος επικοινωνίας: dmelissa@otenet.gr

Περίληψη

Ο Θαλάσσιος Χωροταξικός Σχεδιασμός έχει διεπιστημονικό χαρακτήρα, συνιστά ένα δια τομεακό μέσο πολιτικής, απαιτεί μια διακρατική συνεργασία και αποσκοπεί κυρίως στο προσδιορισμό των χρήσεων στο θαλάσσιο χώρο και στη διατήρηση της βιωσιμότητας του οικοσυστήματος, προκειμένου να διασφαλιστούν οι δραστηριότητες που ενεργοποιούνται σ' αυτόν. Η ανάγκη ομοφωνίας στην ορολογία έχει επισημανθεί από το 2006, ενώ το 2008 η ναυτιλιακή πολιτική στην Ευρωπαϊκή Ένωση διεξάγεται στο πλαίσιο της Κοινής Περιβαλλοντικής Πολιτικής.

Λέξεις κλειδιά Θαλάσσιος Χωροταξικός Σχεδιασμός

1 Η ΟΔΗΓΙΑ ΠΛΑΙΣΙΟ ΓΙΑ ΤΟΝ ΘΑΛΑΣΣΙΟ ΧΩΡΟΤΑΞΙΚΟ ΣΧΕΔΙΑΣΜΟ

Η ανακοίνωση της Επιτροπής το 2008 για έναν οδικό χάρτη για τον θαλάσσιο χωροταξικό σχεδιασμό και την επίτευξη κοινών αρχών στην ΕΕ (COM(2008) 791 τελικό), και η οδηγία πλαίσιο για τη θαλάσσια στρατηγική (2008/56 ΕΚ) αποτέλεσαν τον περιβαλλοντικό πυλώνα της ευρωπαϊκής θαλάσσιας πολιτικής και έθεσε τις βασικές προϋποθέσεις για την εκπόνηση της οδηγίας 2014/89/ΕΚ για το θαλάσσιο χωροταξικό σχεδιασμό.

Η οδηγία πλαίσιο για τη θαλάσσια στρατηγική (2008/56 ΕΚ) ενσωματώθηκε στην ελληνική έννομη τάξη με το ν. 3983/2011, ενώ η οδηγία 2014/89 έχει ενσωματωθεί με το ν.4546/2018 «Ενσωμάτωση στην ελληνική νομοθεσία της Οδηγίας 2014/89/ΕΕ περί θεσπίσεως πλαισίου για το θαλάσσιο χωροταξικό σχεδιασμό, και άλλες διατάξεις» . Η καθυστέρηση αυτή είχε προκριθεί εύλογα από την πολιτική ηγεσία να ενσωματωθεί είτε προηγουμένως είτε μαζί και η Σύμβαση της Βαρκελώνης και ειδικότερα, το Πρωτόκολλο για την ολοκληρωμένη διαχείριση των παράκτιων ζωνών ή περιοχών της Μεσογείου (απόφαση του Συμβουλίου της 4ης Δεκεμβρίου 2008) που αποσκοπεί στο χωρικό σχεδιασμό για τη θαλάσσια και τη χερσαία ζώνη.

Βέβαια, η εκπόνηση των παραπάνω νομοθετημάτων για μια ολοκληρωμένη θαλάσσια πολιτική στην Ε.Ε., τροφοδοτήθηκε από τη «πράσινο βίβλο για τη μελλοντική θαλάσσια πολιτική» και τη «γαλάζια Βίβλο», καθώς επίσης, καθοριστικό ρόλο διαδραματίζουν οι κοινοτικές οδηγίες για τους οικοτόπους, τα πτηνά, την περιβαλλοντική αδειοδότηση.

Η ανάγκη για μια κοινή αποδεκτή ορολογία επισημαίνεται ήδη από το 2006 από τη Διακυβερνητική Ωκεανογραφική Επιτροπή της Unesco, στην οποία βασίζεται η κοινοτική οδηγία 2014/89, και ειδικότερα το άρθρο 3 για την εννοιολογική αποσαφήνιση του Θαλάσσιου Χωροταξικού Σχεδιασμού.

Ο Θαλάσσιος Χωροταξικός Σχεδιασμός έχει διεπιστημονικό χαρακτήρα, συνιστά ένα διατομεακό μέσο πολιτικής, απαιτεί μια διακρατική συνεργασία και αποσκοπεί κυρίως στο προσδιορισμό των χρήσεων στο θαλάσσιο χώρο και στη διατήρηση της βιωσιμότητας του οικοσυστήματος, προκειμένου να διασφαλιστούν οι δραστηριότητες που ενεργοποιούνται σ' αυτόν.

Συχνά τίθεται στη θεωρία ο ιδιαίτερα ενδιαφέρον προβληματισμός, εάν ο θαλάσσιος χωροταξικός σχεδιασμός αντιστοιχεί στο χαρακτήρα των Ειδικών Χωρικών Πλαισίων και στα Περιφερειακά Πλαίσια και το περαιτέρω ερώτημα, εάν το τυπικό περιεχόμενό του μπορεί να καλυφθεί: α) από τη χωρική διάρθρωση παραγωγικών και αναπτυξιακών κλάδων, όπως η αλιεία, ο τουρισμός, οι θαλάσσιες μεταφορές, οι Ανανεώσιμες Πηγές Ενέργειας κ.λπ., β) από την οργάνωση περιοχών ειδικής σημασίας και την προώθηση προγραμμάτων διακρατικής σημασίας. Μέχρι σήμερα δίνεται η εντύπωση ότι ο Θαλάσσιος Χωροταξικός Σχεδιασμός προσεγγίζει περισσότερο το κανονιστικό και νοηματικό περιεχόμενο του Ειδικού Χωρικού Πλαισίου.

Θα πρέπει να τονιστεί σε αυτό το σημείο ότι, η θεωρία έχει επιχειρήσει μια σειρά ομαδοποιήσεις για τις θαλάσσιες χρήσεις, όπως με βάση τον τρισδιάστατο χαρακτήρα «επιφάνεια - υδάτινη στήλη - βυθός» - και η σημερινή συζήτηση σήμερα ανέδειξε και την τέταρτη διάσταση, δηλαδή το χρόνο.

Περαιτέρω ομαδοποίηση διενεργείται επίσης στη θεωρία με βάση τη διάρκεια ή τη περιοδικότητα της χρήσης, όπως η αλιεία, ή με βάση την κινητικότητά τους, το μέγεθος, δηλαδή τη μικρή, μεσαία ή μεγάλη επιφάνεια.

2 ΥΛΟΠΟΙΗΣΗ ΤΟΥ ΘΑΛΑΣΣΙΟΥ ΣΧΕΔΙΑΣΜΟΥ

Ο θαλάσσιος σχεδιασμός έχει το πλεονέκτημα, ότι εφόσον λείπουν οι ιδιωτικές εκτάσεις, θα υλοποιηθεί σε δημόσιο χώρο, σε μία ενιαία και αδιαφοροποίητη υδάτινη επιφάνεια, στην οποία θα αναπτυχθούν συνδυαστικά όλες οι χρήσεις από το βυθό μέχρι την επιφάνεια. Η Πολιτεία οφείλει να συντονίσει, έτσι, να επιτευχθεί η αρμονική συνύπαρξη των ανταγωνιστικών χρήσεων στη θαλάσσιο χώρο, και τούτο επιτυγχάνεται μόνο με τη συναίνεση.

Ευνόητο είναι, ότι πρέπει στη συνέχεια οι μηχανισμοί συντονισμού, όπως οι διαφορετικοί συναρμόδιοι φορείς, να μπορούν να λειτουργήσουν συμπληρωματικά και με συνέργεια, έτσι ώστε, να μην επαναληφθεί το σημερινό φαινόμενο, σε μισό αιώνα από τη θέσπιση του α.ν. 2344/1940 να έχει χαραχθεί μόνο το 12% της ελληνικής ακτογραμμής.

3 ΣΥΜΠΛΗΡΩΜΑΤΙΚΟΤΗΤΑ ΤΟΥ ΧΕΡΣΑΙΟΥ ΚΑΙ ΘΑΛΑΣΣΙΟΥ ΧΩΡΟΤΑΞΙΚΟΥ ΣΧΕΔΙΑΣΜΟΥ

Περαιτέρω, οι παράκτιες περιοχές χαρακτηρίζονται από τη δυναμική αλληλοεπίδραση της στεριάς και της θάλασσας που αποτυπώνει και τη δυναμική αλληλεξάρτηση των φυσικών οικοσυστημάτων και των ανθρώπινων δραστηριοτήτων.

Επομένως επιβάλλεται η συμπληρωματικότητα των χερσαίου και θαλάσσιου χωροταξικού σχεδιασμού, στο βαθμό μάλιστα που η αλληλοεπίδραση αυτή γίνεται πιο αντιληπτή, όταν οι ανθρωπογενείς επεμβάσεις στο χερσαίο μέτωπο γίνονται αντιληπτές στο θαλάσσιο, όπως, για παράδειγμα, η ρύπανση από την ξηρά, που επιδρά αρνητικά σε βιοτόπους και σε είδη παράκτιας και ανοικτής θάλασσας.

Και αντίστροφα, ακραία καιρικά φαινόμενα και φυσικές καταστροφές (τσουνάμι) επηρεάζουν αντίστοιχα το χερσαίο μέτωπο. Ωστόσο η αλληλεξάρτηση δεν μπορεί να μας οδηγήσει στην προέκταση των ρυθμίσεων του χερσαίου μετώπου στο θαλάσσιο, στον βαθμό που η τρίτη διάσταση, δηλαδή το βάθος, με τα ρεύματα και τα υποθαλάσσια κοιτάσματα, διαφοροποιείται από το χερσαίο χώρο.

Επομένως, στο κανονιστικό περιεχόμενο τόσο της Οδηγίας 2014/89 όσο και του Πρωτοκόλλου της Βαρκελώνης για την ολοκληρωμένη Διαχείριση Παράκτιας ζώνης, επισημαίνεται η αλληλοεπίδραση θάλασσας και ξηράς και η προτεραιότητα να διασφαλίζεται η Καλή Περιβαλλοντική Κατάστασή τους, όπως επιτάσσει μάλιστα και η Οδηγία 2008/56 ΕΚ για τη θαλάσσια στρατηγική.

Τηλεγραφικά μόνο να επισημάνω ότι ο θαλάσσιος χωροταξικός σχεδιασμός έχει περισσότερο χωρικό χαρακτήρα, και η Ολοκληρωμένη Διαχείριση της Παράκτιας Ζώνης ή Περιοχών (Πρωτόκολλο Βαρκελώνης) διαχειριστικό χαρακτήρα.

Πάντως, στην πληρέστερη κύρωση τόσο της ολοκληρωμένης διαχείρισης των παράκτιων περιοχών του 8ου Πρωτοκόλλου της Βαρκελώνης, όσο και στην ενσωμάτωση της Οδηγίας 2014/89, θα συμβάλει καθοριστικά η θέσπιση του ειδικού πλαισίου για τον Τουρισμό, που βρίσκεται ακόμη σε εκκρεμότητα, καθώς επίσης η θέσπιση, επιτέλους, του ειδικού πλαισίου για τον παράκτιο και νησιωτικό χώρο.

Τέλος η κοινοτική οδηγία 2014/89/ΕΚ για το θαλάσσιο χωροταξικό σχεδιασμό αργά ή γρήγορα θα ενσωματωθεί στην ελληνική έννομη τάξη. Σημασία έχει να μην αποτελέσει και αυτή η ενσωμάτωση ακόμη ένα νομοθέτημα απροβλημάτιστης αντιγραφής της ελληνικής μετάφρασης της οδηγίας που θα στερείται οποιασδήποτε νομοτεχνικής μεθόδου. Μάλιστα, εάν το νομοθέτημα αυτό αναμειχθεί και με άλλες άσχετες διατάξεις, γεγονός πολύ συνηθισμένο, που δηλώνει την ακόμη μια φορά έλλειψη οποιασδήποτε σχεδιασμού στη νομοθεσία της εκάστοτε πολιτικής, εν κατακλείδι θα καταστεί προβληματική η εφαρμογή του θαλάσσιου χωροταξικού σχεδιασμού στη χώρα με τεράστιες επιπτώσεις σε όλες εκείνες τις δραστηριότητες που επιδιώκει την αρμονική συνύπαρξή τους.

Βιβλιογραφικές αναφορές

Vassenhoven L (2017) Maritime Spatial Planning.

Σερράος Κ, Μέλισσας Δ (2018): Maritime Spatial Planning, Epilogue, pp 131.

Broadening the policy framework: from ICZM to MSP

H. Coccossis*

University of Thessaly, Volos, 38334, Greece
*Corresponding author: hkok@uth.gr

Abstract

Coastal areas have attracted considerable attention due to their significance for a broad range of human activities, for the importance of natural ecosystems and their intricate interdependence. In recent years, the special attention paid to the ocean space, from an ecosystem perspective but also from an economic potential side bringing new perspectives but also new challenges in policy making. An outcome of such concerns is a proliferation of interests in developing relevant policy frameworks from Integrated Coastal Zone Management to Maritime Spatial Planning, taking advantage of spatial planning perspectives across nations and regions. A key issue is the development of relevant policy contexts and programs towards managing coastal and maritime areas. Although in principle the approach is understandable, highlighting its character as comprehensive and integrating, there are significant problems and challenges in practice as it requires new innovative structures, processes and tools for policy related decision-making beyond established experiences, systems and practices.

Keywords ICZM, MSP, Spatial planning.

1 BROADENING PERSPECTIVES

It is a well-established perspective nowadays that the development of human activities in intricately related to environmental quality issues such as the natural resources and ecosystem structure and dynamics. Such a relationship is particularly important to take into consideration in certain areas characterized by such sensitivities and dynamic changes, such as the coastal areas or areas where such relationships are particularly complex and constantly changing, such as the ocean space and the seas.

Coastal areas are particularly attractive for the development of various human activities particularly those benefiting from access to the sea or a land/sea interface. The economies of intermodal transport provide opportunities for port development for example which creates agglomeration economies attracting a variety of activities leading eventually to urbanization. Such a concentration of human activities often leads to conflicts among uses but may also have significant impacts on the environment, particularly coastal resources and ecosystems. Coastal cities, particularly port cities. In other cases, the land/sea interface creates advantages for the location of fishing and aquaculture or tourism depending on the particularities of the coastal area, activities which also may lead to conflicts among uses and pressures for coastal development and urbanization.

The sea space is also complex with intensive dynamics from an ecosystem perspective and is increasingly attracting the interest for the development of human activities as well. The globalization of the economy brought in pressures to develop further human activities (such as extraction of materials or energy resource development, etc.) but also an increasing interest to protect ecosystems and the sea space, beyond national jurisdictions. So, the seas have been increasingly at the center of interest, as well both from an ecosystem management and a social and economic development point of view. In the European Union context such a turn has stimulated also what is known as a "blue economy" perspective seeking to bring-in benefits from the development of sea activities stimulating economic development through innovation, the creation of new jobs and taking advantage of a focus on ecosystem management, as part of an integrated maritime policy.

Both, the increasing concerns for coastal areas and the seas have brought forward the necessity to properly manage and plan for the development of human activities and the protection of resources and ecosystems. From a spatial planning perspective, as an approach to recognize the particularities of space in development policy, these concerns have led to what has been established as Integrated Coastal Area Management and Marine (Maritime) Spatial Planning.

2 COASTAL AND MARITIME PLANNING PERSPECTIVES

Integrated Coastal Area Management (ICAM) has already attracted the attention of policy making at various levels, national and supra-national, since the eighties, leading to the development of relevant policy frameworks and structures. ICAM is a dynamic process focusing on the necessity to establish goals, principles and priorities to guide development of human activities and infrastructure towards sustainable development in coastal areas. Integration emphasizes looking across sectors and linking to ecosystem functions. Management emphasizes the adoption of flexibility in decision-making so as to reflect the changing dynamics of coastal areas. In the Mediterranean this has been a part of the Mediterranean Action Plan of UNEP (United Nations Environment Programme) as the 8th Protocol, stimulating member states to introduce management plans for coastal areas. The basic principles of ICAM are that, a coastal area is unique as a resource system which requires special management and planning, the land-sea interface should be considered as an integrating force in coastal resource systems, land and sea uses should be planned and managed in combination, coastal management and planning boundaries should be issue-based and adaptive, all levels of government should be involved in coastal planning and management, economic and social benefit evaluation, and public participation form important components of coastal area management, conservation is an important goal in sustainable coastal development and multi-sectoral approaches are essential to the sustainable use of resources as they involve multi-sectoral interactions (UNEP/MAP 2001).

In recent years, the special attention paid to sea space, normally beyond territorial regulatory systems, initially from an ecosystem perspective, related to the protection of the environment, but also from an economic potential side, has led to a special attention to the maritime sector as space of special policy concerns (Ehler and Douvere 2009). Whether labelled as integrated maritime policy or blue economy or any other name such a perspective has brought an ecosystem based management basis seeking eventually a spatial dimension which has been often characterized as Marine (or Maritime) Spatial Planning, bringing new perspectives but also new challenges in policy making (Kerr et.al. 2014). MSP has been adopted in the European Union with a view to secure energy supplies, promote the development of maritime transport and support the development of fisheries and aquaculture while ensuring progress towards environmental protection. In this context, MSP through organizing sea space is expected to contribute to the development of marine energy sources, the development of new and renewable energies and the interconnection among energy networks, seeking to improve energy efficiency. In addition, it is expected to safeguard efficient and cost-effective maritime routes throughout Europe, improving port accessibility and transport safety but also support the development of fisheries. It is also expected to strengthen environmental protection through rational use of natural resources, halting the loss of biodiversity and degradation of ecosystem services and reduce marine pollution. MSP is foreseen to contribute to climate change adaptation.

An outcome of such concerns is a proliferation of interests in developing relevant policy frameworks from Integrated Coastal Zone Management to Maritime Spatial Planning, taking advantage of spatial planning perspectives across nations and regions. A key issue is the development of relevant policy contexts and programs with the aim to highlight the opportunities, conflicts and challenges in managing coastal and maritime areas (Garcia Sanabria 2014). Both, ICAM and MSP adopt an ecosystem-based approach seeking to respect and preserve ecosystems and promote sustainable development of human activities, facilitating the coexistence of coastal and maritime uses, thus, preventing conflicts between competing activities (CEC 2014). There is an obvious need for linking ICAM and MSP as they refer to policies for a space which is integrated, highly interacting and necessitates similar approaches emphasizing management, meaning a flexible and adaptable system of making decisions about priorities and rules. Both relate to the need to develop human activities and protect the environment recognizing the characteristics and dynamics of space as key factors in policy making. Thus, both relate to spatial planning.

3 SPATIAL PLANNING CHALLENGES

Spatial planning, is in general a well established public policy process of organizing human activities, related infrastructure and human settlements by setting goals, principles and priorities, as well as rules in the form of spatial plans (at various levels). The new perspectives highlight the necessity to extend traditional spatial planning concerns over pressures, impacts and conflicts among human activities and natural resources and ecosystems in areas which are particular as to the sensitivity to interactions but also quite dynamic in terms of their spatial dimensions challenging long established traditions and experiences in land-use planning and territorial development strategies, introducing a management approach. Although in principle the approach is understandable, highlighting its character as comprehensive and integrating, there are significant problems and challenges in practice as it requires new innovative structures, processes and tools for policy related decision-making beyond established experiences, systems and practices across the globe (Kidd and Ellis 2012).

ICAM and MSP have broadened the scope but also enriched in a sense traditional spatial planning linking a management perspective and strengthening the environmental dimension plus extending the spatial scope. At the same time, however, they have brought in new challenges as established tools and decision-making processes do not necessarily apply as such in the types of spatial areas.
The coastal area and the sea are quite different from territorial space where the main task is to regulate the location and intensity of development in private and public properties. At sea and to a great extent in coastal areas space (and resources) are part of a wider public interest as a principle, so traditional tools of zoning are not necessarily the best solutions. Furthermore, while in land much of the interest is essentially horizontal (territorial surface concerns) at sea there is a third dimension (depth) and the dynamics are more volatile, hence, even the relationship of ecosystem structures and dynamics and human activities and related infrastructure. A key issue is therefore space and conceptualizations, challenging the role and character of spatial planning. The main challenges of spatial planning in its broadening concept concern the basic "object" of planning (the coastal and marine space) and its 'new' character (the need for "a management approach"). At sea and along the coasts the spatial area boundaries are fuzzy, so there is no as such, but a dynamic, fluid, space constantly changing so it cannot be subject to traditional tools such "zoning" as there is a third dimension, the depth. So, the scope and purpose of planning and the appropriate policy tools as well as the institutional framework (structure/procedures) need to be re-invented.

The Mediterranean is an interesting case for such an approach as it has established for a long time ... strong coastal urbanization, established regional cooperation in environmental protection, established contexts for integrated coastal area mangement but also new pressures for maritime spatial planning. Greece is also a case of special interest essentially due to its extensive coastline and island regions. So seeking the potential of spatial planning for coastal areas and maritime space at both regional and national spatial entities could be interesting to seek the opportunities and constraints for spatial plnning and policy making focusing especially on the capacity to proceed with action and implementation.

What is particularly interesting in this context though is the opening-up of new perspectives for coastal cities, especially port cities, as key factors benefitting and contributing to new approaches in spatial planning on the coasts and at sea.

References

Barbanti A, Gissi E, Musco F, Sarretta A, Morelli M, Fraschetti S, Lipizer M, Mosetti R, Vassilopoulou V, Mezek S, Coccossis H, Sedioli O Campostrini P (2017) Towards marine spatial planning implementation in the Adriatic and Ionian Region in Marine Spatial Planning: Methodologies, Environmental issues and Current Trends Kitsiou D. and M. Karydis (eds.). Nova Science Publishers 323-350.

Commission of the European Communities (CEC) (2014) Directive 2014/89/EU of the European Parliament and of the Council of 23 July 2014 establishing a framework for maritime spatial planning, Off.J.Eur.Union L257 (2014) 135–145.

Ehler C, Douvere F (2009) Marine spatial planning: a step-by-step approach toward ecosystem-based management. Intergovernmental Oceanographic Commission Manual and Guides No. 53, ICAM Dossier no. 6. Paris: UNESCO

Garcia Sanabria J (2014) The Scope of Marine Spatial Planning and Integrated Coastal Zone Management: New Challenges for the Future, Journal of Coastal Zone Management, vol. 17 e 10.4172/1410-5217.1000e109

Kerr S, Johnson K, Side JC (2014) Planning at the edge: Integrating across the land sea divide, Marine Policy, vol. 47, pp. 117-125.

Kidd S, Ellis G (2012) From the Land to Sea and Back Again? Using Terrestrial Planning to Understand the Process of Marine Spatial Planning, Journal of Environmental Policy and Planning, vol. 14, pp. 49-66

United Nations Environment Programme/ Priority Actions Programme (UNEP/MAP/PAP) (2001) White Paper Coastal Zone Management in the Mediterranean, Split, Priority Actions Programme,

The coasts at the front of the city of Attica Basin: Landforms coastal uses and management proposals under the principles of integrated coastal management

Ch. L. Anagnostou[1*], A. G. Petropoulos[2] & A. N. Kikaki[1]

[1]Institute of Oceanography, Hellenic Centre for Marine Research, 46.7 km Athens-Sounio Avenue, Mavro Lithari, 19013 Anavyssos, Greece,
[2]Faculty of Geology and Geoenvironment, National and Kapodistrian University of Athens, Panepistimiopolis, 15784 Athens, Greece,
*Corresponding author: chanag@hcmr.gr

Abstract

The state of a part of the coasts in the front of Attica basin cities (Greece) is discussed. Physical characteristics of the coasts and the anthropogenic interventions on the coasts are presented, using aerial photos, Google Earth images and field observations. The examined coastal area is extended in a length of 17,6 km. Marinas, small ports, wave defense works cover 27,2% of the coastline, not accessible coasts, due to constructed fences cover 34.2% of the coastline, commercialized beaches 5%. Free access beaches cover the rest 33.6%. Obviously, it is a need for management of the coastal zone in the study area. The principles of the Integrated Coastal Zone Management are proposed as basis to formulate strategic management plans and actions. Plans and ctions taking into account the sustainability, that means to ensure that natural resources remain available to future generations.

Keywords Coastal front, Big cities, Integrated management

1 INTRODUCTION – SCOPE OF THE WORK - STUDY AREA

In the frame of this presentation the state of a part of the coasts in the front of Attica basin cities will be discussed. This coastal area is extended from Palaio Faliro to Vouliagmeni (Fig.1). The coasts are part of the coastal zone, which include the drainage basins influencing the coasts (s. Fig 1.a and 1.b). Trying to study the state of the coasts of the area mentioned above, we have to calculate the anthropogenic interventions in the area. The physical characteristics of the coasts, as well as the anthropogenic interventions on the coasts are classified and qualified in the frame of this presentation.

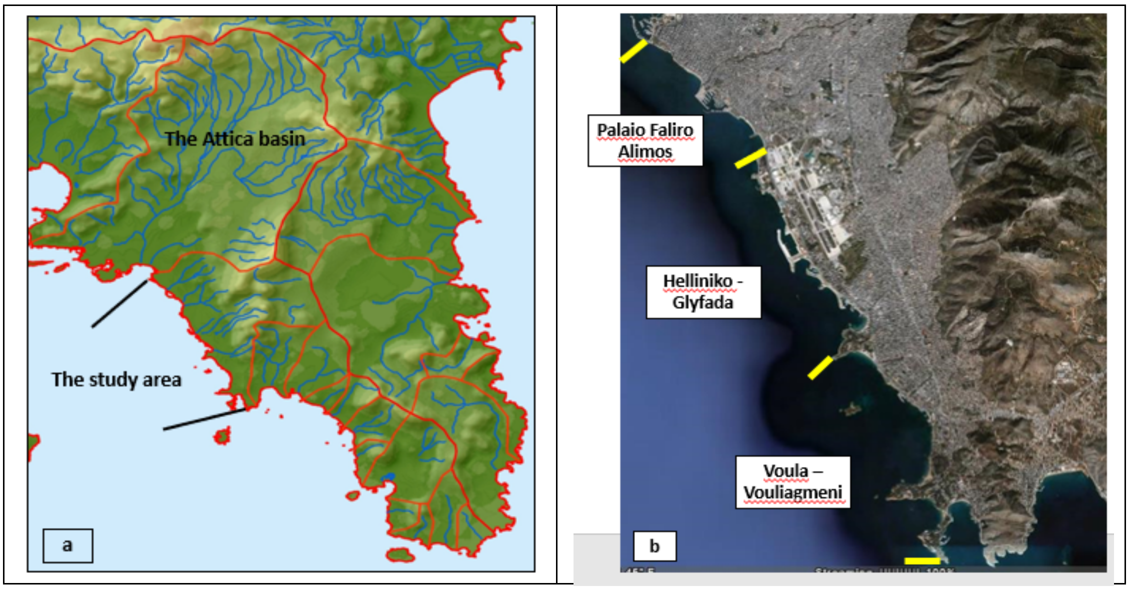

Figure 1 a. Map showing the boundaries of the Attica basin, its drainage system and the coasts studied in the frame of this work, b) The coastal area is divided into three units. Important anthropogenic interventions are also recognized.

2 METHODS

Images from GOOGLE EARTH and aerial photos are used to identify the timeless changes in the coasts. Field observations are carried out in order to classify and quantify the coastal forms and the human activities on coasts. Existing scientific as well as general information is included towards this approach. For the formulation of management practices in study area, the principles of the protocol of the Integrated Coastal Zone Management (ICZM) are used. For a better presentation of the results of the work, the study area is divided into three units (Fig. 1b): a. Palaio Faliro -Alimos, b. Helliniko – Glyfada, c. Voula – Vouliagmeni.

3 LAND FORMS, COASTAL USES OF THE STUDY AREA

The geology of the study area shows post-alpidic formations consisting on of marls, sandstones and siltstones. The mountainous hinterland is covert with metamorphic rocks, marbles and schists. The geology structure and the tectonic of the extended study area resulted on the mountainous relief of Hymettus and the lowland from the mountain to the sea front.

This structure leads to the formation of three coastal types: rocky coasts, cliff coasts and depositional coasts. In many cases cliffs are associated with a depositional coast in the frond of the cliffs. The materials of the depositional coasts are sands (fine sands to coarser sands), gravels, rocky fragments.

Staying in the scope of the present work the characteristics of the coasts (natural and anthropogenic) are classified (Table 1). Table 1 summarizes our study results regarding coastal characteristics mapped in a geographical sense from NW to SE, from Palaio Faliro to Vouliagmeni.

Table 1 Classification of coastal characteristics for the front of Palaio Faliro to Vouliagmeni area.

Geographical parts of the coastal area / Coastal characteristics	A. Palaio Faliro - Alimos	B. Elliniko - Glyfada	C. Voula – Vouliagmeni	Sum
-Length of the coastline	4,6 km	6,7 km	6,3 km	17,6 km
-Human interventions (marinas, wave defence works, etc)	2.40 km [52,0%]	2,21 km [33,0%]	0,19 km [3,0%]	4,80 km [27,2%]
-Not accessible coasts due to constructed fences		3,49 km [52,0%]	2,52 km [40,0%]	6,01 km [34,2%]
-Commercialized closed beaches			0,88 km [14,0%]	0,88 km [5,0%]
-Free access beaches	2,20 km [48,0%]	1,0 km [15,0%]	2,71 km [43,0%]	5,91 km [33,6%]

The coastal characteristics are classified in four groups a) human interventions, b) not accessible coasts due to constructed fences, c) commercialized closed beaches, d) free access beaches.

To gain an idea about the evolution of the coast in the study area aerial photos from 1938 are correlated with Google earth images of 2018 (80 years' time-space). In Figure 2 the images of the geographic units: a. Palaio Faliro - Alimos, b. Helliniko – Glyfada, c. Voula – Vouliagmeni are presented indicating major changes in coastal area between years 1938 and 2018.

Unit a: Palaio Faliro – Alimos

The coast extends in a length of 4.6km. In the land area 1938 Palaio Faliro and Kalamaki settlements are recognized. Extended agricultural land area is also identified. Small coastal interventions (small jetties) are also recognized. In the image of 2018 marinas are figured: Flisvos marina in NW and Alimos marina in Kalamaki coast. Southeasterly a groin separates the sand beach in two parts. The human interventions have occupied more than 50% of the coastline length. The cultivated land is totally changed, covered from the extension of the human settlements.

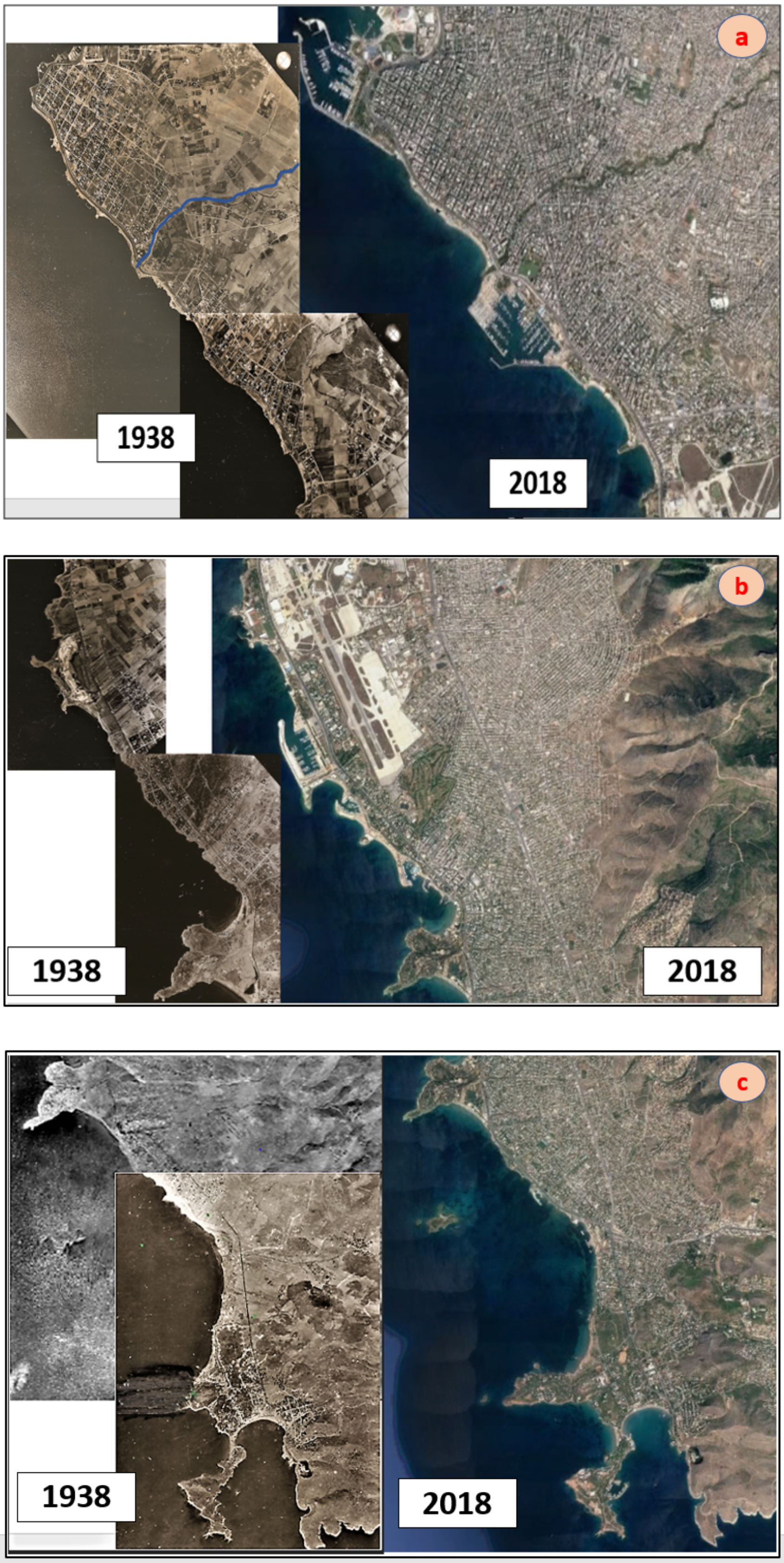

Figure 2 Correlation of the status changes of the coastal area along the study area for the years 1938 and 2018. The images are ordered following the division of the area in the three geographic units: a. Palaio Faliro -Alimos, b. Helliniko – Glyfada, c. Voula – Vouliagmeni.

Unite b: Ellinikon – Glyfada
The coast is extended in a length of 6.7 km. In the image of 1938, we have a landscape without significant interventions along the coasts and the Glyfada city in an initial stage. Most of the land area is used for agriculture. Eighty years later (2018) the area is totally covered from anthropogenic activities: marinas, ports, the former Attica airport, parallel to the coasts and extension of the cities Glyfada and Hellinikon to NE. Only 15% of the coast is free to access beach.

Unit c: Voula – Vouliagmeni
The coast along the Voula – Vouliagmeni area is extended in a length of 6.3 km. The area of Voula – Vouliagmeni figured in the first aerial photo (1938) is more or less a natural area, small settlements of the Voula and Vouliagmeni villages are recognized as well as agricultural areas and free natural landscape. Eighty years later (2018) the area is totally covered from the village's expansion in all directions. Along the coasts a fishery port as well as some human constructions are recognized. 43% of the coast is free to access coast.

4 SUGGESTIONS FOR POLICY ACTIONS BASED ON THE PRINCIPLES OF THE INTEGRATED COASTAL ZONE MANAGEMENT (ICZM)

Focusing on the last 80 years (1938-2018) dynamic of the development of the SE Attica coastal zone area we can identify the most important driving force for this development. This is the high rate of population growth and the following this population growth, large-scale commercial activities, which degrade land resources and act also to the devastating of the coastal resources.

The need for integrated management of coastal area is obvious. The development of management strategies is needed to control the impacts of human interventions on the environment and to address issues of resource use conflicts. In the case of our study the land-sea interaction has to be addressed. The principles of the Integrated Coastal Zone Management (ICZM) can fulfill this scope. The ICZM system is applied for controlling human activities that affect the quality of the coastal environment and indirectly the human's perception for the coast, the boundary line between land and sea. It is basic for coastal management planning to recognize how activities on land affect environmental conditions of the sea. The management zone has to be extended from coastal hinterlands and lowlands, the "dry side" to the coastal waters, the "wet side". The human interventions on the coasts have to be well planned, adding to social prosperity of the coastal communities. Destructions of the environmental diversity of the coastal areas will have sooner or later a negative impact for the society.

The one-dimensional development in the Attica coastal front, applied in the last 80 years has to change totally. Another policy in all administrative levels is needed, a policy to support coastal resources and nature conservation. One has to be recognized: modification of the hinterlands has a high potential affecting on the resources of coastal zones (dams across rivers, landfill for different uses, recreative installations, airports, harbors, etc). The main philosophy of the actions has to be the sustainable management use, that means to ensure that renewable resources remain available to future generations.

Based on the principles of the Integrated Coastal Zone Management (ICZM) we try to formulate some concrete measures that they can be part of future planning.

a. Decentralization plans for the gigantic city of Attica basin

b. Mobilization of the citizens to participate in the planning procedures
Participation by major stakeholders, including the general public, is needed to involve all interests in the processes of programme formulation and implementation of actions related to coastal zone management.

c. Focusing on the coastal zone of the study area – Examples

- New development plans for the Alimos marina
For the Alimos marina interventions are planned (NTUA, 2017) following the old development mentality applied in the previous period. Plans based on the economic growth, without to take into account the social prosperity. In an area of 210.000 m^2 on the land zone of the marina touristic infrastructures are planned (hotels, restaurants, supermarkets, coffee shops, etc.). These plans are out of all the principles of the Integrated Coastal Zone Management. All the levels of planning have to

open these plans to the society and to motivate citizens participation. Public participation has to be important factor for the planners and the decision makers.

-Master plan for the development of the former Hellinikon Airport
Master plan for the development of the former Hellinikon Airport is also based on the perception of economic growth. The same philosophy: hotels, restaurants, apartments, etc. The planers left aside the local society. Human intervention on the coastal zone far away from the coastal communities

-Free access to the coastal front in the area of Voula – Vouliagmeni

References

Clark JR (1997) Integrated management of the coastal zones. -FAO-Food and Agriculture Organization of the UN, 152p.

NTUA (2017) Integrated management plan for the Attica coastal zone. -Technical Report, 113p.

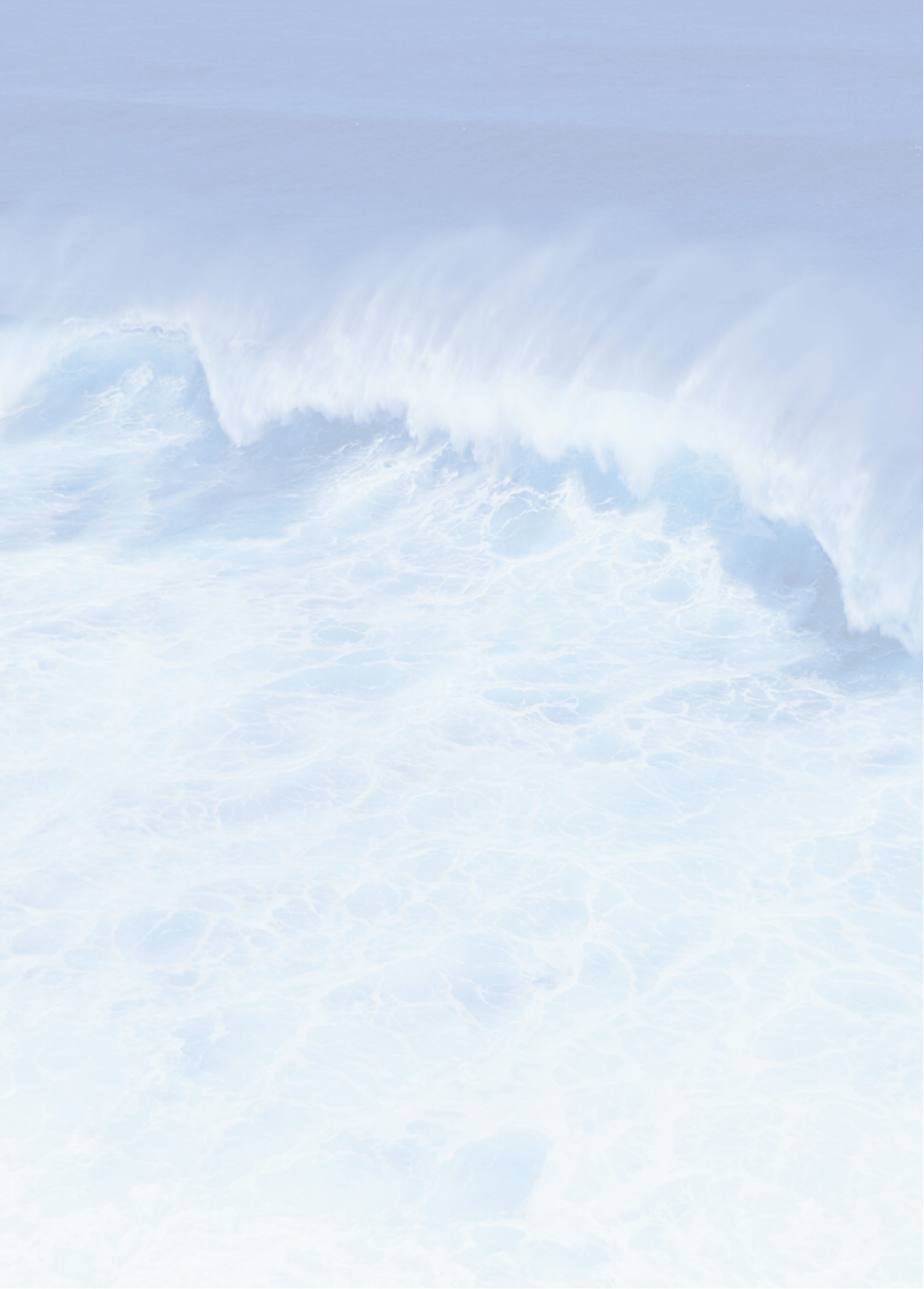

Comparative analysis of six coastal urban industrial areas in Greece regarding their vulnerability to coastal flooding

Ch. Giannakidou[1,*], D. Diakoulaki[1], C.D. Memos[2]

[1]Lab. of Industrial and Energy Economics, School of Chemical Engineering, National Technical University of Athens, Greece
[2]Lab. of Harbour Works, School of Civil Engineering, National Technical University of Athens, Greece
*Corresponding author: cgiannak@central.ntua.gr

Abstract

The scope of this article is to present a methodology developed to assess the coastal flooding vulnerability at urban domains with industrial installations within their area. As the climate change brings new data in the research field, an evaluation tool for assessing the cumulative impact of coastal flooding is expected to have an important contribution in the decision-making process. The industrial activity in the urban space could affect severely the vulnerability and it should be considered in designing the risk management plans in these areas. Coastal flooding can be a threat to life and to socioeconomic and environmental assets, whereas the additional impacts of an industrial accident due to coastal flooding may aggravate the threat. Therefore, there is a need to integrate tools able to consider, at different complexity levels, the interactions between several parameters in order to effectively assess the vulnerability of such areas. This paper illustrates the use of a composite vulnerability index in the risk assessment process. This index is applied at six (6) urban areas with vivid industrial characteristics in Greece and its results have been used in a comparative analysis to highlight the importance of the index's modules, as well as the weighting values of the parameters.

Keywords Vulnerability, Coastal flooding, Decision-making tool, Industries.

1 INTRODUCTION

For assessing vulnerability to coastal flooding, indicators have been proved crucial in representing the relevant variables and processes involved. They consist a support tool that often simplifies the understanding of the distribution and the variations observed in the vulnerability assessment process (Adger, 2006). The purpose of establishing an indicator set is to convey information that is easy to understand, and which can be analyzed quickly. Flooding is the result of a variety of factors that include environmental, social, and economic aspects (Kryvasheyeu et al., 2016). Therefore, generating an appropriate indicator system to evaluate vulnerability in quantitative terms is a challenging process. In risk perceptions the understanding of vulnerability is very broad and subjective. For the needs of this article, the vulnerability is defined as the susceptibility of a system to be affected or damaged as proposed by Villagran de Leon (2006). The use of indicator approaches is a common method to evaluate the vulnerability in the field of natural disaster risk assessment. Followingly, the internationally recognized indices that are used in vulnerability assessment are presented in brief

1.1 Environmental Sustainability Index – ESI

The ESI benchmarks the ability of nations to protect the environment over the next several decades. The 2005 ESI integrates 76 variables into 21 indicators of environmental sustainability for 146 countries (Saisana, 2014). These indicators fall into the following five broad categories: environmental systems, reducing environmental stresses, reducing human vulnerability to environmental stresses, societal and institutional capacity to respond to environmental challenges, and global stewardship.

1.2 Environment Quality Index – EQI

The EQI was developed to improve our understanding of the relationship between environmental conditions and human health for all counties in the U.S. using indicators from the chemical, natural, built and social environment. Included were five environmental domains: air, water, land, built and sociodemographic (Lobdell et al., 2014).

1.3 Environmental Vulnerability Index - EVI

The EVI has been developed by the South Pacific Applied Geoscience Commission (SOPAC), the United Nations Environment Programme (UNEP) and their partners. This index is designed to be used with economic and social vulnerability indices to provide insights into the processes that can negatively influence the sustainable development of countries. The EVI uses 50 smart indicators for estimating the vulnerability of the environment of a country to future shocks (Kaly et al., 2004).

1.4 World Risk Index – WRI

The WRI states the risk of disaster in consequence of extreme natural events for 172 of the world's countries. It is calculated on a country-by-country basis through the multiplication of exposure and vulnerability. Exposure covers threats of the population and other certain protected entities due to earthquakes, cyclones, floods, droughts and sea-level rise. Vulnerability encompasses the societal sphere and is comprised of three components, susceptibility, coping, and adaptation, which are weighted equally in the calculation (Welle and Birkmann, 2015).

1.5 Disaster Risk Index – DRI

The DRI enables the calculation of the average risk of death per country in large- and medium-scale disasters associated with earthquakes, tropical cyclones and floods, based on data from 1980 to 2000. It also enables the identification of a number of socio-economic and environmental variables that are correlated with risk to death and which may point to causal processes of disaster risk (UNDP, 2004). In the DRI, countries are indexed for each hazard type according to their degree of physical exposure, their degree of relative vulnerability and their degree of risk.

1.6 Climate Vulnerability Index -CVI

The CVI is a holistic and interdisciplinary tool developed to provide a clearer understanding of how climate and other global impacts on water resources are likely to influence human populations. It requires the calculation of a baseline score which takes account of a wide range of relevant factors, clustered within 6 core components, referred to as Global Impact Factors (GIFs), these are: Geospatial variability, Resource quantification, Accessibility and property rights, Utilisation and economic efficiency, Capacity of people and institutions, and Ecological integrity maintenance (Sullivan and Byambaa, 2013).

After taking into consideration these indices and their parameters, a new vulnerability index has been synthesized, the coastal urban industrial vulnerability index (CUIVI), to assess the vulnerability of urban coastal zones that incorporate industrial activities due to coastal flooding events as a result of the additional exposure to climate change. The scope of CUIVI is to find the most prominent and effective indicators in assessing the vulnerability depending on the scale of the problem and its specific conditions. Its main objective is to support significantly the decision-making process regarding the location and the license of industries that handle hazardous chemical substances, as well as to identify the appropriate mitigation measures.

2 THE COASTAL URBAN INDUSTRIAL VULNERABILITY INDEX (CUIVI)

The proposed structure of CUIVI contains six distinct modules that are considered to affect mostly the vulnerability of the system under study: 1. Physical system characteristics. 2. Environmental quality. 3. Economic features, assessing the economic impacts caused. 4. Industrial activity, assessing the preparedness of existing or planned industrial activities in mitigating the impacts due to coastal flooding. 5. Socio-demographic characteristics, reflecting the social and demographic characteristics that may impact the adaptability of a study area. 6. Administrative and management features. Each module consists of a set of parameters that are applicable in order to succeed a representative result that would be useful in the hands of decision-makers. It should be mentioned that the parameters presented in table 1 are not the whole set of indicators that form CUIVI and its modules. These are only the applicable ones in the study areas and the most fitting ones to the specific features of the problem. Therefore, CUIVI can differentiate when problems of another scale or specific features are studied. The following table presents the modules and the selected parameters of CUIVI for the initial vulnerability assessment to coastal flooding of six urban coastal areas in Greece with industrial activities in their zones. Moreover, every parameter is sorted regarding its role in the exposure (E), susceptibility (S), and resilience (R) of the study areas.

Table 1 Modules, Parameters and their role in the exposure (E), susceptibility (S), and resilience (R)

Module	Parameters	Units	E/S/R
1.Physical system characteristics	1. Sea Level Rise	mm/yr	E
	2. Storm Surge	cm	E
	3. River Discharge	m3/s	E
	4. Foreshore Slope	%	E
	5. Coastal erosion	m^2	E
	6. Coastline length	km	E
	7. Wave exposure	%	E
2.Environmental quality	1. Urbanisation	%	S
	2. Distance from environemental protected areas	km	R
	3. Sulfur dioxide (SO2) concentrations	$\mu g/m^3$	S
	4. Total suspended particulate concentrations	$\mu g/m^3$	S
3.Economic features	1. Yearly household income	€/yr	R
	2. GDP per capita	€/p	R
	3. Employment in secondary industry	%	S
	4. Unemployment	%	S
4.Industrial activity	1. Number of industrial establishments	#	S
	2. Annual turnover	€/yr	R
	3. Number of employees	#	S
	4. Number of industrial establishments under SEVESO III EU Directive	#	S
5.Socio-demographic characteristics	1. Population	p	S
	2. Hospital beds/1000 inhabitants	#/p	R
	3. Number of tourist accommodation establishments	#	S
	4. Museum visitors	p	S
	5. Depended household members	%	S
6.Administrative and management features	1. Distance form Authorities responsible for the emergency planning in case of a technological accident	km	S
	2. Number of people working for civil protection	p	R
	3. Public information actions	#	R

The calculation of each module of CUIVI is based on the general formula of Flood Vulnerability Index (FVI) as described in eq.1.

$$FVI = \frac{E \cdot S}{R} \quad (1)$$

The final value (Vtot) of the index for each area it is calculated as the sum of values of each module (V1, V2, …V6) as shown in eq. 2.

$$Vtot = \frac{V_1+V_2+V_3+V_4+V_5+V_6}{6} \quad (2)$$

2.1 Application of CUIVI

The CUIVI has been implemented in six urban coastal areas in Greece with industrial activities in their zones for the initial assessment of their vulnerability to coastal flooding. Specifically, the studied areas are parts of Elefsina (E), Thessaloniki (T), Rio-Patras (R), Heraklion (H), Volos (V), and Chryssoupolis-Kavala (C). The selected urban zones incorporate industrial activities, and they lay under the 50m contour line. In some cases, when big technical works exist, such as roads, railways, etc., the area's limit has been taken in lower elevation, as these constructions work as boundary concerning the coastal flooding. Comparing the scoring of each city, some valuable conclusions are highlighted to strengthen the resilience of these areas. The application of the index shows the importance of every module into the assessment of the vulnerability in case these areas are affected by a coastal flooding event. The values of the parameters used for the calculations of each module are normalised following the equation 3, as shown below.

$$NV_i = \frac{V_i}{V_{imax}} \tag{3}$$

where Vi represents the value of the parameter i and Vimax represents the maximum value from the set of values given to parameter i for each area. It should be mentioned that depending on the source of the data some of the values were expressed in grades from 1-4, i.e. for storm surge, wave exposure, yearly household income, etc. The normalised values are subsequently used for the calculation of Vtot. In table 2 are presented the results of the calculations for each module and the total value of CUIVI for each area.

Table 2 Calculated value of each module

	E	T	R	H	V	C
V1	3,5	5,0	4,5	5,5	4,0	4,5
V2	3,0	2,5	1,3	2,3	2,0	1,5
V3	1,3	1,0	0,8	0,6	0,8	1,3
V4	3,0	3,0	2,0	2,6	3,0	5,0
V5	3,0	3,3	4,5	6,0	4,5	3,7
V6	0,3	0,1	0,5	0,3	0,6	1,3
Vtot	2,4	2,5	2,3	2,9	2,5	2,9

3 RESULTS AND DISCUSSION

The results of the CUIVI calculation, as shown in Figure 1, rank Heraklion and Chryssoupolis-Kavala as the most vulnerable areas among the studied domains, when Rio-Patras is the most resilient one. In the case of Heraklion, as shown in table 3, the most vulnerable modules are the socio-demographic characteristics and the physical system characteristics. When for Chryssoupolis-Kavala the vulnerable modules are the industrial activity one, as well as the physical system characteristics.

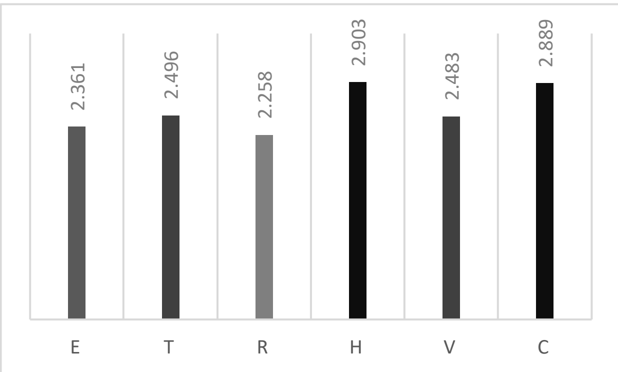

Figure 1 CUIVI results for the studied areas

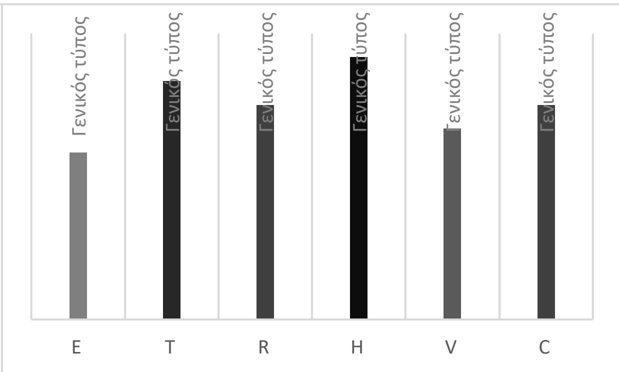

Figure 2 V1 – Physical system characteristics

Looking in detail the results of the physical characteristics module, presented in figure 2, Heraklion and Thessaloniki are more exposed areas to coastal flooding due to their geomorphology. As both areas are part of big cities, they have a relatively good performance in Administrative and management features module. The poor performance towards resilience of Heraklion in the socio-demographic characteristics module, as shown in figure 3, is due to the additional susceptibility, because of the high rates of the touristic activity, as shown from the parameters “Number of tourist accommodation establishments” and “Museum visitors”. The higher number of visitors induces higher vulnerability, as in the area people are unprepared in case of an emergency.

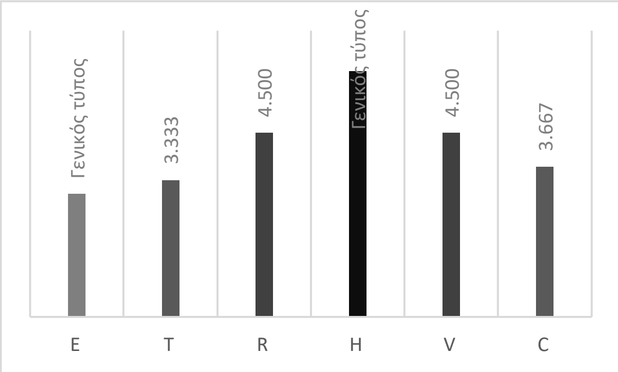

Figure 3 V5 – Socio-demographic characteristics

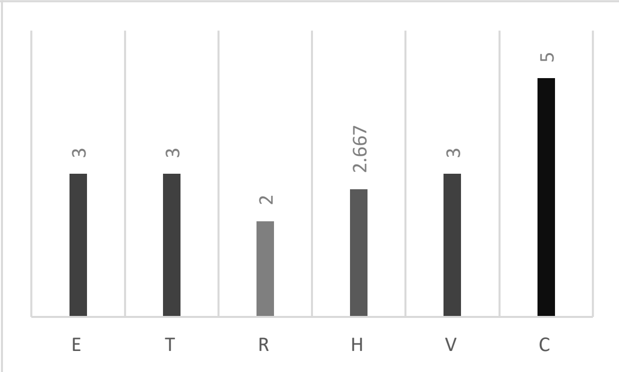

Figure 4 V3 – Industrial activity

Chryssoupolis-Kavala has a poor performance in the core module of the problem studied in this article, which is also presented in figure 3. There is a big number of industries handling hazardous substances, while the annual turnover of the secondary sector is rather low. That raises significantly the vulnerability of the area. On the other hand, Rio-Patras seems to be a resilient area although its vulnerability in the physical system characteristics module is ranked third. Something that probably contributes to its resilience is the fact that there is a low number of establishments under the SEVESO III EU Directive.

Finally, it should be noted that CUIVI is an unweighted index. Every parameter counts equally to the result. The findings of its application urge the need of adopting weights regarding the influence each module has to the final scoring. Weighting the indicators used can lead to safer choices in decision making process. The adoption of weight for every parameter and every module that formulate the CUIVI should be preferred even for an initial estimation of the problem studied.

4 CONCLUSIONS

In this paper, it has been presented the application of the unweighted composite index CUIVI in six urban coastal areas in Greece, where industries are implanted within the studied zones. The proposed index has been proved easy to apply, fast to calculate, and adjustable to the problem’s special features. For safer proposals in the decision-making process weights for each parameter and each module should be adopted.

References

Adger WN (2006) Vulnerability. Global Environmental Change, 16, pp. 268-281.

Kaly UL, Pratt CR and Mitchell J (2004). The Demonstration Environmental Vulnerability Index (EVI) 2004. SOPAC Technical Report 384, 323 pp.

Kryvasheyeu Y, Chen H, Obradovich N, Moro E, Hentenryck PV, Fowler J, Cebrian M, (2016) Rapid assessment of disaster damage using social media activity. Sci. Adv. 2, e1500779, doi: 10.1126/sciadv.1500779.

Lobdell D, Jagai J, Messer L, Rappazzo K, Messier K, Smith G, Pierson S, Rosenbaum B, and Murphy M (2014) Environmental Quality Index - Overview Report. U.S. Environmental Protection Agency, Washington, DC, EPA/600/R-14/305.

Saisana M (2014) Environmental Sustainability Index (ESI). In: Michalos AC (eds) Encyclopedia of Quality of Life and Well-Being Research. Springer, Dordrecht

Sullivan CA and Byambaa E (2013) The application of the Climate Vulnerability Index in Mongolia. Paper presented to the workshop of climate adaptation, UNECE, Geneva.

UNDP (2004) Reducing Disaster Risk: A Challenge for Development. New York: United Nations Development Programme Bureau for Crisis Prevention & Recovery

Villagran de Leon JC (2006) Vulnerability - A Conceptual and Methodological Review, SOURCE - Publication Series of UNU-EHS, United Nations University.

Welle T and Birkmann J (2015) The World Risk Index – An Approach to Assess Risk and Vulnerability on a Global Scale. Journal of Extreme Events. Volume 2.

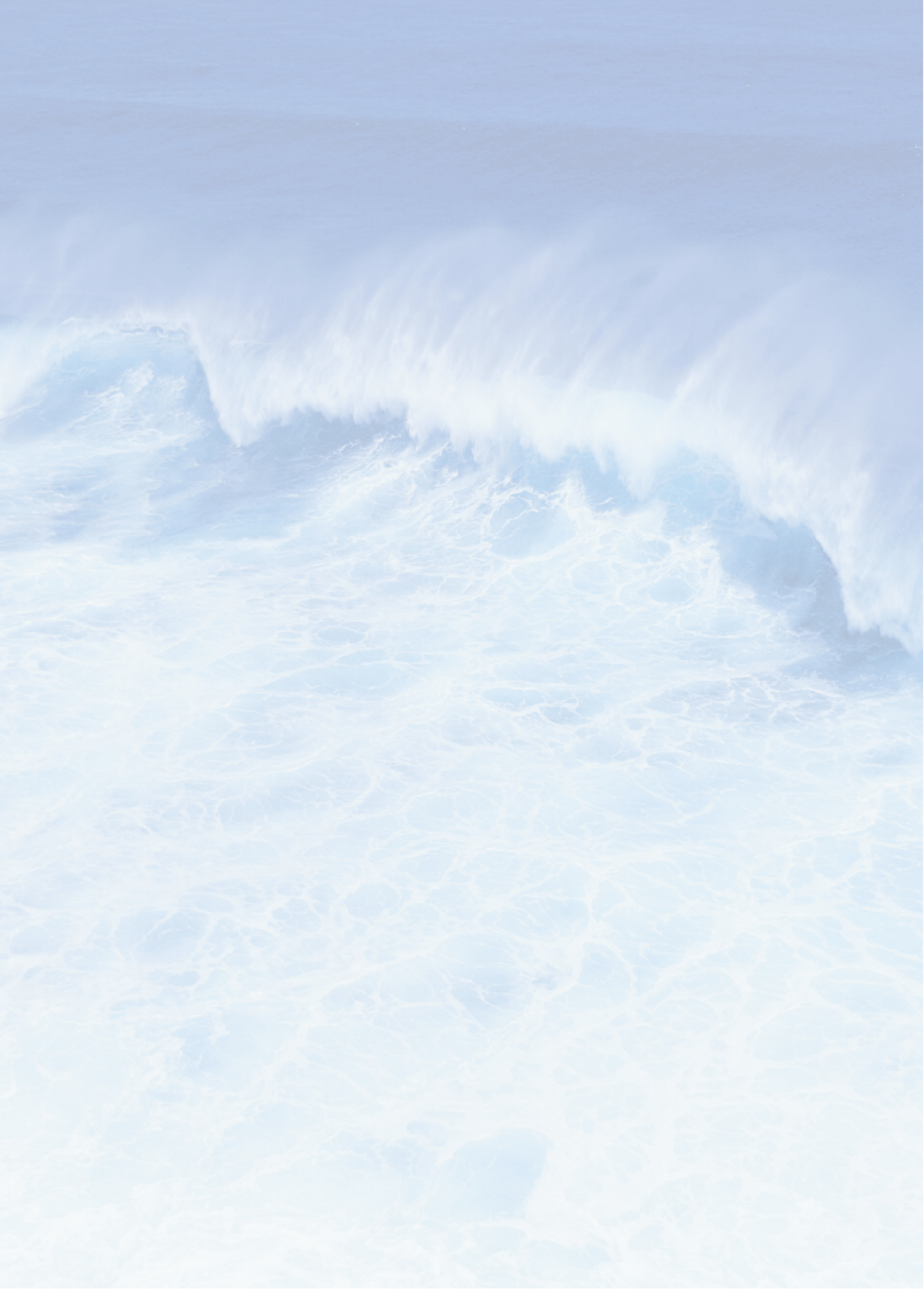

Χωρικό σύστημα λήψης αποφάσεων για την πόλη και το λιμάνι του Πειραιά

Γ. Κουμπαράκης*

Ερευνητής ΕΜΠ, Πτυχιούχος Γεωγραφίας - MSC ΕΜΠ, Υπ. Δρ ΕΜΠ, giwrgoskoumparakis@gmail.com
*Υπεύθυνος επικοινωνίας: giwrgoskoumparakis@gmail.com

Περίληψη

Στόχος της παρούσας ανακοίνωσης είναι η δημιουργία ενός ηλεκτρονικού περιβάλλοντος υποστήριξης των επενδύσεων ως μέρος μιας συνολικής αναπτυξιακής πολιτικής για την πόλη και το λιμάνι του Πειραιά, η οποία θα είναι δυνατή να προσελκύσει επενδύσεις και να συμβάλει στην τοπική ανάπτυξη και κατ' επέκταση στην εθνική. Το Χωρικό Σύστημα Λήψης Αποφάσεων που περιγράφεται αναλυτικά στην παρούσα εργασία στοχεύει στην ολοκληρωμένη ενημέρωση των ενδιαφερόμενων επενδυτών σχετικά με τις περιοχές στις οποίες θα δύνανται να αναπτύξουν επενδυτική δραστηριότητα αλλά και τις περιοχές οι οποίες υπόκεινται σε περιορισμούς ως προς την ανάπτυξης επενδυτικής δραστηριότητας σε αυτές, είτε λόγω παροντικών ιδιαιτεροτήτων είτε λόγω μελλοντικών εργασιών που πρόκειται να συμβούν σε αυτές. Επιπρόσθετα η παρούσα εργασία στοχεύει στην αναβάθμιση των πληροφοριών ενημέρωσης που ο Δήμος Πειραιά θα παρέχει προς ενδιαφερόμενους επενδυτές μέσω της προσθήκης υπηρεσίας συνολικής ενημέρωσης των ενδιαφερόμενων επενδυτών για το χωροταξικό, πολεοδομικό και περιβαλλοντολογικό θεσμικό, στρατηγικό και κανονιστικό πλαίσιο που διέπει τις χρήσεις γης στις περιοχές ενδιαφέροντος τουριστικής αναπτύξεως, καθώς και για το στρατηγικό σχεδιασμό στις περιοχές αυτές. Μέσα από την υλοποίηση του εν λόγω Χωρικού Συστήματος Λήψης Αποφάσεων για την πόλη και το λιμάνι του Πειραιά, ο Δήμος Πειραιά θα αποκτήσει την ικανότητα να διαθέσει σε κάθε ενδιαφερόμενο επενδυτή το σύνολο των προαναφερθεισών πληροφοριών για οποιαδήποτε περιοχή αναπτυξιακού ενδιαφέροντος, κατά τρόπο συγκροτημένο, συγκεντρωτικό, συνεκτικό και πλήρη.

1 ΕΙΣΑΓΩΓΗ

Τα τελευταία χρόνια, υπάρχει ένα μεταβαλλόμενο περιβάλλον όσον αφορά τον χώρο και τις κοινωνικό-οικονομικές δραστηριότητες, όπως η αύξηση του πληθυσμού και των περιβαλλοντικών προβλημάτων, τις ανάγκες για υποδομές, την ανεξέλεγκτη οικοδομική δραστηριότητα, την αύξηση της βιομηχανίας, του μαζικού τουρισμού, την περιθωριοποίηση των υπανάπτυκτων περιφερειών κτλ, όπου δημιουργεί στις πολιτικές εξουσίες (εθνικές, περιφερειακές, τοπικές) αλλά και σε διάφορους οργανισμούς, την ανάγκη λήψης κάποιας απόφασης για την αντιμετώπιση κάποιου προβλήματος που παρουσιάζεται στον χώρο , τόσο σε τοπικό επίπεδο αλλά πολλές φορές και σε παγκόσμιο.

Αρχικά, για να δοθεί μία λύση σε ένα πρόβλημα, πρέπει να προηγηθεί μία λεπτομερής ανάλυση του προβλήματος έτσι ώστε να γνωρίζουμε σε άριστο επίπεδο τις συνιστώσες του και έπειτα να αντιμετωπισθεί ανάλογα. Επομένως η συλλογή πληροφοριών για την αντιμετώπιση χωρικών προβλημάτων είναι μείζονος σημασίας, ιδιαίτερα το τελευταίο διάστημα όπου η ανάγκη συλλογής δεδομένων και πληροφοριών γίνεται ιδιαίτερα πιεστική, για τα προβλήματα που αναφέρθηκαν παραπάνω. Επίσης μη ξεχνάμε πως η καλύτερη αντιμετώπιση ενός προβλήματος είναι η πρόληψη του. Έτσι λοιπόν, συλλέγοντας συνεχώς δεδομένα και αξιόπιστες πληροφορίες που αφορούν ένα χώρο, υπάρχει η δυνατότητα οποιαδήποτε στιγμή , εάν παρουσιαστεί κάποιο πρόβλημα, να είμαστε σε θέση να ληφθεί κάποια απόφαση ή να "προλάβουμε" κάποιο πρόβλημα που θα παρουσιαστεί στο κοντινό μέλλον σ' αυτή την περιοχή.

Ένα εργαλείο συλλογής δεδομένων και στοιχείων είναι οι Βάσεις δεδομένων, είτε σε έντυπη είτε σε ηλεκτρονική μορφή, όμως ο μοναδικός τρόπος αξιοποίησης τους είναι απλά η αποθήκευση και η ανάκτηση των δεδομένων που περιέχουν. Μπορεί μία βάση δεδομένων να περιέχει γεωγραφικές, κοινωνικό-οικονομικές, περιβαλλοντικές κτλ πληροφορίες όμως δεν είναι δυνατή η παρουσίαση αυτών των πληροφοριών σε σχέση με τον χώρο, για τον λόγο αυτό, αναπτύχθηκαν τα Συστήματα Γεωγραφικών Πληροφοριών. (Μανιάτης,1993).

Η ιστορία των Χωρικών Συστημάτων Λήψης Απόφασης (ΧΣΛΑ - Spatial Decision Support System SDSS), ξεκίνησε περίπου το 1987 όταν προτάθηκαν για την επίλυση χωρικών ημι-δομημένων προβλημάτων, των οποίων οι επιλογές απόφασης ήταν πολλές και τα κριτήρια αξιολόγησης δεν ήταν πλήρως γνωστά. Σκοπός τους ήταν να βοηθήσουν τα άτομα μιας ομάδας στην διαδικασία λήψης μίας απόφασης, στα κριτήρια αξιολόγησης, στην εύρεση των εναλλακτικών αποφάσεων, τον εντοπισμό και την επιλογή της βέλτιστης απόφασης. (http://www.institute.redlands.edu/sds/welcome.html).

Συστήματα Λήψης Απόφασης είναι επιφορτισμένα με τη στήριξητης λήψης μιας απόφασης, μέσω της λειτουργίας ενός μοντέλου και με τη διαχείριση δεδομένων που βρίσκονται αποθηκευμένα σε μια βάση. Όμως απο τα Συστήματα Λήψης Απόφασης απουσιάζει ο χωρικός χαρακτήρας. Όλες τις προηγούμενες ελλείψεις αμβλύνονται με την εισαγωγή της τεχνολογίας των Χωρικών Συστημάτων Λήψης Απόφασης, ή, Spatial Decision Support System.Ως χωρικά συστήματα λήψης, απόφασης ονομάζονται τα διαδραστικά (interactive) υπολογιστικά συστήματα, τα οποία σχεδιάζονται ώστε να υποστηρίξουν έναν, ή, περισσότερους χρήστες, που λαμβάνουν μέρος στις διαδικασίες σχεδιασμού (design) στην επιλογή της πιο αποτελεσματικής απόφασης (higher effectiveness) στην προσπάθεια επίλυσης ενός ημι – δομημένου χωρικού προβλήματος λήψης απόφασης.. Τα χωρικά συστήματα υποστήριξης απόφασης κινούνται προς την επίλυση προβλημάτων και την υποστήριξη της λήψης κατάλληλων αποφάσεων σε θέματα, όπου συμμετέχει ο χωρικός παράγοντας. Αυτά συστήματα διακρίνονται σε ορισμένες κατηγορίες, με μέτρο διαφοροποίησης, είτε τα προς επίλυση προβλήματα, ή, την αρχιτεκτονική τους. Αδρομερώς, ως προς την αρχιτεκτονική τους, χωρικά συστήματα υποστήριξης απόφασης διακρίνονται σε: Stand – alone SDSS: όλο το σύστημα είναι εγκατεστημένο σε ένα και μόνο υπολογιστή και είναι δομημένα κατά τέτοιο τρόπο, ώστε να υποστηρίζουν και να εξυπηρετούν τις ανάγκες ενός μόνο χρήστη. Network SDSS: διάφορα δομικά στοιχεία του συστήματος υποστήριξης απόφασης βρίσκονται εγκατεστημένα σε πολλούς υπολογιστές και επομένως η απόφαση καθορίζεται απο τις απόψεις και τις παραμέτρους περισσοτέρων του ενός χρηστών. Ως προς τα προβλήματα που επιλύονται, τα χωρικά συστήματα υποστήριξης απόφασης διακρίνονται σε: Συστήματα επεξεργασίας χωρικών δεδομένων (Spatial Data Processing Systems): Αυτά τα συστήματα πλοηγούνται μέσα σε δεδομένα, όπου με τη χρήση κατάλληλων περιορισμών, κριτηρίων και στρατηγικών επιλύουν συγκεκριμένα προβλήματα, χωρίς τη συμμετοχή του χρήστη. Χωρικά Συστήματα Λήψεως Αποφάσεων (Spatial Decision Support Systems): Επιλύουν ημι – δομημένα, ή, κακώς δομημένα προβλήματα. Χρησιμοποιούν μια κατάλληλη μοντελοποίηση, ώστε να προβούν στη λήψη της καλύτερης απόφασης. Χωρικά Έμπειρα Συστήματα (Spatial Expert Systems): Όλη η γνώσης βάσης ενός έμπειρου επαγγελματία πάνω σε ένα συγκεκριμένο τομέα κωδικοποιείται σε κανόνες (Rules) με στόχο την επίλυση εξειδικευμένων προβλημάτων και τη δυνατότητα παίδευσης απείρων πάνω στη δεδομένη θεματολογία. (Ξενάκης,2007)

2 ΚΑΛΑ ΠΑΡΑΔΕΙΓΜΑΤΑ

Στην παρούσα εργασία μελετήθηκαν διεξοδικά κάποια παραδείγματα καλών πρακτικών Χωρικών Συστημάτων Λήψης Απόφασης, η μελέτη των οποίων συνέβαλλε καθοριστικά στη διαμόρφωση της τελική πρότασης για το σύστημα και παρουσιάζονται στη συνέχεια.

What if?

Αυτό το ΧΣΛΑ μπορεί να λειτουργήσει με δεδομένα ΣΓΠ, για την προετοιμασία ενός μακροχρόνιου προγραμματισμού μίας περιοχής. Αυτά τα δεδομένα μπορεί να είναι: χρήσεις γής, ο πληθυσμός της περιοχής, η απασχόληση, η ανάλυση κυκλοφορίας, προβλέψεις πληθυσμού και απασχόλησης κτλ. Επιτρέπει επίσης στους χρήστες γρήγορα και εύκολα να προσδιορίσουν τις επιπτώσεις εναλλακτικών πολιτικών όπως για παράδειγμα ο έλεγχος της αστικής ανάπτυξης, το ποσοστό διατήρησης της γεωργικής γης κτλ μέσω κατανοητών χαρτών και πινάκων. **(http://www.whatifinc.biz/)**

INDEX

Αυτό το ΧΣΛΑ είναι μία ολοκληρωμένη σουίτα ενός διαδραστικού εργαλείου σχεδιασμού για τη στήριξη λήψης αποφάσεων σε όλες τις φάσεις σχεδιασμού και ανάπτυξης μίας περιοχής. Μερικές ενέργειες που μπορεί να υποστηρίξει είναι πχ στην αξιολόγησης των συνθηκών μιας περιοχής, στον σχεδιασμό μελλοντικών σεναρίων, στην παρακολούθηση της εφαρμογής των εγκεκριμένων σχεδίων κτλ. **(http://www.crit.com/)**

Marine Integrated Decision Analysis System (MIDAS)
Αυτό το ΧΣΛΑ είναι ένα εργαλείο λογισμικού που αναπτύχθηκε για τρεις κύριους στόχους: (1) να βοηθήσει τη διαχείριση των θαλάσσιων περιοχών τόσο από μεριά των σχεδιαστών όσο και από μεριάς των διαχειριστών, έτσι ώστε να μπορούν να σχεδιάσουν ανάλογα με τα προβλήματα της περιοχής (2) για την εκτίμηση πιθανών επιπτώσεων της διαχείριση των θαλάσσιων περιοχών που βασίζεται στο οικολογικό και στο κοινωνικοοικονομικό περιβάλλον, και τέλος (3) για την παροχή συμβουλών διαχείρισης, αναθεωρήσεις σχεδίων κτλ που θα οδηγήσουν στη βελτιστοποίηση των αποτελεσμάτων και των εκροών. (**http://people.bu.edu/suchi/midas/index.html**)

IDRISI Taiga
Αυτό το ΧΣΛΑ, είναι ένα ολοκληρωμένο πρόγραμμα που συνδυάζει τα ΣΓΠ και την επεξεργασίας εικόνων. Το πρόγραμμα παρέχει στον χρήστη περισσότερα από 300 εργαλεία που τον βοηθάνε να αναλύσει και να προβάλει χωρικά δεδομένα. Ένα εργαλείο του, το «Land Change Modeler» είναι ένα εργαλείο όπου μπορεί να αναλύσει, και να προβλέψει τις επιπτώσεις των αλλαγών των χρήσεων γης στο οικοσύστημα και την βιοποικιλότητα της περιοχής. Τα παραδείγματα εφαρμογής που θα μπορούσαν να παρουσιαστούν είναι πάρα πολλά, γι' αυτό θεωρήθηκε ότι είναι καλύτερα να παρουσιαστούν επιγραμματικά μερικά από αυτά, και στο επόμενο κεφάλαιο να παρουσιαστεί ένα εκτενέστερα. Το παράδειγμα εφαρμογής που θα παρουσιαστεί παρακάτω λέγεται GRAS και αφορά την ανάλυση, διαχείριση και την λήψη αποφάσεων χώρων αστικού πρασίνου. (**http://www.clarklabs.org**)

Ανάλυση Χωρικού Συστήματος Λήψης Απόφασης GRAS: A Spatial Decision Support System for Green Space Planning
Το GRAS είναι ένα ΧΣΛΑ που δημιουργήθηκε με σκοπό να ενισχύσει την διαδικασία λήψης αποφάσεων για τους χώρους αστικού πρασίνου, να αξιολογήσει την κατάστασή τους και τα οφέλη που προσφέρουν, καθώς επίσης και στο να υποστηρίξει τις διαδικασίες προγραμματισμού, σχεδιασμού και συντήρησης αυτών. Ο προγραμματισμός αναφέρεται στην διαδικασία της πρόβλεψης ή της επιρροής της φυσικής διάταξης (θέση και μέγεθος) των χώρων πρασίνου στο δομημένο περιβάλλον. Ο σχεδιασμός αναφέρεται στην επιλογή των χαρακτηριστικών (εγκαταστάσεις και χαρακτηριστικά) στο πλαίσιο του φυσικού χώρου για την ικανοποίηση των κριτηρίων που έχουν τεθεί και τέλος η συντήρηση περιλαμβάνει τις επαναλαμβανόμενες, περιοδικές ή προγραμματισμένες αναγκαίες εργασίες για την αποκατάσταση, την πρόληψη των ζημιών ή τη διατήρηση των χαρακτηριστικών των πράσινων χώρων. Αναλυτικότερα το GRAS είναι μια πλήρως ολοκληρωμένη GIS εφαρμογή, βασισμένη σε συγκεκριμένα σενάρια, προσομοίωσης, πολλαπλών κριτηρίων και ενός συστήματος αξιολόγησης. Μία άλλη δυνατότητα της εφαρμογής αυτής είναι ότι υποστηρίζει τους χρήστες της, κατά την έρευνα τους για βιώσιμες μελλοντικές επιλογές των πράσινων χώρων εντός του δομημένου περιβάλλοντος και σύγκριση με τις υπάρχοντες. Το GRAS έχει εφαρμοστεί επιτυχώς στην πόλη Eindhoven (Νότια Κάτω Χώρες). Πιο συγκεκριμένα, μοντέλα και εργαλεία του GRAS χρησιμοποιήθηκαν για τον εντοπισμό και τη διάγνωση πιθανών αδυναμιών και προβλήματα στο συνολικό απόθεμα πράσινων χώρων της πόλης. Επίσης χρησιμοποιήθηκε στην αξιολόγηση των υπαρχόντων αποθεμάτων χώρων πρασίνου με στόχο μια μελλοντική «αποθήκη» πράσινων χώρων. Τελικός, το εγχείρημα της εφαρμογής του GRAS, αποδείχθηκε να είναι ένα σταθερό πλαίσιο, ικανό να υποστηρίξει κάθε στάδιο της διαδικασίας λήψης αποφάσεων στους χώρους πρασίνου, του σχεδιασμού τους και της παρακολούθησής τους. (https://www.researchgate.net/publication/226138971_GRAS_A_Spatial_Decision_Support_System_for_Green_Space_Planning)

3 ΤΟ ΧΩΡΙΚΟ ΣΥΣΤΗΜΑ ΛΗΨΗΣ ΑΠΟΦΑΣΕΩΝ ΓΙΑ ΤΗΝ ΠΟΛΗ ΚΑΙ ΤΟ ΛΙΜΑΝΙ ΤΟΥ ΠΕΙΡΑΙΑ

Μια εξαιρετικά σημαντική δραστηριότητα του Δήμου Πειραιά είναι και η χάραξη της αναπτυξιακής πολιτικής και ο επιτελικός σχεδιασμός της ανάπτυξης του Δήμου βάσει της ασκούμενης πολιτικής. Στο πλαίσιο ενίσχυσης της αναπτυξιακής πολιτικής της πόλης και του λιμανιού του Πειραιά αποφασίστηκε, μετά από αναλυτική διερεύνηση της σχέσης της πόλης και του λιμανιού του Πειραιά, αλλά και μετά από ανάλυση των κοινωνικών, πολιτικών, οικονομικών και πολεοδομικών μεταβολών που συντελέστηκαν στην πόλη του Πειραιά, δια μέσου του χρόνου, η δημιουργία ενός «Χωρικού Πληροφοριακού Συστήματος για την πόλη του Πειραιά».

Το «Χωρικό Πληροφοριακό Σύστημα για την πόλη του Πειραιά» στοχεύει στην υποστήριξη των επενδύσεων, και στη συντονισμένης επικοινωνιακής προβολής της εικόνας των επενδυτικών ευκαιριών του Δήμου Πειραιά τόσο στο εσωτερικό όσο και στο εξωτερικό. Επιπρόσθετα στοχεύει στην αναβάθμιση των υπηρεσιών ενημέρωσης που Δήμος Πειραιά παρέχει προς ενδιαφερόμενους επενδυτές μέσω της προσθήκης υπηρεσίας συνολικής ενημέρωσης των ενδιαφερόμενων επενδυτών για το χωροταξικό, πολεοδομικό και περιβαλλοντολογικό θεσμικό και κανονιστικό πλαίσιο που διέπει τη χρήση γης στις περιοχές ενδιαφέροντος τουριστικής αναπτύξεως, καθώς και για το ήδη υφιστάμενο επενδυτικό περιβάλλον στις περιοχές αυτές. Μέσα από την υλοποίηση του εν λόγω Συστήματος, ο Δήμος Πειραιά θα αποκτήσει την ικανότητα να διαθέσει σε κάθε ενδιαφερόμενο επενδυτή το σύνολο των προαναφερθεισών πληροφοριών για οποιαδήποτε έκταση αναπτυξιακού ενδιαφέροντος, κατά τρόπο συγκροτημένο, συγκεντρωτικό, συνεκτικό και πλήρη. Πέραν αυτών των πληροφοριών, ο Δήμος Πειραιά θα δύναται να παρέχει –μέσω της εφαρμογής– πρόσθετες πληροφορίες επιχειρηματικού ενδιαφέροντος.

Ειδικότερα, ο Δήμος Πειραιά θα αποκτήσει την επιχειρησιακή ικανότητα να διαθέσει σε κάθε ενδιαφερόμενο επενδυτή το σύνολο των προαναφερθεισών πληροφοριών για οποιαδήποτε έκταση αναπτυξιακού ενδιαφέροντος, κατά τρόπο συγκροτημένο, συγκεντρωτικό, συνεκτικό και πλήρη. Μέσω του προτεινόμενου Χωρικού Συστήματος Λήψης Αποφάσεων, θα είναι δυνατή η εύρεση του συνόλου των πληροφοριών, σε ότι αφορά:

- τον αιγιαλό και την παραλία,
- τα εγκεκριμένα Ρυθμιστικά Σχέδια,
- τα Γενικά Πολεοδομικά Σχέδια,
- τα Σχέδια Χωρικής και Οικιστικής Οργάνωσης Ανοικτής Πόλης,
- τις δράσεις της Στρατηγική για τη Γαλάζια Ανάπτυξη
- τις δράσεις της Ολοκληρωμένη Χωρική Επένδυσης
- τις επενδυτικές δράσεις της COSCO για τον ΟΛΠ ΑΕ
- τις Ζώνες Οικιστικού Ελέγχου,
- τις περιοχές NATURA,
- τις ζώνες προστασίας αρχαιολογικών χώρων,
- τους ιστορικούς τόπους,
- τα φυσικά πάρκα περιοχών οικοανάπτυξης,
- τις δασικές περιοχές
- άλλες περιβαλλοντικά ευαίσθητες περιοχές,
- τη χερσαία ζώνη λιμένα Πειραιά

Οι ανωτέρω πληροφορίες θα αποτελούν επίπεδα που θα υπερτίθενται πάνω στο ενιαία επεξεργασμένο υπόβαθρο (1945) ορθοφωτοχαρτών του Κτηματολογίου (2006 – 2015). Πέραν αυτών των πληροφοριών, η υπηρεσία θα παρέχει –μέσω της εφαρμογής– πρόσθετες πληροφορίες επιχειρηματικού ενδιαφέροντος. Συγκεκριμένα, θα απεικονίζονται οι υφιστάμενες ή αναπτυσσόμενες ήδη εγκαταστάσεις τουριστικού ενδιαφέροντος, όπως:

- ξενοδοχεία,
- μαρίνες,
- κατοικίες,
- κτίρια γραφείων,
- τράπεζες,
- νοσοκομεία,
- εγκαταστάσεις τουρισμού και αναψυχής,
- επιχειρηματικά πάρκα,
- θεματικά πάρκα,
- εμπορικά κέντρα,

Η γνώση των ανωτέρω πρόκειται να καθιστά την απόφαση για μία ενδεχόμενη επένδυση τεχνικά και οικονομικά ευσταθή. Στη συνέχεια αναφορικά με το, εν λόγω Σύστημα, θα περιγραφούν:

- Η Αρχιτεκτονική του Συστήματος
- Η λογική του Συστήματος
- Οι Λειτουργικές απαιτήσεις του συστήματος

- Το Υποσύστημα Υποστήριξης Επιχειρηματικών αποφάσεων
- Οι Ενδεικτικές Περιπτώσεις για το Υποσύστημα Επιχειρηματικών Αναφορών
- Το Υποσύστημα Γεωγραφικής Βάσης δεδομένων (GIS)
- Οι Λειτουργικές απαιτήσεις Υποσυστήματος Γεωγραφικής Βάσης Δεδομένων
- Οι Προσφερόμενες Ψηφιακές Υπηρεσίες

Ευχαριστίες
Ευχαριστώ ιδιαίτερα τον Άγγελο Σιόλα, Θωμά Χατζηχρήστο και Ευθύμιο Μπακογιάννη για την καθοριστικής σημασίας συνδρομή τους στην εν λόγω εργασία

Βιβλιογραφικές Αναφορές

Ξενάκης Θεόδωρος, Μεταπτυχιακή Διπλωματική Ανάπτυξη Χωρικού Συστήματος Υποστήριξης Απόφασης για τη Χωροθέτηση Αιολικών Πάρκων (σύστημα HUMAN XORASYS), Αθήνα 2007, σελ. 133-134,137-138 (http://dspace.lib.ntua.gr/bitstream/123456789/553/1/xenakist_sdss.pdf)
Maniatis Y., “ Geographic Information System”, Geo - Cadastre, Ziti publications, Thessaloniki, 1993, p. 25.
(http://www.institute.redlands.edu/sds/welcome.html)
(http://www.whatifinc.biz/)
(http://www.crit.com/)
(http://people.bu.edu/suchi/midas/index.html)
(http://www.clarklabs.org)
(https://www.researchgate.net/publication/226138971_GRAS_A_Spatial_Decision_Support_System_for_Green_Space_Planning)

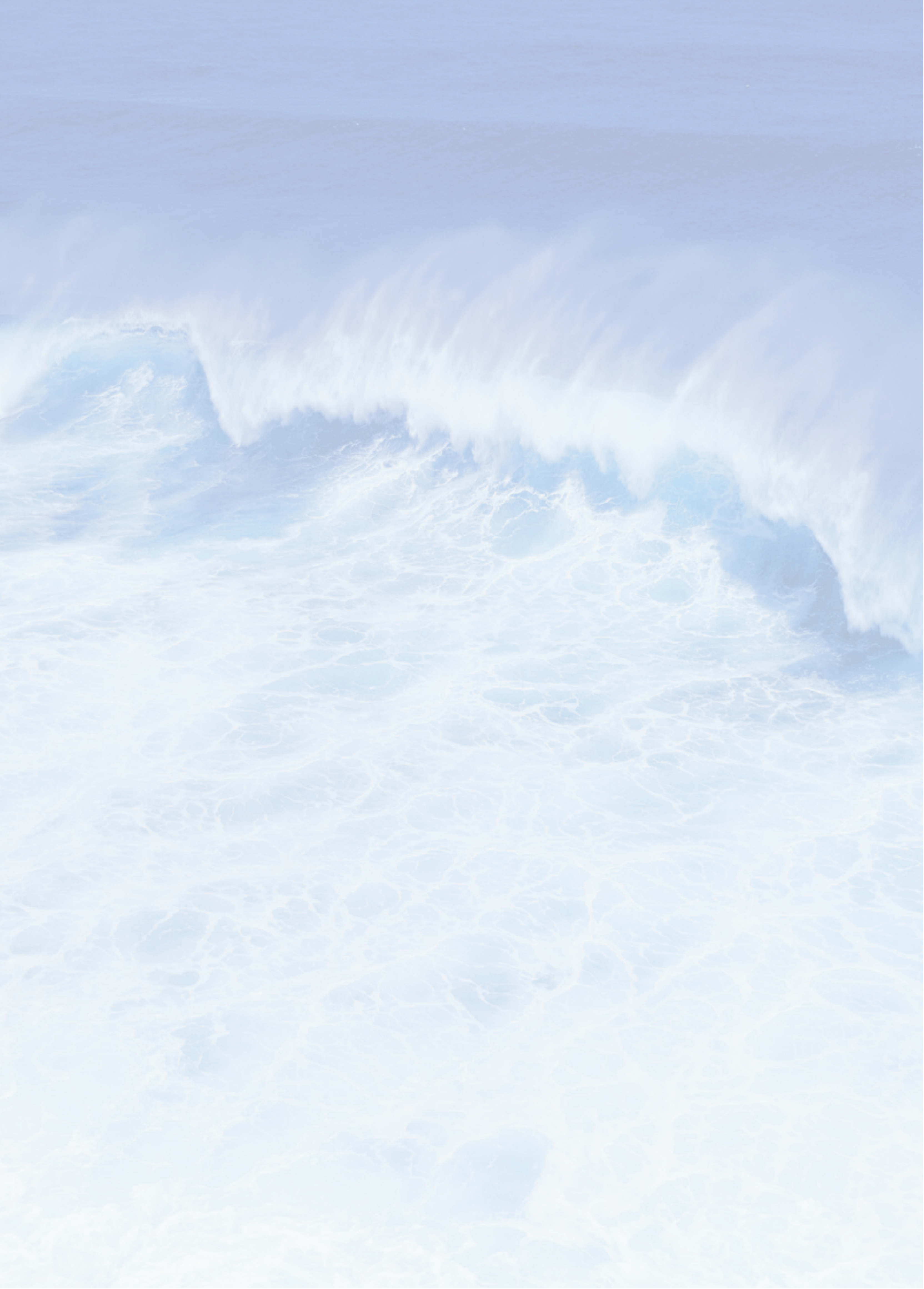

Coastal geomorphological changes in a semi-enclosed bay, induced by recreational interventions

S. Petrakis[1,2*], G. Alexandrakis[2], N. Rempis[2,3], N. Kampanis[2]

[1]Laboratory of Physical Geography, Department of Geology & Geoenvironment, NKUA, Panepistimioupolis Zografou, 15784, Greece
[2]Coastal & Marine Research Lab, Institute of Applied & Computational Mathematics, Foundation for Research & Technology-Hellas, Vasilika Vouton, Crete, 70013, Greece
[3]Department of Geography, University of the Aegean, University Hill, Mytilene, 81100, Greece
[*]Corresponding author: spetrakis@geol.uoa.gr

Abstract

Elounda bay (NE Crete, Greece) is an important coastal area, incorporating sites of significant historical/cultural values. Additionally, Elounda Bay plays a very important role in the economy of the island, since it hosts large-scale tourism facilities. The local economy is based almost entirely on tourism, by exploiting the nearby beaches, in a total coastal front of about 7 km. The continued growth of tourism in the area eventually resulted in the need for additional interventions in the coastal zone and subsequently in increased pressures in the coastal environment. The result from the aforementioned interventions was the significant alteration of the morphology of the coastline by increasing man-made areas through time. During the last seven decades, the area occupied by coastal structures has quadrupled, whereas landwards the area covered by settlements has octupled. In the meantime, the area lost due to erosion has been calculated to be about 14000 m^2, most of it affecting natural and artificial beaches in front of tourism facilities, mainly in areas where coastal interventions have been settled. The erosion phenomena where not induced primarily by climate or natural factors, but are mainly anthropogenic related.

Keywords Coastal structures, Tourism settlements, Anthropogenic pressures, Coastal erosion.

1 INTRODUCTION

The Island of Crete is one of the top tourism destinations in Europe. According to the latest report from the Institute of the Greek Tourism Confederation (INSETE, 2019), 4 million arrivals of foreign and domestic tourists was recorded during 2017, in an island with a local population of 600 thousand residents. Furthermore, more than 24 million tourism accommodations were registered during 2017, which accounts to ¼ of total tourism accommodations in Greece. In Lasithi prefecture, with a local population of 75 thousands, the arrivals for 2017 were 650 thousands and the overnights 3.5 million. The above numbers clearly depict the tourism pressure applying in the area, during (mostly) the summer season (April-October). According to socioeconomic studies (e.g. Alexandrakis, 2014), the average value of a beach in northern Crete is estimated at 18.5 €/m^2/day. On the other hand, Crete, and especially its northern coast is relatively vulnerable to erosion (Alexandrakis, 2014). Furthermore, according to Monioudi et al. (2014), on the basis of two sea level rise (SLR) scenarios (0.26 m and 0.82 m by 2100), the beaches of E. Crete will be significantly affected. For the 0.26 m SLR scenario, 16% of the beaches will retreat by more than half of their maximum dry width, whereas for the SLR of 0.82 m, the corresponding percentage will reach 76%, with consequent loss on the local economy of E. Crete.

2 STUDY AREA

The area under investigation is the coastal front of the Elounda Bay, E. Crete, in a length of about 7 km (Figure 1). The majority (85.6%) of the coastline is characterized as Low vulnerability area, consisting mainly of rocky coasts, steep slopes, and man-made structures. A very small percentage (0.3%) is classified as Medium vulnerability area, whereas High and Very High vulnerability areas correspond to 7.8 % and 5.8 % of the total coastline length respectively, mainly beaches and soft rocky coasts (Alexandrakis et al., 2014). The areas of High and Very High vulnerability ranks are those where large tourism settlements have been constructed and thus, undertake the majority of the tourist flows. The area is surrounded by various sites of cultural and archaeological interest, such as ancient cities and facilities (towers, reservoirs, churches, fortresses), dating from the Minoan era (27th-15th Cen. B.C.), where the -now submerged- city of Olous was present, and followed by posterior cities from Arab (8th Cen. A.C.), Venetian (13th-14th Cen. A.C.), and Othoman invaders (15th-19th Cen. A.C.). The most important historical monument is the Spinalonga fortress, located on a small island at the center of the bay. It has recently been nominated to enter the UNESCO organization as a Natural Cultural Heritage.

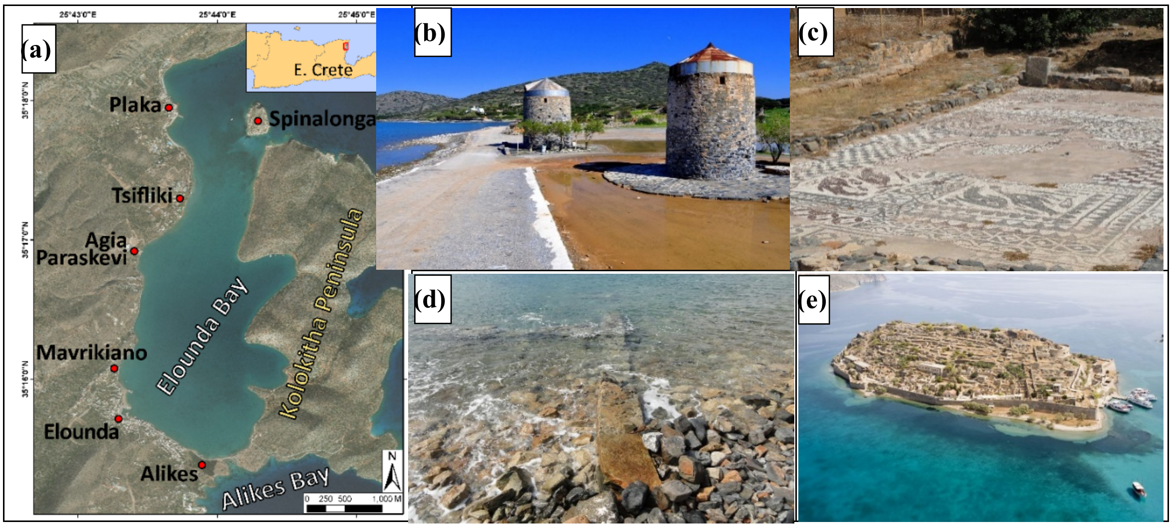

Figure 1 Study area of Elounda Bay (a) and the surrounding settlements: b) historical windmills, c) early Byzantine era Mosaic, d) submerged Roman era fortress, e) Spinalonga Islet

The tourism development of the area started during the 1970's and has been rapidly expanding to the present, heavily affecting the coastal zone, mainly through large-scale tourism settlements (hotels, taverns, beach-bars etc) and coastal constructions (coastal roads, groynes, small ports, artificial beaches etc). The aforementioned development is also reflected to the local population (Figure 2a), which, according to the Hellenic Statistical Authority's censuses, has doubled during the years 1971-2011. The facilities and coastal works construction follows this development pattern, showing an exponential rate of construction during the last 50 years (Petrakis and Rempis, 2018) (Figure 2b).

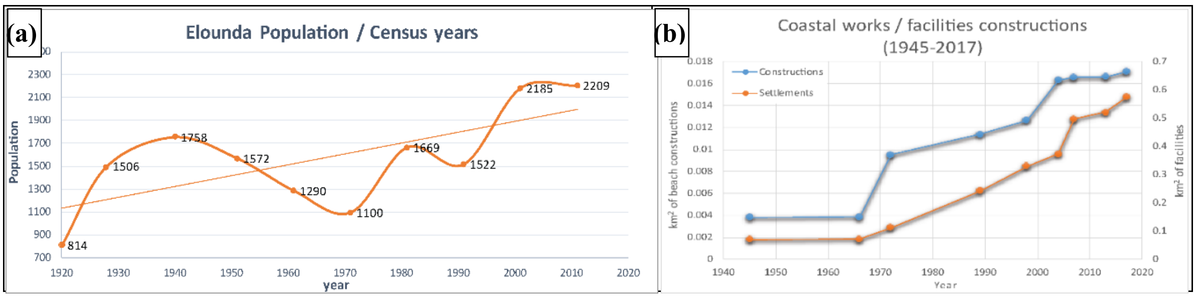

Figure 2 Evolution of population of the municipality of Elounda, 1920 – 2011 (a) and construction of facilities and coastal works, 1945 – 2017 (b)

3 METHODS

In order to assess the changes of the coastal front in Elounda bay, aerial photos (from the years 1945, 1966, 1972, 1989, 1998 and 2004) and satellite images (from the years 2007, 2013 and 2017) of the area were analyzed in a Geographic Information System, covering a period of 72 years. The comparison of coastlines revealed changes, ranked in three categories: (i) loss (erosion), (ii) gain (accretion) and (iii) artificial gain (coastal constructions). Additionally, the coastal works (coastal walls, ports, groynes etc) were mapped and correlated to the urban fabric expansion through time (Figure 3), in order to assess the positive or negative result of the installations on various areas. A correlation of the measured shoreline changes was estimated, by applying a wave model for the area, with climatic data from the Wind and Wave Atlas of the Hellenic Seas (Soukissian et al., 2007).

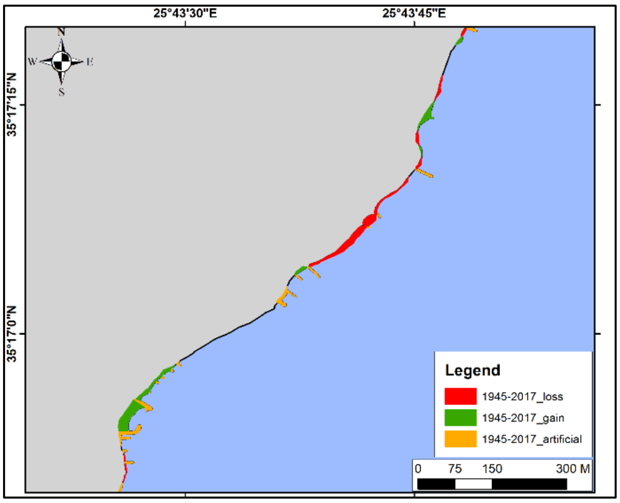

Figure 3 An example of analysis on coastal works and land loss/gain/artificial gain

The area is also subject to "local" waves, generated by small sized renting boats travelling from Plaka and Elounda to Spinalonga Islet, reaching to about 70 transfers per day, from April to November each year. According to unpublished data owned by the authors, the speed of about 6 knots with which the boats travel to and from Spinalonga, generates waves with a height of about 0.3 m and period of about 3 sec, corresponding to a constant wind of about 3 Beauforts for a period of 9 months. These waves affect mostly the southern and central part of the study area.

4 RESULTS

The waves affecting the study area, due to the morphology of the surrounding and the Kolokitha Peninsula which "barricades" the bay, are mainly of N (mostly through diffraction), NE and E direction. Their offshore force is significantly reduced at the NE entrance of the Bay, with the exception of the E wind generated waves which affect the northern part of the area (Plaka and Agia Marina) unobstructed, resulting to the wave heights and periods depicted in Table 1. The most frequent waves affecting the area (F=12.89%) derive from waves of N direction with height and period of 0.4 m and 3 sec, respectively. Accordingly, the most frequent waves of NE and E direction have heights and periods of 1.3 m – 3.2 sec and 1.5 m – 3.75 sec, respectively. The maximum waves affecting the majority of the Bay are of NE direction, occur rarely (F=0.44%) and have height – period of 3.4 m – 6.8 sec, respectively. The rather low wave energy reaching the southern area of the Bay is able to oscillate the fine sediments that consist the beaches and, thus, change the shoreline position over time.

Table 1 Wave characteristics of N, NE and E direction

Direction	U (m/s)	F (%)	H_s (m)	T_s (sec)	H (m)	T (sec)	D (deg.)
N	13,5	12,89	1.52	6.00	0.4	3.0	76
	19	7,89	2.31	6,89	0.6	3.6	79
	24,5	4,44	3.16	7,64	1.25	4.4	81
	30,5	1,78	4.14	8,35	1.5	5.5	84
	37	0,56	5.25	9.03	1.6	5.2	87
	41	0,44	5.96	9.41	1.8	5.5	89
NE	8,5	4,22	0,59	4,06	1,3	3,2	65
	13,5	3,22	1,9	6,96	1,5	4,8	70
	19	1,56	2,9	7,99	3,2	6,2	79
	24,5	0,44	3,96	8,86	3,4	6,8	86
E	8,5	4,78	0,71	4,37	1,5	3,75	90
	13,5	2,33	1,25	5,28	1,7	4,2	90
	19	0,67	1,9	6,06	1,9	4,8	90
	24,5	0,33	2,6	6,72	2,3	5,2	90

	37	0,11	4,32	7,94	3,3	6,5	90
	41	0.03	4,9	8,28	3,8	6,8	90

Key. U: wind speed, F: annual frequency, Hs: offshore wave height, Ts: offshore wave period, H: wave height inside the Bay, T: wave period inside the Bay, D: shoreline approaching direction of the wave

Six areas of the Elounda Bay, affected significantly by the human intervention, were selected in order to quantify the change of the coastal zone during the last 72 years. Plaka (Figure 4a), Agia Marina (Figure 4b), Driros (Figure 4c), Agia Paraskevi (Figure 5a), Elounda (Figure 5b) and Poros (Figure 5c).

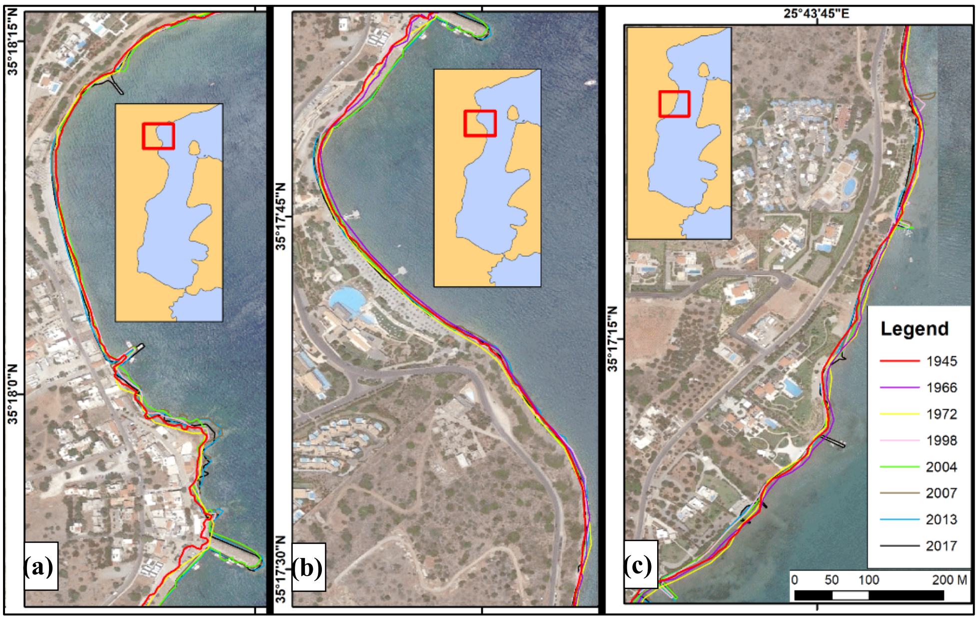

Figure 4 Coastline displacement in the areas of Plaka (a), Agia Marina (b) and Driros (c)

Plaka beach is located at the northern part of the Bay. It consists of cobbles and has a length of 220 m and width of about 12 m. The observed average erosion is about 3 m, whereas the maximum erosion is at its N part (8 m). During the last 4-5 years the area NE of the beach is being built, causing instability to the conglomerate formation on which the constructions are based. Furthermore, the coastal area in front of the town of Plaka undergoes significant wave excavations, causing instability of the coastal settlements. The erosional phenomena are rather strong at this part, since, in contrast to the southern coastal area, the NE and E wind-generated waves strike the coast unimpeded.

Agia Marina beach is located south of Plaka, consists of rounded cobbles and has a length of 280 m and width of about 16 m. No man-made coastal protection constructions are present. The observed average erosion is about 5 m, whereas the maximum erosion occurs at its N part (10 m).

Driros beach is the beach with the most coastal works in the area. The average erosion is about 6 m, whereas it reaches up to 15 m in some places. Several groynes have been constructed along the coast, but have not managed to tackle the erosion.

There is no observed erosion in *Agia Paraskevi*'s coastal front. Two artificial beaches have been built along the coast, through nourishment between groynes, the northern one at the early 2000's and the southern in 2007. Both seem to function rather well, whereas there is no obvious impact in nearby coasts, with the exception of the north part of the northern one, where an erosion of about 2-3 m is observed after the creation of the beach.

The *Elounda port* was constructed at about 1970, whereas during the 1980's it was expanded at its present form. With the creation of a 100 m long groyne north of the port, a 25 m width beach was created, serving as the municipality beach of Elounda. The majority of the southern coastal front of

Elounda is protected by a coastal wall, which seems to work well with the wave regime affecting the area.

The *Alikes area* was serving as a salt-pans until 1972. The area, due to its very low relief, is subjected to ephemeral movement of the coastline, but seems to have been in balance during the last decades, with a small erosion of 1-2 m to be observed.

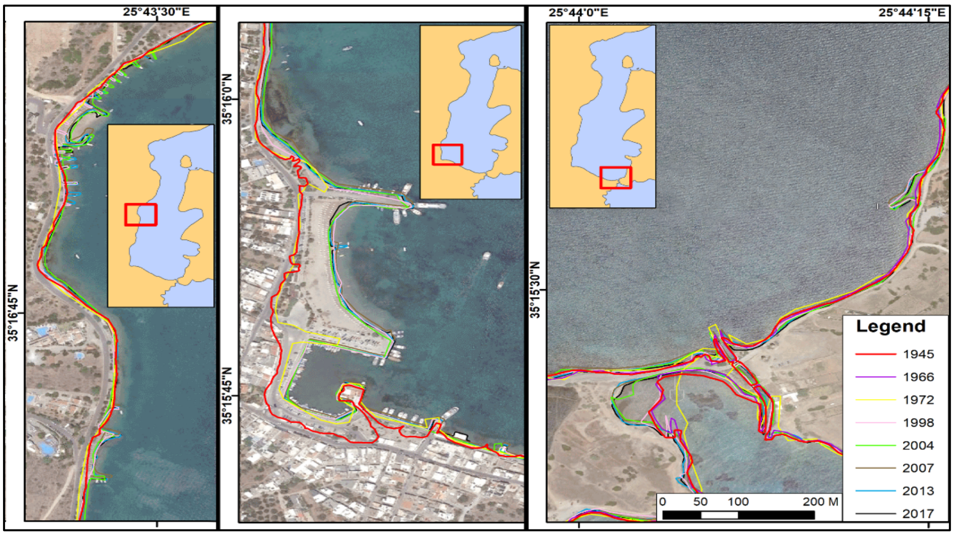

Figure 5 Coastline displacement in the areas of Agia Paraskevi (a), Elounda (b) and Alikes (c)

5 CONCLUSIONS

The coastal front of Elounda Bay is a heavily affected area, due to the inland settlements and the coastal works built for the protection of the shoreline and the control of sediments, mainly for tourism purposes (creation / constrain of beaches serving the tourists and local population). Most of the coastal constructions do not serve effectively their purpose, as erosion seems to continue, mainly at the northern and central part of the area.

Acknowledgments

This work was supported by the HELLAS CH «Synergy ELI - LASERLAB Europe, HiPER & IPERION-CH.gr» (Secretariat for Research & Technology, 5 NSRF 2014-2020 Grant No 002735)

References

Alexandrakis, G., 2014. Estimation of the Climatic Change Impact To Beach Tourism Using Joined Vulnerability Analysis and Econometric Modeling, in: ADAPTtoCLIMATE.

Alexandrakis, G., Petrakis, S., Ghionis, G., Kampanis, N., Poulos, S.E., 2014. Natural and human induced indicators in coastal vulnerability and risk assessment, in: 10th International Congress of the Hellenic Geographical Society. pp. 644–655.

INSETE, 2019. Key Figures of Crete Region.

Monioudi, I., Karditsa, A., Chatzipavlis, A., Alexandrakis, G., Andreadis, O. P., Velegrakis, A., Poulos, S., Ghionis, G., Petrakis, S., Sifnioti, D., Hasiotis, T., Lipakis, M., Kampanis, N., Karambas, T., and Marinos, E. (2014) Assessment of the vulnerability of the eastern Cretan beaches (Greece) to sea level rise. Reg. Envir. Change, 16, 1951-1962. doi: 10.1007/s10113-014-0730-9

Petrakis, S., Rempis, N., 2018. Cultural heritage degradation and socioeconomics impacts due to coastal erosion . Evidence from Elounda , Crete Island., in: EGU General Assembly. p. 4754.

Soukisian, T., Hatsinaki, M., Korres, G., Papadopoulos, A., Kallos, G. et al. 2007. Wind and wave atlas of the Hellenic Seas. Hellenic Centre for Marine Research, Athens, 300 pp.

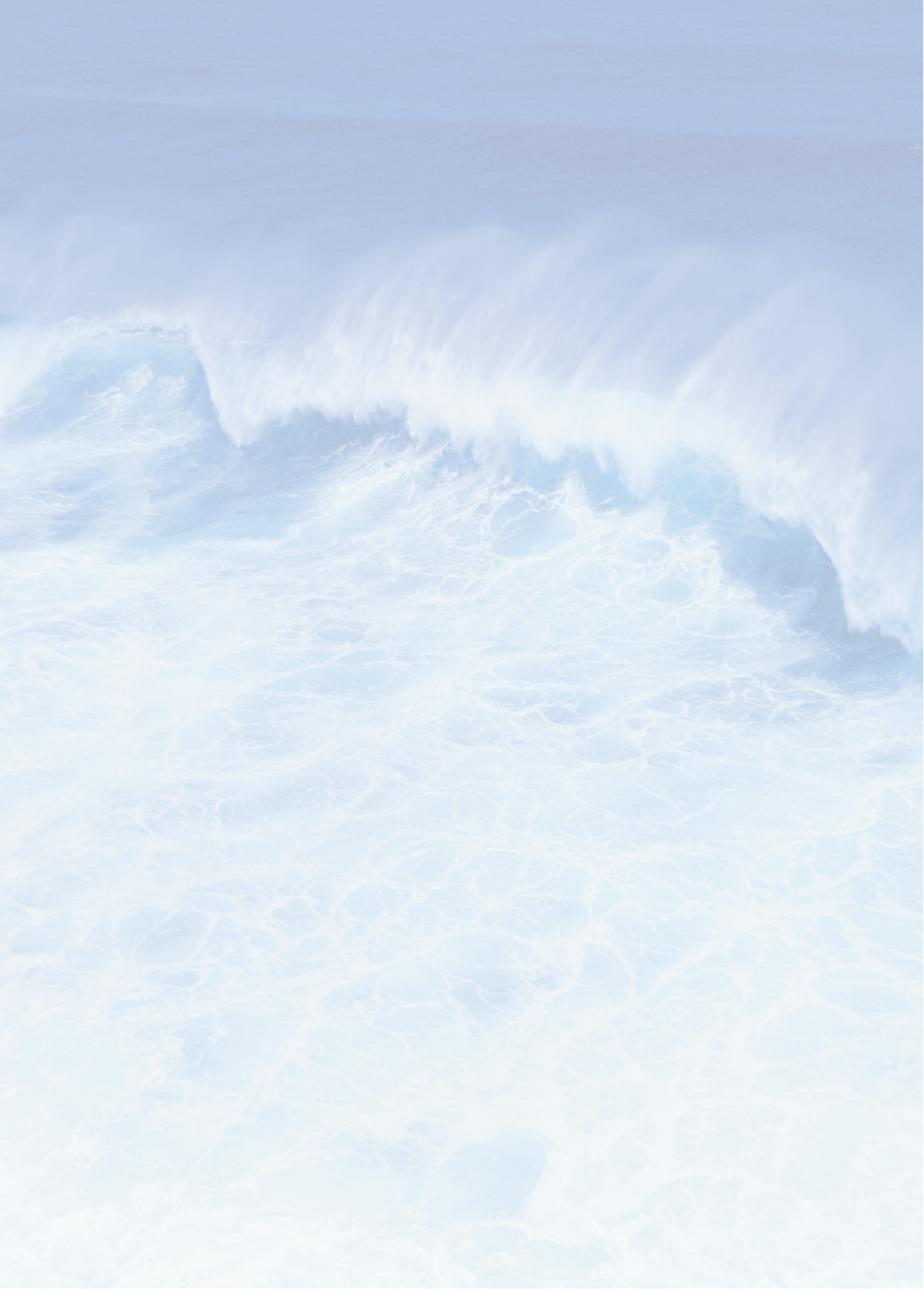

Sub session 4.2: Application of ICZM

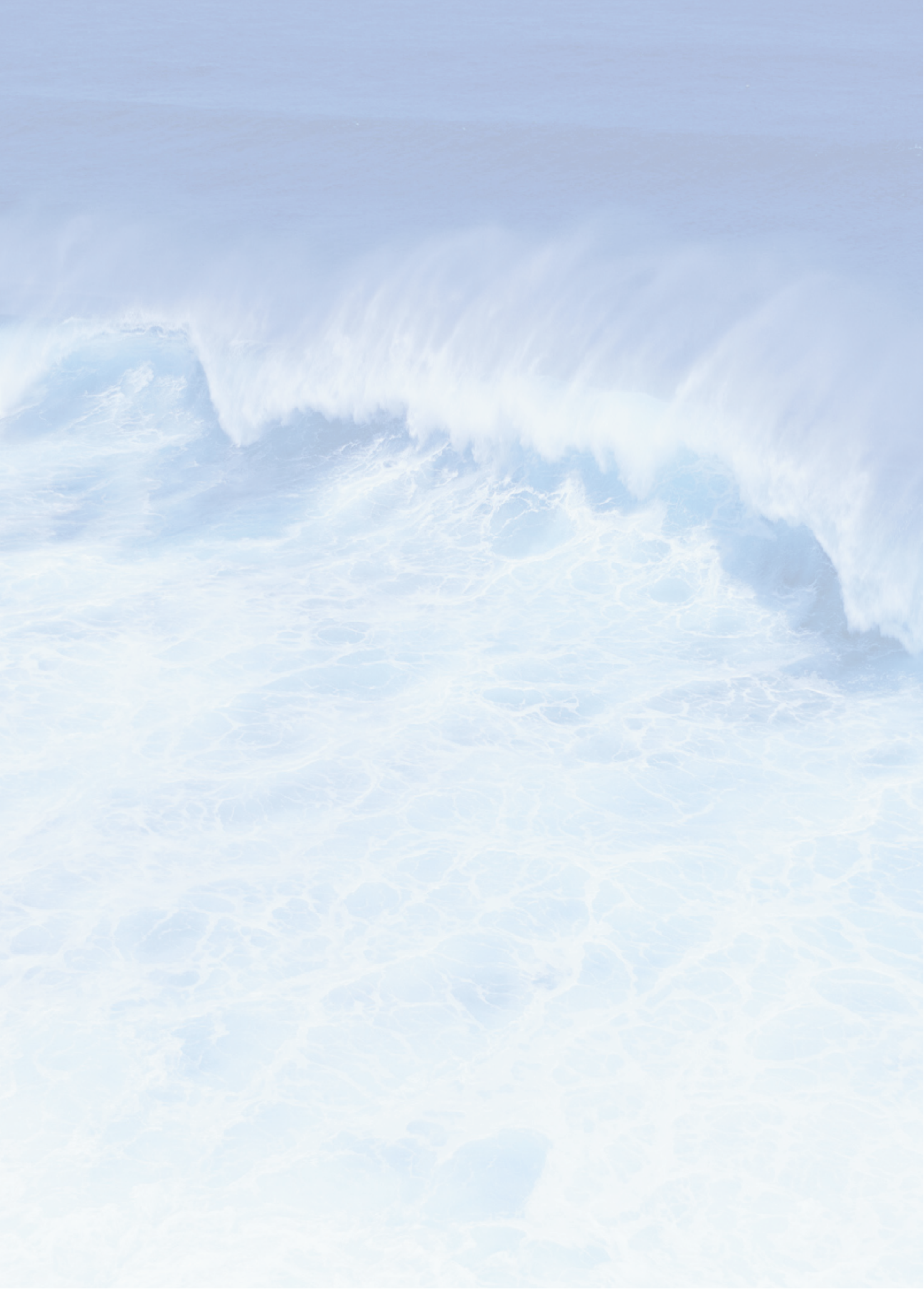

Μέτρα βελτίωσης και προοπτικές ανάπτυξης μαρίνας δήμου Γλυφάδας Αττικής

Ν. Αλαμανής[1], Χ. Δρυμώνας[1], Η. Μυλόζης[1], Κ. Λαζογιάννης[2], Γ. Παπαγεωργίου[1], Εμμ. Βασιλάκης[2], Ι. Αλεξόπουλος[3], Σ. Κωτσόπουλος[1] και Ι. Χουλιάρας[1]

[1]Γενικό Τμήμα, Πανεπιστήμιο Θεσσαλίας, 41110 Λάρισα, Ελλάδα
[2]Τομέας Γεωγραφίας – Κλιματολογίας, Τμήμα Γεωλογίας & Γεωπεριβάλλοντος, Πανεπιστήμιο Αθηνών, Πανεπιστημιούπολη Ζωγράφου, 15784, Ελλάδα
[3]Τομέας Γεωφυσικής και Γεωθερμίας, Τμήμα Γεωλογίας & Γεωπεριβάλλοντος, Πανεπιστήμιο Αθηνών, Πανεπιστημιούπολη Ζωγράφου, 15784, Ελλάδα

Περίληψη

Η Ελλάδα, εδώ και αρκετά χρόνια, έχει θέσει ως προτεραιότητά της την ενίσχυση του θαλάσσιου τουρισμού, όπως είναι ο τουρισμός των σκαφών αναψυχής για την εξυπηρέτηση του οποίου δημιουργήθηκαν τουριστικοί λιμένες (μαρίνες). Στις σημαντικότερες μαρίνες της χώρας συγκαταλέγεται η μαρίνα Γλυφάδας τα έργα της οποίας ξεκίνησαν στο παραλιακό μέτωπο μετά το 1960 αλλάζοντας έτσι την μορφή και την ρυμοτομία της περιοχής. Βασικός στόχος της παρούσας εργασίας είναι η διερεύνηση των μέτρων βελτίωσης καθώς και των προοπτικών ανάπτυξης της μαρίνας Γλυφάδας που αποτελείται από 4 λεκάνες όντας μία από τις πιο όμορφες και εξελιγμένες μαρίνες της χώρας αφού αποτελεί σημαντικό πόλο έλξης τουριστικών σκαφών. Για τον λόγο αυτόν πραγματοποιήθηκαν επί τόπου επισκέψεις στον χώρο του λιμένα τόσο στο θαλάσσιο όσο και στο χερσαίο τμήμα της παράκτιας ζώνης του, με σκοπό την καταγραφή της υφιστάμενης κατάστασης, έτσι ώστε να προσεγγισθούν με την μεγαλύτερη δυνατή ακρίβεια τα χαρακτηριστικά και το εύρος των εσωτερικών λιμενικών έργων και εγκαταστάσεων του ανωτέρω τουριστικού λιμένα. Περαιτέρω παρουσιάζονται, επισημαίνονται και ταξινομούνται ανά λεκάνη τυχόν ελλείψεις ή αστοχίες που χρήζουν βελτίωσης έτσι ώστε να συνεχισθούν απρόσκοπτα οι δραστηριότητες στον χώρο της μαρίνας. Τέλος προτείνονται μέτρα βελτίωσης και αναβάθμισης που δύνανται να συμβάλλουν θετικά στην τουριστική και οικονομική ανάπτυξη του λιμένα αλλά και του δήμου Γλυφάδας γενικότερα.

Λέξεις κλειδιά Μαρίνα Γλυφάδας, Τουριστικοί λιμένες, Εξωραϊσμός εσωτερικών λιμενικών έργων, Μέτρα αναβάθμισης, Παράκτια ζώνη.

1 ΕΙΣΑΓΩΓΗ

Η θάλασσα αποτελεί το μεγαλύτερο ελεύθερο πεδίο της γης πάνω στο οποίο η κίνηση και η μεταφορά είναι μια πράξη απλή, οικονομική, ευθύγραμμη και ελεύθερη, και συνεπώς πολύτιμη σε όσους μπορούν να τη χρησιμοποιούν. Οι λιμένες μαζί με τις υποδομές τους (κρηπιδώματα, κτίρια, εσωτερικές εγκαταστάσεις, εμπορευματοκιβώτια, μηχανήματα, εξοπλισμός, οδικά δίκτυα σύνδεσης με την ενδοχώρα κ.α) ως βασικός παράγοντας στην οικονομία των μεταφορών διαδραματίζουν σημαντικό ρόλο στην οικονομική ανάπτυξη και στην ευημερία της χώρας μας.

Ιδιαίτερη βαρύτητα ανάμεσα στις κατηγορίες λιμένων παρουσιάζουν οι τουριστικοί λιμένες που έχουν ως σκοπό την ανάπτυξη του θαλάσσιου τουρισμού υψηλών απαιτήσεων. Για την ακρίβεια «Τουριστικός λιμένας» σκαφών αναψυχής είναι ο χερσαίος και θαλάσσιος χώρος που προορίζεται κατά κύριο λόγο για/και υποστηρίζει λειτουργικά τον ελλιμενισμό σκαφών αναψυχής και ναυταθλητισμού.

Σύμφωνα με την ισχύουσα νομοθεσία οι τουριστικοί λιμένες χωρίζονται στις εξής κατηγορίες: α) Μαρίνες β) Καταφύγια γ) Αγκυροβόλια δ) Ξενοδοχειακοί λιμένες . «Μαρίνα» είναι ο τουριστικός λιμένας που διαθέτει χερσαίες και θαλάσσιες εγκαταστάσεις και υποδομές προδιαγραφών που ορίζονται με απόφαση του Υπουργού Πολιτισμού και Τουρισμού, όπως προβλέπεται στην παρ. 3 του άρθρου 31 του Ν.2160/1993, για την εξυπηρέτηση των σκαφών αναψυχής και των χρηστών τους. Οι οργανωμένες μαρίνες όπως αυτή της Γλυφάδας κατασκευάζονται για την εξυπηρέτηση θαλαμηγών, προσφέρουν υψηλού επιπέδου υπηρεσίες, διαφημίζουν τη χώρα μας, προσελκύουν τουρίστες υψηλού οικονομικού επιπέδου και συμβάλλουν καθοριστικά στην οικονομία μέσω της προστιθέμενης αξίας (δηλ. της δημιουργίας χιλιάδων θέσεων εργασίας, της κατανάλωσης αγαθών και υπηρεσιών, της συγκέντρωσης δημοσίων εσόδων καθώς και της αναβάθμισης του παραλιακού μετώπου).

Σκοπός της εργασίας αυτής, είναι τα μέτρα βελτίωσης καθώς και η προοπτική ανάπτυξης της μαρίνας Γλυφάδας. Για την επίτευξη του στόχου αυτού πραγματοποιήθηκε επιτόπια επίσκεψη στο έργο κατά την οποία ταυτοποιήθηκαν και παρουσιάζονται οι λεκάνες του λιμένα, ενώ παράλληλα μελετήθηκε ο τρόπος λειτουργίας τους καθώς και τα τυχόν προβλήματα που εμφανίζουν. Τέλος με βάση τις πληροφορίες που συγκεντρώθηκαν προέκυψαν χρήσιμα συμπεράσματα καθώς και προτάσεις που αφορούν την βελτίωση και ανάπτυξη της μαρίνας.

2 ΠΕΡΙΓΡΑΦΗ ΜΑΡΙΝΑΣ-ΠΑΡΕΧΟΜΕΝΕΣ ΥΠΗΡΕΣΙΕΣ

Η μαρίνα Γλυφάδας αποτελείται από 4 λεκάνες, την Α, Β, Γ, Δ και έχει γενικά είσοδο με γεωγραφικές συντεταγμένες 37^o 51΄30΄΄ βόρειο πλάτος και 23^o 45΄30΄΄ ανατολικό μήκος. Βρίσκεται δίπλα στις εγκαταστάσεις του Αγίου Κοσμά και κατασκευάστηκε την δεκαετία του '60 από τον Δήμο Γλυφάδας με επιχωματώσεις της ακτής που μέχρι τότε ήταν βραχώδης. Περιλαμβάνει θαλάσσιο χώρο καθώς και χερσαία ζώνη ακτής, δηλαδή αμμώδη παραλία συνολικού μήκους 3 χιλ. και συγκεκριμένα μεταξύ της Α και Β λεκάνης μήκους 250 μ περίπου, μεταξύ Β και Γ λεκάνης μήκους 150 μ. περίπου, μεταξύ Γ και Δ λεκάνης μήκους 300 μ. περίπου και μεταξύ Δ λεκάνης και ορίου μήκους 350 μ. περίπου με όλες τις λιμενικές εγκαταστάσεις και κτιριακές κατασκευές που βρίσκονται στο χώρο της Μαρίνας. Η χωρητικότητα της μαρίνας Γλυφάδας είναι συνολικά 810 σκάφη και πιο συγκεκριμένα ανά λεκάνη:

- Α΄ λεκάνη 180 σκάφη Β΄ λεκάνη 100 σκάφη
- Γ΄ λεκάνη 280 σκάφη Δ΄ λεκάνη 250 σκάφη

Άλλα χαρακτηριστικά στοιχεία είναι:

Α΄Μαρίνα: Εμβαδόν χερσαίας επιφάνειας περίπου 2400 τ.μ., Εμβαδόν υδάτινης επιφάνειας περίπου 7200 τ.μ., Συνολικό μήκος κρηπιδωμάτων 250 μ.

Β΄Μαρίνα: Εμβαδόν χερσαίας επιφάνειας περίπου 3400 τ.μ., Εμβαδόν υδάτινης επιφάνειας περίπου 8800 τ.μ., Συνολικό μήκος κρηπιδωμάτων 385 μ.

Γ΄Μαρίνα: Εμβαδόν χερσαίας επιφάνειας περίπου 5700 τ.μ., Εμβαδόν υδάτινης επιφάνειας περίπου 37000 τ.μ., Συνολικό μήκος κρηπιδωμάτων 1000 μ.

Δ΄Μαρίνα: Εμβαδόν χερσαίας επιφάνειας περίπου 9000 τ.μ., Εμβαδόν υδάτινης επιφάνειας περίπου 37000 τ.μ., Συνολικό μήκος κρηπιδωμάτων 1000 μ.

Σχήμα 1 Οι μαρίνες της Γλυφάδας σήμερα (Πηγή: ESRI)

Η Δ΄ μαρίνα περιλαμβάνει επιπροσθέτως κεκλιμένο επίπεδο (γλίστρα) ώστε να είναι δυνατή η διαδικασία ανέλκυσης/καθέλκυσης σκαφών ενώ σε κάθε λεκάνη της μαρίνας περιλαμβάνεται και μία λέμβος υπηρεσίας για την υπόδειξη της θέσης ελλιμενισμού. Οι λεκάνες μπορούν να φιλοξενήσουν όλους τους τύπους σκαφών (σκάφη αναψυχής και ναυταθλητισμού, επαγγελματικά σκάφη, ιστιοπλοϊκά, λέμβοι κ.ά.) έως 35μ. ενώ τα τέλη ελλιμενισμού ποικίλουν ανάλογα με την κατηγορία των σκαφών, το μήκος του σκάφους, την εποχή ελλιμενισμού, τον χρόνο παραμονής στις εγκαταστάσεις της μαρίνας καθώς και τον λόγο μεγίστου πλάτους προς μέγιστο ύψος B/L που για τα συμβατικά σκάφη κυμαίνεται μεταξύ του 0,30 και 0,38. Εκτός από τις υπηρεσίες ελλιμενισμού, στον χώρο υπάρχουν διαθέσιμες και πρόσθετες υπηρεσίες όπως: παροχή ηλεκτρικού ρεύματος, παροχή νερού, υπηρεσίες ανεφοδιασμού, φωτισμός, ασφάλεια, υπηρεσίες καθαριότητας, τηλεπικοινωνίες, ενώ επιπροσθέτως δίνεται η δυνατότητα για επισκευές σκαφών μικρής όμως έκτασης, στον χώρο της μαρίνας. Την διαχείριση της μαρίνας έχει αναλάβει το *Τμήμα Διαχείρισης Μαρίνας Γλυφάδας* που υπάγεται στον *Οργανισμό Δήμου Γλυφάδας* και περιλαμβάνει: *το Γραφείο Προϊστάμενου, το Γραφείο Εξυπηρέτησης Κοινού* που στελεχώνεται από 2 διοικητικούς υπαλλήλους και *4 φυλάκια* που απασχολούν 15 φύλακες. Η Μαρίνα αποτελεί και την μεγαλύτερη πηγή εσόδων του Δήμου, με τα ετήσια έσοδα να ανέρχονται σε 1,5 εκατ € και τα έξοδα σε 450.000€. Τα έσοδα προέρχονται κυρίως από τα τέλη ελλιμενισμού και την χρήση των υπολοίπων υπηρεσιών και τα έξοδα αφορούν αμοιβές προσωπικού, κάλυψη παγίων εξόδων και υποχρεώσεων, συντήρηση του λιμένα και προμήθεια εξοπλισμού. Η συγκοινωνία με την ενδοχώρα (από-προς Αθήνα και από-προς αεροδρόμιο) χαρακτηρίζεται ως εξαιρετική και πραγματοποιείται με δημόσια συγκοινωνία, λεωφορεία, τραμ και μετρό.

3 ΚΑΤΑΓΡΑΦΗ ΤΗΣ ΥΠΑΡΧΟΥΣΑΣ ΚΑΤΑΣΤΑΣΗΣ

Στις Α΄ και Β΄ Μαρίνα είναι εμφανής η διάβρωση των προβλητών καθώς και των δεστρών λόγω του έντονου κυματισμού ενώ χρήζει ανακατασκευής ο κεντρικός τάπητας εντός της μαρίνας καθώς έχει υποστεί ζημιά με το πέρασμα των χρόνων. Στην Μαρίνα Β΄ για πρώτη φορά παρατηρήθηκε περιβαλλοντική μόλυνση από τα λύματα των αλιευτικών και των τουριστικών πλοιαρίων. Πιο συγκεκριμένα η αύξηση της πράσινης <χλωρίδας> (φυτοπλαγκτόν) στους βράχους υποδηλώνει την ανάπτυξη ευτροφισμού. Ο ευτροφισμός προκαλείται από την έλλειψη ελεύθερου οξυγόνου στο εσωτερικό της θάλασσας με αποτέλεσμα την αύξηση του φυτοπλαγκτόν αφού αυτό δεν καταναλώνεται από τα ψάρια που συνήθως οδηγούνται σε ασφυξία.

Σχήμα 2 Α΄ Μαρίνα Γλυφάδας. Διάβρωση της προβλήτας. (Πηγή: Δρυμώνης-Μυλόζης, 2016).

Σχήμα 3 Β΄ Μαρίνα Γλυφάδας. Οξείδωση των μεταλλικών δεστρών. (Πηγή: Δρυμώνης-Μυλόζης, 2016).

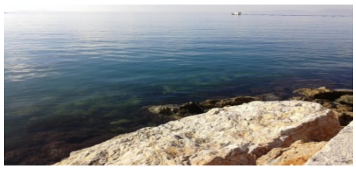

Σχήμα 4 Β΄ Μαρίνα Γλυφάδας. Ανάπτυξη ευτροφισμού (Πηγή: Δρυμώνης-Μυλόζης, 2016).

Στις Μαρίνα Β΄ και Γ΄ παρατηρήθηκε έντονη αλιευτική δράση που με τις πρόχειρες κατασκευές που κατά τόπους εμφανίζονται (Σχ. 5) περιορίζεται η αισθητική του λιμένα. Να σημειωθεί ότι στην μαρίνα Γ΄ παρατηρήθηκε μείωση του αρχικού βάθους της λόγω φερτών υλών ενώ από τις προβλεπόμενες εγκαταστάσεις, λείπουν οι υπηρεσίες αποθήκευσης για τους πελάτες.

Σχήμα 5 Β΄ Μαρίνα Γλυφάδας. Ερασιτεχνική αλιευτική δράση (Πηγή: Δρυμώνης-Μυλόζης, 2016).

Σχήμα 6 Γ΄ Μαρίνα Γλυφάδας. Διάβρωση προβλήτας και ερασιτεχνική αλιευτική δράση. (Πηγή: Δρυμώνης-Μυλόζης, 2016).

Η προβλήτα της μαρίνας Δ΄ χρήζει εσωτερικών επισκευών ενώ παρουσιάζονται ίχνη μόλυνσης δίπλα στην ακτή της Γλυφάδας που δέχεται καθημερινά μεγάλο αριθμό επισκεπτών. (Σχ.7 και Σχ.8).

Σχήμα 7 Δ΄ μαρίνα Γλυφάδας. Ανάγκη επισκευής της προβλήτας λόγω διάβρωσης. (Πηγή: Δρυμώνης-Μυλόζης, 2016).

Σχήμα 8 Δ΄ μαρίνα Γλυφάδας. Είναι εμφανή τα ίχνη μόλυνσης της ακτής. (Πηγή: Δρυμώνης-Μυλόζης, 2016).

Ιδιαιτέρως πρέπει να δοθεί βαρύτητα στην ηχορύπανση διότι διαταράσσει τους ζωντανούς οργανισμούς κοντά στην μαρίνα καθώς επίσης τους ενοίκους αλλά και τους περαστικούς που βρίσκονται στον χώρο του τουριστικού λιμένα. Τέλος ιδιαίτερα σημαντική είναι η αναβάθμιση των μέτρων πυροπροστασίας στον λιμένα που έχει ήδη δρομολογηθεί.

4 ΠΡΟΤΑΣΕΙΣ ΒΕΛΤΙΩΣΗΣ ΚΑΙ ΑΝΑΒΑΘΜΙΣΗΣ

1) Νυκτερινός φωτισμός. Επειδή σε πολλά σημεία του λιμένα η έλλειψη φωτισμού είναι εξαιρετικά αισθητή προτείνεται δημιουργία ζωνών νυχτερινού φωτισμού σε όλη τη διάμετρο του λιμένα.
2) Κατασκευή χώρων στάθμευσης. Ένα από τα σημαντικότερα προβλήματα του λιμένα είναι η έλλειψη επαρκών χώρων στάθμευσης και κατά συνέπεια κρίνεται αναγκαία η κατασκευή επιπλέον χώρων στάθμευσης
3) Κατασκευή ποδηλατοδρόμου. Ο λιμένας της Γλυφάδας είναι ιδιαίτερα αρεστός για τους ποδηλάτες των νοτίων προαστίων. Παρόλα αυτά ακόμα δεν έχει κατασκευαστεί καμία υποδομή όσον αφορά την

εξυπηρέτηση των πολιτών που προτιμούν ως μέσο μεταφοράς το ποδήλατο. Η κατασκευή ποδηλατοδρόμου κρίνεται απαραίτητη.

4) Κατασκευή χώρων πρασίνου. Ο λιμένας αποτελεί ιδανική τοποθεσία για κατασκευή χώρου πρασίνου σε όλο το μήκος του για την ευχάριστη διαμονή των επισκεπτών αλλά πολύ περισσότερο των δημοτών. Η επιπλέον φύτευση ιδαίτερα στις παραλίες (με αλμυρίκια, λεβάντες, πεύκα) θα αναβάθμιζε την αισθητική του λιμένα αλλά και το περιβάλλον γενικότερα.
5) Περιβαλλοντική διαχείριση. Πολύ σημαντικό πρόβλημα το οποίο έχει ήδη αναφερθεί και παραπάνω είναι η μόλυνση των ακτών και του λιμένα (σε αρχικό στάδιο). Η αντιμετώπιση είναι καθήκον όλων των πολιτών και πρέπει να δρομολογηθεί άμεσα η περιβαλλοντική αποκατάσταση των ακτών της μαρίνας.
6) Κατασκευή χώρων αναψυχής. Σημαντικό ρόλο στην εξυγίανση και αναβάθμιση του λιμένα θα ήταν η δημιουργία χώρων αναψυχής όπως λούνα παρκ, παιδικές χαρές, περίπτερα, παγκάκια κατά μήκος του λιμένα ιδιαίτερα κατά τους καλοκαιρινούς μήνες.
7) Ερασιτεχνική αλιεία. Η κατασκευή αλιευτικών χώρων (για ερασιτέχνες αλιείς) καθώς και η εξεύρεση καλύτερων χώρων για τους ομίλους της ιστιοπλοΐας είναι απαραίτητοι για την περιοχή.
8) Ανακατασκευή κτιρίων. Τα κτίρια της λιμενικής υπηρεσίας χρειάζονται επειγόντως ανακαίνιση καθώς και αύξηση του προσωπικού και συνεπώς κρίνεται απαραίτητη η ανακατασκευή τους.

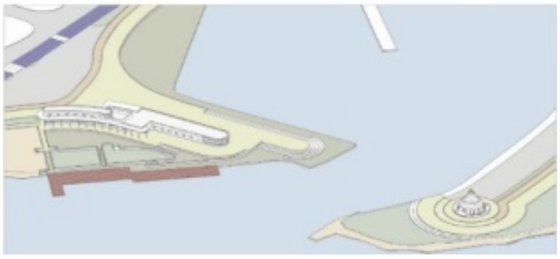

Σχήμα 9 Σχέδιο ανακατασκευής κτιρίων λιμενικής υπηρεσίας (Πηγή: προκαταρκτική μελέτη διαμόρφωσης παραλίας Γλυφάδας)

9) Χώροι ενημέρωσης επισκεπτών. Η κατασκευή χώρων ενημέρωσης επισκεπτών (κιόσκια) όπου θα δίνονται πληροφορίες στους επισκέπτες ιδιαίτερα τους θερινούς μήνες θα συμβάλλει θετικά στην αναβάθμιση του λιμένα.
10) Συντήρηση σκαφών. Η δημιουργία επιπλέον χώρων μεταφοράς σκαφών για την συντήρησή τους θα βελτίωνε κατά πολύ τις υπηρεσίες του λιμένα.
11) Δημιουργία σταθμού πρώτων βοηθειών. Η μαρίνα Γλυφάδας καθ' όλη τη διάρκεια του έτους αποτελεί πόλο έλξης για όλο τον πληθυσμό του λεκανοπεδίου. Κρίνεται συνεπώς ως πρώτη προτεραιότητα η δημιουργία σταθμού πρώτων βοηθειών τόσο για τους λουομένους όσο και για τους εργαζομένους και χρήστες της μαρίνας ενώ ταυτόχρονα θα ήταν αναγκαία η δημιουργία ειδικών μονοπατιών για τους ανάπηρους επισκέπτες της μαρίνας.
12) Ανακατασκευή τάπητα μώλων και προβλητών. Οι μώλοι καθώς και οι προβλήτες σε πολλά σημεία τους όπως προκύπτει από τα ανωτέρω σχήματα έχουν υποστεί έντονη διάβρωση με αποτέλεσμα να χρήζουν άμεσης επιδιόρθωσης όπως συνέβη στην Β΄ μαρίνα το 2004 όπου έγινε μερική ανακατασκευή των κρηπιδωμάτων συνολικού μήκους 356 μέτρων.
13) Προσθήκη ξύλινων προβλητών. Η προσθήκη ξύλινων προβλητών στις μαρίνες Α΄, Β΄, Γ΄ (όπως στην μαρίνα Δ΄) θα συμβάλλει θετικά στον εξωραισμό και στην αισθητική αναβάθμιση του λιμένος.
14) Ηχορύπανση. Η αντιμετώπιση της ηχορύπανσης με τοποθέτηση ηχομόνωσης και ηχοπαγίδων και σημάνσεων-όπου αυτό είναι εφικτό-θα αναβαθμίσει τους χώρους αναψυχής του λιμένα.
15) Πυροπροστασία. Ιδιαίτερα σημαντική είναι η βελτίωση των μέτρων πυροπροστασίας στον λιμένα που σύμφωνα με πληροφορίες έχουν ήδη δρομολογηθεί με χρηματοδότηση από την Περιφέρεια Αττικής.
16) Διαδικτυακή υποδομή. Είναι απαραίτητη η δημιουργία υποδομής για πληρέστερη σύνδεση με το διαδίκτυο καθώς και τοποθέτηση κάμερας ασφαλείας για πληρέστερη φύλαξη της μαρίνας και των σκαφών.

5 ΙΣΧΥΡΑ ΚΑΙ ΑΣΘΕΝΗ ΣΗΜΕΙΑ ΜΑΡΙΝΑΣ ΓΛΥΦΑΔΑΣ

Στα ισχυρά σημεία της Μαρίνας Γλυφάδας συγκαταλέγονται η γεωγραφική της θέση, η μικρή απόσταση από τα νησιά του Αργοσαρωνικού καθώς και ο αριθμός των σκαφών που μπορεί να φιλοξενήσει, κυρίως όμως τα χαμηλά τέλη ελλιμενισμού (Κωνσταντίνου, 2007). Επίσης στα ισχυρά σημεία μπορούν να συμπεριληφθούν το κλίμα και η ήρεμη θάλασσα, το μήκος της ακτής και ο αριθμός των παραλιών καθώς και ο συνδυασμός του yachting με τα θαλάσσια σπορ. Ιδιαίτερα σημαντικό στοιχείο αποτελεί η εύκολη πρόσβαση στην ενδοχώρα (Αθήνα-Πειραιάς-αεροδρόμιο) καθώς και η ύπαρξη τοπικής αγοράς με μεγάλα καταστήματα και εμπορικά κέντρα.

Στα αδύνατα σημεία συμπεριλαμβάνονται η έλλειψη χώρων υγιεινής και μέσων πυροπροστασίας, ο χαμηλός φωτισμός, η ελλιπής ηχομόνωση και η μη επαρκής φύτευση καθώς και η μικρή αναλογία θέσεων ελλιμενισμού και μήκους ακτογραμμής. (Στοιχεία από Swot Analysis Μαρίνας Γλυφάδας και κλάδου yachting στην Ελλάδα). (Κωνσταντίνου, 2007, Λιόκαρης, 2016).

6 ΣΥΜΠΕΡΑΣΜΑΤΑ

1. Οι ακτές του Σαρωνικού αποτελούν, ιστορικά, γεωγραφικά αλλά και κοινωνικό-οικονομικά, οργανικό τμήμα της ευρύτερης χωρικής ενότητας της Αττικής. Η μαρίνα Γλυφάδας λόγω της θέσης της, κοντά στο εμπορικό κέντρο του δήμου Γλυφάδας, αλλά και στα όρια των ανοιχτών αστικών ακτών κολύμβησης, μπορεί να αξιολογηθεί θετικά ως ενδιάμεσος σταθμός θαλάσσιας συγκοινωνίας που θα εξυπηρετούσε μετακινήσεις μικρής κλίμακας.
2. Η προστιθέμενη αξία των τουριστικών λιμένων είναι η θετική συμβολή στην Οικονομία και την Κοινωνία της χώρας μας. Ιδιαίτερη βαρύτητα στην θαλάσσια οικονομία παρουσιάζει η Μαρίνα Γλυφάδας καθώς κατέχει περίοπτη γεωγραφική θέση και προσελκύει κάθε χρόνο μεγάλο αριθμό σκαφών και επισκεπτών.
3. Στη Γλυφάδα λειτουργούν σε πολύ άμεση σχέση μεταξύ τους τέσσερις μικρότερης κλίμακας μαρίνες, έχοντας σαν αποτέλεσμα τη δημιουργία ενός συμπαγούς πόλου τουριστικής λιμενικής εγκατάστασης στα όρια του δήμου, με την καθοδήγηση του οποίου έχουν επιτευχθεί κατ' έτος σημαντικά έσοδα.
4. Στα πλαίσια αναβάθμισης της ιδιαίτερης ταυτότητας του παραλιακού μετώπου, την προστασία και εξυγίανση παράκτιων χερσαίων και θαλάσσιων οικοσυστημάτων, τις ισχυρές πολεοδομικές και περιβαλλοντικές συνδέσεις με τον αστικό ιστό καθώς και τις προτάσεις βελτίωσης που έχουν ήδη διατυπωθεί ανωτέρω η προοπτική ανάπτυξης της Μαρίνας Γλυφάδας διαφαίνεται εξαιρετική τόσο σε βραχυπρόθεσμο όσο και σε μακροπρόθεσμο χρονικό ορίζοντα.

Βιβλιογραφικές Αναφορές

Δημητρακόπουλος Σ (2018) Η μαρίνα Αλίμου και η συμβολή της στην τουριστική ανάπτυξη. Πτυχιακή Εργασία. ΑΤΕΙ Πειραιά, ΣΔΟ, Τμήμα Διοίκησης Επιχειρήσεων. Αθήνα, 2018.

Δρυμώνης Χ, Μυλόζης Η (2016. Προοπτική Ανάπτυξης λιμένος (μαρίνας) Γλυφάδας. ΑΤΕΙ Θεσσαλίας. ΣΤΕΦ. Τμήμα Πολιτικών Μηχανικών Τ.Ε (Λάρισας). Λάρισα, 2016.

Εθνικό Μετσόβιο Πολυτεχνείο. Σχολή Αρχιτεκτόνων Μηχανικών. Εργαστήριο Αστικού Περιβάλλοντος (2017) Σχέδιο Ολοκληρωμένης Διαχείρισης Ακτών Αττικής Στρατηγικές και κατευθύνσεις για την Χωρική Ενότητα: ΣΕΦ - Αγία Μαρίνα Κρωπίας. Αθήνα, Ιούνιος, 2017.

Ευαγγελίδου Μ, Κλουτσινιώτη Κ (2009) Προκαταρκτική Μελέτη Διαμόρφωσης Παραλίας Γλυφάδας. Υ.ΠΕ.ΧΩ.Δ.Ε. Οργανισμός ρυθμιστικού σχεδίου και προστασίας περιβάλλοντος Αθήνας.

Ζαγανάκης Ζ (2015) Κατασκευή και Υπηρεσίες Μαρίνων στην Ελλάδα. Διδάγματα από Ευρωπαϊκές Περιπτώσεις. Πανεπιστήμιο Πειραιώς. Τμήμα Ναυτιλιακών Σπουδών. Πρόγραμμα μεταπτυχιακών σπουδών στην ναυτιλία. Πειραιάς, 2015.

Ζερβάκης Ν (2015) Τεχνοοικονομική Μελέτη Βελτίωσης Τουριστικού Λιμένα: η περίπτωση της Σητείας. Διπλωματική Εργασία. Πολυτεχνείο Κρήτης. Τμήμα Μηχανικών Παραγωγής και Διοίκησης. Χανιά, 2015.

Κωνσταντίνου Ν (2007) Οργάνωση και Διαχείριση των Τουριστικών Λιμένων Σκαφών Αναψυχής. Οι Περιπτώσεις του Δήμου Γλυφάδας και Αλίμου. Εθνική Σχολή Τοπικής Αυτοδιοίκησης. Τμήμα Οικονομικής Διαχείρισης. Τελική Εργασία. Αθήνα, Σεπτέμβριος, 2007.

Μανώλογλου ΣΜ (2017) Ο Τομέας της Ιδιωτικής Θαλάσσιας Περιήγησης (yachting) στην Ελλάδα. Τάσεις και Προοπτικές Ανάπτυξης. Ευρωπαϊκό Κέντρο Αριστείας Jean Monnet. Εθνικό και Καποδιστριακό Πανεπιστήμιο Αθηνών. Μάρτιος, 2017.

Λιόκαρης Μ (2015) Θαλάσσιος Τουρισμός στην Ελλάδα: Μελέτη Περίπτωσης για τις Μαρίνες Αττικής. Πτυχιακή Εργασία. Πανεπιστήμιο Αιγαίου. Τμήμα Διοίκησης Επιχειρήσεων. Χίος, 2015.

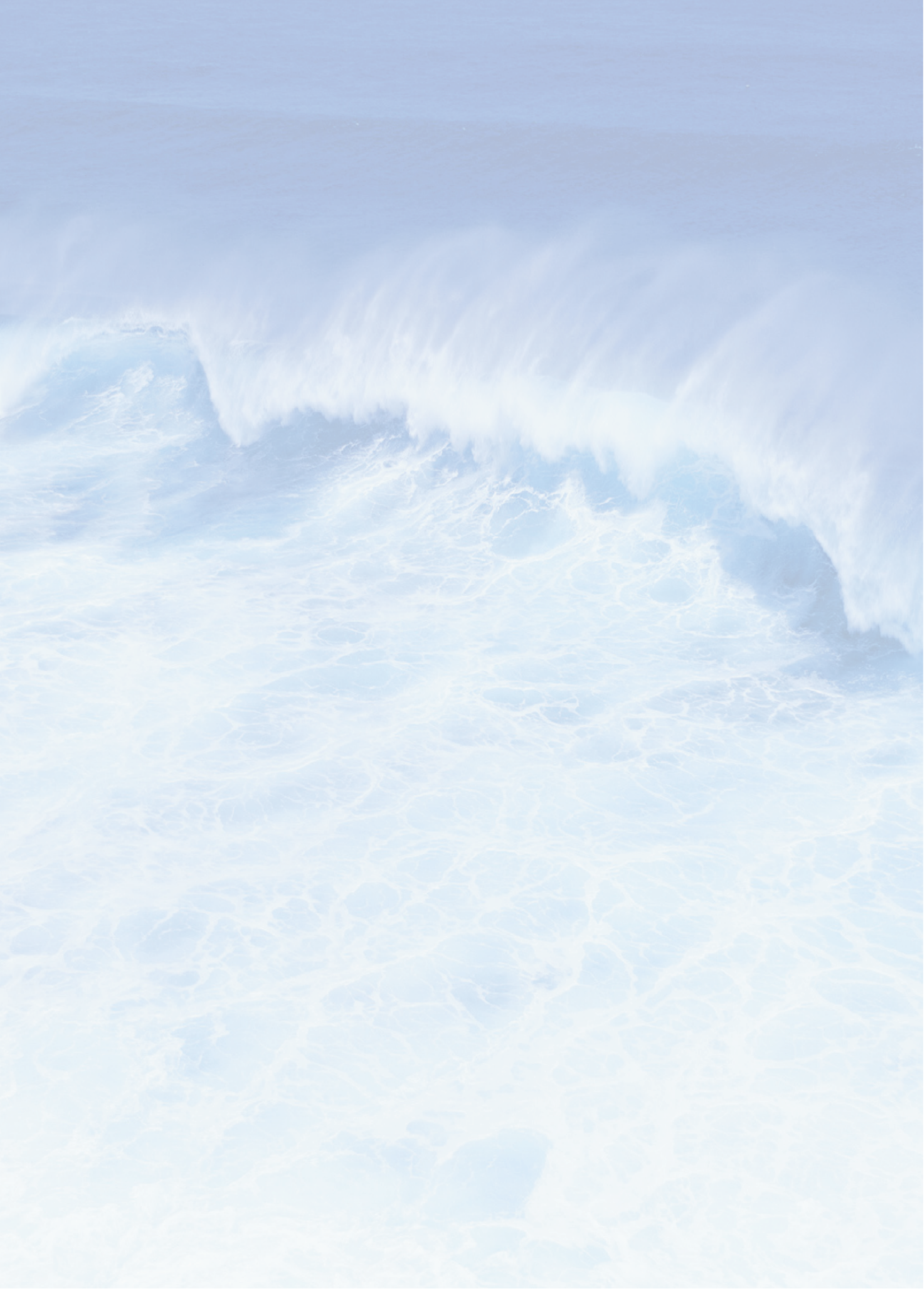

Ανάπτυξη του παράκτιου μετώπου του μητροπολιτικού πόλου Ελληνικού – Αγίου Κοσμά – Το Ελληνικό

Α.Μ. Μπουτάτης[1*], Χ.Δ. Σολομωνίδης[1], Ι.Α. Ρογκάν[1], Μ.Κ. Χονδρός[2], Μ.Ν. Καλπύρη[1]

[1]Ρογκάν & Συνεργάτες, Βαλέττα 9, Τ.Κ. 15771 Αθήνα, Ελλάδα
[2]Εργαστήριο Λιμενικών Έργων, ΕΜΠ, Τ.Κ. 15773 Αθήνα, Ελλάδα
[*]Υπεύθυνος επικοινωνίας: aboutatis@roganassoc.gr

Περίληψη

Η παρούσα μελέτη με τίτλο «Σύνταξη του Απαιτούμενου Φακέλου των Προτεινόμενων Λιμενικών Έργων του Παράκτιου Μετώπου του Μητροπολιτικού Πόλου Ελληνικού – Αγίου Κοσμά», αποτελεί μέρος του γενικότερου έργου «Ανάπτυξη του Μητροπολιτικού Πόλου Ελληνικού – Αγίου Κοσμά» Αντικείμενό της αποτελεί η σύνταξη Φακέλου με στόχο την αδειοδότηση των προτεινόμενων λιμενικών έργων και περιλαμβάνει τις εξής επιμέρους υποστηρικτικές μελέτες:

- Σύνταξη βυθομετρικών – Τοπογραφικών Διαγραμμάτων
- Υποβρύχια Βιολογική Έρευνα
- Χημικές Αναλύσεις Ιζημάτων – Στηλών Νερού
- Υποβρύχια επιθεώρηση Υφιστάμενων Λιμενικών Υποδομών
- Ακτομηχανική Μελέτη
- Προμελέτη Λιμενικών Έργων
- Υποστήριξη του μελετητή εκπόνησης της Μελέτη Περιβαλλοντικών Επιπτώσεων (ΜΠΕ) για την περιβαλλοντική αδειοδότηση των έργων του παράκτιου μετώπου

Στα πλαίσια της Ακτομηχανικής Μελέτης, πέραν της ακτομηχανικής διερεύνησης της υφιστάμενης κατάστασης, προτάθηκαν και διερευνήθηκαν τέσσερα (4) εναλλακτικά σενάρια τα οποία περιλαμβάνουν διαφορετικές διατάξεις και τύπους έργων. Λαμβάνοντας σοβαρά υπόψη τα αποτελέσματα της Υποβρύχιας Βιολογικής Έρευνας, των Χημικών Αναλύσεων Ιζημάτων και Στηλών Νερού και της Υποβρύχιας Επιθεώρησης, ακολούθησε η εκπόνηση της Μελέτης Περιβαλλοντικών Επιπτώσεων (ΜΠΕ) κατά την οποία εξετάστηκαν οι επιπτώσεις των εναλλακτικών προτάσεων, όσον αφορά στα λιμενικά έργα, στο περιβάλλον τόσο κατά τη διάρκεια κατασκευής όσο και κατά τη διάρκεια λειτουργίας τους. Τέλος με την συγγραφή της έκθεσης Προμελέτης Λιμενικών Έργων έγινε εκτενής περιγραφή του συνόλου των προτεινόμενων εναλλακτικών προτάσεων και επιλέχθηκε η βέλτιστη.

1 ΕΙΣΑΓΩΓΗ

«Το Ελληνικό» αποτελεί το μεγαλύτερο έργο αστικής ανάπλασης στην Ευρώπη. Το όραμά για την ανάπτυξη του, είναι ο σχεδιασμός ενός πρωτοποριακού έργου για την Αθήνα, με ιδιαίτερη έμφαση στη δημιουργία ενός μητροπολιτικού πάρκου διεθνούς εμβέλειας, καθώς και την ανάδειξη του παράκτιου μετώπου με ελεύθερη πρόσβαση για όλους. Η συνολική επένδυση ύψους 8 δις. ευρώ, έκτασης 6.200.000 τ.μ., θα αποτελέσει ένα νέο σημείο αναφοράς και έναν νέο προορισμό για την πόλη της Αθήνας.

Η μελέτη ανατέθηκε από την ανώνυμη εταιρεία με επωνυμία «LAMDA Development Ανώνυμη Εταιρεία Συμμετοχών και Αξιοποίησης Ακινήτων» και το διακριτικό τίτλο «LAMDA DEVELOPMENT S.A.», στην ανώνυμη εταιρεία «ΡΟΓΚΑΝ ΚΑΙ ΣΥΝΕΡΓΑΤΕΣ Α.Ε.», Μελέτες – επιβλέψεις Τεχνικών Έργων, την 1η Μαρτίου 2018, στην Αθήνα.

2 ΜΑΘΗΜΑΤΙΚΗ ΠΡΟΣΟΜΟΙΩΣΗ ΤΩΝ ΑΚΤΟΜΗΧΑΝΙΚΩΝ ΔΙΕΡΓΑΣΙΩΝ ΣΤΗΝ ΠΕΡΙΟΧΗ ΤΩΝ ΕΡΓΩΝ

Η χρήση των μαθηματικών ομοιωμάτων τεκμηριώνει με τον καλύτερο δυνατό τρόπο την αναγκαιότητα των προτεινόμενων έργων λιμενικών και έργων προστασίας ακτής. Στη μελέτη προσομοιώθηκε η κυματική διαταραχή στο παράκτιο πεδίο, η γένεση και ανάπτυξη κυματογενών ρευμάτων καθώς και οι τάσεις στερεομεταφοράς.

2.1 Προσδιορισμός Συνθηκών στην περιοχή μελέτης

- Βυθομετρία περιοχής μελέτης

Εκπονήθηκε βυθομετρική αποτύπωση της περιοχής μελέτης παράλληλα με την ακτογραμμή, έως την ισοβαθή των -12,0μ, καλύπτοντας ένα πλάτος περίπου 800-900μ από την ακτογραμμή. Επιπλέον έγινε συμπλήρωση των υπόλοιπων βαθυμετρικών δεδομένων στα πιο βαθιά νερά έως την ισοβαθή των -40μ αλλά και στα «ανοιχτά», με την αξιοποίηση ναυτικών χαρτών.

- Ανεμολογική δίαιτα περιοχής μελέτης και ευρύτερης περιοχής

Για την ευρύτερη περιοχή μελέτης, κρίσιμοι από απόψεως δημιουργίας κυματισμών αναδείχθηκαν οι άνεμοι προερχόμενοι από Νοτιοανατολικά, Νότια, Νοτιοδυτικά, Δυτικά Βορειοδυτικά. Τα αναπτύγματα πελάγους, φτάνουν, για Νότιες και Νοτιοανατολικές πνοές ανέμων, έως το σύμπλεγμα των Κυκλάδων και την δυτική Κρήτη. Για το λόγο αυτό, για τις Νοτιοανατολικές και Νότιες διευθύνσεις αναζητήθηκαν ανεμολογικά δεδομένα από τη Μήλο και τη Σούδα (Κρήτης) αντίστοιχα. Ενώ για τις υπόλοιπες διευθύνσεις, Νοτιοδυτικά, Δυτικά και Βορειοδυτικά χρησιμοποιούνται τα ανεμολογικά δεδομένα του μετεωρολογικού σταθμού του Ελληνικού.

- Κυματικό κλίμα στα ανοιχτά και ωκεανογραφικά δεδομένα (στάθμη θάλασσας, παλίρροια και ρεύματα)

Ο προσδιορισμό των κυματισμών στην περιοχή μελέτης έγινε με δύο μεθοδολογίες. Πρώτα, χρησιμοποιήθηκε το σύστημα μαθηματικών ρουτινών ACES (Automatic Coastal Engineering System) και σε συνέχεια, εφαρμόσθηκε το μοντέλο MIKE21 SW (Spectral Wave). Το συμπεράσματα που προέκυψε είναι πως τα αποτελέσματα των δύο μεθοδολογιών προκύπτουν αρκετά κοντά μεταξύ τους. Τελικά αξιοποιούύνται τα αποτελέσματα του μοντέλου MIKE21 SW για τους εξής λόγους:

1. Αφενός στις περισσότερες περιπτώσεις τα αποτελέσματα του μοντέλου έδινα ύψος κύματος μεγαλύτερο από τα αντίστοιχα των σχέσεων της μεθόδου SMB
2. Αφετέρου το μοντέλο λαμβάνει υπόψη του και προσομοιώνει μια σειρά φυσικών φαινομένων και διεργασιών σε αντίθεση με τις σχέσεις της μεθόδου SMB(την ύπαρξη βραχονησίδων, μικρών και μεγάλων νήσων). Προσομοιώνει επίσης, την κυματογένεση λόγω ανέμου, τις μη γραμμικές αλληλεπιδράσεις κυματισμών, τη διάχυση λόγω θραύσης κυματισμών στα ανοιχτά και στα ρηχά, τη διάχυση λόγω τριβής πυθμένα και τη διάθλαση και ρήχωση λόγω μεταβολής του βάθους

Πίνακας 1: Κυματικά δεδομένα εισόδου στα αριθμητικά μοντέλα προσομοίωσης των παράκτιων διεργασιών

ΝΑ & Ν 186°				ΝΔ 210°				Δ 264°				ΒΔ 293°			
α/α	f (%)	Hs(m)	Tp(s)	α/α	f (%)	Hs(m)	Tp(s)	α/α	f (%)	Hs(m)	Tp(s)	α/α	f (%)	Hs(m)	Tp(s)
1	0.59	1.50	4.02	6	0.04	1.61	3.89	9	0.05	1.33	3.46	11	0.02	1.46	3.26
2	0.25	2.16	4.78	7	0.01	2.40	4.57	10	0.01	2.01	4.04	12	0.02	2.07	3.73
3	0.08	2.99	5.71	8	0.01	3.41	5.24								
4	0.02	4.12	6.65												
5	0.02	5.59	7.06												
Σύνολο:	**0.964**				**0.054**				**0.054**				**0.036**		

Επιπλέον λήφθηκαν υπόψη στατιστικά στοιχεία από το πλησιέστερο παλιρροιόμετρο στο λιμένα Πειραιά, όσον αφορά τη διακύμανση της στάθμης της θάλασσας.

- Προβλέψεις μεταβολής κρίσιμων παραμέτρων λόγω κλιματικής αλλαγής

Στα πλαίσια πρόσφατου ερευνητικού έργου (Galiatsatou et al. 2014) σε σχέση με την επίδραση της κλιματικής αλλαγής στη στάθμη και το κυματικό κλίμα των ελληνικών θαλασσών, έγινε ανάλυση και εκτίμηση των μεταβολών, με χρήση σύγχρονων μοντέλων περιοχικής και τοπικής κλίμακας έως το έτος 2100. Έχοντας υπόψη τα αποτελέσματα, λήφθηκαν οι εξής παραδοχές:

- Αύξηση της Μέσης Στάθμης Θάλασσας κατά 0.20μ.
- Αύξηση της Μέγιστης Στάθμης κατά 9% λόγω της μετεωρολογικής παλίρροιας (storm surge).
- Αύξηση του σημαντικού ύψους κύματος Hs στα «ανοιχτά» κατά 6%. της

- Χαρακτηριστικά ιζήματος περιοχής μελέτης

Στην περιοχή μελέτης πραγματοποιήθηκαν δειγματοληψίες και κοκκομετρική ανάλυση των δειγμάτων σύμφωνα με τα οποία, ο τύπος εδάφους που κυριαρχεί είναι τύπου SP (άμμος κακής διαβάθμισης με χαλίκια) ,εκτός μίας περιοχής στην οποία βρέθηκε έδαφος τύπου GP (χαλίκι κακής διαβάθμισης με μίγμα άμμου-χαλικιού.).

2.2 Μαθηματική Προσομοίωση Κυματικών και Υδροδυναμικών Συνθηκών

Έχοντας ως βάση όλα τα παραπάνω, γίνεται προσομοίωση των παράκτιων διεργασιών για την υφιστάμενη κατάσταση χωρίς την παρουσία των προτεινόμενων ακτομηχανικών και λιμενικών έργων. Συγκεκριμένα προσδιορίζεται το κυματικό πεδίο τόσο στα ανοιχτά όσο και στην παράκτια ζώνη. Στη συνέχεια προσομοιώνεται το υδροδυναμικό πεδίο και το πεδίο τάσεων στερεομεταφοράς, αποδίδοντας τις περιοχές με τάσεις απόθεσης ή διάβρωσης. Τέλος, εκπονείται νέα κύκλος προσομοιώσεων με την παρουσία των ακτομηχανικών και λιμενικών έργων με στόχο τη διερεύνηση της συμπεριφοράς αυτών στις παράκτιες διεργασίες και τη βελτιστοποίησή τους.

2.2.1 Βυθομετρικό Υπόβαθρο

Για το σενάριο της υφιστάμενης κατάστασης, χρησιμοποιήθηκαν τα βαθυμετρικά δεδομένα της πρόσφατης βυθομετρικής αποτύπωσης. Με βάση αυτά κατασκευάστηκε χωρικά μεταβλητό πλέγμα 61.694 κόμβων και 119.102 στοιχείων, που αναπαριστά πιστά τη βαθυμετρία. Αντίστοιχα κατασκευάστηκαν χωρικά μεταβλητά πλέγματα για τα εναλλακτικά σενάρια τα οποία περιλαμβάνουν τα προτεινόμενα έργα.

2.2.2 Μοντέλο Μετασχηματισμού Κυματισμών

Για την μεταφορά του κυματικού κλίματος στην παράκτια ζώνη χρησιμοποιήθηκε το μοντέλο MIKE 21 SW (D.H.I. 2017),. Το μοντέλο περιγράφει την διάδοση στις παράκτιες περιοχές, λαμβάνοντας υπόψη τα φαινόμενα της διαθλάσεως, περιθλάσεως και της ρηχώσεως λόγω μεταβολής της βαθυμετρίας, και την απώλεια ενέργειας, λόγω τριβής βυθού και θραύσεως των κυματισμών.

2.2.3 Υδροδυναμικό Μοντέλο

Για κάθε κυματικό πεδίο, προσδιορίστηκε με την χρήση δισδιάστατου υδροδυναμικού μοντέλου MIKE 21 FM-HD (D.H.I. 2017) που αναπτύχθηκε από το Danish Hydraulic Institute, το ανυσματικό πεδίο ταχυτήτων των κυματογενών ρευμάτων. Το μοντέλο υπολογίζει την κυματογενή κυκλοφορία την οφειλόμενη τόσο στην θραύση των κυματισμών όσο και σε τυχόν υπάρχοντα ρεύματα, στη δράση του ανέμου.

2.2.4 Μοντέλο Στερεομεταφοράς

Στη βάση της κυματογενούς κυκλοφορίας που υπολογίσθηκε στο προηγούμενο βήμα, θα προσδιορισθεί με το μαθηματικό μοντέλο MIKE 21 ST (D.H.I. 2017), που αναπτύχθηκε από το Danish Hydraulic Institute (D.H.I.), ο ρυθμός στερεομεταφοράς, αλλά και ο αρχικός ρυθμός διαβρώσεως ή εναποθέσεως ιζήματος, σε κάθε σημείο του δισδιάστατου κανάβου της περιοχής ενδιαφέροντος. Επίσης υπολογίζεται ο ρυθμός μεταβολής της βαθυμετρίας.

2.3 Αποτελέσματα και συμπεράσματα Ακτομηχανικής Μελέτης

Από τη διερεύνηση της υφιστάμενης κατάστασης συμπεραίνουμε ότι οι κυματισμοί Νοτιοανατολικής – Νότιας διεύθυνσης είναι οι εντονότεροι, με μέγιστες ταχύτητες ρευμάτων της τάξεως του 1 m/s. Διαπιστώθηκαν εναλλασσόμενες τάσεις διάβρωσης και απόθεσης στο μεγαλύτερο μέρος τα ακτής, με εντονότερο το φαινόμενο της απόθεσης στις υφιστάμενες ακτές.

Όσον αφορά την κλιματική αλλαγή εξετάστηκαν δύο σενάρια. το πρώτο έχει μεγάλη πιθανότητα εμφάνισης ενώ το δεύτερο, πιο ακραίο, έχει σημαντικά μικρότερη πιθανότητα εμφάνισης. Σύμφωνα με τα αποτελέσματα, παρατηρούνται ελαφρώς για το πρώτο, και σημαντικά για το δεύτερο, μεγαλύτεροι κυματισμοί κοντά στην ακτογραμμή. Σε σχέση με το υδροδυναμικό πεδίο παρατηρούνται μικρότερες ταχύτητες ρεύματος και ότι το εύρος της ζώνης ανάπτυξης των ρευμάτων μειώνεται. Σε σχέση με τις τάσεις στερεομεταφοράς, παρατηρείται τοπικά, αύξηση της τάσης διάβρωσης και μείωση της τάσης απόθεσης, συμπεραίνοντας ότι η ακτή χωρίς την παρουσία έργων προστασίας είναι μελλοντικά ευάλωτη στη διάβρωση λόγω κλιματικής αλλαγής.

Από τη διερεύνηση των εναλλακτικών διατάξεων προκύπτει πως, για όλες τις εναλλακτικές παρατηρούνται τάσεις απόθεσης στις ακτές που θα δημιουργηθούν, ενώ δεν αποτυπώνονται τάσεις απόθεσης στις εισόδους των προτεινόμενων λιμενικών εγκαταστάσεων.

Συγκρίνοντας τις εναλλακτικές σύμφωνα με τα αποτελέσματα του μοντέλου και σε συνάρτηση με την ανάγκη για εναρμόνιση των λιμενικών έργων με τα υπόλοιπα έργα τις ευρύτερη μελέτης επιλέχθηκε η αποδοτικότερη διάταξη των έργων.

Για την επιλεγείσα διάταξη , εξετάστηκαν τα δυο σενάρια κλιματικής αλλαγής. Σύμφωνα με τα αποτελέσματα, υπάρχει μεγαλύτερη μετάδοση κυματικής ενέργειας πάνω από τα έργα προστασία ακτής, ωστόσο παραμένουν λειτουργικά. Σε σχέση με το υδροδυναμικό πεδίο παρατηρούνται μικρότερες ταχύτητες ρεύματος και το εύρος της ζώνης ανάπτυξης των ρευμάτων μειώνεται. Σε σχέση με τις τάσεις στερεομεταφοράς, παρατηρείται (στο ακραίο σενάριο) ότι τα έργα προστασία της ακτής παραμένουν λειτουργικά.

Τέλος, προτάθηκε η θέσπιση προγράμματος παρακολούθησης της εξέλιξης της ακτογραμμής (μέτρηση ρυθμών διάβρωσης) σε όλο το μήκος των ακτών, προκειμένου να εξάγονται ασφαλή συμπεράσματα για την συμπεριφορά της ακτής, και εάν χρειαστεί, να γίνονται τακτικές παρεμβάσεις συμπλήρωσης υλικού.

3 ΠΡΟΤΕΙΝΟΕΜΝΗ ΕΝΑΛΛΑΚΤΙΚΗ ΔΙΑΤΑΞΗ

Τα προτεινόμενα λιμενικά έργα είναι:

- η κατασκευή δύο προβόλων 20 και 28 μέτρων για την οριοθέτηση της εκβολής του χειμάρρου Τραχώνων,
- ο εμπλουτισμός τριών υφιστάμενων ακτών του παραλιακού μετώπου συνολικού μήκους περίπου 500 μέτρων και η δημιουργία μίας ενιαίας ακτής, ελεύθερης πρόσβασης, μήκους 900 μέτρων,
- η επέκταση και αναβάθμιση των υφιστάμενων λιμενικών εγκαταστάσεων ναυτικών δραστηριοτήτων του ναυτικού ομίλου Αγίου Κοσμά,
- τα έργα επιχώσεων της τάξεως των 19.400 τ.μ. και τα έργα θωράκισης της ακτογραμμής μήκους περίπου 770 μέτρων περίπου για την εγκατάσταση υπερσύγχρονου ενυδρείου και την κατασκευή νέου τουριστικού καταφυγίου χωρητικότητας 150 σκαφών αναψυχής,
- η κατασκευή δύο ύφαλων αποσπασμένων κυματοθραυστών μήκους 210 μέτρων και απόσταση 180 – 190 m από την ακτή και ενός προβόλου μήκους 210 μέτρων με κατεύθυνση από νοτιοανατολικά προς τα βορειοδυτικά και διαπλάτυνση στο τέλος του,
- η δημιουργία επιχώσεων επί του προβόλου για τις ανάγκες κατασκευής πισίνας τύπου infinity pool διαμέτρου 85 μέτρων και πεζόδρομου πρόσβασης,
- η καθαίρεση υφιστάμενων κατασκευών από τον αιγιαλό.

Εικόνα 1: Παράκτιο Μέτωπο του Μητροπολιτικού Πόλου Ελληνικού – Αγίου Κοσμά

4 ΑΝΤΙΚΤΥΠΟ ΤΩΝ ΕΡΓΩΝ ΣΤΟ ΠΕΡΙΒΑΛΛΟΝ

Σύμφωνα με τη Μελέτη Περιβαλλοντικών Επιπτώσεων, οι ενδεχόμενες επιπτώσεις από τη λειτουργία των προτεινόμενων έργων, συνολικά, εκτιμώνται ως θετικές. Τα εξεταζόμενα έργα θα συμβάλλουν καθοριστικά στη βελτίωση των ακτομηχανικών συνθηκών, στην αισθητική αναβάθμιση της περιοχής καθώς και της ενίσχυσης δραστηριοτήτων σχετικών με την ψυχαγωγία, τον τουρισμό και το εμπόριο.

Αναπόφευκτη είναι η κατάληψης τμήματος της θαλάσσιας έκτασης για την υλοποίηση κάποιων έργων. Σύμφωνα με τις Υποβρύχιες έρευνες εντοπίσθηκαν στην ευρύτερη θαλάσσια περιοχή λιβάδια Ποσειδωνίας. Τα προτεινόμενα έργα αναπτύσσονται σε περιοχή (βάθος, γεωγραφικό στίγμα) που παρουσιάζει μεμονωμένες συστάδες Ποσειδωνίας, ενώ η επιφάνεια κατάληψής τους είναι μιαρότερη από το 1% της Ποσειδωνίας που απαντάται στο υπό μελέτη μέτωπο και σε απόσταση από την ακτή έως 3 χλμ..

Η περιοχή βρίσκεται εκτός των ορίων και σε σημαντική απόσταση από προστατευόμενες ή ευαίσθητες από πλευράς φυσικών χαρακτηριστικών περιοχές. Επιπλέον, κατά τη διάρκεια της κατασκευής αλλά και της λειτουργίας των έργων, δεν προβλέπεται κανένα έργο στη χερσόνησού του Αγίου Κοσμά η οποία είναι κηρυγμένος αρχαιολογικός χώρος. Επίσης για ότι τυχόν ανευρεθεί θα ακολουθηθούν οι νόμιμές διαδικασίες.

Τέλος το όλο εγχείρημα θα τονώσει την οικονομία και την απασχόληση και θα γίνει σημαντικός πόλος έλξης μεγάλου κύματος τουριστών, σε πανευρωπαϊκό επίπεδο.

Βιβλιογραφικές Αναφορές

DHI (2017) MIKE 21 WAVES, USER GUIDE. Danish Hydraulic Institute Water & Environment, Denmark.

DHI (2017) MIKE 21 HYDRODYNAMIC, USER GUIDE. Danish Hydraulic Institute Water & Environment, Denmark.

DHI (2017) MIKE 21 SEDIMENT TRANSPORT, USER GUIDE. Danish Hydraulic Institute Water & Environment, Denmark.

Galiatsatou P, Prinos P (2014) Estimation of extreme values of wave height and storm surge under climate change. Technical Report WP 3.2, Research Program CCSEAWAVS (in Greek). http://thalis-ccseawavs.web.auth.gr/en/

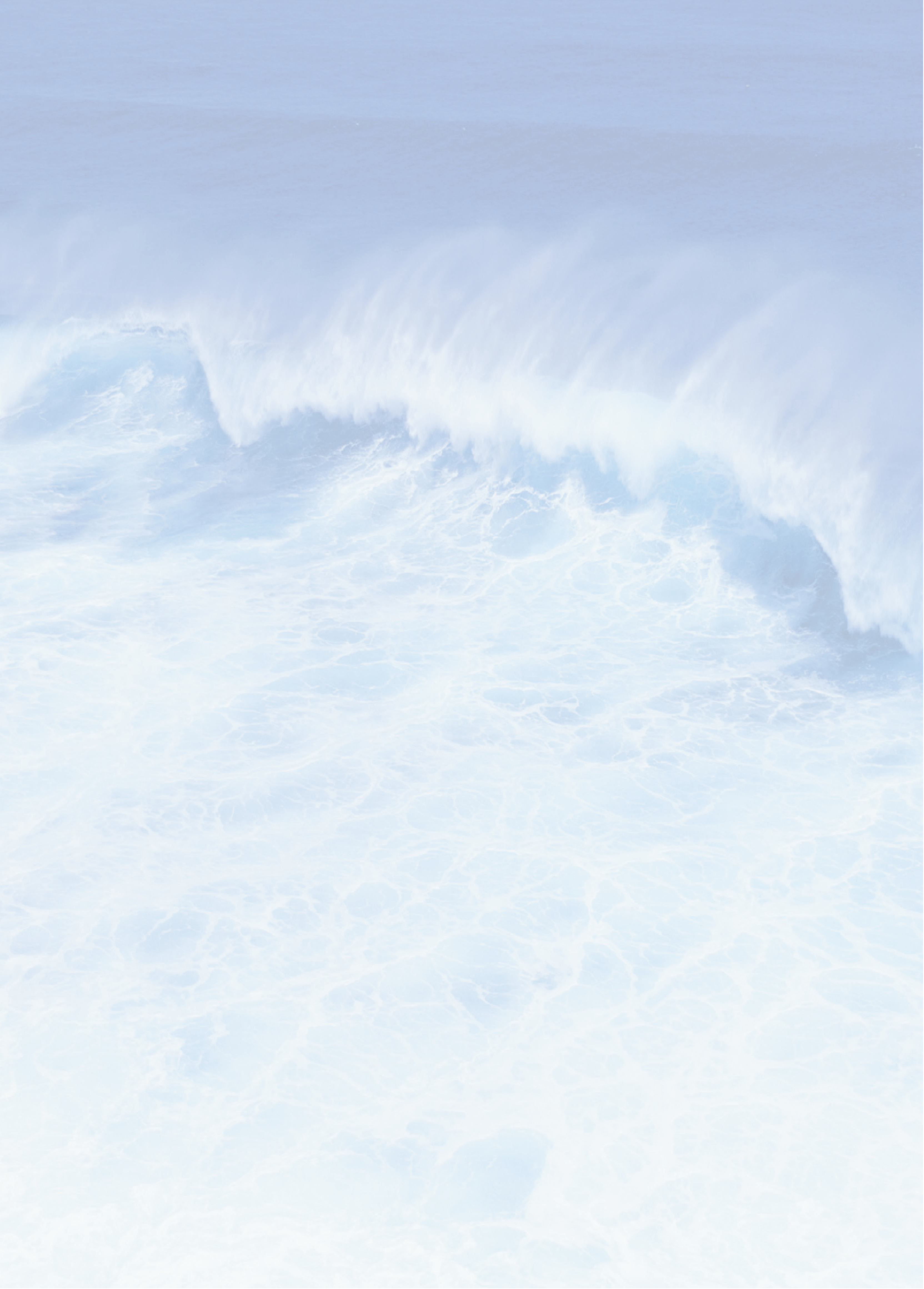

Design, construction and legal framework of an Artificial Surfing Reef (ASR) in Marathon bay, Attica

V.I. Chalastani[1], V.K. Tsoukala[1] and D. Melissas[2]

[1]Laboratory of Harbour Works, Department of Water Resources and Environmental Engineering, School of Civil Engineering, National Technical University of Athens (NTUA), Zografou 15780, Greece.
[2]Department of Urban and Regional Planning, School of Architecture, National Technical University of Athens (NTUA), Patission Complex 10682, Greece.
[*]Corresponding author: vanesachala@hotmail.com

Abstract

The study encompasses a preliminary design for a submerged multi-purpose artificial reef, also known as artificial surfing reef (ASR). The reef is designed to be constructed off the coast of Marathon Bay, Attica. The three main purposes of this reef are: to stabilize the shoreline, in order to protect it against erosion peril; to provide a stable habitat for marine life; and to create a surfing reef break. Bearing the above three goals in mind, the project is examined along three main axes. As results, a salient with amplitude of 122 m and length of 976 m is predicted along the shoreline. In addition, the ASR (165 m length, 30 m width) is designed using geosynthetic sand-filled containers, which provide an excellent environment for the development of the local, protected by law marine species. It has to be mentioned that the analysis of the reef is conducted using theoretical methods and the computer wave model MIKE 21 and predicted that the reef would produce good waves, suitable for a broad range of surfers. Finally, legal due diligence on obtaining environmental approval for the construction of the ASR is carried out, due to the fact that the site is protected by law.

Keywords ASR, Reef, Surfing, Marathon bay.

1 INTRODUCTION

1.1 The study area

The area examined is Marathon Bay, located at a distance of 45 km from the center of Athens, on the northeastern part of Attica, Greece. The site's proximity to the city of Athens constitutes an asset while planning the area's development. Its historic value is high, as one of the most emblematic battles between the Greeks and the Persians has taken place there in 490 BC. The classic Marathon race starts from this area to end up to the Panathenaic Stadium and attracts thousands of athletes from all around the world every year. In parallel, Marathon serves as the most important coastal ecosystem of Attica with a great variety of habitats, species and types of landscape. The latter was the reason for the establishment of the National Park of Schinias – Marathon in 2000 by presidential decree, and the formation of a management plan of the area, which is divided into eight zones of protection. Among them, the marine area of the Park is a bay of shallow waters on the bottom of which we encounter *Posidonia oceanica*, a seagrass species which is endemic in the Mediterranean Sea. *Posidonia oceanica* serves as a refugee for the diversified marine fauna of the area, which in the underwater meadows of *Posidonia* is alive and reproductive. The value of the site is acknowledged not only on a national but also on a European level, as the marine area of the Park is found in the list of the *Natura2000* sites. These sites are protected by the Greek law and every intervention within their boundaries has to follow a particular legal framework. Among the numerous assets of the area, one could add the construction of the Schinias Olympic Rowing and Canoeing Centre which is built to host the rowing and canoe sprint events at the 2004 Summer Olympics. However, after 2004, the area is facing constant degradation, basically due to the unapproved construction and the uncontrolled waste disposal. The effects of such actions on the coastal environment when combined with the impacts of overfishing, plastic litter, ghost nets, trawling and climate change are severe. The coastal area has already started to face erosion while the protected species of *Posidonia* is declining in population.

1.2 The surfing activity

Surfing is considered as one of the oldest activities. It is believed that the indigenous fishermen of Polynesia were learning to ride the high waves with the use of wooden boards driven by the wind. Subsequently, the activity is further evolved, especially in Hawaii. Today, surfing constitutes a sports activity which demands skill and attracts thousands of people around the globe. Apart from being such an activity, surfing has the unique characteristic of forming culture around it. People are constantly travelling to find the best beach and the best wave to ride. The sport firstly appeared in Greece in the early '90s, in the coastal area of Epirus. However, the interest of people regarding the matter, and the fact that surfing is a water sport with no seasonal limitation –it can be exercised both during summer and winter- led to the identification of multiple areas around the country, as suitable for surfing. The most visited remain the ones of the Ionian Sea, but those of the central Aegean Sea and the west Peloponnese are chosen by the athletes for practice. The activity is highly popular, especially among young people who do not hesitate to travel, explore and invest in order to acquire the best surfing experience.

1.3 The Artificial Surfing Reefs (ASRs)

Various techniques have been identified and implemented as a response to the construction of heavy and traditional structures, such as breakwaters, in the coastal landscape, to protect the shoreline from erosion. Among them, the method of beach nourishment is considered as cost-effective. However, it has severe impacts to the marine habitats and species (Auld and Schubel 1978), due to the turbulence associated to the process. On the other hand, the artificial reefs constitute an environmentally-friendly and resilient solution that assist the reproduction of the local marine flora and fauna while providing the desired protection from erosion. In addition, they can be designed in a way to create waves suitable for surfing. Therefore, they are named ASRs and act as an economic asset to enhance tourism and sustain the economy. The constantly increasing interest in surfing leads to the rise of ASRs' design and construction.

1.4 The surfing parameters

There are some parameters, crucial for the prediction of conditions suitable for surfing activity. Among them, there are some widely-used in various coastal engineering applications, such as the wave breaking height, the wave peel angle, the wave breaking intensity and the wave section length. However, these notions are further explored and expanded to be applied for surfing applications. For instance, the wave peel angle has to be such to create a "pocket" where the surfer will enter to practice his manoeuvres, and the range of angles defines the level of practicing (Figure 1a). In addition, as far as it concerns the wave breaking intensity, except for the Irribaren number, which predicts the type of breaking, something more is needed to predict the type of "tube" created when the type of breaking is the one of *plunging*. The latter is the vortex ratio that also defines the level of skills needed for the activity (Figure 1b).

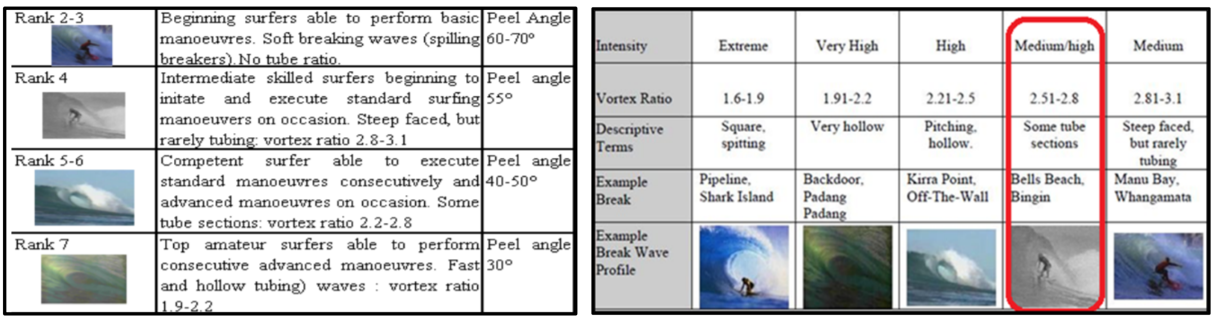

Rank 2-3	Beginning surfers able to perform basic manoeuvres. Soft breaking waves (spilling breakers). No tube ratio.	Peel Angle 60-70°
Rank 4	Intermediate skilled surfers beginning to initate and execute standard surfing manoeuvers on occasion. Steep faced, but rarely tubing: vortex ratio 2.8-3.1	Peel angle 55°
Rank 5-6	Competent surfer able to execute standard manoeuvres consecutively and advanced manoeuvres on occasion. Some tube sections: vortex ratio 2.2-2.8	Peel angle 40-50°
Rank 7	Top amateur surfers able to perform consecutive advanced manoeuvres. Fast and hollow tubing) waves : vortex ratio 1.9-2.2	Peel angle 30°

(a)

Intensity	Extreme	Very High	High	Medium/high	Medium
Vortex Ratio	1.6-1.9	1.91-2.2	2.21-2.5	2.51-2.8	2.81-3.1
Descriptive Terms	Square, spitting	Very hollow	Pitching, hollow.	Some tube sections	Steep faced, but rarely tubing
Example Break	Pipeline, Shark Island	Backdoor, Padang Padang	Kirra Point, Off-The-Wall	Bells Beach, Bingin	Manu Bay, Whangamata
Example Break Wave Profile					

(b)

Figure 1 Examples of surfing parameters: a) ASRs' degree of difficulty ranking for surfing reefs (Hutt et al. 2001), b) Classification of the wave breaking intensity (Mead and Black 2001a).

2 METHODOLOGY

The four (4) main goals that the reef should achieve are: (i) to create surfing conditions at the Marathon bay, (ii) to provide a friendly environment for the protection of *Posidonia oceanica* and the reproduction of marine fauna in the area; (iii) to protect the coast from erosion and (iv) to be designed according to the national environmental regulation, in order for it to be feasible to be deployed.

2.1 The primary data

The necessary *wind data* is obtained from the Hellenic National Meteorological Service (HNMS). The data concerned the station of Marathon for the years 1986-1997 and it is the monthly and annual frequencies of the wind intensity for every wind direction. Finally, due to the geographical position of the bay, the wind directions affecting the area are the Southern, the Southeastern and the Eastern, with a maximum intensity of eight (8) on the Beaufort scale. The first step for acquiring the *wave conditions* in the study area is to calculate the fetch length for every one of the three (3) principal wave directions. Subsequently, the Sverdrup-Munk-Bretchneider (SMB) model is used to obtain the significant wave period and the significant wave height. For the Southern wind direction, the significant wave period is T_s=4.6 sec and the significant wave height is H_s=1.56m at a -20 m depth. The breaking depth is h_b= 1.95 m.

2.2 The wave model MIKE 21

In order for the wave characteristics close to the shoreline to be defined, the model MIKE 21- version of Parabolic Mild Slope (PMS) is used. The model is a linear refraction-diffraction model based on a parabolic approximation to the elliptic mild slope equation. The model takes into account the effects of refraction and shoaling due to varying depth, diffraction along the perpendicular to the predominant wave direction and energy dissipation due to bottom friction and wave breaking (DHI 2017). MIKE 21 PMS takes into account, among others, the phenomena of shoaling, refraction, diffraction and wave breaking. The primary input is the bathymetry (Figure 2) and the wave characteristics in deep waters. The model permits the introduction of waves only from the western boundary and has better response when these are parallel to the x axis of the model grid. In our case, the principal southern wave direction is perpendicular to the eastern boundary of the grid and the grid dimensions are 5 m by 5 m which are chosen according to the wave length in deep waters. The basic output data from the model are integral wave parameters such as the root mean square wave height, the peak wave period and the mean wave direction.

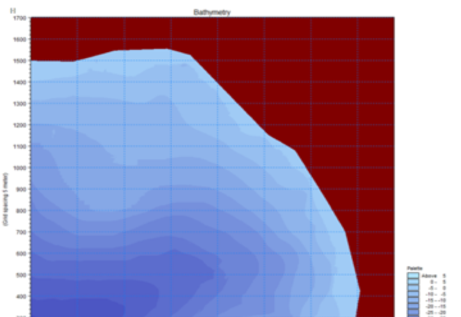

Figure 2 The bathymetry of the area as it is depicted by the model. The grid spacing is 5 m. Red color is for land and the range of depths in the palette is from -65 (deep blue) to above 5 (light blue).

2.3 The legislative framework

The site examined is protected by law, due to the fact that it is part of the European network of protected areas *NATURA2000*. Therefore, any intervention in the site is subject to specific environmental restrictions. In the context of proposing a solution which is technically feasible, the legal due diligence on obtaining environmental approval for the construction of the ASR is carried out. For this reason, the legislative framework of the National Park of Marathon Bay and of all the Greek areas included in the *NATURA2000* framework is analyzed. Subsequently, the steps and documents to be provided to the authorities are created and collected respectively.

3 RESULTS

Once the design of the reef is crystallized, a method for its deployment has to be considered. Therefore, the ASR is designed using geosynthetic sand-filled containers, with an estimated duration life of approximately 40 years, which provide an excellent environment for the development of the local, marine flora and fauna. In particular, this technique enhances conservation in the area, as *Posidonia oceanica* is growing on the containers and thus serving as an ideal refuge for a variety of fish and oysters. The process followed is the Rapid Accurate Deployment (Mead 2003). Subsequently, the national legal framework is explored in depth to understand the administrative steps need to be followed in order for the reef to be constructed.

3.1 Design of the Reef

The main result of the analysis is the design of a V-shape ASR (165 m length, 30 m width) placed on the bottom of the sea. The two parts of the ASR (i.e. left and right) are designed with different directions in order to create different ranges of breaking wave heights and angles as well as different types of surfing tubes. Therefore, most types of surfers (except for the professional ones) could use the ASR. The layout of the reef is shown in Figure 3.

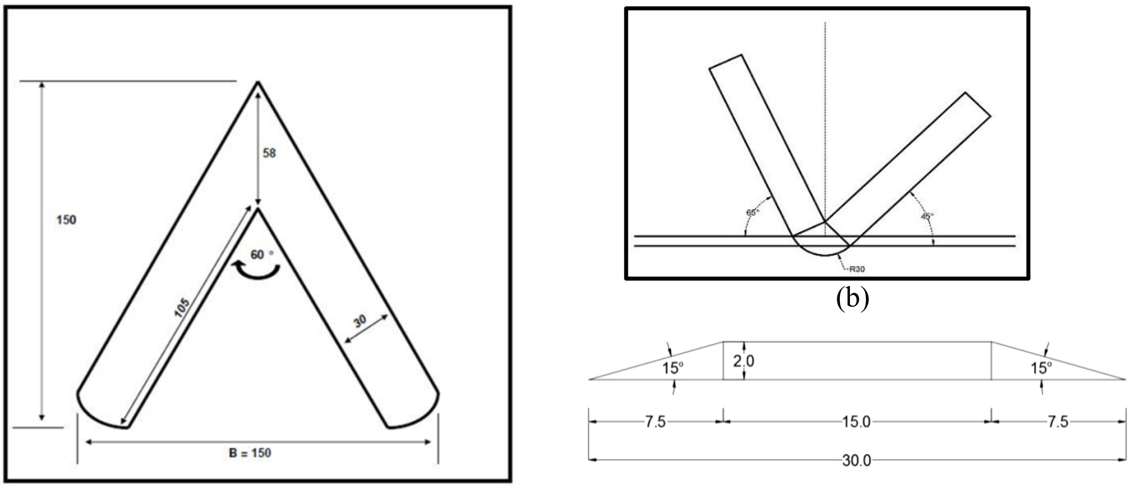

(a) (c)

Figure 3 Characteristics of the ASR: (a) initial geometrical characteristics (2 sides of 165 m length and 30 m width each), (b) Final layout of the ASR; The right side produces waves for competent surfers and the left one for beginners, (c) Section of one side of the reef. The reef has a curved vertical profile

3.1.1 Geometrical characteristics

Firstly, the geometrical characteristics of the reef are chosen arbitrarily. A V-shape reef is decided. The two (2) sides of the reef are of 165 m length and 30 m width each. The right side is to produce waves for the highest ranks of surfing skills whereas the left one for the lowest groups (Hutt et al. 2001). These characteristics are subsequently examined in order to create the formation of a salient as a beach response to erosion. In parallel, the geometry has to be such so as for a tombolo formation to be avoided in all cases. A crucial parameter for the final formation for moderating beach erosion is the distance of the reef from the shoreline. The empirical formulas of Black and Andrews (2001) and the Coastal Engineering Manual Guideline (CEM 2011) are used to predict the magnitude of the salient and the distance of the reef from the coast. We ended up with a salient with amplitude of 122 m and length of 976 m is predicted along the shoreline to address the problem of erosion. The reef is placed at 300 m off the coast of Marathon bay, at a depth of approximately -3 m.

3.1.2 Direction of the reef's sides

As far as it concerns the direction of the two (2) sides of the reef, that is calculated according to the Hutt classification (Hutt et al. 2001). For ranks 2-6, the wave breaking angles are ranging between 75° to 40° respectively. Therefore, the right side is designed at a direction of 45° relatively to the direction of the waves (ranks 5-6; competent surfers; Figure 1) whereas the left one at a direction of 65^o (ranks 2-3; beginners; Figure 1).

3.1.3 Slope of the reef's sides

Regarding the slope of the sides of the reef, the Irribaren ratio is not enough to predict the magnitude of breaking intensity and for this reason, the vortex ratio is used. A medium to high breaking intensity (vortex ratio of 2.51-2.8; Figure 1b) is chosen to define the desired slope at the direction of the wave. The final layout of the slopes of the reef is shown in Figure 3c. The slope of 15^o in each side is diminishing from the 2 m height of the reef to the bottom of the sea in order to acquire the desired curved profile (Mead and Black 2001).

3.2 Legal Due Diligence

The main legal axes of interest are the *Presidential Decree of 3.7.2000* and the *Law with number 4014 of 2011*. The Decree states the marine area of Marathon bay as of particular ecological importance and it characterizes the area as a protected zone where only marine recreational activities, research and monitoring are allowed. In addition, the second article of the Law 4014/2011 encloses interventions in marine areas in the 9th group among 12. Constructions in *"NATURA2000"* sites are included in the second group of separation, among two (2). The first article of the same regulation defines the actions need to be taken for each of the two (2) groups of separation in order for such an intervention to be effected. In our case, except for the Environmental Impact Assessment, a Special Ecological Evaluation needs also to be conducted.

4 CONCLUSIONS

The area examined is currently facing multiple challenges. The deployment of the ASR could address them in a holistic way as it will control the erosion, it will build resilience by improving the local marine life and it will serve as the main asset of the area to attract tourism. Furthermore, the connection of the reef to the Schinias Olympic Rowing and Canoeing Centre could be effected through the creation of light structures in the terrestrial part of the National Park. The area could then provide a complete environmentally-friendly touristic experience, as athletes and people could spend the whole day there, firstly at the Rowing and Canoeing Centre for rowing and walks and subsequently at the beach for surfing, and vice versa. The local development plan could be focused on this axis. The protection and further growing of the marine life is to be effected through the deployment of the reef and that is a viable alternative to the degradation of the area. Finally, any such work should explore the feasibility of the suggested constructions, both technically and legally. In order to acquire the full spectrum of the aforementioned feasibility, the legal overview of the reef is created. The outcome is very encouraging, as it is found that despite the predictions, such an intervention in a marine protected area is possible, and that particular structures such as the one proposed could be deployed in a protected area while following the steps.

References

Auld AH Schubel JR (1978) Effects of suspended sediment on fish eggs and larvae: A laboratory assessment. Estuarine and Coastal Marine Science, Vol 6, Issue 2, February 1978, Pages 153–164

Black KP, Anrews CJ (2001) Sandy shoreline response to offshore obstacles, Part 1: Salient and tombolo geometry and shape. In: Black KP. (*ed.*), Natural and Artificial Reefs for Surfing and Coastal Protection. Journal of Coastal Research, Special Issue No. 29, pp. 82-93.

Coastal Engineering Manual (CEM) (2006) U.S. Army Corps of Engineers, Washington, D.C. http://chl.erdc.usace.army.mil/cem.

DHI (2012) User Guide and Reference Manual. Danish Hydraulic Institute, Water and Environment, Denmark.

Hutt JA, Black KP, Mead ST (2001) Classification of surf breaks in relation to surfing skill.

Mead ST, Black KP, (2001) Field studies leading to the bathymetric classification of world-class surfing breaks. In: Black KP (*ed.*), Natural and Artificial Reefs for Surfing and Coastal Protection. Journal of Coastal Research, Special Issue No. 29, pp. 5-20.

Mead ST (2003) Surfing Science. *Proceedings of the 3rd International Symposium,* Raglan, New Zealand. June 2003.

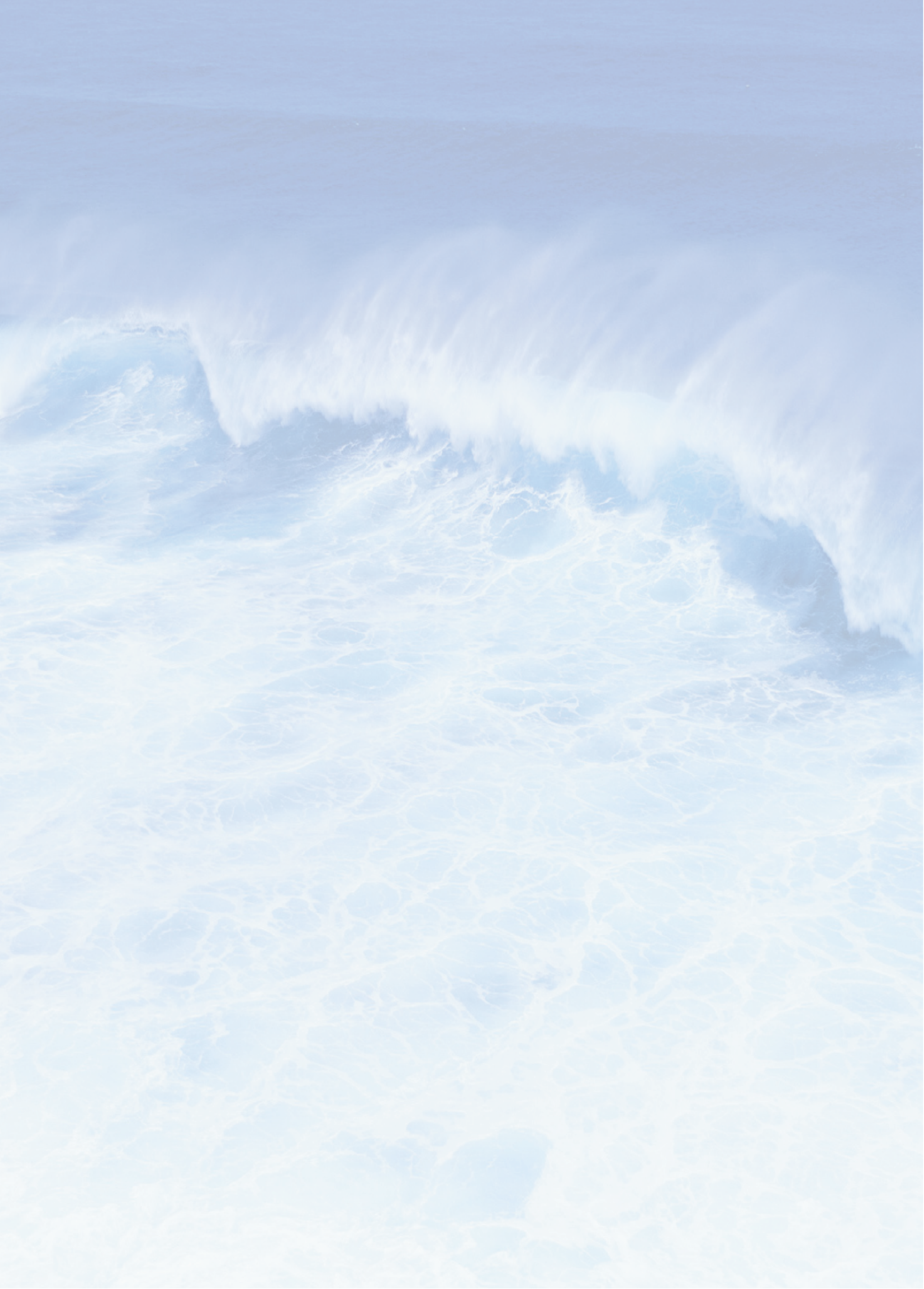

Ιεράρχηση εναλλακτικών παρεμβάσεων έναντι προβλημάτων διάβρωσης

Δ. Χαρχούση[1*], Μ.Π. Παπαδοπούλου[1], Β. Τσουκαλά[2]

[1]Εργαστήριο Φυσικής Γεωγραφίας και Περιβαλλοντικών Επιπτώσεων, Σχολή Αγρονόμων Τοπογράφων Μηχανικών, Εθνικό Μετσόβιο Πολυτεχνείο, Αθήνα, 15773, Ελλάδα
[2]Εργαστήριο Λιμενικών Έργων, Σχολή Πολιτικών Μηχανικών, Εθνικό Μετσόβιο Πολυτεχνείο, Αθήνα, 15773, Ελλάδα
[*]Υπεύθυνος επικοινωνίας: charchousi@gmail.com

Περίληψη

Οι μέθοδοι πολυκριτηριακής ανάλυσης αποτελούν ένα ευρέως διαδεδομένο εργαλείο αξιολόγησης εναλλακτικών λύσεων, οι οποίες βασίζονται στην απόδοση κάθε εναλλακτικής σε σχέση με ένα σύνολο κριτηρίων. Στόχος της παρούσας εργασίας είναι η ιεράρχηση εναλλακτικών έργων παρέμβασης στο παράκτιο περιβάλλον με τη χρήση πολυκριτηριακών προσεγγίσεων. Συγκεκριμένα, η εργασία στοχεύει στην επιλογή της βέλτιστης εναλλακτικής παρέμβασης που θα συμβάλλει στην προστασία του παράκτιου τμήματος από την Παραλία Αυλίδας έως το Βαθύ του Δήμου Χαλκίδας και το μετριασμό των συνεπειών διάβρωσης που παρατηρούνται κατά μήκος της ακτογραμμής. Για τη σταθεροποίηση και την αποκατάσταση των προβλημάτων διάβρωσης προτάθηκαν 5 τεχνικές λύσεις οι οποίες περιλαμβάνουν συστήματα προβόλων και κυματοθραυστών. Η αποτελεσματικότητα των λύσεων αυτών έναντι του φαινομένου της διάβρωσης αξιολογήθηκε μέσω της ανάπτυξης μαθηματικού μοντέλου προσομοίωσης του παράκτιου συστήματος. Κατά την πολυκριτηριακή ανάλυση, αξιολογήθηκε και η μηδενική λύση ώστε να αποτιμηθούν οι επιπτώσεις της διάβρωσης με βάση τη διαχρονική εξέλιξη της υφιστάμενης κατάστασης. Η ανάλυση βασίστηκε στην απόδοση των εναλλακτικών λύσεων με βάση δώδεκα τεχνικά, περιβαλλοντικά, κοινωνικά και οικονομικά κριτήρια. Για λόγους πληρότητας, αναπτύχθηκαν και μελετήθηκαν δύο σενάρια, τα οποία διαφοροποιούνται ως προς τη βαρύτητα των κριτηρίων. Επιπλέον, για κάθε σενάριο, οι εναλλακτικές λύσεις αξιολογήθηκαν με δύο μεθόδους της οικογένειας PROMETHEE (PROMETHEE I και PROMETHEE II). Η εναλλακτική λύση που προτείνει την ανάπτυξη ενός συστήματος 13 προβόλων μήκους 30m αποδείχθηκε η βέλτιστη υπό το πρίσμα όλων των εξεταζόμενων σεναρίων και μεθόδων. Συμπερασματικά, οι πολυκριτηριακές μέθοδοι PROMETHEE αποδείχθηκαν χρήσιμες για την ταυτόχρονη αξιολόγηση ποιοτικών και ποσοτικών κριτηρίων. Ωστόσο, το πιο κρίσιμο βήμα για την αποτελεσματικότητα της ανάλυσης είναι η επιλογή κατάλληλων και αντιπροσωπευτικών κριτηρίων.

Λέξεις κλειδιά Πολυκριτηριακή ανάλυση, Μέθοδοι PROMETHEE, Παράκτιο περιβάλλον.

1 ΕΙΣΑΓΩΓΗ

Η διάβρωση των ακτών αποτελεί σημαντική απειλή για τη βιωσιμότητα των παράκτιων κοινοτήτων, υποδομών και οικοσυστημάτων. Για τη σταθεροποίηση και την αποκατάσταση των προβλημάτων διάβρωσης υιοθετούνται έργα «έντονης» ή «ήπιας» παρέμβασης όπως η κατασκευή κυματοθραυστών ή η τεχνητή αναπλήρωση ακτών αντίστοιχα. Συχνά περισσότερες από μία τεχνικές λύσεις αξιολογούνται και αποδεικνύονται αποτελεσματικές για την προστασία των παράκτιων περιοχών έναντι των διαβρωτικών φαινομένων και η τελική επιλογή πραγματοποιείται με βάση κοινωνικά, περιβαλλοντικά και οικονομικά κριτήρια.

Η παρούσα εργασία εστιάζει στην αξιολόγηση εναλλακτικών παρεμβάσεων που αποσκοπούν στην απομείωση των αρνητικών επιπτώσεων των διαβρωτικών φαινομένων κατά μήκος της ακτογραμμής από την Παραλία Αυλίδας έως το Βαθύ του Δήμου Χαλκίδας. Για το σκοπό αυτό, πραγματοποιήθηκε πολυκριτηριακή ανάλυση όλων των προτεινόμενων τεχνικών λύσεων στην περιοχή παρέμβασης με τη χρήση του λογισμικού Visual PROMETHEE (VPSolutions 2013), ένα λογισμικό το οποίο υποστηρίζει την εφαρμογή της πολυκριτηριακής μεθόδου απόφασης PROMETHEE (Brans κ.ά. 1986).

2 ΠΕΡΙΟΧΗ ΠΑΡΕΜΒΑΣΗΣ

2.1 Γενικά χαρακτηριστικά

Το παράκτιο μέτωπο από την Παραλία Αυλίδας έως το Βαθύ του Δήμου Χαλκίδας αποτελεί την περιοχή παρέμβασης (Εικόνα 1). Στην περιοχή είναι εμφανής η ανθρωπογενής δραστηριότητα, ενώ ιδιαίτερα σημαντική είναι και η τουριστική της αξία. Στην περιοχή παρέμβασης, η οποία διαβρέχεται από τον Νότιο Ευβοϊκό κόλπο, είναι εμφανείς οι επιπτώσεις των διαβρωτικών φαινομένων κατά μήκος της ακτογραμμής.

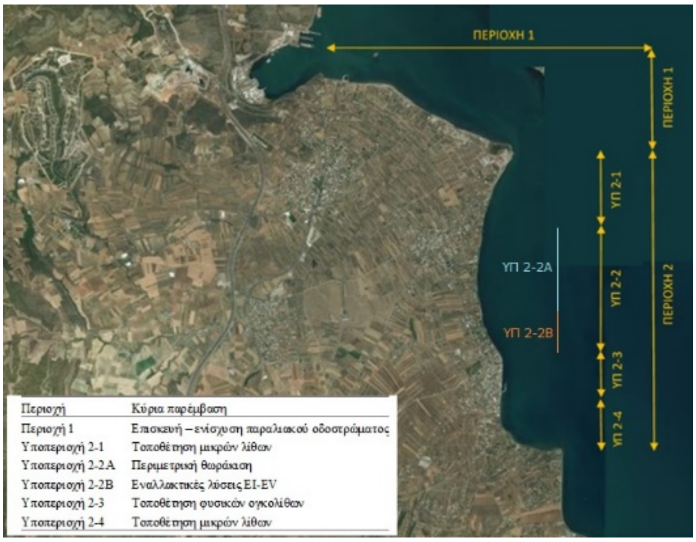

Εικόνα 1 Περιοχή μελέτης (Υπόβαθρο: Google Earth)

2.2 Περιγραφή των προτεινόμενων έργων παρέμβασης

Στα πλαίσια της πολυκριτηριακής ανάλυσης αξιολογούνται έξι εναλλακτικές λύσεις: α) η μηδενική λύση και β) 5 τεχνικές προτάσεις για τη σταθεροποίηση και την αποκατάσταση των προβλημάτων διάβρωσης στην περιοχή μελέτης. Οι τεχνικές προτάσεις αφορούν σε ένα σύνολο επεμβάσεων κατά μήκος της ακτογραμμής που ενδέχεται να περιλαμβάνουν την τοποθέτηση μικρών λίθων, την περιμετρική θωράκιση παράκτιου μετώπου και την τοποθέτηση φυσικών ογκολίθων. Η πλειονότητα των παρεμβάσεων είναι κοινές σε όλες τις προτάσεις, ωστόσο διαφοροποιούνται ως προς την προτεινόμενη μέθοδο παρέμβασης στην Υποπεριοχή 2-2Β (Εικόνα 1). Η αποτελεσματικότητα των παρεμβάσεων έναντι του φαινομένου της διάβρωσης έχει αξιολογηθεί μέσω της ανάπτυξης μαθηματικού μοντέλου προσομοίωσης του παράκτιου συστήματος (ΥΥΜ, 2018). Στη συνέχεια της εργασίας οι έξι εναλλακτικές λύσεις αναφέρονται ως Μ, ΕΙ, ΕΙΙ, ΕΙΙΙ, ΕΙV, ΕV αντίστοιχα με βάση την προτεινόμενη λύση για την περιοχή παρέμβασης Υποπεριοχή 2-2Β. Συγκεκριμένα:

- Μ – ΜΗΔΕΝΙΚΗ ΠΑΡΕΜΒΑΣΗ: Προτείνεται η παρακολούθηση της διαχρονικής εξέλιξης της υφιστάμενης κατάστασης χωρίς καμία επέμβαση
- ΕΙ – ΣΥΣΤΗΜΑ 5 ΠΡΟΒΟΛΩΝ 30 m: Προτείνεται στην Υποπεριοχή 2-2Β η αφαίρεση των υφιστάμενων προβόλων και η κατασκευή προβόλων κάθετων προς την ακτογραμμή, μήκους 30 m
- ΕΙΙ – ΣΥΣΤΗΜΑ 5 ΠΡΟΒΟΛΩΝ 60 m: Προτείνεται στην Υποπεριοχή 2-2Β η αφαίρεση των υφιστάμενων προβόλων και η κατασκευή προβόλων κάθετων προς την ακτογραμμή, μήκους 60 m
- ΕΙΙΙ – ΣΥΣΤΗΜΑ 4 ΕΞΑΛΩΝ ΚΥΜΑΤΟΘΡΑΥΣΤΩΝ: Προτείνεται στην Υποπεριοχή 2-2Β η αφαίρεση των υφιστάμενων προβόλων και η κατασκευή συστήματος 4 αποσπασμένων κυματοθραυστών χαμηλής στέψεως
- ΕΙV – ΣΥΣΤΗΜΑ 4 ΙΣΑΛΩΝ ΚΥΜΑΤΟΘΡΑΥΣΤΩΝ: Προτείνεται στην Υποπεριοχή 2-2Β η αφαίρεση των υφιστάμενων προβόλων και η κατασκευή συστήματος 4 ίσαλων αποσπασμένων κυματοθραυστών.
- ΕV – ΣΥΣΤΗΜΑ 13 ΠΡΟΒΟΛΩΝ 30m: Προτείνεται στην Υποπεριοχή 2-2Β η ανακατασκευή των υφιστάμενων προβόλων και η τοποθέτηση επιπλέον προβόλων που θα δημιουργούν ένα σύστημα δεκατριών συνολικά προβόλων, μήκους 30 m που θα εκτείνονται έως την ισοβαθή των 2 m.

3 ΜΕΘΟΔΟΛΟΓΙΑ

3.1 Η μέθοδος PROMETHEE

Η μέθοδος PROMETHEE (Preference Ranking Organization Method for Enrichment Evaluations) είναι μία μέθοδος που προτιμάται στη διαδικασία λήψης αποφάσεων προβλημάτων περιβαλλοντικού σχεδιασμού (Geneletti και van Duren 2008, Betrie κ.ά. 2013) καθώς δίνει τη δυνατότητα να οριστούν πλήθος κριτηρίων, ποιοτικών και ποσοτικών, με βάση τα οποία θα γίνει η συγκριτική αξιολόγηση και ιεράρχηση πλήθους εναλλακτικών λύσεων. Κατά την εφαρμογή της μεθόδου PROMETHEE, οι εναλλακτικές λύσεις συγκρίνονται ανά ζεύγη για κάθε κριτήριο αξιολόγησης, προκειμένου να δημιουργηθεί μία κατάταξή σύμφωνα με το σύνολο των κριτηρίων. Στην παρούσα εργασία, εφαρμόστηκαν δύο μέθοδοι της οικογένειας PROMETHEE, α) η μέθοδος PROMETHEE I (partial ranking) και β) η μέθοδος PROMETHEE II (complete ranking). Η κατάταξη των εναλλακτικών λύσεων και για τις δύο μεθόδους πραγματοποιείται με βάση τις τιμές των ροών εκροής φ+(α) και των ροών εισροής φ-(α). Συγκεκριμένα, η κατάταξη για τη μέθοδο PROMETHEE I βασίζεται στη σύγκριση ανάμεσα στις τιμές των ροών εκροής φ+(α) και των ροών εισροής φ-(α), ενώ για τη μέθοδο PROMETHEE II μέσω του υπολογισμού της καθαρής ροής (διαφορά μεταξύ των ροών εκροής και εισροής). Ο προσδιορισμός της προτιμητέας λύσης μπορεί να απεικονιστεί γραφικά μέσω διαγραμμάτων όπου μία λύση Α θεωρείται προτιμητέα όταν η γραμμή που ενώνει τις τιμές των ροών εκροής φ+(α) και των ροών εισροής φ-(α) της λύσης Α υπερτερεί πλήρως έναντι της αντίστοιχης γραμμής της λύσης Β. Όταν οι γραμμές των δύο λύσεων τέμνονται τότε αυτές είναι ασύγκριτες (δεν υπερισχύει κάποια). Ο εντοπισμός της προτιμητέας λύσης στο διάγραμμα της μεθόδου PROMETHEE II είναι ευκολότερος καθώς η προτιμητέα λύση είναι αυτή με τη μεγαλύτερη καθαρή ροή.

3.2 Κριτήρια περιβαλλοντικής αξιολόγησης των προτεινόμενων παρεμβάσεων

Η αξιολόγηση των έξι εναλλακτικών λύσεων που προτάθηκαν για την απομείωση των επιπτώσεων των διαβρωτικών φαινομένων στην περιοχή παρέμβασης πραγματοποιήθηκε βάσει περιβαλλοντικών, κοινωνικών και οικονομικών κριτηρίων. Τα κριτήρια επιλέχθηκαν ώστε να καλύπτουν στο μεγαλύτερο εύρος τις πιθανές επιπτώσεις των προτεινόμενων λύσεων στο φυσικό, κοινωνικό και οικονομικό περιβάλλον. Για κάθε κριτήριο καθορίστηκαν ένας ή περισσότεροι δείκτες ώστε να πραγματοποιείται ευκολότερα και ακριβέστερα η αξιολόγηση του κριτηρίου (Πίνακας 1).

Πίνακας 1 Κριτήρια και δείκτες αξιολόγησης

Είδος κριτηρίων	Κριτήριο	Δείκτης
Περιβαλλοντικά	K1. Προστασία βιοποικιλότητας, χλωρίδας, πανίδας	C1. Απώλεια-Υποβάθμιση οικοσυστημάτων
	K2. Προστασία εδαφών και ποιοτική αποκατάσταση	C2. Αλλοίωση της ακτογραμμής
		C3. Μείωση των παραλιών/παράκτια γη
		C4. Υποβάθμιση ποιότητας εδαφικού υλικού
	K3. Προστασία θαλάσσιων υδάτων και ποιοτική/ποσοτική βελτίωση	C5. Ύπαρξη οχετών– σημειακές/διάχυτες πηγές ρύπανσης
Κοινωνικά	K4. Βελτίωση ποιότητας ζωής και υγείας κατοίκων	C6. Διαμόρφωση–δημιουργία χώρων αναψυχής, πεζοδρομίων, ποδηλατοδρόμων
		C7. Πρόσβαση στις παραλίες (ράμπες/κλίμακες)
	K5. Προστασία και ανάδειξη τουριστικού προϊόντος περιοχής	C8. Δημιουργία πόλων έλξης
Οικονομικά	K6. Διάχυση οφέλους στην κοινωνία	C9. Δημιουργία θέσεων απασχόλησης
	K7. Οικονομική αποτίμηση	C10. Κόστος παρεμβάσεων
		C11. Παρεμπόδιση διέλευσης στον κόλπο/αλιείας
	K8. Προστασία και ενίσχυση υλικών περιουσιακών στοιχείων	C12. Αξίες γης

3.3 Κριτήρια περιβαλλοντικής αξιολόγησης των προτεινόμενων παρεμβάσεων

Η οπτική κάθε ενδιαφερόμενου μέρους/εμπλεκόμενου στην αξιολόγηση των εναλλακτικών λύσεων ενός περιβαλλοντικού προβλήματος εισάγεται στο λογισμικό με τη χρήση των συντελεστών βαρύτητας των κριτηρίων. Στην παρούσα εργασία, αναπτύχθηκαν δύο σενάρια τα οποία διαφοροποιούνται ως προς τις τιμές των συντελεστών βαρύτητας. Μέσω της διαδικασίας αυτής μπορεί να ελεγχθεί η ευρωστία της ιεράρχησης των εναλλακτικών λύσεων. Στο Σενάριο Α, θεωρήθηκε ότι όλοι οι δείκτες είναι το ίδιο σημαντικοί για την ιεράρχηση των προτεινόμενων λύσεων. Επομένως, κάθε ένα από τα δώδεκα κριτήρια έλαβε τον ίδιο συντελεστή βαρύτητας. Κατά το Σενάριο Β, θεωρήθηκε ότι οι τρεις κύριες κατηγορίες κριτηρίων (περιβαλλοντικά, κοινωνικά, οικονομικά) είναι εξίσου σημαντικές για την τελική απόφαση. Επομένως, κάθε μία από τις κατηγορίες αυτές έχει συντελεστή βαρύτητας 33,3%. Στη συνέχεια το ποσοστό αυτό επιμερίστηκε ισόποσα στους επιμέρους δείκτες της (C_i) κάθε κατηγορίας κριτηρίων.

3.4 Κριτήρια περιβαλλοντικής αξιολόγησης των προτεινόμενων παρεμβάσεων

Η επίδοση κάθε εναλλακτικής λύσης σε κάθε κριτήριο εισάγεται στο λογισμικό μέσω του πίνακα αξιολόγησης. Ο πίνακας αξιολόγησης συμπληρώνεται είτε με ποσοτικές είτε με ποιοτικές τιμές για κάθε εναλλακτική λύση ως προς κάθε δείκτη. Η αξιολόγηση των ποσοτικών δεικτών πραγματοποιήθηκε με βάση μία 5-βάθμια κλίμακα η οποία δημιουργήθηκε στα πλαίσια της ανάλυσης για κάθε δείκτη. Αντίστοιχα, οι ποιοτικοί δείκτες αξιολογήθηκαν με τις τιμές ΝΑΙ/ΟΧΙ.

4 ΠΕΡΙΟΧΗ ΠΑΡΕΜΒΑΣΗΣ

4.1 Αξιολόγηση των προτεινόμενων παρεμβάσεων (Σενάριο Α)

Στην Εικόνα 4 απεικονίζεται η κατάταξη των εναλλακτικών λύσεων βάσει των μεθόδων PROMETHEE I και II, αντίστοιχα, για το σενάριο Α κατά το οποίο όλα οι δείκτες θεωρούνται ισοδύναμοι. Η εναλλακτική λύση EV (σύστημα 13 προβόλων 30 m) είναι προτιμητέα σε σχέση με όλες τις υπόλοιπες εναλλακτικές σύμφωνα και με τις δύο μεθόδους. Στη σειρά κατάταξης των λύσεων ακολουθεί η λύση EI (σύστημα 5 προβόλων 30 m) ενώ τελευταία στην κατάταξη είναι η μηδενική λύση.

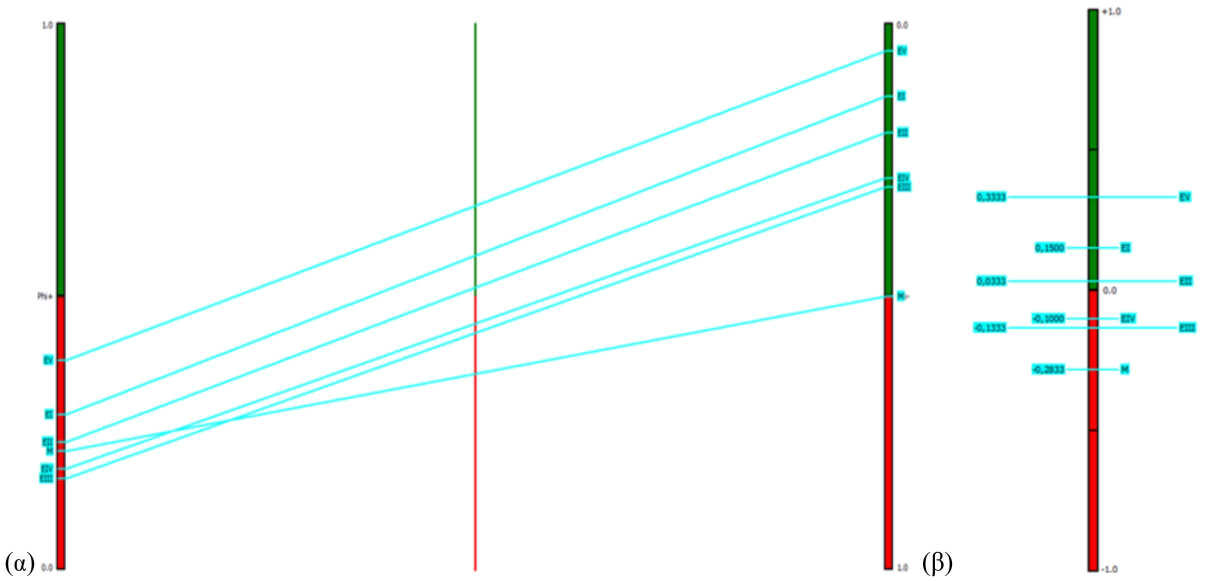

Εικόνα 4 Κατάταξη εναλλακτικών λύσεων υπό το Σενάριο Α: α) Βάσει της μεθόδου PROMOTHEE I, β) Βάσει της μεθόδου PROMOTHEE II

4.1 Αξιολόγηση των προτεινόμενων παρεμβάσεων (Σενάριο Β)

Τα αποτελέσματα της πολυκριτηριακής ανάλυσης για το Σενάριο Β, το σενάριο δηλαδή όπου οι τρεις κύριες κατηγορίες κριτηρίων είναι ισοδύναμα σημαντικές, παρουσιάζονται στην Εικόνα 5. Η εναλλακτική λύση EV (σύστημα 13 προβόλων 3 0m) είναι προτιμητέα σε σχέση με όλες τις υπόλοιπες εναλλακτικές με βάση τη μέθοδο PROMETHEE I αλλά και τη μέθοδο PROMETHEE II.

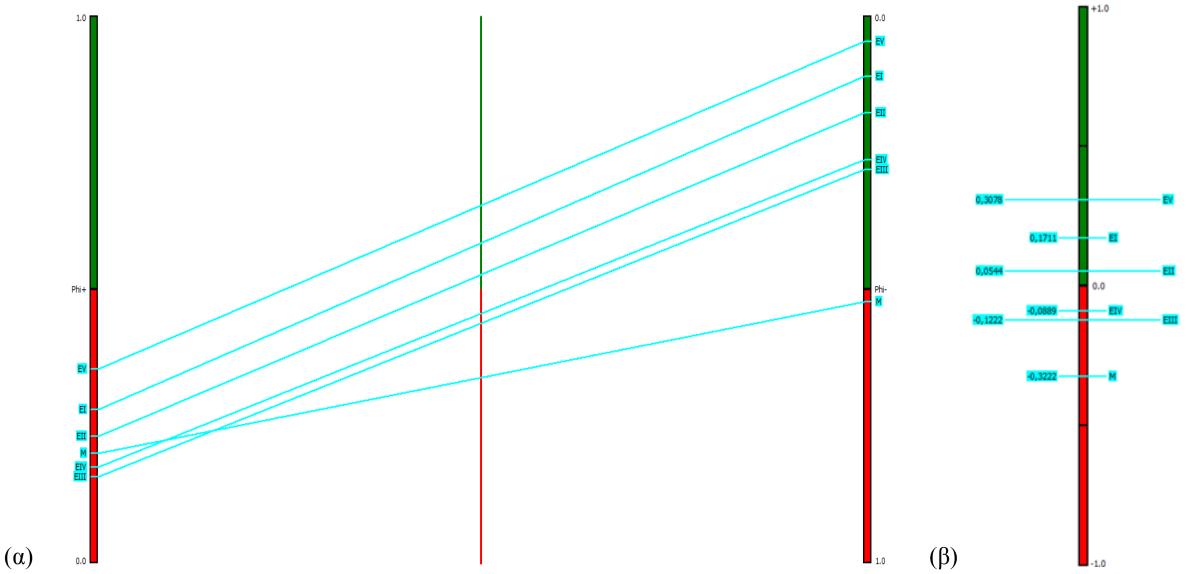

Εικόνα 5 Κατάταξη εναλλακτικών λύσεων υπό το Σενάριο Β: α) Βάσει της μεθόδου PROMOTHEE I, β) Βάσει της μεθόδου PROMOTHEE II

5 ΣΥΜΠΕΡΑΣΜΑΤΑ

Οι έξι εναλλακτικές λύσεις - συμπεριλαμβανομένης και της μηδενικής - που προτάθηκαν για την απομείωση των αρνητικών επιπτώσεων των διαβρωτικών φαινομένων που παρατηρούνται στην περιοχή μελέτης αξιολογήθηκαν με βάση τεχνικά, περιβαλλοντικά και κοινωνικο-οικονομικά κριτήρια. Η αξιολόγηση πραγματοποιήθηκε με τη χρήση του λογισμικού Visual PROMETHEE μέσω του οποίου εφαρμόστηκαν οι μέθοδοι PROMETHEE I και II.

Τα αποτελέσματα της πολυκριτηριακής ανάλυσης κατέδειξαν ότι η εναλλακτική λύση EV (σύστημα 13 προβόλων μήκους 30 m) αποτελεί την πιο ενδεδειγμένη λύση σε σχέση με όλες τις υπόλοιπες εναλλακτικές που εξετάστηκαν με τις δυο μεθόδους (PROMETHEE I και II). Τέλος, η ανάλυση ευαισθησίας (Σενάρια Α και Β) κατέδειξε ότι η εναλλακτική λύση EV αποτελεί μια εύρωστη λύση για το υπό εξέταση πρόβλημα σχεδιασμού, καθώς και για τα δύο σενάρια κρίθηκε ως η πιο προτιμητέα λύση.

Βιβλιογραφικές Αναφορές

Betrie GD, Sadiq R, Morin KA, Tesfamariam S (2013) Selection of remedial alternatives for mine sites: A multicriteria decision analysis approach. Journal of Environmental Management 119:36-46. doi.org/10.1016/j.jenvman.2013.01.024.

Brans JP, Vincke Ph, Mareshal B (1986) How to select and how to rank projects: The PROMETHEE method. European Journal of Operational Research. 24:228-238.

Geneletti D, van Duren IC (2008) Protected area zoning for conservation and use: a combination of spatial multicriteria and multiobjective evaluation. Landscape and urban planning 85(2):97-110.

VPSolutions (2013) Visual PROMETHEE 1.4 Manual. Available via DIALOG. http://www.promethee-gaia.net/assets/vpmanual.pdf. Accessed 05 Apr 2019

Υπουργείο Υποδομών και Μεταφορών (ΥΥΜ), Δ/νση Λιμενικών Υποδομών, Τμήμα Σχεδιασμού Προγραμματισμού και Μελετών (2018) Καταγραφή – αξιολόγηση και ιεράρχηση προβλημάτων διάβρωσης της ακτής Παραλία Αυλίδας έως Βαθύ του Δήμου Χαλκίδας και οργάνωση του σχεδιασμού προστασίας. Στάδια Β & Γ: Εξέταση εναλλακτικών λύσεων & κατάταξη παρεμβάσεων ανάλογα με την προτεραιότητα τους. Τεχνική έκθεση. Αθήνα.

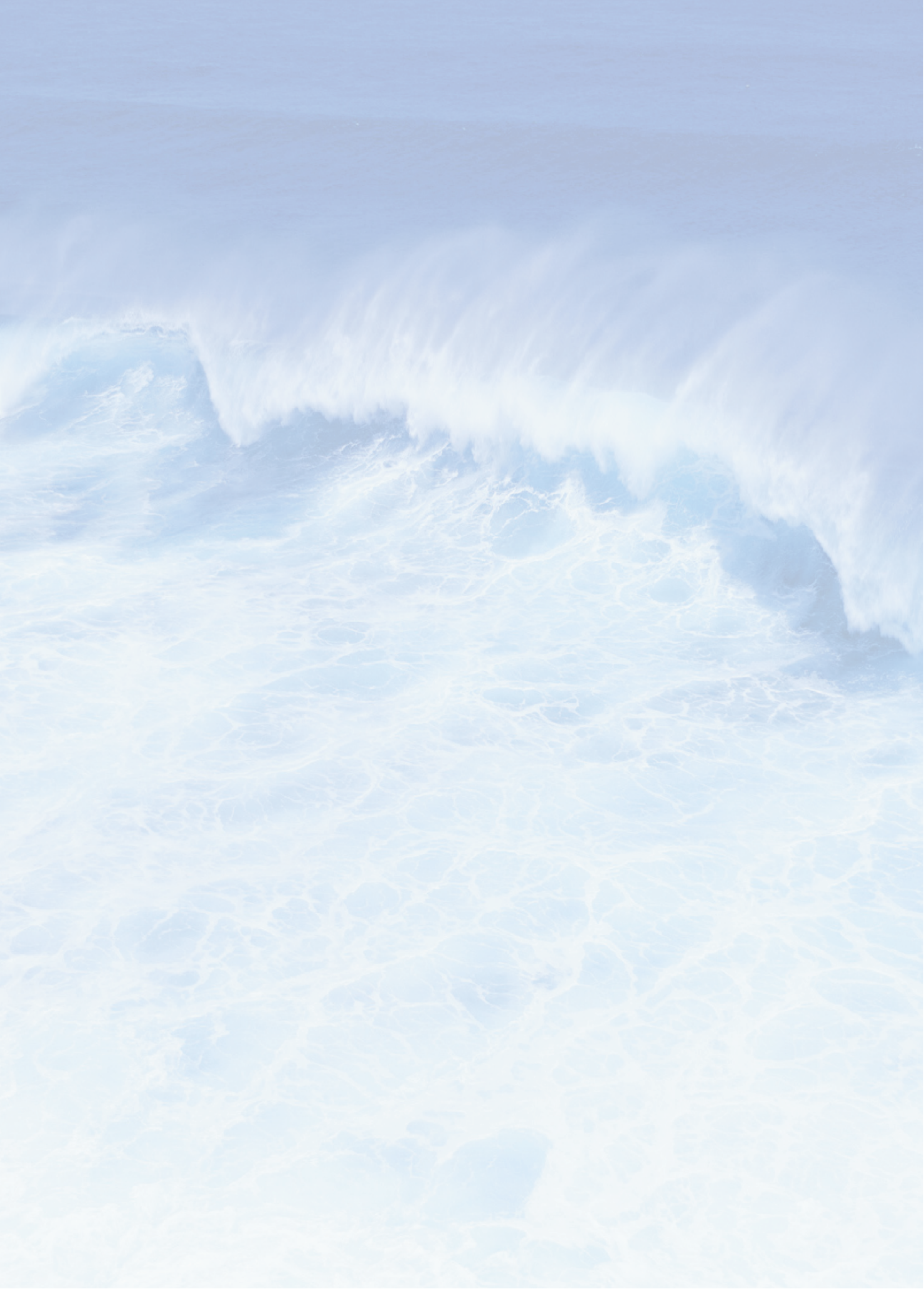

Ας ξεκινήσουμε με ένα εκατομμύριο!

Ι. Δουλάκης
Δημοτικό Λιμενικό Ταμείο Αριστοτέλη, Ιερισσός Νομού Χαλκιδικής, 63075, Ελλάδα
Ι. Δουλάκης: ioannis.doulakis@gmail.com

ΠΕΡΙΛΗΨΗ

Η κατάθεση μιας μικρής εμπειρίας από τη διαχείριση κάποιων μικρών λιμένων και οι μεγάλες προσδοκίες που αυτή δημιούργησε για ένα καλύτερο μέλλον είναι η επιδίωξη της παρούσας εισήγησης. Μικρής κλίμακας παρεμβάσεις αλλάζουν εντυπωσιακά την εικόνα και δίνουν το στίγμα μιας άλλης προοπτικής σε έναν τόπο με πλήθος αναξιοποίητα συγκριτικά πλεονεκτήματα. Διαθέσιμα στοιχεία δείχνουν ότι τα λιμενικά έργα μπορούν να γίνουν όχημα ανάπτυξης με πολλαπλά οικονομικά και κοινωνικά οφέλη για τις τοπικές κοινωνίες και ένας δημόσιος Φορέας δηλώνει πρόθυμος να αντιμετωπίσει την πρόκληση.

Λέξεις κλειδιά: Τοπικές κοινωνίες, Λιμενικές υποδομές

Θέσαμε ως τίτλο της εισήγησής μας το ποσό του ενός εκατομμυρίου όχι μόνο γιατί το εκατομμύριο στη γλώσσα του λαού ταυτίζεται με την ευημερία αλλά και επειδή όντως τόσα περίπου ήταν τα ίδια έσοδα του Δημοτικού Λιμενικού Ταμείου Αριστοτέλη κατά τα τέσσερα πρώτα χρόνια της λειτουργίας του. Τα έσοδα αυτά προέρχονται κατά κύριο λόγο από τέλη που επιβαρύνουν επισκέπτες στην περιοχή και επομένως πρόκειται για εισροή χρημάτων και διοχετεύτηκαν για τη συντήρηση και αναβάθμιση των λιμενικών υποδομών, κυρίως μάλιστα μέσω της τοπικής αγοράς. Θα μπορούσαμε λοιπόν να ισχυριστούμε ότι ο Φορέας ενίσχυσε την τοπική κοινωνία με μία οικονομική ένεση περίπου 2.000.000€, αφού αφενός διέθεσε το ποσό του 1.000.000€ στην τοπική αγορά ενώ αφετέρου εμπλούτισε τις υφιστάμενες λιμενικές υποδομές με ίσης αξίας παρεμβάσεις. Προκειμένου δε να αναδειχθεί η δυναμική που κρύβεται στο ποσό αυτό αξίζει να αναφέρουμε ότι αντιστοιχεί σε ποσοστό άνω του 5% των συνολικών ιδίων εσόδων του οικείου Δήμου Αριστοτέλη για το ίδιο χρονικό διάστημα. Αξιοσημείωτος επίσης είναι ο ρυθμός αύξησης των εσόδων του Φορέα όπως απεικονίζεται στο συγκριτικό πίνακα απολογιστικών στοιχείων που αφορά τα ίδια έσοδα του Φορέα.

Πίνακας 2 Συγκριτικά απολογιστικά στοιχεία ιδίων εσόδων 2015-2018 (Πρωτογενή δεδομένα)

2015	2016	2017	2018
198.804,27 €	236.192,43 €	261.213,72 €	289.474,27 €

Μια συνολική αύξηση δηλαδή περίπου 45%, ενώ τίποτα δεν προοιωνίζει μια διαφορετική εξέλιξη στο μέλλον. Το αντίθετο μάλιστα. Πεποίθησή μας είναι ότι η αύξηση αυτή θα συνεχιστεί και ίσως με πιο εντυπωσιακούς ρυθμούς. Η αισιοδοξία μας δε αυτή πηγάζει από την εξέταση δεδομένων πάνω σε δύο άξονες. Πρώτον, σε ποιες συνθήκες επιτεύχθηκε η ανωτέρω διαχείριση και δεύτερον σε ποιες προοπτικές βασίζεται ο σχεδιασμός για το προσεχές και το απώτερο μέλλον.

Ξεκινώντας με τον πρώτο άξονα, θεωρούμε ότι πρέπει κατ' αρχήν, να… συστηθούμε! Να σας παρουσιάσουμε ποιοι και τι ακριβώς είμαστε, ώστε να βοηθηθείτε στην κατανόηση του μεγέθους, της αποστολής, των δυνατοτήτων και των περιορισμών που μας χαρακτηρίζουν και διέπουν τη λειτουργία μας. Το Δημοτικό Λιμενικό Ταμείο Αριστοτέλη είναι ένα Δημοτικό Νομικό Πρόσωπο Δημοσίου Δικαίου, ένας Φορέας Διοίκησης και Εκμετάλλευσης Λιμένων στα γεωγραφικά όρια ενός Δήμου, εποπτευόμενος από τον οικείο Ο.Τ.Α.. Προκειμένου να μην κουράζουμε με λεπτομέρειες θα μπορούσαμε να συνοψίσουμε τα χαρακτηριστικά της φύσης του Φορέα ως εξής: Πρόκειται για έναν οργανισμό στενά συνδεδεμένο με την Τοπική Αυτοδιοίκηση Α΄ βαθμού, γεγονός που εκτιμούμε ως εξαιρετικά θετικό, καθώς τουλάχιστον θεωρητικά κανείς δεν μπορεί να γνωρίζει και να αγαπά έναν τόπο περισσότερο από τους ίδιους τους ανθρώπους του, που ωστόσο μοιραία φέρει στο σώμα του και τα αρνητικά χαρακτηριστικά του δημοσίου τομέα στην Ελλάδα και δη αυτά της Τοπικής Αυτοδιοίκησης, που φυσικά αποτελούν ανασταλτικό παράγοντα για μια εύρυθμη λειτουργία.

Θεωρούμε επίσης άξιο αναφοράς, το γεγονός ότι ο Φορέας μας, ιδρύθηκε, στο μέσον περίπου μιας περιόδου κρίσης η οποία πέραν όλων των άλλων συνοδεύτηκε από βαθιά οικονομική ύφεση, πολιτική αστάθεια και πλήθος διαρθρωτικών μεταρρυθμίσεων. Σε μια στιγμή δηλαδή που ο οικείος Ο.Τ.Α. λόγω της υποχρηματοδότησης και της υποστελέχωσής του ελάχιστα μπορούσε να υποστηρίξει το εγχείρημα της οργάνωσης και λειτουργίας ενός καινούριου Φορέα. Την ίδια στιγμή που οι μνημονιακές δεσμεύσεις της χώρας καθιστούσαν ανέφικτη και την πιο στοιχειώδη προϋπόθεση για τη λειτουργία του, την πρόσληψη δηλαδή προσωπικού για τη στελέχωση των Υπηρεσιών του! Στη χρονιά εκείνη που επιβλήθηκαν οι γνωστοί περιορισμοί κίνησης κεφαλαίων.

Εν τούτοις, το Δημοτικό Λιμενικό Ταμείο Αριστοτέλη σε ένα διάστημα περίπου έξι μηνών άρχισε να λειτουργεί. Η κατάσταση που έπρεπε να διαχειριστεί ήταν εξίσου απογοητευτική. Από τους δέκα χώρους με λιμενικές εγκαταστάσεις στα γεωγραφικά του όρια μόνο δύο διέθεταν τη βασική προϋπόθεση που του έδιναν την καθ' ύλην αρμοδιότητα σ’ αυτούς. Τον καθορισμό ή την εξομοίωση χώρου με Ζώνη Λιμένα. Επιπλέον οι φυσικές υποδομές των χώρων αυτών ήταν στο σύνολό τους ανεπαρκείς, φθαρμένες, χρονίως ασυντήρητες, οι περισσότερες κατασκευασμένες χωρίς αδειοδότηση ή καθ’ υπέρβαση αυτής. Θεωρούμε ότι δεν υπερβάλλουμε αν ισχυριστούμε ότι αρχίσαμε να λειτουργούμε όχι από μηδενική βάση αλλά από ελλειμματικό υπόβαθρο.

Από το σημείο όμως αυτό, για να περάσουμε στο δεύτερο άξονα, αρχίζει να διαφαίνεται και η σε λανθάνουσα κατάσταση ευρισκόμενη δυναμική των λιμένων μας. Όλα διέθεταν κάποιες εγκαταστάσεις και κάποιες υποδομές, όλα φιλοξενούσαν οικονομική δραστηριότητα, χωρίς όμως στοιχειώδη οργάνωση, συντονισμό, σχεδιασμό, στρατηγική. Στην πραγματικότητα απουσίαζε παντελώς ένας Φορέας Διοίκησης και Εκμετάλλευσης των χώρων αυτών και αυτό το ρόλο κληθήκαμε να διαδραματίσουμε.

Επιγραμματικά παρουσιάζουμε τα αποτελέσματα των πρωτοβουλιών του Φορέα σε ορισμένους τομείς της δραστηριότητας που συνήθως αναπτύσσεται στους λιμένες με παρεμβάσεις που στόχο είχαν τον εξορθολογισμό δαπανών και εσόδων, την τυποποίηση των διαδικασιών και την αναπτυξιακή προοπτική των χώρων αρμοδιότητας.

Πίνακας 3 Έσοδα-Έξοδα από ηλεκτροδότηση-υδροδότηση κατά τα έτη 2016-2018 (Πρωτογενή δεδομένα).

2016		**2017**		**2018**	
ΕΣΟΔΑ	**ΕΞΟΔΑ**	**ΕΣΟΔΑ**	**ΕΞΟΔΑ**	**ΕΣΟΔΑ**	**ΕΞΟΔΑ**
17,70 €	22.419,16 €	6.543,77 €	21.746,61	7.797,24 €	20.926,70 €

Πίνακας 4 Έσοδα από παραχωρήσεις χώρων κατά τα έτη 2015-2018 (Πρωτογενή δεδομένα)

2015	*2016*	*2017*	*2018*
600,00	*1.279,20*	*3.297,64*	*28.064,74*

Πίνακας 5 Έσοδα από Τέλη-Π.Δ.Ε. κατά τα έτη 2015-2018 2018 (Πρωτογενή δεδομένα).

ΕΙΔΟΣ ΕΣΟΔΟΥ	2015	2016	2017	2018
ΤΕΛΗ	0 €	0 €	12.844,97 €	16.827,62 €
Π.Δ.Ε. ΠΟΡΟΙ	-	32.000,00 €	70.000,00 €	123.600,00 €

Από την ανάγνωση των αποτελεσμάτων αυτών γίνεται φανερό ότι επιτεύχθηκε σημαντική αύξηση εσόδων σε τομείς με μεγάλη υστέρηση, αύξηση η οποία μεταφράζεται σε δημιουργία ή ενίσχυση άμεσων και έμμεσων θέσεων εργασίας, βελτίωση των υφιστάμενων υποδομών τόσο αισθητικά όσο και λειτουργικά και το κυριότερο σε οργάνωση της λιμενικής δραστηριότητας σε έναν κύκλο αυτοτροφοδοτούμενο και αυτάρκη καθώς ο Φορέας λειτουργεί αποκλειστικά με ίδια έσοδα.

Φυσικά ούτε τα ποσά που αναφέρθηκαν ούτε οι υποδομές που δημιουργήθηκαν είναι τέτοιας τάξεως μεγέθους που να δικαιολογούν ενθουσιασμό παρά μόνο εάν εκληφθούν ως ενδείξεις ή καλύτερα ως τροχιοδεικτικά στοιχεία μιας αναπτυξιακής πορείας η οποία και αποτελεί το κύριο αντικείμενο των επιδιώξεων του Φορέα μας από την ίδρυσή του. Σχετικές μελέτες και έρευνες που έχουν εκπονηθεί από διάφορους φορείς επί του γενικότερου αντικειμένου, σε σχέση δηλαδή με τη σημασία, το οικονομικό δυναμικό και τις προοπτικές ανάπτυξης των δραστηριοτήτων που σχετίζονται με τις λιμενικές υποδομές όπως η αλιεία, ο θαλάσσιος τουρισμός και ειδικότερα η κρουαζιέρα και το yachting, καταδεικνύουν σαφώς: α) Το πλούσιο οικονομικό δυναμικό που αυτές διαθέτουν, β) την αυξητική τάση που παρουσιάζουν σε ευρωπαϊκό και παγκόσμιο επίπεδο, γ) τα πολλαπλασιαστικά οφέλη που αποκομίζουν οι τοπικές κοινωνίες από την συνάφειά τους, δ) το έλλειμμα που παρουσιάζει η χώρα μας σε υποδομές φιλοξενίας τέτοιων δραστηριοτήτων και ε) τα συγκριτικά πλεονεκτήματα της Ελλάδας στο συγκεκριμένο πεδίο (Γκιζάκης κ.α. 2012) (Μυλωνάς 2012) (Μανώλογλου 2017).

Φαίνεται λοιπόν ότι η χώρα μας ενώ διαθέτει τα συγκριτικά πλεονεκτήματα που την καθιστούν προνομιούχο και εξαιρετικά ελκυστικό προορισμό, δεν απολαμβάνει παρά ένα μικρό μερίδιο από αυτό που δυνητικά της αναλογεί σε μια δυναμικά αναπτυσσόμενη αγορά εξ αιτίας της υστέρησης που εμφανίζει στον ανταγωνισμό. Αν όμως μπορούν τα ανταγωνιστικά πλεονεκτήματα να αντισταθμίσουν ή και να υπερκεράσουν τα συγκριτικά, τι θα μπορούσε να επιτευχθεί από το συνδυασμό αυτών των δύο;

Σε μια προσπάθεια να εξειδικεύσουμε την αναζήτησή μας στη δική μας μικρή τοπική κοινωνία θεωρούμε απαραίτητο να παρουσιάσουμε έστω συνοπτικά τα χαρακτηριστικά του τόπου μας και τα συγκριτικά πλεονεκτήματα που αυτός, κατά τη γνώμη μας, διαθέτει. Ο Δήμος Αριστοτέλη είναι ένας ηπειρωτικός δήμος που όμως διαθέτει περισσότερα από 240 χιλιόμετρα ακτογραμμής. Ταυτόχρονα συγκεντρώνει ελκυστικές ιδιαιτερότητες όπως το παγκόσμιας ακτινοβολίας Άγιο Όρος το οποίο είναι επισκέψιμο μόνο δια θαλάσσης και οι λιμένες που αποτελούν τις αποκλειστικές πύλες εισόδου-εξόδου προς και από αυτό, συμπεριλαμβάνονται στους χώρους αρμοδιότητας του Φορέα μας, ενώ η επιβατική κίνηση που συνδέεται με το Άγιο Όρος ξεπερνά τις 700.000 από-επιβιβάσεις ετησίως (Πρωτογενή δεδομένα). Τη γενέτειρα και ταυτόχρονα την τελευταία κατοικία του μεγαλύτερου φιλοσόφου όλων των εποχών Αριστοτέλη, η οποία βρίσκεται σε απόσταση αναπνοής από τον παραθαλάσσιο οικισμό της Ολυμπιάδας και μερικών δεκάδων μέτρων από το λιμάνι της. Τη μοναδικής ιστορικής σημασίας Διώρυγα του Ξέρξη που διαπερνά το γραφικό οικισμό των Νέων Ρόδων δίπλα ακριβώς από το σημερινό λιμανάκι. Την Αμμουλιανή, το μοναδικό κατοικημένο νησί της Κεντρικής Μακεδονίας και πόλο έλξης δεκάδων χιλιάδων Ελλήνων και ξένων επισκεπτών ετησίως. Την μακραίωνη παράδοση στη ναυπηγική τέχνη με τα διάσημα Καρνάγια της Ιερισσού όπου μέχρι και σήμερα κατασκευάζονται και συντηρούνται παραδοσιακά ξύλινα σκάφη αλλά και σύγχρονα. Την αλιεία με ένα αξιόλογο στόλο μέσης και παράκτιας αλιείας, αλλά και την όχι άδικη φήμη του σπάνιου ψαρότοπου. Τα γραφικά Πυργαδίκια στο μυχό του Σιγγιτικού κόλπου καθώς και σπάνιας ομορφιάς παραλίες σε συναρπαστική εγγύτητα με το πράσινο του ορεινού όγκου και πολλούς -επίσημα αναγνωρισμένους 38- εξαιρετικής σημασίας αρχαιολογικούς χώρους.

Στον αντίποδα ακριβώς των πλεονεκτημάτων αυτών βρίσκεται δυστυχώς η ανεπάρκεια υποδομών και ιδιαίτερα λιμενικών, που θα μπορούσαν να υποστηρίξουν τη φέρουσα ικανότητα της περιοχής συμβάλλοντας ουσιαστικά στην πορεία του τόπου προς μια υγιή, βιώσιμη και αειφόρο ανάπτυξη. Σε ένα δήμο με ολοφάνερα τουριστικό χαρακτήρα, που διαθέτει σύμφωνα με στοιχεία του Ξ.Ε.Ε. 67 ξενοδοχειακές μονάδες με 3.894 δωμάτια και 7.609 κλίνες εκ των οποίων 3 μονάδες 5αστέρων με 232 δωμάτια και 489 κλίνες, δεν υπάρχει ούτε ένας τουριστικός λιμένας, ιδιωτικός ή δημόσιος, η επιβατική κίνηση εξυπηρετείται από οριακού μεγέθους και ασφάλειας προβλήτες και μόνο ένα από τα 9 λιμάνια όλης της περιοχής προσφέρει ασφαλές καταφύγιο από όλους τους ανέμους!

Αυτά, τη στιγμή που σύμφωνα με διαθέσιμα στοιχεία, για κάθε 100 θέσεις ελλιμενισμού σε ένα λιμένα αναψυχής, αντιστοιχούν 4,36 άμεσες θέσεις εργασίας και 100 έμμεσες, ενώ κατά προσέγγιση αντιστοιχεί και μία θέση εργασίας ανά σκάφος (Γκιζάκης κ.α. 2012). Ταυτόχρονα, για κάθε 100 € που ξοδεύει ένας τουρίστας σε μαρίνα, αντιστοιχούν περίπου 450€ στην τοπική οικονομία (Μανωλόγλου 2017), ενώ το ποσό που εκτιμάται ότι δαπανά ημερησίως κάθε επιβάτης κρουαζιέρας για κάθε ενδιάμεσο λιμένα προσέγγισης φθάνει τα 80€ (Μυλωνάς 2012). Πολλαπλάσια βεβαίως είναι τα ποσά στους λιμένες αφετηρίας καθώς συνδέονται με περισσότερους κλάδους της τοπικής οικονομίας.

Η μεγάλη δε αντίφαση στην περίπτωσή μας είναι ότι η περιοχή στερείται τόσων δυνητικών προσόδων όταν οι ίδιες έρευνες δείχνουν ότι περιοχές με τα δικά της χαρακτηριστικά –μη κοσμικές- αποτελούν τους κυριότερους προορισμούς (75%) (Γκιζάκης κ.α. 2012) για τα σκάφη αναψυχής, ενώ στην περίπτωση της κρουαζιέρας στην Ελλάδα, εξαιρετικά σημαντικό πρόβλημα θεωρείται η απουσία νέων προορισμών. Αν όμως το Κατάκολο και η Αρχαία Ολυμπία δέχονται κατά μέσο όρο 500.000 επιβάτες κρουαζιέρας ετησίως (Μπέλλος 2019) γιατί το Άγιο Όρος και ο Αριστοτέλης μαζί, δεν θα μπορούσαν να διεκδικήσουν το δικό τους μερίδιο στην αγορά; Και τι θα σήμαινε αυτό για την τοπική οικονομία; Με μια υπόθεση προσέλκυσης μόλις του 1% των επιβατών κρουαζιέρας που επισκέπτονται την Ελλάδα με στοιχεία του 2018 έχουμε 4.788.642*1%*80=3.830.913,6€! Στον τομέα της ήδη υφιστάμενης στην περιοχή δραστηριότητας της ημερήσιας κρουαζιέρας, καθώς οι λιμένες μας καταγράφουν περίπου 110.000 επιβάτες ετησίως, μόνο όμως οι μισοί ξεκινούν από αυτούς, η ενίσχυση του home porting θα μπορούσε να διπλασιάσει τα έσοδα. Το ανύπαρκτο σήμερα yachting θα μπορούσε επίσης να συνεισφέρει εντυπωσιακά, δεδομένου ότι τα έσοδα των 22 μαρίνων στην Ελλάδα ανέρχονται στα 50.000.000€ ετησίως ενώ άλλα 300.000.000€ περίπου διαχέονται στους επαγγελματίες του χώρου. Αναλογικά μία μαρίνα στο μέσο όρο των υφιστάμενων θα απέφερε περί τα 2.000.000€ έσοδα και άλλα 13.000.000€ όφελος στην τοπική οικονομία. Κατά παρόμοιο τρόπο, η ανάπτυξη παραδοσιακών και νέων μορφών τουρισμού, θαλάσσιου και μη, όπως ο αλιευτικός, ο καταδυτικός, ο γαστρονομικός, ο θρησκευτικός, ο αρχαιολογικός κλπ. καθώς και η βελτίωση της προσβασιμότητας (υδατοδρόμια, λιμάνια), με τη δημιουργία των κατάλληλων λιμενικών υποδομών υποδοχής και φιλοξενίας, υπόσχεται ένα άθροισμα πολλών εκατομμυρίων για την τοπική κοινωνία.

Τείνουμε λοιπόν να καταλήξουμε στο συμπέρασμα ότι είναι εφικτό, ένας υγιής Δημόσιος Φορέας, όπως το Δημοτικό Λιμενικό Ταμείο Αριστοτέλη, ειδικά στην παρούσα χρονική συγκυρία, σε τοπικό επίπεδο, να λειτουργήσει ως ο κεντρικός παράγοντας για τη δημιουργία και την ανάπτυξη ενός top-down cluster (Μπαρμπαδήμου 2017), που με επίκεντρο τη δημιουργία νέων και τον εκσυγχρονισμό των υφιστάμενων λιμενικών υποδομών θα προσελκύσει γύρω του συστάδες επιχειρήσεων, δίνοντας το έναυσμα για μια εντυπωσιακή και αλματώδη ανάπτυξη.

Υπό το πρίσμα αυτής της αντίληψης, ο φορέας μας ήδη εκπονεί σειρά μελετών και γενικότερα κινείται στην κατεύθυνση της προετοιμασίας και ωρίμανσης λιμενικών έργων, επιδιώκοντας να προσελκύσει χρηματοδοτικά εργαλεία για την υλοποίησή τους ενώ ταυτόχρονα παρεμβαίνει στο μέτρο των δυνατοτήτων του βελτιώνοντας και καθιστώντας ελκυστικότερους τους χώρους δικαιοδοσίας του. Με βάση τις σχεδιαζόμενες δράσεις και με την επιφύλαξη της υλοποίησής τους, θεωρούμε ρεαλιστικό στόχο ένα μέσο ρυθμό ανάπτυξης της τάξης του 25% με τα εξής αποτελέσματα σε βάθος πενταετίας και δεκαετίας αντίστοιχα:

Πίνακας 6 Πίνακας στοχοθεσίας πενταετίας/δεκαετίας (Πρωτογενή δεδομένα)

2024			**2029**		
ΙΔΙΑ ΕΣΟΔΑ ΔΛΤΑ	**ΟΦΕΛΟΣ ΤΟΠΙΚΗΣ ΚΟΙΝΩΝΙΑΣ**	**ΔΙΑΧΥΣΗ ΣΤΗΝ ΤΟΠΙΚΗ ΟΙΚΟΝΟΜΙΑ**	**ΙΔΙΑ ΕΣΟΔΑ ΔΛΤΑ**	**ΟΦΕΛΟΣ ΤΟΠΙΚΗΣ ΚΟΙΝΩΝΙΑΣ**	**ΔΙΑΧΥΣΗ ΣΤΗΝ ΤΟΠΙΚΗ ΟΙΚΟΝΟΜΙΑ**
890.000 €	1.800.000 €	9.000.000 €	2.600.000 €	5.200.000 €	25.000.000

Προφανώς υπάρχουν και κάποια μεγάλα εμπόδια στην υλοποίηση ενός τέτοιου σχεδιασμού, τα κυριότερα εκ των οποίων εντοπίζονται στο μεγάλο κόστος που συνεπάγονται τα περισσότερα λιμενικά έργα και στις θεσμικές δυσκολίες που συναντούν τόσο οι δημόσιοι φορείς όσο και οι επίδοξοι επενδυτές. Ίσως όμως το σημαντικότερο πρόβλημα έως σήμερα να αποτελεί η ίδια η έλλειψη στρατηγικού σχεδιασμού σε τοπικό αλλά και σε περιφερειακό επίπεδο (Μ.Ο.Δ. 2006). Αυτό ακριβώς το έλλειμμα φιλοδοξεί να καλύψει ο Φορέας μας, στοχεύοντας σε δράσεις εναρμονισμένες στις πρόσφατες Οδηγίες της Ευρωπαϊκής Ένωσης (ΟΔΗΓΙΑ 214/89/ΕΕ) και τα Προγράμματα που συγχρηματοδοτεί με το Ελληνικό Κράτος, ενώ ταυτόχρονα οι θεσμικές αλλαγές που προωθούνται βαθμιαία στην χώρα, γεννούν καλές ελπίδες για την επιτυχία του στόχου μας.
Έχουμε λοιπόν ένα φιλόδοξο σχέδιο που μοιάζει και θα μπορούσε να λέγεται νέο “new deal”!

Βιβλιογραφικές Αναφορές

Μονάδα Οργάνωσης της Διαχείρισης Αναπτυξιακών Προγραμμάτων (Μ.Ο.Δ.) (2006) Απογραφή και αξιολόγηση της ασκηθείσας περιφερειακής πολιτικής στην Ελλάδα μετά την ένταξή της στην Ε.Ε. με έμφαση στα προγράμματα Δημοσίων Επενδύσεων και στα προγράμματα Περιφερειακής Ανάπτυξης.

Γκιζάκης Κ, Χριστοδούλοου Α, Παπαδοπούλου Γ, Καρρά Α, Μπαρδής Κ. (2012) Έρευνα για την ανάδειξη της σημασίας των σκαφών αναψυχής στον θαλάσσιο τουρισμό και την εθνική οικονομία, Κέντρο Ερευνών του Πανεπιστημίου Πειραιώς, Ερευνητικό Εργαστήριο Ναυτιλιακής Οικονομίας, Διοίκησης και Ναυτιλιακών Ατυχημάτων.

Μυλωνάς Π. (2012) Κλαδικές Μελέτες, Εθνική Τράπεζα της Ελλάδος.

Μανώλογλου Σ (2017) Ο τομέας της ιδιωτικής θαλάσσιας περιήγησης (yachting) στην Ελλάδα – Τάσεις και προοπτικές ανάπτυξης, Ευρωπαϊκό Κέντρο Αριστείας JEAN MONMENT-Εθνικό Καποδιστριακό Πανεπιστήμιο Αθηνών, Αθήνα.

Μπαρμπαδήμου Λ (2017) Πολιτικές ενίσχυσης του ναυτιλιακού πλέγματος-cluster. Η Ευρωπαϊκή εμπειρία και η ελληνική πρακτική. Διπλωματική εργασία που υποβλήθηκε στο Τμήμα Ναυτιλιακών Σπουδών του Πανεπιστημίου Πειραιώς ως μέρος των απαιτήσεων για την απόκτηση του Μεταπτυχιακού Διπλώματος Ειδίκευσης στην Ναυτιλία. Πανεπιστήμιο Πειραιώς, Πειραιάς.

Μπέλλος Η (2019) Μειωμένες οι εισπράξεις για την ελληνική κρουαζιέρα το 2018. Η Καθημερινή.

http://www.kathimerini.gr/1003544/article/oikonomia/epixeirhseis/meiwmenes-oi-eispra3eis-gia-thn-ellhnikh-kroyaziera-to-2018. Accessed 09 Jan 2019

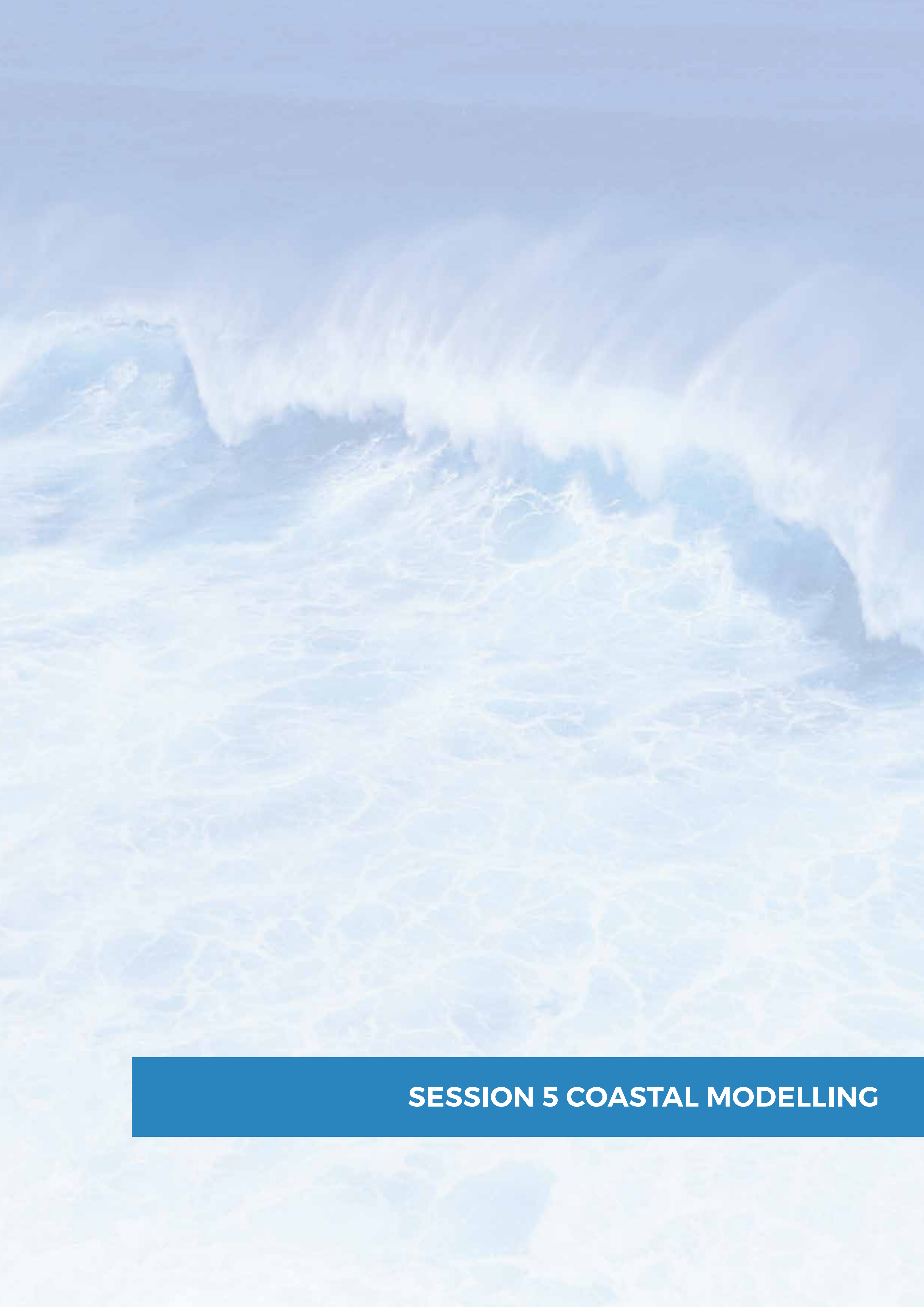

SESSION 5 COASTAL MODELLING

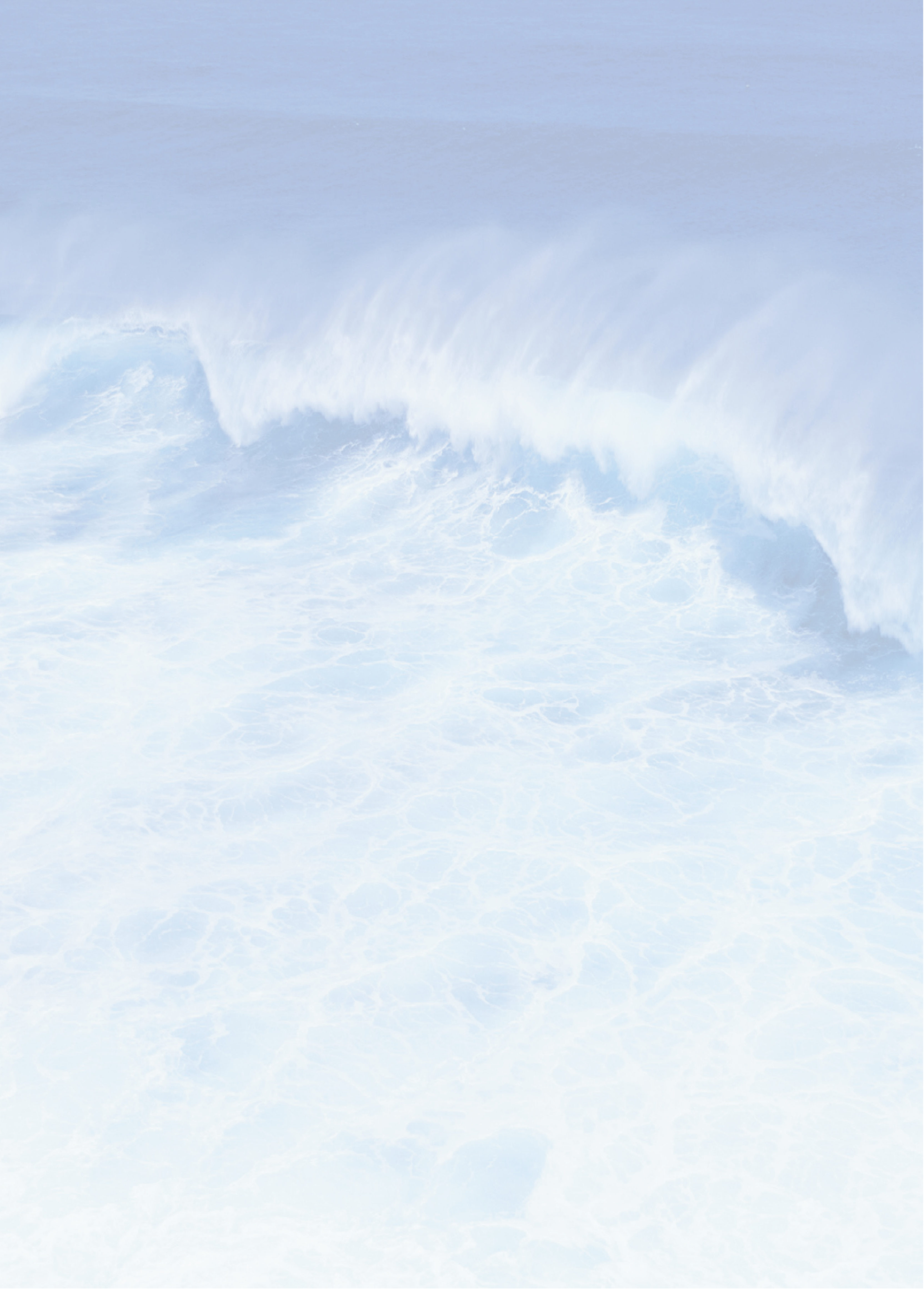

Advanced numerical model for the design of coastal protection structures

A.-Ch. Tsiaras, Th. Karambas*,

Laboratory of Maritime Engineering, Division of Hydraulics and Environmental Engineering, School of Civil Engineering, Aristotle University of Thessaloniki, 54124, Thessaloniki, Greece
*Corresponding author: karambas@civil.auth.gr

Abstract

An advanced nonlinear wave, sediment transport and bed morphology evolution 2DH model, for the design of coastal protection structures, has been developed. The extended Boussinesq equations, including higher order non-linear terms, which can describe the propagation of highly nonlinear waves in the shoaling region, surf and swash zone, are used. The bed and suspended load transport are estimated with a quasi-steady semi-empirical formulation for an oscillatory flow combined with a superimposed current under an arbitrary angle, involving phase-lag effects in the sheet flow layer. Model results are compared with experimental data showing good agreement between numerical simulations and measurements. The methodology can be applied to the design of coastal protection structures.

Keywords Coastal Protection Structures, Numerical Models, Boussinesq

1 1 WAVE AND CURRENT MODULE

The Boussinesq equations have been shown to be capable of reproducing successfully the wave phenomena that affect the morphology of the coastal area. The classical Boussinesq equations have been extended so as to be able to include higher order non-linear terms, which can describe better the propagation of highly nonlinear waves in the shoaling zone. Apart from that, the linear dispersion characteristics of the equations have been improved in order to describe the nonlinear wave propagation from deeper waters (Zou, 1999). Wave energy dissipation due to wave breaking is based on a significant characteristic of a breaker: the presence of the surface roller. Dissipation due to the wave breaking is introduced as an excess momentum term due to the non-uniform velocity distribution (Schäffer et al., 1993), based on a simplified velocity profile where the surface roller is being transported with the wave celerity. In the swash zone, the 'dry bed' boundary condition is used to simulate runup according to (Militello et al., 2004). The bottom shear stresses term are approximated by the use of the formulae proposed by Kobayashi et al. (2007):

$$\tau_{bx} = \frac{1}{2}\rho f_b \sigma_T^2 G_{bx} \qquad \tau_{by} = \frac{1}{2}\rho f_b \sigma_T^2 G_{by} \tag{1}$$

with σ_T is the standard deviation of the oscillatory horizontal velocity, f_b is the bottom friction factor, and

$$G_{bx} = \frac{U_c}{\sigma_T}\left[1.16^2 + \left(\frac{U_c}{\sigma_T}\right)^2\right]^{0.5} \qquad G_{by} = \frac{V_c}{\sigma_T}\left[1.16^2 + \left(\frac{V_c}{\sigma_T}\right)^2\right]^{0.5}$$

where U_c and V_c are the depth averaged current velocities, estimated after time-averaging the instantaneous velocities (according to Karambas and Karathanassi, 2004).

The governing equations are finite-differenced utilizing a high-order predictor-corrector scheme that employs a third-order explicit Adams-Bashforth predictor step and a fourth-order implicit Adams-Moulton corrector step (Wei and Kirby, 1995). The corrector step is iterated until the desirable convergence is achieved. First order spatial derivatives are discretized to fourth-order accuracy. Figure 1 shows a snapshot of the computed free surface elevation for the case of waves propagating near a detached breakwater.

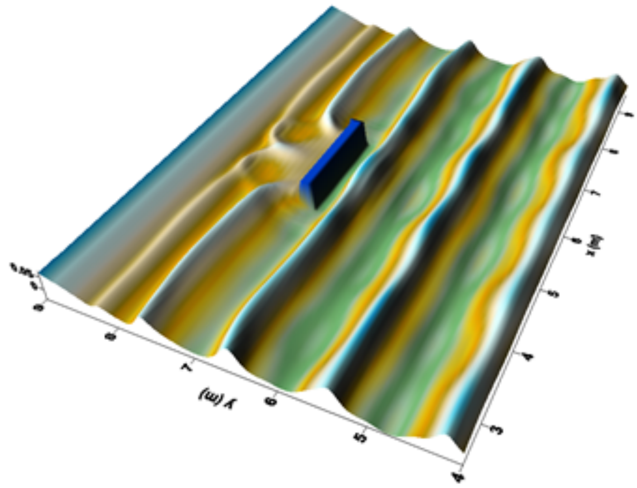

Figure 1 Wave propagation near a detached emerged breakwtater: snapshot of the computed free surface elevation

2 SEDIMENT TRANSPORT MODULE

A transport rate formula involving unsteady aspects of the sand transport phenomenon presented by Dibajnia and Watanabe (1998) is adopted. The formula estimates the sheet flow sand transport rates and has been generalised by them for the bed load as well as for the suspended load over ripples (Dibajnia and Watanabe, 1998). In Dibajnia et al (2001) the formula has been modified to estimate sand transport rate under irregular sheet flow conditions.

In a 2DH wave-current coexisting field the total velocity field can be represented by the vector $\mathbf{u_c}$ which lasts for an interval of T_c, followed by the vector $\mathbf{u_t}$ which lasts for an interval of T_t. The sediment transport vector $\mathbf{q_b}$ is now estimated by (Dibajnia et al., 2001):

$$\frac{\mathbf{q_b}}{w_s\, d_{50}} = \alpha_{DW} \frac{\mathbf{u_c} T_c \left(\Omega_c + \Omega'_t\right) + \mathbf{u_t} T_t \left(\Omega_t + \Omega'_c\right)}{\left(T_c + T_t\right)\sqrt{(s-1)gd_{50}}} \tag{2}$$

where w_s is the sediment fall velocity, α_{DW} is a proportionality coefficient, s is the relative density of the sediment and d_{50} the median grain size and $\mathbf{u_c}=(u_c, v_c)$and $\mathbf{u_t}=(u_t, v_t)$ are the equivalent root-mean-square velocity amplitudes for the positive (crest) and negative (through) portions of the velocity profile, defined as:

$$u_c^2 = \frac{2}{T_c}\int_{t_0}^{t_0+T_c} u_{ou}^2\, dt\ , \qquad u_t^2 = \frac{2}{T_t}\int_{t_0+T_c}^{t_0+T} u_{ou}^2\, dt$$

$$v_c^2 = \frac{2}{T_c}\int_{t_0}^{t_0+T_c} v_{ou}^2\, dt\ , \qquad v_t^2 = \frac{2}{T_t}\int_{t_0+T_c}^{t_0+T} v_{ou}^2\, dt \tag{3}$$

where $T=T_c+T_t$, u_{ou} and v_{ou} are the bottom velocities $u_{ou}=u_{ow}+U_c$, $v_{ou}=v_{ow}+ V_c$ (u_{ow} and v_{ow} are the oscillatory component of the near-bottom velocities).

Values of the Ω_j are given in Dibajnia et al. (2001).

The above formulations ignores an obvious effect, i.e. the additional stirring of sediment by the surface breaking-induced turbulence which penetrates toward the bottom. This additional stirring is simulated adopting the Bailard formula after the consideration that the dissipation mechanism is the wave breaking. As in Karambas and Koutitas (2002) we can assume a time-averaged approach for the estimation of the suspended load induced by wave breaking. Thus the total submerged weight transport rate can be estimated from (1989, Karambas and Koutitas, 2002):

$$\mathbf{q_s} = \frac{1}{a}\frac{b\varepsilon_s \overline{D}\mathbf{U_c}}{w_s} \tag{4}$$

where $\overline{D}$ is the dissipation of wave energy due to breaking $\mathbf{U_c}=(U_c, V_c)$, $\varepsilon_s=0.01$, $a=(1-n)(s-1)\rho g$, n = the porosity of the sediment, ρ the density of the water and $b=0.2$.
Swash zone sediment transport is modelled as in Karambas (2006).

The nearshore morphological changes are calculated by solving the conservation of sediment transport equation:

$$\frac{\partial z_b}{\partial t} = -\frac{\partial}{\partial x}\left(q_x - 5|q_x|\frac{\partial z_b}{\partial x}\right) - \frac{\partial}{\partial y}\left(q_y - 5|q_y|\frac{\partial z_b}{\partial y}\right) \tag{5}$$

where z_b is the local bottom elevation and q_x, q_y are the total volumetric longshore and cross-shore sediment transport rates (sum of bed and suspended load, derived from eqs 2 and 4).

The following methodology has been adopted for the estimation of the morphology evolution: first, the initial bathymetry was inserted into the model so as to estimate the wave and current field, which are used by the sediment transport model for the calculations of the sediment transport rates. Then, the bathymetry was updated according to the sediment movement, by solving the conservation of sediment transport equation. This procedure was repeated until the state of equilibrium was reached or after a specific period.

3 COMPARISON WITH MEASUREMETS - CONCLUSIONS

Model results are compared with experimental data concerning morphology evolution behind detached breakwaters (Ming and Chiew 2000) and coastal accretion and erosion due to the presence of a groin (Badiei et al., 1995).

Baidei et al. (1995) employed a series of mobile bed process models (in order to investigate the impact of groins on nearshore morphology under the attack of obliquely incident random waves. Two series of tests were carried out at the Queen’s University Coastal Engineering Laboratory (QUCERL) and the Hydraulic Laboratory of the National Research Council of Canada (NRCC). The physical model regarded an initially plane sloping beach (1:10 slope), composed of D_{50} = 0.12 mm sand grains. In this work, the case of a single groin was modeled (Test NT2), exposed to waves of H_{s0} = 0.08 m deep water significant wave height, T_p = 1.15 s peak period and θ_0 = 11.6° deep water incident wave angle, for a total duration of 12 h after groin installation. In Figure 2 the comparison between experimental data and numerical results is shown. Model predictions and measurements are in good agreement.

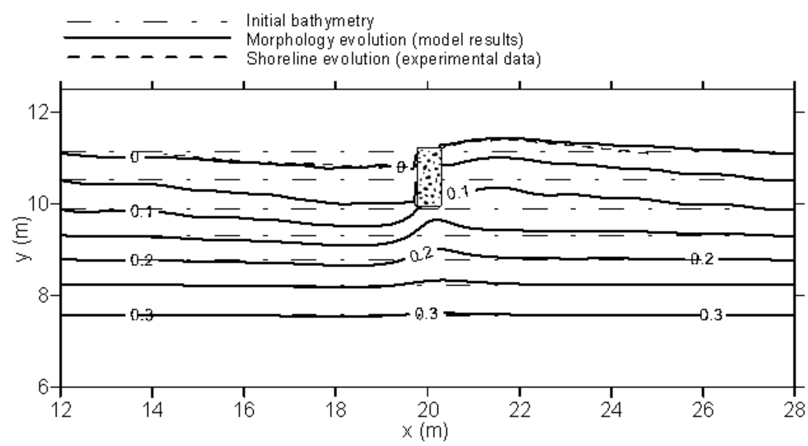

Figure 2 Comparison between the computed and measured shoreline and bathymetry evolution (contours represent the final bathymetry) for Test NT2 of Baidei et al. (1995) .

The present model is also verified against the laboratory experiments, by Ming and Chiew (2000) which depict the bathymetry changes behind a detached breakwater. The experiments were conducted in a wave basin that was 10 m long, 5 m wide, and 0.7 m high. A plunger-type wavemaker was used to generate monochromatic waves. Sponge was placed behind the wavemaker to minimize wave reflection. The 6 m long beach consisted of uniformly distributed sand with a median grain size of d_{50} = 0.25 mm. The test duration was approximately 15 h, which also was the duration needed for the beach to reach equilibrium. The period of the incident wave was T=0.85 s and the height H_o=0.05 m.

In Fig 3, model results are compared with experimental data of Test 10 (breakwater length=0.90 m, distance from the shoreline 0.90 m). Model results and laboratory data agree quite well.

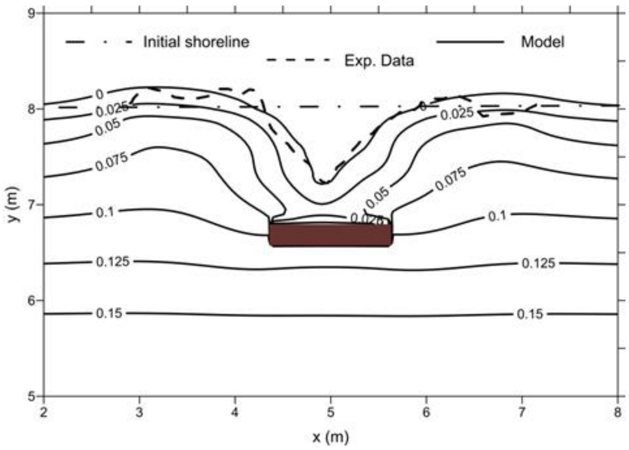

Figure 3 Morphology evolution behind a detached breakwater. Comparison of model results and experimental data by Ming and Chiew (2000) Test 10.

Similarly the model has been applied for other tests (resulting to salient or tombolo formation) showing good agreement with measurements. In addition model predictions agree with the tombolo/salient criteria for emerged detached breakwaters found in the literature.

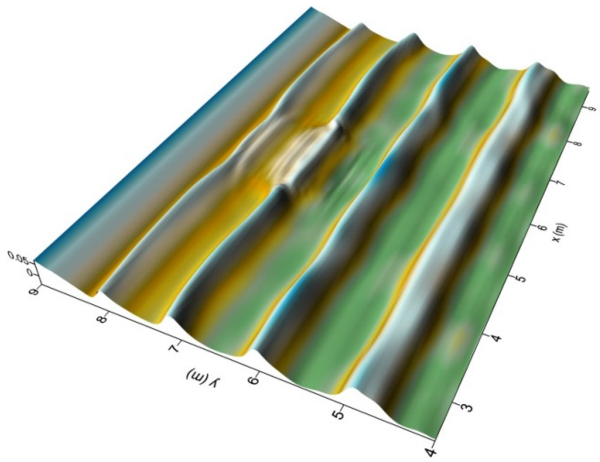

Figure 4 Wave propagation near a detached submerged breakwtater: snapshot of the computed free surface elevation

The methodology is also applied to simulate the morphological changes behind submerged breakwaters. The same wave and morphology conditions (as in Ming and Chiew case), with only difference the use of submerged breakwaters instead of emerged ones (Figure 4). In this way some interesting conclusions, for the conceptual design of submerged breakwaters, can be derived. In Fig 5 the initial breaking wave induced current filed and the morphology evolution behind a submerged breakwater are shown. This net transport of water into the lee zone causes a water level rise and is balanced mainly by outgoing currents at the heads of the structures. Consequently the main flow pattern is characterized by an onshore flow over the submerged breakwater, an offshore flow at the gaps (eroding rip currents) and two nearshore eddies similar to those formed in the case of emerged breakwaters. The first two flow patterns do not exist in the latter case, while the third flow pattern is not extended up to the structure.

The applications also resulted to useful conclusions concerning the role of the transmission coefficient and the net mass influx over the breakwater.

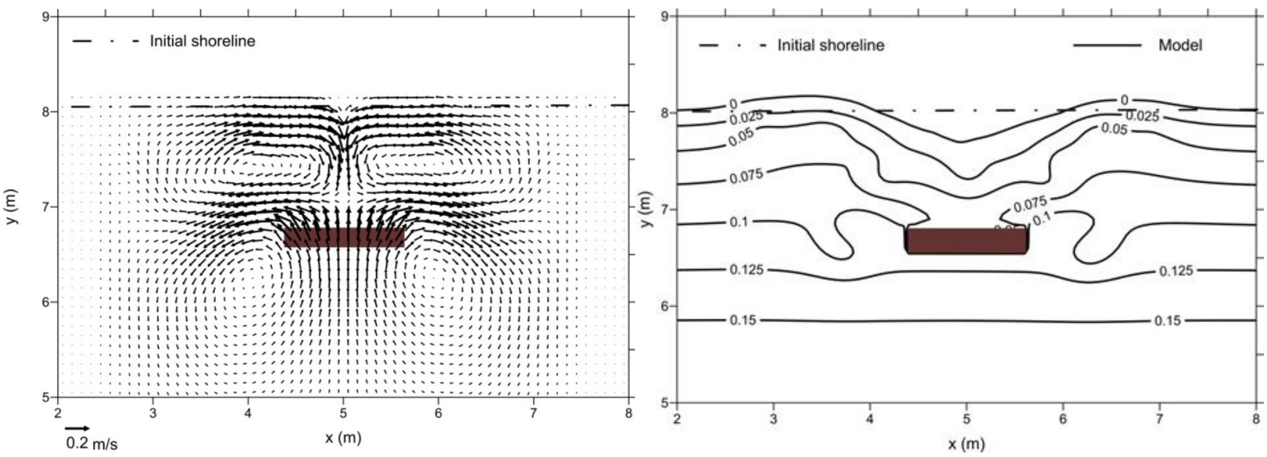

Figure 5 Initial breaking wave induced current filed and morphology evolution behind a submerged breakwater (breakwater length=0.90 m, distance from the shoreline 0.90 m, transmission coefficient K_t=0.40).

The verification of the model indicates that the proposed methodology can be applied to the design of coastal protection structures.

References

Badiei, P.; Kamphuis, J. Hamilton, D. Physical experiments on the effects of groins on shore morphology 1995 Proceedings of the 24th International Conference on Coastal Engineering, Kobe, Japan, October 23-28: pp 1782-1796.

Dibajnia M. and Watanabe A. (1998) Transport rate under irregular sheet flow conditions. Coastal Engineering, vol. 35, pp. 167-183.

Dibajnia M., Moriya T. and Watanabe A. (2001) A representative wave model for estimation of nearshore local transport rate. Coastal Engineering Journal, vol. 43, no 1, pp. 1-38.

Karambas Th. V. and Koutitas C. (2002) Surf and swash zone morphology evolution induced by nonlinear waves. Journal of Waterway, Port, Coastal, and Ocean Engineering, vol 128, no 3, pp 102-113.

Karambas Th. V. and E.K. Karathanassi (2004) Boussinesq modeling of Longshore currents and sediment transport, Journal of Waterway, Port, Coastal and Ocean Engineering, American Society of Civil Engineers (ASCE), Vol. 130, no 6, pp. 277-286.

Karambas Th. V. (2006) Prediction of sediment transport in the swash zone by using a nonlinear wave model, Continental Shelf Research, 26, pp. 599-609.

Kobayashi, N., Agarwal, A., and Johnson, B. (2007) Longshore Current and Sediment Transport on Beaches. J. Waterw., Port, Coastal, Ocean Eng., 133(4), 296–304

Militello A., C. W. Reed, A.K. Zundel, N. C. Kraus (2004) Two-Dimensional Depth-Averaged circulation model M2D: version 2.0, Report 1, US Army Corps of Engineers, ERDC/CHL TR-04-2.

Ming D. and Y-M. Chiew (2000) Shoreline changes behind detached breakwater, Journal of Waterway, Port, Coastal, and Ocean Engineering, Vol. 126, No. 2, 63-70.

Schäffer H. A., Madsen P.A. and Deigaard R. (1993) A Boussinesq model for waves breaking in shallow water, Coastal Engineering, 20, pp. 185-202.

Wei G. and Kirby T. (1995) Time-dependent numerical code for extended Boussinesq equations. Journal of Waterway, Port, Coastal, and Ocean Engineering, vol. 121, no 5, pp. 251-261
Zou Z.L. (1999) Higher order Boussinesq equations, Ocean Engineering, 26, pp. 767-792.

Αριθμητική προσομοίωση παράκτιας στερεομεταφοράς με ομοίωμα τύπου Boussinesq

Γ. Κλωνάρης[1*], Κ. Μέμος[2]

[1]Department of Geography, Ghent University, 9000 Ghent, Belgium
[2]Σχολή Πολιτικών Μηχανικών, Ε.Μ.Π., Ζωγράφος, 157 80, Ελλάδα
[*]Υπεύθυνος επικοινωνίας: Georgios.Klonaris@UGent.be

Περίληψη

Στην παρούσα εργασία παρουσιάζεται ένα σύνθετο αριθμητικό μοντέλο για την προσομοίωση της παράκτιας στερεομεταφοράς και εξέλιξης της μορφολογίας του πυθμένα λόγω κυματισμών και ρευμάτων. Το σύνθετο αυτό εργαλείο εφαρμόζεται σε μία και δύο οριζόντιες διαστάσεις και βασίζεται σε ένα κυματικό μοντέλο τύπου Boussinesq υψηλής μη γραμμικότητας και βελτιωμένης διασποράς. Το μοντέλο έχει επεκταθεί στις ζώνες θραύσης και διαβροχής, με αποτέλεσμα το πεδίο εφαρμογής του να καλύπτει ολόκληρη την παράκτια ζώνη. Ο υπολογισμός του φορτίου πυθμένα βασίζεται σε σύγχρονες ημι-εμπειρικές σχέσεις, ενώ το φορτίο σε αιώρηση προκύπτει από την επίλυση μιας εξίσωσης μετάθεσης-διάχυσης. Η εκτίμηση της στερεομεταφοράς στη ζώνη διαβροχής βασίζεται σε μια προσέγγιση με αναλογία προς τη βαλλιστική θεωρία. Το ενοποιημένο μοντέλο στερεομεταφοράς εφαρμόζεται για το συνδυασμό κυμάτων και ρευμάτων και λαμβάνει υπόψη την κυματική ασυμμετρία και φαινόμενα υστέρησης του ιζήματος. Η εξέλιξη της βυθομετρίας προσομοιώνεται με την επίλυση της εξίσωσης ισοζυγίου των φερτών σε χρονικές κλίμακες των μορφολογικών διεργασιών. Το μοντέλο επαληθεύτηκε με πειραματικές μετρήσεις και έδειξε, σε γενικές γραμμές, ικανοποιητική απόκριση.

Λέξεις κλειδιά Μοντέλο Boussinesq, Στερεομεταφορά, Παράκτια μορφολογία, Διάβρωση ακτών.

1 ΕΙΣΑΓΩΓΗ

Η κατανόηση των σύνθετων μορφοδυναμικών διεργασιών είναι ύψιστης σημασίας για την επίλυση των προβλημάτων της παράκτιας μηχανικής. Η μεγάλη πλειοψηφία των μοντέλων στερεομεταφοράς και μορφολογίας που έχουν παρουσιαστεί λαμβάνουν ως δεδομένα εισόδου τα αποτελέσματα ολοκληρωμένων στην περίοδο κυματικών μοντέλων (phase-averaged models). Στην υπολογιστική αυτή πορεία, φαινόμενα όπως η κυματική ασυμμετρία και οι μη γραμμικές κυματικές αλληλεπιδράσεις λαμβάνονται υπόψη μόνο προσεγγιστικά. Επιπλέον, τα επιμέρους υπο-μοντέλα εφαρμόζονται από το χρήστη ξεχωριστά το ένα από το άλλο. Η διαδικασία αυτή είναι επίπονη και χρονοβόρα, με αποτέλεσμα πολλές φορές στην πράξη να υπολογίζονται μόνο οι αρχικοί ρυθμοί διάβρωσης και απόθεσης. Στην παρούσα εργασία παρουσιάζεται ένα σύνθετο εργαλείο για τη μελέτη της παράκτιας μορφολογίας που έχει ως βάση ένα κυματικό μοντέλο τύπου Boussinesq. Ο συνδυασμός ενός τέτοιου κυματικού μοντέλου με ένα μοντέλο στερεομεταφοράς αποτελεί αντικείμενο σύγχρονης έρευνας, καθώς επιτρέπει τη βαθύτερη εξέταση των βραχυχρόνιων ακτομηχανικών διεργασιών.

2 ΠΕΡΙΓΡΑΦΗ ΤΟΥ ΣΥΝΘΕΤΟΥ ΑΡΙΘΜΗΤΙΚΟΥ ΜΟΝΤΕΛΟΥ

Στην παρούσα ερευνητική εργασία αναπτύχθηκε ένα σύνθετο αριθμητικό μοντέλο που συνδυάζει τέσσερα υπο-μοντέλα σε μία ενιαία μορφή. Το σύνθετο αυτό εργαλείο περιλαμβάνει: κυματικό μοντέλο, υδροδυναμικό μοντέλο για την προσομοίωση των κυματογενών ρευμάτων, μοντέλο παράκτιας στερεομεταφοράς και μοντέλο μορφοδυναμικής. Τα υπο-μοντέλα εφαρμόζονται διαδοχικά, το ένα μετά το άλλο, σε μία αυτοματοποιημένη και ενοποιημένη διαδικασία. Η εφαρμογή της αποτελεσματικής μεθόδου που βασίζεται στον ‘morphological acceleration factor’ (Morfac), f_{MOR}, επιτρέπει την προσομοίωση μορφολογικών μεταβολών σε μεγαλύτερες παράκτιες περιοχές και χρονικές κλίμακες (Lesser κ.ά., 2004).

2.1 Κυματικό και υδροδυναμικό μοντέλο
Το κυματικό μοντέλο είναι τύπου Boussinesq με βελτιωμένα χαρακτηριστικά διασποράς και υψηλής μη γραμμικότητας. Περιλαμβάνει ένα σύστημα εξισώσεων σε μία (1DH) ή δύο (2DH) οριζόντιες διαστάσεις, εκφρασμένων ως προς την ανύψωση της ελεύθερης επιφάνειας ζ και τη μέση κατά βάθος οριζόντια ταχύτητα, $\boldsymbol{U} = (U, V)$. Το παρόν μοντέλο μπορεί να προσομοιώσει την κυματική διάδοση σε ολόκληρο το εύρος των βαθών, από τα βαθειά έως τα ρηχά. Επιπλέον, επεκτάθηκε ώστε να εφαρμόζεται στις ζώνες θραύσης και διαβροχής. Συγκεκριμένα, η διδιάστατη έκδοση του μοντέλου περιλαμβάνει την εξίσωση συνέχειας (Εξ. 1) και ορμής (Εξ. 2):

$$\beta\zeta_t + \nabla \cdot (\Lambda \boldsymbol{U}) = 0 \tag{1}$$

$$\boldsymbol{U}_t + (\boldsymbol{U} \cdot \nabla)\boldsymbol{U} + \mathrm{g}\nabla\zeta = \boldsymbol{\psi_I} + \boldsymbol{\psi_{II}} + \boldsymbol{\psi_{III}} + \boldsymbol{F_{br}} - \frac{\boldsymbol{\tau_b}}{d+\zeta} + \boldsymbol{F_{eddy}} + \boldsymbol{F_{sp}} \tag{2}$$

όπου ο δείκτης t υποδηλώνει παραγώγιση ως προς το χρόνο, g είναι η επιτάχυνση της βαρύτητας, d το βάθος ηρεμίας, $\boldsymbol{\psi_I}$, $\boldsymbol{\psi_{II}}$, $\boldsymbol{\psi_{III}}$ είναι όροι διασποράς και μη-γραμμικότητας ανώτερης τάξης, $\boldsymbol{F_{br}}$ ο όρος θραύσης σύμφωνα με το μοντέλο τυρβώδους συνεκτικότητας, $\boldsymbol{\tau_b}$ η τριβή πυθμένα, $\boldsymbol{F_{eddy}}$ ο όρος τυρβώδους ανάμιξης και $\boldsymbol{F_{sp}}$ ο όρος απόσβεσης για τα απορροφητικά όρια του πεδίου. Τέλος, οι μεταβλητές β και Λ προκύπτουν από την εφαρμογή της μεθόδου των «σχισμών» για την προσομοίωση της αναρρίχησης και καταρρίχησης των κυματισμών. Περισσότερες λεπτομέρειες περιγράφονται στην εργασία των Klonaris κ.ά. (2016).

Το αριθμητικό σχήμα επίλυσης είναι ένα γενικευμένο σχήμα πρόβλεψης-διόρθωσης πολλαπλών βημάτων. Το στάδιο πρόβλεψης είναι 3ης τάξης, ενώ η διόρθωση 4ης τάξης. Η γένεση των κυματισμών επιτυγχάνεται με την εφαρμογή της μεθόδου της συνάρτησης πηγής.

Λόγω του μη-γραμμικού χαρακτήρα του, το μοντέλο μπορεί να εκτιμήσει το πεδίο των κυματογενών ρευμάτων απευθείας, χωρίς την ανάγκη για ρητό υπολογισμό των τάσεων ακτινοβολίας. Επίσης, συνδυάζοντας τα μοντέλα θραύσης της τυρβώδους συνεκτικότητας και του επιφανειακού κυλίνδρου (surface roller), λαμβάνεται υπόψη προσεγγιστικά ο μηχανισμός του undertow. Συγκεκριμένα, υπολογίζεται η μέση κατά βάθος τιμή του και η τιμή του κοντά στον πυθμένα (βλ. Putrevu και Svendsen, 1993).

2.2 Μοντέλο στερεομεταφοράς και μορφολογίας πυθμένα
Για τον υπολογισμό του φορτίου πυθμένα, $\boldsymbol{q_{sb}}$, στη ζώνη θραύσης και στα ανοιχτά εφαρμόζονται οι ημι-εμπειρικές σχέσεις των Camenen και Larson (2007) που ισχύουν για συνδυασμό κυμάτων και ρεύματος. Συγκεκριμένα:

$$\frac{q_{sb,w}}{\sqrt{(s-1)\mathrm{g}d_{50}{}^3}} = \alpha_\mathrm{w} \frac{\theta_{cw,net}}{\sqrt{|\theta_{cw,net}|}} \theta_{cw,m} \exp\left(-\mathrm{b}\frac{\theta_{cr}}{\theta_{cw}}\right) \tag{3}$$

$$\frac{q_{sb,n}}{\sqrt{(s-1)\mathrm{g}d_{50}{}^3}} = \alpha_\mathrm{n} \frac{\theta_{cn}}{\sqrt{|\theta_{cn}|}} \theta_{cw,m} \exp\left(-\mathrm{b}\frac{\theta_{cr}}{\theta_{cw}}\right) \tag{4}$$

όπου οι δείκτες w και n αναφέρονται, αντίστοιχα, στη διεύθυνση του κύματος και στην κάθετη σε αυτή διεύθυνση, d_{50} είναι η μέση διάμετρος των κόκκων του υλικού του πυθμένα, α_w, α_n και b είναι εμπειρικοί συντελεστές, s είναι ο λόγος της πυκνότητας του ιζήματος προς την πυκνότητα του νερού, $\theta_{cw,m}$, θ_{cw}, θ_{cr} είναι η μέση χρονικά απόλυτη τιμή, η μέγιστη και η κρίσιμη τιμή της παραμέτρου Shields, αντίστοιχα. Η παράμετρος Shields στην κάθετη στον κυματισμό διεύθυνση, θ_{cn}, οφείλεται μόνο στο ρεύμα. Οι χρησιμοποιούμενες εξισώσεις είναι από τις λίγες διαθέσιμες στη βιβλιογραφία που λαμβάνουν υπόψη τα μη μόνιμα φαινόμενα υστέρησης κατά την κίνηση του ιζήματος. Αυτό επιτυγχάνεται μέσω της «καθαρής» παραμέτρου Shields, $\theta_{cw,net}$.

Το φορτίο σε αιώρηση υπολογίζεται από την επίλυση της ολοκληρωμένης στο βάθος εξίσωσης μετάθεσης-διάχυσης για τη μέση κατά βάθος συγκέντρωση φερτών στη στήλη νερού, C_{ave}:

$$\frac{\partial(C_{ave}h)}{\partial t}+\frac{\partial(C_{ave}hU)}{\partial x}+\frac{\partial(C_{ave}hV)}{\partial y}=\frac{\partial}{\partial x}\left(K_x h\frac{\partial C_{ave}}{\partial x}\right)+\frac{\partial}{\partial y}\left(K_y h\frac{\partial C_{ave}}{\partial y}\right)+P_r-D_r \tag{5}$$

όπου $h=d+\zeta$ είναι το στιγμιαίο βάθος νερού, $K_x=K_y=5.93u_{*,c}h$ είναι οι συντελεστές διασποράς του ιζήματος, $u_{*,c}$ είναι η ταχύτητα τριβής λόγω ρεύματος, P_r και D_r είναι ο ρυθμός αιώρησης και εναπόθεσης του ιζήματος, αντίστοιχα. Το μέσο χρονικά φορτίο σε αιώρηση ανά μονάδα πλάτους δίνεται από τη σχέση:

$$\boldsymbol{q}_{ss}=\left(\overline{C_{ave}h-K_x h\frac{\partial C_{ave}}{\partial x}}\,,\overline{C_{ave}h-K_y h\frac{\partial C_{ave}}{\partial y}}\right) \tag{6}$$

Περισσότερες λεπτομέρειες για τις εξισώσεις στερεομεταφοράς στη ζώνη θραύσης και ανοιχτά αυτής περιγράφονται στην εργασία των Camenen και Larson (2007). Για τον υπολογισμό του ρυθμού στερεομεταφοράς στη ζώνη διαβροχής εφαρμόζονται οι τύποι των Larson και Wamsley (2007) που βασίζονται σε μια αναλογία προς τη βαλλιστική θεωρία. Η εξέλιξη της τοπογραφίας του πυθμένα προκύπτει από την επίλυση της εξίσωσης ισοζυγίου των φερτών:

$$\frac{\partial d}{\partial t}=\frac{1}{1-n_p}\nabla\cdot\boldsymbol{q}'_{tot} \tag{7}$$

όπου n_p είναι το πορώδες του ιζήματος ($\approx$ 0.4) και $\boldsymbol{q}'_{tot}$ ο τροποποιημένος συνολικός ρυθμός στερεομεταφοράς που λαμβάνει υπόψη την κλίση του πυθμένα. Το χρονικό βήμα επίλυσης της Εξ. (7), Δt_{mor}, είναι πολλαπλάσιο του αντίστοιχου του κυματικού μοντέλου, Δt και συνδέονται με τη σχέση:

$$\Delta t_{mor}=f_{MOR}\cdot\Delta t \tag{8}$$

όπου ο παράγοντας f_{MOR} παίρνει τιμές από 1 έως 20.

3 ΕΠΑΛΗΘΕΥΣΗ ΤΟΥ ΜΟΝΤΕΛΟΥ

3.1 Μονοδιάστατη (1DH) επαλήθευση

Το μοντέλο επαληθεύτηκε με τις πειραματικές μετρήσεις των Kajima κ.ά. (1982), οι οποίες αναφέρονται στην εξέλιξη της μορφολογίας του πυθμένα μιας αρχικά επίπεδης παραλίας. Η πειραματική διάταξη περιλαμβάνει ένα οριζόντιο πυθμένα βάθους 4.50 m, ακολουθούμενο από μία ομοιόμορφη κλίση 1:20. Ο πυθμένας είναι αμμώδης με μέση διάμετρο κόκκων $d_{50}=0.27$ mm. Οι διαδιδόμενοι κυματισμοί έχουν περίοδο $T=6.0$ s και ύψος $H_0=1.00$ m και η διάρκεια του πειράματος είναι 98.1 hrs. Στην Εικόνα 1 αποτυπώνεται η σύγκριση των αποτελεσμάτων του μοντέλου και των μετρήσεων, όσον αφορά το ρυθμό στερεομεταφοράς και την εξέλιξη της βυθομετρίας μετά από 7 hrs κυματικής δράσης.

(a) (b)

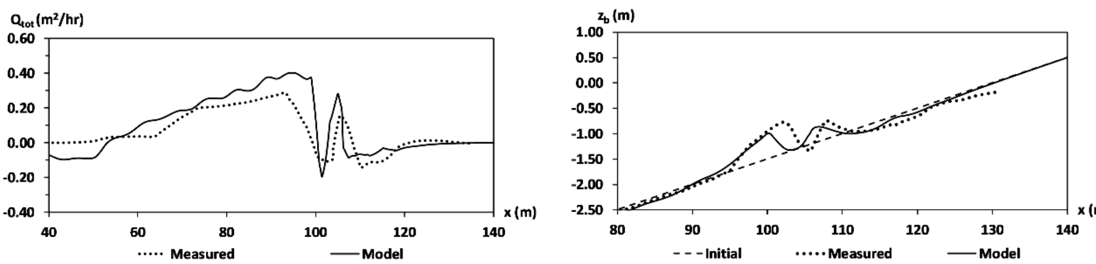

Εικόνα 1 Σύγκριση μεταξύ πειραματικών μετρήσεων των Kajima κ.ά. (1982) και μοντέλου για a) το ρυθμό στερεομεταφοράς μετά από 2 hrs , b) τη μορφολογία του πυθμένα μετά από 7 hrs

Η ακρίβεια του μοντέλου κρίνεται ικανοποιητική καθώς προβλέπει το σχηματισμό του κύριου ύφαλου αναβαθμού. Παρόλα αυτά, η προσάμμωση στην κατάντη παρειά του ύφαλου υποεκτιμάται και αυτό εξηγείται από το γεγονός ότι το μοντέλο υπολογίζει μια πιο απότομη από τη μετρημένη δευτερεύουσα κορυφή στην κατανομή του ρυθμού στερεομεταφοράς. Αντίθετα, ο δευτερεύων ύφαλος και η διάβρωση κατάντη αυτού εκτιμώνται επαρκώς.

Στην Εικόνα 2 παρουσιάζονται αντίστοιχες συγκρίσεις με το πείραμα των Dette κ.ά. (2002) που αναφέρεται στη διάδοση τυχαίων κυματισμών φάσματος TMA με $T_p = 5.5$ s και $H_{m_o} = 1.20$ m, πάνω από αμμώδη πυθμένα με μέση διάμετρο κόκκων $d_{50} = 0.30$ mm.

(a) (b)

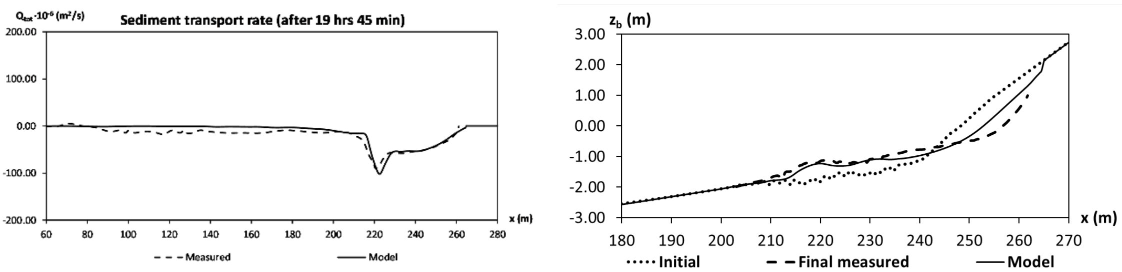

Εικόνα 2 Σύγκριση μεταξύ πειραματικών μετρήσεων των Dette κ.ά. (2002) και μοντέλου για a) το ρυθμό στερεομεταφοράς μετά από 19.75 hrs , b) τη μορφολογία του πυθμένα μετά από 23 hrs

Οι θέσεις απόθεσης και διάβρωσης περιγράφονται ορθά, παρά την υποεκτίμηση της δεύτερης στη ζώνη διαβροχής. Σημειώνεται ότι στις μονοδιάστατες εφαρμογές (1DH) η συνεισφορά της κ.μ.α. στερεομεταφοράς στο ισοζύγιο των φερτών αμελείται.

3.2 Διδιάστατη (2DH) επαλήθευση

Το μοντέλο ελέγχθηκε και με πειραματικές μετρήσεις σε δύο οριζόντιες διαστάσεις. Ένα από τα πειράματα που χρησιμοποιήθηκαν είναι αυτό των Gravens και Wang (2007) που αναφέρεται σε πλάγια πρόσπτωση σύνθετων κυματισμών φάσματος TMA με $T_p = 5.5$ s και $H_{m_o} = 1.20$ m, πάνω από αμμώδη πυθμένα με μέση διάμετρο κόκκων $d_{50} = 0.15$ mm. Η πειραματική διάταξη και η εξέλιξη της βυθομετρίας φαίνονται στην Εικόνα 3, ενώ στην Εικόνα 4 παρουσιάζονται συγκρίσεις των αποτελεσμάτων του μοντέλου με τις πειραματικές μετρήσεις όσον αφορά το ύψος κύματος και το κ.μ.α. κυματογενές ρεύμα. Η ακρίβεια του μοντέλου είναι ικανοποιητική, καθώς το πλάτος του σχηματιζόμενου salient υπολογίζεται σωστά, όπως και οι θέσεις απόθεσης/διάβρωσης.

(a) (b)

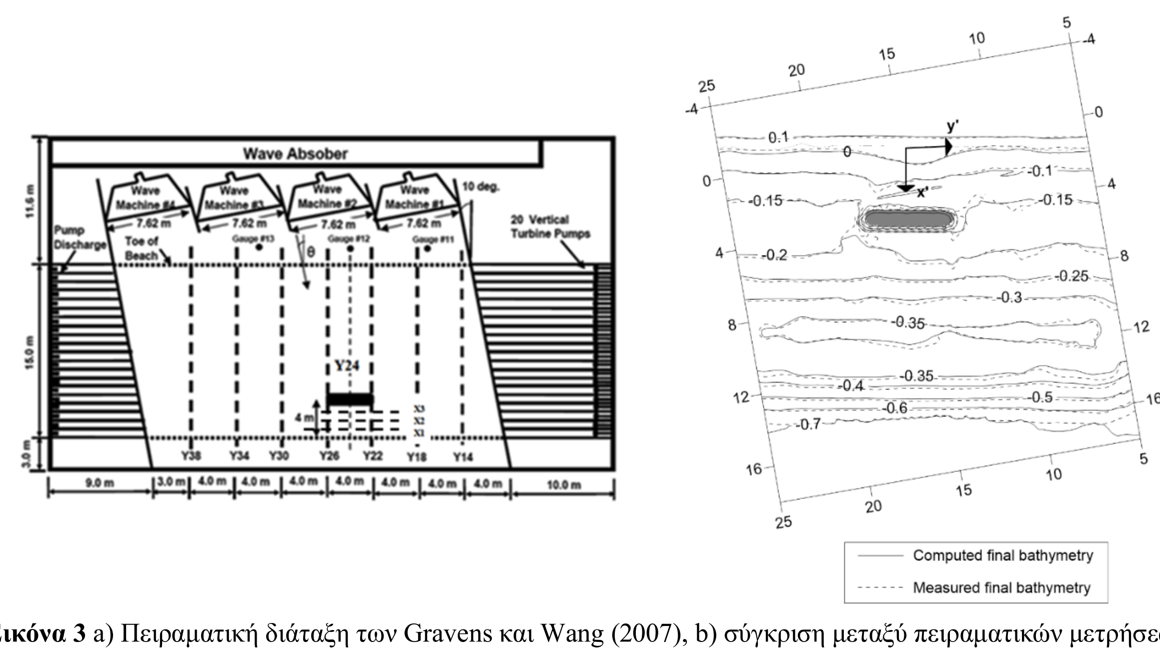

Εικόνα 3 a) Πειραματική διάταξη των Gravens και Wang (2007), b) σύγκριση μεταξύ πειραματικών μετρήσεων και αποτελεσμάτων του μοντέλου σχετικά με την τελική βυθομετρία (ισοβαθείς σε cm)

(a) (b)

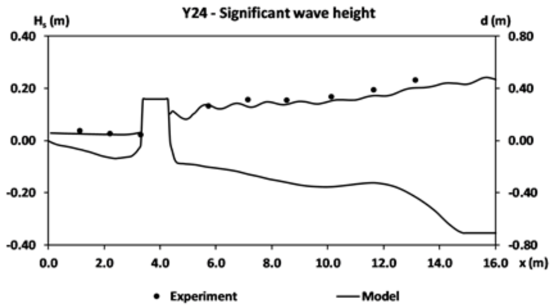

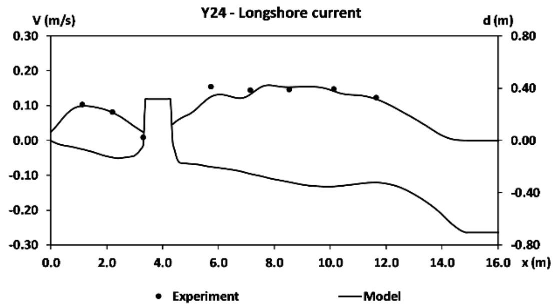

Εικόνα 4 Σύγκριση μεταξύ των πειραματικών μετρήσεων και των αποτελεσμάτων του μοντέλου κατά μήκος της διατομής Y24 όσον αφορά α) το σημαντικό ύψος κύματος, b) την ταχύτητα του κ.μ.α. κυματογενούς ρεύματος

4 ΣΥΜΠΕΡΑΣΜΑΤΑ

Ο συνδυασμός ενός μη ολοκληρωμένου στην περίοδο (phase-resolving) κυματικού μοντέλου με ένα μοντέλο στερεομεταφοράς αποτελεί ένα δύσκολο, αλλά χρήσιμο εγχείρημα. Το παρόν μοντέλο Boussinesq είναι υψηλής μη γραμμικότητας και συνεπώς μπορεί να περιγράψει με ακρίβεια την κυματική ασυμμετρία και τις μη γραμμικές κυματικές αλληλεπιδράσεις, φαινόμενα ιδιαιτέρως σημαντικά για την ορθή εκτίμηση της παράκτιας στερεομεταφοράς. Επιπλέον, η χρήση σύγχρονων σχέσεων για τον υπολογισμό αυτής επιτρέπει την περιγραφή των φαινομένων υστέρησης στην απόκριση του ιζήματος. Επίσης, επιβεβαιώνεται ότι η εφαρμογή της μεθόδου που βασίζεται στον Morfac επιτρέπει την προσομοίωση μορφολογικών μεταβολών αναφερόμενων σε χρονικές κλίμακες της τάξης ωρών ή λίγων ημερών. Συμπερασματικά, ο ολοκληρωμένος χαρακτήρας του μοντέλου, η δυνατότητα εφαρμογής του σε ολόκληρη την παράκτια ζώνη από τα βαθειά νερά έως τη ζώνη διαβροχής και η εκτενής επαλήθευση των αποτελεσμάτων του το καθιστούν ένα αξιόπιστο εργαλείο για τη μελέτη σύνθετων υδροδυναμικών και μορφοδυναμικών διεργασιών.

Βιβλιογραφικές Αναφορές

Camenen, B, Larson, M (2007) A unified sediment transport formulation for coastal inlet application. Tech. rep. ERDC/CHL CR-07-1, U.S. Army Engineer Research and Development Center, Vicksburg, MS, U.S.A., 231 pp.

Dette, HH, Larson, M, Murphy, J, Newe, J, Peters, K, Reniers, A, Steetzel, H (2002) Application of prototype flume tests for beach nourishment assessment. Coast. Eng. 47(2):137-177. doi: 10.1016/S0378-3839(02)00124-2

Gravens, MB, Wang, P (2007) Data report: laboratory testing of longshore sand transport by waves and currents; morphology change behind headland structures. Tech. Rep., ERDC/CHL TR-07-8, Coastal and Hydraulics Laboratory, U.S. Army Engineer Research and Development Center, Vicksburg, MS, U.S.A.

Kajima, R, Shimizu, T, Maruyama, K, Saito, S (1982) Experiments on beach profile change with a large wave flume. In: Edge BL (ed) Proc. 18th Int. Conf. on Coastal Engineering, Cape Town, South Africa, part II, chapter 85, pp. 1385-1404. doi: 10.9753/icce.v18.%25p

Klonaris, GTh, Memos, CD, Drønen, NK (2016) High-order Boussinesq-type model for integrated nearshore dynamics. J. Waterw. Port Coast. Ocean Eng. 142(6):04016010. doi: 10.1061/(ASCE)WW.1943-5460.0000349

Larson, M, Wamsley, TV (2007) A formula for longshore sediment transport in the swash. In: Proceedings Coastal Sediments '07, ASCE, New Orleans, U.S.A., pp. 1924–1937. doi: 10.1061/40926(239)151

Lesser, GR, Roelvink, JA, van Kester, JATM., Stelling, GS (2004) Development and validation of a three-dimensional morphological model. Coast. Eng. 51(8–9):883–915 (October). doi:10.1016/j.coastaleng.2004.07.014

Putrevu, U, Svendsen, IA (1993) Vertical structure of the undertow outside the surf zone. J. Geophys. Res. 98(C12):22707–22716. doi: 10.1029/93JC02399

Morphodynamics of vortex ripples under oscillatory flow conditions

G.A. Leftheriotis*, A.A. Dimas

Department of l Civil Engineering, University of Patras, Patras, Achaia, 26500, Greece
Corresponding author: gleytheriot@upatras.gr

Abstract

In the present study, large-eddy simulations were performed, in order to study in detail the sediment dynamics that occur in oscillatory flow over a rippled bed. Emphasis was given to the development of a morphological module in order to analyze the creation and evolution of ripples. The simulations were based on the numerical solution of the Navier-Stokes equations for incompressible flow and the advection-diffusion equation for the suspended load, while empirical formulas were used for the bed load. The evolution of the bed form was obtained by the numerical solution of the Exner equation. The Immersed Boundary method was implemented for the imposition of fluid and sediment boundary conditions on the bed surface. The numerical model was effectively validated against laboratory measurements involving oscillatory wave motion and sediment transport. Both suspended sediment concentration and bed load transport magnitude increased with increasing values of the mobility parameter, ψ. The numerical model captured phenomena of ripple creation and propagation, resulting in ripple dimensions in agreement with those predicted by empirical equations. Under oblique oscillatory flow conditions, ripples are re-oriented and formed perpendicular to the flow direction.

Keywords Ripples, Sediment transport, Immersed-boundary method, Morphodynamics.

1 INTRODUCTION

In coastal areas, the wave-induced oscillatory flow leads to the modification of the seabed and the generation of small-scale bed forms, generally known as ripples. The geometry of these structures has a strong impact on the wave-induced bottom boundary layer processes, which control sediment transport in coastal areas. Computation of bed and suspended sediment transport rates as well as accurate predictions of the ripple shape under certain flow conditions are fundamental components of coastal engineering studies.

1.1 Bed Morphodynamics Under Oscillatory Flow Conditions

In oscillatory flow over ripples, the behavior of suspended sediment is highly correlated to the development of coherent vortices, generated at the lee side of the ripple during each half-cycle. Sediment is first hurled over the lee vortex, and at flow reversal it is carried by that vortex as it is ejected into the outer flow. According to this vortex formation-ejection mechanism, Bagnold (1946) characterized these bed forms as “vortex ripples”. Under typical oscillatory flow conditions, the external flow is usually assumed to correspond to the near-bed flow of a 2nd order wave

$$U(t) = U_o\left(\cos(\omega t) + B\cos(2\omega t)\right) \tag{1}$$

where U is the dimensional velocity, $U_o = a_o\omega$ is the velocity amplitude, a_o is the orbital amplitude, $\omega=2\pi/T$ is the radial frequency, T is the period, and B is the flow skewness factor. The Reynolds number is defined as Re = $U_o a_o/\nu$, where ν is the water kinematic viscosity, while the mobility parameter is defined as $\psi = U_o^2/[(S\text{-}1)gD_g]$, where S is the sediment specific gravity, g is the gravitational acceleration and D_g is the sand gran diameter.

Studies of ripples under oscillatory flow date back to the end of the 19th century, but the first large-scale experimental studies took place at the late 1950s. After 1990, series of field and laboratory datasets became available with measured sediment concentration and transport in full-scale oscillatory flows at high Reynolds numbers (Ribberink and Al-Salem 1994, Van der Werf et al. 2007). Several numerical studies have also been reported on the coupled fluid flow and sediment transport simulation over ripples. Furthermore, during the last decades, significant progress has been made in understanding bed form dynamics, especially in the topic of ripple morphodynamics. The prediction of ripple formation and geometry has been studied by a number of researchers (Giri and Shimizu 2006, Marieu et al. 2008, Nienhuis et al. 2014).

The objective of the present study is to assess the effect of the mobility parameter and the sand grain size on sediment transport over orbital vortex ripples and to analyze the mechanisms regarding the morphodynamical development of vortex ripples.

2 METHODOLOGY

2.1 Hydrodynamics

In LES, the governing fluid flow equations, in non-dimensional form using U_o and a_o, are the continuity $\partial u_i/\partial x_i = 0$ and the Navier-Stokes equations

$$\frac{\partial u_i}{\partial t} + \frac{\partial}{\partial x_j}\left(u_i u_j\right) = -\frac{\partial p}{\partial x_i} - \frac{\partial \tau_{ij}}{\partial x_j} + \frac{1}{\mathrm{Re}}\frac{\partial^2 u_i}{\partial x_j \partial x_j} + f_i \tag{2}$$

where x_i are the spatial coordinates, u_i are the corresponding resolved velocity components, t is the time, p is the dynamic pressure, τ_{ij} are the subgrid-scale (SGS) stresses, Re is the Reynolds number, and f_i is a source term associated with the implementation of the Immersed Boundary (IB) method for the enforcement of the non-slip velocity boundary condition on the bed surface.

2.2 Sediment Transport

In the present study, both bed and suspended sediment transport was considered. The bed load transport rate q_b was computed using the semi-empirical formula in Engelund and Fredsøe (1976) for the dimensionless bed load transport rate parameter Φ_b. The evolution of sediment in suspension was modeled using a dimensionless advection-diffusion equation for the volumetric concentration, c, of the suspended sediment

$$\frac{\partial c}{\partial t} + u_j\frac{\partial c}{\partial x_j} - \frac{W_s}{U_o}\frac{\partial c}{\partial x_3} = -\frac{\partial \chi_j}{\partial x_j} + \frac{1}{\mathrm{Re}\cdot\sigma}\frac{\partial^2 c}{\partial x_j \partial x_j} + f_c \tag{3}$$

where W_s is the dimensional settling velocity of the sediment, χ_j is the SGS turbulent flux of sediment, σ is the Schmidt number, and f_c is a source term associated with the implementation of the IB method for the enforcement of the appropriate sediment concentration boundary condition on the bed surface. The boundary condition for Eq. 3 on the bed was set according to the model in Fredsøe and Deigaard (1992), and a Dirichlet condition was imposed at a dimensionless distance of $2D_g/a_o$ above the bed.

2.3 Bed Morphodynamics

The coupling between the evolution of the bed morphology and the sediment transport mechanisms was obtained by the numerical solution of the conservation of sediment mass equation (also called the Exner equation), expressed as

$$\frac{\partial h}{\partial t} = -\left(\frac{\partial q_{x_1}}{\partial x_1} + \frac{\partial q_{x_2}}{\partial x_2}\right) \tag{4}$$

where h is the bed level and q_{xi} is the total sediment flux in the horizontal directions, which comprises both bed, q_b, and suspended load, q_s, transport rates.

2.4 Immersed-Boundary Method

For the spatial discretization, 2nd order central finite differences on a staggered Cartesian grid were used, while boundary conditions on the bed surface were imposed using the IB method. The IB method is explained in detail in Balaras (2004). The basic feature of the method is that boundary surfaces, like the rippled bed in the present application, do not coincide with any grid lines but are immersed in the computational domain. Thus, the computational domain includes both the fluid and the solid phases. The imposition of the boundary conditions on the bed surface is achieved by appropriately reconstructing the solution in the vicinity of the boundary through an additional source term f in the governing Eqs. 1 – 2. The main advantage of the method is that efficient Cartesian solvers can be applied around complex boundaries. The solution is reconstructed on the forcing points, which are the grid points that belong to the fluid phase and are the nearest ones to the immersed boundary.

3 RESULTS

The present numerical model was validated in terms of oscillatory flow and sediment transport over ripples as presented in Dimas & Leftheriotis (2019).

3.1 Oscillatory Flow Over Ripples

Results are presented for oscillatory flow over fixed ripples with dimensions based on three values of ψ (= 20, 50 and 80) and for three cases of a_o/D_g (= 250, 500 and 1000) that span the range of typical values for vortex ripples in the orbital regime. A total of nine cases were simulated in an effort to assess the influence of the mobility parameter and the grain size on sediment transport dynamics and loads. The Reynolds number was equal to Re = 2.3×10^4 which corresponds to turbulent flow over the ripples, and B = 0.176 as in Van der Werf et al. (2007).

For ψ = 20, the bed load transport is active close to the ripple crests due to flow separation. As ψ increases, the magnitude of q_b increases due to the increase of U_o, while the bed load transport is active practically over the whole length of the ripples, as it is influenced during each half-cycle by the lee vortices. The effect of ψ on the magnitude of Φ_b is similar to the one on q_b, while the effect of a_o/D_g on the magnitude of Φ_b is weak. This is demonstrated in Figure 1 (left) where the net bed load parameter $\langle\Phi_b\rangle$ is shown for all cases, where $\langle\rangle$ = period-, ripple-span- and ripple-length-averaged, hereafter. The effect of a_o/D_g on $\langle\Phi_b\rangle$ is negligible, while the effect of ψ on $\langle\Phi_b\rangle$ is stronger in the range $20 \le \psi \le 50$. In all cases, the net bed load is positive, i.e. in the onshore direction.

In all cases, the suspended load transport rate q_s is in the offshore direction, it increases with increasing ψ and/or a_o/D_g, and it is active practically over the whole length of the ripples. This is shown in Figure 1 (right) where the net suspended load parameter $\langle\Phi_s\rangle$ is shown to be negative for all cases. In the examined range $20 \le \psi \le 80$, the effect of a_o/D_g on $\langle\Phi_s\rangle$ is strong unlike its effect on $\langle\Phi_b\rangle$.

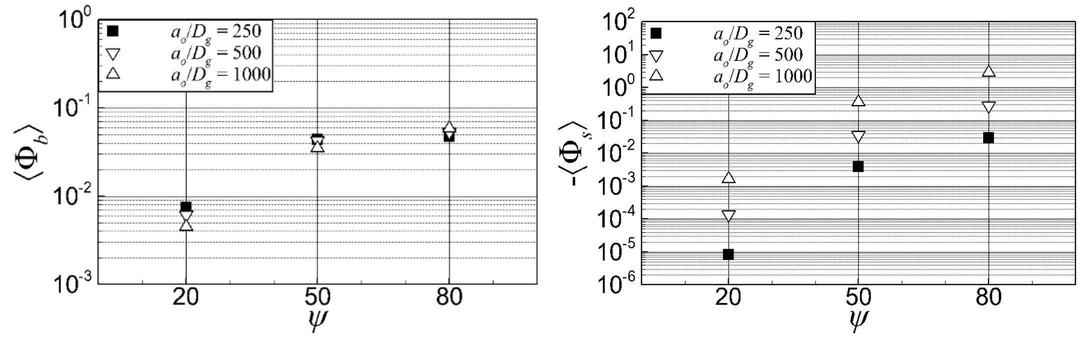

Figure 1 The net bed load parameter $\langle\Phi_b\rangle$ (left) and net suspended load parameter $\langle\Phi_s\rangle$ (right) as function of the mobility parameter ψ and the relative sand grain size a_o/D_g

The ratio of the net bed load parameter to the net total sediment load parameter is shown in Figure 2. The magnitude of the net total sediment load parameter is defined as $|\langle\Phi_{tot}\rangle| = |\langle\Phi_b\rangle| + |\langle\Phi_s\rangle|$. The relative contribution of bed or suspended load to the total sediment load depends on both ψ and a_o/D_g.

The extreme cases are: (a) $\psi \leq 20$ and $a_o/D_g \leq 500$ where the bed load is dominant, and (b) $\psi \geq 80$ and $a_o/D_g \geq 1000$ where the suspended load is dominant.

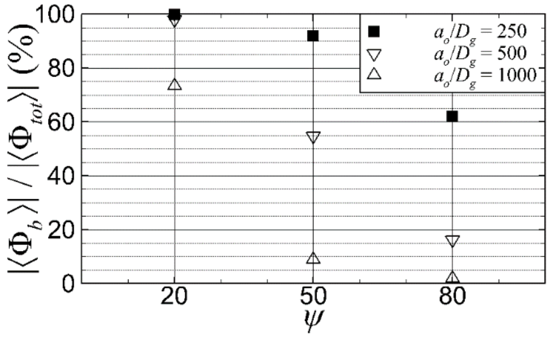

Figure 2 The ratio of the net bed load parameter to net total sediment load parameter $|\langle\Phi_b\rangle|/|\langle\Phi_{tot}\rangle|$ as a function of the mobility parameter ψ and the relative sand grain size a_o/D_g

3.2 Vortex Ripples Morphodynamics

In the second part of the present work, the morphological evolution of the rippled bed was examined under hydrodynamic/sediment forcing. In this approach, the shape of the bed form was allowed to change. Every N time steps of coupled flow and suspended sediment simulation, the bed morphology was updated by means of the total sediment transport rate. Ripple creation and propagation from semi-flat or random beds is examined, as well as ripples adapting to changing water conditions, after changing the flow direction and using different values of the mobility parameter.

Figure 3 illustrates an example of ripple creation and propagation from an initially semi-flat bed with a small perturbation in the middle of the computational domain. The mobility parameter, ψ = 50, corresponds to ripples with $L_r/a_o = 0.895$ (L_r is the ripple length). The domain length in both horizontal directions was set equal to $2.685 \cdot a_o$, in order to capture the development of three consecutive ripples in the streamwise direction, after saturation is reached. During the first 30 waves, the initial hump grows in height and expands in the spanwise direction, while a number of smaller perturbations are created and propagate on each side of it. After 50 wave cycles, the computational domain is almost fully covered in ripples that present spanwise two-dimensionality. At 100 wave cycles, the bed comprises four consequent ripples, which is close to the predicted final form. The rippled bed finally converges to its equilibrium geometry, composed of 3 ripples with length of $0.895 \cdot a_o$ and height of $0.12 \cdot a_o$, at about 300 wave cycles.

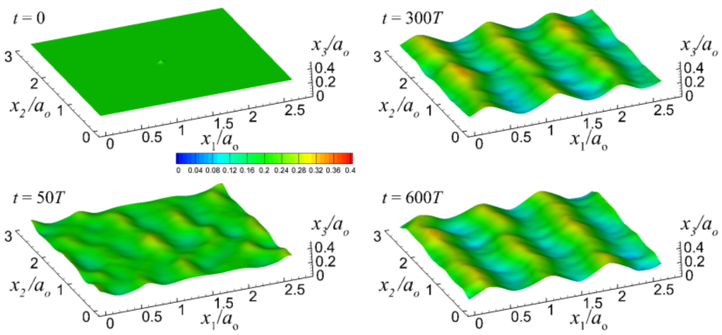

Figure 3 Ripple creation and evolution initiating from a flat bed for ψ = 50.

Finally, ripple re-orientation was examined. The equilibrium profile that resulted from the previous simulation (Figure 3, $t = 600 \cdot T$) was used as initial bed geometry. The simulation set-up, apart from the flow direction, is the same. Figure 4 shows the morphodynamics development for the specific simulation. The initial ripples are corrupted due to the oblique flow and as a result, smaller ripples are created. The ripples are formed perpendicular to the flow direction and merge with each other resulting in the formation of larger ripples, which continue to grow until they reach an equilibrium profile, when ripples with $L_r/a_o \approx 1.2$ and $h_r/a_o \approx 0.14$ (h_r is the ripple height) are formed perpendicular to the flow direction.

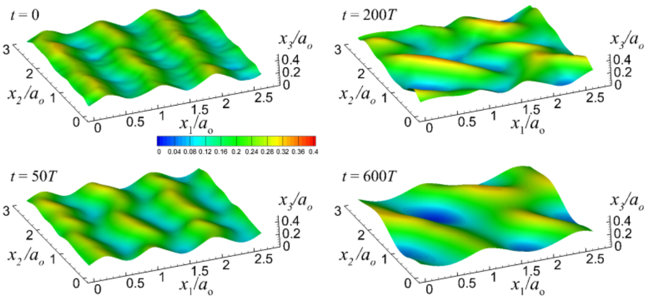

Figure 4 Ripple re-orientation initiating from the equilibrium profile that resulted from numerical simulation, under oblique oscillatory flow (45°) with the initial ripple crest, for $\psi = 50$.

4 CONCLUSIONS

A well-resolved LES model was employed for the coupled simulation of the turbulent oscillatory flow and the bed and suspended sediment transport over fixed vortex ripples. Nine cases were simulated at Re = 2.3×10^4, in the ranges $20 \le \psi \le 80$ and $250 \le a_o/D_g \le 1000$. For bed sediment transport, the net load was always in the onshore direction, while the effect of ψ on the net bed load was stronger for $\psi < 50$. For suspended sediment transport, the net load was always in the offshore direction, and its magnitude increased with increasing ψ and increasing a_o/D_g. The relative contribution of bed load versus suspended load on the total sediment load was found to depend on both ψ and a_o/D_g.

Numerical simulations of the morphological evolution of a sandy bed were also conducted. Ripple creation and propagation from semi-flat beds were examined, until the bed form reaches an equilibrium shape, adapting to oscillatory flow conditions based on ψ. The numerical model captures phenomena of ripple creation, growth, merging and migration, resulting in equilibrium ripples with wavelengths in agreement with those predicted by empirical equations. Under oblique oscillatory flow conditions, ripples are re-oriented and formed perpendicular to the flow direction.

Acknowledgements

This work was funded by the matching contribution (5231) of GSRT to the Initial Training Network SEDITRANS, implemented within the 7th Framework Programme of the European Commission, and was also supported by computational time granted from the Greek Research & Technology Network (GRNET) in the National HPC facility ARIS under project ID CoastHPC.

References

Bagnold RA (1946) Motion of waves in shallow water, interaction between waves and sand bottoms. Proceedings of the Royal Society A 187(1008): 1-15.

Balaras E (2004) Modeling complex boundaries using an external force field on fixed Cartesian grids in large-eddy simulations, Computers & Fluids 33: 375-404.

Dimas AA, Leftheriotis GA (2019) Mobility parameter and sand grain size effect on sediment transport over vortex ripples in the orbital regime, J. Geophys. Res. Earth Surf. 124 (1): 2-20.

Engelund F, Fredsøe J (1976) A sediment transport model for straight alluvial channels. Hydrol. Res. 7(5): 293-306.

Fredsøe J, Deigaard R (1992) Mechanics of coastal sediment transport. Singapore: World Scientific.

Giri S, Shimizu Y (2006) Numerical computation of sand dune migration with free surface flow. Water Resour. Res. 42: W10422.

Marieu V, Bonneton P, Foster DL, Ardhuin F (2008) Modeling of vortex ripple morphodynamics, J. Geophys. Res. 113: C09007.

Nienhuis JH, Perron JT, Kao JCT, Myrow PM (2014) Wavelength selection and symmetry breaking in orbital wave ripples, J. Geophys. Res. Earth Surf. 119: 2239-2257.

Ribberink JS, Al-Salem AA (1994) Sediment transport in oscillatory boundary layers in cases of rippled bed and sheet flow. J. Geophys. Res. 99(C6): 12707-12727.

Van der Werf JJ, Doucette JS, O'Donoghue T, Ribberink JS (2007) Detailed measurements of velocities and suspended sand concentrations over full-scale ripples in regular oscillatory flow. J. Geophys. Res. 112: F02012.

Flow over three-dimensional bed formations

I.A. Chalmoukis*, A.A. Dimas

Department of Civil Engineering, University of Patras, Patras, Achaia, 26500, Greece
*Corresponding author: ichalmoukis@upatras.gr

Abstract

The objective of this study is to simulate the turbulent flow over three-dimensional (3D) bed formations by means of an advanced Navier-Stokes solver and compare the deviation of the turbulence statistics with respect to the corresponding ones for two-dimensional cases. The discretization of the Navier-Stokes equations is done on a Cartesian grid where the bed surface is an interface immersed in the numerical grid, following the 3D immersed-boundary (IB) method. As a result, the implementation of the boundary conditions is achieved through additional terms in the Navier-Stokes equations at the nodes closest to the boundaries, which are called forcing points. The spatial discretization is based on the use of finite differences on a staggered grid for the dependent variables (u, v, w, p), and a two-stage time-splitting method is employed for the velocity-pressure coupling. To validate the accuracy of the computational model, simulations have been conducted for turbulent uniform flow over 3D dunes and the numerical results were compared to numerical simulations and experimental results in the literature. Specifically, good agreement was found in the comparison with existing numerical and experimental results where the dune dimensions are L_{xm} = 0.8 m and H_m = 0.04 m where L_{xm} is the mean dune length and H_m is the mean dune height. The Reynolds number is Re = $U_{bulk}\ h_{max}/v$ = 78,000 where U_{bulk} is the mean bulk velocity, h_{max} is the maximum water depth, and v is the water kinematic viscisity. In addition, 4 cases of fixed vortex ripples (one 2D and three 3D) were examined at Re = 20,000. Results are presented for the phase-averaged vorticity and turbulent kinetic energy (TKE). We concluded that even though the spanwise changes of the streamwise ripple steepness results into more energetic conditions locally, the spatially-averaged TKE is lower than from the corresponding 2D case. Nevertheless, diffusion of the TKE due to the 3D bottoms leads to higher quantities above one ripple height.

Keywords Three-dimensional ripples, Turbulent flow, Immersed-boundary method.

1 INTRODUCTION

In coastal areas, the wave-induced oscillatory flow modifies the sandy seabed and generates small-scale symmetric bed forms, generally known as ripples. Under typical oscillatory flow conditions, the external flow is usually assumed to correspond to the near-bed flow of a 2nd order wave

$$U(t) = U_o\left(\cos(\omega t) + B\cos(2\omega t)\right) \tag{1}$$

where U is the dimensional velocity, $U_o = a_o\omega$ is the velocity amplitude, a_o is the orbital amplitude, ω=2π/T is the radial frequency, T is the period, and B is the flow skewness factor. The Reynolds number is defined as Re = $U_o a_o/v$, where v is the water kinematic viscosity.

Several numerical studies have been reported on the oscillatory flow over 2D rippled bottoms (Fredsoe et al. 1999, Scandura et al. 2000, Grigoriadis et al. 2012). More recently, Nienhuis et al. (2014) presented a combined experimental/numerical study. They found that the ripples were in a dynamic equilibrium and they adapted to changing wave conditions by shortening or lengthening gradually their length via transient 3D morphologies. In general, most of research to date has been focused on the study of the oscillatory flow over 2D ripples. However, natural ripples are usually 3D and they can exhibit cross-stream variations in the streamwise crest location leading to differences in ripple length and steepness. Hence, the motivation of this work is to extend the present understanding acquired from previous studies, by performing large-eddy simulations (LES) over a set of different 3D ripples (see Figure 1 and Table 1). These fixed 3D ripples are consistent with observations made in the experiments of Nienhuis et al. (2014) and though simpler in some respects, incorporate observed features of natural random ripples, while maintaining enough similarity to previously studied 2D ripples to allow comparisons.

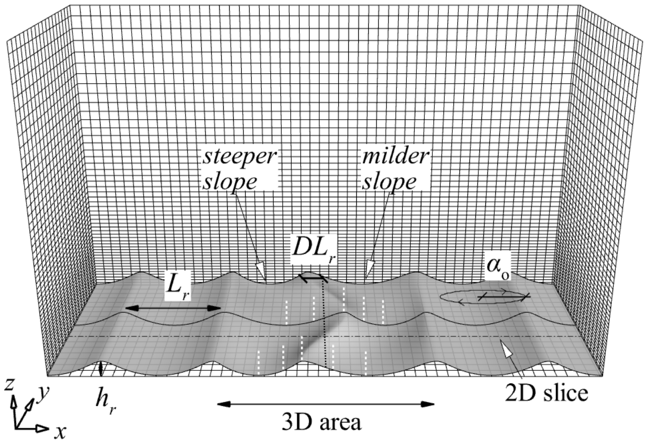

Figure 1 Sketch of a 3D vortex ripple formation with the grid (every 5th node is shown) and the selected stations (white dashed lines). Numbering of the ripple crests is from left to right.

Table 1 Geometric characterics of the rippled bed cases

Case	Width	3D Ripple length
B2_DL0	2 L_r	2 L_r
B2_DL005	2 L_r	$L_r \pm 0.05\ L_r$
B2_DL01	2 L_r	$L_r \pm 0.1\ L_r$
B2_DL02	2 L_r	$L_r \pm 0.2\ L_r$

2 METHODOLOGY

2.1 Hydrodynamics

In LES, the governing fluid flow equations, in non-dimensional form using U_o and a_o, are the continuity $\partial u_i/\partial x_i = 0$ and the Navier-Stokes equations

$$\frac{\partial u_i}{\partial t} + \frac{\partial}{\partial x_j}\left(u_i u_j\right) = -\frac{\partial p}{\partial x_i} - \frac{\partial \tau_{ij}}{\partial x_j} + \frac{1}{\mathrm{Re}}\frac{\partial^2 u_i}{\partial x_j \partial x_j} + f_i \qquad (2)$$

where x_i are the spatial coordinates, u_i are the corresponding resolved velocity components, t is the time, p is the dynamic pressure, τ_{ij} are the subgrid-scale (SGS) stresses, Re is the Reynolds number, and f_i is a source term associated with the implementation of the Immersed Boundary (IB) method (Gilmanov et al. 2003) for the enforcement of the non-slip velocity boundary condition on the bed surface. Their discretization is done on a Cartesian grid where the bed surface is an interface immersed in the numerical grid, following the 3D immersed-boundary (IB) method. The spatial discretization is based on the use of finite differences on a staggered grid for the dependent variables (u, v, w, p), and a two-stage time-splitting method is employed for the velocity-pressure coupling. The dynamic pressure is split to the imposed dynamic pressure of the external flow and the dynamic pressure correction due to the presence of the bed surface.

2.2 Immersed-Boundary Method

To ensure the application of the no slip condition on the seabed, the IB method is utilized. The main characteristic of this method is that the bottom interface is not aligned with the numerical grid and the imposition of the boundary conditions is achieved by additional forcing terms in the Navier-Stokes equation. In this study, the immersed surface is discretized using an unstructural triangular mesh (Figure 2).

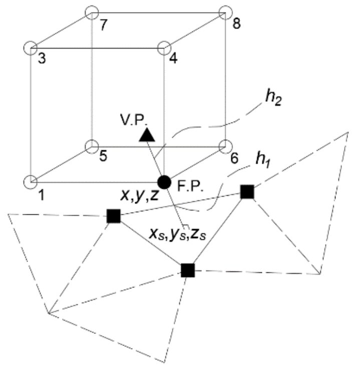

Figure 2 Schematic representation of a forcing point, its closest three immersed boundary points (rectangular-symbol) and its virtual point

3 RESULTS

3.1 Unidirectional Flow over 3D Dunes

To validate the accuracy of the computational model, simulations were conducted for turbulent uniform flow over 3D dunes and the numerical results were matched well to previous numerical simulations (Xie et al. 2013) and existing experimental results (Maddux et al. 2003). For this selected case, the Reynolds number was Re = $U_{bulk}\ h_{max}\ /\ \nu$ = 78,000 where U_{bulk} is the bulk velocity (= 0.36m/sec), h_{max} is the maximum water depth (= 0.193m), and ν is the water kinematic viscosity. The large value of this case Reynolds number makes it suitable to prove the reliability of the implemented LES approach. The dune dimensions were: mean length L_{xm} = 0.8 m, and mean height H_m = 0.04 m. In Figure 3, the two numerical results are almost identical, while, in Figure 4, the present LES results match better the experimental data in Maddux et al. (2003) than the corresponding results of Xie et al. (2013), probably due to the finer mesh that was used in this study.

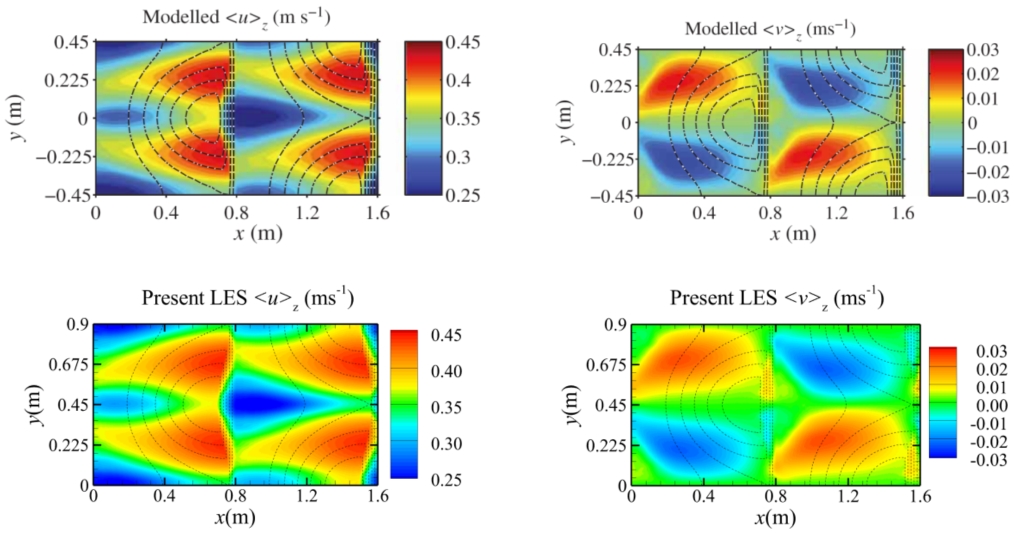

Figure 3 Depth-averaged streamwise (left) and spanwise (right) velocity between numerical results in Xie et al. (2013) (top) and present LES (bottom). Lines denote the elevation of the dune surface.

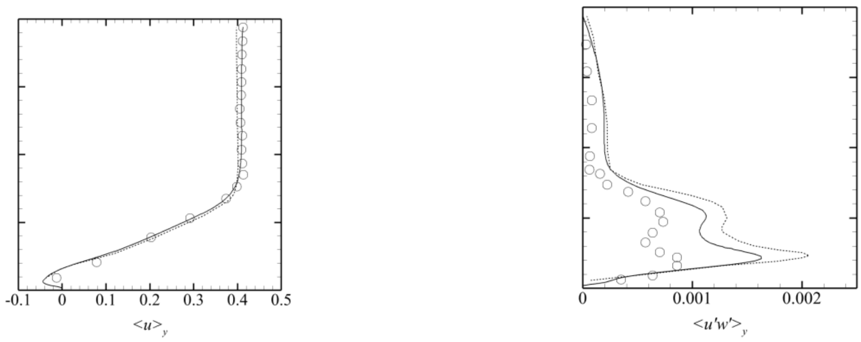

Figure 4 Spanwise-averaged streamwise velocities (left) and Reynolds shear stresses (right) between present LES results (solid line), Maddux et al. (2003) (symbols) and Xie et al. (2013) (dashed line)

3.2 Oscillatory Flow over 3D Vortex Ripples

Four cases of vortex ripples (one 2D and one 3D) were examined for oscillatory flow at Reynolds number Re = 20,000. The non-dimensional ripple height was $h_r/\alpha_o = 0.18$ and length, $L_r/\alpha_o = 1.25$.

To assess parametrically the effects of the 3D bottom on the oscillatory flow, we studied three different cases by changing gradually the middle ripple length, and comparing them with the 2D bottom configuration. In Figure 5, we correlate the spanwise vorticity with the turbulent kinetic energy. In particular, larger vortical structures are created and higher ejection of turbulent kinetic energy (TKE) is present on steeper regions due to locally higher favorable pressure gradient. However, when we spatially-averaged the TKE over the 3D region, we found that even though the spanwise changes of the streamwise ripple steepness results into more energetic conditions locally (Figure 5), the spatially-averaged TKE is lower than from the corresponding 2D case (Figure 6). Nevertheless, diffusion of the TKE due to the 3D bottoms leads to higher quantities above one ripple height (Figure 6).

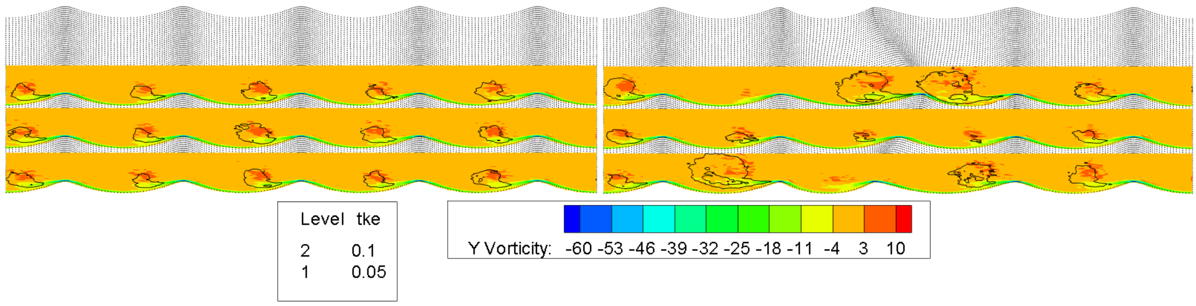

Figure 5 Vorticity contours and turbulent kinetic energy lines on three xz-planes for cases B2_DL0 (left) and B2_DL02 (right) at $t = 12T/32$ above the rippled bed.

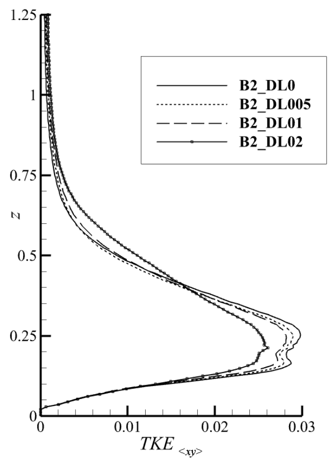

Figure 6 Spatially-averaged turbulent kinetic energy at $t = 12T/32$ for the four simulated cases

4 CONCLUSIONS

A first step towards the study of ripples that more closely resemble the transient 3D sandy bottoms found in nature was presented here. It could be argued that a more variable rippled bed would produce more chaotic and energetic flow than the mathematically defined symmetric ripples. However, starting from simple 3D bottom geometries, the decomposition of the complex flow and transport mechanisms is more achievable. In this study, LES of oscillatory flow over 3D rippled beds have been presented using the IB method to incorporate the bottom. The code was validated against numerical and experimental results concerning unidirectional flow over 3D dunes. Flow and turbulence statistics results over 3D vortex ripples are reported at Re = 20,000. The effect of the spanwise variation of the ripple length was examined and it was found that steeper regions were always associated locally with stronger turbulence levels and larger recirculation regions. In addition, the 3D bottom induces spanwise secondary flow that is responsible for the sediment transport and the rearrangement of the sandy seabed.

Aknowledgements

This work was funded by the matching contribution (5231) of GSRT to the Initial Training Network SEDITRANS, implemented within the 7th Framework Programme of the European Commission, and was also supported by computational time granted from the Greek Research & Technology Network (GRNET) in the National HPC facility ARIS under project ID CoastHPC.

References

Fredsøe J, Anderson KH, Sumer BM (1999) Wave plus current over a ripple-covered bed. Coastal Engineering, 38(4): 177-221.

Gilmanov A, Sotiropoulos F, Balaras E (2003) A general reconstruction algorithm for simulating flows with complex 3D immersed boundaries on Cartesian grids. Journal of Computational Physics, 191: 660-669.

Grigoriadis DGE, Dimas AA, Balaras E (2012) Large-eddy simulation of wave turbulent boundary layer over rippled bed. Coastal Engineering, 60: 174-189.

Maddux TB, Nelson JM, McLean SR (2003) Turbulent flow over three-dimensional dunes: 1. Free surface and flow response. Journal of Geophysical Research, 108: 1-10.

Nienhuis JH, Perron JT Kao JCT, Myrow PM (2014) Wavelength selection and symmetry breaking in orbital wave ripples. Journal of Geophysical Research - Earth Surface 119: 2239-2257.

Scandura P, Vittori G, Blondeaux P (2000) Three-dimensional oscillatory flow over steep ripples. Journal of Fluid Mechanics 412: 355-378.

Xie Z, Lin B, Falconer RA, Maddux TB (2013) Large-eddy simulation of turbulent open-channel flow over three-dimensional dunes. Journal of Hydraulic Research 51: 494-505.

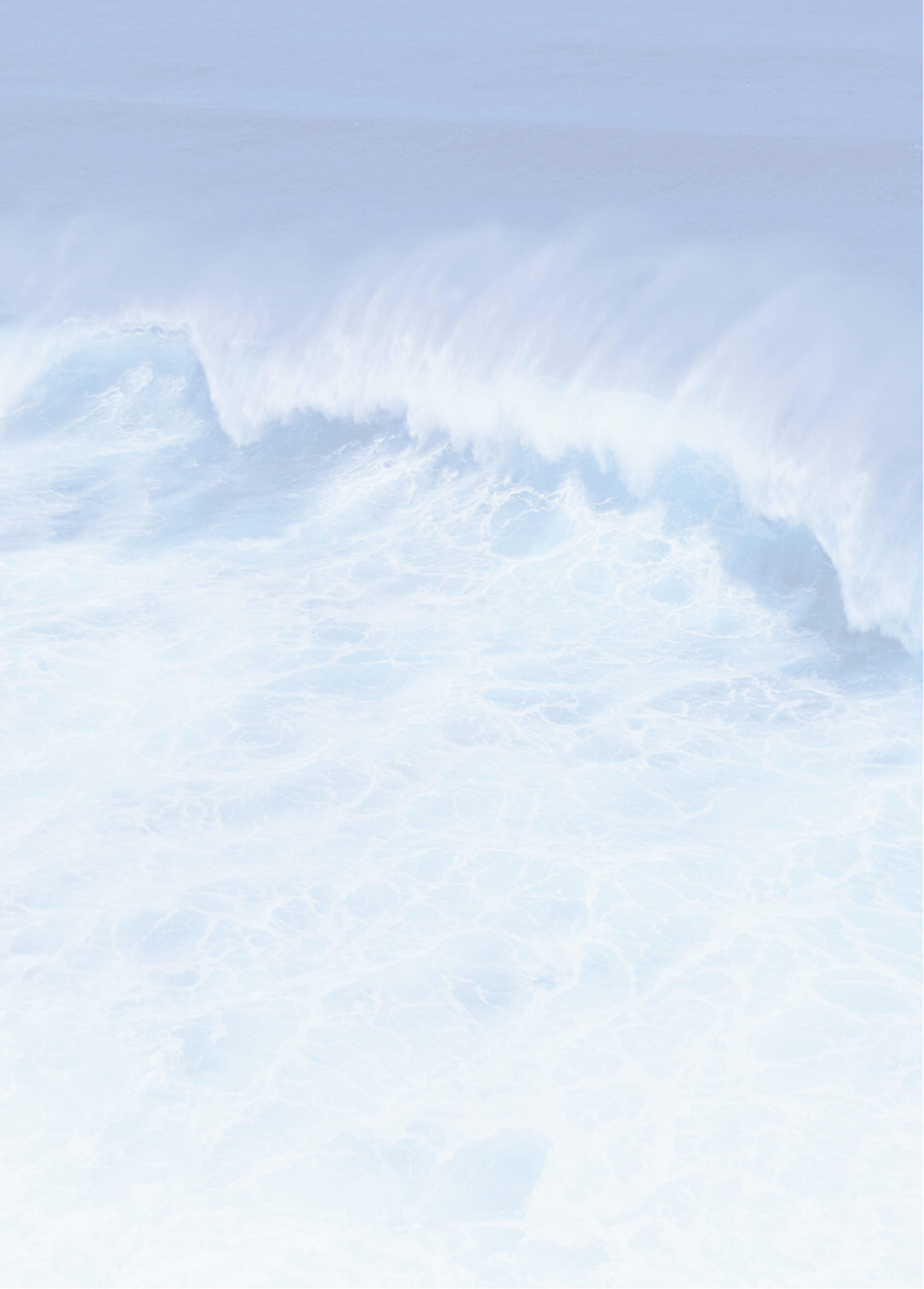

Numerical approaches for the evaluation of sediment transport mechanisms on a shallow sloping sea bottom

V. Afentoulis[1*], A. Papadimitriou[1], M. Benoit[2], V. Tsoukala[1]

[1]Laboratory of Harbour Works, Department of Water Resources and Environmental Engineering, School of Civil Engineering, National Technical University of Athens, Iroon Polytechniou 5, 15780 Athens, Greece.
[2]Aix Marseille Univ., CNRS, Centrale Marseille, Institut de Recherche sur les Phénomènes Hors-Equilibre (IRPHE), 49 rue F. Joliot-Curie, 13013 Marseille, France
[*]Corresponding author: afvas@central.ntua.gr

Abstract

The seabed evolution due to wave–current interaction is examined in the case of a gently sloping bottom in a shallow water coastal area. In this study, an attempt has been made to estimate bed level changes over a time period of 96 hours, under accretive and erosive wave sequences. A numerical model based on the non-linear shallow water equations (NSWE) is utilized in order to simulate the wave propagation and hydrodynamic conditions. Two different approaches are used for the detailed investigation of sediment transport and seabed-fluid interactions. It is shown that the numerical approximation performs reasonably well, as the erosive sequence is characterized by an offshore sediment movement while the sandbar is driven shoreward under accretive wave conditions. The simulation is carried out on a variable coastal bathymetry corresponding to the wave basin experiments of Michallet et al. (2013) at LHF facility (Grenoble INP, France). The obtained results are qualitatively compared with laboratory observations.

Keywords Sediment transport, Numerical simulation, Morphodynamics, Coastal hydrodynamics.

1 INTRODUCTION

The evolution of seabed under the combined action of waves and currents has been extensively studied, but until nowadays is still not fully understood. Historically, many studies have been carried out on the sediment transport pathway investigation, generation and migration of different bed forms, such as ripples and dunes (Sleath 1984), (Nielsen 1992), (Fredsøe and Deigaard 1992), (Soulsby 1997), and (Van Rijn 1993, 2007). Due to the complex nature of these phenomena, it is difficult to strictly interpret their mechanisms with a rational theory. Sand fluxes can be generated and driven by the combination of steady flows (currents) and oscillatory flows (waves). However, several other processes need to be taken into consideration, such as the mean water level variations (tide, wave set-up and set-down), breaking effects, and influence of the bed slope and form (Camenen and Larroudé 2003).

The main objective of the present study is to provide a comprehensive understanding of seabed-fluid interactions, using numerical modeling approaches. Hence, a numerical model is employed to simulate the hydrodynamic conditions and morphological seabed changes under erosive and accretive wave sequences. In order to assess the interaction between hydrodynamic and morphodynamic processes, the wave-current-bed evolution system is evaluated in an interactive mode, by considering the feedback on the former from the latter (Wang et al. 2012). Thus, a significant difference of the initial wave height distribution is observed due to the bathymetry changes, while topographically controlled currents are generated as a result of this interaction. It is worth pointing out that the effects of swash and groundwater dynamics in the unsaturated zone of beach is beyond the scope of the present work. Furthermore, measurements and observations from laboratory experiments have been used in order to verify the accuracy and credibility of the numerical approach.

1.1 General model setup

The simulation is carried out on a variable coastal bathymetry corresponding to the wave basin experiments of Michallet et al. (2013) at LHF facility (Grenoble INP, France). Figure 1 depicts the 3D bottom topography colored map and the alongshore-averaged beach profiles at the three main stages of the experiments. The applied initial wave climates, defined by their significant wave height and peak period, are divided into two main categories: energetic conditions (A: Hm0 = 23 cm / Tp = 2.3 s) and moderate conditions with a large period (B: Hm0 = 18 cm / Tp = 3.5 s). These wave characteristics correspond to the so-called down-state and up-state wave transitions respectively (i.e. the change from high to low wave energy in the case of the accretive sequence and the change from low to high wave energy in the case of the erosive sequence). The still water depth is set to h_0= 0.765 m and the length and time scales are 1/10 and $\approx 1/\sqrt{10}$ respectively, using Froude similarity law. Fine sand is considered, with specific gravity (G_s) of 2.65 and a median diameter (d_{50}) of 0.166 mm which corresponds to a settling velocity (w_s) = 2 cm/s. The total simulation time is 96.4 hours and it is divided into two parts, 62 hours duration of B wave conditions and 34.4 hours duration of A wave conditions. In order to create alongshore nonuniformity in the wave breaking spatial pattern, the wave directional spreading at the inlet varies from 20 to 30 degrees.

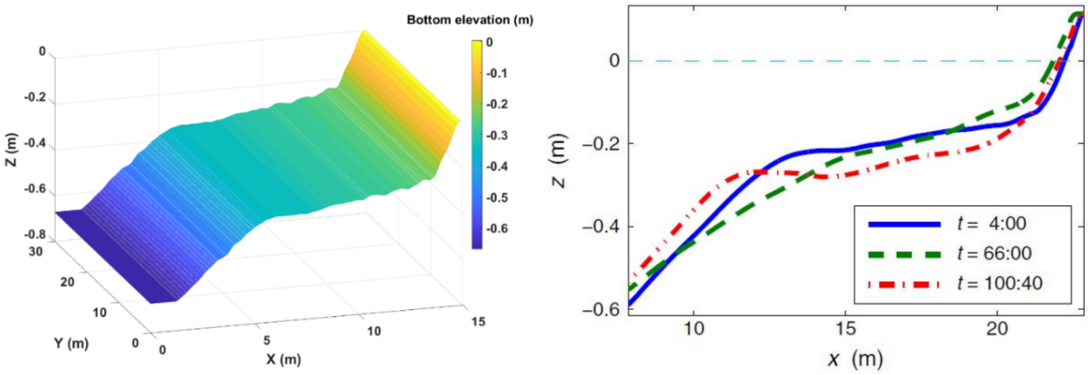

Figure 1 3D bathymetry colored elevation map (left). Alongshore-averaged beach profiles at the three main stages of the experiments (Michallet et al. 2013) (right).

2 HYDRODYNAMICS

For the assessment of hydrodynamic conditions, a model that solves the two-dimensional non-linear shallow water equations (NSWE) in conservative form is applied (Marche and Bonneton 2006), (Marche et al. 2007). These equations are discretized by a finite volume formulation, which preserves steady state solutions on non-flat sea beds in the absence of perturbations. The main advantage of this numerical approach is that breaking events can be modeled as the development of a free-surface and current discontinuity (Bonneton et al. 2010). It is noted, however, that dispersion effects are not considered, which is a limitation of this approach. A wave-maker is implemented for the generation of irregular waves using directional spectral data. These irregular waves are obtained by superposing a series of wave components with different frequencies and directions, using random phases. In Figure 2 the evolution of wave height distribution during the erosive sequence is shown. The change of the computed significant wave height is due to the wave-bed evolution joint actions.

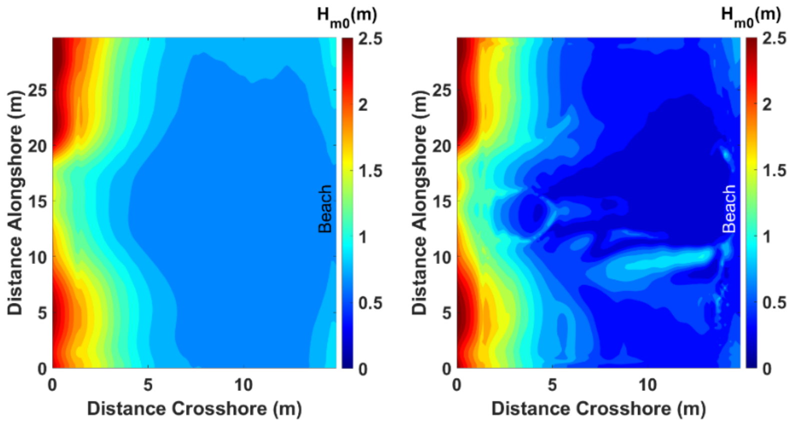

Figure 2 Map of computed significant wave height at the beginning (left) and at the end (right) of the erosive sequence.

3 MORPHODYNAMICS

In the present work, the mode of sediment movement is investigated using two different transport approaches. The first one is based on a quasi-steady approximation suggested by Ribberink (1998) for the estimation of bed load transport, while the suspended transport is calculated from Camenen and Larson's (2005, 2007, 2008) formula. The second approach is based on Soulsby-Van Rijn approximation (Soulsby 1997). This formula applies to total (bed and suspended load) sediment transport in combined waves and currents on sloping beds. Averaged sediment fluxes are obtained, by integrating the transport load over 50 wave periods. Furthermore, a slope limiting methodology is applied to control the maximum bottom slope, which is considered equal to the sediment repose angle (≈32 deg) (Bailard and Inman 1981).

3.1 Ribberink's and Camenen – Larson's methods

3.1.1 Bed load transport

Ribberink suggested a model of bed load transport where the solid flux is proportional to a function of the difference between the actual time-dependent bed shear stress and the critical bed shear stress. This formula is described by the following expression for the sand transport rate:

$$q_{SB} = m_{Rib}\sqrt{(s-1)gd^3}\left\langle \left(\left|\overrightarrow{\theta(t)}\right| - \theta_{cr}\right)^{n_{Rib}} \frac{\overrightarrow{\theta(t)}}{|\theta(t)|}\right\rangle \tag{1}$$

where, $\overrightarrow{\theta(t)} = 0.5 f_{cw}|u(t)|\overrightarrow{u(t)}/[(s-1)gd]$ is the time-dependent Shields parameter with the instantaneous velocity $\overrightarrow{u(t)} = \overrightarrow{U_c} + \overrightarrow{u_W(t)}$, s the relative density of sediment and f_{cw} the wave – current friction factor. $\langle\,\rangle$: time-averaged over several wave periods; and m_{Rib} = 11, n_{Rib} = 1.65: adjusted coefficients.

3.1.2 Suspended load transport

The Camenen and Larson (2005, 2007, 2008) transport rate formula is adopted for estimating suspended load. This formula is described by the following expression for the suspended load transport:

$$q_{SB} = U_C \frac{c_R \varepsilon}{W_s}\left[1 - e^{-\frac{W_s h}{\varepsilon}}\right] \tag{2}$$

where, $c_R = 3.51^{-3} e^{-0.3 d_*} \theta_{cw,m} e^{-4.5\frac{\theta_{cr}}{\theta_{cw}}}$ is the reference concentration at the bottom with $d_* = \sqrt[3]{(s-1)g/v^2} d_{50}$ the dimensionless grain size, v the kinematic viscosity of water, $\theta_{cw,m}$ and θ_{cw} the mean and maximum Shields parameters due to wave-current interaction and ε the sediment diffusivity.

3.2 Soulsby-Van Rijn's method

Soulsby-Van Rijn's formula (Soulsby, 1997) was derived for total (suspended and bed load) sediment transport in combined wave and currents on horizontal and sloping beds. This approach is described by the following expression for the sand transport rate:

$$q_t = A_s \bar{U} \left[\left(\bar{U}^2 + \frac{0.018}{C_D} U_{RMS}{}^2 \right)^{\frac{1}{2}} - \bar{U}_{CR} \right]^{2.4} (1 - 1.6 tan\beta) \tag{3}$$

where, $\boldsymbol{A_S = A_{SB} + A_{Ss}}$ with $\boldsymbol{A_{SB} = \frac{0.005h(\frac{d50}{h})^{1.2}}{[(s-1)gd_{50}]^{1.2}}}$ and $\boldsymbol{A_{SS} = \frac{0.012 d_{50} d_*^{-0.6}}{[(s-1)gd_{50}]^{1.2}}}$. $\boldsymbol{\bar{U}}$ is the depth averaged velocity, $\boldsymbol{U_{RMS}}$ the root-mean-square wave orbital velocity, $\boldsymbol{C_D}$ the drag coefficient due to current alone, $\boldsymbol{\bar{U}_{CR}}$ the threshold current velocity and $\boldsymbol{\beta}$ the bed slope.

4 RESULTS AND DISCUSSION

The sea bed evolution at the end of the accretive and erosive sequence using Ribberink's and Camenen – Larson's formulas is presented in Figure 3, while the results corresponding to the Soulsby's approximation are depicted in Figure 4. In Figure 5 alongshore-averaged beach profiles are demonstrated, as obtained using the two methods. It is observed that the numerical approximation performs reasonably well, as the erosive sequence is characterized by an offshore sediment movement while the sandbar is driven shoreward under accretive wave conditions. The obtained results show a good agreement between the two different applied methods, as the identified accretive and erosion areas in Figure 3 and in Figure 4 look similar. However, small discrepancies around the offshore zone are noticed during the accretion sequence. The intensity and direction of the wave-induced currents are determinant for the morphological changes of the sea bottom. The flow is characterized by a rip current, which has a shore-normal orientation and a magnitude of about 0.05 m/s and 0.1 m/s during the accretion and erosive sequence respectively. The intensity of the seaward current causes an offshore sandbar migration under energetic wave conditions. The mean circulations obtained during the experiments of Michallet et al. (2013) have a same mean flow magnitude but their directions are highly variable during each sequence. This is to some extent due to the imposed wave conditions of the experiment, where the wavemaker is designed to have a varying damping at the center of the wave front. Thus, the seabed alongshore nonuniformity obtained by the numerical simulation is more intense. Seabed changes at the end of each numerical simulation (Figure 5) are in the same order of magnitude with the measured ones (Figure 3), between -0.1 m and +0.1 m. Overall, a good agreement between both experimental and numerical results is achieved, as the seabed adapts correctly to the wave climate changes. Further numerical investigations are needed to investigate the transition from the dissipative to the reflective beach state and back again, considering the intermediate sub-states according to the work of Wright and Short (1984).

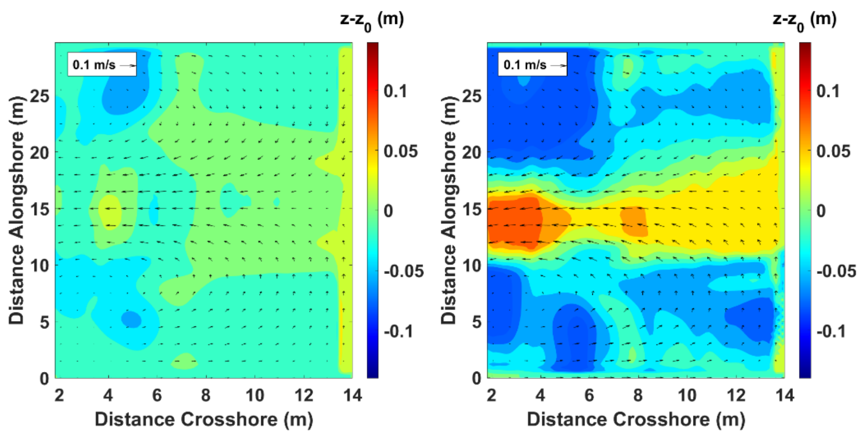

Figure 3 Map of bottom changes and associated mean flow field (vectors) at the end of the accretive (left) and at the end of the erosive sequence (right) using Ribberink's and Camenen – Larson's formulas.

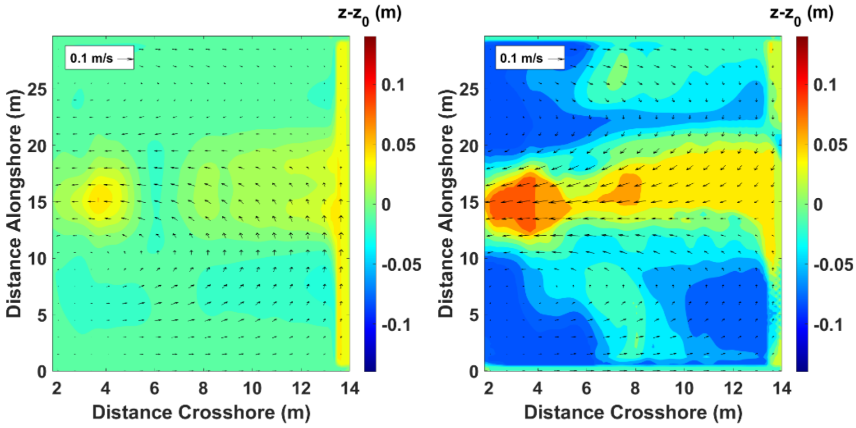

Figure 4 Map of bottom changes and associated mean flow field (vectors) at the end of the accretive (left) and at the end of the erosive sequence (right) using Soulsby's formula.

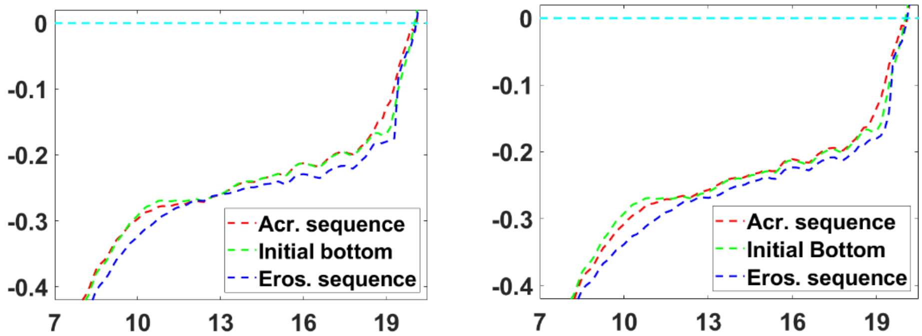

Figure 5 Alongshore-averaged beach profiles at the two main stages of the simulation using Soulsby's formula (left) and Ribberink's and Camenen – Larson's formulas (right).

References

Bailard JA, Inman DL (1981) An energetics bedload model for a plane sloping beach: local transport. Journal of Geophysical Research Atmosperes 86(C3) : 2035-2043. doi : 10.1029/JC086iC03p02035

Bonneton P, Bruneau N, Castelle B, Marche F (2010) Large-scale vorticity generation due to dissipating waves in the surf zone. Discrete and Continuous Dynamical Systems - Series B 13(4):729-738. doi:10.3934/dcdsb.2010.13.729

Camenen B, Larroudé P (2003) Comparison of sediment transport formulae for the coastal environment. Coastal Engineering 48(2): 111-132. doi:10.1016/S0378-3839(03)00002-4

Camenen B, Larson M. (2005) A general formula for non-cohesive bed load sediment transport. Estuarine, Coastal and Shelf Science 63(1-2): 249-260. doi:10.1016/j.ecss.2004.10.019

Camenen B, Larson M (2007) A unified sediment transport formulation for coastal inlet application. Technical report ERDC/CHL CR-07-1. US Army Engineer Research and Development Center. Vicksburg, MS

Camenen B, Larson M (2008) A general formula for noncohesive suspended sediment transport. Journal of Coastal Research 24(3): 615-627. doi: 10.2112/06-0694.1

Fredsøe J, Deigaard R (1992) Mechanics of coastal sediment transport. World Scientific, Singapore

Marche F, Bonneton P (2007) A simple and efficient well-balanced model for 2DH bore propagation and run-up over a sloping beach. Paper presented at the 30th International Conference of Coastal Engineering, World Scientific, Singapore

Marche F, Bonneton P, Fabrie P, Seguin N (2007) Evaluation of well-balanced bore-capturing schemes for 2D wetting and drying processes. International Journal for Numerical Methods in Fluids 53(5): 867-894. doi:10.1002/fld.1311

Michallet H, Castelle B, Barthélemy E, Berni C, Bonneton P (2013) Physical modeling of three-dimensional intermediate beach morphodynamics. J. Geophys. Res. Earth Surf. 118(2): 1045–1059. doi:10.1002/jgrf.20078

Nielsen P (1992) Coastal bottom boundary layers and sediment transport. World Scientific, Singapore
Ribberink JS (1998) Bed-load transport for steady flows and unsteady oscillatory flows. Coastal Engineering 34(1-2): 59-82. doi: 10.1016/S0378-3839(98)00013-1
Soulsby R (1997) Dynamics of marine sands: a manual for practical applications. Thomas Telford, London
Sleath JFA (1984) Sea bed mechanics. Wiley, New York.
Van Rijn LC (1993). Principles of sediment transport in rivers, estuaries, and coastal seas. Aqua Publications, The Netherlands
Van Rijn LC (2007) Principles of sediment transport in rivers, estuaries, and coastal seas. Aqua Publications, The Netherlands
Wang JY, Tang HS, Fang HW (2013) A fully coupled method for simulation of wave-current-seabed systems. Communications in Nonlinear Science and Numerical Simulation, 18(7): 1694-1709
Wright LD, Short AD (1984) Morphodynamic variability of surf zones and beaches: A synthesis. Marine Geology 56(1-4): 93-118. doi: 10.1016/0025-3227(84)90008-2

Numerical simulation of berm and dune erosion, cross-shore profile evolution and scour in front of breakwaters using OpenFOAM

N. Karagiannis*, Th. Karampas, C. Koutitas

Department of l Civil Engineering, Aristotle University of Thessaloniki, Thessaloniki, 54124, Greece
*Corresponding author: nkarag@civil.auth.gr

Abstract

A challenging approach to sediment transport numerical simulation is hereby presented following authors' previous works, (Karagiannis et al. 2016, 2017) and concerns the numerical simulation of berm and dune erosion due to wave overtopping and sediment overwash and the cross-shore profile evolution under breaking waves, as well as the scour prediction in front of vertical breakwaters. A repetitive approach of coupling two numerical models, a hydrodynamic one, synthesized on the OpenFOAM platform and a morphodynamic one developed in FORTRAN, is used here. The former is used for the wave propagation, while the latter one yields the new cross-shore seabed formation using the results of the first model. The above process is repeated until the equilibrium profile is achieved.

Keywords Cross-shore profile evolution, Dunes erosion, OpenFOAM, Numerical simulation.

1 INTRODUCTION

The influence of hydrodynamic processes to the seabed morphological evolution in the coastal zones is of great research interest while waves propagation being the main culprit behind any morphological changes of the seabed. Either breaking waves propagating over the surf and swash zones, or standing waves formation in front of coastal structures, can have devastating effects to the beach and the coastal structures respectively. Nourishment projects with wide berms and high dunes can shield the coastal areas against storms, but in case of a storm event these formations can be completely eroded. Hence, the prediction of the morphological evolution of the seabed is of great importance, as it can provide with substantial information for the accurate design of the preventing solutions. The numerical models constitute a great tool to that purpose, once properly developed and validated.

A challenging approach of coupling two numerical models has been developed and implemented here, following authors' previous works (Karagiannis et al., 2016, 2017). First, a hydrodynamic numerical model, synthesized on the OpenFOAM platform, has been developed and implemented for the wave propagation, while a second one, developed in FORTRAN, has been implemented to predict the sediment transport and morphological evolution of the seabed, using the hydrodynamic results of the first model. The method used in this work is iterative. The new bathymetry, which is the result of the second model, is used by the first model and this process is repeated until convergence, namely morphological equilibrium of the seabed.

The numerical results are compared satisfactorily to experimental data for the cases of berm and dune erosion (Figlus et al. 2011), cross-shore profile evolution (Dette et al. 1998) and scour in front of vertical breakwater (Xie 1981), while validation of the hydrodynamic model is presented as well (Roeber 2010).

2 HYDRODYNAMIC MODEL - GOVERNING EQUATIONS

This section provides the governing equations of the hydrodynamic mathematical model, which is synthesized on the OpenFOAM basis and solves the Reynold Averaged Navier – Stokes (RANS) equations numerically using the Finite Volume Method. Free surface is tracked by the VOF method, while the k-ω SST turbulence model, (modified from the one in OpenFOAM libraries, so that the density will be included in the equations), is used for the simulation of the turbulence effects.

2.1 Continuity and RANS equations

The mathematical model solves the continuity equation along with RANS equations, as follows:

$$\frac{\partial U_{\mathrm{i}}}{\partial \mathrm{x}_{\mathrm{i}}}=0 \tag{1}$$

$$\frac{\partial(\rho \mathrm{U}_{\mathrm{i}})}{\partial \mathrm{x}_{\mathrm{i}}}+\rho U_{\mathrm{j}}\frac{\partial U_{\mathrm{i}}}{\partial \mathrm{x}_{\mathrm{j}}}=-\frac{\partial \mathrm{p}}{\partial \mathrm{x}_{\mathrm{i}}}+\rho \mathrm{g}_{\mathrm{i}}+\frac{\partial}{\partial \mathrm{x}_{\mathrm{j}}}\left[\mu\left(\frac{\partial U_{\mathrm{i}}}{\partial \mathrm{x}_{\mathrm{j}}}+\frac{\partial U_{\mathrm{j}}}{\partial \mathrm{x}_{\mathrm{i}}}\right)-\rho\overline{u_i{}'u_j{}'}\right]+\sigma_T \kappa_\gamma \frac{\partial \gamma}{\partial \mathrm{x}_{\mathrm{i}}} \tag{2}$$

where U is the velocity, ρ is the density, g is the gravity acceleration, p is the pressure, μ is the dynamic viscosity, and $-\rho\overline{u_i{}'u_j{}'}$ is the Reynolds stress tensor. The last term in equation (2) represents the surface tension effect.

2.2 Volume of fluid (VOF) equations

Volume of fluid method (Hirt and Nichols, 1981) is provided by OpenFOAM for the "tracking" of the free surface. According to this method, each free surface computational cell is divided in two parts, one representing the air volume and the other equal to water volume. The calculation of the water-air portion in every cell is possible with the help of the scalar quantity γ, with its value fluctuating between 0 and 1, depending on the content of the cells and is given by:

$$\frac{\partial \gamma}{\partial t}+\frac{\partial(\gamma \mathrm{U}_{\mathrm{i}})}{\partial \mathrm{x}_{\mathrm{i}}}+\frac{\partial[\gamma(1-\gamma)\mathrm{U}r_{\mathrm{i}}]}{\partial \mathrm{x}_{\mathrm{i}}}=0 \tag{3}$$

where U_r is a relative velocity and the quantities like density or viscosity are now given by:

$$\rho=\gamma\rho_{water}+(1-\gamma)\rho_{air}, \quad \mu=\gamma\mu_{water}+(1-\gamma)\mu_{air} \tag{4}$$

2.3 Turbulence modelling

The transport equations for the k-ω SST model are as follows (Menter F. R., 1993-1994):

$$\mu_t=\frac{\rho\alpha_1 k}{\max(\alpha_1\omega, S\mathrm{F}_2)} \tag{5}$$

$$\frac{\partial(\rho k)}{\partial t}+\frac{\partial(\rho k U_i)}{\partial x_i}=P_k-\beta^*\rho k\omega+\frac{\partial}{\partial \mathrm{x}_i}\left[(\mu+\sigma_k\mu_t)\frac{\partial k}{\partial \mathrm{x}_i}\right] \tag{6}$$

$$\frac{\partial(\rho\omega)}{\partial t}+\frac{\partial(\rho\omega U_i)}{\partial x_i}=\alpha S^2-\beta\rho\omega^2+\frac{\partial}{\partial \mathrm{x}_j}\left[(\mu+\sigma_\omega\mu_t)\frac{\partial \omega}{\partial \mathrm{x}_j}\right]++2(1-\ \mathrm{F}_1)\rho\sigma_{\omega 2}\frac{1}{\omega}\frac{\partial k}{\partial x_i}\frac{\partial \omega}{\partial x_i} \tag{7}$$

where k is the turbulent kinetic energy and ω is the dissipation rate. The rest coefficients are given in literature.

2.4 Wave generation and absorption

The wave theories applied to the respective experiments have been implemented through the additional toolbox waves2Foam. Moreover, sponge layers from waves2Foam libraries are implemented at the left and right end of the computational domain in order to avoid wave reflection which would affect the numerical results (wave absorption).

The wave attenuation at the sponge layers is described by the following equation:

$$a_R(\chi_R)=1-\frac{\exp(\chi_R^{3.5})\, ibed\ -1}{\exp(1)-1} \quad \gamma\iota\alpha\ \chi_R\in[0;1] \tag{8}$$

where the α_R is used in the following equation:

$$\varphi=a_R\varphi_{computed}+(1-a_R)\,\varphi_{target} \tag{9}$$

where φ may be the velocity or the quantity γ from the VOF equation.

3 MORPHODYNAMIC MODEL - GOVERNING EQUATIONS

The mode of sediment movement on the coast is usually divided into bed load, suspended load and sheet flow transport. The bed load transport (q_b or the non-dimensional Φ_b) is estimated with a quasi-steady, semi-empirical formulation, developed by Camenen, and Larson, (2007):

$$\Phi_b = \begin{cases} \dfrac{q_{b,w}}{\sqrt{(s-1)gd_{50}^3}} = a_w \dfrac{\theta_{cw,net}}{\sqrt{|\theta_{cw,net}|}} \theta_{cw,m} exp\left(-b_w \dfrac{\theta_{cr}}{\theta_{cw}}\right) \\ \dfrac{q_{b,n}}{\sqrt{(s-1)gd_{50}^3}} = a_n \dfrac{\theta_{cn}}{\sqrt{|\theta_{cn}|}} \theta_{cw,m} exp\left(-b_w \dfrac{\theta_{cr}}{\theta_{cw}}\right) \end{cases} \tag{10}$$

where the subscripts *w* and *n* correspond, respectively, to the wave direction and the direction normal to the wave direction, s $(= \rho_s/\rho)$ is the relative density, d_{50} the median grain size, a_w, a_n and b are empirical coefficients (Camenen and Larson 2007), $\theta_{cw,m}$ and θ_{cw} the mean and maximum Shields parameters due to wave-current interaction, θ_{cn} the current-related Shields parameter in the direction normal to the wave direction, and θ_{cr} the critical Shields parameter for the inception of transport. All parameters are calculated and presented by Camenen and Larson (2007). Phase-lag effects in the sheet flow layer are taken into account in $\theta_{cw,net}$ calculation.

The suspended sediment load (q_s) can be obtained (Camenen and Larson 2007):

$$q_{s,w} = U_{cw,net}\, c_R \frac{\varepsilon}{w_s}\left[1 - exp\left(-\frac{w_s d}{\varepsilon}\right)\right] \tag{11}$$

$$q_{s,n} = U_c sin\varphi\, c_R \frac{\varepsilon}{w_s}\left[1 - exp\left(-\frac{w_s d}{\varepsilon}\right)\right] \tag{12}$$

where c_R is the reference concentration at the bottom, ε the sediment diffusivity, w_s the sediment fall and $U_{cw,net}$, the net mean current (wave-current interaction). Finally, following the calculation of sediment transport rates, the conservation of sediment transport is applied (Leont'yev, 1996):

$$\frac{\partial z_b}{\partial t} = -\frac{\partial}{\partial x}\left(q_x - \varepsilon_{slope}|q_x|\frac{\partial z_b}{\partial x}\right) - \frac{\partial}{\partial y}\left(q_y - \varepsilon_{slope}|q_y|\frac{\partial z_b}{\partial y}\right) \tag{13}$$

where z_b is the local bottom elevation and $q_x(=q_{s,x}+q_{b,x})$, q_y $(=q_{s,y}+q_{b,y})$ are the volumetric sediment transport rates in *x* and *y* horizontal directions respectively and ε_{slope} coefficient related to the slope.

4 RESULTS – DISCUSSION

4.1 Solitary wave over exposed sloping reef (comparison with Roeber et al. 2010)

The implemented geometry is presented in Fig.1 according to Roeber et al. (2010) experiment, with a *1/12* reef slope, *20cm* reef crest exposed by 6cm over the still water level and then submerged by *14cm* flat bed. The depth is *2,5m* while a solitary wave of *0,75m* amplitude is generated at the inlet with cyclic boundary condition. As depicted in Fig.1, the numerical results for surface elevation match satisfactorily the experimental data (2 instantaneous surface elevation results are depicted in Fig.1 before and after breaking).

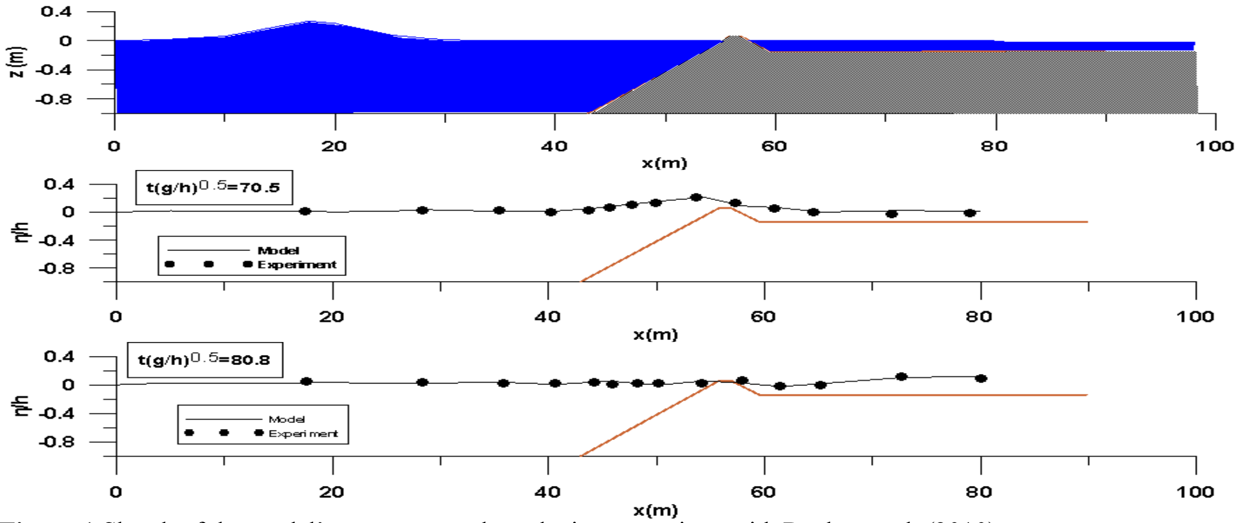

Figure 1 Sketch of the model's geometry and results in comparison with Roeber et al. (2010)

4.2 Berm and dunes profile evolution – erosion (comparison with Figlus et al. 2011)

The implemented geometry is presented according to Figlus et al. (2011) experiment, for the berm and dune (BD) case as depicted in Fig.2, where the flume section was *23m* long and *1.15m* wide with a low-crested vertical wall at the landward end. Irregular waves of Jonswap spectrum with H_{mo}*=0,19m* and T_p*=2,6sec* at *1m* depth were implemented, while the specific density and porosity of the sediment is *2,5 and 0,4* respectively and the fall velocity *2cm/sec*. Fig.2 shows the comparison between the numerical results and the experimental ones (Figlus et al. 2011) at 3 different phases, which is quite satisfactory. The initial slope is depicted with the grey solid line, the computed results with blue line and the experimental ones with triangular symbols and dashed grey line.

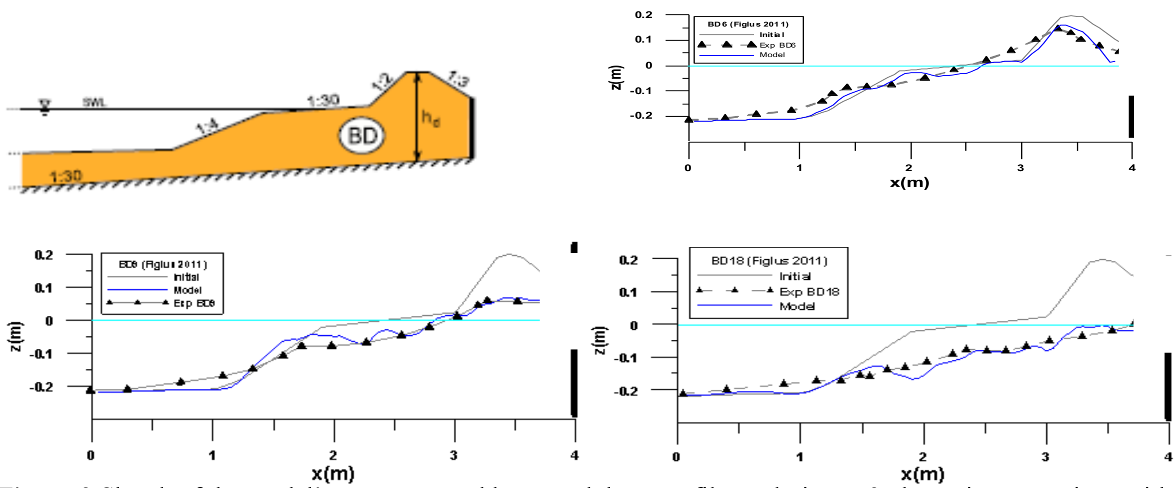

Figure 2 Sketch of the model's geometry and berm and dune profile evolution at 3 phases in comparison with Figlus et al. (2011)

4.3 Cross-shore profile evolution (comparison with Figlus et al. 2011)

A Jonswap wave spectrum was applied with $H_{m0}=1.20m$ and $T_m=5.5s$ at *5m* depth (storm water level) as per the wave characteristics of the SAFE B2 experiment in order to compare the morphodynamic numerical results with the experimental data. The sediment properties are $d_{50}=300\mu m$ and a fall velocity of $w_f=0.042m/sec$. According to Fig.3, the implemented slope is *1:10* for the B2 experiment, while the initial one is given by *h=0.12x2/3*. The numerical results are compared satisfactorily with experimental data (Figure 3).

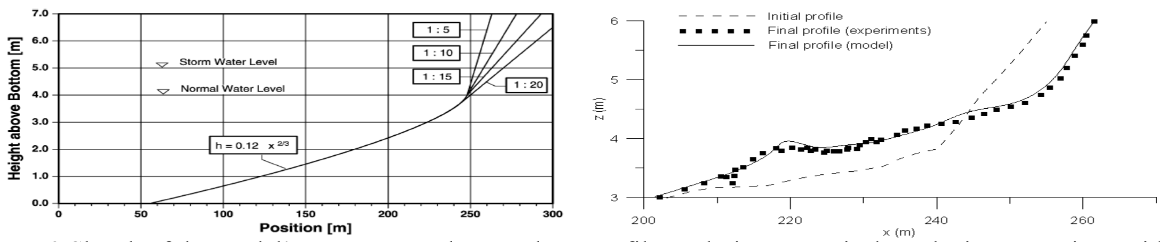

Figure 3 Sketch of the model's geometry and cross-shore profile evolution numerical results in comparison with Dette et al. (2011) SAFE B2 experiment

4.4 Scour in front of vertical breakwater (comparison with Xie 1981)

The implemented geometry is according to Xie (1981) experiment, as depicted in Fig.4, where an initial slope of *1:30* is implemented and the water depth is *30cm* in front of breakwater. Cnoidal waves of *H=0.05m* and *T=1,17sec* were applied, while the grain size is $D_{50} = 0.106mm$. Figure 4 shows the instantaneous surface elevation at *t=29,86sec* as well as the corresponding velocity vectors, with the formation of the standing wave being clear. The scour was found numerically at *1,3cm*, which matches Xie (1981) experiment (Fig.4).

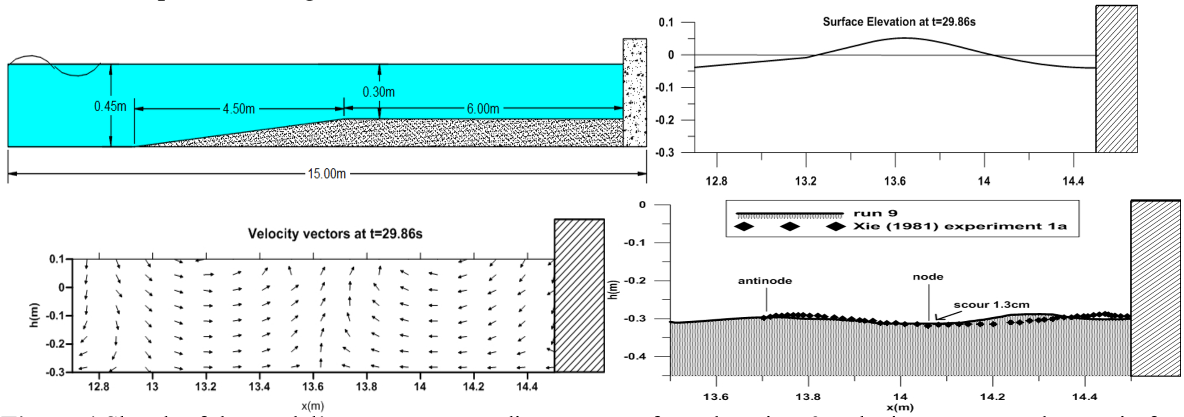

Figure 4 Sketch of the model's geometry, standing wave surface elevation & velocity vectors and scour in front of breakwater results in comparison with Xie (1981) 1a. experiment

References

Camenen B., Larson M. (2007): A unified sediment transport formulation for coastal inlet application, Technical report ERDC/CHL CR-07-1, US Army Engineer Research and Development Center, Vicksburg, MS.

Dette H.H., Peters K. and Newe J. (1998). ″ Large wave flume experiment '96/97.″ MAST III – SAFE Project, Report No. 825.

Figlus J., Kobayashi N., Gralher C., Iranzo V. (2011): Wave-induced Overwash and Destruction of Sand Dunes, Proceedings of 32nd Coastal Engineering Conference, Sediment, 34, 113

Hirt C.W. & Nichols B.D. (1981). "Volume of fluid (VOF) method for the dynamics of free boundaries", Journal of Computational Physics, 39 (1), 201-225.

Jacobsen N., Fuhrman D., Fredsøe J. (2012): A Wave Generation Toolbox for the Open-Source CFD Library: OpenFoam. Int. J. Numerl. Meth. Fluids, 70(9): 1073–1088.

Karagiannis N., Karampas T., Koutitas C. (2016): Numerical simulation of cross-shore profile evolution using OpenFoam, Coastal Engineering Proceedings (ICCE 2016), n.35, p. sediment 22

Karagiannis N., Karampas T., Koutitas C. (2017): Numerical simulation of sediment transport in surf and swash zones using OpenFoam, Proceedings of Coastal Dynamics 2017, n.26, 1747-1757

Karagiannis N., Karambas T., Koutitas C. (2016). "Numerical simulation of scour in front of a breakwater using OpenFoam", Proc 4th IAHR Europe Congress, 27 - 29 July, 2016, Liege, Belgium, 309-315

Menter, F.R. (1993). "Zonal Two Equation k-ω Turbulence Models for Aerodynamic Flows", *AIAA Paper,* 93-2906.

Menter, F.R. (1994). "Two-Equation Eddy-Viscosity Turbulence Models for Engineering Applications", *AIAA Journal*, vol. 32, no 8. pp. 1598-1605.

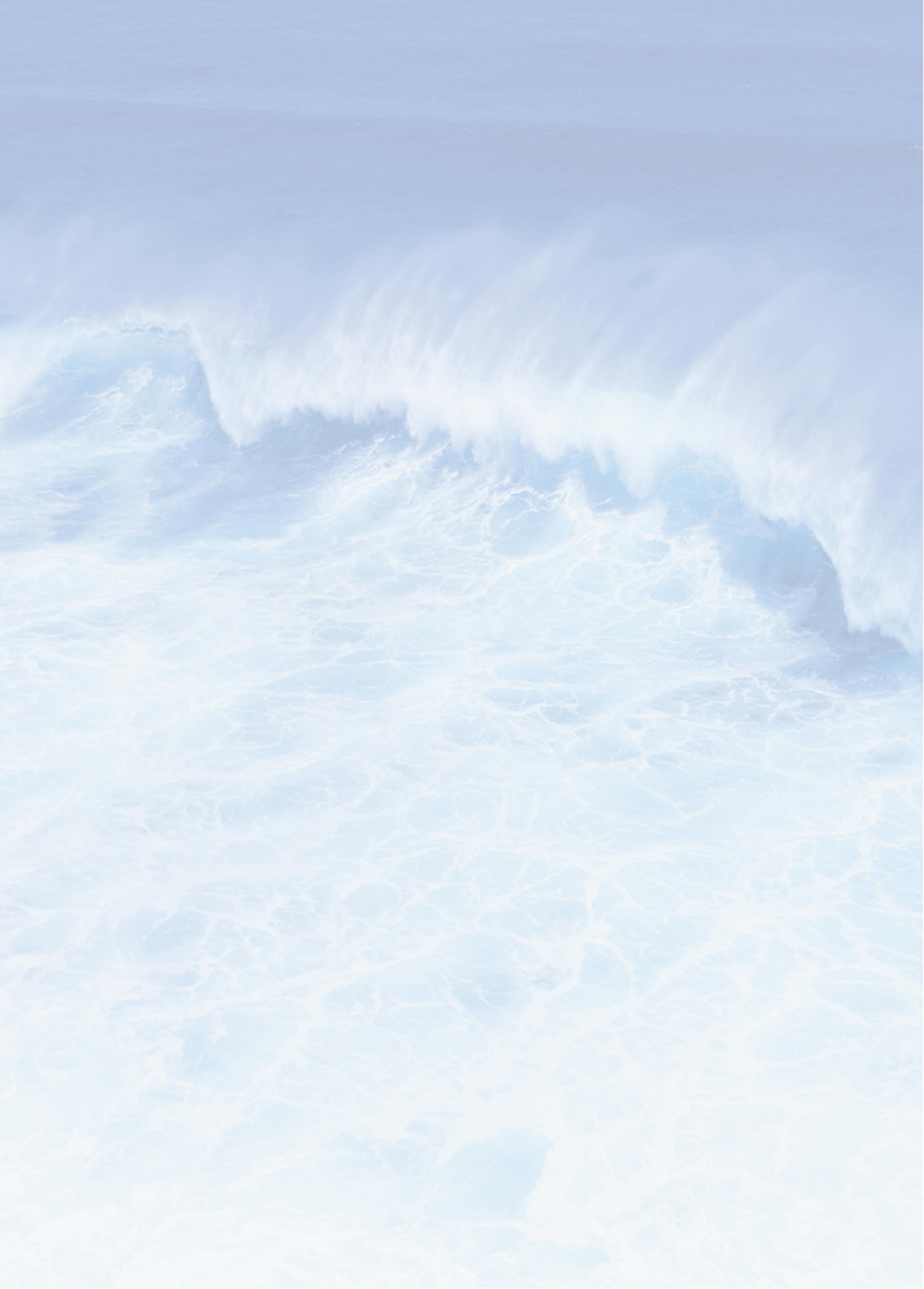

An investigation of the morphodynamic evolution of Oroklini beach in Cyprus via an innovative semi-analytical solution to the One-Line model

A. Valsamidis[1,*], C. Michailides[2], G.C. Georgiou[2]

[1]College of Engineering, Swansea University, Swansea, Wales, SA1 8EN, UK
[2] Department of Civil Engineering and Geomatics, Cyprus University of Technology, Limassol, 3036, Cyprus
[3] Department of Mathematics and Statistics, University of Cyprus, Cyprus, Nicosia, 20537, Cyprus
[*]Corresponding author: antonios.valsamidis@swansea.ac.uk

Abstract

Semi-analytical solutions to the One-Line model may be applied to assess the shoreline evolution of complicated coastal systems. In this work, Oroklini beach in Cyprus, which suffers from erosion problems, was firstly simulated via a simple semi-analytical model suitable for assessing morphodynamic evolution in groyne compartments and results confirmed the beach erosion occurring in this area. Then, a more sophisticated semi-analytical model which includes successive groyne compartments and may be used for the investigation of the performance of groyne-fields was developed and consequently applied in Oroklini beach considering a hypothetical impermeable groyne in the middle of the shorefront. In this case, the simulation that took place showed that the erosion phenomenon in Oroklini beach had significantly been mitigated.

Keywords One-Line model, Beach erosion, Semi-analytical model, Groyne.

1 INTRODUCTION

1.1 Erosion problems in Cyprus

Coastal zones are socially and economically very important especially for Cyprus where economic growth has been mostly based on activities that take place close to the coastal areas. At the same time and apart from human interventions, these zones are subjected to several environmental hazards and wave action, which may cause coastal erosion. Specifically, 20% of the total length of Cyprus shorelines which is 92,338 m, has suffered due to erosion an average retreat of 14.0 meters during the last 50 years (the maximum observed erosion was equal to 260 m). Thus, prediction and quantification of the morphodynamic evolution of coastal areas is important for coastal management decisions and the investigation of the performance of different coastal defence schemes that potentially could be applied.

1.2 The One-Line model

The One-Line model is a process-based shoreline model which can be used for predicting beach evolution, and has been proved to be a successful tool for Coastal Engineering applications during the last three decades. Its main advantages are the low requirement of input-data and the high computational efficiency. Specifically, the knowledge of some surveyed historical shoreline positions corresponding a specific case-study, and the related recorded wave-data, is sufficient for applying the model. On the other hand, detailed modeling techniques incorporated into widely used software packages, for instance, DELFT 3D or MIKE, require a significantly larger amount of input-data, including full bathymetry with respect to a particular case-study, and in addition, long computational times for assessing the corresponding beach morphodynamic evolution.

The One-Line model was firstly developed by Pelarnd-Considere (1956) for the analytical assessment of shoreline evolution near a groyne which is caused by constant wave forcing. It is based on the continuity of mass equation and an equation which describes the longshore sediment movement (for instance, CERC 1984; Kamphuis 2000; or Bayram et al. 2007). A fundamental assumption of the One-Line model theory is that the bathymetric contours move parallel to the shoreline and the longshore sediment movement takes place up to a specific depth, namely, the depth of closure.

Solutions to the One-Line model can be either analytical or numerical. Analytical methods incorporate some assumptions, like small wave angle relatively to the shoreline orientation, a smooth shoreline curve and constant wave forcing (e.g. Valsamidis and Reeve 2017). The combination of these assumptions with the continuity of mass equation and a longshore sediment transport formula, yields the diffusion equation (Equation 1):

$$\frac{\partial y}{\partial t} = \varepsilon \frac{\partial^2 y}{\partial x^2} \qquad (1)$$

where ε is the diffusion coefficient; x is the longshore distance on an axis X parallel to the shore normal; and y is the vertical distance on a Y axis corresponding to the shoreline position.

The diffusion equation (Equation 1) can be solved analytically considering specific initial and boundary conditions. This way, solutions to the One-Line model can be produced describing the shoreline evolution of particular coastal systems that are under investigation.

Analytical methods are limited to theoretical and oversimplified case-studies. On the other hand, numerical solutions to the One-line model are not restricted by the aforementioned assumptions. Thus, they can be used to simulate realistically more complicated coastal systems. In this work, analytical solutions to the One-Line model will be presented which are evaluated for all but the simplest cases numerically. For this reason, they are termed 'semi-analytical'. Contrary to the analytical solutions, the semi-analytical ones can incorporate time-varying wave data and are capable of assessing more complicated coastal systems than the analytical solutions can do. An application of semi-analytical solutions will be presented with respect to Oroklini beach in Cyprus. Oroklini beach is presented in the following section.

2 CASE-STUDY

The construction of Larnaca port has caused a general erosive trend to its north-east side. A part of this coastal system will be studied in this work, which lies about 3 km away of Larnaca port and is near to Oroklini area (Figure 1):

Figure 1 The location of the case-study relatively to Larnaca Port.

The section of Oroklini beach under study extends *1150m* north-eastwards of a revetment up to a groyne near hotel 'Lenios' (Figure 2). Oroklini beach is a touristic resort where water sports take place. The seabed cross-shore slope is about 1%.

Figure 2 Eastern and western boundaries of the case-study.

3 METHODOLOGY

The area under investigation is regarded as a groyne compartment since it is confined between two structures, namely a revetment and a groyne (Figure 2). Both structures are assumed to totally block sediment movement along the shore, thus the case-study is considered isolated from the lateral coastal areas. As the available surveyed historical shoreline data indicate an erosion trend along the shore except for the beach section near the groyne where an accretional trend prevails, the performance of a coastal defence scheme that could potentially mitigate the observed erosion phenomenon, was investigated, specifically, a groyne placed in the middle of this beach section. Therefore, a more sophisticated semi-analytical model is introduced which is a combination of the simpler semi-analytical solution to the One-Line model by Zacharioudaki and Reeve (2008) so as a groyne-field to be developed, via the deployment of the right internal boundary condition (Figure 3):

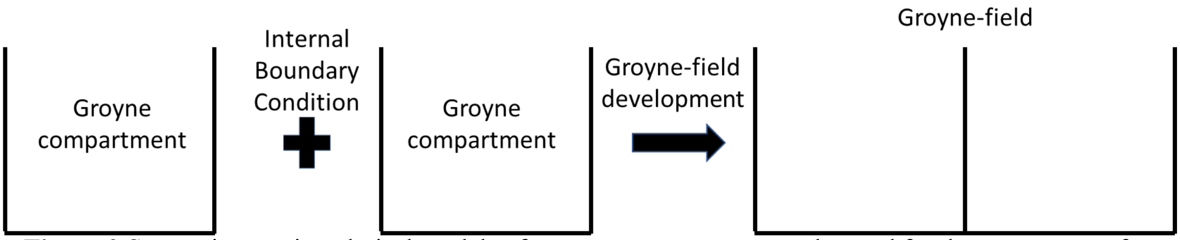

Figure 3 Successive semi-analytical models of groyne compartments can be used for the assessment of a groyne-field.

Two surveyed historical shoreline positions in 2014 and 2018, respectively, were available for the simulation process, plus wave data corresponding to the time period: 2014-2018.

4 RESULTS

Initially, Oroklini beach was simulated as a groyne compartment via the semi-analytical solution by Zacharioudaki and Reeve (2008); results are presented in Figure 4 and are in agreement with the general observations which were conducted by other Coastal Engineers regarding this area (e.g. Rogan and Associates, 2012). According to these observations an accretion trend is identified near the groyne on the left-hand side of the case-study (Figure 4), while an erosion trend is dominant along the rest shorefront. It is worth noting that the surveyed shoreline position in 2018 shows an accretion trend in the middle of the case-study. This phenomenon might imply coastal processes that evolve in a small time-scale and have no apparent effect over a long period of time.

Then, an impermeable groyne which permits sediment bypassing at the tip of its offshore-ward tip was hypothetically applied *575m* away from the left boundary of the case-study, dividing this way the beach into two groyne compartments, and the new semi-analytical model was consequently applied. Results are presented in Figure 5.

From Figure 5 it is obvious that the presence of an internal groyne at *x=575m* had as an effect the mitigation of the erosion phenomenon on the right-hand side groyne compartment to the degree that it was almost eliminated. Regarding the left-hand side groyne compartment, an expected erosion trend occurred on the downdrift side of the internal groyne, while accretion appeared on the left boundary of the case-study.

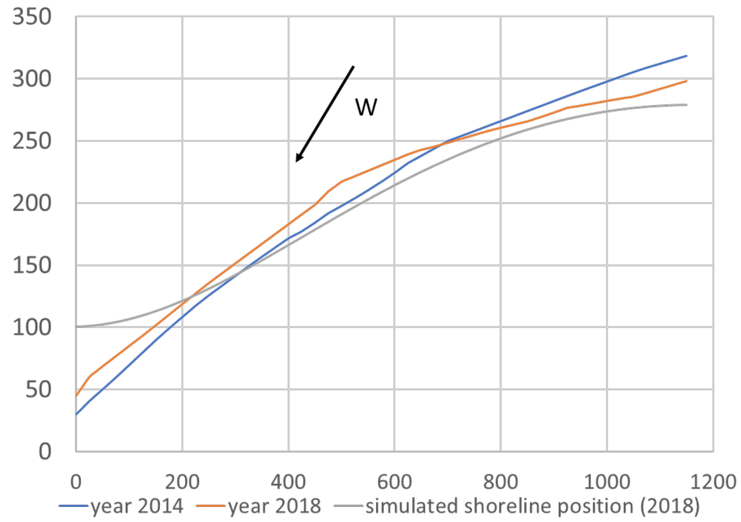

Figure 4 Simulation of Oroklini shoreline in the time-period 2014-2018. The predominant wave direction is noted.

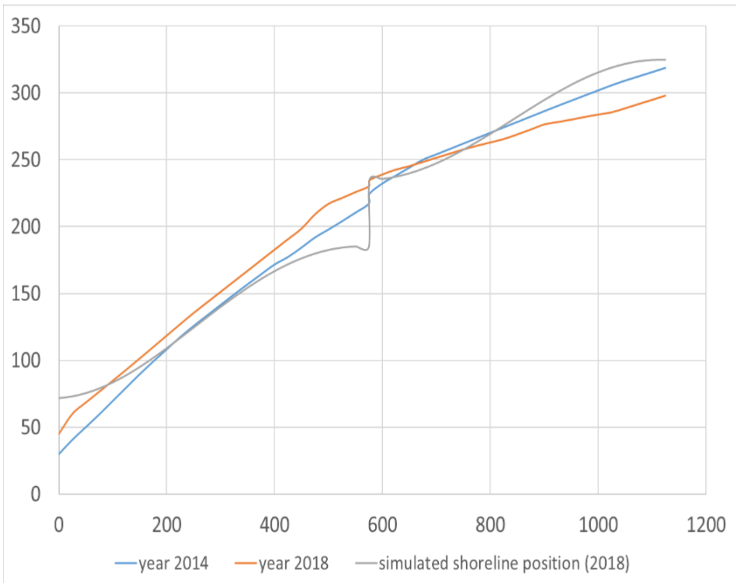

Figure 5 Simulation of Oroklini shoreline in the time-period 2014-2018, considering a groyne at $x=575m$.

5 DISCUSSION - CONCLUSIONS

The morphodynamic evolution of Oroklini beach was initially simulated via a semi-analytical solution to the One-Line model (Zacharioudaki and Reeve 2008), which has been specifically developed for assessing the shoreline evolution in groyne compartments. Then, a more sophisticated semi-analytical model was introduced which is capable of assessing successive groyne compartments that form a groyne-field. The latter model can be used for investigating the performance of groyne-fields. The application of the new model in Oroklini beach, taking into account a hypothetical groyne in the middle of the coastline had as a result the mitigation of the erosion phenomenon which occurs along the shore, except for the downdrift side of the internal groyne.

Aiming at further developing the new semi-analytical model, and subsequently, describing in a more accurate and realistic way a variety of different coastal systems, the simpler semi-analytical solution to the One-Line model regarding shoreline evolution in a beach section which is restricted by a groyne on the one side while the other side extends to a theoretically infinite distance (Reeve 2006), will be incorporated into the new model.

The semi-analytical solutions that were presented in this work cannot be considered a substitute to numerical modeling. However, they may be used for validating numerical models for simplified cases before the latter are applied considering the full complexity of the coastal system under investigation (Hanson and Kraus 1989).

References

Bayram, A, Larson, M and Hanson H (2007) A new formula for the total longshore sediment transport rate. Coastal Engineering, 54:700-710. doi:10.1016/j.coastaleng.2007.04.001.

CERC (1984) Shore protection manual. U. S., Corps of Engineers, Vicksburg.

Hanson, H, and Kraus, NC (1989) Genesis: Generalized Model For Simulating Shoreline Change. U. S., Corps of Engineers, Vicksburg.

Kamphuis, JW (2000) Introduction to coastal engineering and management. World Scientific Publishing Co. Pte. Ltd, Kingstone.

Pelnard-Considere, R (1956) Essai de theorie de l’evolution des forms de rivages en plage de sable et de galets. Societe Hydrotechnique de France, Proc., 4th Journees de l’Hydraulique, les Energies de la Mer, Question III, Rapprot No. 1, 289–298 (in French).

Reeve, DE (2006) Explicit Expression for Beach Response to Non-Stationary Forcing near a Groyne. Journal of Waterway, Port, Coastal, and Ocean Engineering, 132:125-132. doi: 10.1061/(ASCE)733-950X(2006)132:2(125).

Rogan and Associates (2012) Ακτομηχανική Διερεύνηση με μαθηματικά ομοιώματα στα πλαίσια της μελέτης προστασίας και βελτίωσης της ακτής του παραλιακού μετώπου λιμένα Λάρνακας – Διυλιστηρίων Ορόκλινης, NTUA, Athens (in Greek).

Valsamidis, A and Reeve, DE (2017) Modelling shoreline evolution in the vicinity of a groyne and a river. Journal of Coastal Research: 410 - 415. doi: 10.1016/j.csr.2016.11.010.

Zacharioudaki, A, and Reeve, DE, (2008) Semianalytical Solutions of Shoreline Response to Time-Varying Wave Conditions. Journal of Waterway, Port, Coastal, and Ocean Engineering, 134: 265-274. doi: 10.1061/(ASCE)0733-950X(2008)134:5(265).

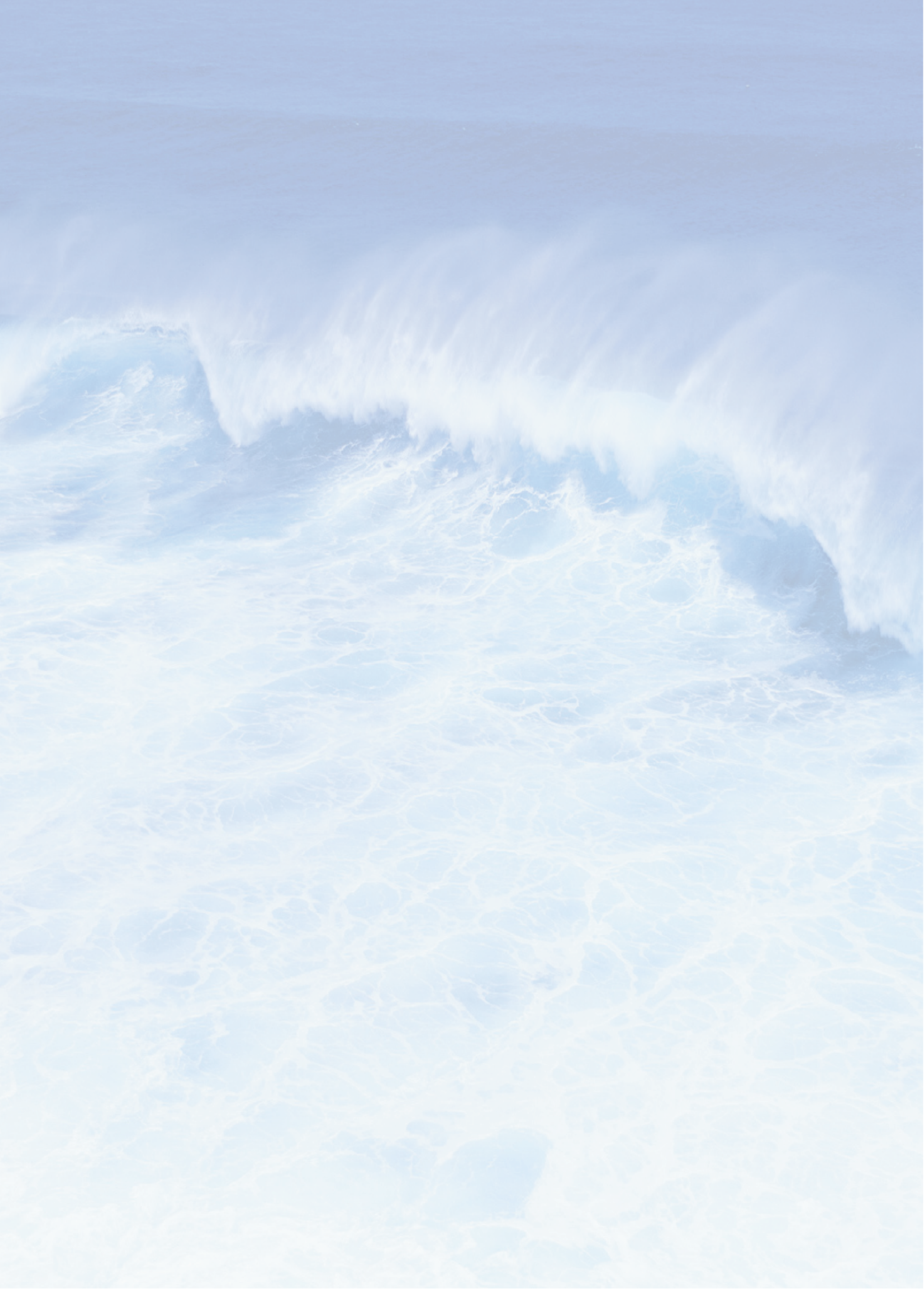

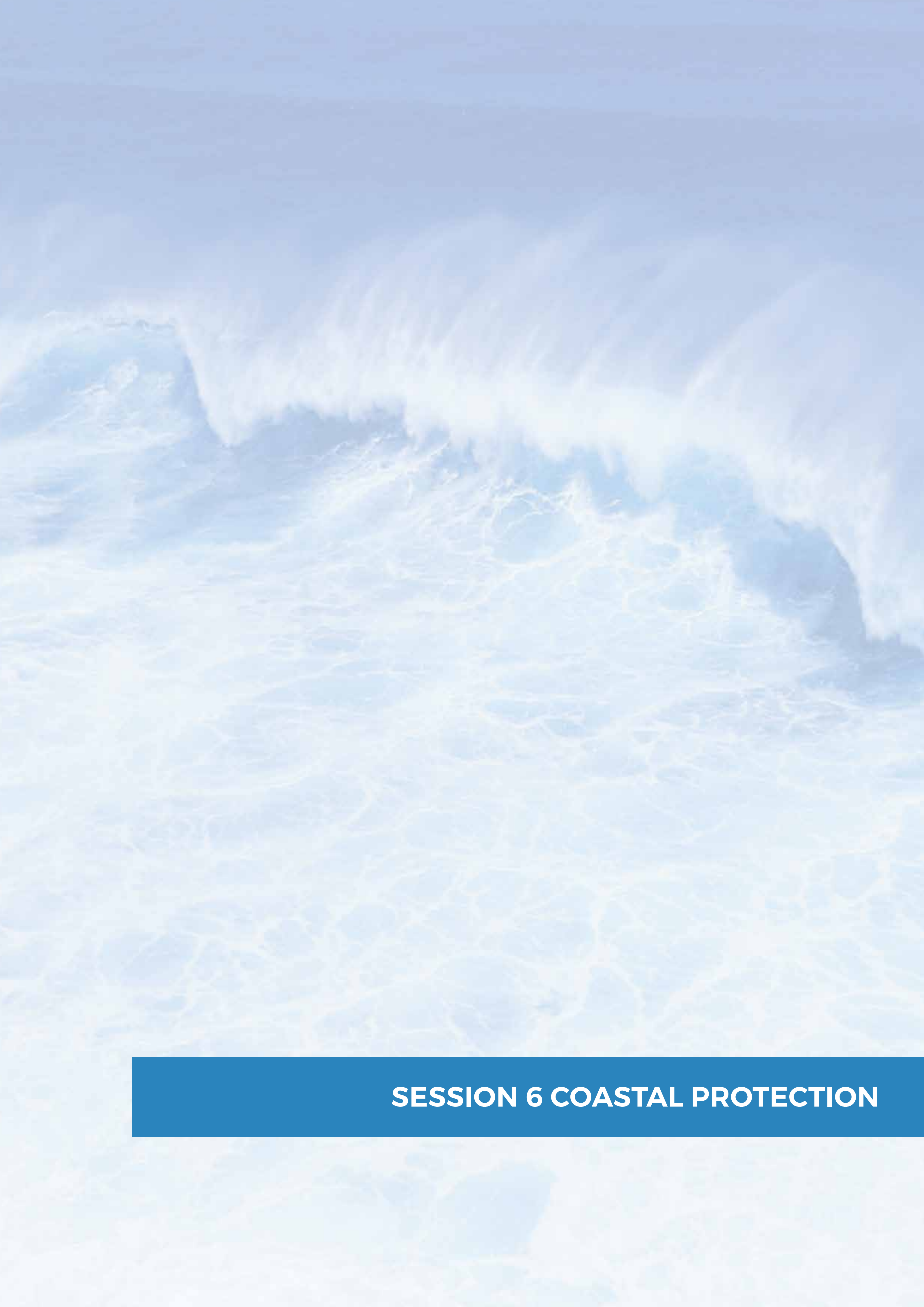

SESSION 6 COASTAL PROTECTION

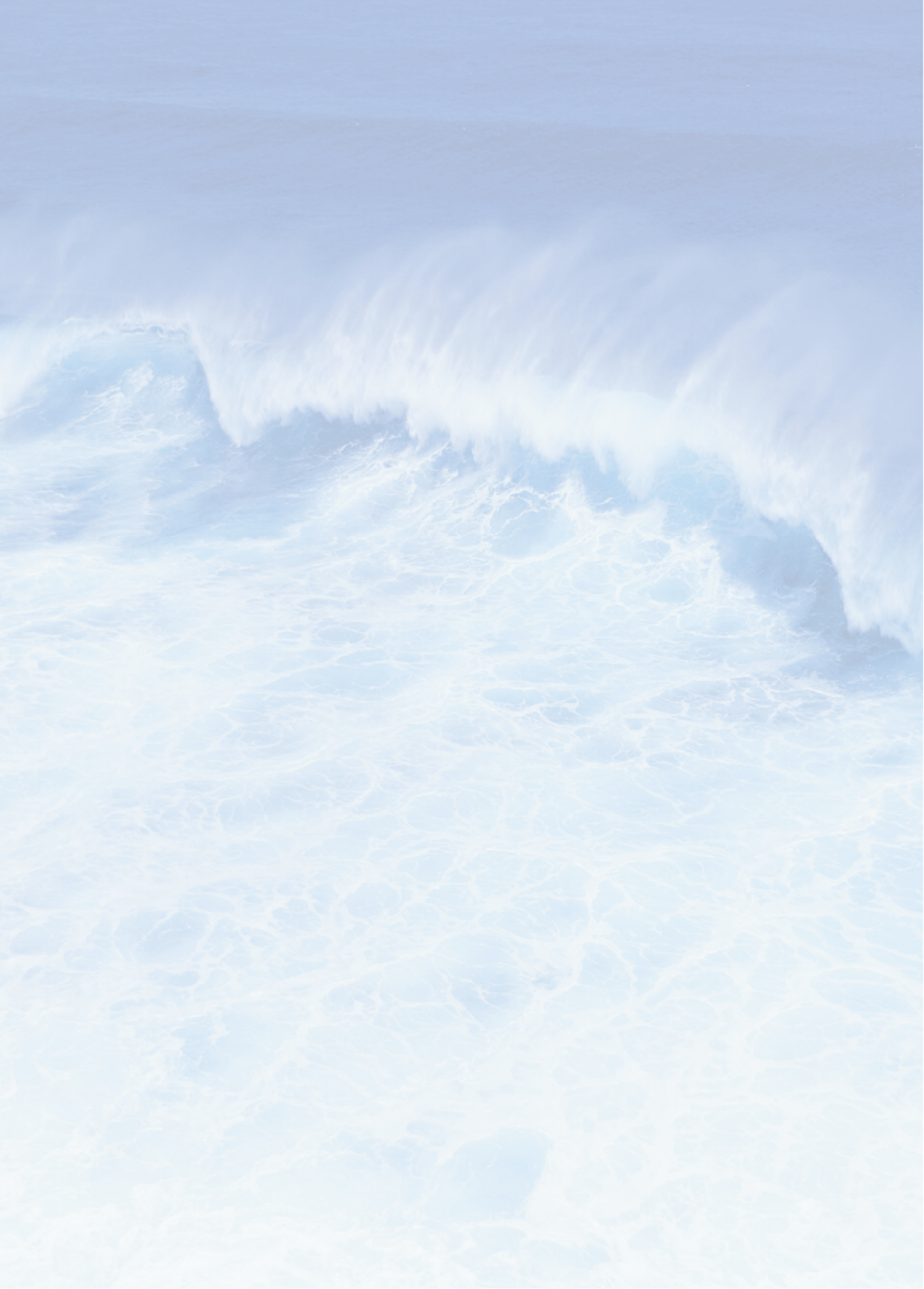

Evaluation of impacts in coastal morphology induced by different coastal structures using high-resolution coastal simulation Software

C.A. Kapopoulos[1*], F. Karathanasi[2,3]

[1]Ch. Kapopoulos & Associates Co., Aquaterra, Patras, Peloponnese, 26221, Greece
[2]Institute of Oceanography, Hellenic Centre for Marine Research, Anavyssos, 19013, Greece
[3]School of Naval Architecture & Marine Eng., National Technical University of Athens, Athens, 15780, Greece
[*]Corresponding author: ckapo@aquaterra.gr

Abstract

The study of coastal morphology variations is becoming of high priority due to the impacts in the coastal environment imposed either from climate change or anthropogenic activities. The increasing number of coastal structures is a main factor responsible for changes in coastal morphology. Prediction of these changes becomes extremely important especially when considering impacts near the coast. In most of cases changes in coastal morphology are studied in low resolution when elaborating coastal studies and environmental impact assessments (EIA). High resolution coastal morphology analysis is a high-cost, financially and computationally, task. As a consequence, there is lack of information in predicting morphological changes responsible for short-term and consequently, long-term adverse impacts and therefore knowledge gap is embedded in coastal studies and management reports especially near the coastline. Grid spacing becomes important especially when conducting relevant hydrodynamic and morphological analyses for evaluating impacts due to the presence of different types of nearshore structures. Coarse computational grids are not adequate to describe local bedload sediment transport and distribution patterns accurately. Use of high-resolution simulation near the coast remains a challenge for the coastal engineer due to the effort and time needed for specific projects and applications. When high-resolution modeling of seabed and shoreline evolution is considered even two dimensions can be adequate providing significant information even at the phase of preliminary structural design. In this paper changes in nearshore morphology are investigated in respect to erosion defense coastal structures using Aphrodite3D and MIKE 21 high-resolution simulations. Two-dimensional morphological analysis is considered.

Keywords High-resolution coastal modeling, Morphodynamic analysis, Nearshore impact mitigation, Impact prediction.

1 INTRODUCTION

Morphological changes near the coast is the outcome of several physical processes originated mainly from hydrodynamic conditions and there is need to be addressed especially when nearshore engineering structures already exist or are planned. Differences in direction of incoming waves, which result in different wave-current fields, contribute to sediment transport and nearshore morphological changes influencing each coastal project and activity. Accurate predictions of hydrodynamic conditions and sediment transport rates are rather difficult, as coastal-environmental functions and processes encapsulate a large number of interdependent functions that pose a high volume of parameters and combinations that need to be simultaneously examined in detail.

This paper has a twofold aim: i) to evaluate numerical modeling results on local morphological changes and hydrodynamic conditions at the coastal segment of Kalamaki beach in Western Achaia Municipality, Peloponnese, Greece as appears in Figure 1, from a new high-resolution numerical model, Aphrodite3D standard orthogonal mesh, under development by Aquaterra Engineering Company (Greece), with the well-known and widely used 2D model, MIKE 21 Coupled Model FM (Danish Hydrologic Institute), recently applied at another Greek coastal area (Karathanasi and Belibassakis 2019), under selected wave conditions as regards mean wave direction, significant wave height and wave period, as also appears in Figure 1, and; ii) investigate the morphodynamic changes induced from specific types of coastal defense structures near the coast in the short term, enabling the understanding of main processes at the Kalamaki coast. The coastal defense structures that are examined include two groups of three detached breakwaters located at the western and eastern side of the examined coast.

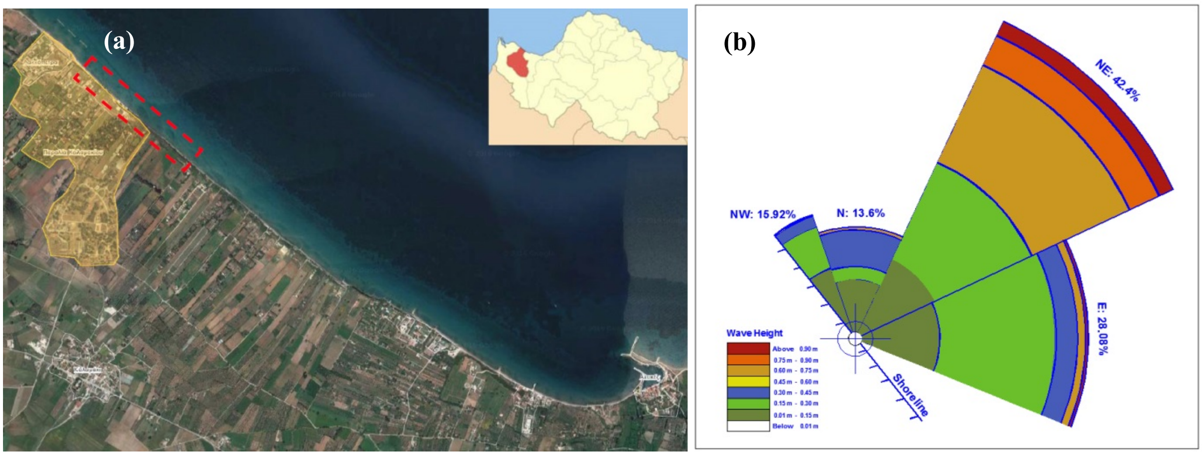

Figure 1 Coastal region of study the Western Achaia area, Greece: a) Study area, b) Rose diagram of significant wave height and direction (Patras station)

2 COASTAL HYDRODYNAMICS AND MORPHODYNAMICS

Environmental conditions, sediment properties, human intervention and their interaction play an important role in coastal hydrodynamics. Different formulations, based mostly on empirical parameters have been developed to express complex processes active in the coastal zone. As the waves reach shallow waters (*$d/L < 0.05$*), non-linear effects are evident as a result of shoaling, refraction, diffraction and bottom friction, that influence the wave characteristics.

These natural changes lead to problems, e.g. coastal erosion, when the area that is affected is important for human activities. To avoid excessive or unwanted morphodynamic changes at a desired location, proper understanding of the coastal hydrodynamics and morphodynamics of the area is necessary before planning any type of infrastructure. Based on the solution of the incompressible Reynolds averaged Navier-Stokes equations the local continuity equation integrated over depth (2D) are used (Shallow water equations) for Aphrodite3D (Kapopoulos 2017) as well as for MIKE21 (Danish Hydrologic Institute).

2.1 Sediment Transport

2.2.1 Sediment Properties

The fall velocity (w_s) of a particle depends on its size, density and magnitude of drag coefficient C_D :

$$w_s = \sqrt{\frac{4(s-1)gD}{3C_D}} \tag{4}$$

where s is the relative density of the sediment and D is the sediment grain size, τ_b is the shear stress on the grains. The critical shear stress describes the point of initiation of motion. The equilibrium of forces, whether vertical, horizontal or moment equilibrium is considered, gives an expression of the form:

$$\rho_{(s} - \rho)gD^3 \sim \tau_{b,cr}D^2, \tag{5}$$

where ρ_s is the density of sediment and ρ is the density of fluid. From the previous proportionality, the critical Shields parameter θ_{cr} can be deduced:

$$\theta_{cr} = \left(\frac{\tau_{b,cr}}{\rho_{(s} - \rho)gD}\right) = C. \tag{6}$$

The constant C is determined experimentally. For sand positioned smoothly on a flat bed, *C~0.05*. For the Aphrodite3D model the seabed morphology is calculated from the bedload sediment transport formula (Leont'yev, 1996):

$$\frac{\partial z_b}{\partial t} = -\frac{\partial}{\partial x}\left(q_x - 2|q_x|\frac{\partial z_b}{\partial x}\right) - \frac{\partial}{\partial y}\left(q_y - 2|q_y|\frac{\partial z_b}{\partial y}\right)$$

where z_b is the local increasement of the seabed and q_x, q_y are the bedload sediment transport rates in the longshore and cross-shore directions respectively in relation to the sediment transport rate

$$q_{x,y} = \frac{i_{x,y}}{(\rho_s - \rho)gN}$$

where N is the volumetric sediment concentration ($N=0.60$) and ρ_s , ρ the sediment and water densities respectively. The terms i_x , i_y correspond to the transport rates (Bailard 1981, Karambas 1998)

$$i_{xt} < \left[\frac{\varepsilon_b}{tan\varphi}\left(\frac{u_o}{u_{ot}} + \frac{d_x}{tan\varphi}\right)\omega_b + \varepsilon_s\frac{u_{ot}}{w}\left(\frac{u_o}{u_{ot}} + \varepsilon_s d_x\frac{u_{ot}}{w}\right)\omega_t\right] > \quad i_{yt}$$

$$< \left[\frac{\varepsilon_b}{tan\varphi}\left(\frac{v_o}{u_{ot}} + \frac{d_y}{tan\varphi}\right)\omega_b + \varepsilon_s\frac{u_{ot}}{w}\left(\frac{v_o}{u_{ot}} + \varepsilon_s d_y\frac{u_{ot}}{w}\right)\omega_t\right] >$$

where <> indicates time averaging over the wave period, w is the grain settlement velocity, φ the angle of the sediment grains internal friction, u_o, v_o the current velocity near the seabed, d_x, d_y the seabed slope in x,y directions respectively, and u_{ot}, ω_b are given from the formulas $u_{ot} = \sqrt{u_o^2 + v_o^2}$ and $\omega_b = C_f \rho u_{ot}^3$, respectively, and ω_t is the total rate of energy dissipation (Leont'yev, 1996) defined by

$$\omega_t = \omega_b + De^{3/2(1-\frac{h}{H})},$$

where H is the wave height ($Hrms$) and D is the mean dissipation rate of wave energy per unit area.

3 NUMERICAL MODEL

3.1 Finite difference equations

The finite difference scheme is used to solve the partial differential equations. The method is not unconditionally stable when it is applied to the set of two dimensional, vertically averaged flow equations especially in areas of arbitrary bathymetry and irregular boundaries. A time-step limitation is necessary to ensure numerical stability. The Courant number C_r, has to be lower than 2 in order to achieve stability.

$$C_r = \Delta t\sqrt{gh_{max}}\sqrt{\frac{1}{\Delta x^2} + \frac{1}{\Delta y^2}}$$

where Δt is the time-step of the finite-difference scheme, $\Delta x, \Delta y$ the horizontal grid spacing in the x,y directions respectively and h_{max} the maximum water depth of the numerical study area. The discretization of the partial differential equations for the shallow water equations finite difference method has been well described (Karambas and Koutitas 2002).

3.2 Application to the seabed of smooth geometry and simulation results

Both software models were applied to a smooth seabed geometry with a first group of three detached breakwaters at the western part of the study area, each one of 75m length, 4m width at the crest and 25m of spacing between successive structures, located at a distance of 100m from the nearly straight shoreline (measured perpendicular to the shoreline) and a second group of three detached breakwaters at the eastern part of the study area with each breakwater of 85m length, 6m width at the crest and 25m spacing between successive structures, located at a distance of 130m from the shoreline. The length of the model area is 3000m (x-direction) and its width is 500m (y-direction). The mean seabed slope is s=0.033. The grain size of the seabed sediments was kept the same for all simulations D_{50}=0.20mm. Two representative wave scenarios were investigated through numerical modeling modelling and the corresponding wave parameters, used as input to the coastal models, are presented in Table 1. The coast is subjected to erosion and breakwaters are designed to mitigate erosion at the central part of this coastal region. All structures are examined with breakwaters crest emerging at 1m above mean water level (MWL).

Table 1 Structural option, wave climate conditions, time of simulation for numerical calculations

	Wave scenarios	Hs [m]	T_p [s]	θ_w [deg]	t_s [sec]
1	Scenario1 (SC1)	2.3	5.3	320	6400
2	Scenario2 (SC2)	2.5	5.8	50	6400

Given the examined wave scenarios, different wave current flow patterns and seabed morphology changes are calculated as well as different sediment transport rates. This paper focuses on nearshore flow and morphological changes where the presence of emerging breakwaters produces flow patterns transformation. Seabed and shoreline morphology, as produced by the MIKE21, is shown in Figure 2.

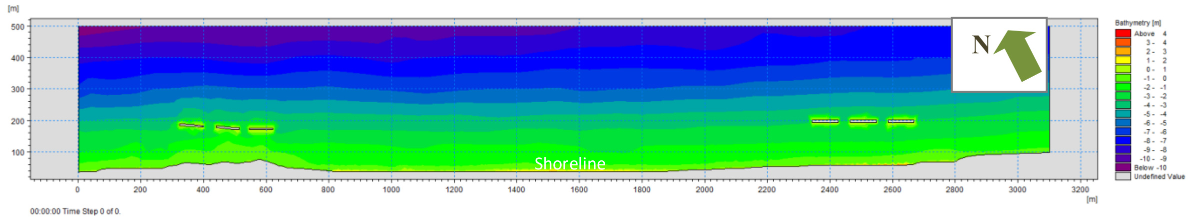

Figure 2 Coastal modeling area, initial seabed bathymetry, shoreline and breakwaters geometry from MIKE21

Hydrodynamic modeling starts after determining relevant physical and numerical parameters. After executing calculations for wave forcing conditions of two hours (t_s = 6400 sec) for both wave scenarios, the spatial distribution of the hydrodynamic conditions and sediment transport field at the last timestep of the simulation are presented and discussed only for SC2. Specifically, in Figure 3 the spatial distribution of current speed and direction is shown for both models. The produced pattern of current speed and direction from the two models resembles considerably; the current speed at the central part of the coast around the isobath of -1m is close to 0.5 m/s and is characterized by an eastern direction. However, at the upstream side of the breakwaters higher values of current speed are estimated from MIKE21 compared to Aphrodite3D.

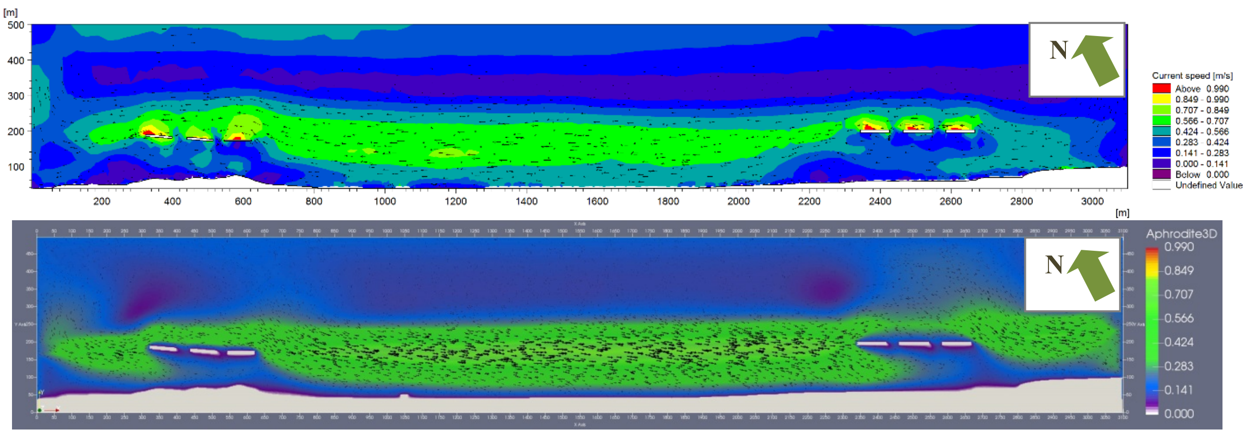

Figure 3 Spatial distribution of wave currents (speed and direction) from Aphrodite3D simulation (upper panel) and MIKE21 simulation (lower panel) for SC2 and the two groups of detached breakwaters

In Figure 4 the spatial distribution of bed level at the last timestep of the simulation is depicted for both models. The presented outputs show that there are small changes on the entire shoreline and only locally some obvious erosion patterns in the upstream side of breakwaters, better presented by Aphrodite3D simulation.

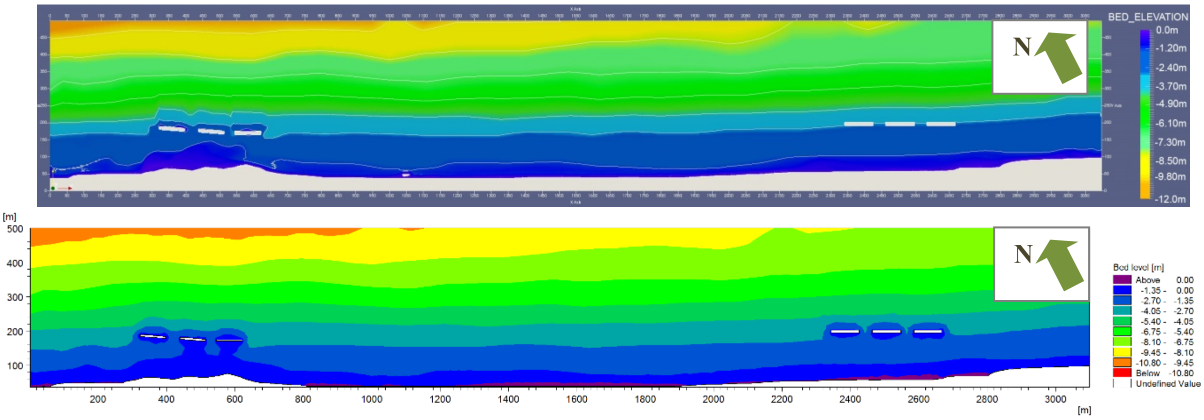

Figure 4 Spatial distribution of bed level from (a) Aphrodite3D simulation (upper panel) and (b) MIKE21 simulation (lower panel) for SC2 and the two groups of detached breakwaters

4 CONCLUSIONS

In this paper the wave current flow transformation due to the presence of two groups of breakwaters on a sandy beach and their impact on local changes in coastal morphology is examined. In particular, two 2DH dynamic modelling software products are used for simulating the hydrodynamic conditions of the Western Achaia region, focusing on Kalamaki coast, in order to predict local morphology changes for two wave scenarios. The wave current flow and the bedload sediment transport equations are solved by using a finite volume method based on non-overlapping triangular elements in MIKE21 while in Aphrodite3D software the equations are solved by using the finite differences method on an orthogonal high-resolution mesh. Results from the present analysis showed comparable results regarding wave current circulation and seabed-shoreline evolution patterns for the two different modeling software products, under the discrete wave forcing scenarios examined in this paper. Future work will focus on the further expansion of present hydrodynamic and seabed-shoreline evolution computations of the studied site to additional wave forcing scenarios as well as to different types of erosion defense structures considering also soft protection approaches.

Acknowledgements

F. Karathanasi would like to thank E. Mousoulis from DHI-Greece for providing the software license for MIKE 21.

References

Chen JL, Shi F, Hsu TJ, Kirby JT (2014) **NearCoM-TVD – a quasi-3D nearshore circulation and sediment transport model.** Coast. Eng., 91:200-212.

Goudas C, Kapopoulos Ch, Psarropoulou E (2011) Soft Shore Protection: Evaluation of experimental applications, Paper presented at the MEDCOAST Conference, Rhodes, Greece.

Goudas C, Kapopoulos Ch, Psarropoulou E (2008) Integrated Coastal Zone Management-The Global Challenge, In: Krishnamurthy R Soft Shore Protection: Theory and Practice, Research Publishing, Singapore, p 285-304.

Kapopoulos Ch (2017) Application of Aphrodite3D coastal simulation software to generate high-resolution nearshore current circulation and seabed evolution. Paper presented at the 15th International Conference on Environmental Science and Technology, Rhodes, Greece.

Karambas ThV, Koutitas C (2002) Surf and swash zone morphology evolution induced by nonlinear waves. J. of Waterway, Port, Coastal, and Ocean Eng., 102-113.

Karambas ThV (2012) Design of detached breakwaters for coastal protection: development and application of an advanced numerical model'. Paper presented at the 33rd International Conference on Coastal Engineering.

Karathanasi FE, Belibassakis KA (2019) A cost-effective method for estimating long-term effects of waves on beach erosion with application to Sitia Bay, Crete. Oceanologia 61(2):276-290. doi: 10.1016/j.oceano.2018.12.001

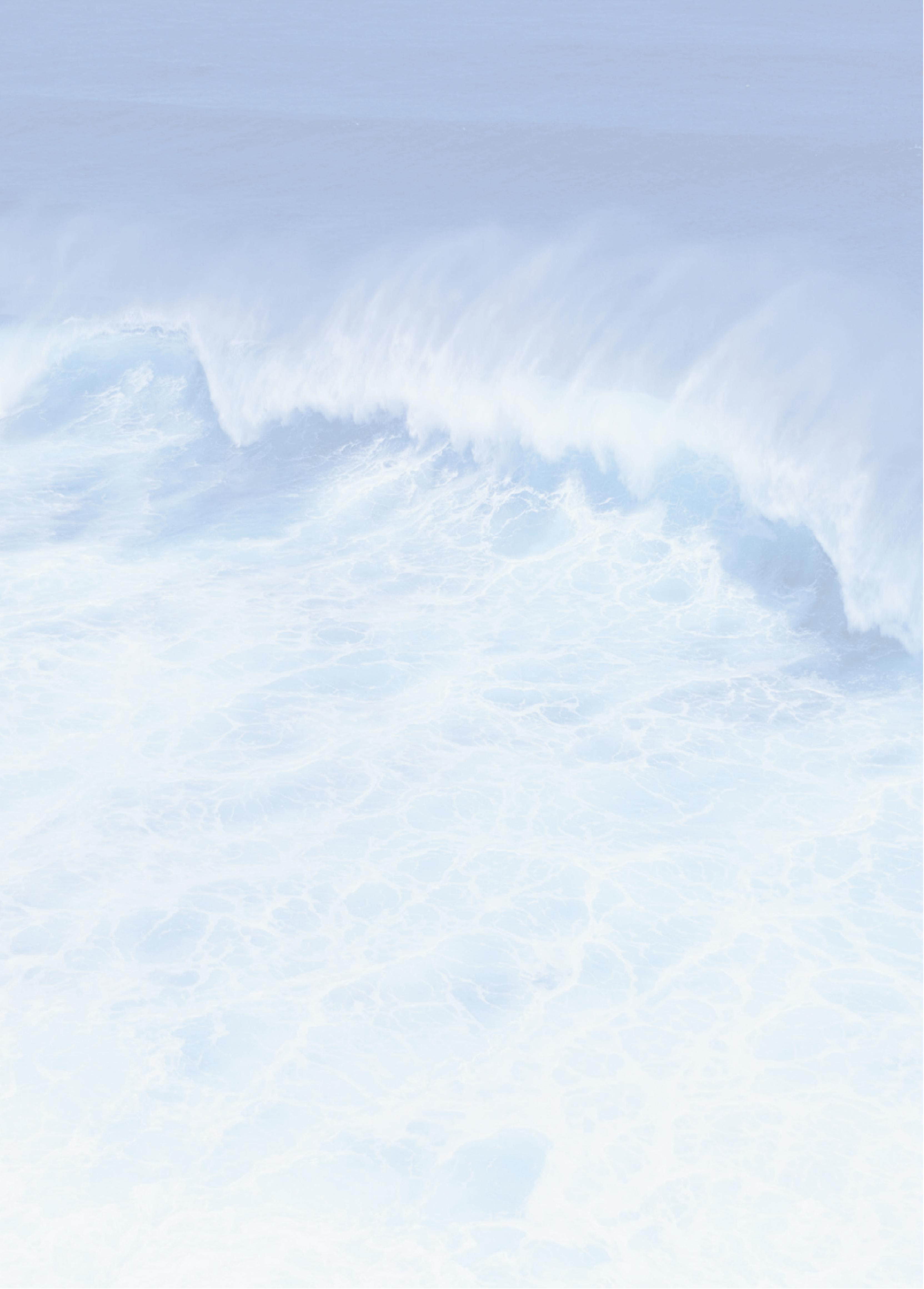

A numerical analysis method for addressing wave-structure interaction effects

C. Michailides

Department of Civil Engineering and Geomatics, Cyprus University of Technology, Limassol, 3036, Cyprus
*Corresponding author: c.michailides@cut.ac.cy

Abstract

For addressing wave-structure interaction effects potential flow or incompressible flow models can be used. Response calculation accuracy and computational costs contradict each other. In the present paper, a combined numerical analysis method for addressing efficiently the wave-structure interaction effects is discussed. The numerical analysis method couples a computational fluid dynamics model and a finite element method model; the viscous damping model that is used from the finite element model is continuously updated during the solution of the equation of motion of a multibody floating system. The proposed numerical method for estimating the viscous damping loads efficiently provides high accuracy and at the same time low computational cost.

Keywords Wave-structure-interaction, Viscous damping, Hydrodynamics.

1 INTRODUCTION

1.1 General considerations that address the problem

The global outlook for oil and gas demand is uncertain but looks set to play a major role in global energy out to 2040; offshore oil and gas sector will support this role. Renewables are the largest source of energy growth and are set to penetrate the global energy system more quickly than any fuel in human history. Offshore wind turbines are significantly contributing into this growth and are expecting to dominate into renewables up to 2040 (WindEurope, 2018). In addition to the offshore oil and gas structures and systems that already have been developed and installed, but are still being developing with a growing rate, ocean renewable energy systems (e.g. offshore wind turbines, wave energy converters, combined/hybrid concepts) are currently in the consideration, assessment and design phase.

A huge development of coastal and offshore structures and systems is anticipated for the years to come; in order to meet efficiently this development one word should be assured, safety. Analysis and design methods covering the whole life-cycle range of coastal and offshore structures are continuously redeveloped and reassessed always in connection with the rest technological aspects. Appropriate numerical methods for the analysis of those structures and systems and calculation of the wave-structure interaction effects during conception, design, installation, operation, maintenance, and dismantling should be used.

1.2 Specific considerations and contribution of the paper

Analysis and design of coastal and offshore structures is an equally demanding and challenging task. Response calculation accuracy and computational costs contradict each other. Accuracy is required at a maximum level while computational cost is very important when we reach the design phase of a coastal and offshore structure and a big number of analysis cycle iterations for a big number of operating and extreme environmental conditions are required to be performed. Wave-structure interaction effects and resulting excitation wave loads should be appropriately addressed within the limitations of computational capacity and time.

For the analysis and design of coastal and offshore structures wave loads by using potential flow theory are commonly calculated and used. The calculated wave loads are afterwards used as input data from finite element model tools for the solution of the equation of motion of a marine structure, its analysis and design. Very common the viscous effects are taken in consideration as distributed drag type loads since this is permitted according to international standards (DNV, 2010). On the other hand, the modelling of the dynamics of the fluid flow with the use of computational fluid dynamics methods provides high fidelity accuracy and calculation of the excitation wave loads but is still considered to be relatively computationally expensive. A clear contrast exists between computational cost and accuracy (Figure 1).

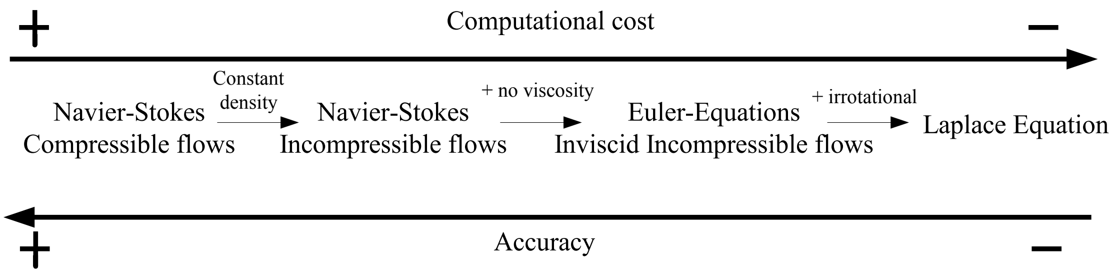

Figure 1 Accuracy and computational cost contradiction for addressing wave-structure interaction effects

In the present paper, a combined numerical analysis method for addressing efficiently the wave-structure interaction effects is discussed. The combined method is based on both finite element method and computational fluid dynamics and is applied for studying the response of a moored floating structure. The amount of data that needs to be communicated and the coupling method between the finite element model and computational fluid dynamics model is also of practical importance and is discussed. The computational fluid dynamics model is solving the Navier-Stokes equations considering incompressible fluid while the finite element model uses the modified Cummins Equation for solving the equation of motion of the moored floating structure in time domain. The combined method couples data calculated with the computational fluid dynamics model with the finite element model by means of high fidelity calculation of the viscous damping quantities (van der Vegt JJ, 1984; Faltinsen, 1993; Weller, 2012). A clear improvement of the calculated response is observed.

2 DESCRIPTION OF THE NUMERICAL METHOD

2.1 Description of the numerical models and their interconnections

The numerical method that has been used in the present paper is generic but for the purpose of the present paper has been applied in a moored multibody floating structure that operates as a wave energy converter. The first body of the multibody structure is a floating cylinder while the second is a fully submerged body. The two bodies behave rigidly and are connected with two vertical mooring lines that operate as tendons (Figure 3a). The mooring line system station keeps the floating structure and numerically provides horizontal and heave stiffness. Since the predictions of the present numerical method will be compared against experimental data, the numerical analysis was performed at model scale using geometry information and details of the multibody structure that are presented in Costello et al. (2014).

The numerical model brings together different numerical analysis techniques and tries to increase the accuracy of the calculated response but at the same time keeping the computational cost at low level. When studying wave structure interaction problems both components of the hydrodynamic damping, namely, the radiation damping and the viscous damping should be accounted. The viscous damping cannot be calculated when potential flow theory is used. On the other hand with the use of a computational fluid dynamics model the viscous damping can be quantified with good accuracy when appropriate model development has been made (e.g. grid size, viscous model etc.).

The numerical method that has been used in the present paper consists of: (a) a potential flow model for the calculation of the hydrodynamic coefficients in frequency domain with the use of potential theory, (b) a 3D computational fluid dynamics model for taking into account the effects of incompressible flow after appropriate mathematical analysis of results derived with this model and (c) a 3D finite element model for solving the equation of motion of the floating structure in time domain capable for the estimation of the response of all structural components of the structure. In Figure 2 an outline and interconnections between the different used models are presented.

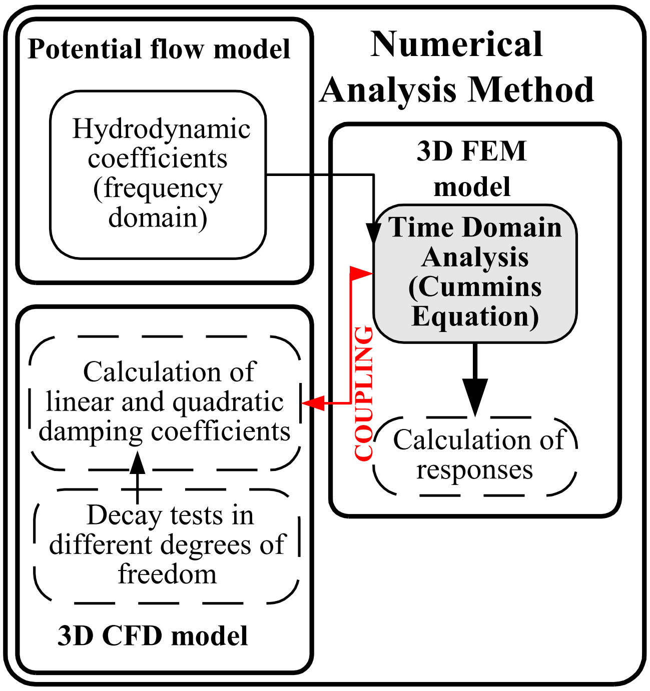

Figure 2 Numerical analysis and coupling method

2.2 Description of the numerical models

Potential theory is used for the estimation of the hydrodynamic coefficients of the two floaters, namely, added mass, radiation damping, hydrostatic stiffness and excitation forces in frequency domain. All those coefficients are used by the 3D FEM model while the added mass is calculated for infinite frequency. The tendons that connect the two floating bodies and the mooring line system are modelled with the use of appropriate two node finite elements but by ignoring their hydrodynamic properties and characteristics.

With regards to the 3D CFD model, the model is developed in order to be capable for solving the Navier-Stokes equations in time along with free surface modelling and immersed boundary method. The code solves incompressible viscous flow using the Navier-Stokes equations and the mass conservation equation:

$$\rho\left(\frac{\partial \mathbf{V}}{\partial t}+\nabla\cdot(\mathbf{VV})\right)=-\nabla p+\nabla\cdot\mu\left(\nabla\mathbf{V}+\nabla\mathbf{V}^{T}\right)+\rho\mathbf{g}+\mathbf{F} \quad (1)$$

$$\nabla\cdot\mathbf{V}=0 \quad (2)$$

where V is velocity of the fluid, p is the pressure, μ is the viscosity, ρ is the density, g is the gravitational acceleration and F represents the forces applied due to the presence of the structure in the computational domain.

With the FEM model the following equation of motion of the floating structure is solved in the time domain:

$$\left[M+\alpha(\infty)\right]\ddot{x}+B_1\dot{x}+B_2 f(\dot{x})+\int_0^t\left[h(t-\tau)\right](\dot{x})+Kx=F_{wave} \quad (3)$$

where M is the structural mass, α is the added mass that corresponds to infinite frequency, B_1 and B_2 are the linear and quadratic damping coefficients simulating the hydrodynamic damping, K is the summation of hydrostatic stiffness and stiffness related with the mooring lines system and F_{wave} is the excitation wave load. Details about the solution methods used of Eq. 3 are presented in Karimirad et al. (2018).

With the use of the 3D computational fluid dynamics model and by performing decay tests in the degrees of freedom of interest linear, B_1, and quadratic, B_2, damping coefficients can be calculated. For the calculation of those coefficients different methods can be used as reported in Faltinsen O (1993) and Nematbakhsh et al. (2015). In the present paper the PQ-method proposed by van der Vegt JJ (1984) is used. With this method decay tests are required in order to calculate the mean relative motion decrement of the decay tests. Successive amplitudes of the decay curve are used to determine the p and q coefficients for the estimation of the B_1 and B_2 damping coefficients. It is noted that the hydrodynamic damping can be reproduced accurately with linear and quadratic damping terms. For the calculation of the B_1 and B_2 coefficients the following equations are used:

$$B_1 = 2p \times \frac{M}{T_n} \quad (4)$$

$$B_2 = \frac{3}{8} qM \quad (5)$$

where M is the total mass of the floater (e.g. structural mass and added mass) and T_n is the natural frequency of the floater for the examined degree of freedom calculated with the decay test.

For the calculation of the p and q coefficients the decay curve of a specific motion of the floater is used. Points with coordinates $\left[\left(\Phi_{i+1}+\Phi_i\right)\times 0.5, \left(\Phi_i-\Phi_{i+1}\right)/\left(\Phi_{i+1}+\Phi_i\right)\times 0.5\right]$ are calculated and plotted where Φ is the amplitude of the motion of the decay curve. The slope of the fitted line of those points corresponds to the q value while the intercept of the same line with the vertical axis of the plot corresponds to the p value.

In the literature the B_1 and B_2 calculated with the use of computational fluid dynamics or experiments and are given as input to the FEM solver as constant values for solving the equation of motion in all time duration of the analysis. For floaters that the decay test includes a big number of oscillations and consequently different velocities of the floater, the calculation of a mean value for both B_1 and B_2 for all those oscillations and afterwards its use for the solution of equation of motion is conservative. In the present paper three different pairs of B_1 and B_2 are calculated that correspond to three ranges of the velocity of the floater. Depending to the velocity of the floater the relevant pair of B_1 and B_2 is used in the analysis made by the FEM model and consequently the computational fluid dynamics and FEM models are directly coupled at every time step of the analysis.

3 RESULTS FROM APPLICATION OF THE DEVELOPED METHOD, DISCUSSION AND CONCLUSIONS

The developed method has been applied for the case of the floating structure as presented in Figure 3a. A 3D CFD model (Figure 3b) has been developed and decay tests have been performed for the surge and heave motions of the cylinder floater. Based on the decay tests of the heave motion (Figure 3c) and surge motion three pairs of B1 and B2 have been calculated that correspond to three different velocities of the cylinder. With the use of those three pairs and by coupling them for the solution of Eq. 3 the heave Response Amplitude Operator (RAO) has been calculated and compared against relevant experimental data (Figure 4a); a very good agreement is observed. For specific irregular wave time series, in Figure 4b a comparison of the heave response of the cylinder floater is presented between the finite element model with the use of the proposed hydrodynamic model and the same finite element model but with the only potential damping model. A clear difference is observed on the heave response between the two damping models. Same differences exist for rest responses as far as internal loads of tendons, motions and relative heave motion between the two floaters that have connection with the produced power. Viscous damping is clearly a very important factor for performing wave-structure interaction analysis and calculate the response of floating structures. Efforts should be made for the inclusion of viscous damping effects when using potential flow. The proposed method for estimating the viscous damping loads efficiently provides high accuracy and at the same time low computational cost.

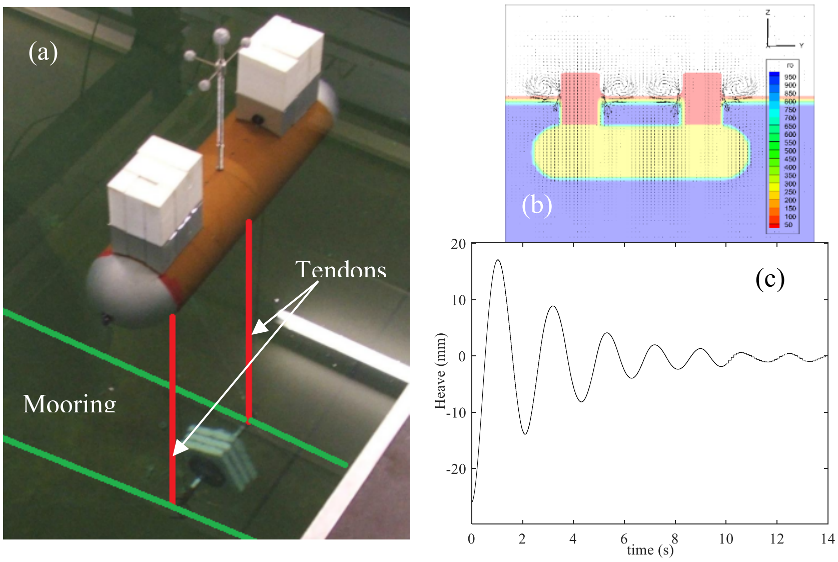

Figure 3 (a) The multibody floating system under study, (b) Image from the CFD model and (c) Heave decay test

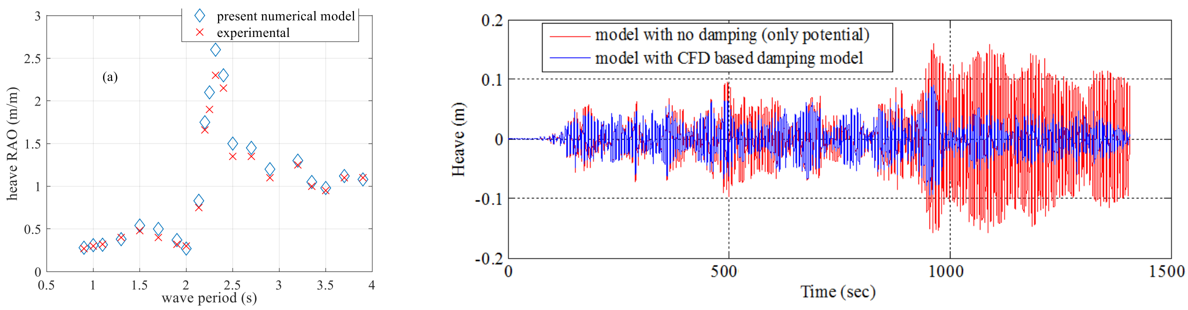

(a) (b)

Figure 4. (a) Comparison of heave RAO of the cylinder floater and (b) Comparison of the heave motion of the cylinder with different hydrodynamic damping models

References

Costello R, Padeletti D, Davidson J and Ringwood JV (2014) Comparison of numerical simulations with experimental measurements for the response of a modified submerged horizontal cylinder moored in waves. Paper presented at the 33rd International Conference on Ocean, Offshore and Arctic Engineering, CA.

DNV (2010) Recommended Practice – Environmental Conditions and Environmental Loads. DNV-RP-C205. Høvik, Norway.

Faltinsen O (1993) Sea loads on ships and offshore structures. Cambridge University Press.

Karimirad M, Michailides C and Nematbakhsh A (2018) Offshore Mechanics: Structural and Fluid Dynamics for Recent Applications. John Wiley & Sons, Ltd.

Nematbakhsh A, Michailides C, Gao Z and Moan T (2015) Comparison of Experimental Data of a Moored Multibody Wave Energy Device With a Hybrid CFD and BIEM Numerical Analysis Framework. Paper presented at the 34th International Conference on Ocean, Offshore and Arctic Engineering, St. John's, Newfoundland, Canada.

van der Vegt JJ (1984) Slinger gedrag van schepen. KIVI Lecture on Seakeeping.

Weller S (2012) Analysis of the DeepCwind model tests and a first attempt to simulate a semi-submersible floating wind platform with aNySIM. MARIN, Wageningen, The Netherlands. Technical Report No. 24602-MSG-1.

WindEurope (2018) Offshore Wind in Europe Key trends and statistics 2018. https://windeurope-.org/wp-content/uploads/files/about-wind/statistics/WindEurope-Annual-Offshore-Statistics-2018.pdf. Accessed 10 Apr 2019.

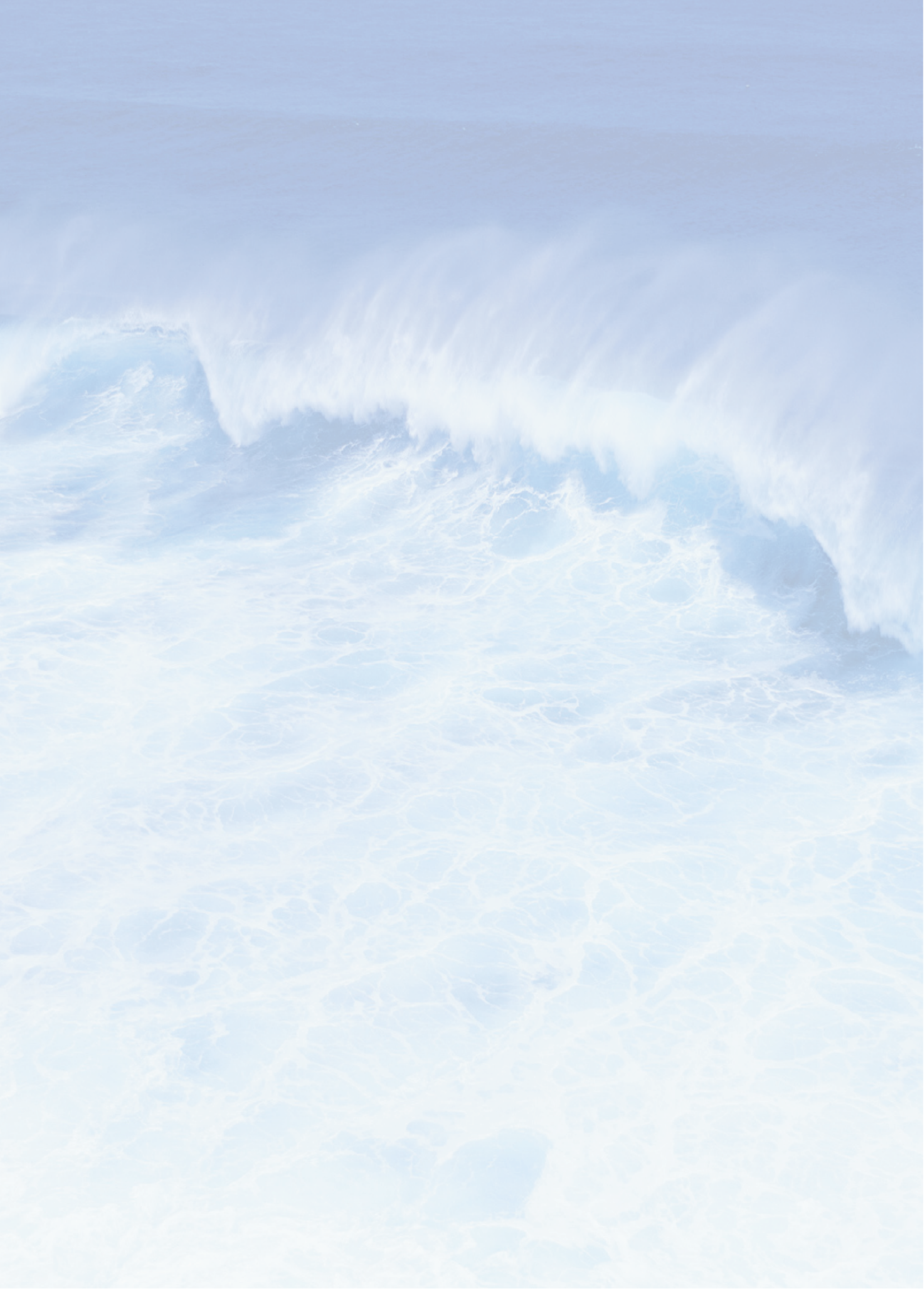

Nearshore processes induced by oblique irregular waves in the vicinity of a segmented, detached, zero-freeboard breakwater

M.V. Fotia, A.A. Dimas*

Department of Civil Engineering, University of Patras, Patras, 26500, Greece
*Corresponding author: adimas@upatras.gr

Abstract

The objective of this study was to assess the effectiveness in coastal protection of a segmented, detached, zero-freeboard breakwater (ZFB) using the non-hydrostatic model of the software XBeach. Specifically, the modification of the hydrodynamic processes in the sheltered area of the ZFB was studied for several irregular wave cases including cross-shore and oblique wave incidence. The results indicated that the effectiveness of the ZFB was weakly affected by the angle of wave incidence, therefore, the dominant design parameter is the wave height in terms of wave overtopping and transmission. For cross-shore wave incidence, rip-current speed increased with increasing incident wave height, while the longshore speed near the shoreline in the sheltered area of the ZFB decreased with increasing incident wave height. For oblique waves, the rip-current was intense at the upstream roundhead of each ZFB segment. The wave setup in the sheltered area of the ZFB increased with increasing incident wave height, while it was not affected much by the angle of wave incidence.

Keywords Segmented, Detached, Zero-freeboard breakwater, XBeach.

1 INTRODUCTION

The use of detached, low-crested breakwaters for coastal protection has increased due to their low aesthetical impact. The objective of this study was to assess the effectiveness in coastal protection of a segmented, detached, zero-freeboard breakwater (ZFB). Several irregular wave cases were examined, including cross-shore and oblique incidence, by means of numerical simulations using the non-hydrostatic model of the software XBeach (Roelvink 2015).

2 METHODOLOGY

The non-hydrostatic module of XBeach is a phase-resolving numerical model of the Nonlinear Swallow Water equations coupled to a Poisson equation solver for the dynamic pressure. In the present study it was verified that the model captures well the processes of wave overtopping above the ZFB crest, wave diffraction by the ZFB roundhead, wave setup in the sheltered leeside area of the ZFB, and wave runup on the swash zone of the beach. The wave breaking model of XBeach was calibrated for three cases of incident waves breaking on a beach of constant slope 1/15, without the presence of a breakwater, in comparison with existing experimental measurements.

3 RESULTS

The non-hydrostatic model of XBeach was applied at prototype scale on a segmented, detached ZFB on a beach of constant slope 1/15. In the longshore direction, the computational domain included one segment of the ZFB, while its lateral boundaries were located in the centerline of the gaps between the specific segment and the two neighboring ones in order to facilitate the use of periodic boundary conditions. The length of the ZFB measured at its crest level was 90 m, the crest width was 15.6 m, while its leeward toe was at depth of 5.8 m, i.e. 87 m from the shoreline. The length of each gap between segments of the ZFB was 45 m, hence the length of the computational domain in the longshore direction was 135 m. A snapshot of the computational domain and grid in the vicinity of the ZFB segment is shown in Figure 1.

Incident irregular waves (JONSWAP spectrum) of characteristic height 1.6 m, 3.8 m and 4.8 m, and deep-water incidence angles of 0°, 22.5° and 45° were examined. Typical results of cross-shore and oblique wave incidence are shown in Figures 3-5. It was observed that wave diffraction is more intense for the two cases with the smaller heights, while for the case with the larger height wave transmission is the dominant process. Wave transmission increases with increasing incident wave height.

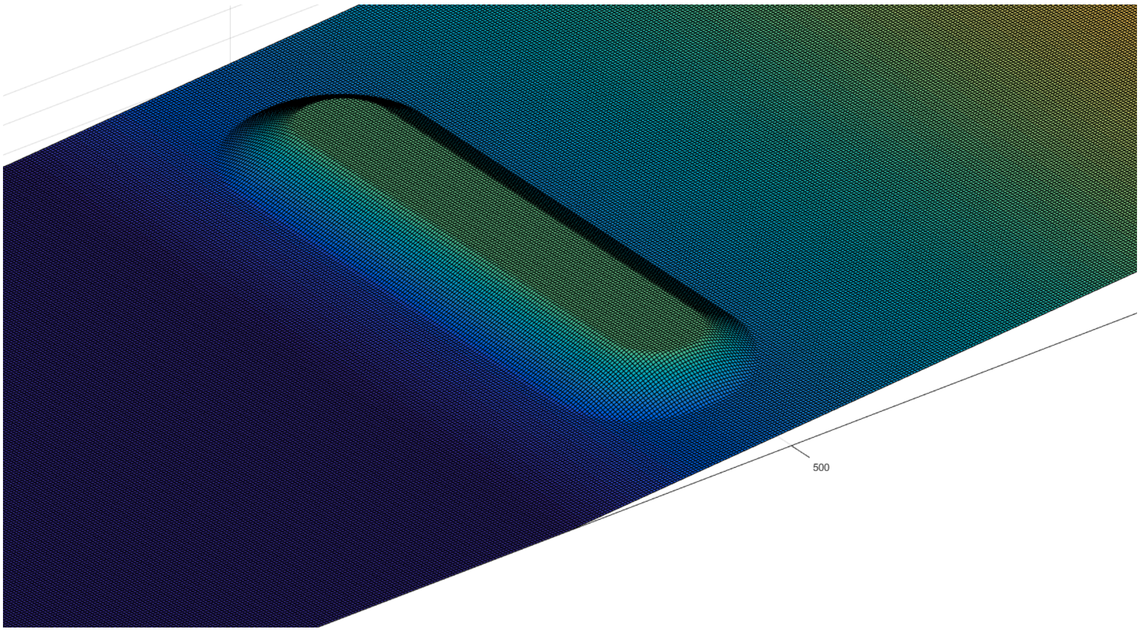

Figure 1 The computational grid in the vicinity of the ZFB segment on the beach of slope 1/15

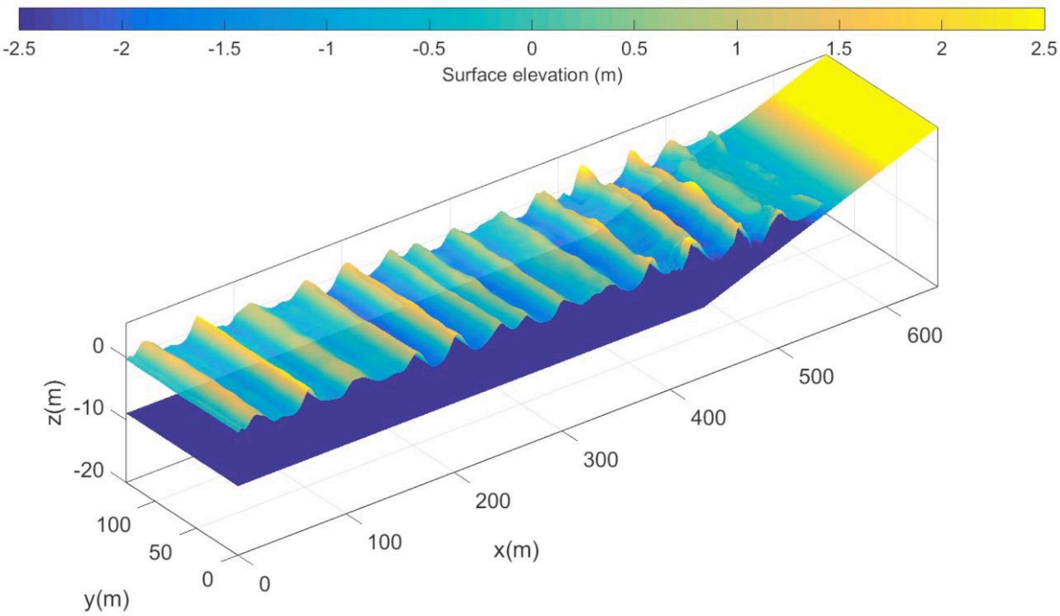

Figure 2 Free surface elevation snapshot of cross-shore irregular wave incidence with characteristic height of 3.8 m; the ZFB is at x ≈ 500 m

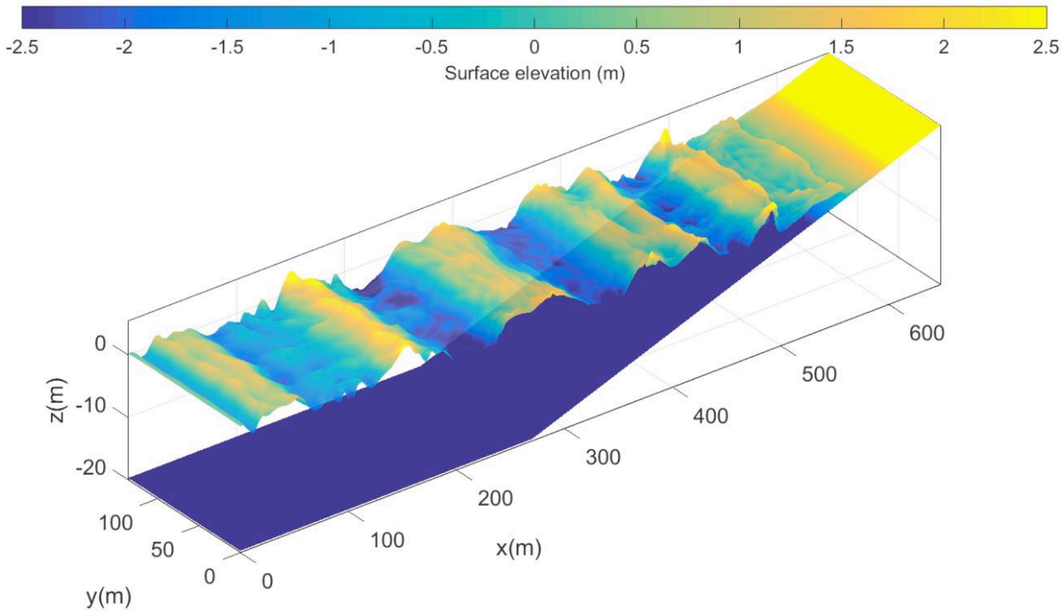

Figure 3 Free surface elevation snapshot of cross-shore irregular wave incidence with characteristic height of 4.8 m; the ZFB is at x ≈ 500 m

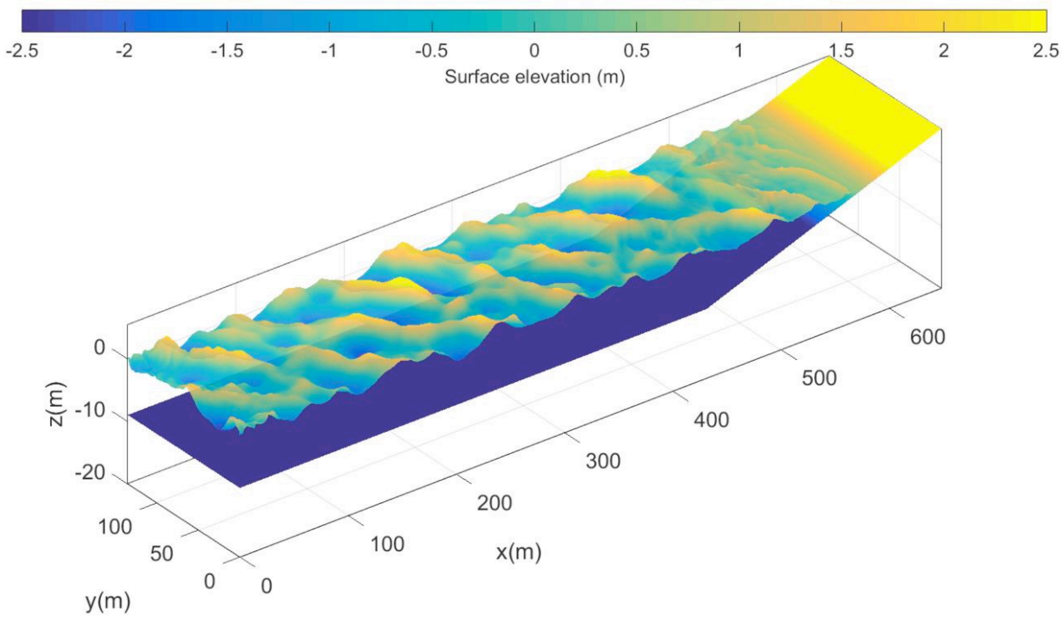

Figure 4 Free surface elevation snapshot of oblique irregular wave incidence at angle of 45° with characteristic height of 3.8 m; the ZFB is at x ≈ 500 m

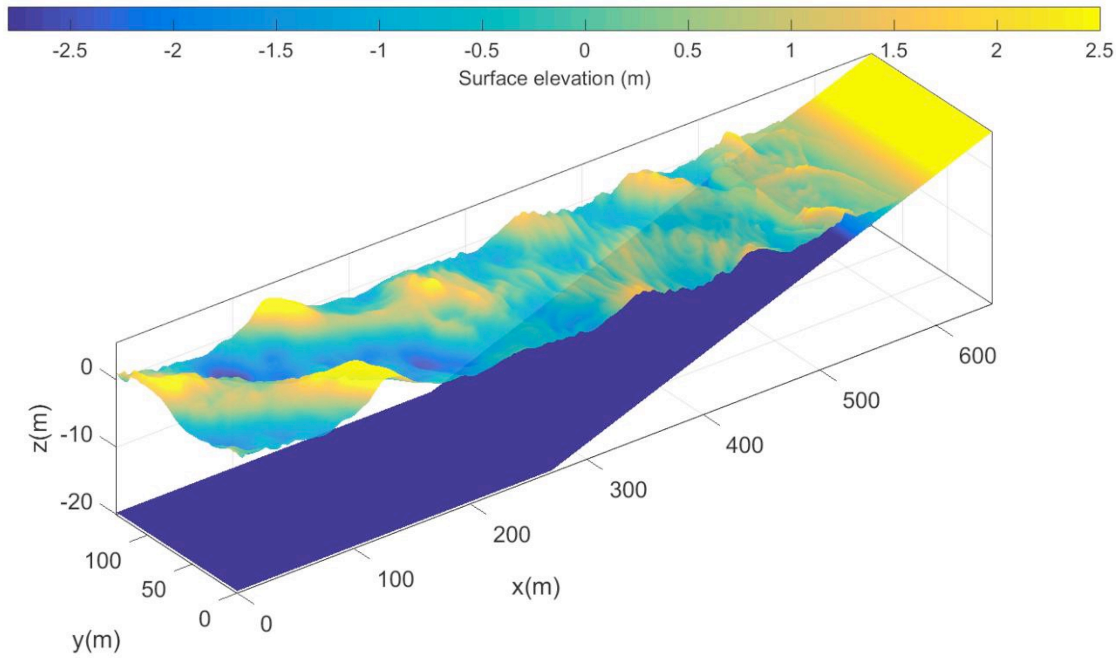

Figure 5 Free surface elevation snapshot of oblique irregular wave incidence at angle of 45° with characteristic height of 4.8 m; the ZFB is at x ≈ 500 m

Typical results of wave-generated currents are shown in Figures 6-7. For cross-shore wave incidence (Figure 6), two counter-rotating circulation cells are formed in the sheltered area of the ZFB. For oblique wave incidence (Figure 7), the rip current is intense at the upstream roundhead of the ZFB segment, while the generation of the longshore current dominates over the appearance of circulation cells in the sheltered area of the ZFB.

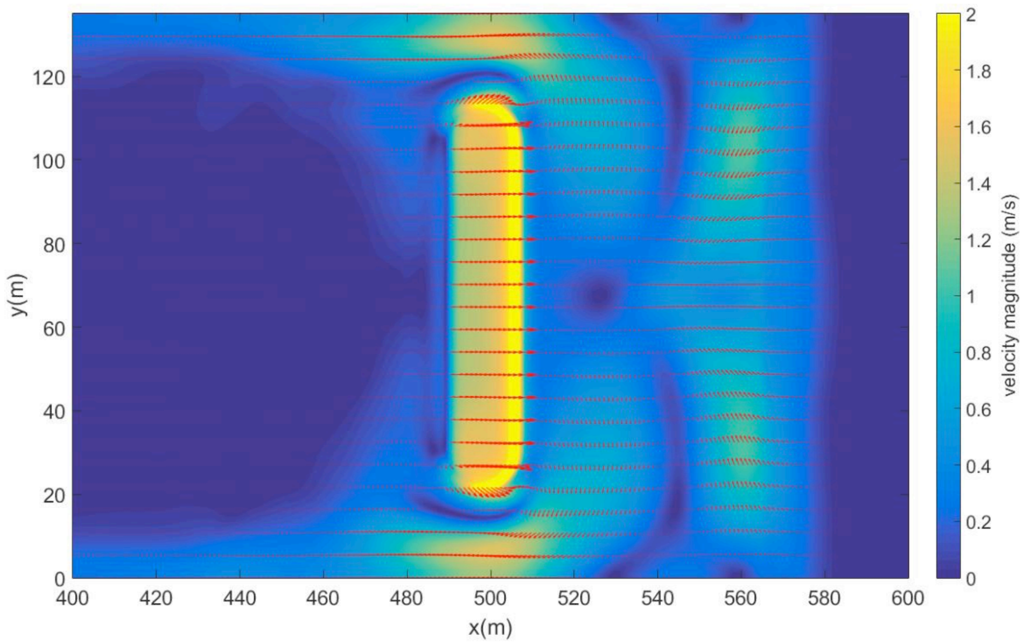

Figure 6 Wave-induced currents for cross-shore irregular wave incidence with characteristic height of 3.8 m; the ZFB is at x ≈ 500 m

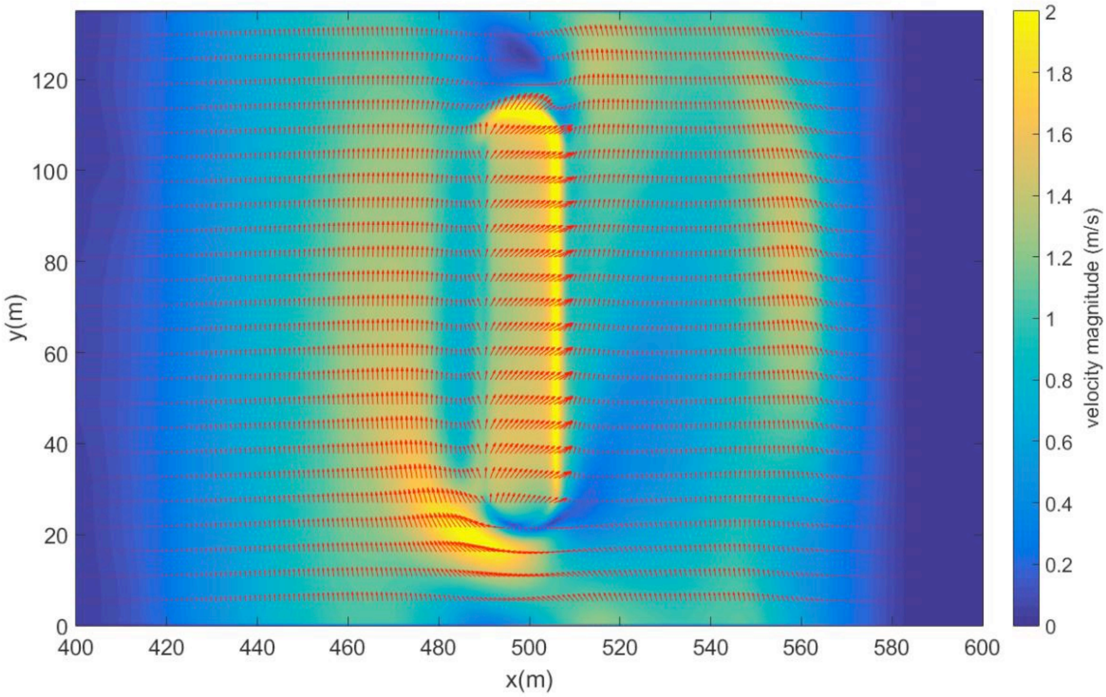

Figure 7 Wave-induced currents for oblique irregular wave incidence at angle of 45° with characteristic height of 3.8 m; the ZFB is at x ≈ 500 m

Wave setup increases in the leeside area of the ZFB as the incident wave height increases, while the incident wave direction does not influence the wave setup. In the upstream roundhead, wave set-down was observed and it was correlated to energy dissipation, while at the downstream roundhead weak wave setup occurred.

4 CONCLUSIONS

The numerical results indicated that the effectiveness of the ZFB was weakly affected by the angle of wave incidence, therefore, the dominant design parameter is the wave height in terms of wave overtopping and transmission, while wave reflection increased with decreasing wave steepness. For cross-shore wave incidence, rip-current speed increased with increasing incident wave height, while the longshore speed near the shoreline in the sheltered area of the ZFB decreased with increasing incident wave height. For oblique waves, the rip-current was intense at the upstream roundhead of each ZFB segment. The wave setup in the sheltered area of the ZFB increased with increasing incident wave height, while it was not affected much by the angle of wave incidence. In the gaps between segments and the seaward area of the ZFB, wave set-down was observed and it was correlated to energy dissipation. For oblique waves, wave set-down occurred only at the upstream roundhead of each ZFB segment, while at the downstream roundhead weak wave setup occurred.

References

Roelvink D (2015) XBeach Technical Reference - Kingsday Release. Deltares, Unesco-IHE Institute for Water Education, TU Delft.

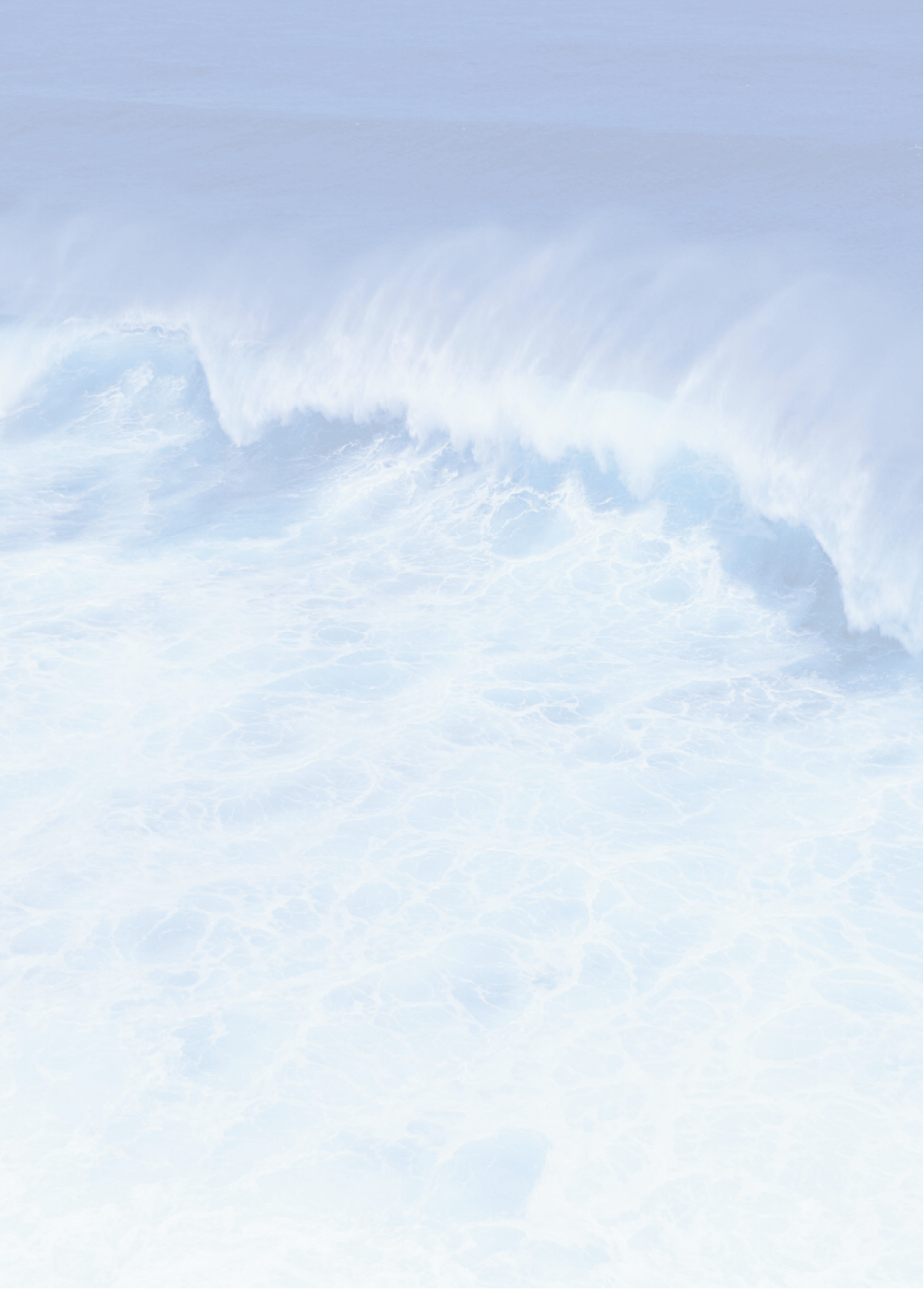

Reliability analysis of rubble mound breakwaters
An easy-to-use methodology

D.I. Malliouri[1*], C.D. Memos[1], T.H. Soukissian[2], V.K. Tsoukala[1]

[1]Department of Civil Engineering, National Technical University of Athens, Zografos, Attiki, 15780, Greece
[2]Institute of Oceanography, Hellenic Centre for Marine Research, Anavyssos, Attiki, 19013, Greece
[*]Corresponding author: dimall@central.ntua.gr

Abstract

An easy-for-application probabilistic methodology is presented aiming at estimating the reliability of coastal structures such as rubble mound breakwaters during their lifetime. This methodology uses the joint probability density function of all stochastic load variables involved in the reliability function of each element of the structure, in order that the system failure probability be extracted. Besides, in this method the correlation between all statistically dependent random variables can be taken into consideration. Then, based on the structure of the breakwaters' fault tree that describes the linking of the individual failure mechanisms to the system's failure, the latter's probability of failure can be computed by taking also into account the statistical correlation of these modes of failure. The aforementioned methodology has been applied to a sample of wave data at the structure's location generated for this purpose. The data were derived from wave measurements in deep waters, covering a period of 12 years, obtained from an oceanographic buoy, located in the central Aegean off Mykonos island. The proposed methodology's results were then compared with those of advanced fully probabilistic methods and showed satisfactory agreement.

Keywords Reliability, Probabilistic methods, Rubble mound breakwater, Statistical correlation.

1 INTRODUCTION AND THEORETICAL BACKGROUND

The reliability based design methods for coastal structures are divided into four categories, related to their accuracy in determining the reliability of the structural elements and the consideration of all involved uncertainties (U.S. Army Corps of Engineers 2006):

- Deterministic method (Level 0)
- Semi-Probabilistic Method (Level I)
- Probabilistic Methods with Approximations (Level II)
- Fully Probabilistic Methods (Level III)

Conventional design practice for coastal structures is often deterministic in nature, and its reliability is based on the exceedance probability of the design wave load. Specifically, the notion of design wave parameters and especially that of wave height associated with a certain return period is adopted (Burcharth and Liu 1996).

The loads considered for the design of coastal structures, should be based on the probabilistic representation of the long-term wave climate and sea level conditions at the structure's location. However, such wave measurements covering a period of several decades are often rare. Therefore, regarding the wave climate at the structure's location, there is a need to estimate these data under a fully probabilistic framework using measurements in deep waters (e.g. Malliouri et al. 2019) or wind data in the wave generation area (e.g. Malliouri et al. 2017).

The reliability of an element depends on the safety margin between the strength (i.e. resistance R) and the load or action A. The reliability function g describes the relation between resistance and action an element and is formulated as follows:

$$g = R - A \tag{1}$$

Thus, the probability of failure of a structural element (P_f) and the reliability of that element (N) are defined by Eq. 2 & 3 respectively.

$$P_f = Prob(g < 0) = Prob(A > R) \quad (2)$$

$$N = 1 - P_f \quad (3)$$

A deterministic calculation method uses nominal values of the basic variables. Often a global safety factor γ is applied to deal with the unknown uncertainties in the basic variables and to provide a safety margin between strength and load. Thus, the reliability inequality is formulated as:

$$R_{nom} \geq \gamma A_{nom} \quad (4)$$

where: R_{nom} and A_{nom} are the nominal values for strength and action respectively. In the deterministic calculation, the load variables correspond to certain return periods, which can be extracted from measurements. The latter often cover a period of data usually shorter than the return period of interest. In general, the longer period of measurements makes the estimated return values more reliable.

In the semi-probabilistic approach, partial safety factors developed initially by PIANC (1992) are implemented for strength and load via the following relation, creating by this way a safety margin:

$$\frac{R_{nom}}{\gamma_r} \geq \gamma_A A_{nom} \quad (5)$$

where: γ_r and γ_A are the partial safety factors for strength R_{nom} and load A_{nom} respectively.

In short, according to PIANC (1992), partial safety factors are calibrated with the following input:

- Design Lifetime T_L (=20, 50 or 100 years)
- Acceptable probability of failure P_f (=0.01, 0.05, 0.10, 0.20, or 0.40)

Another possibility of estimating the reliability of an element is to use a Level II method which is a probabilistic method with approximations. Its calculations are based on a rather iterative and complex process, making thus Levell II methods difficult to apply, especially if the random variables are non-normally distributed and statistically correlated, and the failure function is not linear.

When a fully probabilistic method is applied, e.g. Direct Integration Method (DIM), Monte Carlo Method (MCM), the failure probability of an element can be calculated accurately based on the probabilistic framework of all stochastic variables involved. The core problem of DIM is the exact estimation of the joint probability density function (pdf) of these variables. Given that the marginal pdfs of the variables considered are known, the calculation of their joint pdf is necessary only if these variables are correlated, otherwise their joint pdf is equal to the multiplication product of the marginal pdfs of the variables.

In case of correlated variables, an efficient way to capture their correlation is to apply the conditional probability model in order to calculate the joint pdf. The said model can be illustrated by the total probability law applied indicatively to two variables, but can be also applied to more than two correlated variables as well:

$$f_{X_1,X_2}(x_1, x_2) = f_{X_1|X_2}(x_1|x_2) f_{X_2}(x_2) \quad (6)$$

where $f_{X_1,X_2}(x_1, x_2)$ is the joint pdf of the stochastic variables X_1, X_2, $f_{X_1|X_2}(x_1|x_2)$ is the conditional pdf of X_2 given X_1, and $f_{X_2}(x_2)$ is the marginal pdf of X_2.

Given that $f_{\bar{X}}$ is the joint pdf of all stochastic variables involved, i.e. of the vector $\bar{X} = (X_1, X_2, \dots, X_n)$, the probability of failure can be calculated via the following integral:

$$P_f = \int_{g(\bar{x})<0} f_{\bar{X}}(\bar{x}) d\bar{x} \tag{7}$$

MCM is based on a large number of simulations N, a part of which (N_f) leads to element's failure. Thus, it is assumed that provided N is a high enough number, P_f attains acceptable convergence and is computed as:

$$P_f = \frac{N_f}{N} \tag{8}$$

2 METHODOLOGY

The proposed easy-for-application methodology is based on the advanced fully probabilistic methods (Level III) and generates an artificial sample of wave data of significant wave height H_s, mean wave period T_m, and mean wave direction θ_m at the structure's location, which can be representative of the real population covering a certain time period. The method can be easily applied when wave measurements or wave data in deep waters are available. In this case a wave propagation model has to be applied, e.g. a fast and simple linear model via integration of short- with long-term wave statistics (Malliouri et al. 2019). For reasons of simplicity, mean sea level conditions have not been taken into consideration in this study. However, the said methodology can well be expanded to include that parameter.

The steps for the generation of the artificial sample at the structure's location based on "stratified random sampling" are listed below:

(1) Calculation of the total number of sea sates in the data set (denoted by N_d) in deep waters
(2) Grouping of the initial data into joint classes of H_s, T_m, θ_m of adequately small bin size and estimation of the frequency of each joint class
(3) Selection of the reduced sum of sea states of the new dataset (denoted by M_d)
(4) Calculation of the new frequencies of the joint classes of the new dataset by rounding to the nearest integer the product of the initial frequencies of each joint class by M_d, divided by N_d
(5) To obtain the new dataset of H_s, T_m, and θ_m, a sample of M_d sea states can be estimated, by generating a number of groups of H_s, T_m, and θ_m between the limits of each class, equal to the new frequency of each class (step 4)
(6) Estimation of the wave data at the structure's location by propagating the new dataset (step 5) from deep waters towards the structure's location
(7) Application of the conditional model of the above three variables to wave data (step 6) in order that the joint pdf of the three variables at the structure's location be estimated
(8) Calculation of the new frequencies of each joint class, by rounding to the nearest integer the product of the joint probability of each class (step 7) by an adequately large number N (step 1)
(9) To obtain the artificial data set of H_s, T_m, and θ_m at the structure's location, a sample of N sea states can be estimated, by generating a number of groups of H_s, T_m, and θ_m between the limits of each class, equal to the new frequency of each joint class (step 8)

The accuracy of the artificial sample depends on the bin size of the joint classes, which should be adequately small, and the total sum of the reduced sample M, which should be adequately large. These two conditions make the random sample generated more representative of the real population and also avoid elimination of the most extreme and rare events in the artificial sample.

Besides, a fault tree has to be considered that depends on the structure under design. In this study, a rubble mound breakwater's fault tree was adopted of a series system that consists of three failure modes, i.e. the sea side armour failure, the toe instability, and the rear side armour failure. Then, a design methodology should be applied based on MCM, thus number N should be adequately large to achieve convergence of P_f estimated via Eq. 8. The statistical correlation of the three failure modes can also be considered by checking if the elements fail simultaneously, i.e. under the same wave conditions (see Table 1).

Table 1 Estimation of modes of failure and system's failure frequency (based on Everts 2016)

Sea state	Sea side armour failure	Toe failure	Rear side armour failure	System failure
1	1	0	1	1
2	0	0	0	0
3	0	1	1	1
.	.	.	.	.
.	.	.	.	.
N	1	0	0	1
Total	N_s	N_t	N_r	N_f

3 EXAMPLE OF APPLICATION

The aforementioned methodology was applied to measured wave data obtained from an oceanographic buoy that belongs to the POSEIDON Marine Monitoring Network operating under the responsibility of the Hellenic Centre of Marine Research (HCMR), see Soukissian and Chronis 2000. The buoy is located at the depth of 140 m in deep waters (37.51 °N, 25.46 °E) in the central Aegean off Mykonos island. The wave measurements cover a period of 12 years (2000-11) and the recording interval is 3 h.

The mean and standard deviation of H_s and T_m, and their linear correlation parameter $r(T_m, H_s)$ of the artificial sample in deep waters are compared with those of the original data, presented in Table 2. The latter are also compared with the sample generated by MCM. The joint distribution of these two variables (see iso-probability density contours in Figure 1) has been derived from the original data set, while the other two samples are extracted from this joint distribution. Furthermore, the three populations have been compared in Figure 1 showing good agreement.

Table 2 Comparison of the two data sets developed by the easy-to-use methodology and MCM in deep waters with the original data set

Data set	Mean H_s (m)	Std H_s (m)	Mean T_m (s)	Std T_m (s)	$r(T_m, H_s)$
Original	1.08	0.75	3.87	0.88	0.91
Ease-to-use	1.08	0.74	3.89	0.85	0.91
MCM	1.07	0.72	3.90	0.83	0.90

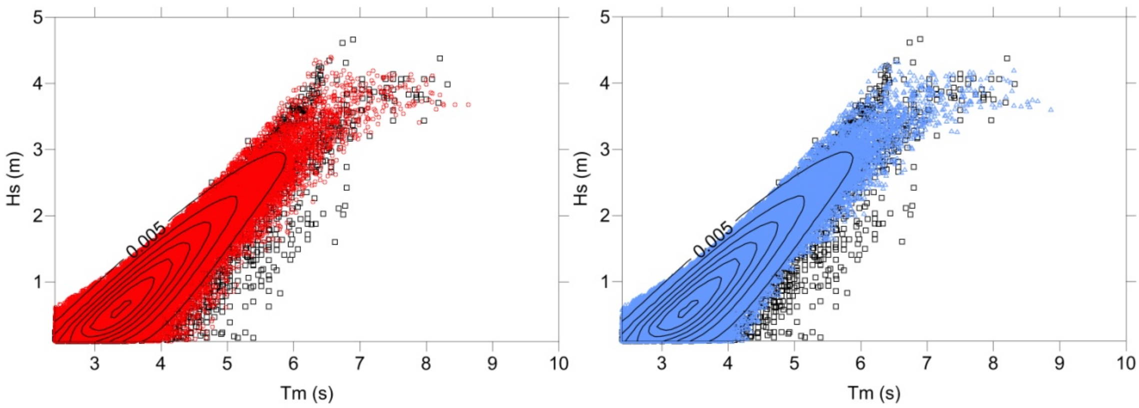

Figure 1 Comparison of the original data (black squares) in deep waters with those generated by Easy-for-application Method (red circles) (left) and MCM (cyan triangles) (right) (iso-probability density contour step 0.01/m/s)

The new dataset at the structure's location (at the depth of 6 m) was generated by considering the parameter M equal to 1500 sea states in deep waters (adjusted to our computer capacities), bin size equal to 0.20 m for H_s, 0.2 s for T_m and 10° for θ_m, and by applying the linear propagation model (Malliouri et al. 2019).

The design requirements that need to be specified firstly are the allowable probability of failure, considered in this example 0.20 for deterministic design, and the design Lifetime T_L of the rubble mound breakwater which is considered equal to 20 years taking into account that the measured data cover 12 years and trying thus to avoid including high uncertainties during time extrapolations.

The deterministic design method applied is based on an omni-directional extreme value model for H_s that considers waves coming from the open sea towards the structure (referring to the 56% of the total data from all directions including lack of waves). Therefore, by applying this model and assuming the return value of H_s that corresponds to the return period of 100 years as design storm event for the deterministic design, H_s^{100} is estimated at 4.31 m, and the most probable T_m associated to H_s^{100} is 7.95 s. The exceedance probability of H_s^{100}, P_e, during the Lifetime is 0.1813, thus is lower than the allowable probability considered. This is estimated given that only extreme events are considered. However, the corresponding probability if all events are taken into account is equal to $3.42*10^{-6}$ at 1 year, considering that H_s^{100} is exceeded on average once every m observations, where m is the total number of observations in 100 years. Besides, P_e of H_s^{100} during the structure's Lifetime is estimated at $6.85*10^{-5}$ via time extrapolation.

The nominal stone mass derived from the preliminary design of a rubble mound breakwater considering initial damage, is equal to 6.0 t for sea-side armour, 1.4 t for toe and 5.8 t for rear-side armour units. Then, the easy-for-application probabilistic method's result of system's failure probability was computed and compared with fully probabilistic methods, as presented in Table 3. As it can be observed, the proposed probabilistic methodology's result is very close to those of fully probabilistic methods. Besides, it is noted that probabilistic methods of Level III are more accurate than deterministic or semi-probabilistic design since they consider the whole data under a probabilistic framework, the fault tree, and the statistical correlation of wave parameters and failure mechanisms.

Table 3 Comparison of estimated P_f during the structure Lifetime via the easy-for-application probabilistic method with other methods

Design Method	Easy-to-use Method	MCM	DIM
Initial Damage	$1.96*10^{-4}$	$2.56*10^{-4}$	$1.79*10^{-4}$
Intermediate damage	$1.14*10^{-5}$	$2.85*10^{-5}$	$1.74*10^{-5}$
Failure	$8.91*10^{-7}$	$9.99*10^{-7}$	$9.81*10^{-7}$
Complete Failure	$1.38*10^{-8}$	$1.51*10^{-8}$	$1.40*10^{-8}$

4 CONCLUSIONS

An easy-for-application probabilistic methodology that tackles a variety of significant current issues for the design of coastal structures is derived based on existing advanced reliability methods. Also, some other design issues have been discussed and clarified.

References

Burcharth HF, Liu Z (1996) Design Wave Height Related to Structure Lifetime. Paper presented at the 25th International Coastal Engineering Conference: ICCE '96, Orlando, Florida.

Everts PS (2016) Probabilistic design of a rubble mound breakwater. MSc Thesis, Delft University of Technology.

Malliouri D, Afentoulis V, Bonaros V, Memos C, Tsoukala V (2017) Integrated design of coastal structures and adaptation to climate change hazards. Paper presented at the 15th International Conference on Environmental Science and Technology, Rhodes.

Malliouri D, Memos C, Tampalis N, Soukissian T, Tsoukala V (2019) Integrating short- and long-term statistics for short-crested waves in deep and intermediate waters. Applied Ocean Research 82(3):346–361. doi: 10.1016/j.apor.2018.11.004.

PIANC (1992). Analysis of rubble mound breakwaters; report of working group 12 (PTC II).

Soukissian T, Chronis G (2000) Poseidon: A marine environmental monitoring, forecasting and information system: For the Greek seas, Mediterr. Mar. Sci., 1(1):71-78. doi: 10.12681/mms.12.

U.S. Army Corps of Engineers (2006) Coastal engineering manual. Washington, D.C.

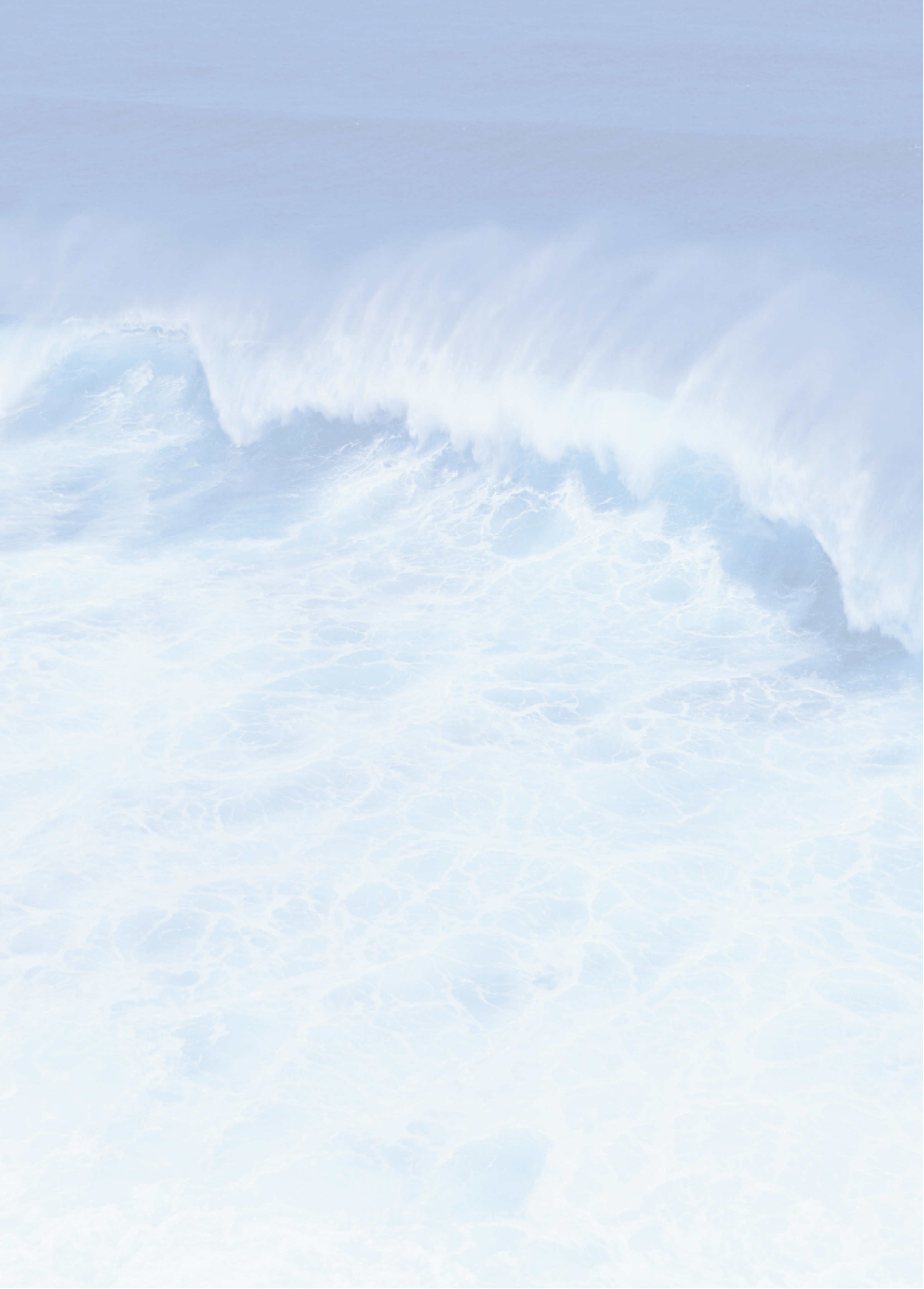

Wave transmission over a narrow crested submerged breakwater with steep slopes

E.G. Repousis* and C.D. Memos

School of Civil Engineering, National Technical University of Athens, Athens, Zografos, 15780, Greece
*Corresponding author: elpirep@hotmail.com

Abstract

As an alternative to emerged detached breakwaters, coastline stabilization can be enhanced by abstracting incoming wave energy by submerged homogeneous breakwaters, most effective in micro-tidal environments of a moderate wave climate exposure. In this regard, a narrow crested submerged permeable rubble mound breakwater with steep slopes is studied herein in terms of technical efficiency, as such type configurations seem to aggregate a series of environmental advantages, but do not produce for certain cases the main desired effect on beach protection from wave impact. Keeping up with the main priority on dealing with beach erosion, but environmental limitations are also present, a structural modification is proposed. This is to decrease the permeability through incorporating a core in the center of the structure. Its subsequent effect on the decrease of wave transmission coefficient was examined through 2-D experiments on physical models of testing scale around 1:10 involving regular and irregular waves. The relevant data analysis, indicated that a rather small core inside a narrow crested permeable rubble mound submerged breakwater with steep slopes, gives a relatively non-negligible extra reduction of transmitted wave energy, furthering the acceptance of submerged breakwaters in the realm of environmental-friendly coastal interventions.

Keywords Submerged breakwaters, Homogeneous breakwaters, Rubble mound, Wave transmission.

1 INTRODUCTION

Nowadays, the need for protecting the shore from wave action is one of the most frequent yet complex issues scientists, engineers, and managers have to deal with. Considering past experience, conventional installations as emerged shore-parallel breakwaters consist a widespread practice in dealing with beach erosion generated by the wind waves' scouring effect on the littoral terrain. Such infrastructure commonly interposed in the surf zone, function as a dissipative barrier for wave loads approaching the swash zone and have proven to significantly decrease the transmitted wave energy and thus its potential erosive sequence. Despite their overall acceptability, it has been observed that emerged breakwaters are usually followed by a significant environmental impact mostly related to their bulky and coarse layout, including low level of water renewal, degradation of the aesthetic value of the landscape, occupation of relatively large seabed areas, sedimentary imbalance like disruption of normal sand grain distribution and local accretion of high-density minerals and heavy metals, local high intensity currents, production of beach erosion pockets, etc. As environmental awareness gradually increases, submerged breakwaters have become a shore protection alternative aiming in confining such side effects most effectively in micro-tidal sea regions (Mediterranean Sea, Baltic Sea and Caribbean) of up to average wave regime exposure. Beyond protecting the coast, it has been deduced that especially permeable rubble mound submerged breakwaters (SPBs) may function similarly to natural reefs as they tend to attract marine life.

In concern to minimizing impact on the environment, submerged breakwaters of high permeability, narrow crest and steep slopes seem to aggregate the environmental advantages mentioned previously, but do not comply under certain conditions with the main goal of protecting sufficiently the coast from erosion due to wave energy impact. Narrow crested permeable breakwaters are considered those with a crest width of 3 to 5 times the mean diameter of the armour unit used and are often referred in the literature as homogeneous submerged rubble mounds or reef-type breakwaters. They seem to have a threshold on wave energy reduction less than a quarter of the total incoming energy for marginally effective free board, thus making engineers cautious in proposing such structures when beach erosion management is the main aim.

For cases as the latter a modification is proposed in this study for widening the structure's applicability range, but still retaining their eco-hydraulic nature. This is to decrease the permeability in the center of the structure through incorporating a core. This layout resembling a state between a homogeneous permeable submerged rubble mound and a conventional low crested breakwaters' design, keeps up with the environmentally friendly character of the narrow crested permeable submerged breakwater, i.e. its small dimensions compared to other adopted breakwater configurations, and sufficient voids and hollows functioning as an artificial habitat for marine life through increased porosity in the structure in conjunction to adequate water circulation capability. By selecting a lower stone unit mean diameter than the outer layer, and of wide grading, the core decreases the transmitted waves through the structure thus enhancing shore protection. For example, Metallinos et al. (2016) by filling the pores of a rubble mound submerged breakwater's physical model with material of smaller gradation reproduced fully impermeable conditions in terms of wave propagation although a significant level of porosity remained.

Focusing on the primary issue of submerged rubble mounds' behaviour on wave energy dissipation, several studies including laboratory investigations on wave transmission and relevant reviews, either independently or as an extension of Low Crested rubble mound breakwaters (LCS) can be found in the literature (Van der Meer and Daemen 1994, D'Angremond et al. 1996, Briganti et al. 2004, Makris & Memos 2007, Buccino & Calabrese 2007, Tomasicchio & D'Alessandro 2013). In all these attempts, technical efficiency is evaluated through the percentage of wave energy abstraction induced by the SPBs, through water surface elevation analysis of the waves propagating over such rubble mounds where a prime quantitative parameter of beach protection measured was the wave transmission coefficient (K_t). Also, numerical models have been used to calculate K_t for some cases of submerged rubble mounds (e.g. Metallinos et al. 2016). A point of interest is that most advanced proposed formulae estimating wave energy abstraction do not consider directly the porosity of the breakwater, and they have been plotted by calibrating semi-empirical equations to a series of different experimental data-sets emphasising on LCS of conventional armour and core layering. Besides inconsistencies of such formulae mostly due to underestimating the factor of core permeability most prominent for narrow crested submerged rubble mounds, a common conclusion point of the above efforts is that main parameters affecting wave energy attenuation due to their presence in regard to certain bathymetry and wave climate, are the crest width, seaward and leeward slope angle, armour unit diameter and particularly free board.

Especially for SPBs, two main wave energy dissipation mechanisms have been observed, i.e. wave breaking (Calabrese et al. 2008) and water flow/wave transmission through and over. However, despite proposed K_t equations, a systematic experimental investigation on wave transmission for one-layer, homogeneous SPBs leading to a K_t parameterization that considers combined phenomena like wave breaker type evolution and turbulent flow within the structure is still to be examined. Considering the above, in order to investigate the proposed SPB design behaviour, experiments were carried out and as expected each of the existing semi-empirical formulae presented certain limitations and inaccuracies compared to this experimental data. A part of that study is only included herein for reasons of brevity.

2 LABORATORY EXPERIMENTS

2.1 Experimental Setup

Evaluation of the proposed SPB's behaviour on wave transmission compared to its homogeneous SPB counterpart, was performed through 2-D experiments involving regular and irregular waves under breaking and non-breaking conditions. Measurements were obtained from free surface elevation experiments that took place in a canal constructed inside a 3-dimensional basin in the Laboratory of Harbor Works at National Technical University of Athens, Greece. Two physical models of the same overall dimensions, the first one without and the other with a core, were constructed and tested subsequently in a canal comprised of two metal sheet walls 4.00 m long, distanced to a 0.80 m width, placed in the wave basin. The wave generator constructed by HR Wallingford is capable to produce both regular and irregular waves, of a wave period spectrum from 1.0 to 2.0 sec (f=1÷0.5 Hz) with wave heights' range depending on the water depth. Further details for the canal facility inside the basin can be found in the experimental work by Memos et al. (2018).

In order to study the differences of wave transmission coefficient above a narrow crested SPB with or without a core, sets of experiments were performed by keeping all parameters constant and modifying only the stone unit mean diameter (d_{n50}) in the inner center of the first model. Initially, for simulating the SPB without the core, the structure was made of natural angular stones with d_{n50}=0.12 m, obtaining a porosity around 0.50. After that, for representing the proposed modified SPB physical model incorporating a core, the gaps between the stones located on the center of the bottom layers for the part of equal width to the crest and two thirds of the breakwater's height were filled with gravel of d_{n50}=0.015 m. Decrease of the overall d_{n50} in this inner section's part also decreased its porosity to around 0.25, pursued for simulating impermeable conditions for the core in terms of obstructing precedent waves' penetration and smooth propagation. As already mentioned, the two rubble mounds followed the same outline geometry and dimensions were representative for narrow crested SPBs. Their height (h_s) was 0.35 m, the crest width 0.30 m and sloping 1:1.5 at both sides (Figure 1). Water depths used were 0.45 m and 0.50 m with free boards (R_c) of 0.10 m and 0.15 m respectively. The wave maker paddle was located 7.5 m from the upstream toe of the SPB models and a dissipative layer, made of gravel beach, was formed starting at 3.5 m from the downstream toe. Testing scale was around 1:10 following Froude scaling similarity and the submerged bars were designed as statically stable.

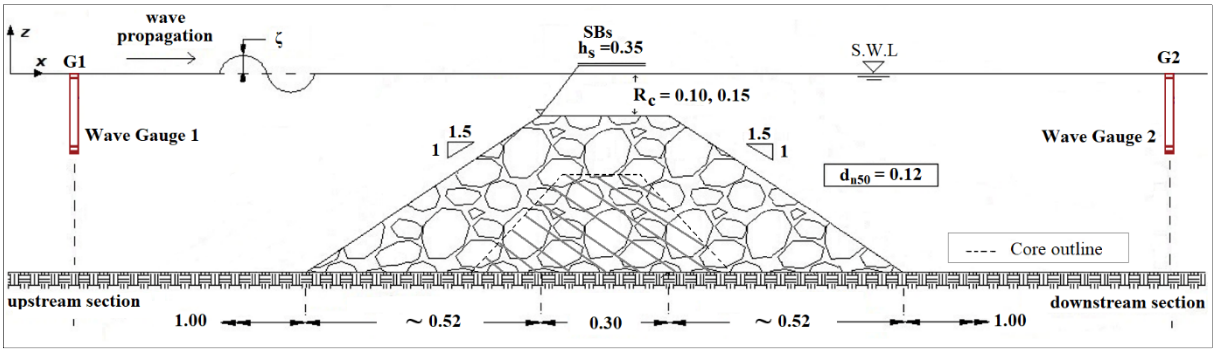

Figure 1 Layout of the physical rubble mound models tested and location of wave gauges (lengths in m).

2.2 Instrumentation

Two resistant-type wave gauges were used to measure water surface elevation (ζ), placed at two specific locations along the canal. As shown in Figure 1. Gauge 1 (G1), used to measure the characteristics of the incident wave, was placed 1.0 m up-wave from the offshore slope toe and Gauge 2 (G2) was positioned 1.0 m inshore from the downslope toe of the SPBs in order to take measurements of the transmitted wave characteristics. The wave gauges were calibrated before each run in order to prevent deviations of the correlation coefficients from linearity. The gauge signals were recorded by a personal computer loaded with WaveData acquisition and analysis software of HR Wallingford. In each run, data were recorded simultaneously from the two stations at a sampling frequency of 50 Hz (dt=0.02 sec), and in total 8,200 data points per gauge for each regular wave run and 45,000 data points respectively for the irregular ones were taken. Wave breaking occurrence was visually observed and noted down.

2.3 Wave Tests

Regular and random waves propagating in waters of intermediate depth were used for the tests. In order to distinguish the influence of the core on wave transmission coefficient, it was essential to perform tests for both breaking and non-breaking events with waves from long to short periods. During preliminary testing of the rubble mounds, discontinuities in wave transmission were observed, most discrete for regular wave runs and for certain wave periods, arguably due also to resonance effects for permeable conditions between wave and submerged structures' geometry, a sort of which also evidenced for emerged rubble mounds by Memos et al. (2018). Under that conceptual basis, this study concentrates also on the wave period parameter. In regard to the application range of SPBs, wave periods ranging from1.15 sec to 2.0 sec were examined. Wave heights for each period were selected (ranging from 0.06 m to 0.13 m) in order to obtain wave steepness values roughly between 0.002 and 0.008, suitable for investigating the wave period influence to K_t. Wave steepness (ε_g) is approached herein as H_i/gT^2, where H_i the incident wave height, T the relevant wave period and g the gravitational acceleration.

3 RESULTS AND DISCUSSION

3.1 Experimental Data Analysis

For regular waves, a total of thirty two different combinations, with eight pairs of different wave heights and periods matching for two different structures and for two water depths, of 0.45 m and 0.5 m respectively, was assorted from the initial dataset. For irregular waves, a total of forty different combinations of a four different ten-pairs dataset was analysed respectively. Beyond the irregular cases, in the regular ones, significant incident wave height (H_{is}) and significant transmitted wave height (H_t) were also calculated through spectral analysis of the free surface elevation timeseries as considerable nonlinearities existed, expected due to the wave interaction with the structures. For all wave runs, K_t was measured equal to H_t divided by H_{is}. Each K_t value was correlated with $\varepsilon_g = H_{si}/gT^2$, where T was set as the spectral peak period (T_p) for the irregular waves. All pairs of incoming wave height and period correspond to G1 measurements.

3.2 Results

The experimental data that were sorted and analysed, were considered satisfactory for a preliminary examination, on the contribution of the modified SPB design to its technical efficiency. Experiments showed that the modification proposed herein by incorporating a rather small core inside a narrow crested rubble-mound SPB with steep slopes, leads to technically adequate wave transmission coefficients behind the structure and thus extends the scope of such structures when coastal management sets priority on dealing with beach erosion, but environmental limitations are also present. Results of K_t are shown in Figures 2 and 3 for regular and irregular waves, respectively.

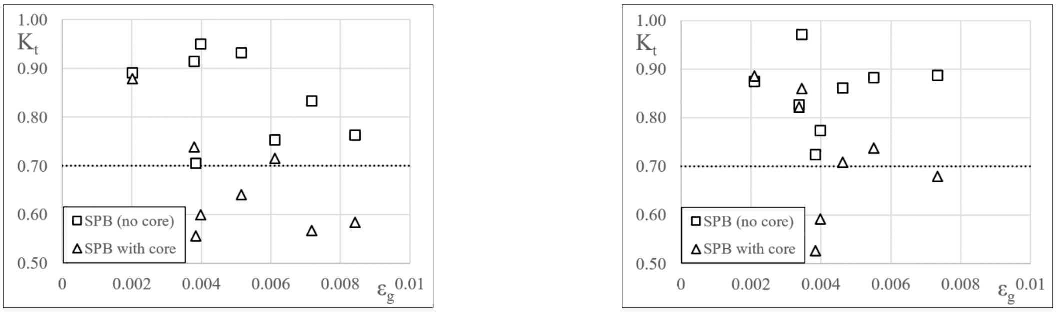

(a) (b)

Figure 2 (a) Comparison of K_t measured values for SPB with and without core, R_c = 0.10 m, regular waves. (b) Comparison of K_t measured values for SPB with and without core, R_c = 0.15 m, regular waves.

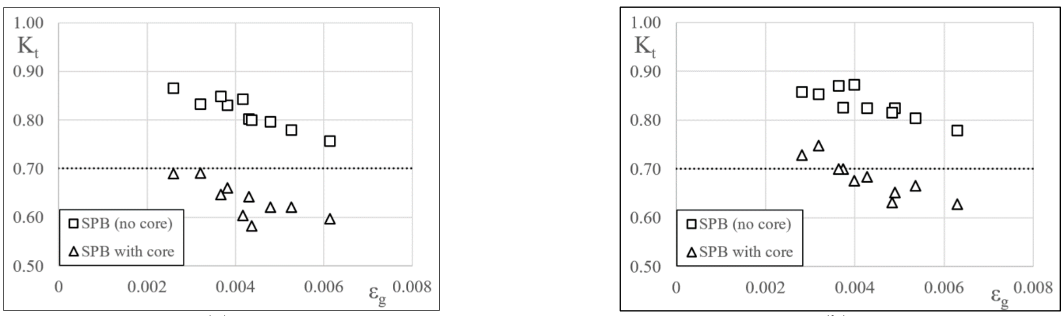

(a) (b)

Figure 3 (a) Comparison of K_t measured values for SPB with and without core, R_c = 0.10 m, irregular waves. (b) Comparison of K_t measured values for SPB with and without core, R_c = 0.15 m, irregular waves.

3.3 Discussion

It can be seen that in both regular and irregular waves the same wave energy dissipation trend is at place, i.e. the core can reduce the transmission coefficient by about 20% or more depending on the actual configuration. In a few runs, however especially for the higher free board and for regular waves, no reduction on that coefficient was observed. This apparently is due to the relatively low wave steepness in the runs (ε_g less than 0.4%), where wave transmission is quite high irrespectively of the actual features of the structure. Following the graphs for regular waves (Figure 2), experimental results confirm a kind of discontinuity for the K_t values for roughly the same wave steepness (ε_g values close to 0.4%) for the SPB layout tested herein. Further study is required in order to examine the processes governing these certain deviations.

In terms of the structure's stability, the core's material sizing should comply with the layer grading criteria similarly to conventional breakwaters. Nevertheless, since the core material is subject due to its reduced height, to lower hydrodynamic and washout actions than the emergent counterpart structure, further research is justified on the said criteria.

Summarizing, in the effort of furthering the applicability of submerged breakwaters to a wider range of cases, the proposed submerged structure in this study is one more step in supporting such infrastructure as technically adequate for coast defense.

Acknowledgements

The authors acknowledge the support of the Direction and staff of the Laboratory of Harbour Works, NTUA, and especially Panagiotis Margaronis, for the technical assistance he provided during the experiments.

References

Briganti R, Van der Meer JW, Buccino M, Calabrese M (2004) Wave transmission behind low crested structures. Proc. Coastal Structures, Portland, Oregon, ASCE.

Buccino M, Calabrese M (2007) Conceptual approach for the prediction of wave transmission at low crested breakwaters. J Waterw Port Coast 133:213–224. doi:10.1061/ASCE0733-950X2007133:3213

Calabrese M, Buccino M, Pasanisi F (2008) Wave breaking macrofeatures on a submerged rubble mound breakwater. J Hydro Environ Res 1:216–225. doi: 10.1016/j.jher.2007.11.003

D'Angremond K, Van der Meer JW, De Jong RJ (1996) Wave transmission at low crested structures. Proc. 25th Int. Conf. on Coastal Engineering, ASCE 3305–3318.

Makris C, Memos C (2007) Wave Transmission over Submerged Breakwaters: Performance of Formulae and Models. Paper presented at the 16th International Offshore and Polar Engineering Conference, Lisbon, Portugal, 2007.

Memos C, Malliouri D, Kazakidou E, Tsoukala V (2018) Impact of wavelength on the stability of rubble mound breakwaters. Paper presented at the 7th International Conference on the Application of Physical Modelling in Coastal and Port Engineering and Science, Santander, Spain.

Metallinos A, Repousis E, Memos C (2016) Wave propagation over a submerged porous breakwater with steep slopes. J Ocean Eng 111:424-438. doi:10.1016/j.oceaneng.2015.11.015

Tomasicchio GR, D'Alessandro F (2013) Wave energy transmission through and over low crested breakwaters. J Coastal Res, special issue 65. doi: 10.2112/SI65-068.1

Van der Meer JW, Daemen IF (1994) Stability and wave transmission at low crested rubble mound structures. J Waterw Port Coast 120:1–19.

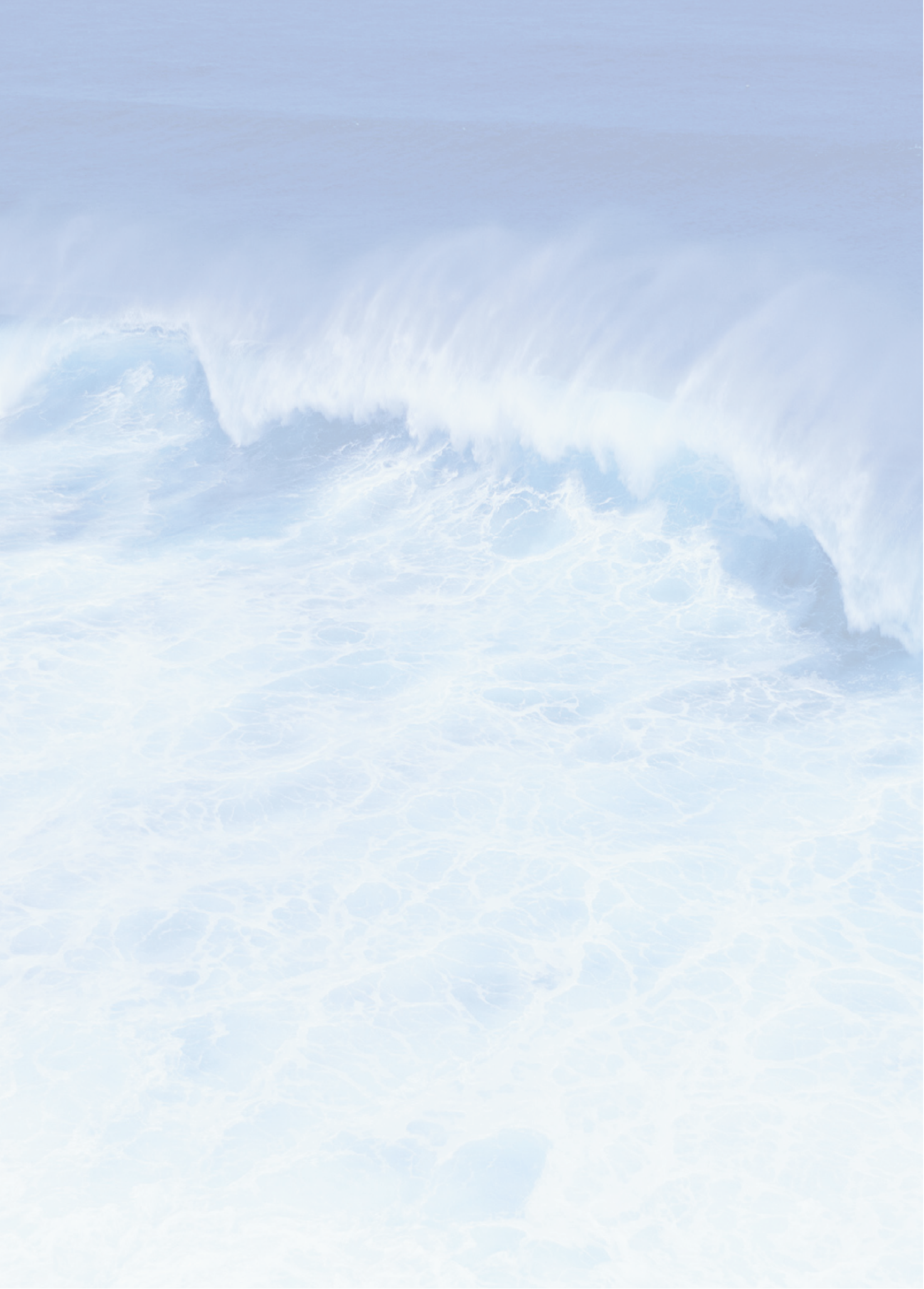

Experimental investigation of sandbag structures in the swash zone as a mild method of coastal protection

I. Biliani[*], A.A. Dimas

Department of Civil Engineering, University of Patras, Patras, 26223, Greece
[*]Corresponding author: irenebvbvbv@gmail.com

Abstract

The present study is an experimental investigation to determine the operational limits for the use of sandbags in the swash zone as a mild method of coastal protection. Different flow conditions were examined with the same geometric scale of 1/20 through Froude similarity. The first set of experiments was conducted in an open channel flume under steady flow loading for different values of the sandbag dimensions and the seaward slope of the sandbag structure. The second set of experiments was conducted in a wave basin under wave loading. Critical velocity and water depth measurements were compared to values in the literature. The comparison revealed that the stability of sandbag structures is controlled by the surf similarity parameter. Moreover, the critical stability and the operational limit of the sandbag structures were identified.

Keywords Sandbags, Coastal Protection, Critical Stability, Operational Limit.

1 INTRODUCTION

The increase of coastal erosion and coastline retreat in recent years is expected to continue in the future as the contributing geological and marine processes may be enhanced due to climate change. The use of sandbags in coastal protection is not new and it remains an alternative environmentally-friendly method. Sandbags comprise natural materials, since they are usually filled with sand from the coast to be protected. The main goal of sandbag structures is to slow down the intense erosion phenomena. Initially, sandbag structures were designed according to modifications of the original Hudson stability formula, which is used for rubble mound breakwaters. Recio and Oumeraci (2007) proposed a process-based stability formula, whose parameters have to be adopted according to the sandbad dimensions.

The purpose of this paper is to determine the operational limits for the use sandbag structures for coastal protection. Experimental measurements were carried out for different flow conditions: i) under steady flow load, in order to compute the critical velocity and water depth, and ii)under monochromatic wave load, in order to compute the critical wave characteristics. The examined parameters of the sandbag structures were the dimensions of the sandbags and the seaward slope of the sandbag structures.

2 EXPERIMENTAL SET UP

The experimental tests were conducted in the Hydraulic Engineering Laboratory of the Department of Civil Engineering, at the University of Patras (Greece).

2.1 Preparation of Sandbags

Froude similarity was used for the experiments under geometric scale of 1/20. Two sizes of sandbags were considered in accordance to an existing application in Australia (Hornsey et al. 2011).The dimensions and properties of the sandbags used are shown in Table 1. The geotextile for both models corresponds to non-woven sandbags, which has relatively lower friction in comparison to woven geotextile. The sand in the sandbags was clean river sand that had to be sifted out to size 0.1 to 0.2 mm. After filling the models geotextile with the sifted sand, they had to be sealed and properly sealed with no flapping areas.

Table 1 Properties of model sandbags

	Model A	Model B
Length (m)	0.1	0.15
Width (m)	0.05	0.075
Height (m)	0.02	0.04
Weight (kg)	0.213	0.431
Volume (m^3)	$0.15*10^{-3}$	$0.3*10^{-3}$
Density (kg/m^3)	1420	1437
Relative Density	0.385	0.402

Model sandbags were placed horizontally in a trapezoidal shape with sand fill ratio of about 100%. The sandbag structures had 2 sandbags width and 4 sandbags height. To maximize the friction between sandbags, they were placed in an alternating pattern. To achieve that, 5×2 sandbags were placed in the 1st and 3rd sandbag layers from the bottom and 4×2 sandbags were placed in the 2nd and 4th layers for model tests A (sum of 36 sandbags for model A), while 4×2 and 3×2 sandbags, respectively, for model tests B (sum of 28 sandbags for model B).Two sets of experiments were conducted in order to take into account both steady flow and wave loading.

2.2 Open Channel Flume Experiments

The first model tests were conducted in an open channel flume (PLINT) 8 m net long, 0.3 m wide and 0.4 m deep. Based on the geometrical scale of 1/20, the maximum water depth was 8 m according to Froude similarity. Two wooden slopes of tanα = 1/2 and 1/1 were installed inthe flume in order to provide the desired support for the sandbag structures. The crest width was 0.1 m and the crest height was 0.14 m, for both wooden slopes. Four experimental scenarios were considered: 1) model A with tanα = 1/2,2)model A with tanα = 1/1, 3) model B with tanα =1/2,and 4) model B with tanα = 1/1.

The velocity measurements where performed with a thin Pitot tube, which could be placed between sandbags, and can measure model velocities up to 1.5 m/s, which is within the required velocity range. The velocity was measured over the whole depth at three stations: (A) upstream of the sandbag structure, (B) at distance l_c upstream of the sandbag structure toe, and (C) above the crest of the sandbag structure. Further details on the structure are presented in Figure 1. Water depth measurements were carried out with a thin ruler in stations A, B, and C.

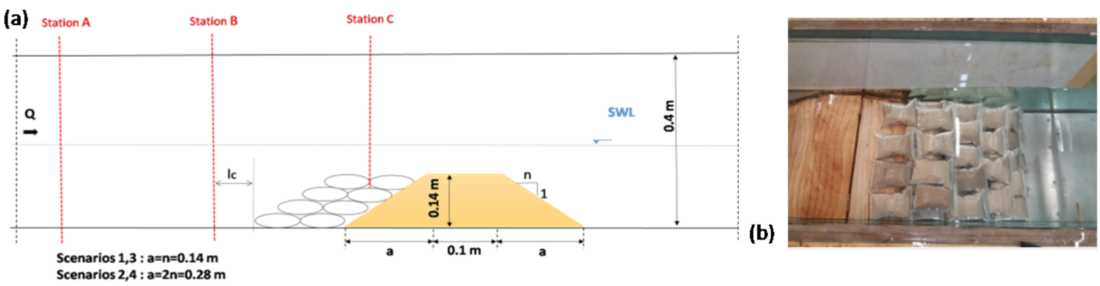

Figure 1 Open channel flume experiment: (a) sketch in model dimensions, and (b) photo

2.3 Wave Basin Experiments

The second model tests were conducted in a wave basin of 12 m long, 4 m width, and water depth of 1.05 m. The wave-maker reproduced monochromatic waves (Stokes) for 4 wave scenarios (Table 2). The sandbag structure was placed on a beach with slope 1/15 and was supported landward by a rock-armored slope with tanα = 1/2 and rocks with nominal model diameter of 0.04 m. Further details of the experimental setup are shown in Figure 2. The sandbag structure was identical to the one of case (1) of the open channel flume.

Table 2 Incident wave scenarios considered in the wave basin where H is the wave height, T is the wave period, L is the wavelength and H/L is the wave steepness.

Case	H (m)	T (s)	L (m)	H/L
WC1	0.04	0.72	0.8	0.05
WC2	0.05	0.8	1	0.05
WC3	0.04	0.93	1.34	0.03
WC4	0.05	1.03	1.67	0.03

For the second set of experiments, velocities measurements were carried out using a side looking Acoustic Doppler Velocimeter (ADV). The ADV method, samples velocities every 0.2 sec, 5 cm away from the instrument, in order to avoid any influence of its presence in the water. The ADV was placed 5 cm away from the centerline of the model sandbags, l_c distance away from the sandbag structure, collecting data for the whole water depth every 1 cm.

Velocity measurements were also taken with the thin Pitot tube. The Pitot tube was also placed in the centerline of the model sandbag structure on top the sandbags. This time, instead of recording the time series, the maximum velocity was measured after the full development of the wave conditions. The Pitot tube is capable of measuring one velocity component, whereas the ADV system is recording all 3 velocity components. The ADV method samples volumes of 0.3 cm^3, thus making it impossible to record velocities close to the free surface or inside porous structures. Free surface elevation conditions were recorded using wave gauges. Three wave gauges (WG1, 2, and 3) were located along the centerline of the sandbag structure as shown in Figure 2a.

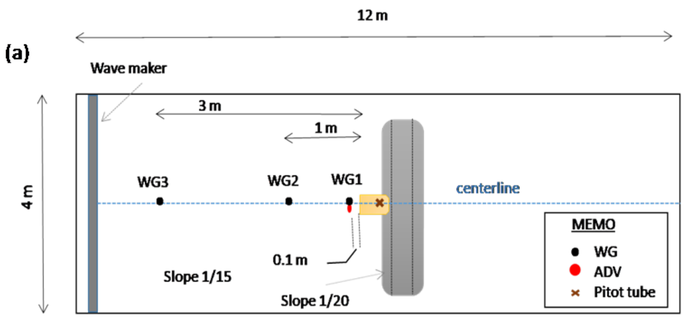

Figure 2 Wave basin experiment: (a) plan-view sketch, and (b) photo

3 RESULTS

3.1 Open Channel Results

The results included the identification of two discrete velocities: the critical velocity and the operational velocity. The critical velocity was defined as the minimum velocity at which incipient motion of the sandbags was observed. During the experiments, the incipient motion was identified as a slight sliding movement of the middle crest sandbag without loss of structure stability. The operational velocity was defined as the maximum velocity at which no sandbag motion was observed. Similarly definitions were used for the critical and the operational water depth.

Typical velocity profiles along the open channel are shown in Figure 3 for the critical stability state of scenario 3.The velocity profiles at station (C) above the sandbag structure crest (14 cm) for both critical and operational states of all scenarios are shown in Figure 4. In all scenarios, inside the top layer of sandbags scenarios, the velocities are about 2 times smaller than the velocities far above the structure crest. The critical and operational velocities of all scenarios upstream and above the sandbag structures are summarized in Table 3. On average, the critical velocity was 1.1 times the operational velocity, while the critical water depth was 1.05 times the operational depth in the present experiments (Table 3).

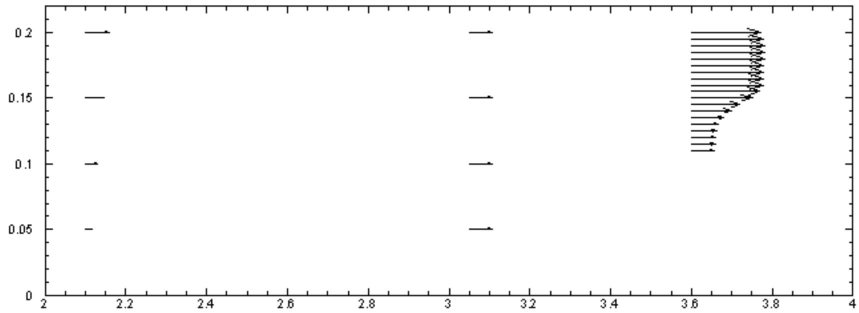

Figure 3 Typical vertical profiles of velocity upstream and over the sandbag structure for the critical state of scenario 3; the sand bag structure toe is at x = 3.35 m, while its crest is at y = 0.14 m

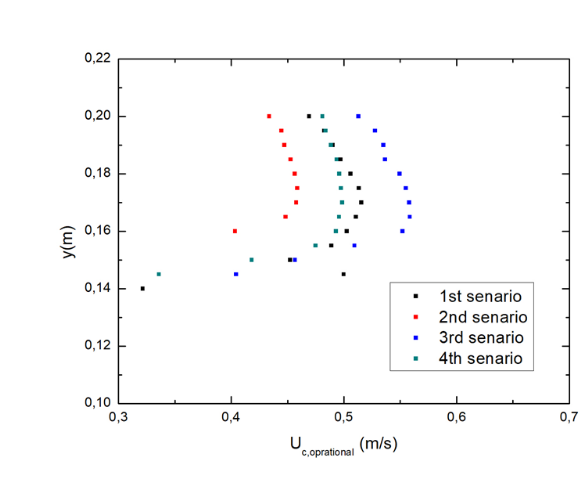

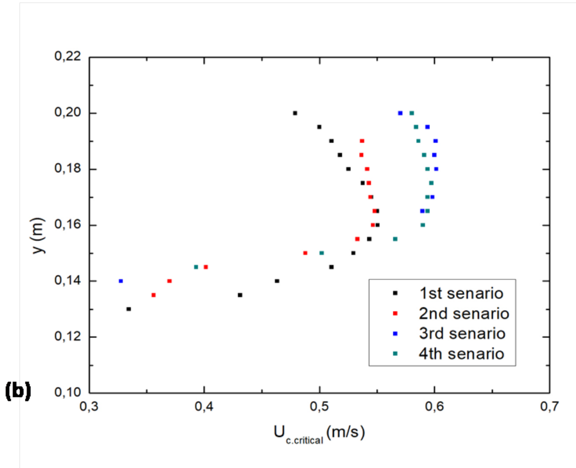

Figure 4 Vertical profiles of (a) operational velocity and (b) critical velocity of the open channel steady flow above the sandbag structure crest

Table 3 Critical and operational results of the open channel experiments

Scenario	**Sandbag**	**tan*a***	**Operational Limits** *d_i*(m)	*U_i*(m/s)	*U_c* (m/s)	**Critical Limits** *d_i*(m)	*U_i*(m/s)	*U_c* (m/s)
1	A	1/2	0.22	0.15	0.51	0.23	0.18	0.56
2	A	1/1	0.20	0.156	0.46	0.21	0.18	0.55
3	B	1/2	0.23	0.17	0.56	0.24	0.19	0.61
4	B	1/1	0.22	0.20	0.5	0.23	0.25	0.59

3.2 Wave Loads Results

Based on the results of the open channel flow for scenario 1 (sandbag A and tanα=1/2) where $U_{i,\text{critical}}$=0.18 m/s and $U_{i,\text{operational}}$ =0.15 m/s, the wave scenarios of Table 2 were considered in order to identify the critical stability and the operational states of the sandbag structure. It was found that scenarios WC1 and WC2 were in the operational regime, while scenarios WC3 and WC4 were in the critical stability regime. Therefore, it was deduced that the critical wave parameter is the wave steepness; the sandbag structure stability decreases with decreasing the wave steepness.

Similar conclusions were drawn by previous researchers who identified the surf similarity parameter $\xi_o = \tan\alpha(H/L)^{-1/2}$ as the critical one to identify the critical stability state of sandbag structures. Specifically, Oumeraci et al. (2002) proposed upper and down stability limits as functions of ξ_o for zero-freeboard structures (Figure 5a). Our operational scenarios WC1 and WC2 are within these stability limits, while our critical scenarios WC3 and WC4 are outside these stability limits (Figure 5a) indicating that the formula in Oumeraci et al. (2002) is conservative in terms of the stability of the sandbag structure.

In contrast to the small scale experiments in Oumeraci et al. (2002), Dassanayake and Oumeraci (2012) conducted large scale experiments of different sandbag structures with different geotextiles under wave attack. Critical stability nomograms were generated for different sandbag structure geometries and sandbag properties. The corresponding nomogram for non-woven geotextiles under regular wave load and zero-freeboard sand bag structure is shown in Figure 5b.Our operational scenarios WC1 and WC2 are indeed below the incipient motion limit, while our critical scenarios WC3 and WC4 are exactly on the incipient motion limit. Therefore, our results are in completed agreement to the predictions of the empirical formula in Dassanayake and Oumeraci (2012).

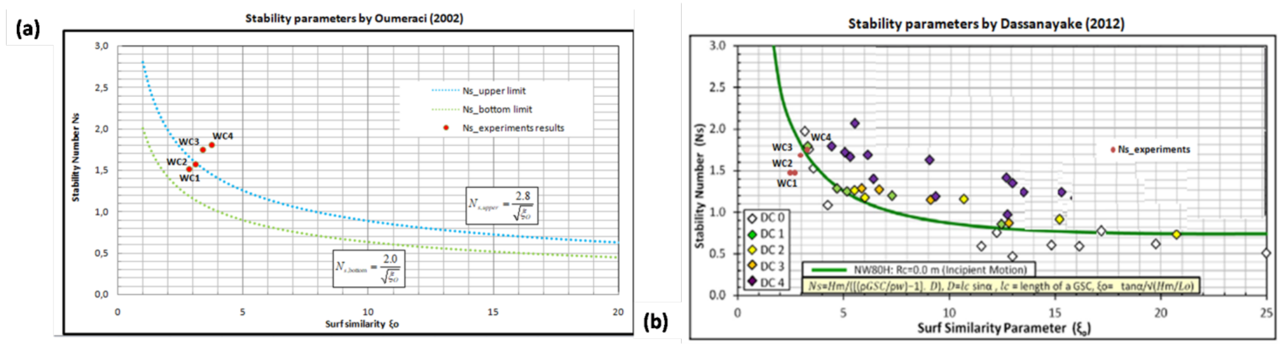

Figure 5 Comparison of experimental results with the empirical formulas in (a) Oumeraci et al. (2002) for zero-freeboard sandbag structures, and (b) Dassanayake and Oumeraci (2012) for zero-freeboard sandbag structures, non-woven geotextiles, and 80%filled sandbags

4 CONCLUSIONS

The stability of sandbag structures, to be used as a mild method of coastal protection, was studied experimentally both under steady flow and wave load. The critical and the operational states of the structures were identified and it was found, in agreement to Dassanayake and Oumeraci (2012), that the stability limit under wave load depends on the surf similarity parameter.

References

Dassanayake DT, Oumeraci H (2012) Engineering properties of geotextile and sand containers and their effect on hydraulic stability and damage development of low-crested/submerged structures. International Journal of Ocean and Climate Systems(3): 135-150.

Hornsey WP, Carley JT, Coghlan IR, Cox RJ (2011) Geotextile and container shoreline protection systems: Design and applications. Geotextiles and Geomembranes 29(4): 425-439.

Oumeraci H, Hinz M, Bleck M, Korthenhaus A (2002)Sand-filled geotextile containers for shore protection. Proc. Coastal Structures 2003, Portland, Oregon, USA.
Recio J, Oumeraci H (2007) Effect of the deformation on the hydraulic stability of coastal structures made of geotextile sand containers. Geotextile and Geomembranes 25(4-5): 278-292.

Experimental study of the wave generated current field in the vicinity of a segmented, detached rubble -mound, zero-freeboard breakwater

K.A. Galani*, A.A. Dimas

Department of Civil Engineering, University of Patras, Patras, 26500, Greece
*Corresponding author: kgalani@upatras.gr

Abstract

Low-crested breakwaters are widely used for coastal protection against erosion, they are usually constructed parallel to the shoreline and they behave as dampers of wave energy that will finally reach the shoreline. The aim of the present work is the experimental study of the flow developed in the vicinity of a detached, rubble-mound, zero-freeboard breakwater (ZFB). Experiments were conducted in a wave basin 12 m long, 7 m wide and 1.05 m deep. The wave basin is equipped with a paddle wavemaker, controlled by an Active Wave Absorption Control System for wave generation with concurrent absorption of reflected waves directed back to the paddle. The physical model of the detached, rubble mound ZFB was constructed using two rows of rocks with a median diameter of $D_{n,50}$ = 4 cm in the armor layer (crest, slopes and roundhead) and it was placed above a steep sloping beach of 1/15. Five cases of incoming regular waves were examined and velocity measurements were obtained in the vicinity of the ZFB using both ADV and PIV. Velocity measurements were used to extract the wave-generated current field around the ZFB with emphasis in the vicinity of the breakwater roundhead where a strong rip current developed, with velocities in the range of 0.10 to 0.46 m/s, depending on the incoming wave characteristics. The rip current presented a non uniform vertical distribution and its magnitude increased linearly from the slope bottom towards the free surface.

Keywords Detached zero-freeboard breakwater, Wave-generated current field, Rip current.

1 INTRODUCTION

Low-crested breakwaters (LCBs) are widely used as a coastal protection measure against erosion. Such a structure can operate either individually or as part of an array of segmented, detached, low-crested breakwaters, and it is placed parallel to the shoreline and at a distance from it. The basic function of coastal breakwaters is the reduction of wave energy that will eventually end up on the shoreline, due to wave breaking on the seaward slope or on the crest of the structure, to reflection of wave energy from the seaward slope towards the open sea and to energy dissipation inside the structure's porosity or to friction with the rough surface of the seaward slope.

For the proper design of such structures, information on the flow characteristics developing in their vicinity is crucial. Several studies have been carried out, trying to illuminate and understand the physical processes and mechanisms governing such flows. In particular, Wind and Vreugdenhil (1986) performed experimental measurements in order to understand the mechanisms governing the rip current development near coastal structures (e.g. groynes) and to study the spatial and temporal scale of such currents. Petti et al. (1994) studied experimentally the large scale vortices developed by waves breaking above a submerged breakwater. Mory and Hamm (1997) performed measurements of wave height, surface elevation and wave generated currents around a detached breakwater for incoming regular and irregular waves. Haas and Svendsen (2002) studied experimentally the vertical structure of rip currents developed near longshore bars. Kramer et al. (2005) performed experiments in order to study the waves - LCB interaction, in terms of flow velocity and turbulence developing near LCBs within the European Project DELOS. DELOS results regarding waves, wave runup, overtopping and currents around LCBs were presented in Zanuttigh and Lamberti (2006). Vicinanza et al. (2009) studied experimentally the combined effect of transmission/diffraction on wave transformation and induced currents in the sheltered area of a single detached LCB. Finally, Kim et al. (2016) experimentally studied the rip current developing near the tip of a submerged breakwater, while they also performed LES simulations in order to predict the generation of rip currents.

It can be easily realized that coastal hydrodynamic circulation near LCBs has attracted the interest of many researchers. A marginal case of LCB is the Zero-Freeboard breakwaters (ZFBs), the crest level of which matches the Still Water Level (SWL). Some studies on the hydrodynamic circulation around ZFB breakwaters exist; their number however is considerably smaller in comparison to the emerged/submerged cases of LCBs. The aim of the present study is the experimental investigation of the impact of a rubble-mound ZFB breakwater on the hydrodynamic circulation above a steep-sloping beach of 1/15, and specifically of the wave-generated currents' field in the vicinity of the structure. Emphasis is given to the structure and intensity of the rip current developing near the heads of the ZFB breakwater.

2 EXPERIMENTAL SETUP

Experiments were conducted in the wave basin of the Hydraulic Engineering Laboratory, Department of Civil Engineering, University of Patras, which is 12 m long, 7 m wide, and has a maximum still water depth of 1.05 m. The wave basin is equipped with a paddle wavemaker, controlled by an Active Wave Absorption Control System (Schäffer and Hyllested, 1999) for wave generation with concurrent absorption of reflected waves directed back to the paddle.

Opposite to the wavemaker, a physical model of a segmented, detached, rubble-mound ZFB was placed above a constant sloping beach of 1:15 and between water depths d = 18 cm (seaward toe) and d = 12.6 cm (leeward toe). The shape, dimensions and location of the ZFB are shown in Figs 1 and 2. The armor layer of the ZFB consisted of two rows of rocks with nominal diameter Dn50 = 4 cm, while the core of the ZFB was impermeable as it was formed by a framed steel sheet. The weight of the rocks of the armor layer was selected using the corresponding formula in Van der Meer (1990), assuming a design wave height of 0.12 m. Wave guide walls at 4 m apart were also placed in the wave basin (Fig. 1) in order to model a hypothetical prototype segmented, detached ZFB; each wave guide corresponds to the symmetry plane in the middle of the gap between ZFB segments.

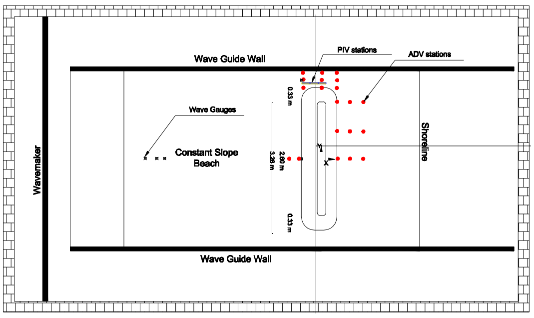

Figure 5 Sketch of the experimental setup (plane view) of the segmented, detached ZFB on a steep beach of slope 1/15; Velocity and surface elevation measurements positions are shown.

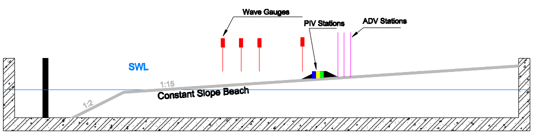

Figure 6 Sketch of the experimental setup (side view) of the segmented, detached ZFB on a steep beach of slope 1/15; Velocity and surface elevation measurements positions are shown.

Five cases of incoming regular waves were examined. The parameters of the wave cases are summarized in Table 1 where H is the wave height at the wavemaker. Free surface elevation measurements were performed using wave gauges of the resistance-type, while velocity measurements were obtained in the vicinity of the ZFB using both Acoustic Doppler Velocimetry (ADV) and Particle Image Velocimetry (PIV).

Table 1 Incident wave height, H and period, T at the wavemaker depth of 1.05 m and the incident wave breaking depth, d_b on the beach before the ZFB installation. The breaking point was identified visually.

Wave Case	H (m)	T (s)	d_b (m)
1	0.10	1	0.110
2	0.10	1.5	0.125
3	0.10	2	0.115
4	0.08	1.5	0.090
5	0.12	1.5	0.150

The PIV apparatus used was an underwater planar PIV system, which was supported by a platform above the water surface. The main components of the PIV system were a double-pulsed Nd: YAG laser head, an optics system and a digital 12-bit CCD camera. The laser head was attached on the platform, while the housings of the optics system were totally submerged and attached to the platform via thin vertical tubes. The CCD camera with a full image resolution of 5 million px was also operated fully submerged into the water. Adjustments in the laser head and the CCD camera settings were made remotely using the PIV software. For the flow visualization, hollow glass spheres with a mean diameter of 10 μm and a density of 1.1 g/cc were used as seeding particles. The calculation of the instantaneous velocity vector fields was achieved by determining the displacement of the seeding particles though a two-frame, multi-pass cross-correlation. PIV measurements were performed in three vertical FOVs along the ZFB gap centerline (Fig. 2). ADV measurements were performed by means of a 16-MHz MicroADV probe with three side-looking acoustic receivers and one acoustic transmitter. The recording frequency was set equal to 50 Hz, while measurements were conducted at twenty stations around the ZFB, nine stations at ZFB leeside, nine stations at the ZFB gap and two seaward the ZFB model. At each ADV station, velocity measurements were obtained at several depths starting from 2.2 cm above the slope bed and moving upwards up to the trough level with a step of 1 cm. Velocity measurements were initiated after quasi-steady wave conditions were established inside the wave tank, and particularly after 150 s from the initiation of wave generation.

3 RESULTS

PIV instantaneous velocity vector fields and ADV instantaneous velocity timeseries were period-averaged to obtain the current field developed in the vicinity of the ZFB, by taking into consideration 60 consecutive wave periods. Fig. 3 presents the wave-generated current field in the vicinity of the ZFB for incoming regular waves with H = 0.10 m and T = 2 s. Due to symmetry, only half of the sheltered area is shown. In the ZFB leeside and specifically along the transverse symmetry axis of the model (Y=0), a wave-generated current is observed with a seaward direction close to the slope bottom and an alongshore direction near the free surface. The driving mechanism for the current generation is the wave transmission above the ZFB crest. Due to wave transmission, a significant volume of fluid overleaps the structure's crest, thus a mass-flow towards the shoreline is created. In order to balance this mass-flow, a cross-shore wave-generated current develops with seaward direction. At the ZFB level and near the free surface this cross-shore current "collides" with the volume of fluid overtopping the ZFB at the time, and the current is forced to turn and move parallel to the shoreline. In case where more than one detached ZFB are in series, the wave-generated current moving alongshore meets the corresponding current of the neighboring ZFB, these two currents contribute and divert towards deep water through the gap between the ZFBs. The result of all this interaction is the development of two superficial counterclockwise vortices in the ZFB leeside. The wave-generated current field shown in Fig. 3 is typical for all the incoming wave cases tested. The main difference observed for different incoming wave characteristics is the magnitude of the wave-generated currents. Regarding the cross-shore wave-generated current, it was observed that its magnitude increases with increasing incoming wave period and decreasing incoming wave height. As for the rip current, generated near the tip of the ZFB model, it presented larger velocities for wave cases 2 and 5 (Table 1). This was attributed to the fact that the driving mechanism for the rip current generation was the wave setup established in the ZFB leeside, which was measured to be larger in wave cases 2 and 5 (Galani and Dimas, 2018).

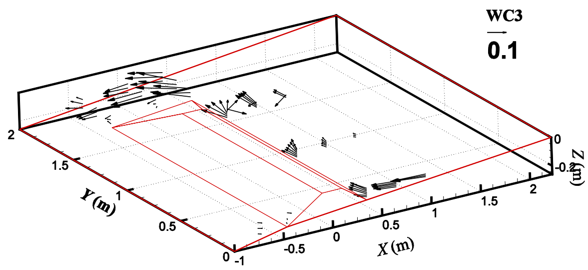

Figure 3 Wave generated current field near the ZFB for incoming regular waves with $H = 0.10$ m and $T = 2$ s.

Fig. 4 presents the period-averaged horizontal velocity vector fields and magnitude contour plots of the rip current developing in the ZFB gap at FOV A, B and C (blue, yellow and green window, respectively; Fig. 2) for all wave cases tested (Table 1). It is observed that the rip current is a strong cross-shore current with magnitudes up to 0.46 m/s. In general, the rip current has a non uniform vertical distribution and more specifically its magnitude increases linearly from the slope bottom towards the free surface. In the FOV with the smaller depth (FOV C, green window; Fig. 2), rip current velocity is large enough to "sweep" the entire water column in the majority of wave cases tested. At larger depths (FOV A and B, blue and yellow window, respectively; Fig 2), the rip current is directed seaward by moving mostly close to the free surface. These observations are in line with the observations of Haas and Svendsen (2002), who have studied the rip current developing above a submerged bar and have found that the rip current is practically uniform in depth inside the surf zone, while upstream the surf zone it presents larger velocities near the free surface than close to the sea bed.

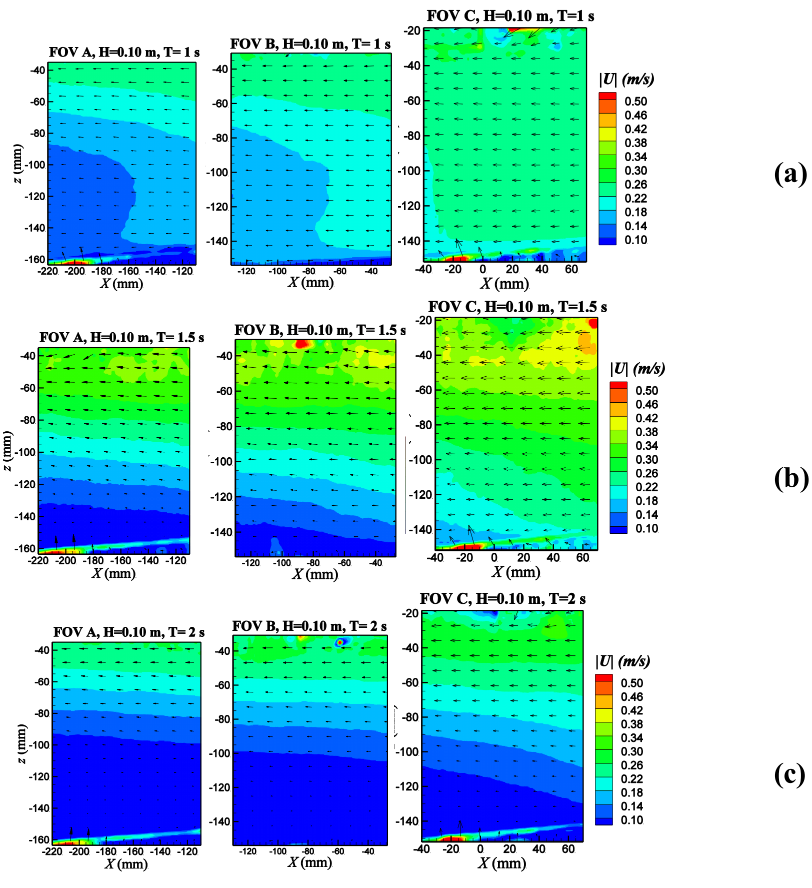

Figure 4 Period-averaged horizontal velocity vector fields and magnitude contour plots of the rip current developing in the ZFB gap at three adjacent vertical planes (FOV A, B and C, blue, yellow and green window, respectively; Fig. 2) for incoming (a) wave case 1, (b) wave case 2, (c) wave case 3, (d) wave case 4 and (e) wave case 5 (Table 1).

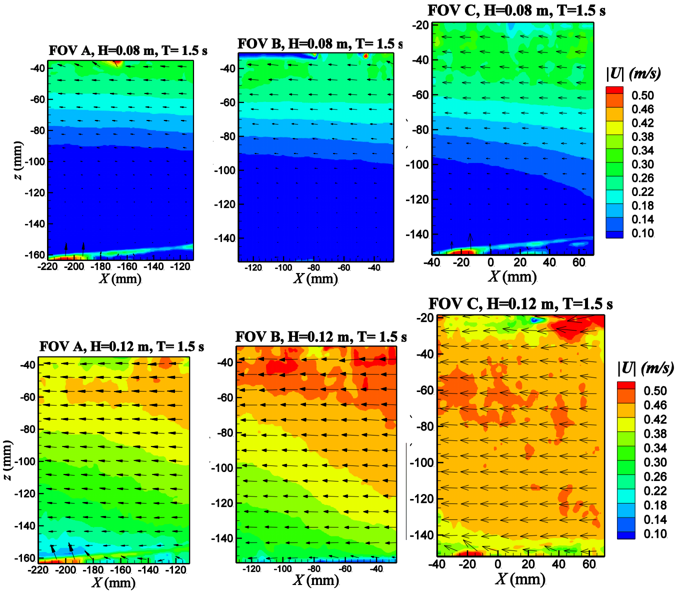

(d)

(e)

Figure 4 (*Continued*).

Acknowledgements

This work was funded by the matching contribution (5231) of GSRT to the Initial Training Network SEDITRANS, implemented within the 7th Framework Programme of the European Commission.

References

Galani K.A. and Dimas A.A. (2018). "Experimental Study of the flow induced by waves in the vicinity of a detached low-crested (zero-freeboard) breakwater". Proc. 36th Int. Conf. Coastal Eng., ASCE, Baltimore, Maryland.

Haas, K.A. and I.A. Svendsen (2002). "Laboratory Measurements of the Vertical Structure of Rip Currents". J. of Geophysical Research. Vol. 107 (C5), pp. 15-1 - 15-19.

Kim, I.H., W.D. Lee, S. Shin, J.H. Kim, D.S. Hur and W.C. Cho (2016). "Study on Rip Current Generated by Submerged Breakwaters: Field Observation and Numerical Simulation". J. of Coastal Research. Special Issue No. 75, pp. 1352-1356.

Kramer M., Zanuttigh B., van der Meer J.W., Vidal C., Gironella F.X. (2005). "Laboratory experiments on low – crested structures", Coastal Engineering, Vol. 52, pp. 867 – 885.

Mory, M. and Hamm, L. (1997). "Wave height, setup and currents around a detached breakwater submitted to regular or random wave forcing", Coastal Engineering, vol. 31, pp. 77 - 96.

Petti, M., Quinn, P. A., Liberatore, G., and Easson, W. J. (1994). "Wave Velocity Field Measurements over a Submerged Breakwater", Coastal Engineering, pp. 525 – 539.

Schäffer, H.A., and Hyllested, P., 1999. Reflection analysis using an active wave absorption control system. Proc. Coastal Structures '99, Santander, Spain, pp. 93-99.

Van der Meer, J.W., 1990. Data on wave transmission due to overtopping. Delft Hydraulics, Rep. no H986, prepared for CUR C67.

Vicinanza, D., Cáceres, I., Buccino, M.nGironella, X., Calabrese, M., (2009). "Wave disturbance behind low-crested structures: Diffraction and overtopping effects". Coastal Eng. Vol. 56, pp. 1173-1185.

Wind, H.G. and C.B. Vreugdenhil (1986). "Rip - Current Generation Near Structures". J. of Fluid Mechanics. Vol. 171, pp. 459-476.

Zanuttigh, B., Lamberti, A., (2006). "Experimental analysis and numerical simulations of waves and current flows around low-crested rubble-mound structures". J. Waterway, Port, Coastal, Ocean Eng. Vol. 132(1), pp. 10 - 27.

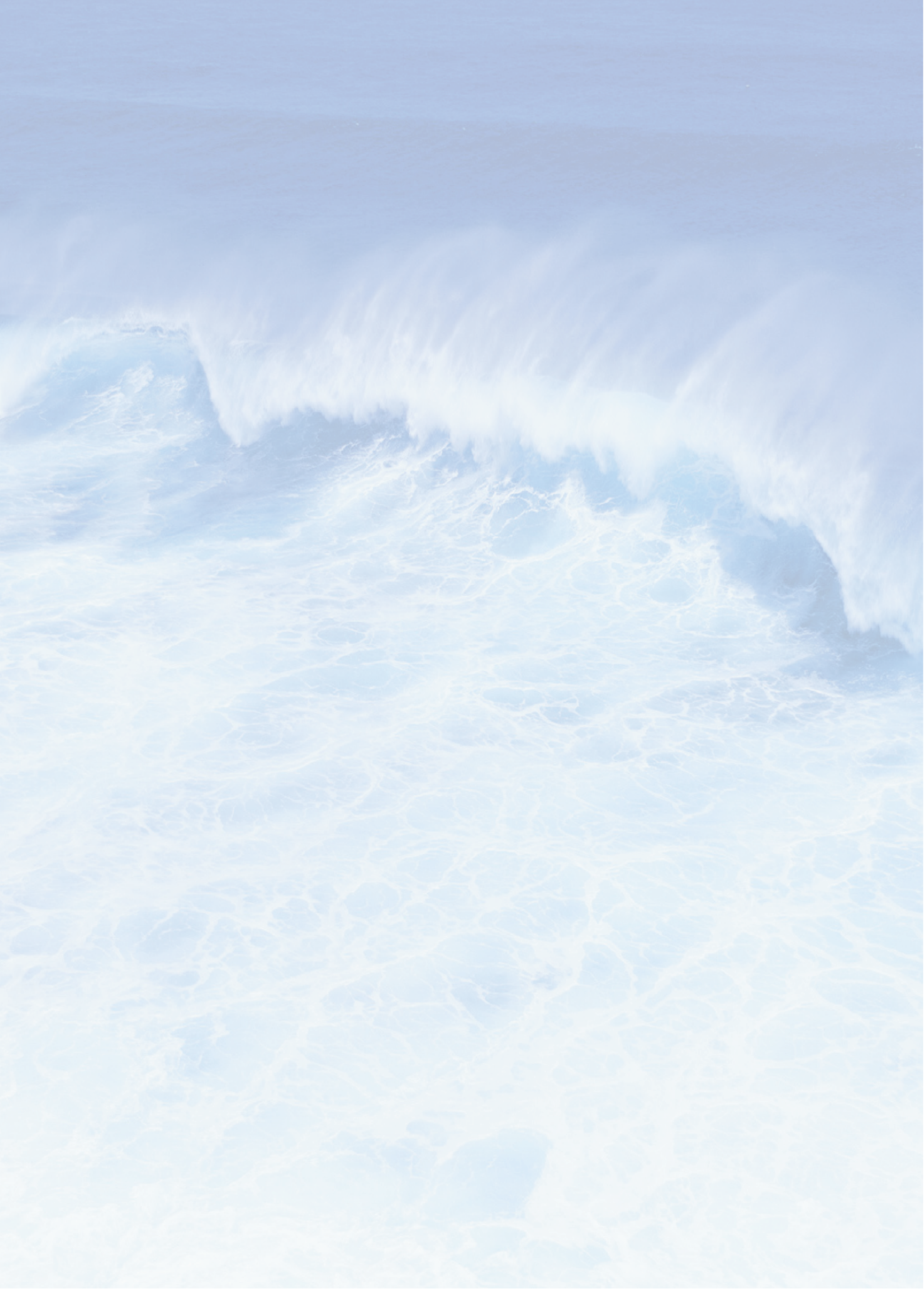

Assessing failure probabilities of rubble mound breakwaters for extreme conditions under climate change

P. Galiatsatou[1*], C. Makris[2], D. Kokkinos[1], P. Prinos[1]

[1]Lab of Hydraulics, School of Civil Engineering, Aristotle University of Thessaloniki (AUTh), Thessaloniki, 54124, Greece
[2]Lab of Maritime Engineering, School of Civil Engineering, AUTh, 54124, Thessaloniki, Greece
[*]Corresponding author: pgaliats@civil.auth.gr

Abstract

In the present work, the performance of a selected conventional rubble mound breakwater to different failure mechanisms under extreme conditions associated with climate change, is investigated. The nonstationary Generalized Extreme Value distribution (GEV) is fitted to annual extremes of offshore significant wave heights and sea surface heights due to storm surges at the site of the defence. Extracted distributions for extreme waves are transferred to the breakwater site by means of a statistical approach. Time-dependent future failure probabilities of the structure are assessed for different failure mechanisms within the general framework of nonstationary reliability analysis. Failure probability estimates are used to determine future periods of increased vulnerability of the studied structure to different ultimate limit states. The analysis defines critical failure mechanisms and proves that the assumption of stationarity underestimates the total failure probability of the structure under extreme marine conditions.

Keywords Reliability, Rubble mound breakwater, Climate change, Extreme value theory.

1 INTRODUCTION

Global climate change is expected to cause significant long-term changes in mean sea level (MSL), wave height and storm variability (IPCC 2007, 2012). The general inception of a changing climate with extreme marine events of higher intensity and frequency and MSL rise increases vulnerability and exposure of port and harbour structures to different failure modes, resulting in their inability to fulfill their requirements. Increased future hydraulic loadings, combined with the limited residual service lifetime of many of them, and the fact that economic activity is assembled in these areas, creates a need for a reliable estimation of failure probabilities of such defences under future extreme marine conditions.

Although the majority of scientific studies examining climate change effects in the Mediterranean has focused on the variability and long-term trends in MSL (*i.e.* Adloff et al. 2015), changes in extreme storm surges and waves under climate change started to gain interest quite recently (*i.e.* Benetazzo et al. 2012, Galiatsatou et al. 2016, Makris et al. 2016). The effects of climate change on coastal and port or harbour structures received considerable attention only during the last decade (*i.e.* Suh et al. 2013, Isobe 2013, Burcharth et al. 2014).

Risk-based approaches are currently gaining ground in the process of evaluating safety of coastal structures subject to increased marine conditions. Reliability analysis, corresponding to assessing failure probabilities of such defences, forms an inherent part of a risk-based approach to designing new or evaluating the performance of existing coastal structures (*i.e.* Dai Viet et al. 2008, Kim and Suh 2010, Naulin et al. 2015, Galiatsatou et al. 2018). The vast majority of these studies focus on specific variables of the marine climate (*i.e.* MSL rise or wave climate) and do not consider nonstationarities of marine climate variables under future climate conditions.

In the present work, the performance of a selected conventional rubble mound breakwater to different failure mechanisms under extreme marine conditions associated with climate change, is investigated. Failure probabilities of the structure are assessed for different failure mechanisms, considering variations in MSL, wave climate and storm surge, within the general framework of nonstationary reliability analysis.

2 METHODOLOGY

2.1 Extraction and analysis of extreme sea states at port or harbour sites

The boundary conditions for designing or evaluating the safety of port or harbour protection structures mainly include the hydraulic conditions at the site of the defence. Collapse of the defence is associated with Ultimate Limit States (ULS) happening under extreme marine conditions. To capture nonstationarity in the univariate marine extremes, a time-dependent Generalized Extreme Value (GEV) distribution (Galiatsatou et al. 2019) is fitted to deepwater significant wave height (H_s) annual maximum events. To estimate the parameters of the nonstationary distributions a 50-years length moving time window with an annual time step is used. The derived parameter estimates correspond to the last year of each 50-years period. Appropriate nonstationary distribution functions are also fitted to extreme sea level heights due to storm surge (*SLH*) at the site of the structure (Makris et al. 2018).

The abovementioned nonstationary univariate distributions for extreme H_s are then transferred to the site of the breakwater following an approach proposed by Suh et al. (2013). The latter is based on the assumption that H_s distributions in coastal water reduce in the mean and in the standard deviation compared with the deepwater waves, so that their coefficient of variation remains constant. However, the shape of their distribution does not undergo any significant changes. This procedure, which also considers design quantities of the existing structure, is implemented for each moving window to extract time-dependent estimates of all GEV parameters in the study area.

2.2 Assessment of nonstationary failure probabilities under climate change

Principal failure mechanisms of conventional rubble mound breakwaters include failure or instability of the windward armour layer, failure of the leeward slope, scouring of the toe, excessive overtopping, the slip cycle, sliding and tilting of existing superstructures, and excessive settlement. Three failure modes are considered here as the main types of instability under extreme marine conditions, namely instability of the windward primary armour layer, excessive overtopping, and scouring of the breakwater toe. Reliability analysis hinges on the use of the probability of failure, P_f, as a measure of the structure performance. The reliability function, Z, for a certain limit state is defined as the difference between the resistance of the structure and the load it is exposed to. The failure domain is defined for $Z \leq 0$. Reliability functions contain variables of the marine climate at the windward side of the breakwater, as well as variables describing geometrical and material properties of the studied structure. Level II reliability methods, including the linearization of the reliability function at an appropriately defined design point of the failure space, are used in this work to assess time-dependent P_f for the limit states.

The reliability function for hydraulic stability of a windward primary armour layer composed of accropodes is based on the stability formula of Van der Meer (1998), using a safety factor of 1.5:

$$Z_{stability} = 2.5 \cdot \Delta \cdot D_n - H_{su} \tag{1}$$

where $\Delta = (\rho_{ac}/\rho_w) - 1$ and ρ_{ac} and ρ_w are accropode and water densities [ton/m^3], D_n [m] is the characteristic diameter of armour stone units, and H_{su} [m] is the significant wave height in front of the studied breakwater corresponding to its ULS. The reliability function for excessive wave overtopping is based on the formula of EurOtop (2007):

$$Z_{overtopping} = q - 0.2 \cdot C_r \cdot \exp\left(-\frac{2.3 \cdot R_c}{\gamma_f \cdot H_{su}}\right)\sqrt{g H_{su}{}^3} \; with \; R_c = H_{crest} - MSLR - TR_{max} - SLH \tag{2}$$

where q [m^2/s] is the maximum allowable overtopping discharge, $C_r = 3.06 \cdot exp(-B/H_{su})$ is the reduction factor due to effect of armoured crest berm of width B [m], γ_f is the influence factor for crest armour units, and R_c [m] is the freeboard height resulting when subtracting MSL rise, $MSLR$ [m], maximum tidal range, TR_{max}, and storm surge, SLH [m], from crest level height, H_{crest} [m]. The reliability function for toe stability is based on the formula proposed by Van der Meer et al. (1995):

$$Z_{scouring} = \left(0.24\frac{h_t}{D_{n50}} + 1.6\right) N_{od}{}^{0.15} \Delta D_{n50} - H_{su} \ with\ h_t = d + MSLR + TR_{mean} + SLH \quad (3)$$

where h_t [m] is the total water depth at the breakwater toe, D_{n50} [m] is the characteristic diameter of toe elements, N_{od} is the number of displaced units within a strip with width D_{n50}, d [m] is the depth of the water column from MSL to breakwater toe, and TR_{mean} [m] is the mean tidal range of the area.

3 STUDY AREA AND AVAILABLE DATASETS

The selected conventional rubble mound structure is located at the port of Alexandroupolis in the northern Greek coast of the Aegean Sea. The southern windward breakwater protects the port from waves of south and southwestern origin. Its newly constructed part of length 1155m has a primary armour layer made of Accropode blocks with unit volume of 5m^3. The breakwater has been designed for deepwater H_s=5.25m and peak spectral period T_p=9s, and for a maximum incident H_s=4m locally at the breakwater site. The water depth in front of the breakwater toe is d=5m, its crest level height H_{crest}=5.10m, and its crest width B=7.7m. Its windward and leeward slopes are 3/4. The breakwater toe consists of rocks with maximum weight of 6tons. The necessary wave and *SLH* data used in this paper cover a period of 150 years (1951-2100) and are derived from 3-hourly simulation results for the Greek Seas, produced by SWAN wave model and the high-resolution two-dimensional, barotropic, storm surge model GreCSS (Makris et al. 2016). Forcing of wind and atmospheric pressure fields are derived from dynamically downscaled simulations with Regional Climate Model RegCM3, and future climate projections are based on IPCC-A1B emissions scenario (IPCC 2007).

The Aegean Sea is a semi-enclosed water basin labelled as a marginal sea, with rather low maxima of storm surge-induced sea levels in the coastal zone, identifying H_s extremes as the primary cause of port downtime (stoppage of operations within the basins due to malfunction of the protection system). Wave height events of directions affecting the port of Alexandroupolis, exceeding a threshold of 1.5m for durations more than six hours, were initially selected at a representative point of the SWAN model grid in the offshore area of the study site. Waves have been corrected for bias (Makris et al. 2016) and annual maxima were extracted to be fitted by the nonstationary GEV distribution (see Sect. 2.1). Nearshore storm-driven *SLH* corresponding to the respective annual maxima of H_s was also used in the analysis. A five-day window of *SLH* data was used, covering the time of corresponding records of H_s maxima by 2.5 days bilaterally, and extracted data was fitted by the nonstationary GEV distribution. To assess the MSL rise in the Aegean Sea (used in Eqs. 2-3), both a steric and a component of mass addition due to ice melting were considered, resulting to a total value of 25cm by 2100 (Galiatsatou et al. 2019). The maximum tidal range near the port of Alexandroupolis is considered to be TR_{max}=0.66m while the respective mean tidal range is TR_{mean}=0.24m (HNHS 2011).

4 RESULTS

The nonstationary GEV distribution was first fitted to extreme deepwater H_s and nearshore *SLH* and parameters of the fitted 50-year windows were estimated using L-moments. Figure 1 presents time-dependent estimates of 100-years return levels of H_s and SLH for the selected study site, together with their associated 95% confidence intervals estimated using a parametric bootstrap approach.

H_s return level estimates present an increasing trend in the first half of the 21st century, with their maximum values in the interval 2040-2055. A second peak in H_s extremes appears around 2065-2070, while H_s decreases rapidly at the end of the century. Most probable estimates of H_s vary more than 33% within the 21st century, while predictions in the mid-century appear highly uncertain (very wide 95% confidence intervals). GEV distributions of deepwater H_s extremes have been then transferred to the studied breakwater site (see Sect. 2.1). SLH extremes at the breakwater site show quite similar variation to the respective deepwater H_s estimates. They present an evident increasing trend in the interval 2020-2040, and a decreasing one in 2070-2100. Two peaks in SLH extremes can be distinguished, around 2040 and 2065, while predictions in the interval 2040-2070 are characterized by increased uncertainty.

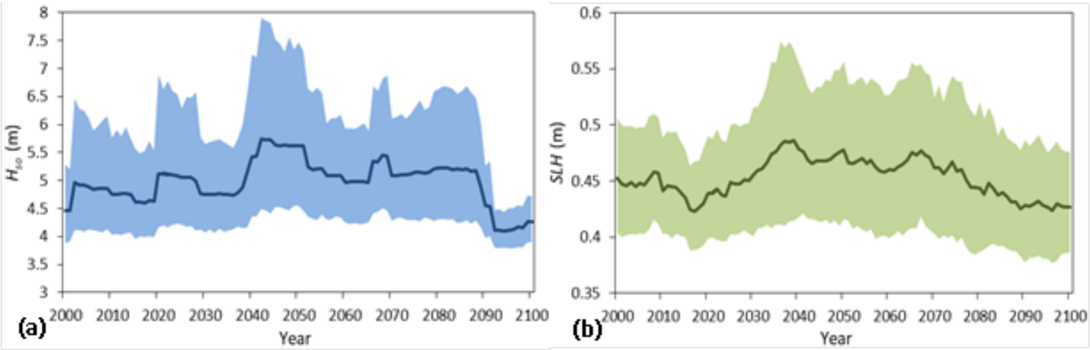

Figure 1 Time-dependent 100-years return level estimates with 95% confidence intervals for: a) H_s in the offshore area, b) Nearshore *SLH* at the port of Alexandroupolis

Figure 2a presents nonstationary P_f estimates for the three selected failure mechanisms (see Sect. 2.2). In Eq. 2 the maximum allowable overtopping discharge q=5 l/sm (EurOtop 2007), while the number of displaced units in Eq. 3 is N_{od}=0.5, corresponding to negligible damages at the breakwater toe. Estimated probabilities for all failure mechanisms present a bimodal behavior, showing discrete peaks in the intervals of maximum H_s. Therefore, P_f of all three mechanisms vary considerably within the 21st century. Excessive overtopping seems to be the governing failure mechanisms for the entire study period, followed by scouring of the breakwater toe and by instability of primary armour layer of the structure. The highest P_f correspond to return periods of 81, 104, and 140 years, for overtopping, scouring of the breakwater toe and instability of its primary armour layer, respectively. It should be noted that even if the structure can be considered quite safe for present marine conditions (P_f for all failure mechanisms are very low, corresponding to return periods of less than 1000 years), it seems to be exposed to severe marine conditions in the future. Considering the excessive overtopping ULS, P_f in the interval 2065-2070 are estimated higher compared to the respective ones in the middle of the century, identifying the significant contribution of $MSLR$ and SLH in determining failure conditions.
Figure 2b presents estimates of total failure probability P_{ftotal} considering the three ULS as independent or perfectly dependent. It also includes P_{ftotal} estimates from the series of 150 (1951-2100) and 100 (2001-2100) years, considering stationarity of marine conditions. Lower and upper bounds of these intervals correspond to perfect dependence or independence of ULS. The highest failure probabilities correspond to return periods of 36 and 81 years, for independent or perfectly dependent ULS, respectively. The stationarity assumption significantly underestimates P_{ftotal} reaching 82% and 64% when failure probabilities are estimated from 150 and 100 years, respectively.

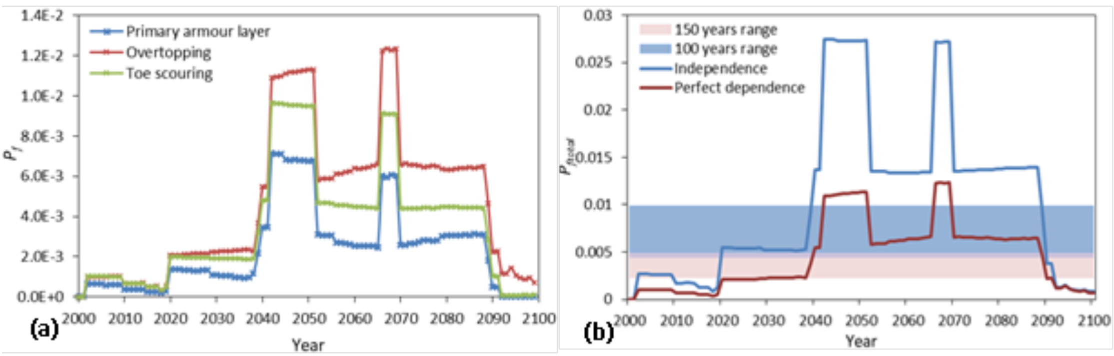

Figure 2 Time-dependent estimates of: a) Failure probabilities for three failure mechanisms (ULS), b) Total failure probability for independent and perfectly dependent failure mechanisms

5 CONCLUSIONS

In the present work failure probabilities of an indicative rubble mound breakwater protecting a Greek port against increasing future marine hazards and related escalating exposure to downtime risks are estimated within a nonstationary extreme value analysis framework. The results concern time-dependent P_f estimates for three main ULS, which are intercompared and used to determine future periods of increased vulnerability of the studied structure to extreme marine hazards. Excessive overtopping ULS seems to be the most critical for the collapse of the studied defence. This failure mechanism identifies a period around 1965-1970, with the highest P_f, where all variables of the marine climate (H_s, $MSLR$ and SLH) have a significant contribution to port downtime. Total failure probabilities are quite high for the future periods 2040-2055 and 2065-2070, with the highest values corresponding to a return period of 36 years for independent ULS. Estimating P_{fotal} within a nonstationary reliability framework assists in avoiding underestimation of future marine hazard effects on port and harbour structures. It should be noted that only selected ULS are considered in the present work. Excessive wave height inside the port/harbour basin during normal weather conditions causes port downtime without severe collapse of defence structures, and can be regarded as Serviceability Limit State (SLS). Such limit states can significantly affect P_{fotal} of Greek ports and harbours.

References

Adloff F et al. (2015) Mediterranean Sea response to climate change in an ensemble of twenty first century scenarios. Clim Dynam 45(9-10): 2775-2802. doi:10.1007/s00382-015-2507-3

Benetazzo A et al. (2012) Wave climate of the Adriatic Sea: a future scenario simulation. Nat Hazard Earth Sys Sci 12(6): 2065-2076. doi:10.5194/nhess-12-2065-2012

Burcharth H F, Andersen T L, Lara J L (2014) Upgrade of coastal defence structures against increased loadings caused by climate change: A first methodological approach. Coast Eng 87: 112–121.

Dai Viet N, Verhagen H J, van Gelder P, Vrijling J K (2008) Conceptual Design for the Breakwater System of the South of Doson Naval Base: Optimization versus Deterministic Design. Paper presented at PIANC-COPEDEC VII, Dubai, United Arab Emirates.

EurOtop (2007) Wave Overtopping of Sea Defences and Related Structures: Assessment Manual. EA, Bristol, UK, ENW,Utrecht, The Netherlands, KFKI, Hamburg, Germany.

Galiatsatou P et al. (2016) Modelling nonstationary extreme wave heights in present and future climates of Greek Seas. Water Sci Eng 9(1): 21-32. doi:10.1016/j.wse.2016. 03.001

Galiatsatou P, Makris C Prinos P (2018) Optimized Reliability Based Upgrading of Rubble Mound Breakwaters in a Changing Climate. J Mar Sci Eng 6(3): 92. doi:10.3390/jmse6030092

Galiatsatou P, Makris C, Prinos P Kokkinos D (2019) Nonstationary joint probability analysis of extreme marine variables to assess design water levels at the shoreline in a changing climate. Nat Haz (accepted, under revision).

HNHS (2011) Statistical data of sea level in Hellenic Ports. Hellenic Navy Hydrographic Service, Athens, Greece. (in Greek) https://www.hnhs.gr/en/online-2/2015-05-16-18-51-00

IPCC (2007) Climate change 2007: The Scientific Basis, Contribution of Working Group I to the Fourth Assessment Report of IPCC. Cambridge University Press, USA.

IPCC (2012) Managing the Risks of Extreme Events and Disasters to Advance Climate change Adaptation. A Special Report of Working Groups I & II of IPCC. Cambridge University Press, USA.

Isobe M (2013) Impact of global warming on coastal structures in shallow water. Ocean Eng 71: 51–57. doi:10.1016/j.oceaneng.2012.12.032

Kim TM, Suh KD (2010) Reliability analysis of breakwater armor blocks: Case study in Korea. Coast Eng J 52: 331–350. doi:10.1142/S0578563410002208

Makris C et al. (2016) Climate change effects on the marine characteristics of the Aegean and Ionian Seas. Ocean Dyn 66(12): 1603-1635. doi:10.1007/s10236-016-008-1

Makris C et al. (2018) Climate change impacts on the coastal sea level extremes of the east-central Mediterranean Sea. Paper presented at the XIV PRE Conference, Thessaloniki, Greece.

Naulin M, Kortenhaus A, Oumeraci H (2015) Reliability-based flood defense analysis in an integrated risk assessment. Coast Eng J 57: 1540005. doi:10.1142/S0578563415400057

Suh KD, Kim SW, Kim S, Cheon S (2013) Effects of climate change on stability of caisson breakwaters in different water depths. Ocean Eng 71: 103–112.

Van der Meer J W (1988) Deterministic and probabilistic design of breakwater armor layers. J Waterw Port Coast Ocean Eng 114: 66–80. doi:10.1061/(ASCE)0733-950X (1988)114:1(66)

Van der Meer JW, D'Angremond K, Gerding E (1995) Toe structure stability of rubble mound breakwaters. Adv Coast Struct Brkwtr, 308–321. doi:10.1680/aicsab.25097.0029

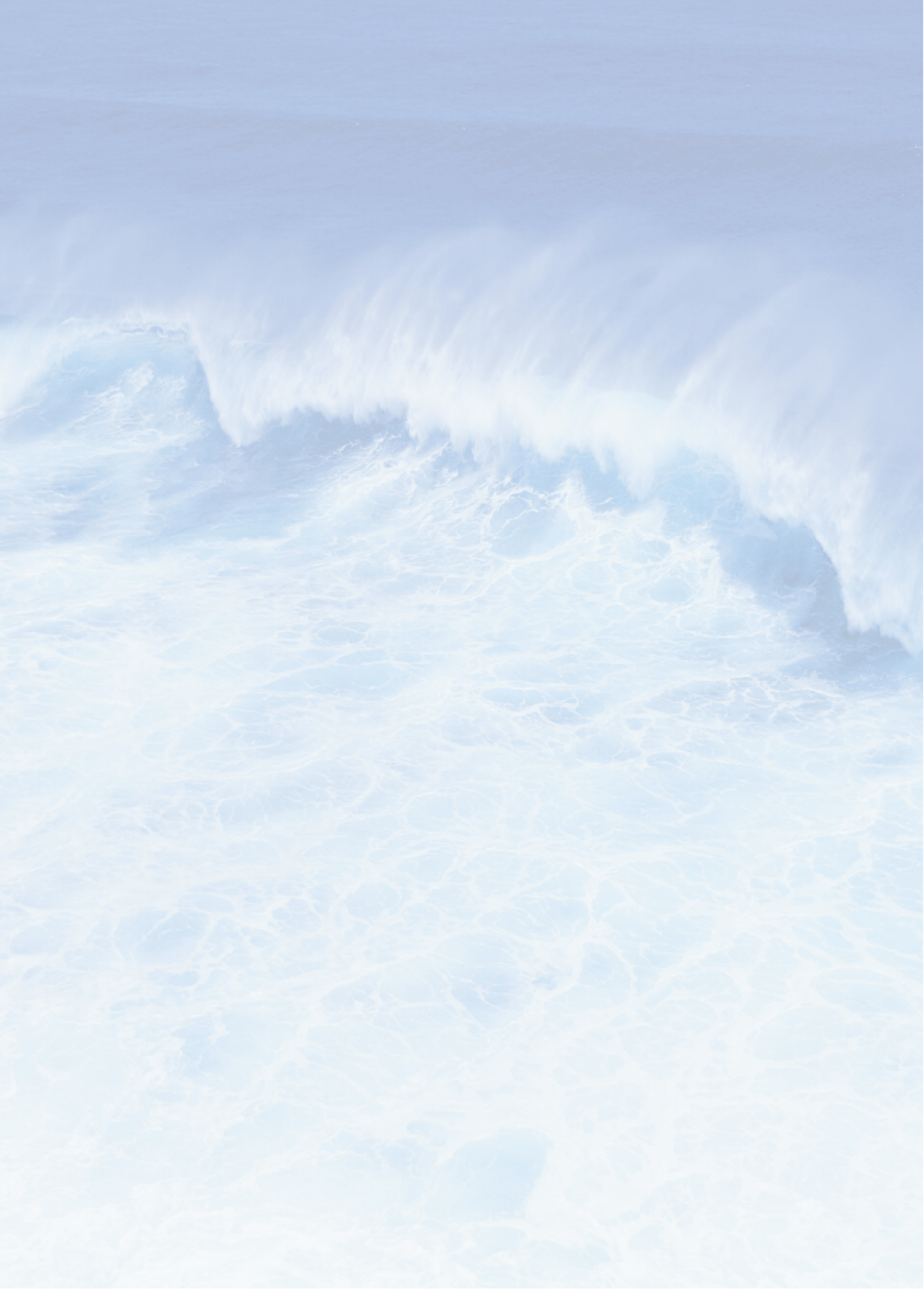

SESSION 7 DESIGN CRITERIA AND CLIMATE CHANGE

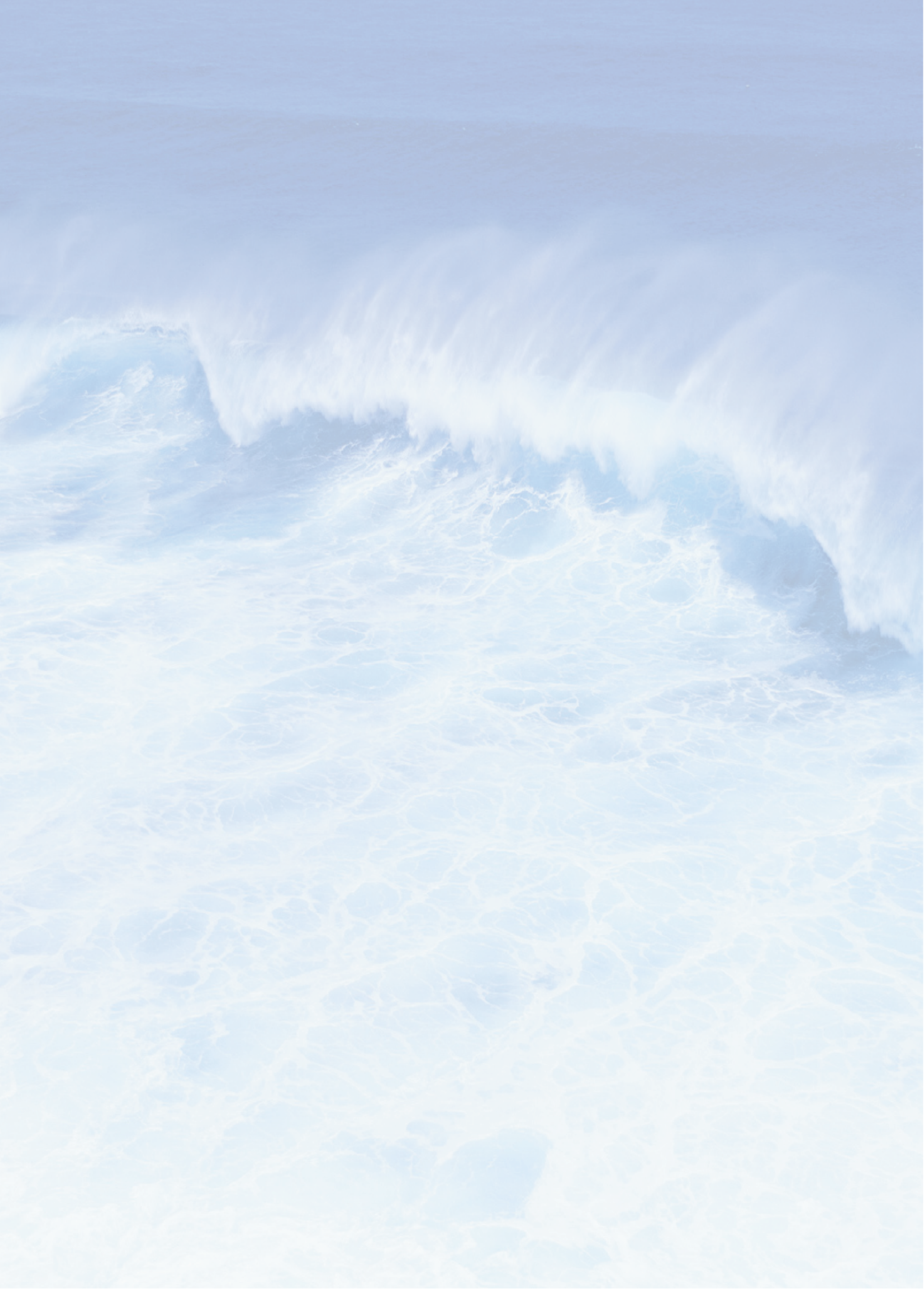

Sub session 7.1: Design Guidelines and Proposals

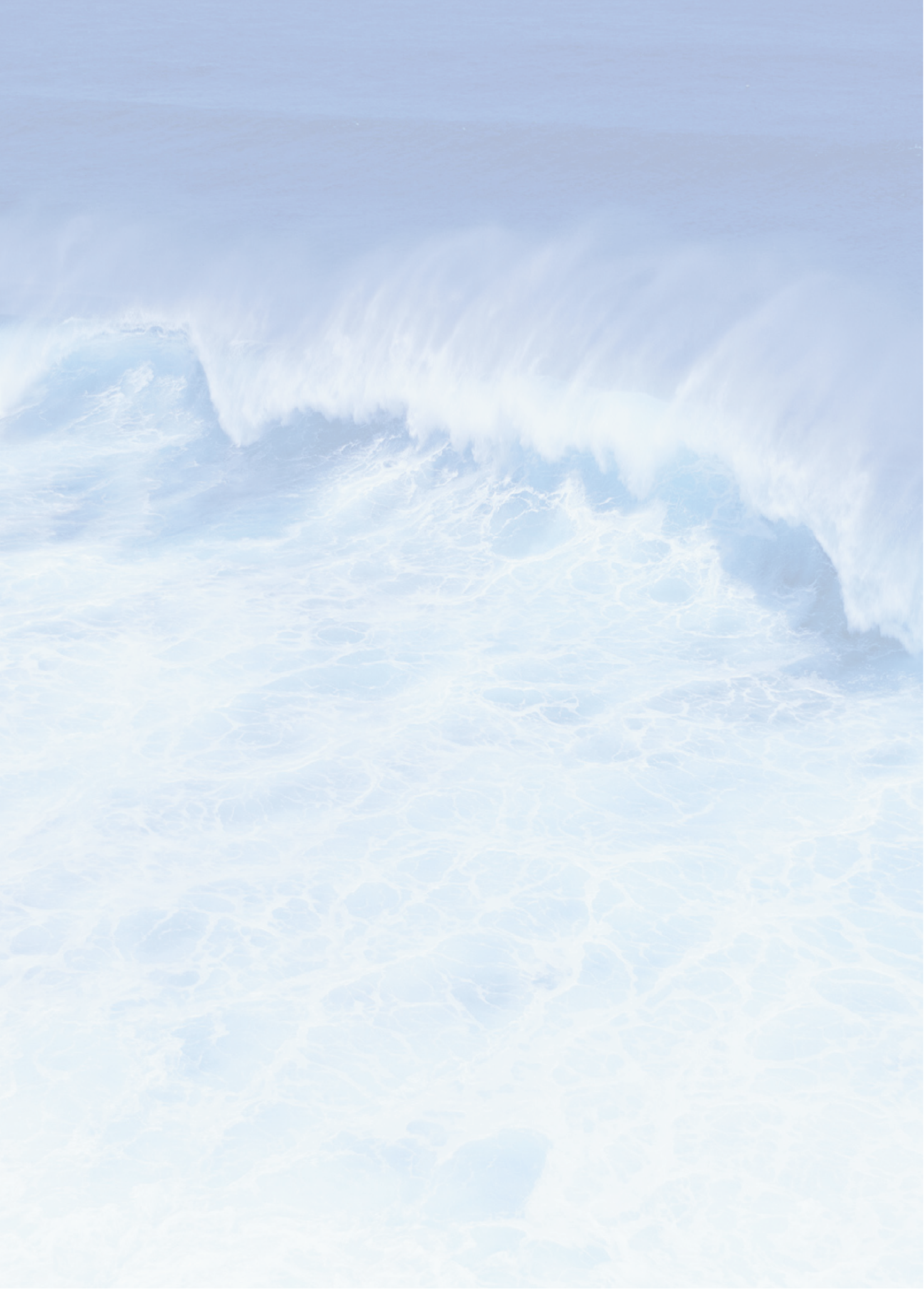

«Δράσεις κυμάτων και ρευμάτων στις παράκτιες κατασκευές»
Ο υπό διαμόρφωση νέος Ευρωκώδικας

Κ.Δ. Μέμος[1,2*], Δ.Ι. Μαλλιούρη[1]

[1]Εργαστήριο Λιμενικών Έργων, Εθνικό Μετσόβιο Πολυτεχνείο, Ζωγράφος, 15780, Ελλάδα
[2]Scientia Maris, Ζωγράφος, 15772, Ελλάδα
[*]Υπεύθυνος επικοινωνίας: cmemos@mail.ntua.gr

Περίληψη

Το παρόν άρθρο παρουσιάζει τα βασικά στοιχεία του υπό επεξεργασία νέου Ευρωκώδικα που αφορά τις δράσεις κυμάτων και ρευμάτων σε παράκτια έργα. Εντοπίζονται σημεία απόκλισης του νέου Ευρωκώδικα από το υπόλοιπο σύστημα Ευρωκωδίκων και αναφέρονται οι λόγοι για τις αναγκαίες αυτές αποκλίσεις, μία από τις οποίες αναφέρεται στην παραδοσιακή μέθοδο υπολογισμού των παράκτιων έργων. Δίδεται μία εκτενέστερη περιγραφή της εφαρμογής της πλήρους πιθανοτικής μεθόδου στην περιοχή των θαλασσίων έργων και δίδεται μια πρόταση απλουστευμένης μεθόδου ικανοποιητικής ακρίβειας που αναφέρεται στον υπολογισμό των κυματικών δράσεων, ο οποίος και παράγει το κυριότερο μέρος της συνολικής αβεβαιότητας που υπεισέρχεται στους υπολογισμούς. Η μεθοδολογία αυτή δεν έχει τεθεί ακόμη προς διαβούλευση στη σχετική ομάδα σύνταξης του νέου Ευρωκώδικα. Το έργο της ομάδας εμπειρογνωμόνων έχει ξεκινήσει από το φθινόπωρο του 2017 και είναι τριετούς διάρκειας. Χρηματοδοτείται από την Ευρωπαϊκή Επιτροπή σύμφωνα με την παραγγελία M/515 προς την Ευρωπαϊκή Επιτροπή Τυποποίησης (CEN), ενώ παρακολουθείται από την επιτροπή CEN/TC 1 “Structural Eurocodes – Actions on Structures”.

Λέξεις κλειδιά Ευρωκώδικας, Παράκτια έργα, Κυματικές δράσεις, Πιθανοτικός υπολογισμός.

1 ΕΙΣΑΓΩΓΗ

Η Ευρωπαϊκή Επιτροπή για την Τυποποίηση (CEN) έχει προχωρήσει στην ανάπτυξη ενός προγράμματος επικαιροποίησης των Ευρωκωδίκων και ενοποίησης της τυποποίησης στην Ευρώπη. Στο υπό εξέλιξη αυτό πρόγραμμα έχει ενταχθεί και η παραγωγή μερικών νέων Ευρωκωδίκων, μεταξύ των οποίων αυτός που αναφέρεται στο αντικείμενο της παράκτιας μηχανικής και ασχολείται με τις «Δράσεις Κυμάτων και Ρευμάτων στις Παράκτιες Κατασκευές». Η σύνταξη του εν λόγω Ευρωκώδικα γίνεται από ομάδα Ευρωπαίων ειδικών υπό την παρακολούθηση του μηχανισμού των Ευρωκωδίκων και με τη βοήθεια άλλης παρόμοιας ομάδας εμπειρογνωμόνων. Οι εργασίες σύνταξης ξεκίνησαν τον Σεπτέμβριο 2017 και το τελικό σχέδιο του κειμένου έχει προγραμματισθεί να είναι έτοιμο τον Ιούνιο 2020.

2 ΑΝΤΙΚΕΙΜΕΝΟ

Ο Ευρωκώδικας θα αναφέρεται σε δράσεις ρευμάτων και ανεμογενών κυματισμών περιλαμβανομένης της ρεστίας επί παράκτιων κατασκευών, στις οποίες περιλαμβάνονται και τα έργα προστασίας λιμένων λόγω των ομοιοτήτων τους με τα αντίστοιχα παράκτια έργα. Ειδικότερα περιλαμβάνονται κυματοθραύστες, έργα παράκτιας προστασίας, έργα επί πασσάλων, πλωτές κατασκευές, όλα στην παράκτια ζώνη. Το πλέον σημαντικό αντικείμενο του Κώδικα είναι όμως τα κεφάλαιά του για τις βασικές αρχές σχεδιασμού των έργων αυτών, τον καθορισμό των περιβαλλοντικών φορτίσεων, τον πιθανοτικό σχεδιασμό και το σχεδιασμό με υποβοήθηση από ελέγχους σε φυσικό ομοίωμα. Ο όρος <δράσεις> κυμάτων και ρευμάτων περιλαμβάνει εκτός από τις κλασικές εξωτερικές <δυνάμεις> επί των κατασκευών τις έννοιες της κυματικής <υπερπήδησης> των έργων, την γενική ή τοπική <διάβρωση> του πυθμένα ή τμήματος του έργου από τη δράση κυμάτων και ρευμάτων, καθώς και άλλες δευτερεύουσες δράσεις ανάλογα με την συγκεκριμένη κατασκευή. Στο παρόν άρθρο θα περιορισθούμε στις κλασικές δυνάμεις επί των έργων και ειδικότερα επί κυματοθραυστών με πρανή, δηλαδή σε ένα κεντρικό ζήτημα που απασχολεί τους μηχανικούς.

Ο Κώδικας μπορεί να περιέχει υλικό υποχρεωτικής η προαιρετικής συμμόρφωσης υπό τύπο οδηγίας. Προβλεπόμενοι χρήστες του είναι γραφεία μελετών, επιβλέπουσες υπηρεσίες, κατασκευαστές παράκτιων έργων και γενικότερα πολιτικοί μηχανικοί στην Ευρώπη και παγκοσμίως.

3 ΒΑΣΙΚΕΣ ΚΑΤΕΥΘΥΝΣΕΙΣ

Μερικές από τις βασικές κατευθύνσεις που έχουν δοθεί στην ομάδα συγγραφής του υπό συζήτηση Ευρωκώδικα δίδονται στη συνέχεια:

(α) Ο υπό διαμόρφωση Ευρωκώδικας θα πρέπει να στηρίζεται στο Διεθνές Πρότυπο ISO 21650:2007 που ασχολείται με το ίδιο αντικείμενο. Αξίζει να προστεθεί εδώ πως με την πρόοδο του έργου ο χαρακτήρας του υπό δημιουργία Κώδικα στοχεύει περισσότερο στον καθορισμό των δράσεων παρά σε τυπολόγιο σχεδιασμού, όπως το ISO. Έτσι η συνάφεια με αυτό είναι πλέον ασθενής.

(β) Ο Κώδικας θα πρέπει να εντάσσεται αρμονικά στο υπάρχον σύστημα της σειράς των Ευρωκωδίκων. Η εν λόγω παραίνεση θα πρέπει ευλόγως να ικανοποιηθεί στο κείμενο τόσο του νέου Κώδικα όσο και μέσω παρεμβάσεων σε άλλους τυχόν Ευρωκώδικες. Ένα σημαντικό ζήτημα αφορά την ομογενοποίηση των κριτηρίων σχεδιασμού για όλα τα έργα αρμοδιότητος πολιτικού μηχανικού.

(γ) Θα πρέπει να παρέχει ένα πλήρη καθορισμό των θαλάσσιων περιβαλλοντικών συνθηκών σχεδιασμού. Όπως αναφέρθηκε, αυτή η κατεύθυνση θα είναι πράγματι, εφόσον πραγματοποιηθεί, πολύ σημαντική προσφορά προς τον σχετικό επαγγελματικό χώρο. Η πορεία της ομάδος εργασίας κατευθύνεται προς την πλήρη υλοποίηση του εν λόγω αιτήματος.

(δ) Ο νέος Ευρωκώδικας θα πρέπει να ενθαρρύνει τους μηχανικούς στη χρήση πιθανοτικών μεθόδων υψηλής ακρίβειας, όπου αυτό είναι αναγκαίο. Παρομοίως, η ομάδα συγγραφής εργάζεται προς την κατεύθυνση αυτή και μερικά πρώτα αποτελέσματα θα παρουσιασθούν στη συνέχεια.

4 ΚΕΝΤΡΙΚΟ ΖΗΤΗΜΑ ΣΧΕΔΙΑΣΜΟΥ

Ίσως το πλέον ουσιώδες θέμα σχεδιασμού των παράκτιων έργων αφορά την τυποποίηση του αναγκαίου επιπέδου αξιοπιστίας του κάθε έργου, το οποίο σε γενικές γραμμές ταυτίζεται με την πιθανότητα αστοχίας του. Ο υπολογισμός της αξιοπιστίας αυτής είναι σύνθετη διαδικασία εφόσον σε ένα πρώτο επίπεδο παραδοσιακής προσέγγισης γίνεται αντιληπτό ότι οι δράσεις κυμάτων και ρευμάτων επί των παράκτιων κατασκευών δεν είναι δυνατόν να δοθούν ρητά, στις περισσότερες περιπτώσεις, αλλά σε σχέση με τη συγκεκριμένη κατασκευή και το στοιχείο που σχεδιάζεται. Επιπρόσθετα, οι κυματικές δράσεις είναι εξόχως μη γραμμικές ως προς τα χαρακτηριστικά του κυματισμού, γεγονός που θέτει συχνά περιορισμούς στη χρήση των ημι-εμπειρικών εκφράσεων που χρησιμοποιούνται στους σχετικούς υπολογισμούς. Παράλληλα η βαθμονόμηση των αντίστοιχων μερικών συντελεστών της ημι-πιθανοτικής μεθόδου που δέχονται οι Ευρωκώδικες ως τη βασική μέθοδο υπολογισμού γίνεται πολλαπλώς απροσδιόριστη και σε πολλές περιπτώσεις δεν δύναται να μειώσει ικανοποιητικά το βαθμό προσέγγισης έναντι των απλών παραδοσιακών μεθόδων.

Είναι γενικά παραδεκτό πως το πολύ μεγαλύτερο ποσοστό της ενδεχόμενης αβεβαιότητας των αποτελεσμάτων των υπολογισμών προκύπτει από το τμήμα των περιβαλλοντικών παραμέτρων εισαγωγής σε αντίθεση με τις παραμέτρους αντοχής της κατασκευής. Έτσι στον υπό διαμόρφωση Ευρωκώδικα υιοθετείται η γραμμή της ακριβέστερης περιγραφής των παραμέτρων των δράσεων, αντί να γίνει προσπάθεια βαθμονόμησης των μερικών συντελεστών τόσο της φόρτισης όσο και της αντίδρασης της κατασκευής.

Ο προσδιορισμός των δράσεων γίνεται σε τρία επίπεδα ακρίβειας (ΗΕΑ) αντιστρόφως ανάλογα με τη συνθετότητα της μεθόδου υπολογισμού. Τα επίπεδα αυτά καθορίζονται, σύμφωνα με τις προβλέψεις των Ευρωκωδίκων, από το μέγεθος των επιπτώσεων πιθανής αστοχίας του έργου, αλλά και από την αβεβαιότητα του υδροδυναμικού καθορισμού μίας ή περισσοτέρων καταστάσεων θαλάσσης – κυρίως βέβαια του κυματικού κλίματος. Η μέθοδος σχεδιασμού της κατασκευής (RDA) καθορίζεται από το επίπεδο του υδροδυναμικού υπολογισμού αλλά και από την πρόσθετη αβεβαιότητα που υπεισέρχεται στις σχέσεις υπολογισμού πέραν της αβεβαιότητας υδροδυναμικής πρόβλεψης που έχει ήδη υπεισέλθει στον υπολογισμό των περιβαλλοντικών φορτίσεων. Όπως και στην εκτίμηση των θαλάσσιων καταστάσεων έτσι και στην προτεινόμενη μέθοδο υπολογισμού προβλέπονται τρία επίπεδα συνθετότητας, όπως φαίνεται στον Πίνακα 1.

Πίνακας 1 Προτεινόμενη Μέθοδος Υπολογισμού (RDA)

Επίπεδο ΗΕΑ[1]	Αβεβαιότητα σχέσεων υπολογισμού[2]	
	Χαμηλή-Μέτρια	Υψηλή[3]
HEA-1	DET	RDA-1
HEA-2	RDA-1 ή DET[4]	RDA-2 ή RDA-4
HEA-3	RDA-2	RDA-4

[1] Μέθοδος υδροδυναμικού υπολογισμού

[2] Περιλαμβάνει αβεβαιότητα των σχέσεων που αφορά τον τύπο των δράσεων και των αντιδράσεων της κατασκευής και των επιμέρους στοιχείων της. Δεν περιλαμβάνει αβεβαιότητα που αφορά την ΗΕΑ.

[3] Μπορεί να αφορά τμήμα της κατασκευής, όπως ακρομώλιο, τοίχο στέψης, κλπ.

[4] Εφόσον δεν υπάρχουν τιμές εφαρμογής των μερικών συντελεστών

DET Ντετερμινιστική μέθοδος εφαρμογής ημι-εμπειρικών σχέσεων σε συνδυασμό με κατάλληλη επιλογή της περιόδου επαναφοράς της κύριας δράσης (επίπεδο ΗΕΑ-1)

RDA-1 Ημι-πιθανοτική μέθοδος με χρήση μερικών συντελεστών

RDA-2 Πλήρως πιθανοτική μέθοδος ή κατάλληλη προσέγγισή της

RDA-4 Μέθοδος σχεδιασμού υποστηριζόμενη από εργαστηριακές μετρήσεις

Όπως αναγράφεται στον προηγούμενο Πίνακα η μέθοδος υπολογισμού DET αναφέρεται στην παραδοσιακή μέθοδο υπολογισμού εμπλουτισμένη με την απλή πιθανοτική θεώρηση της περιόδου επαναφοράς (ΗΕΑ-1). Η μέθοδος αυτή παρ' ό,τι δεν προβλέπεται στο σύστημα των Ευρωκωδίκων θεωρήθηκε αναγκαίο να περιληφθεί στο πίνακα των προτεινόμενων μεθόδων λόγω των ιδιαιτεροτήτων των δράσεων του θαλασσίου περιβάλλοντος που αναφέρθηκαν προηγουμένως. Οι προσεγγίσεις RDA-1 (μερικοί συντελεστές), RDA-2, RD-4 περιγράφονται σε γενικές γραμμές στο σύστημα των Ευρωκωδίκων (EN 1990).

5 ΣΧΕΔΙΑΣΜΟΣ ΚΑΙ ΑΞΙΟΠΙΣΤΙΑ ΠΑΡΑΚΤΙΩΝ ΚΑΤΑΣΚΕΥΩΝ

5.1 Μηχανισμοί αστοχίας

Σε κάθε μηχανισμό αστοχίας αντιστοιχεί μία συνάρτηση αξιοπιστίας (ή αστοχίας), η οποία προκύπτει από μία έκφραση αντοχής του σχετιζόμενου στοιχείου της κατασκευής. Οι καίριες μεταβλητές της προαναφερόμενης συνάρτησης αξιοπιστίας θα πρέπει να εξετάζονται για το αν είναι χρονικά εξαρτώμενες. Μια καλή προσέγγιση είναι να συνδέσουμε τις χρονικά εξαρτώμενες μεταβλητές με τις περιβαλλοντικές φορτίσεις και ιδιαίτερα με τις κυματικές φορτίσεις. Συνήθως, οι σημαντικότερες και συνεπώς πιο συνήθεις χρονικά εξαρτώμενες στοχαστικές μεταβλητές, που εμπλέκονται στις συναρτήσεις αξιοπιστίας των μηχανισμών αστοχίας παράκτιων κατασκευών, είναι το σημαντικό ύψος κύματος H_s, η μέση περίοδος κύματος T_m, η κύρια κατεύθυνση των κυματισμών θ_m, η ταχύτητα ρεύματος C και η ανύψωση της μέσης στάθμης της θάλασσας SL που σχετίζεται με το κυματικό πεδίο. Συνεπώς, η πιθανότητα αστοχίας στην περίοδο αναφοράς ενός έτους υπολογίζεται ως εξής:

$$P_{f,1y} = \int_{\Omega(\bar{x})} f_X(\bar{x})\, d\bar{x} \qquad (1)$$

όπου: $\bar{x} = \{H_s\,, T_m, \theta_m;\, C, SL\}$, $f_x(\bar{x})$ η συνάρτηση της από κοινού πυκνότητας πιθανότητας των $\bar{x}$ στην περίοδο αναφοράς του ενός έτους και το $\Omega(\bar{x})$ αποτελεί το χωρίο αστοχίας προσδιοριζόμενο από την οριακή συνάρτηση αστοχίας άμεσα συνδεδεμένη με το μηχανισμό αστοχίας του στοιχείου.

Η πιο συχνή περιβαλλοντική παράμετρος που δεν επηρεάζεται από το κυματικό πεδίο είναι η διακύμανση της στάθμης της θάλασσας εξαιτίας της αστρονομικής παλίρροιας (T). Η μεταβλητή αυτή, παρόλο που είναι ντετερμινιστικής φύσης, μπορεί να συνδυαστεί με τα κύματα με τυχαίο τρόπο. Η πιθανοτική κατανομή της T, $f_T(t)$, εξαρτάται από την τοποθεσία του παράκτιου έργου και τον παλιρροιακό της κύκλο. Συνεπώς, η $f_T(t)$ μπορεί να θεωρηθεί ανεξάρτητη από την χρονική περίοδο αναφοράς και μπορεί να συνδυαστεί με την $f_x(\bar{x})$ της Εξ. 1 ως εξής:

$$P_{f,1y} = \iint_{\Omega(\bar{x},t)} f_X(\bar{x}) f_T(t) d\bar{x} dt \qquad (2)$$

όπου: $\Omega(\bar{x}, t)$ το επεκταμένο χωρίο αστοχίας λόγω της θεώρησης της μεταβλητής T.

5.2 Χρονική προέκταση της πιθανότητας αστοχίας

Η πιθανότητα αστοχίας ενός έτους, αναφορικά με τις χρονικά εξαρτώμενες μεταβλητές, μπορεί να επεκταθεί και να χρησιμοποιηθεί στην εκτίμηση της πιθανότητας αστοχίας σε μεγαλύτερες χρονικές περιόδους, π.χ. στη διάρκεια ζωής του έργου L, σύμφωνα με την ακόλουθη σχέση που βασίζεται στη στατιστική ανάλυση ακραίων γεγονότων:

$$P_{f,L} = 1 - \left(1 - P_{f,1y}\right)^L \qquad (3)$$

Ο υπολογισμός της $P_{f,L}$ μπορεί να πραγματοποιηθεί και στην περίπτωση ταυτόχρονης θεώρησης τόσο χρονικά εξαρτώμενων όσο και μη χρονικά εξαρτώμενων μεταβλητών.

5.3 Αστοχία συστήματος

Η πιθανότητα αστοχίας ενός συστήματος, π.χ. μιας παράκτιας κατασκευής, εξαρτάται από τις πιθανότητες αστοχίας των επιμέρους στοιχείων του. Ένα διάγραμμα αστοχιών (fault tree) σχεδιάζεται αρχικά, το οποίο καθορίζει τη σχέση των μηχανισμών αστοχίας μεταξύ τους και τη σύνδεσή τους με την αστοχία του συστήματος. Το διάγραμμα μπορεί να διακριθεί σε δύο θεμελιώδη υποσυστήματα, το σύστημα αστοχιών σε σειρά και το παράλληλο σύστημα. Στο σειριακό σύστημα, η αστοχία του συστήματος συμβαίνει όταν οποιοδήποτε στοιχείο του συστήματος αστοχεί και συνεπώς η πιθανότητα αστοχίας του συστήματος εκτιμάται ως η πιθανότητα της ένωσης των ενδεχομένων αστοχίας των επιμέρους μηχανισμών. Αντίθετα στο παράλληλο σύστημα, η αστοχία του συστήματος συμβαίνει όταν όλα τα στοιχεία του συστήματος αστοχούν και συνεπώς η πιθανότητα αστοχίας του συστήματος εκτιμάται ως η πιθανότητα της τομής των ενδεχομένων αστοχίας των επιμέρους μηχανισμών. Ένας εύκολος τρόπος για να ληφθεί υπόψη η στατιστική συσχέτιση των μηχανισμών αστοχίας είναι να ελέγχονται όλοι οι μηχανισμοί σε κοινές συνθήκες περιβαλλοντικών φορτίσεων και να εξάγεται με τον τρόπο αυτό η πιθανότητα αστοχίας του συστήματος.

1.1 *5.4 Μέθοδοι υπολογισμού της αξιοπιστίας κατασκευής*

Οι μέθοδοι εκτίμησης της αξιοπιστίας των παράκτιων κατασκευών αναφέρθηκαν συνοπτικά στον Πίνακα 1. Η συμβατική πρακτική σχεδιασμού των παράκτιων κατασκευών είναι κατά βάση ντετερμινιστική (DET) και η εκτίμηση της αξιοπιστίας τους στηρίζεται στην πιθανότητα υπέρβασης του φορτίου σχεδιασμού των παράκτιων κατασκευών στη διάρκεια ζωής τους. Στην ημι-πιθανοτική προσέγγιση (RDA-1), μερικοί συντελεστές ασφαλείας, οι οποίοι αναπτύχθηκαν αρχικά από την PIANC (1992), εφαρμόζονται ξεχωριστά για την αντοχή και την φόρτιση. Και στις δύο αυτές προσεγγίσεις χρησιμοποιείται η έννοια της περιόδου επαναφοράς του φορτίου σχεδιασμού, π.χ. του σημαντικού ύψους κύματος, που εξάγεται συνήθως από ανάλυση ακραίων τιμών.

Πιο ακριβείς μέθοδοι υπολογισμού θεωρούνται οι πλήρως πιθανοτικές μέθοδοι (RDA-2) που αναφέρονται στη συνέχεια. Στις μεθόδους αυτές ανήκουν η Μέθοδος Άμεσης Ολοκλήρωσης (DIM) και η Μέθοδος Monte Carlo (MCM). Η μέθοδος DIM καταναλώνει περισσότερο υπολογιστικό χρόνο και έχει περισσότερες απαιτήσεις σε πόρους ηλεκτρονικού εξοπλισμού.

1.2 5.4.1DIM

Η μέθοδος αυτή χρησιμοποιεί τη συνάρτηση της από κοινού πυκνότητας πιθανότητας όλων των στοχαστικών μεταβλητών που εμπλέκονται στη συνάρτηση αστοχίας. Για τον υπολογισμό της συγκεκριμένης συνάρτησης σε περίπτωση παραμέτρων που παρουσιάζουν στατιστική συσχέτιση μεταξύ τους μπορεί να χρησιμοποιηθεί το μοντέλο δεσμευμένης πιθανότητας. Η Εξ. 1, ύστερα από τη χρήση του μοντέλου αυτού εφαρμοσμένο σε τρεις καίριες μεταβλητές διαμορφώνεται ως ακολούθως:

$$P_{f,1y} = \iiint_{g<0} f_{H_s|T_m|\theta_m}(H_s|T_m|\theta_m) f_{T_m|\theta_m}(T_m|\theta_m) f_{\theta_m}(\theta_m) dH_s dT_m\, d\theta_m \qquad (4)$$

όπου η ανίσωση $g < 0$ ορίζει το χωρίο αστοχίας.

1.3 5.4.2MCM

Η μέθοδος αυτή βασίζεται σε ένα μεγάλο αριθμό προσομοιώσεων N, ένα μέρος του οποίου N_f οδηγεί στην αστοχία του στοιχείου της κατασκευής. Με την προϋπόθεση αυτή ώστε να επιτυγχάνεται μια ικανοποιητική σύγκλιση, η πιθανότητα αστοχίας του συστήματος εκτιμάται ως εξής:

$$P_{f,1y} = \frac{N_f}{N} \tag{5}$$

Στη συγκεκριμένη μέθοδο, προσοχή πρέπει να δοθεί στο ότι οι μεταβλητές πρέπει να ακολουθούν τις πιθανοτικές κατανομές τους και να λαμβάνεται υπόψη η συσχέτιση μεταξύ τους, εφόσον υπάρχει. Για το λόγο η MCM συχνά συνδυάζεται με το πιθανοτικό μοντέλο δεσμευμένης πιθανότητας.

1.4 5.4.3Πρόταση εύκολης εφαρμογής

Στην παρούσα προσέγγιση, χρησιμοποιείται η θεωρητική έκφραση της από κοινού κατανομής των περιβαλλοντικών παραμέτρων, οι οποίες παρουσιάζουν τη μεγαλύτερη αβεβαιότητα σε σχέση με τις μεταβλητές αντίστασης. Η συγκεκριμένη πρόταση μπορεί να εφαρμοστεί σε περίπτωση που υπάρχουν κυματικές μετρήσεις στα βαθειά είτε όταν είναι διαθέσιμα μόνο ανεμολογικά δεδομένα. Ειδικότερα, ο πληθυσμός των κυματικών δεδομένων στα βαθειά επιλέγεται να εκπροσωπηθεί από ένα μικρότερο αλλά αντιπροσωπευτικό δείγμα της τάξης των 1500-2000 εκπροσώπων, αφού πρώτα έχει κατηγοριοποιηθεί σε κλάσεις. Στη συνέχεια, με ένα γρήγορο αλλά ικανοποιητικής ακρίβειας μοντέλο (Malliouri κ.ά. 2019a), η στατιστική πληροφορία του μακροπρόθεσμου κυματικού κλίματος μπορεί να μεταφερθεί από τα βαθειά νερά στη θέση του έργου, χρησιμοποιώντας τη βραχυχρόνια στατιστική πληροφορία για κάθε εκπρόσωπο. Ακολουθεί η περιγραφή της πιθανοτικής κατανομής του δείγματος που αναφέρεται στη θέση του έργου και στη συνέχεια το δείγμα μεγεθύνεται ώστε να αποκτήσει το αρχικό σύνολο δεδομένων εφαρμόζοντας αναλογία στις κλάσεις της κάθε μεταβλητής και παραγωγή τυχαίων αριθμών εντός των ορίων της κάθε κλάσης. Τέλος η πιθανότητα αστοχίας του στοιχείου της κατασκευής υπολογίζεται σύμφωνα με την Εξ. 5. Αναλυτική περιγραφή της μεθόδου παρουσιάζεται στο άρθρο των Malliouri κ.ά. 2019b.

6 ΑΛΛΑ ΘΕΜΑΤΑ ΣΧΕΔΙΑΣΜΟΥ

Πέραν από το κεντρικό ζήτημα σχεδιασμού που αφορά το επιθυμητό επίπεδο αξιοπιστίας των παράκτιων κατασκευών και για το οποίο έγινε λόγος πιο πάνω, έχουν αναδειχθεί κατά τις εργασίες της συντακτικής ομάδος του νέου Κώδικα μια σειρά θεμάτων ενδιαφέροντος για τον σχεδιασμό τέτοιων κατασκευών, όπως ανάδειξη της κυματικής υπερπήδησης ως κριτήριο σχεδιασμού της στέψης του έργου, ανάδειξη της κυματικής περιόδου ως κριτήριο ευστάθειας διαπερατών έργων με πρανή, υπογράμμιση της χαμηλής ευρωστίας των παράκτιων αναχωμάτων και της ανάγκης διαμόρφωσης μεθόδου υπολογισμού της αλλά και σχετικών τιμών-στόχων για την ανάλυση των έργων.

ΑΝΑΓΝΩΡΙΣΗ

Το έργο σύνταξης του νέου Ευρωκώδικα χρηματοδοτείται από την Ευρωπαϊκή Επιτροπή σύμφωνα με την παραγγελία Μ/515 προς την CEN και παρακολουθείται από την τεχνική επιτροπή CEN/TC 250/SC 1 “Structural Eurocodes – Actions on Structures” προς την οποία εκφράζονται ευχαριστίες για τη βοήθειά της.

Βιβλιογραφικές Αναφορές

Malliouri D, Memos C, Tampalis N, Soukissian T, Tsoukala V (2019a) Integrating short- and long-term statistics for short-crested waves in deep and intermediate waters. Applied Ocean Research 82(3):346–361. doi: 10.1016/j.apor.2018.11.004.

Malliouri D, Memos C, Soukissian T, Tsoukala V (2019b) Reliability analysis of rubble mound breakwaters. An easy-to-use Methodology. Paper presented at the 1st International Conference on Design and Management of Port, Coastal and Offshore Works, May 8-11, Athens, Greece.

PIANC (1992) Analysis of rubble mound breakwaters; report of working group 12 (PTC II).

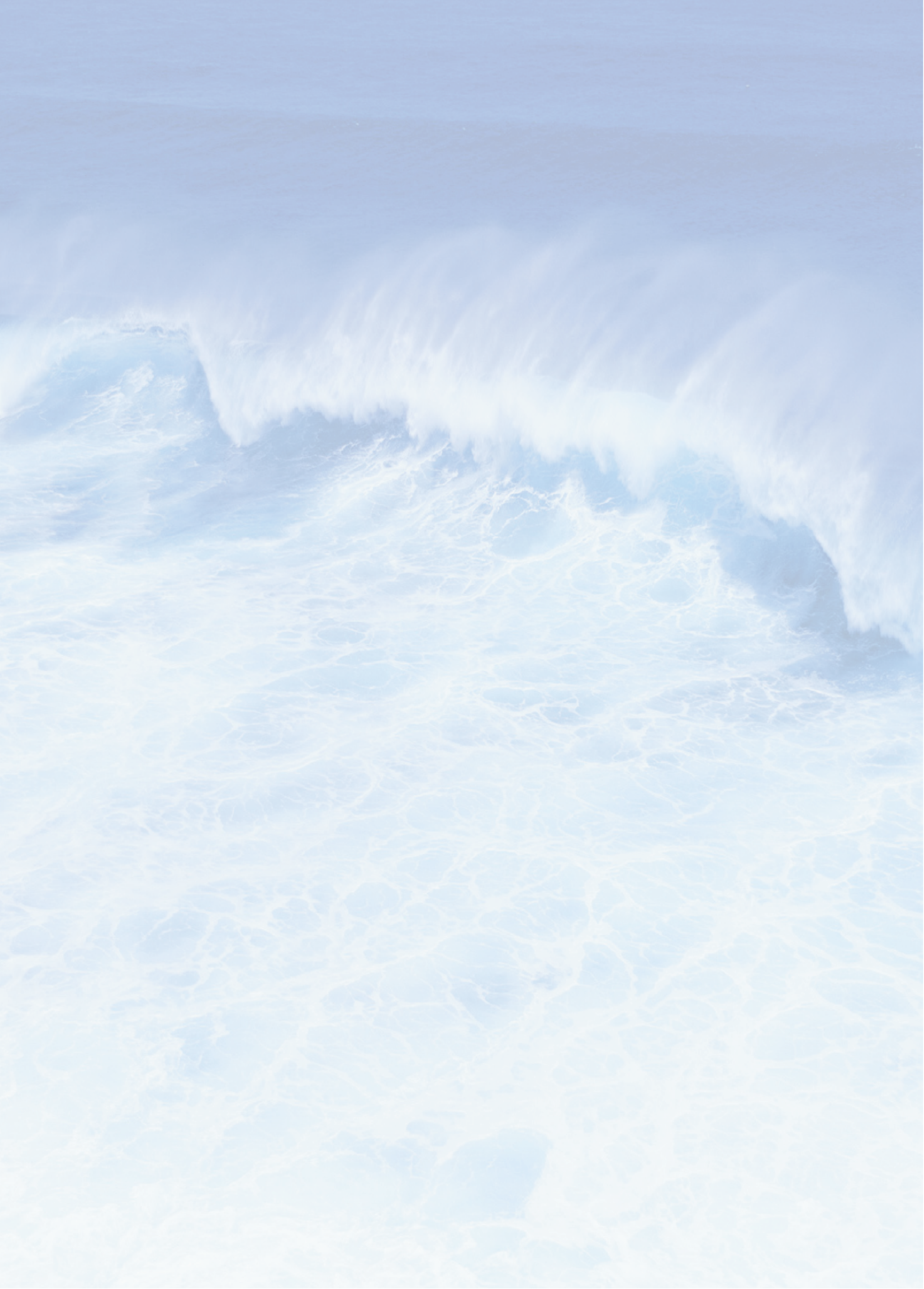

Climate change effects on extreme total water levels of the Greek coastal zone

P. Galiatsatou[1,*], C. Makris[2], D. Kokkinos[1], P. Prinos[1], Y. Krestenitis[2]

[1]Lab of Hydraulics, School of Civil Engineering, Aristotle University of Thessaloniki (AUTh), Thessaloniki, 54124, Greece
[2]Lab of Maritime Engineering, School of Civil Engineering, AUTh, 54124, Thessaloniki, Greece
[*]Corresponding author: pgaliats@civil.auth.gr

Abstract

The nonstationary univariate extreme value theory is implemented on data of sea state characteristics at selected Greek coastal areas of the Aegean Sea to provide reliable estimates of design total water levels (TWLs) on the coast and to assess their temporal variability in the future climate, by adopting a compound event approach. Long-term time series of deep water significant wave height and associated peak spectral wave period corresponding to sea states affecting the coast are used to estimate the wave run-up at the selected coastal areas by means of established empirical formulas. Wave-induced run-up is then added to concomitant five-day maxima of sea level heights due to storm surge, mean sea level rise and astronomical tide records. The resulting structure variable is modeled using a nonstationary Generalized Extreme Value (GEV) distribution to extract time-dependent estimates of extreme TWLs at the shoreline, providing more reliable design values for coastal areas and structures.

Keywords Total Water Level, Nonstationary extremes, Coastal zone, Climate change

1 INTRODUCTION

Global climate change is expected to cause significant long-term changes in storm variability regionally, leading to consequent shifts in mean sea level (MSL), wave climate and storm surge regime. Changes in frequency and severity of future marine conditions can significantly affect vulnerability and exposure of coastal areas to inundation, flooding and erosion hazards. During the last decade climate change effects on the variability and long-term trends in MSL, as well as changes in extreme wave climate and extreme storm surges in the Mediterranean have gained significant interest (*i.e.* Adloff et al. 2015, Tsimplis et al. 2013, Makris et al. 2016).

Estimation of extreme total water level (TWL) at a coastal area assessing the contributions of various components of the marine climate, can provide the boundary conditions for flooding and erosion hazard studies and estimation of the related coastal risks. Very recently, studies focusing on the estimation of TWL at the shoreline started including components to simulate seasonality and interannual variability of the marine climate, as well as considering dependencies between the different variables of TWL (*i.e.* Serafin and Ruggiero 2014, Serafin et al. 2017, Galiatsatou et al. 2019).

Climate change being one of the prominent causes of long-term nonstationarities inherent in marine signals, especially when their extreme levels are of interest, necessitates the use of a nonstationary approach to assess reliable future extremes of TWL on the coast, to be used as input for various impact studies. However, many of the studies in this field assume stationarity of the marine climate variables and/or do not consider their combined impact on coastal areas. In the present work extreme TWLs on the coasts of Greece are assessed by the use of a nonstationary approach to approximate the coastal flooding hazard under climate change conditions. Wave characteristics, sea level heights due to storm surges (SLH), MSL rise, and astronomical tidal range of the study areas are considered in the analysis.

2 METHODOLOGY

Coastal flooding, caused by the combined effect of high water levels (storm surges and astronomical tides), MSL rise and wave action of rough sea states, can result from the combination of large values of more than one of its constituent processes. Therefore, a compound extreme TWL can be a combination of variables that are not necessarily extreme events of themselves (Serafin et al. 2017) and extreme source is not equivalent to extreme impact (Leonard et al. 2014). Therefore, in the present work an impact-based definition of multivariate sea storm events is used, adopting a compound event approach to estimate extreme TWL at the shoreline. Long-term time series of deep water significant wave height H_s and associated peak spectral wave period T_p corresponding to sea states affecting the coast are primarily used to estimate the wave-induced run-up $R_{2\%}$ on the shoreline at selected coastal areas by means of the Stockdon et al. (2006) empirical formula:

$$R_{2\%} = 1.1\left(0.35tan\beta(H_sL_o)^{1/2} + \frac{\left(H_sL_o(0.563tan^2\beta+0.004)\right)^{1/2}}{2}\right) \; or \; R_{2\%} = 0.043(H_sL_o)^{1/2}, \xi < 0.3 \quad (1)$$

where H_s[m] is the deep water significant wave height, L_o[m] is the deep water wave length associated to the peak spectral wave period T_p[s], tanβ is the beach face slope and ξ is the Iribarren number. The TWL at the shoreline results from adding the wave-induced run-up at the shoreline, $R_{2\%}$, the sea level height due to storm surge, SLH, the MSL rise, $MSLR$, and the maximum astronomical tidal range, TR_{max} at the selected study area:

$$TWL = R_{2\%} + SLH + MSLR + TR_{max} \quad (2)$$

Annual maxima of the sum of the two stochastic components of TWL, $R_{2\%}$ and SLH, are extracted and the univariate Extreme Value Theory (EVT) is used to assess extremes of the response variable. The nonstationary Generalized Extreme Value (GEV) distribution is then utilized to model the distribution function of the aforementioned structure variable ($TWL_{stoch} = R_{2\%} + SLH$). All time-dependent distributions are fitted using a 50-year moving time window with an annual time step. The derived parameter estimates correspond to the last year of each 50-years period.

Linear and nonlinear parametric trends are then fitted to extracted parameter estimates and best-fitted models are selected using the Akaike and the Bayesian Information Criterion, as well as tests for statistical significance of the coefficients of the fitted trends (Galiatsatou et al. 2019). Nonstationary design $TWLs$ are then defined as a conditional sum of extracted return level estimates of the structure variable (with or without the fitted parametric trends), astronomical tide, and MSL rise estimates at the selected coastal areas.

3 AVAILABLE DATA

The wave (H_s and T_p) and SLH data used in this paper cover a period of 150 years (1951-2100) and are derived from 3-hourly simulation results for the Greek Seas produced by SWAN wave model and the high-resolution two-dimensional, barotropic, storm surge model GreCSS (Makris et al. 2016). Forcing of wind and atmospheric pressure fields are derived from dynamically downscaled simulations with Regional Climate Model RegCM3, and future climate projections are based on IPCC-A1B emissions scenario (IPCC 2007). After extracting $R_{2\%}$ for all waves heading to the coastal areas of interest, a five-day window (by 2.5 days bilaterally) of concurrent *SLH* is implemented in the analysis, in order to estimate the largest possible response to particular storm events, which usually have a maximum duration of 120 hours in the Mediterranean basin.

Three representative Greek study areas (Makris et al. 2018) have been selected, one in the North Aegean (Area 1) containing the coastal zone of Alexandroupolis city, one in the Central Aegean (Area 2) containing the coastal area of Eresos in the southern Lesvos Island, and one in the South Aegean (Area 3) containing the coastal area of the city of Heraklion in northern Crete. An adequate number of representative cross-shore profiles, with distances 800 to 1000m from each other, were selected at each study area: namely 21, 5 and 18 beach slope profiles for Areas 1, 2 and 3, respectively. Three profiles were studied in each of these areas, corresponding to the maximum (17.1% for Area 1, 16.2% for Area 2, 14.5% for Area 3), and the minimum slopes (1.2% for Area 1, 5.7% for Area 2, 3.0% for Area 3) as well as to slopes close to the median (7.5% for Area 1, 11.6% for Area 2, 8.5% for Area 3).

To assess the MSL rise in the Aegean Sea, both a steric and a component of mass addition due to ice melting were considered, resulting to a total value of 25cm by 2100 (Makris et al. 2016), corresponding to about 2.5mm/year, averaged over the whole Mediterranean. The maximum astronomical tidal range, TR_{max}, is considered equal to 0.66m, 0.44m and 0.40m for the coastal areas of Alexandroupolis, Eresos and Heraklion, respectively (HNHS 2011).

4 RESULTS

The nonstationary analysis of TWL_{stoch} extremes using 50-year moving time windows for all selected cross-shore profiles in all three study areas (see Sect. 2) resulted in obtaining time-dependent estimates of GEV parameters (location, scale and shape) from 2000 to 2100. All parameter estimates were obtained using the L-moments approach. Figure 1 presents such estimates for cross-shore profiles with slopes close to the median value for each study site. Statistically significant (5% significance level) linear trends, as well as best-fitted nonlinear trends for all parameters are also shown in Figure 1. Similar plots were also produced for maximum and minimum slopes, not presented here for the sake of brevity.

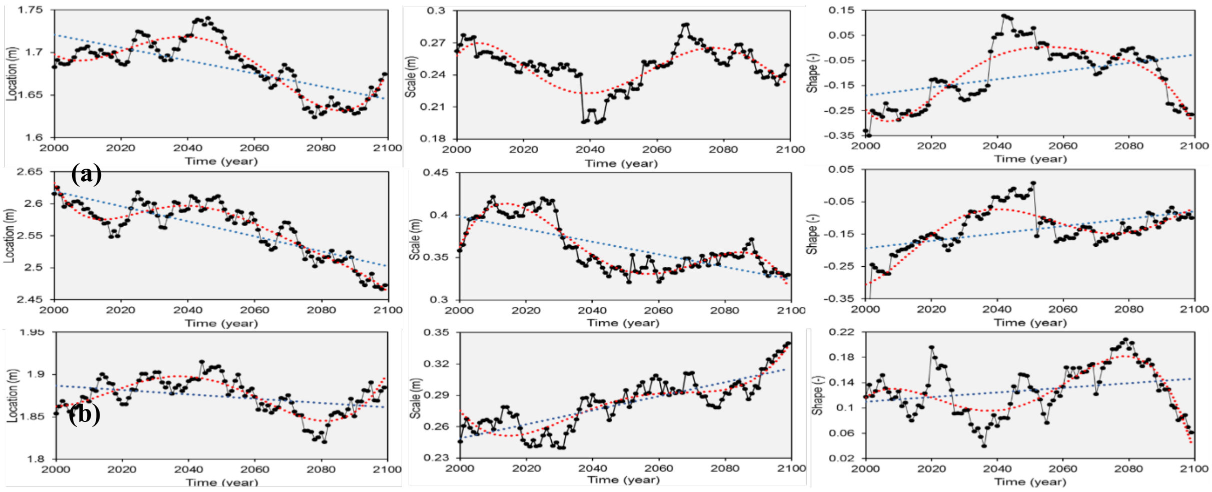

Figure 1 Time-dependent estimates of the GEV location (m), scale (m), and shape (-) parameters fitted to the sum of stochastic components of TWL for cross-shore profiles with slope close to the median for the coastal areas of: a) Alexandroupolis (Area 1), b) Eresos (Area 2), c) Heraklion (Area 3). Blue and red dashed lines represent statistically significant linear and best-fitted nonlinear trends, respectively.

(c)

Statistically significant linear trends have been detected in almost all GEV parameters for all three study areas (except the scale parameter for Area 1). Such trends are decreasing for the location and increasing for the shape parameter in all areas, identifying distribution functions with progressively lower means and heavier tails during the future period. GEV distribution functions seem to present progressively lower variances (represented by the scale parameter) in the future in Area 2, and higher ones in Area 3.

Statistically significant polynomial trends have been also detected in all parameters of the GEV fitted to TWL_{stoch} for all three study areas. In the present work the maximum order of the fitted polynomial trends was set equal to five. All resulting polynomial trends are of order four or five, identifying quite high variability of the GEV parameter estimates with time in all study areas. Larger differences in variations over time among the study coastal areas are observed for the scale parameter, which shrinks or stretches the TWL distribution and the shape parameter, which dictates its limiting behavior. In Area 1 the scale parameter presents a bimodal behavior, peaking at the beginning and after the middle of the 21st century, while during the latter period the shape parameter presents its highest values. In Area 2 the scale parameter decreases considerably after 2020, while highest values of the shape parameter are obtained around the middle of the 21st century. Finally, in Area 3, the scale parameter presents an increasing trend, while heavy tails characterize the distribution of TWL throughout the 21st century.

Figure 2 presents time-dependent 100-years return levels of TWL (Eq. 2) for the period 2000-2100 for cross-shore profiles with slopes close to the median value in all three study areas. Most likely 100-years return levels are presented, together with their associated 95% confidence intervals estimated using a parametric bootstrap approach. Figure 2 also includes most likely 100-years TWL estimates assessed by considering best-fitted nonlinear parametric trends for all GEV parameters. Similar plots were also produced for maximum and minimum slopes, not presented here for the sake of brevity.

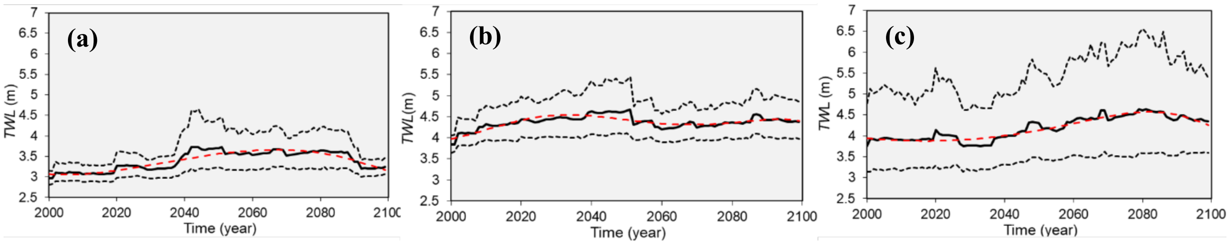

Figure 2 Time-dependent estimates of 100-years TWL for cross-shore profiles with slope close to the median for the coastal areas of: a) Alexandroupolis (Area 1), b) Eresos (Area 2), c) Heraklion (Area 3). Solid black lines represent most likely estimates, and dashed back lines represent their associated 95% confidence intervals. Dashed red lines are most likely 100-years TWL estimates considering nonlinear trends in all GEV parameters.

TWL extremes in Area 1 appear increased in the second half of the 21^{st} century, while uncertainty almost doubles in this interval (apart from the last ten years), with respect to the period 2000-2040. Considering nonlinear trends in GEV parameters, most likely TWL extremes peak in the interval 2065-2070 to the value of 3.6m (2.7m to 6.0m considering minimum and maximum slope). In Area 2 extreme $TWLs$ seem to increase in the first half of the 21^{st} century and decrease in the second one, presenting their highest values (4.7m) around the middle of the century (2.8m to 5.3m considering minimum and maximum slope). When including parametric trends in the GEV parameters, highest values of 100-years TWL estimates appear around 2035. In Area 3 extreme $TWLs$ present their highest values (4.6m) around 2080 (2.8m to 6.6m considering minimum and maximum slope), appearing highly uncertain throughout almost the entire study period. Variability of most likely 100-years TWL estimates in all study areas exceeds 20% in the 21^{st} century, while it increases to more than 35% when upper 95% confidence intervals are considered.

Figure 3 presents TWL return level estimates from 2000 to 2100 corresponding to return periods from 2 to 200 years in the three coastal areas of the northern (Area 1), central (Area 2), and southern (Area 3) Aegean Sea. Estimates shown were produced for cross-shore profiles with slopes close to the median value in all three study areas, considering best-fitted nonlinear parametric trends in the GEV parameters. Similar plots were also produced for maximum and minimum slopes of the cross-shore profiles.

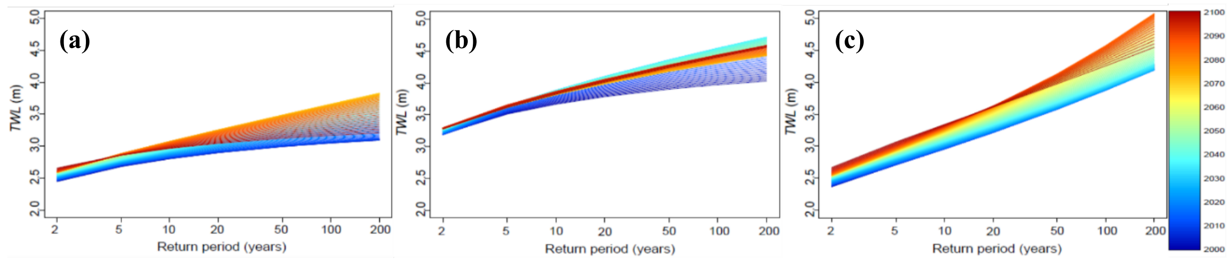

Figure 3 Return level estimates of TWL for cross-shore profiles with slope close to the median for the coastal areas of: a) Alexandroupolis (Area 1), b) Eresos (Area 2), c) Heraklion (Area 3) for the period 2000-2100 considering best-fitted nonlinear trends in all GEV parameters.

In Area 1 TWL return level estimates present an increasing trend until 2065-2070 and a decreasing trend afterwards, for the entire range of probabilities considered. Differences are more pronounced for high return periods. The decrease in TWL values is quite sharp especially for high return periods, leading to short-tailed distributions in the last thirty years of the 21^{st} century. In Area 2 TWL return level estimates associated with low probabilities of occurrence present an abrupt increase in the first half of the 21^{st} century, and decrease slightly afterwards. Short-tailed GEV distribution functions are assigned to the entire study period, enabling the extraction of design values of the response for different impact studies. In Area 3 TWL return level estimates progressively increase during the period 2000-2080. Extreme $TWLs$ are fitted to GEV distribution functions with progressively heavier tails, turning to upper-bounded distribution functions in the last twenty years of the 21st century.

5 CONCLUSIONS

In this study multivariate extreme sea states (storm waves and surges) at selected areas of the Greek coastal zone, representing a possible realization of the future marine climate, are statistically treated via EVT, considering nonstationarity on time scales longer than the seasonal or interannual, possibly attributed to climate change. Furthermore, they are combined with other sources of the coastal flooding hazard, *i.e.* astronomical tides and MSL rise, allowing for a robust derivation of extreme values, which is mainly focused on the associated response function of the TWL in coastal areas of the Aegean Sea. This hopefully allows for safer estimations of the coastal flooding hazards, more reliable design values for coastal protection works and more efficient management of the coastal zone.

The nonstationary analysis of the response function of TWL revealed statistically significant nonlinear trends in all GEV parameters and identified quite a high variability in its estimates in all study areas. TWL peaks appearing after 2060 in northern Aegean Sea imply the rise of extreme southerly winds in the area towards the middle of the 21st century and beyond (Vagenas et al. 2017). Progressive increase of TWL extremes in southern Aegean Sea could be possibly combined with a mild rise of northerly extreme winds after the first half of the 21st century detected in the Aeolian patterns (Galiatsatou et al. 2019). Finally, the projected significant increase in extreme Etesians (*i.e.* local strong meridional winds called "Meltemia"; Maheras 1980) in the first half of the 21st century could possibly explain peaks in TWL extremes in the central Aegean Sea during this period.

References

Adloff F et al. (2015) Mediterranean Sea response to climate change in an ensemble of twenty first century scenarios. Clim Dynam 45(9-10): 2775-2802. doi:10.1007/s00382-015-2507-3.

Galiatsatou P et al. (2019) Nonstationary joint probability analysis of extreme marine variables to assess design water levels at the shoreline in a changing climate. Nat Haz (accepted, under revision).

HNHS (2011) Statistical data of sea level in Hellenic Ports. Hellenic Navy Hydrographic Service, Athens, Greece. (in Greek) https://www.hnhs.gr/en/online-2/2015-05-16-18-51-00.

IPCC (2007) Climate change 2007: The Scientific Basis, Contribution of Working Group I to the Fourth Assessment Report of IPCC. Cambridge University Press, USA.

Leonard M et al. (2014) A compound event framework for understanding extreme impacts. WIRES Clim Change 5: 113-128. doi:10.1002/wcc.252.

Maheras P (1980) The problem of Etesians [Le probleme des Etesiens]. Mediterranée 40:57–66. doi: 10.3406/medit.1980.1955.

Makris C et al. (2016) Climate change effects on the marine characteristics of the Aegean and Ionian Seas. Ocean Dyn 66(12): 1603-1635. doi:10.1007/s10236-016-008-1.

Makris C et al. (2018) Climate change impacts on the coastal sea level extremes of the east-central Mediterranean Sea. Paper presented at the XIV PRE Conference, Thessaloniki, Greece.

Serafin KA and Ruggiero P (2014) Simulating extreme total water levels using a time-dependent extreme value approach. J Geophys Res Oceans 119: 6305-6329. doi:10.1002/2014JC010093.

Serafin KA, Ruggiero P and Stockdon HF (2017) The relative contribution of waves, tides, and nontidal residuals to extreme total water levels on U.S. West Coast sandy beaches. Geophys Res Lett 44: 1839-1847. doi:10.1002/2016GL071020.

Stockdon HF et al. (2006) Empirical parameterization of setup, swash, and runup. Coast Eng 53: 573-588. doi:10.1016/j.coastaleng.2005.12.005.

Tsimplis MN (2013) The effect of the NAO on sea level and on mass changes in the Mediterranean Sea. J Geophys Res Oceans 118(2): 944-952. doi:10.1002/jgrc.20078.

Vagenas C, Anagnostopoulou C and Tolika K (2017) Climatic Study of the Marine Surface Wind Field over the Greek Seas with the Use of a High Resolution RCM Focusing on Extreme Winds. Climate 5(2): 29. doi:10.3390/cli5020029.

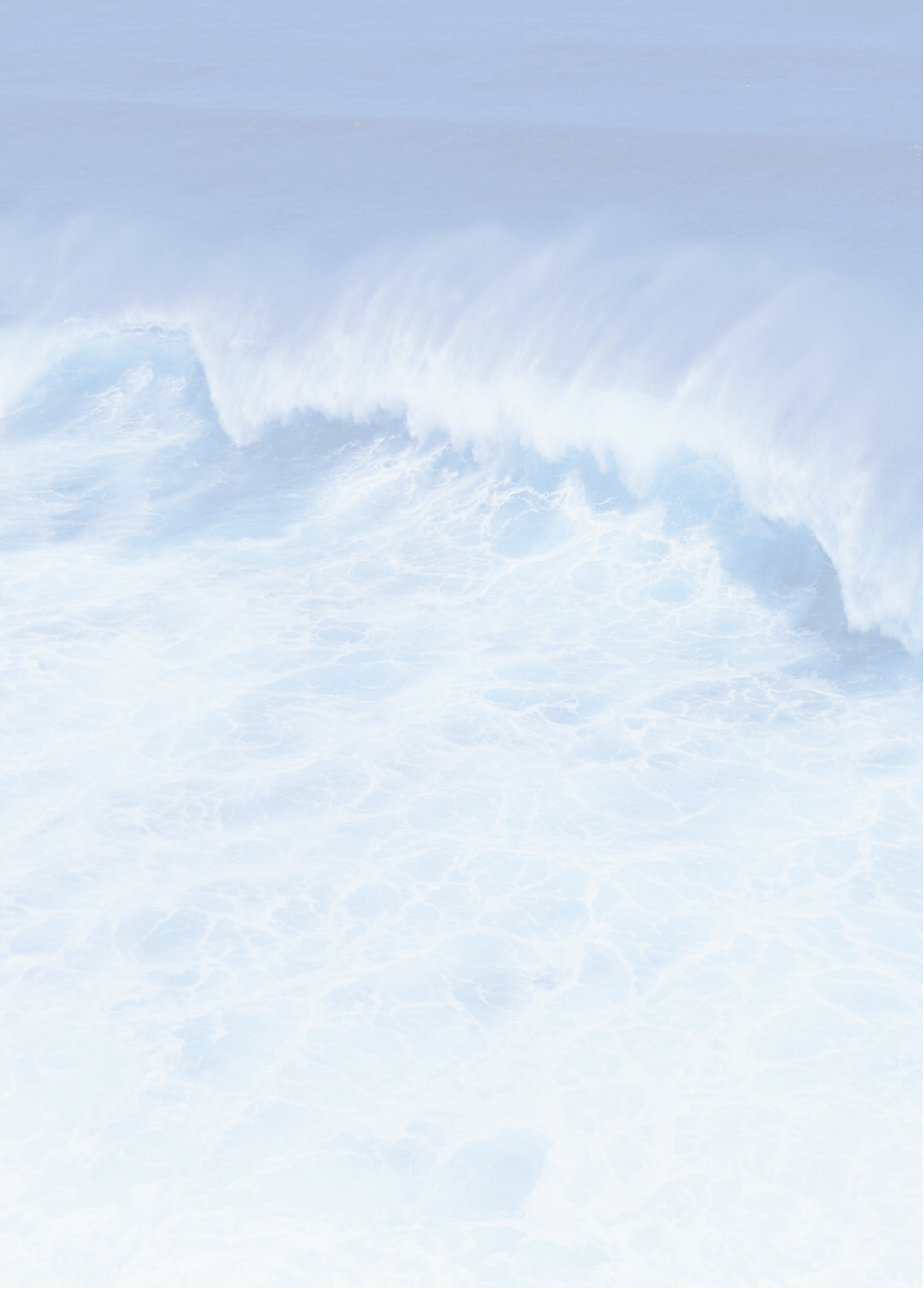

Multivariate metocean design conditions in the Mediterranean and North Seas

T.H. Soukissian[1*], S.A. Mavrakos[2]

[1]Hellenic Centre for Marine Research, Institute of Oceanography, Anavyssos, Attica, 19013, Greece
[2]School of Naval Architecture and Marine Engineering, National Technical University of Athens, Zografos, Greece
[*]Corresponding author: tsouki@hcmr.gr

Abstract

In this work the design environmental conditions at three locations in the Mediterranean Sea and North Sea are provided along with the necessary theoretical background. The analysis of the local wind and wave climate is based on numerical model simulation results obtained by the Era-20C data set, published by the European Centre For Medium-Range Weather Forecasts (ECMWF). The time series that were analysed extend in the period 1980-2010 and correspond to significant wave height H_{m_0}, mean wave direction θ_H, wind speed U_W, mean wind direction θ_U and spectral peak period T_P, all with a recording interval of 3h. The estimation of design values of multivariate random variables is, in principle, an open theoretical field. In contrast to the univariate extreme case, the theory of multivariate extremes is characterized by important theoretical difficulties which have not been resolved yet. In the ocean engineering community, some alternative methods have been proposed for the assessment of this problem. These methods though, are valid under some important theoretical assumptions; however in practice they seem to perform satisfactorily. The most well-known of these methods is based on conditional distributions and transformations of random variables and is used in this work for the estimation of the trivariate design values for H_{m_0}, T_P and U_W.

Keywords Design values, multivariate extremes, Mediterranean Sea, North Sea.

1 INTRODUCTION

In this work the design environmental conditions at three locations in the Mediterranean Sea and North Sea are provided along with the theoretical background. The locations examined are Kassos Isl. (~35.34° N, ~26.80° E, location L1) and Sicily Isl. (~37.30° N, ~12.69° E, location L2) in the Mediterranean Sea and offshore Norway (~59.42° N, ~3.40° E, location L3) in the North Sea. See also Figure 1.

Figure 7 The examined locations L1 and L2 in the Mediterranean Sea (left panel) and location L3 in the North Sea (right panel) (from Google Earth)

All locations are at water depths around 200m. Specifically, the local wind and wave climate along with the univariate and trivariate design values of the significant wave height, wind speed and wave spectral peak period are assessed. The analysis is based on numerical model simulation results obtained by the Era-20C data set, published by the European Centre For Medium-Range Weather Forecasts (ECMWF), see (ERA-20C project). The original simulations extend to a 111-years period (1900-2010). However, to avoid non-stationarity, uncertainty and inhomogeneity issues in the statistical and extreme value analysis, we considered the last 31 years of the available time series, i.e., met-ocean data covering the period 1980-2010. The particular time series that were analyzed correspond to significant wave height H_{m_0}, mean wave direction θ_H, wind speed U_W, mean wind direction θ_U and spectral peak period T_P, all with a recording interval of 3h.

2 STATISTICAL ANALYSIS OF MET-OCEAN PARAMETERS

The statistical analysis refers to H_{m_0}, T_P and U_W. Specifically, the main statistical parameters, the wave and wind rose diagrams and the bivariate frequency histograms of $H_{m_0} - \theta_H$, $U_W - \theta_U$, $H_{m_0} - U_W$, and $H_{m_0} - T_P$ are provided. In Table 1 the main statistical characteristics (sample size N, mean value m, standard deviation s, variation coefficient CV, maximum max, minimum min, skewness Sk and kurtosis Ku) of wave and wind parameters for the examined locations are summarised.

Table 1 Statistical characteristics of wind and wave time series at the examined locations

	Location	N	m	min	max	s	CV	Sk	Ku
	L1		0.948	0.061	5.387	0.602	63.453	1.548	3.499
H_{m_0}, m	L2		0.864	0.024	6.490	0.715	82.809	1.835	4.700
	L3		1.999	0.175	9.774	1.184	59.237	1.292	2.126
	L1		5.466	2.430	11.176	1.106	20.235	0.537	0.464
T_P, s	L2	90584	5.357	2.430	11.066	1.438	26.847	0.571	-0.051
	L3		8.417	3.415	17.875	2.017	23.962	0.508	0.013
	L1		6.495	2.000	18.624	2.661	40.971	0.534	0.076
U_W, m/s	L2		5.834	2.000	20.133	3.010	51.591	0.791	0.194
	L3		7.856	2.000	23.196	3.589	45.680	0.465	-0.333

From the analysis of wind and wave rose diagrams (not shown here) the following conclusions can be drawn: For location L1 the prevailing wave and wind directions lie within the sector [315, 337.5], while winds and waves from the southern sectors are very rare. The most intense winds and sea-states come from the sector [337.5, 360]. Winds and waves in the area seem to be well aligned. For L2 the prevailing wave and wind directions lie within the sector [292.5, 315] and then within the south-eastern sectors, i.e., [135, 157.5]. The most intense sea-states propagate also from the prevailing wave directions, however the maximum significant wave height occurs from 270° wave direction. The most intense wind speeds are observed in the north-north-western directions. For L3 the prevailing wave direction is from the sector [315, 337.5]. Waves propagating from the southern sectors are rather rare, while waves from the [0, 90] sector are very rare, mainly due to the morphology of the area (very limited fetches in these directions). The most intense sea-states propagate also from the [315, 337.5] sector. Winds blow from the sectors [135, 180] and [315, 360]. The most intense wind speeds blow from a variety of sectors; the overall maximum wind speed corresponds to 226°.

3 ESTIMATION OF UNIVARIATE DESIGN VALUES FOR MET-OCEAN PARAMETERS

For the estimation of the univariate design values of met-ocean parameters the block maxima (annual maxima, AM) method will be applied. The underlying distribution for the AM method is the Generalized Extreme Value (GEV) distribution; see also Coles (2001), Soukissian and Kalantzi (2006), Soukissian and Tsalis (2015). By implementing the Maximum Likelihood Method (MLM), the parameters of the GEV distribution for H_{m_0}, T_P and U_W, have been estimated. In Table 2 the design values of the examined parameters are provided for return periods 10-100 years. For design purposes though, the 95% confidence intervals should be also taken into consideration. The detailed results along with the obtained fits are presented in the relevant deliverable report.

Table 2 Design values for significant wave height (m), wind speed (m/s) and spectral peak period (sec) for various return periods (in years) for locations L1, L2 and L3

		Return period									
		10	20	30	40	50	60	70	80	90	100
H_{m_0}	L1	4.89	5.15	5.29	5.39	5.46	5.52	5.58	5.62	5.66	5.69
	L2	5.99	6.41	6.64	6.81	6.93	7.04	7.12	7.20	7.26	7.32
	L3	8.95	9.44	9.70	9.89	10.03	10.15	10.24	10.32	10.39	10.46
U_W	L1	17.81	18.25	18.48	18.64	18.75	18.85	18.92	18.99	19.05	19.10
	L2	18.94	19.50	19.80	20.01	20.16	20.28	20.38	20.46	20.54	20.60
	L3	21.70	22.32	22.68	22.94	23.13	23.30	23.44	23.56	23.66	23.76
T_P	L1	10.35	10.73	10.96	11.13	11.26	11.36	11.46	11.54	11.61	11.67
	L2	10.94	11.00	11.02	11.04	11.04	11.05	11.05	11.06	11.06	11.06
	L3	17.01	17.45	17.68	17.84	17.95	18.04	18.12	18.18	18.23	18.28

4 ESTIMATION OF TRIVARIATE DESIGN VALUES OF MET-OCEAN PARAMETERS

4.1 General

The estimation of design values of multivariate random variables is, in principle, an open theoretical field. In contrast to the univariate extreme case, the theory of multivariate extremes is characterized by important theoretical difficulties which have not been resolved yet. In the ocean engineering community, some alternative methods have been proposed for the assessment of this problem. These methods though, are valid under some important theoretical assumptions; however, in practice they seem to perform satisfactorily. The most well-known of these methods is based on conditional distributions and transformations of random variables and will be used in this work for the estimation of the trivariate design values for H_{m_0}, T_P and U_W.

Let $f_{UHT}(U_W, H_{m_0}, T_P)$ and $F_{UHT}(U_W, H_{m_0}, T_P)$ denote the pdf and the corresponding cdf of the random variables U_W, H_{m_0}, T_P. If T_P is assumed as almost independent from H_{m_0}, f_{UHT} can be expressed as follows:

$$f_{UHT}(U_W, H_{m_0}, T_P) \approx f_U(U_W) f_{H|U}(H_{m_0}|U_W) f_{T|H}(T_P|H_{m_0}), \tag{1}$$

where $f_{X|Y}(X|Y)$ denotes the denotes the conditional distribution of X given Y.

In order to evaluate the joint design values of U_W, H_{m_0}, T_P, the joint distribution (1) must be transformed by implementing the Rosenblatt transformation in a new non-physical space, where U_W, H_{m_0}, T_P will be reflected into Gaussian and independent variables, U_1, U_2, U_3, Rosenblatt (1952). This approach is also described and applied for bivariate extreme values analysis of met-ocean parameters in Cheng et al. (2003), Baarholm et al. (2010), Yang, Chang (2013), Li et al. (2013). To implement the transformations the following mapping is used:

$$F_U(U_W) = \Phi(u_1), F_{H|U}(H_{m_0}|U_W) = \Phi(u_2), F_{T|H}(T_P|H_{m_0}) = \Phi(u_3), \tag{2}$$

where $\Phi(\cdot)$ is the standard normal distribution. For obtaining variables U_1, U_2, U_3, the inverse relations of equations (2) are used. In the new non-physical space $U_1 - U_2 - U_3$, the n-year return period is defined as a circle with radius r provided by the following relation:

$$\Phi(r) = 1 - 1/N_{n-years}, \tag{3}$$

where $N_{n-years}$ is the number of met-ocean "states" expected to occur within n years. In our case, the radius r has been calculated for the *ultimate limit state analysis*, which corresponds to 50 years. For sampling period 3h, from relation (3) we obtain immediately

$$r = \Phi^{-1}\left(1 - {}^{1}/_{(365.25 \times 8 \times n)}\right). \tag{4}$$

To return back to U_W, H_{m_0}, T_P, the following relations are used:

$$U_W = F_U^{-1}(\Phi(u_1)),\ \ H_{m_0} = F_{H|U=u}^{-1}(\Phi(u_2)),\quad T_P = F_{T|H=h}^{-1}(\Phi(u_3)). \tag{5}$$

In general, for the space $U_1 - U_2 - U_3$ all the possible combinations of u_1, u_2, u_3 with return periods n −years can be obtained (i.e., the loci of points u_1, u_2, u_3 that have a distance from the $u_1\ u_2 u_3$ axis start equal to the particular r that corresponds to 50-years). Transformation (5) provides the possible combinations of U_W, H_{m_0}, T_P, with the same return period.

In order to "construct" $f_{UHT}(U_W, H_{m_0}, T_P)$, the estimation of $f_U(U_W)$, $f_{H|U}(H_{m_0}|U_W)$ and $f_{T|H}(T_P|H_{m_0})$ is necessary. Let us note that great care should be paid to the selection of the underlying distributions and parameters; the decisions made in this phase may have important effects on the obtained results.

4.2 Estimation of $f_U(U_W)$, $f_{H|U}(H_{m_0}|U_W)$ and $f_{T|H}(T_P|H_{m_0})$

For the estimation of $f_U(U_W)$, the 2-parameter Weibull pdf is adopted. Weibull has been widely used for the modelling of wind speed. For the estimation of $f_{T|H}(T_P|H_{m_0})$, the log-normal distribution is used with location parameter $\gamma = 0$. In this respect, the H_{m_0} −sample is discretized to different H_{m_0} −classes (bin size 0.5m). The parameters of the log-normal distribution of T_P for the different significant wave height bins are estimated using Maximum Likelihood Method. For conditioning spectral peak period with significant wave height, the parameters of the log-normal distribution for the different bins of significant wave height should be expressed as functions of the latter variable.

The next step is the estimation of $f_{H|U}(H_{m_0}|U_W)$. This task is performed by discretizing the U_W −domain in appropriate "cells" where the estimation of the analytic form of $f_{H|U}(H_{m_0}|U_W)$ will take place. Following Li et al. (2013), $f_{H|U}(H_{m_0}|U_W)$ is modelled through a Weibull distribution function and its parameters for the different bins of wind speed are expressed as functions of the latter variable.

5 NUMERICAL RESULTS

By applying the procedure described in the foregoing sections, the contour surfaces with return periods 50 years have been estimated for the corresponding $U_W - H_{m_0} - T_P$ combinations. In particular, from the 3D 50-year contours of $U_W - H_{m_0} - T_P$, $U_{W,max}$ and $H_{m_0,max}$ have been identified and the corresponding (associated) values of the other two parameters (i.e., H_{m_0}, T_P and U_W, T_P respectively) are provided in Table 3.

Table 3 Environmental conditions on the 50-year contour surfaces with maximum U_W or maximum H_{m_0}

Condition	Parameter	Location L1	Location L2	Location L3
	U_W (m/sec)	18.82	21.80	25.44
Conditions with maximum U_W	H_{m_0} (m)	5.44	7.46	10.34
	T_P (sec)	10.20	11.88	13.56
	U_W (m/sec)	18.76	21.52	25.36
Conditions with maximum H_{m_0}	H_{m_0} (m)	5.48	7.50	10.36
	T_P (sec)	10.28	11.90	13.56

Then, for various threshold values of U_W, the corresponding 2D contours of $H_{m_0} - T_P$ are also provided. Let us note that all curves correspond to the 50 year return period. See Figure 8. The results provided here are very sensitive to the assumptions that have been adopted for the analytic derivation. Selection of different marginal or conditional probability density functions would have led to different results.

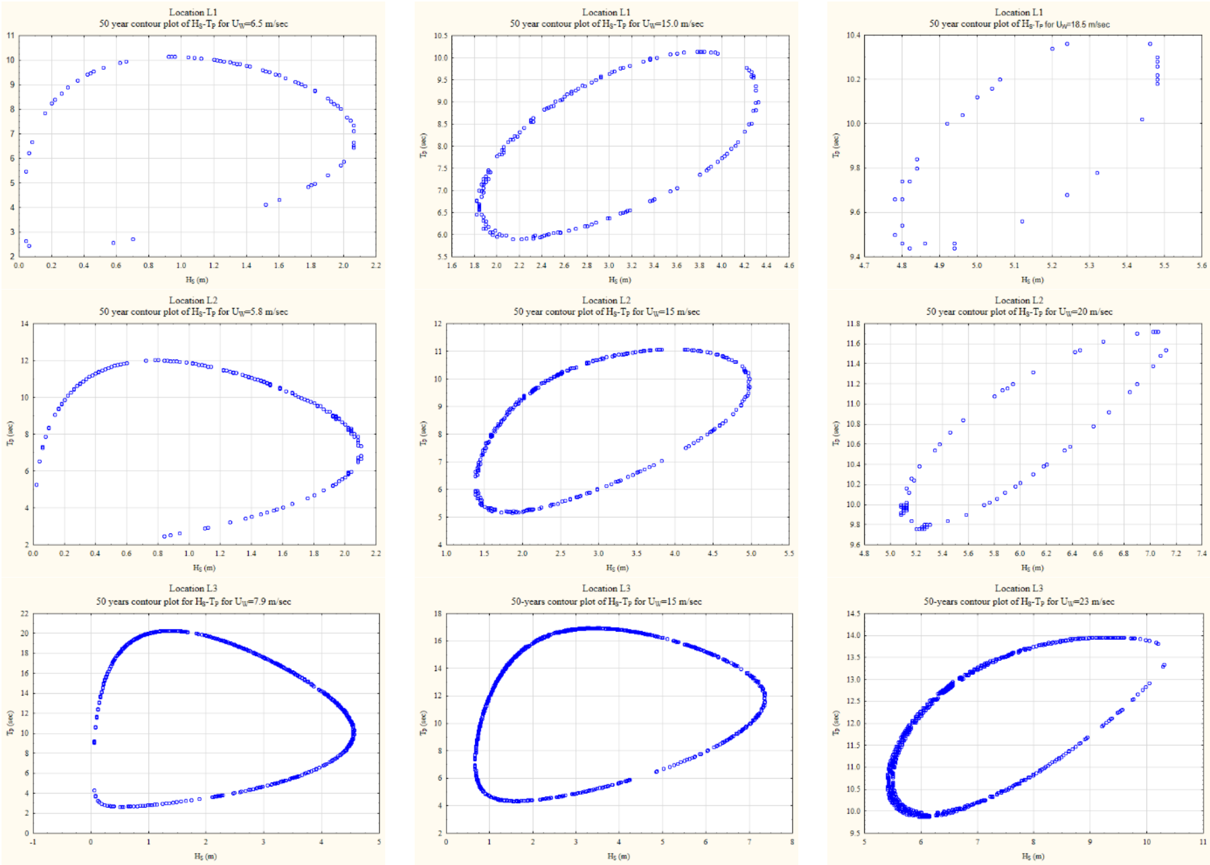

Figure 8 50-year contour surfaces of significant wave height and spectral peak period for different values of wind speed for location L1 (upper row), L2 (middle row) and L3 (lower row)

References

Baarholm GS, Haver S, Økland OD (2010) Combining contours of significant wave height and peak period with platform response distributions for predicting design response. Marine Structures 23(2): 147-163, doi:10.1016/j.marstruc.2010.03.001

Cheng PW, van Bussel GJW, van Kuik GAM, Vugts JH (2003) Reliability-based Design Methods to Determine the Extreme Response Distribution of Offshore Wind Turbines. Wind Energy 6(1), doi:10.1002/we.80

Coles S (2001) An Introduction to Statistical Modelling of Extreme Values. Springer

ERA-20C Project (ECMWF Atmospheric Reanalysis of the 20th Century). Research Data Archive at the National Center for Atmospheric Research, Computational and Information Systems Laboratory. http://dx.doi.org/10.5065/D6VQ30QG.

Li L, Gao Z, Moan T (2013) Joint Environmental Data At Five European Offshore Sites For Design Of Combined Wind And Wave Energy Devices. Paper presented at the 32nd International Conference on Ocean, Offshore and Arctic Engineering, OMAE2013-10156, June 9-14, Nantes, France

Rosenblatt M (1952) Remarks on a multivariate transformation. Ann. Math. Statist., 23(3):470-472

Soukissian TH, Kalantzi G (2006) Extreme value analysis methods used for wave prediction. Paper presented at the 16th International Offshore and Polar Engineering Conference (ISOPE), Vol. III, pp. 10-17, ISBN 1-880653-66−4

Soukissian TH, Tsalis C (2015) The effect of the generalized extreme value distribution parameter estimation methods in extreme wind speed prediction. Natural Hazards, 78:1777-1809, doi:10.1007/s11069-015-1800-0

Yang X, Zhang Q (2013), Joint probability distribution of winds and waves from wave simulation of 20 years (1989-2008) in Bohai Bay. Water Science and Engineering, 6(3): 296-307

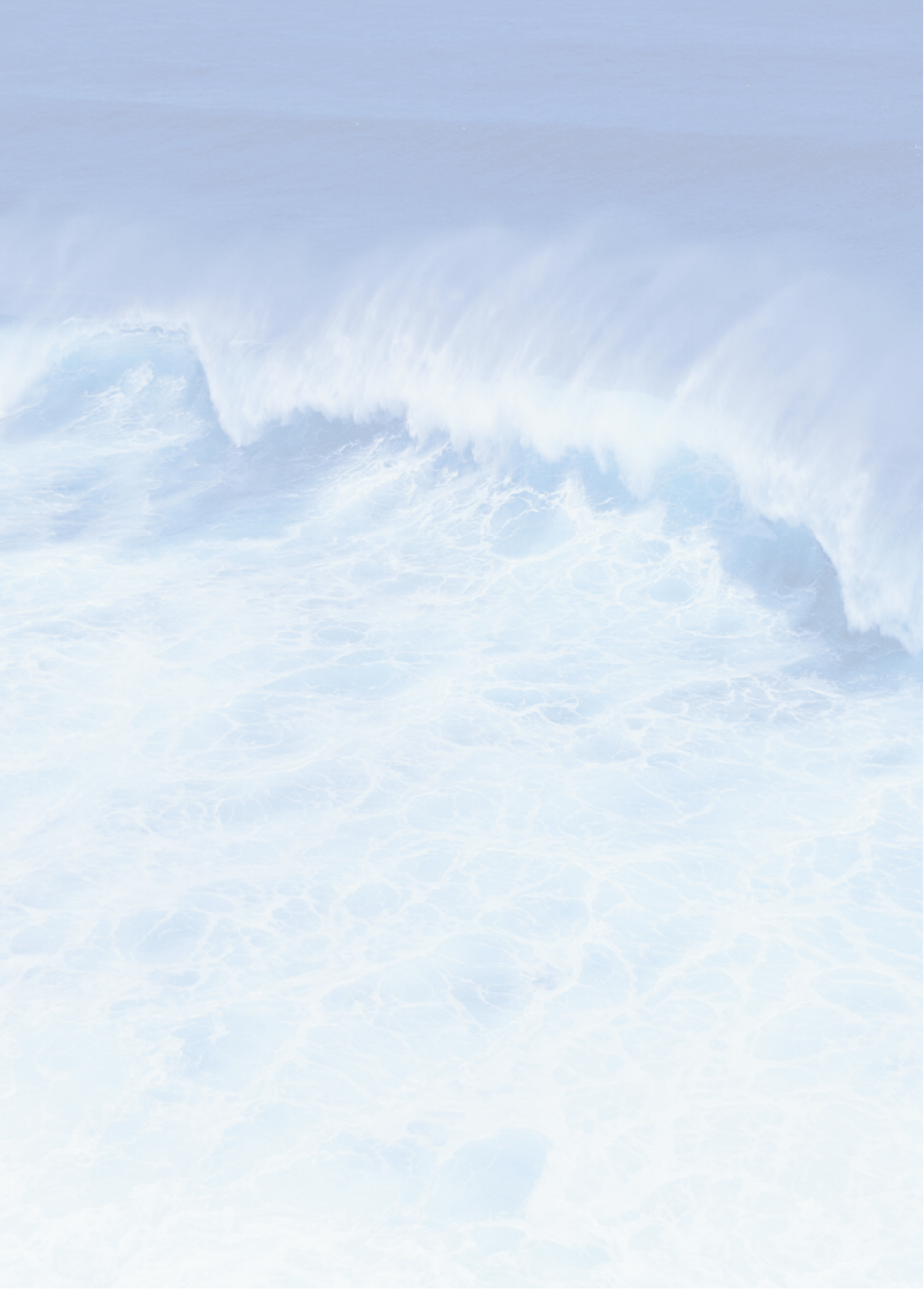

A Smart Data Selection Tool (SDST) for estimating design wave height

M. Chondros[1,2*], A. Metallinos[1,2], C. Memos[1,2], V. Tsoukala[2]

[1]Scientia Maris, Agias Elenis 10, Zografos, 15772, Greece
[2]School of Civil Engineering, National Technical University of Athens, Zografos, 15780, Greece
[*]Corresponding author: michondros@gmail.com

Abstract

A methodology is proposed to efficiently and accurately define design wave heights for corresponding return periods. For this reason a Smart Data Selection Tool is developed in order to wisely choose occurred events, with high wind velocities and sufficient durations and thus capable of generating storm waves. By carrying out a limited number of wave generation and propagation simulations for selected wind blowing events, an array of maximum significant wave heights can be extracted at the location of interest. The proposed methodology is applied offshore of the Port of Rethymno and the resulted maximum wave height was close to the one calculated, over the same period, from large scale hindcast simulations carried out in past projects. This methodology can replace the common practice of estimating design wave heights calculated by means of mean annual wind data instead of an extremal wave height analysis.

Keywords Design wave height, Extreme waves, Wind-waves growth, Storm events.

1 INTRODUCTION

Design wave height is the basic parameter for designing port and coastal structures. The structure longevity or its possible failure strongly depends on this design value. A common practice nowadays, adopted by a large portion of engineers, equalizes design wave height with a significant height calculated by means of offshore wave growth formulas based, however, on mean annual wind data, thus not representing extreme events. This particular practice became attractive due to the ease and quickness of implementation. However, it usually leads to over- or usually under-estimation of the proper dimensions of the material (e.g. armor stones) required to construct coastal and port works. To cover this need an efficient methodology is proposed in the present study able to determine the appropriate design wave height by developing a useful tool.

2 A SMART DATA SELECTION TOOL FOR ESTIMATING DESIGN WAVE HEIGHT

Determination of design wave height is based on statistical analysis of extreme wave heights occurred during the past decades. These data can be acquired either by field measurements or by means of numerical modeling. Nonetheless, there is a significant lack of data sources in Greek seas, since the deployed buoys do not cover but a small portion of the total sea area. On the other hand, offshore wave climate modeling for periods of at least 20 years is an extremely time consuming process that requires significant computational resources, making this option non-applicable.

Therefore, a Smart Data Selection Tool (SDST hereafter) is developed in the present study in order to wisely choose from occurred wind events, giving high velocities and sufficient durations and thus capable of generating storm waves. The SDST scans wind data time series and automatically detects candidate events with duration greater than, say, 6 hrs and average velocities greater than, say, 6Bf. Each event is assigned to a principal direction (e.g. E, NE etc) assuming that the observed wind directions, during the event, lie in the interval ±22.5° from the principal. Obviously, the orientation and morphology of the shoreline indicate a limited number of directions to be investigated, since in these directions the coastal area is exposed to incident waves.

SDST analyses big wind data and yields one or two storm events per year that could lead to extreme wave heights occurrence. Hence, only the more severe storms are considered and specific scenarios of limited number are simulated. Consequently, it becomes evident that the required computing time drops dramatically.

Given the scenarios by the SDST, the spectral wave model TOMAWAC (Benoit et al. 1996) is implemented to simulate the offshore wave generation and propagation and conclude with an array of extreme significant wave heights at a specific point offshore of the coastal area of interest. Each significant height represents a storm event. Afterwards, by choosing the lifetime of the structure, L, and the acceptable risk, R, one can calculate the required design wave height.

In addition to the aforementioned, it should be noted that a probabilistic description of the long-term wave climate is of great significance for the selection of the design parameters for coastal structures. In order to gain this information via estimation of the joint distribution of long-term wave parameters, engineers usually use wave measurements obtained from buoys often located in deep waters or wind data in the wave generation area. In both cases there is a need to transform the long-term wave climate from deep waters to the design structure's location. A simple and fast model is available (Malliouri et al. 2019), which transforms this vital information from deep towards intermediate waters with satisfactory accuracy compared with non-linear models, via integration of short - and long-term wave statistics.

3 CASE STUDY – PORT OF RETHYMNO

3.1 Application of SDST

In order to validate the performance of the proposed SDST a case study is considered herein to calculate the design wave height at a point offshore of the port of Rethymno in Crete Island, Greece (Figure 1).

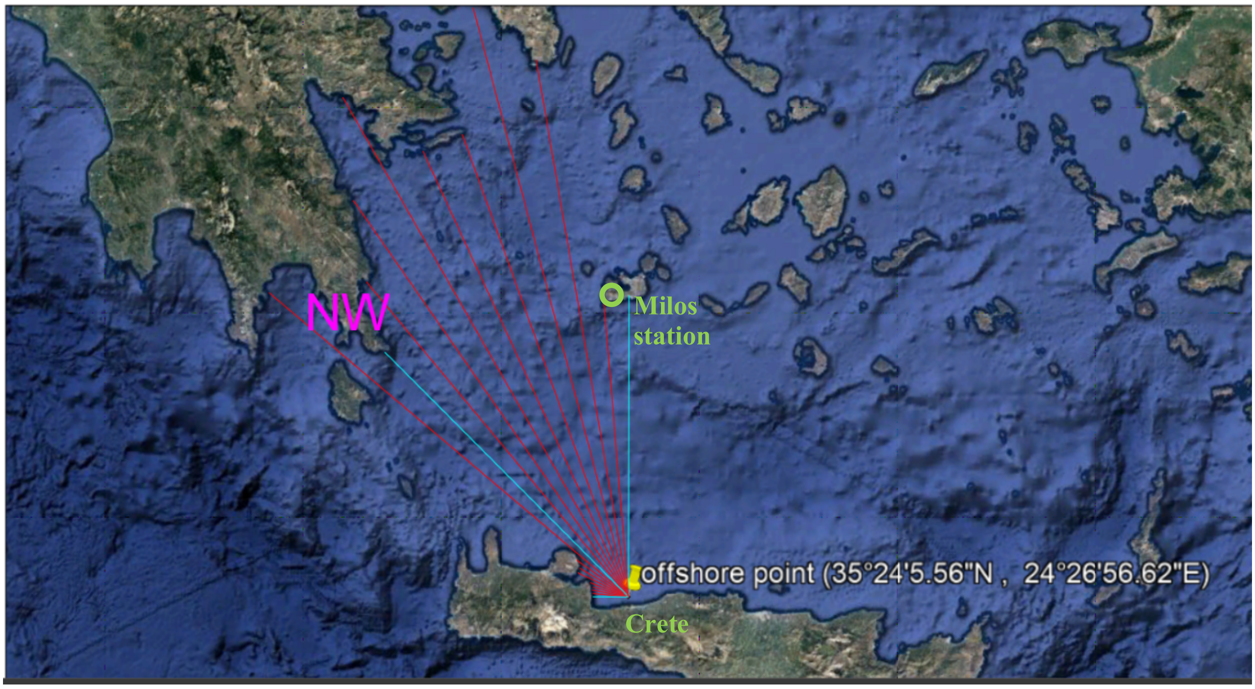

Figure 1 Offshore point of interest in the Aegean Sea and fetch rays

The desired open source (National Centers for Environmental Prediction, National Oceanic and Atmospheric Administration, ncdc.noaa.gov) data include time series of 175.321 wind speed and direction values for a selected 20-year period, 1979-1998, with a time step of 1 hr. The SDST (which is an easily-implemented executable file, coded in MATLAB) is then applied to scan the time series and detect the extreme wind events by assuming a minimum duration of 6 hrs, wind velocities equal or greater than 6Bf (>11 m/s), and the NW as the principal direction. The SDST yielded 19 extreme wind events with durations ranging from 6 to 15 hrs, speeds ranging from 11 to 21 m/s and directions 290 to 340 degrees (counting clockwise from North).

3.2 *Simulation of Wave Generation and Propagation*

Given the 19 events by the SDST, the spectral wave model TOMAWAC (Benoit et al. 1996) is implemented to simulate the offshore wave generation and propagation. The bathymetry of the western Aegean is constructed in flexible mesh, covering an area from the northwestern shoreline of Crete Island up to the Gulf of Saronikos and taking into account the existing small and larger islands. Spatial and temporal wave growth results are illustrated indicatively for the first event in Figure 2. The resulted significant wave heights, occurred during these events at the offshore point of interest, are greater than 2 m, with a maximum of 4.45 m.

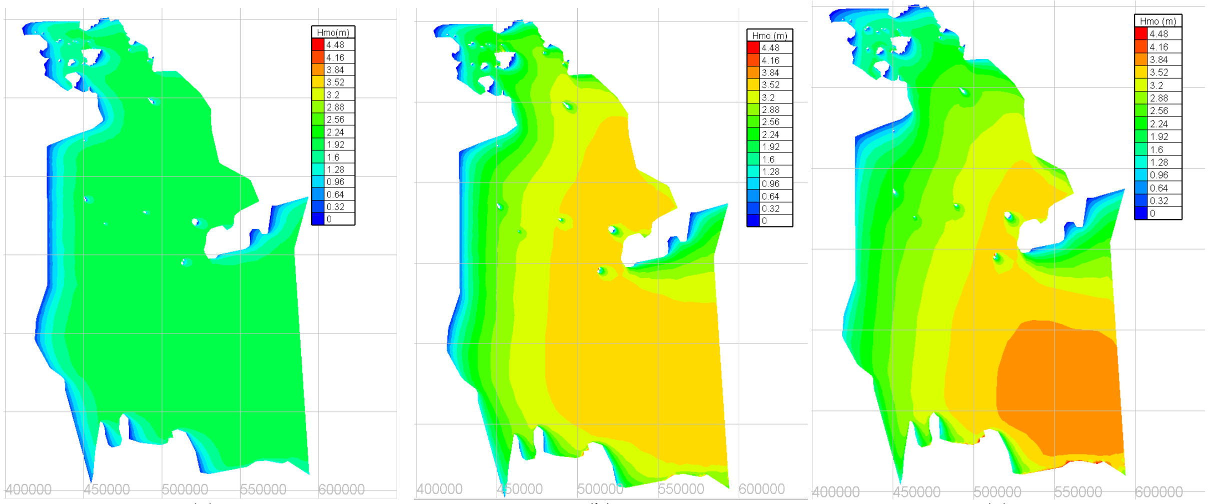

(a) (b) (c)

Figure 2 Indicative spatial wave growth results for the first extreme wind event at: (a) t=3 hrs, (b) t=6 hrs and (c) t=9 hrs; Color palette represents spatial H_s distribution, ranging from 0 m (blue) to 4.5m (red)

3.3 *Extremal Wave Height Analysis*

By applying the approach developed by Goda (1988) to fit probability distributions to the aforementioned array of extreme heights and by choosing the lifetime of the structure, L, and the acceptable risk, R, one can calculate the required design wave height. Two probability distributions are considered herein:

$$\text{Fisher-Tippett Type I:}\quad F\left(H_s \leq \hat{H}_s\right) = e^{-e^{-\left(\frac{\hat{H}_s - B}{A}\right)}} \tag{1}$$

$$\text{Weibull:}\quad F\left(H_s \leq \hat{H}_s\right) = 1 - e^{-\left(\frac{\hat{H}_s - B}{A}\right)^k} \tag{2}$$

where $F\left(H_s \leq \hat{H}_s\right)$ probability of $\hat{H}_s$ not being exceeded, H_s significant wave height, particular value of significant wave height $\left(H_s \leq \hat{H}_s\right)$, B location parameter and A, k scale and shape parameter, respectively.

As mentioned above, the input array of significant wave heights should be extracted from a long-term data source of measurements, hindcasts, or observations. For instance, for return periods, T_r, of 100 years a record length of 40 years is recommended. The reliability of predicted extremes is directly related to the accuracy of available data and the number of years of record. Furthermore, an estimation of confidence intervals is given to provide a quantitative indicator of the level of uncertainty. The approach of Goda (1988) for estimating standard deviation of return value when the true distribution is known is used herein. Goodness-of-fit indicated that Weibull distribution best match the input data, since the correlation factor is 0.937 while for Fisher-Tippett Type I is 0.910. The resulted significant wave heights and the corresponding 90% confidence intervals are presented in Table 1.

The aforementioned methodology is compared with the common practice of calculating the design wave height as the maximum height derived by mean annual wind data, adopted by a large portion of engineers.

Table 1 Design wave height and confidence intervals in relation to return period T_r for two distributions

T_r (yrs)	FT-I H_s (m)	FT-I 90% Conf. intervals		Weibull H_s (m)	Weibull 90% Conf. intervals	
2	2.59	2.16	3.01	2.54	2.10	2.99
5	3.53	2.86	4.20	3.62	2.86	4.39
10	4.15	3.15	5.14	4.23	3.22	5.24
25	4.92	3.48	6.37	4.91	3.62	6.20
50	5.50	3.72	7.28	5.35	3.87	6.84
75	5.81	3.84	7.78	5.58	4.00	7.17
100	6.07	3.95	8.20	5.75	4.10	7.43

In particular, the offshore wave climate is estimated by means of offshore wave growth formulas, i.e. SPM (1984) and Smith (1991), based, however, on mean annual wind data (common practice), thus not representing extreme events. In the case study, examined in this paper, is chosen the station of Hellenic National Meteorological Service located in Milos Island (Figure 1) to obtain mean annual wind data, since it is closer to the wave generation area from NW winds. It is observed that the maximum occurred wind velocity from the NW direction is 10Bf with a mean annual frequency of 0.011%. Furthermore, the linear distances of the Fetch rays, illustrated in Figure 1, were measured and the results are given below. The different H_s results of the two methods are attributed to the different equations on which they are based. Following a conservative approach most engineers use the fetch limited wave heights.

Table 2 Offshore wave height calculated by wave growth formulas

Method	Wind velocity (Bf)	Mean annual frequency of occurrence (%)	Duration limited $\boldsymbol{H_s}$ (m)	Fetch limited $\boldsymbol{H_s}$ (m)
Smith et al. 1991	10	0.011	1.10	6.35
SPM 1984			2.30	6.15

The maximum derived height equals to 6.35m which is significantly larger than the one resulted from the hindcast simulations 4.45 m, and even from a 100-year return period design wave height equal to 5.75 m (Table 1). Such significant deviations are the reason for over- or under- estimation of the coastal structure armoring. For instance, bearing in mind that the exponential power of the wave height, in the well-known Hudson formula, equals to 3, the above “small” deviation of ~0.60 m, leads to +35% greater armor weight requirements.

4 VALIDATION WITH LARGE SCALE HINDCAST SIMULATIONS

In order to verify the SDST results, a comparison is given herein with offshore wave hindcast simulations utilizing a 3-level SWAN (Booij et al. 1999) based scheme illustrated in Figure 3. It was initially developed in the framework of Thales project CCSEAWAVS (Prinos 2014) and the downscaling was carried out in the framework of FP7 - PEARL project (Tsoukala et al. 2016). The simulation scheme uses past and future projections of climatic wind fields for the estimation of wave characteristics with resolution 0.2 x 0.2 degrees in the Mediterranean basin (Level 1). These data provide boundary information for repeating the simulation using a finer mesh 0.05 x 0.05 degrees inside an Eastern Mediterranean subsection (Level 2). Then, a high-resolution 0.005 x 0.005 degrees mesh was applied in the selected coastal region (Level 3).

The wave heights occurred during the selected period, 1979-1998, at the offshore point of interest and from the NW direction, are plotted in Figure 4. The maximum wave height is 4.2 m, which is close to the one estimated by the present approach, 4.45 m, proving its validity.

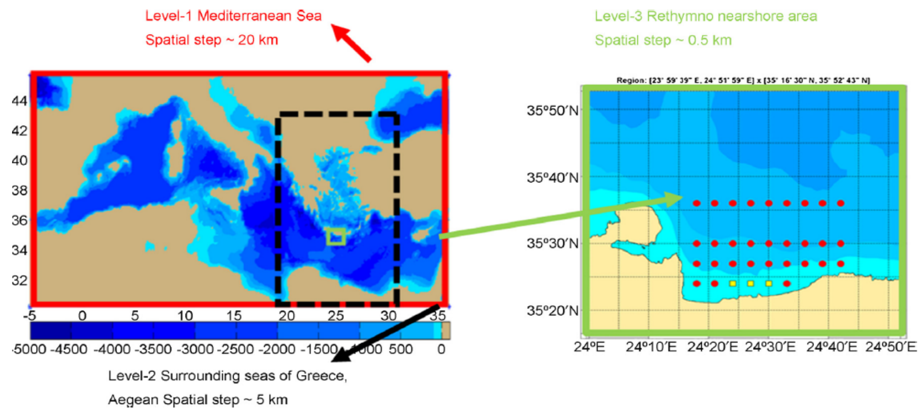

Figure 3 Estimation of offshore wave characteristics using a 3-level downscaling (Tsoukala et al. 2016)

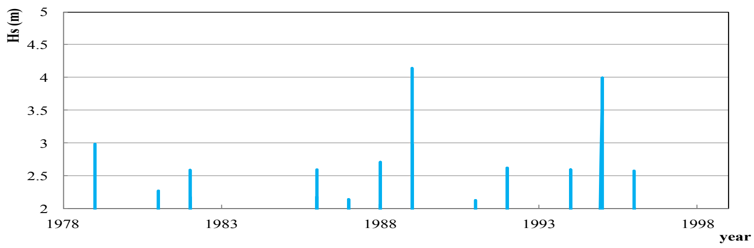

Figure 4 Maximum wave heights occurred during the selected period, 1979-1998, at the offshore point of interest and from the NW direction as calculated by large scale simulations

5 CONCLUSIONS

The Smart Data Selection Tool developed in this paper, in conjunction with open source wind data and a Spectral Wave model, can help engineers estimate the design wave height for a corresponding return period, in absence of long-term field measurements or numerical hindcast modeling results.

References

Benoit M, Marcos F, and Becq F (1996) Development of a third generation shallow-water wave model with unstructured spatial meshing, Proceedings of the 25th International Conference on Coastal Engineering, Orlando, 465–478, ASCE.

Booij N, Ris RC, Holthuijsen LH (1999) A third-generation wave model for coastal regions: 1. Model description and validation. J. Geophys. Res. 104 (C4), 7649—7666

Goda Y (1988) On the Methodology of Selecting Design Wave Height. Proceedings of the Twenty-first Coastal Engineering Conference, American Society of Civil Engineers, Costa del Sol-Malaga, Spain, pp. 899-913.

Malliouri D, Memos C, Tampalis N, Soukissian T, Tsoukala V (2019) Integrating short- and long-term statistics for short-crested waves in deep and intermediate waters. Applied Ocean Research 82(3):346–361. doi: 10.1016/j.apor.2018.11.004

Prinos P (2014) Climate change effects on the Greek seas and coastal areas — the research project THALIS-CCSEAWAVS. In: 6th Panhel- lenic Conference on Coastal Zones Management and Improve-ment, 24—27 November 2014, Athens, 315—324.

Shore Protection Manual (1984) 4th ed., 2 Vols., US Army Engineer Waterways Experiment Station, Coastal Engineering Research Center, US Government Printing Office, Washington, DC, Chapter 3, pp. 24-66.

Smith JM (1991) Wind-Wave Generation on Restricted Fetches, Miscellaneous Paper CERC-91-2, US Army Engineer Waterways Experiment Station, Vicksburg, MS.

Tsoukala VK, Chondros MK, Kapelonis, ZG, Martzikos, N, Lykou, A, Belibassakis K A, Makropoulos Ch (2016) An integrated wave modelling framework for extreme and rare events for climate change in coastal areas – the case of Rethymno, Crete, Journal of Oceanologia Vol. 58, Issue 2, pp. 71-89.

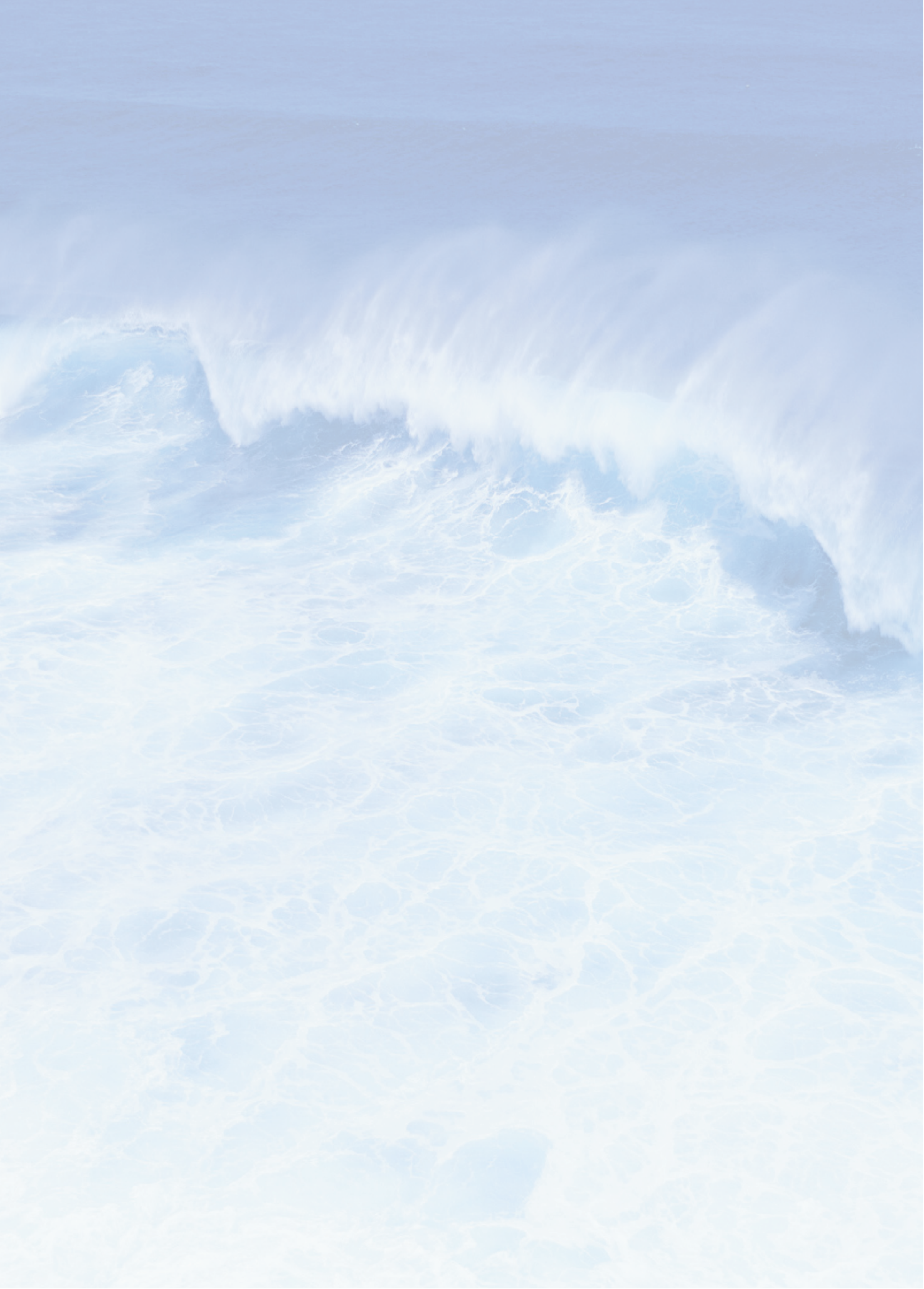

Mediterranean Coastal Storms in a Changing Climate

N. Martzikos[1*], P. Prinos[2], C. Memos[1], V. Tsoukala[1]

[1]Laboratory of Harbour Works, School of Civil Engineering, National Technical University of Athens, Zografos 15780, Greece.
[2]Hydraulics Laboratory, Department of Civil Engineering, Aristotle University of Thessaloniki, Thessaloniki 54124, Greece.
[*]Corresponding author: nmartzikos@central.ntua.gr

Abstract

Coastal storms as extreme hydro-meteorological events have severe impacts on the coasts and consequently affect the coastal communities, attracting considerable interest in research nowadays. Trying to understand these extreme events, the storm analysis is accomplished by studying the significant wave height, the wave period, the storm duration and many other important parameters. The range of storm parameters and their thresholds are valuable for a specific location but also constitutes a rough outline of wave climate during storm events. Here, a buoy dataset from all over the Mediterranean Sea was analysed for describing coastal storm activity and investigating further each storm event about their parameters, the storm duration, their independence and the storm energy. A statistical description and their trends are also presented. A deeper understanding of the risk due to coastal storms was pursued, gaining knowledge on what to expect, how to inform coastal communities and how to protect the coastal areas from coastal storm impacts in a changing climate.

Keywords Mediterranean, Coastal storms, Climate change, Extreme events.

1 INTRODUCTION

Researchers all over the world are focused on coastal storms in order to learn more about these extreme events and study their impacts. The coastal flooding, the beach erosion, the damages of harbour and coastal works are some of the most serious problems faced by coastal communities. The management of such events, the preparedness and an informed society are of great importance and more urgent especially nowadays due to a changing climate.

Considering the coastal storms as storm events with impacts on coastal areas, their identification can be carried out by setting that the significant wave height (H_s) exceeds a certain threshold and remains over this for a minimum time period relevant to the storm duration (D). The above thresholds are varied according to authors, with most common; $1 \leq H_s \leq 4$ m and $6 \leq D \leq 30$ hr, but they are also site-specific, depending on the bathymetry, the synoptic systems, the local characteristics and the exposure of a location to the winds and the big waves (Harley 2017). In addition, recently there has been an increasing interest in the calm period between two consecutive storms, with the meaning of the inter-arrival time between the start of the upcoming event and the end of the previous one (Corbella and Stretch 2013). This value is used to ensure the independence between two events. Also, it is the criterion for considering two events as one, unifying them to a cluster and specifying the storm duration. A storm sequence could be crucial to the beach erosion and the coastal morphology and it is more destructive than isolated events in many cases (Ferreira 2005; Dissanayake et al. 2015; Sénéchal et al. 2017). In this context, the main direction of storm events and their energy are also taken into account. Moreover, the variation of these parameters during a storm is one more limitation that requires special attention.

For the clarification of all the above, a detailed analysis of historical storm events, based on a large dataset, will normally reveal the variation of the above parameters, the importance of reliable thresholds and a better understanding of their processes and their impacts. The aim of this work is to present an integrated statistical analysis of coastal storm events, gaining in this way an insight view of their severity over the Mediterranean and any modifications incurred through the years.

2 CASE STUDY & METHODOLOGY

The extended data analysis of storm events is performed over the Mediterranean Sea. A dataset from 30 buoys recording the wave climate of Greece, Italy, France and Spain is analysed. The data were obtained by Puertos del Estado (www.puertos.es), Copernicus (www.copernicus.eu) and EMODnet (www.emodnet.eu) databases, covering in general a time period since the 1980's. The specific buoy locations in each country are selected according to their vicinity to the coast (Figure 1), in order to focus and analyse coastal storms, differentiating them from the storms in open sea waters.

The identification of storm events is carried out by using the significant wave height (H_s) threshold, fixed in the 95th percentile of the significant wave height timeseries for each location. Following Martzikos et al. (2018), the minimum storm (D) duration was taken as 9 hours, skipping over the events with smaller duration. The inter-arrival time (I) between two independent storm events is set to be greater than 18 hours, where the closest events are considered as one event. The wave period for a storm event is taken as the mean of the corresponding timeseries, while the range of this parameter is short during a storm event. In addition, the storm energy is estimated for each storm event by the Eq. 1, as it was proposed by Dolan and Davis (1992), where t_1 denotes the beginning of a storm event, t_2 the end time and H_s is always greater or equal to the predefined threshold.

$$E = \int_{t_2}^{t_1} H_s^2 dt \qquad (1)$$

Consequently, a statistical analysis of the above parameters is accomplished and the frequency of storm events during 6 months or one year are also estimated. The duration, the inter-arrival time and the storm energy, as well as the range of storm's important parameters and the most extreme events, are described for each location and to a country level.

Figure 1 The location of buoys over the Mediterranean Sea

3 RESULTS

The integrated analysis of 30 different datasets, resulted valuable information about storm activity over the Mediterranean Sea for the last decades. It should be noted, that the major part of the data is gathered with different sampling frequency, ranging from 0.5 to 6 hours (see also Table 1), as well as the different types of data encoding raised an additional difficulty in this effort. For 2728 storm events, which are identified and analysed, their frequency varies during a year according to the location, while the majority of storm events occur during the winter months.

3.1 Descriptive Statistics

For the statistical analysis, the mean value of significant wave height (m_H) and the wave period (m_T) are presented below. The corresponding coefficients of variation CV_H and CV_T are also estimated, in order to investigate the homogeneity of the sample, where the smallest values are preferable. The storm energy (m_E) and the storm duration (m_D) of events are also presented by their mean value.

Finally, the most extreme events are examined, taking the highest 5% of storm events according to the maximum significant wave height and the maximum wave period timeseries for each location and describing them by their mean ($m_{H0.5}$, $m_{T0.5}$). All the above parameters and their descriptive statistics are presented thoroughly in Table 2.

The locations which are affected from long fetches and consequently they are exposed to big waves, appeared with the highest values of significant wave height, such as Cabo Begur in Spain, La Revellata and Catania in Italy. On the other hand, when the water depth was very small, or the locations were sheltered by a bay and they surrounded by shallow waters, they appear with the lowest values, such as Kalamata in Greece and Venezia in Italy. In this context, the aforementioned trends are also the same for the most extreme events, where the mean of significant wave height exceeded the 6 m and the wave period was over 10 s for the most exposed locations. Regarding the duration, it is important to point out that many storm events have mean duration nearly 27 hours, while the shortest events occur in Palermo and La Revellata in Italy and in Marseille in France. The storm energy, as it depends on the H_s and on the duration, is ranged high when the other parameters have also high values.

Table 1 Sampling details and the frequency of storm occurrence in a country level

	Locations	Covering Period [years]	Frequency [hr]	Storms	Storms Oct-March	Storms Apr-Sept	Storms /year
Greece	9	1999-2017	3.0	881	781	100	46
Italy	6	2013-2017	1.0-6.0	83	75	8	17
France	6	2004-2017	0.5	391	329	62	39
Spain	9	1985-2019	1.0	1373	1070	303	40

3.2 Duration & Inter-arrival time

The analysis of duration is accomplished by taking all the events which exceeded the threshold for the significant wave height, even if there were not developed to storms, since they did not overcome the minimum storm duration. The boxplots in Figure 2(a) show the full range of the duration of these exceedances, by the meaning of storm duration. The most exceedances lasted for a time period lower to 25 hours, reinforcing that the minimum storm duration should be defined under of this value. The rectangles inside of boxplots correspond to the interquartile range of storm duration in the dataset of each country, while the segment inside shows the median. The mean value is represented by the dot in the centre of rectangle. The selected threshold of 9 h for the minimum storm duration, is usually between the median and the mean value for all the examined locations.

The inter-arrival time between storm events was also analysed. A storm sequence could be destructive for a coastal zone, but the majority of storm events rarely distinguished by a calm period less than 15 days (360 hours), according to boxplots in Figure 2(b). More specifically, the 50% of storm events in Mediterranean are independent, having an inter-arrival time nearly over of a month (700 hours).

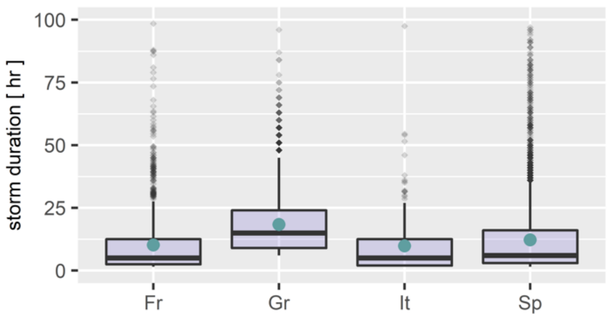

(a)

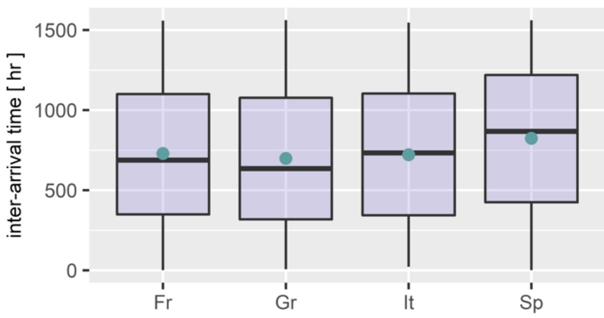

(b)

Figure 2 Boxplots for the full range of variation of the duration of storm events (a) and the inter-arrival time between two consecutive storm events (b)

Table 2 Basic statistics of the most important parameters in a storm event for the examined locations

Location		m_H [m]	CV_H	m_T [s]	CV_T	m_E [m^2/h]	m_D [hr]	$m_{H0.5}$ [m]	$m_{T0.5}$ [s]
Greece	Athos	2.78	0.07	7.41	0.04	267.85	24.89	6.01	10.39
	Lesvos	2.84	0.09	7.22	0.11	174.30	24.25	7.04	14.34
	Skyros	2.88	0.12	7.58	0.07	321.93	32.52	5.02	10.05
	Mykonos	3.05	0.10	8.34	0.08	249.37	25.90	5.81	11.05
	Santorini	3.04	0.24	8.11	0.15	164.57	23.37	6.38	12.36
	Heraklion	2.15	0.18	6.90	0.13	194.75	28.29	4.21	9.14
	Kalamata	0.98	0.09	6.79	0.03	61.80	27.57	3.64	10.89
	Pylos	2.82	0.06	9.14	0.05	297.94	27.00	6.70	12.68
	Zakynthos	2.31	0.10	8.37	0.13	213.57	23.6	7.68	24.96
Italy	Catania	3.92	0.19	10.22	0.12	255.58	37.00	4.96	13.33
	Crotone	1.96	0.06	8.53	0.09	267.78	33.58	6.46	13.33
	Venezia	1.74	0.11	6.31	0.06	67.80	20.69	3.24	10.27
	Palermo	2.79	0.12	8.38	0.07	170.61	18.50	5.49	13.33
	La Revellata	3.68	0.09	9.28	0.09	323.63	18.12	7.70	13.30
	Alistro	3.46	0.34	9.13	0.17	172.56	27.57	5.80	11.80
France	Banyuls	2.56	0.22	8.79	0.06	159.46	26.62	6.72	18.88
	Leucate	2.13	0.13	6.39	0.06	218.07	32.28	7.92	25.90
	Marseille	3.20	0.23	8.30	0.09	135.99	19.43	6.00	14.75
	Nice	2.16	0.19	7.76	0.12	85.23	23.87	3.40	13.30
	Sete	1.98	0.11	6.92	0.07	190.51	29.97	5.18	13.45
	Porquerolles	3.27	0.09	9.71	0.06	188.29	16.45	6.03	11.20
Spain	Barcelona	1.97	0.08	7.97	0.05	142.70	29.46	4.41	11.22
	Malaga	2.24	0.29	7.93	0.15	115.58	34.17	3.96	10.94
	Taragona	1.99	0.23	8.02	0.12	67.31	29.91	3.25	11.01
	Valencia	1.93	0.18	7.38	0.11	116.61	29.67	4.17	13.29
	Cabo De Gata	3.11	0.12	7.96	0.09	226.90	23.69	5.31	10.24
	Dragonera	2.87	0.04	8.36	0.04	324.55	27.24	6.09	12.17
	Cap De Pera	3.47	0.15	8.66	0.11	303.85	27.54	5.97	11.67
	Son Bou	2.03	0.16	5.41	0.08	94.98	26.21	4.13	8.35
	Cabo Begur	3.77	0.06	8.10	0.06	518.06	28.61	7.04	11.15

4 DISCUSSION & CONCLUSIONS

With the above analysis, a deeper understanding of the risk due to coastal storms is pursued, gaining knowledge on what to expect. As result, a new database about storm events in Mediterranean is created and it could be useful to everyone, such engineers, organisations or stakeholders on how to inform coastal communities and how to protect the coastal areas from coastal storm impacts in a changing climate.

A dataset of wave climate timeseries from 30 boys over the Mediterranean was analysed, covering coastal areas from Greece, Italy, France and Spain for the years 1985-2019. A total amount of 2728 storm events were identified and the trends of their important parameters were examined. For each storm event the mean significant wave height, the mean wave period, the energy, the duration and the inter-arrival time from the previous or the upcoming event, were estimated and their descriptive statistics were presented. The frequency of storm occurrence in a year, the number of events during the semesters October-March and April-September and the most extreme storm events were also investigated by the highest 5% of storm events. The results of this investigation show that a number of 35 storm events per year occur in coastal areas, with the most of them to be developed during the semester of October-March. The most extreme storm events usually have significant wave height which exceeds the value of 4 m and the wave period to be over of 8 s.

The limitations of this analysis are mainly the sampling frequency of buoys datasets and the different data encoding, which provided by different databases. The covering time period was very short and different for many locations, resulting that the conclusions of this analysis could not be so general. For this reason, the summary of this analysis at a country level is not very helpful and thus is not included. However, the conclusions for each location are considered very important for everyone who could be interested about the storm activity around a specific location.

The statistical analysis of important parameters for a storm event, give valuable information about the range of significant wave height, the wave period as well as their values at the most extreme events in each location. The results about the mean storm duration are also significant, while the duration is of great importance for the vulnerability of coastal structures and their design. The storm energy is the only variable which its range was not so comprehensible to everyone, while the storm impacts are not clearly associated with this, but it might be helpful in comparison with other locations or with different events.

Finally, it may be concluded that a future work should describe in more detail the storm activity of each location in order to study in depth the coastal storm events, their processes and understand better their potential impacts.

Acknowledgements
This work is part of Mr. Martzikos' PhD thesis and it was supported by the Action: «Enhancing the Human Research Potential through the Implementation of Doctoral Research» of the Operational Programme «Human Resources Development, Education and Lifelong Learning» of NSRF 2014-2020, co-financed by the European Social Fund and the Greek Government.

References

Corbella S, Stretch DD (2013) Simulating a multivariate sea storm using Archimedean copulas. Coast. Eng. 76, 68–78. https://doi.org/10.1016/j.coastaleng.2013.01.011

Dissanayake P, Brown J, Wisse P, Karunarathna H (2015) Effects of storm clustering on beach/dune evolution. Mar. Geol. 370, 63–75. https://doi.org/10.1016/j.margeo.2015.10.010

Dolan R, Davis R (1992) An Intensity Scale for Atlantic Coast Northeast Storms. Journal of Coastal Research 8, 840–853.

Ferreira Ó (2005) Storm Groups versus Extreme Single Storms: Predicted Erosion and Management Consequences. Journal of Coastal Research, 221-227.

Harley M (2017) Coastal Storm Definition, in: Coco, G., Ciavola, P. (Eds.), Coastal Storms. John Wiley & Sons, Ltd, Chichester, UK, pp. 1–21. https://doi.org/10.1002/9781118937099.ch1

Martzikos N, Afentoulis V, Tsoukala V (2018) Storm clustering and classification for the port of Rethymno in Greece. Water Utility Journal 20, 67–79.

Sénéchal N, Castelle B, Bryan K (2017) Storm Clustering and Beach Response, in: Coastal Storms. John Wiley & Sons, Ltd, Chichester, UK, pp. 151–174. https://doi.org/10.1002/9781118937099.ch8

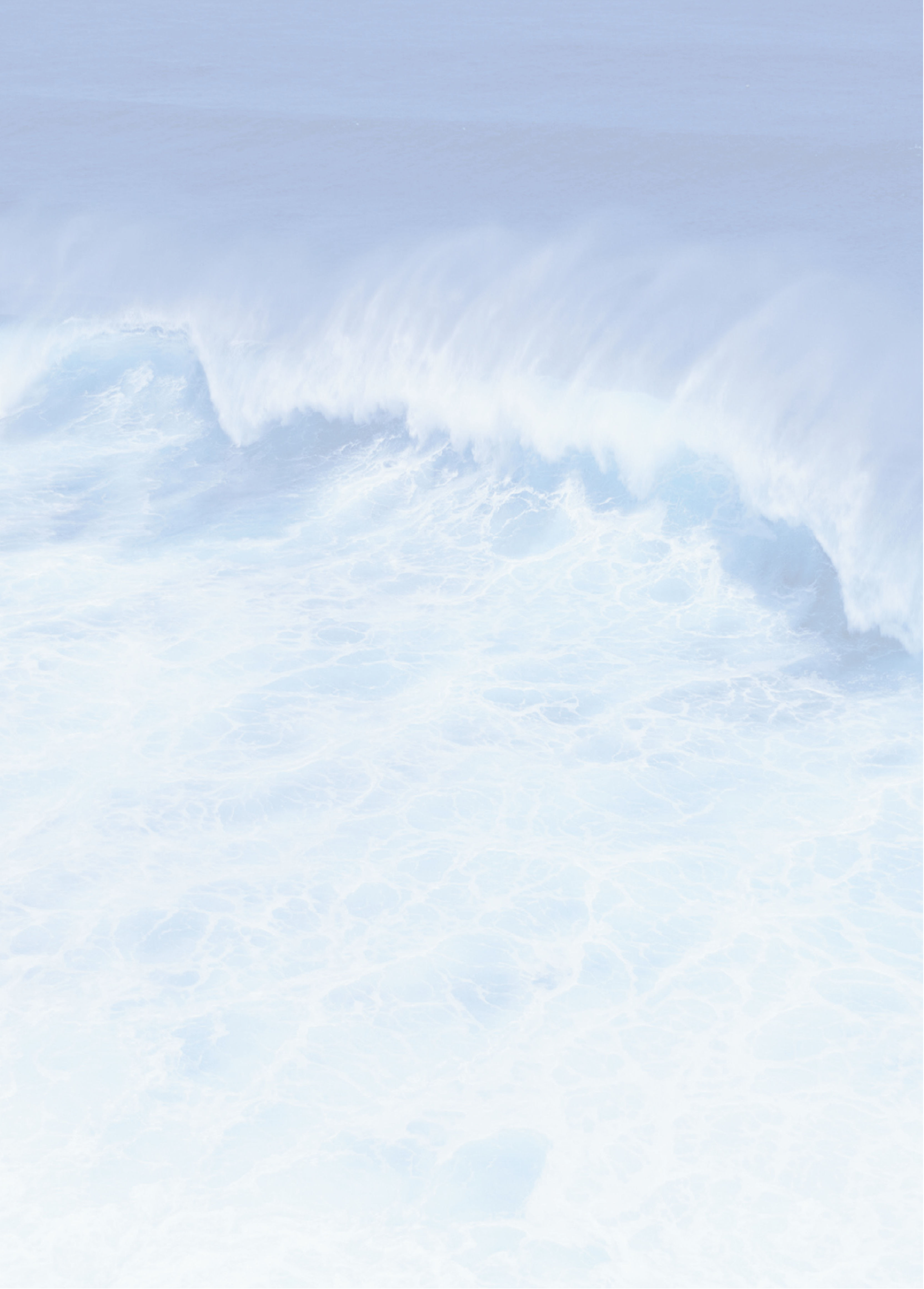

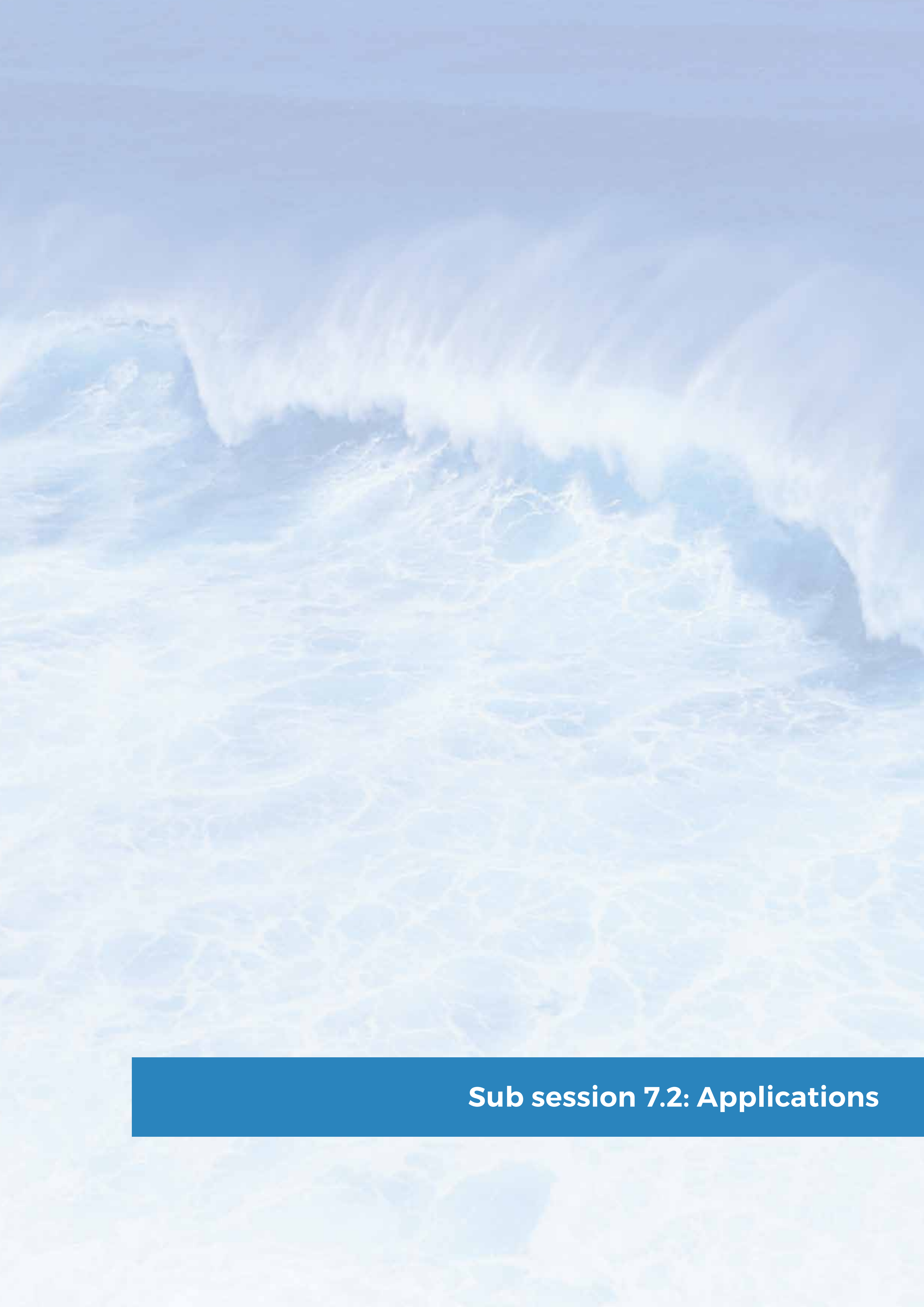

Sub session 7.2: Applications

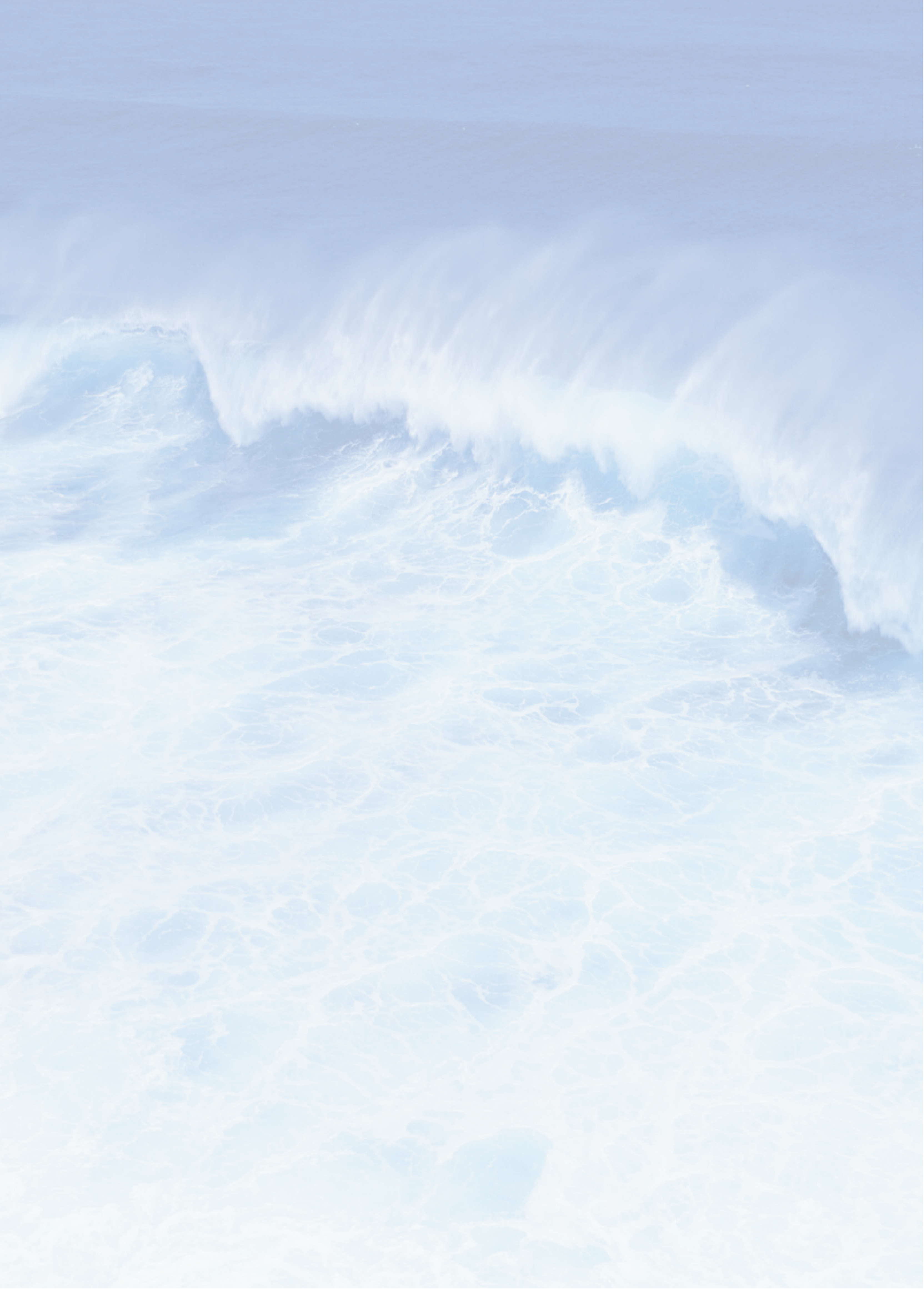

Περιγραφή μεθόδων υδρογραφίας-βαθυμετρίας και η συνεισφορά της στην κατασκευή λιμενικών έργων και διαχείριση της παράκτιας ζώνης

Α. Κ. Μαυραειδόπουλος*

Λιμενολόγος Πολιτικός Μηχ. ΕΜΠ-Υδρογράφος Μηχ. MSc
*Corresponding author: athanasios.mavraeidopoulos@yahoo.com

Περίληψη

Η Υδρογραφία είναι ο κλάδος των εφαρμοσμένων Γεωεπιστημών, που σκοπό έχει την περιγραφή του αναγλύφου του θαλασσίου πυθμένα και των αντικειμένων που βρίσκονται επί αυτού. Πρωταρχικός στόχος της Υδρογραφιας είναι η ασφάλεια της ναυσιπλοΐας και άλλων θαλάσσιων δραστηριοτήτων, όπως η υποστήριξη στην κατασκευή λιμενικών έργων, η θαλάσσια έρευνα, η έρευνα υδρογονανθράκων, δραστηριότητες που σχετίζονται με την προστασία του θαλάσσιου περιβάλλοντος και την διαχείριση της παράκτιας ζώνης. Η συνεισφορά της Υδρογραφίας-βαθυμετρίας στην κατασκευή των λιμενικών έργων θεωρείται κρίσιμος παράγοντας στην οικονομοτεχνική ολοκλήρωση μίας θαλάσσιας κατασκευής, στην ορθολογική διαχείρηση της παράκτιας ζώνης, στην αειφόρο διαχείρηση ενός παράκτιου οικοσυστήματος και γενικότερα στην οικονομική και κοινωνική ανάπτυξη μίας παράκτιας περιοχής.

Λέξεις κλειδιά Υδρογραφία, Έρευνα θαλασσίου πυθμένα, Ασφάλεια ναυσιπλοΐας, Τεχνικές προδιαγραφές ΙΗΟ, παράκτια και υπεράκτια θαλάσσια έργα.

1 ΕΙΣΑΓΩΓΗ

Η ολιστική παρακολούθηση και αντιμετώπιση των ζητημάτων που σχετίζονται με την προστασία και διατήρηση των παράκτιων συστημάτων, εκτιμάται ως πολύ σημαντική για τις χώρες που βρέχονται από θάλασσα, όπως είναι η χώρα μας, η οποία έχει ένα τεράστιο ανάπτυγμα ακτογραμμής μήκους 16.300 χλμ (USA/CIA, 2005), που κατατάσσει την Ελλάδα στην 9η κατά σειρά χώρα με την μεγαλύτερη ακτογραμμή παγκοσμίως. Ένα πολύ σημαντικό εργαλείο για την συστηματική παρακολούθηση και διαχείριση των παραπάνω παράκτιων οικοσυστημάτων αποτελεί η απόδοση της βαθυμετρίας ή της Υδρογραφίας της υπόψη περιοχής. Βασικός σκοπός της επιστήμης της Υδρογραφίας είναι η «Ασφάλεια της Ναυσιπλοΐας». Ωστόσο, οι μέθοδοι υδρογράφησης υποστηρίζουν ένα ευρύτερο φάσμα τεχνκών δραστηριοτήτων μεταξύ των οποίων και η μελέτη και κατασκευή λιμενικών έργων παράκτιων ή υπεράκτιων (I.H.O, 2005).

2 ΕΜΠΛΕΚΟΜΕΝΟΙ ΔΙΕΘΝΕΙΣ ΟΡΓΑΝΙΣΜΟΙ

Ο Διεθνής Ναυτιλιακός Οργανισμός (ΙΜΟ) είναι ο εξειδικευμένος οργανισμός των Ηνωμένων Εθνών, του οποίου κύριο καθήκον είναι η βελτίωση της ασφάλειας και προστασίας της διεθνούς ναυτιλίας και η πρόληψη της προερχόμενης από τα πλοία ρύπανσης. Το σύνθημα του ΙΜΟ συνοψίζει τους στόχους του: «*Σώα, ασφαλής και αποτελεσματική ναυτιλία σε καθαρούς ωκεανούς*».

Το τεχνικό όργανο του Διεθνούς Ναυτιλιακού Οργανισμού, το οποίο ασχολείται με τις προδιαγραφές κατασκευής και διαχείρισης των ναυτικών χαρτών που αποτελούν βασικά προϊόντα που σχετίζονται με τα θέματα της ασφάλειας της ναυσιπλοΐας είναι ο Διεθνής Υδρογραφικός Οργανισμός (International Hydrographic Organization-IHO). Οι βασικοί στόχοι του ΙΗΟ είναι ο συντονισμός των δραστηριοτήτων των ΥΥ των Κρατών-Μελών (Κ-Μ) του, η επίτευξη της μεγαλύτερης δυνατής ομοιογένειας στους εκδιδόμενους ναυτικούς χάρτες και στις λοιπές ναυτιλιακές εκδόσεις, η υιοθέτηση αξιόπιστων και αποτελεσματικών μεθόδων υδρογράφησης για την ορθή εκτέλεση και βέλτιστη αξιοποίηση των υδρογραφικών εργασιών πεδίου, η ανάπτυξη των επιστημών στο πεδίο της υδρογραφίας και των τεχνικών που εφαρμόζονται στην ωκεανογραφία πεδίου.

Ο αντίστοιχος Ευρωπαϊκός τεχνικός οργανισμός που ασχολείται με τα θέματα της ασφάλειας της είναι η Ευρωπαϊκή Υπηρεσία Ασφάλειας της Ναυσιπλοΐας (European Maritime Safety Agency-EMSA). Σκοπός της EMSA είναι η διασφάλιση υψηλού, ομοιόμορφου και αποτελεσματικού επιπέδου ναυτιλιακής ασφάλειας στη θάλασσα, ασφάλειας προσωπικού στη θάλασσα, πρόληψης και άμεσης αντίδρασης στη περίπτωση ρύπανσης, η οποία προκαλείται από τα πλοία, καθώς και η άμεση αντίδραση στη θαλάσσια ρύπανση που προκαλείται από τα πλοία μεταφοράς καυσίμων και από τις εγκαταστάσεις πετρελαίου και φυσικού αερίου.

3 ΣΥΝΕΙΣΦΟΡΑ ΤΗΣ ΥΔΡΟΓΡΑΦΙΑΣ ΣΤΗΝ ΑΣΦΑΛΕΙΑ ΤΗΣ ΝΑΥΣΙΠΛΟΪΑΣ, ΤΗΝ ΚΑΤΑΣΚΕΥΗ ΛΙΜΕΝΙΚΩΝ ΕΡΓΩΝ ΚΑΙ ΣΤΗΝ ΔΙΑΧΕΙΡΙΣΗ ΤΗΣ ΠΑΡΑΚΤΙΑΣ ΖΩΝΗΣ.

1.5 *3.1* *Υδρογραφία και Ασφάλεια της Ναυσιπλοΐας*

Οι θαλάσσιες περιοχές της Ελλάδας αποτελούν θαλάσσιους διαδρόμους επικοινωνίας και μεταφοράς αγαθών μεταξύ Ασίας (μέσω της διώρυγας του Σουέζ), Ευρώπης και Αμερικής (μέσω του Στενού του Γιβραλτάρ) και παρευξείνιων χωρών (μέσω των στενών των Δαρδανελίων). Σύμφωνα με την Ευρωπαϊκή Υπηρεσία Ασφάλειας της Ναυσιπλοΐας (EMSA), οι παράκτιες περιοχές ελληνικού ενδιαφέροντος παρουσιάζουν την μεγαλύτερη συχνότητα ναυτικών ατυχημάτων σε ολόκληρη την Ευρώπη. Επιπρόσθετα, ο μεγαλύτερος αριθμός των ναυτικών ατυχημάτων στις ευρωπαϊκές περιοχές και στην Ελλάδα συμβαίνουν στις παράκτιες περιοχές (28.6%) ή στα εσωτερικά ύδατα και τους λιμένες (42%) των κρατών (European Maritime Safety Agency, 2018).

Το γεγονός αυτό καθιστά τη σημασία της επιστήμης της Υδρογραφίας ως σημαντική για τα ζητήματα της ασφάλειας της ανθρώπινης ζωής στην θάλασσα λαμβανομένου υπόψη, ότι σύμφωνα με την Σύμβαση SOLAS/I.M.O, οι κυβερνήσεις πλέον υποχρεώνονται στην συνεχή παροχή Υδρογραφικών Υπηρεσιών και προϊόντων. Οι σημαντικότεροι παράγοντες που επέβαλαν την ανάγκη για επαρκή υδρογραφική κάλυψη και την τυποποίηση στην παραγωγή ναυτικών χαρτών και εκδόσεων όπως προβλέπει το άρθρο V της SOLAS είναι η κατασκευή σκαφών εξαιρετικά μεγάλου βυθίσματος, όπως είναι για παράδειγμα τα supertankers τ. Ultra Large Crude Carrier-ULCC (Mavraeidopoulos A., *et al.,* 2017). Άλλοι σημαντικοί παράγοντες που επιβάλλουν την συνεχή υδρογραφική και βαθυμετρική κάλυψη και παραγωγή αντίστοιχων χαρτογραφικών προϊόντων είναι η συνεχώς αυξανόμενη ανάγκη για προστασία του θαλάσσιου και παράκτιου περιβάλλοντος, η αλλαγή των συνήθων θαλάσσιων εμπορικών οδών, η αυξανόμενη σπουδαιότητα των υποθαλάσσιων πηγών ενέργειας, η Σύμβαση των ΗΕ για το Δίκαιο της Θάλασσας που επηρεάζει περιοχές εθνικής δικαιοδοσίας.

1.6 *3.2* *Υδρογραφία και Θαλάσσια (Παράκτια & Υπεράκτια) Έργα*

Οι μέθοδοι υδρογράφησης θαλασσίων περιοχών δύνανται να χρησιμοποιηθούν όχι μόνο για την παραγωγή των ναυτικών χαρτών (έντυπων ή ηλεκτρονικών) αλλά και για άλλες δραστηριότητες όπως είναι η κατασκευή λιμενικών έργων ή τεχνικών έργων διαχείρισης της παράκτιας ζώνης μίας περιοχής. Οι επιπτώσεις της υδρογραφίας-βαθυμετρίας στην μελέτη και κατασκευή των τεχνικών έργων λιμένων εκτιμώνται επίσης ως πολύ σημαντικές. Τόσο κατά την φάση του σχεδιασμού ενός λιμενικού έργου όσο και κατά τα διάφορα στάδια κατασκευής και φυσικά και κατά την φάση της παραλαβής του απαιτείται η διενέργεια βαθυμετρικής αποτύπωσης, προκειμένου διαπιστωθούν οι στάθμες θεμελίωσης, υπολογιστεί ο όγκος των ποσοτήτων των εκσκαφών, γίνει προσδιορισμός του τελικού βάθους στις θέσεις πρόσδεσης των σκαφών, καθώς και να ελεχθεί το βάθος της ευρύτερης περιοχής προσέγγισης στο εκάστοτε λιμενικό έργο, προκειμένου εξασφαλιστεί η ασφαλής προσέγγιση σε αυτό.

Επίσης, κατά την διάρκεια λειτουργίας ενός λιμενικού έργου η πληροφορία της βαθυμετρίας είναι πολύ κρίσιμη για την διατήρηση της προσβασιμότητας και διατήρησης χρήσης των λιμένων και των λοιπών θαλασσίων εγκαταστάσεων. Η συνεχής βαθυμετρική παρακολούθηση και η ενδεχόμενη μεταβολή των βαθών αποτελεί έγκαιρη ειδοποίηση για την αναγκαιότητα συντήρησης των λιμενικών εγκαταστάσεων. Η βαθυμετρία αποτελεί επίσης πολύ σημαντική πληροφορία για μία ακτομηχανική μελέτη που αφορά στον υπολογισμό του χρόνου που επίκειται να προσαμμωθεί μία παράκτια περιοχή ενδιαφέροντος και ποια θα είναι η ποσότητα εκσκαφής/εξυγίανσης (sediment budget) της.

Αναφορικά με την περιβαλλοντική διαχείριση μίας παράκτιας ζώνης, επίσης είναι πολλά τα οφέλη από την εκτέλεση λεπτομερών υδρογραφικών-βαθυμετρικών αποτυπώσεων. Η ορθολογική χωροθέτηση έργων στην παράκτια ζώνη επηρεάζει ένα πολύ μεγάλο ποσοστό του πληθυσμού μίας χώρας και ταυτόχρονα την οικονομική της ανάπτυξη. Στις παράκτιες περιοχές ζει και δραστηριοποιείται το 70% περίπου του παγκόσμιου πληθυσμού, ενώ η εκτιμώμενη αξία των οικονομικών ιδιωτικών περιουσιακών στοιχείων στην Ευρώπη σε απόσταση 500 μέτρων από τη θάλασσα ανέρχεται σε 500 έως 1000 δισεκατομμύρια ευρώ (European Environment Agency, 2018).

4 ΠΕΡΙΓΡΑΦΗ ΜΕΘΟΔΩΝ ΥΔΡΟΓΡΑΦΙΑΣ-ΒΑΘΥΜΕΤΡΙΑΣ

Ο συνήθης εξοπλισμός μέτρησης-έρευνας που χρησιμοποιείται στο πλαίσιο των υδρογραφικών μεθόδων αποτελείται από ακουστικά συστήματα. Τα κυριότερα υδρογραφικά συστήματα είναι οι υδρογραφικές βολίδες, τα ηχοβολιστικά (Η/Β) μονής δέσμης (Singlebeam Echosounders), τα Η/Β πολλαπλής δέσμης (Multibeam Echosounders), ενώ σταδιακά έδαφος κερδίζουν, οι οπτικές μέθοδοι βαθυμετρίας με χρήση LIDARs ή η εξαγωγή βαθυμετρίας από πολυφασματικές ή SAR δορυφορικές εικόνες (Εικ. 1). Ωστόσο, για την επίτευξη της επιθυμητής ακρίβειας των μετρήσεων απαιτείται συνήθως και συμπληρωματικός εξοπλισμός που συνίσταται συνήθως από κατάλληλο Υδρογραφικό λογισμικό, συστήματα που διορθώνουν την απόκλιση του Υ/Γ σκάφους από το οριζόντιο επίπεδο, ψηφιακές γυροπυξίδες, δορυφορικά ή ακουστικά συστήματα προσδιορισμού θέσης, συστήματα που μετρούν την μεταβολή της ταχύτητας του ήχου συναρτήσει του βάθους, παλιρροιογράφοι, κοκ. Σε ειδικές περιπτώσεις ερευνών, εκτός από τα προαναφερθέντα συστήματα βαθυμετρίας χρησιμοποιούνται και επιπλέον συστήματα έρευνας του ανάγλυφου του θαλάσσιου πυθμένα. Τα σημαντικότερα συστήματα έρευνας θαλασσίου πυθμένα είναι το πλευρικό ηχοβολιστικό (Side Scan Sonar), τα ηχοβολιστικά πολλαπλής δέσμης, μαγνητόμετρα, σεισμικά συστήματα, γρίποι κοκ. Οι τάσεις που επικρατούν στις σύγχρονες υδρογραφήσεις είναι η απόκτηση περισσοτέρων δεδομένων υψηλότερης ακρίβειας και συλλογή περισσότερων δεδομένων με μεγαλύτερες ταχύτητες. Ωστόσο, υφίστανται διάφοροι παράγοντες που περιορίζουν την επίτευξη της μέγιστης δυνατής ακρίβειας και ταχύτητας συλλογής των δεδομένων, όπως για παράδειγμα το μέγεθος του ακουστικού αποτυπώματος του χρησιμοποιούμενου συστήματος στον πυθμένα, η μη χρήση του καταλληλότερου εξοπλισμού μέσα στην θάλασσα.

5 ΤΕΧΝΙΚΕΣ ΠΡΟΔΙΑΓΡΑΦΕΣ ΙΗΟ

Ο ΙΗΟ για να αντιμετωπίσει τα ζητήματα της ασφάλειας της ναυσιπλοΐας αύξησε την τυποποίηση των ναυτικών χαρτών, οι οποίοι παράγονται από υδρογραφικά/βαθυμετρικά δεδομένα πεδίου. Παράλληλα, καθόρισε πρότυπα για την εκτέλεση των υδρογραφικών μεθόδων, τα οποία περιγράφονται στην ειδική έκδοση του Οργανισμού με τίτλο «IHO Standards for Hydrographic Surveys-Special Publication No. 44» (International Hydrographic Organization, 2008). Σύμφωνα με τις διεθνείς προδιαγραφές, οι υδρογραφικές εργασίες κατηγοριοποιούνται με βάση την σπουδαιότητα των περιοχών ερεύνης για την ασφάλεια της ναυσιπλοΐας. Οι εν λόγω προδιαγραφές αποτελούν τα «ελάχιστα πρότυπα» (minimum standards) για τη διεξαγωγή συμβατικών υδρογραφικών ερευνών και ταξινομούνται σε τέσσερις (4) κατηγορίες. Ειδικότερα, οι προτεινόμενες από τον ΙΗΟ κατηγορίες υδρογραφικών εργασιών είναι η «Special Order Surveys» (Ειδικής Κατηγορίας Υδρογραφικές Έρευνες), η «Order 1a» (Κατηγορία 1α), η «Order 1b» (Κατηγορία 1β) και η «Order 2» (Κατηγορία 2). Ερμηνεύοντας τις προδιαγραφές του Διεθνούς Υδρογραφικού Οργανισμού για την εκτέλεση βαθυμετρήσεων, προκύπτει ότι η κύρια προσπάθεια εστιάζεται στις παράκτιες περιοχές, δηλαδή σε περιοχές με ρηχά ή σχετικά ρηχά ύδατα, βάθους έως και 40 μέτρων. Στις εν λόγω παράκτιες περιοχές υπάρχει μεγάλη πιθανότητα να συμβεί κάποιο ναυτικό ατύχημα, το οποίο μπορεί να προκαλέσει καταστροφή του θαλάσσιου και παράκτιου περιβάλλοντος, με αρνητικό αντίκτυπο στην θαλάσσια οικονομία του παράκτιου κράτους.

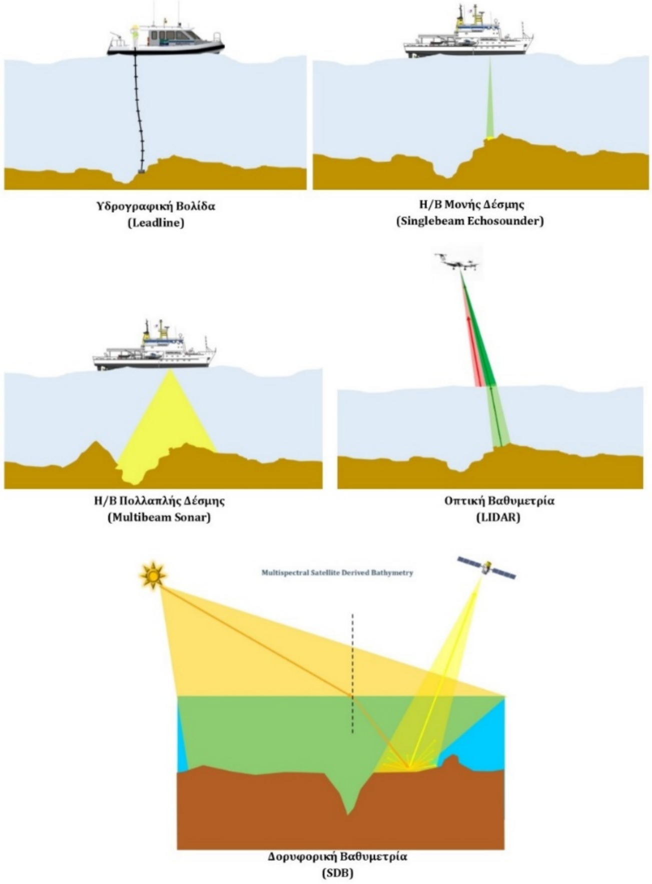

Εικόνα 1 Μέθοδοι Υδρογραφίας-Βαθυμετρίας

Για τους λόγους αυτούς, οι πιο απαιτητικές κατηγορίες από πλευράς κατακόρυφης και οριζοντιογραφικής ακρίβειας είναι η «Ειδική Κατηγορία» και η «Κατηγορία 1α» υδρογραφικών ερευνών. Για αυτό το λόγο και στις δύο περιπτώσεις («Ειδική Κατηγορία» και «Κατηγορία 1α), είναι απαραίτητη η πλήρης έρευνα (100%) του θαλάσσιου πυθμένα. Ωστόσο, και η περίπτωση εκτέλεσης βαθυμετρικών αποτυπώσεων για την κατασκευή ή εγκατάσταση υπεράκτιων έργων συχνά απαιτεί αυστηρότερες προδιαγραφές ακρίβειας ακόμα και σε μεγαλύτερα βάθη. Στην ουσία, σε αντίθεση με ότι προβλέπει ο IHO για την κατασκευή ναυτικών χαρτών, στις υπεράκτιες περιοχές, όταν πρόκειται να μελετηθούν ή κατασκευαστούν θαλάσσια έργα και εγκαταστάσεις απαιτείται να εφαρμόζονται τα πρότυπα της Ειδικής ή της 1α Κατηγορίας.
Οι υπόψη προδιαγραφές του IHO δεν είναι υποχρεωτικές για τους μη κρατικούς φορείς, όπως για παράδειγμα τεχνικές εταιρείες, επιστημονικούς φορείς ή άλλους μη κυβερνητικούς οργανισμούς, ωστόσο κάνοντας χρήση αυτών εξασφαλίζεται η προτυποποίηση της εκτέλεσης των βαθυμετρικών αποτυπώσεων σύμφωνα με τα εν ισχύ διεθνή πρότυπα του IHO.

6 ΣΥΖΗΤΗΣΗ

Το εμπόριο με πλοία εξακολουθεί να είναι ο κύριος τρόπος μεταφοράς αγαθών για το Διεθνές εμπόριο, αφού πάνω από το 80% του Παγκόσμιου εμπορίου πραγματοποιείται διά θαλάσσης. Ταυτόχρονα διαπιστώνεται μία συνεχής αύξηση του διεθνούς εμπορίου τα τελευταία δέκα (10) έτη (2008-2018), γεγονός που υποδηλώνει την σημαντικότητα ύπαρξης κατάλληλων λιμενικών υποδομών στις χώρες αυτές. Παράλληλα, η αυξανόμενη τάση εξόρυξης και επεξεργασίας πετρελαιοειδών και φυσικού αερίου από θαλάσσιες περιοχές, απαιτεί σύγχρονες και επαρκείς λιμενικές εγκαταστάσεις, μέσω των οποίων θα αποθηκεύονται και εν συνεχεία θα μεταφέρονται τα προϊόντα αυτά προς τις χώρες καταναλωτές (U.N. Trade & Development Report, 2018). Όσο διενεργείται εντοπισμός νέων κοιτασμάτων, τόσο θα αυξάνεται και το ενδιαφέρον των μεγάλων χωρών για επενδύσεις σε υποδομές που αφορούν στην ασφαλή και ταχεία μεταφορά των εν λόγω φυσικών πόρων. Κατάλληλες λιμενικές υποδομές απαιτούν τακτή παρακολούθηση και έγκαιρη συντήρηση των θαλασσίων διαύλων προσέγγισης λιμενικών εγκαταστάσεων ή των υφιστάμενων λιμένων, κατασκευή μεγαλύτερων προβλητών ή/και κρηπιδωμάτων, σύγχρονες διαδικασίες διαχείρισης τερματικών σταθμών αγαθών - επιβατών, επικαιροποιημένους ναυτικούς χάρτες με νέα υδρογραφικά/βαθυμετρικά δεδομένα.

7 ΕΠΙΛΟΓΟΣ

Συμπερασματικά, η συνεισφορά των μεθόδων της Υδρογραφίας-βαθυμετρίας στην κατασκευή τεχνικών έργων λιμένων τόσο των παράκτιων όσο και των υπεράκτιων είναι υψηλή. Η κατασκευή κατάλληλων λιμενικών υποδομών συνδέεται άμεσα με την οικονομική και κοινωνική ανάπτυξη ενός παράκτιου κράτους. Οι επενδύσεις σε λιμενικά έργα και υδρογραφικές έρευνες αφορούν στο σύνολο του κοινωνικού συνόλου και όχι σε μία συγκεκριμένη ομάδα πολιτών ή μία επαγγελματική συντεχνία. Ειδικότερα, οι επενδύσεις στην υδρογραφία σώζουν ανθρώπινες ζωές, υποστηρίζουν την εθνική οικονομία αφού επιτρέπουν την διαχείριση της παράκτιας ζώνης με ορθολογικό τρόπο, προσδίδοντας στο παράκτιο και υπεράκτιο περιβάλλον αειφόρο συμπεριφορά.

References

Commission U (2018) Generalized System of Preferences: Possible Modifications, 2017 Review. Ανάκτηση από USITC: https://www.usitc.gov/publications/332/pub4827_0.pdf (last acessed September 2018).

Development U N (2018) Trade and development reportR 2018. New York and Geneva: UNCTAD.

European Environment Agency (2018) Ανάκτηση από Ευρωπαϊκό Οργανισμός Περιβάλλοντος: https://www.eea.europa.eu (last acessed December 13 2018).

European Maritime Safety Agency (2018) Annual Overview of Marine Casualties and Incidents 2018. EMSA.

IMO (2018) Basic Documents (Vol. I). London.

International Hydrographic Bureau (2005) Manual on Hydrography. Monaco: IHO.

International Hydrographic Organization (2008) IHO Standards for Hydrographic Surveys - S 44 (5th edition.). Monaco: International Hydrographic Bureau.

International Hydrographic Organization (2018). IHO Publications. Ανάκτηση από International Hydrographic Organization: https://www.iho.int/iho_pubs/misc/M-2_3.0.7_E_06142018.pdf (last acessed 2018 June).

International Maritime Organisation (2010) I.M.O. Basic Documents (Vol. I). London: I.M.O.

Mavraeidopoulos AK, Pallikaris A, Oikonomou E (2017) Satellite Derived Bathymetry (SDB) and Safety of Navigation. (I. H. Bureau,) The International Hydrographic Review, 17, 7-19.

USA/CIA (2017), Ανάκτηση από Central Intelligence Agency: https://www.cia.gov/library/-publications/the-world-factbook/

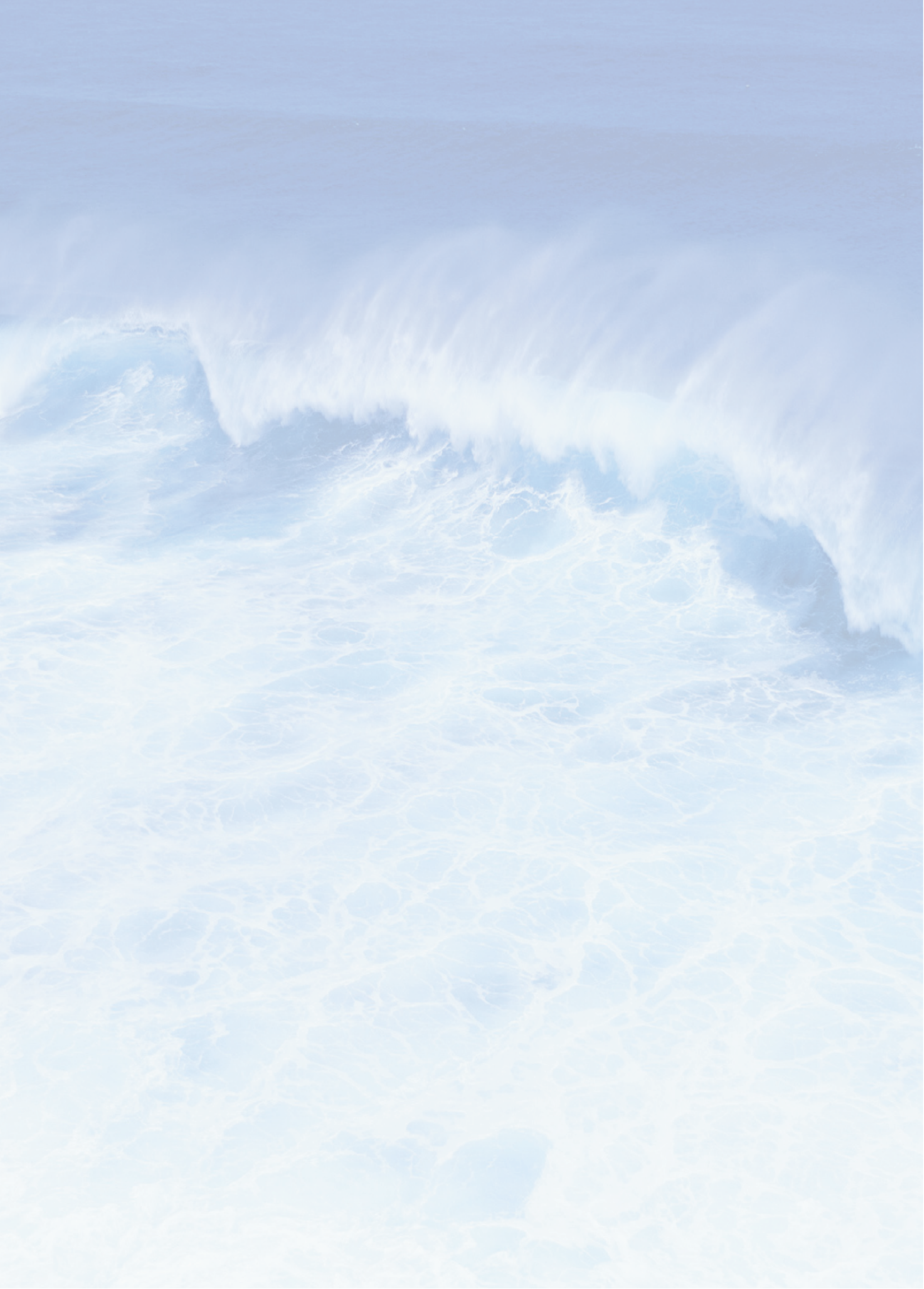

Διερεύνηση της επίδρασης της κλιματικής αλλαγής στις κυματικές συνθήκες και την υδροδυναμική κυκλοφορία του Κορινθιακού κόλπου

Ε.Ν. Κυπραίου*, Α.Α. Δήμας

Τμήμα Πολιτικών Μηχανικών, Πανεπιστήμιο Πατρών, Πάτρα, 26500., Ελλάδα
*Υπεύθυνος επικοινωνίας: evakypraiou@hotmail.com

Περίληψη

Αντικείμενο της παρούσας εργασίας είναι η διερεύνηση της επίδρασης της κλιματικής αλλαγής στις κυματικές συνθήκες και την υδροδυναμική κυκλοφορία του Κορινθιακού Κόλπου. Στόχος είναι να αποτιμηθεί η μελλοντική ισορροπία των παράκτιων περιοχών του Κορινθιακού Κόλπου, οι οποίες ήδη παρουσιάζουν προβλήματα διάβρωσης υπό το συνδυασμό περιβαλλοντικών φορτίσεων (κύματα, ρεύματα, στερεομεταφορά), παράκτιων έργων και λιμενικών υποδομώ. Για το σκοπό αυτό πραγματοποιήθηκε προσομοίωση των σημερινών και των μελλοντικών κλιματικών συνθηκών της ευρύτερης περιοχής του Κορινθιακού Κόλπου, με το περιοχικό κλιματικό μοντέλο RegCM, σύμφωνα με τα σενάρια εκπομπών αερίων του θερμοκηπίου RCPs (RCP2.6, RCP4.5 και RCP8.5). Η γένεση και η ανάπτυξη των κυματισμών καθώς και μεταβολή της ελεύθερης επιφάνειας και η ροή των υδάτων λόγω της δράσης του ανέμου προσομοιώθηκαν με το αριθμητικό πρόγραμμα MIKE21.

Λέξεις κλειδιά Κλιματική Αλλαγή, Κορινθιακός Κόλπος, RegCM, MIKE21

1 ΕΙΣΑΓΩΓΗ

Ο όρος «Κλιματική Αλλαγή» (Κ.Α.) κατά τη Διακυβερνητική Επιτροπή για την Κλιματική Αλλαγή αναφέρεται σε κάθε αλλαγή του κλίματος με την πάροδο του χρόνου, είτε αυτή οφείλεται σε φυσική μεταβλητότητα, είτε είναι αποτέλεσμα της ανθρώπινης δραστηριότητας (IPCC, 2007). Οι επιπτώσεις της Κ.Α. αναμένεται να πλήξουν την ανοιχτή θάλασσα και την παράκτια ζώνη. Οι σημαντικότερες από αυτές είναι η άνοδος της στάθμης της θάλασσας, η αύξηση της συχνότητας των ακραίων καιρικών φαινομένων που οδηγούν στην εμφάνιση ισχυρών θυελλών στη λεκάνη της Μεσογείου, υψηλότερα κύματα και ισχυρότερα ρεύματα στην παράκτια ζώνη, μεγάλες διακυμάνσεις της στάθμης της θάλασσας (μετεωρολογική παλίρροια = storm surge), καθώς και αύξηση του ρυθμού διάβρωσης στις παραλίες με λεπτόκοκκη άμμο και οι ταχύτατες μορφολογικές αλλαγές τους (Ζαχαριάδου, 2013).

Η διάβρωση της παράκτιας ζώνης αποτελεί συχνό φαινόμενο στον Ελλαδικό χώρο με επιπτώσεις σε περιβαλλοντικό, κοινωνικό και οικονομικό επίπεδο. Χαρακτηριστικό παράδειγμα αποτελεί ο Κορινθιακός Κόλπος. Αντικείμενο της παρούσας εργασίας, είναι η προσομοίωση των ανεμολογικών χαρακτηριστικών στην περιοχή του Κορινθιακού Κόλπου λόγω του φαινομένου της Κ.Α., σύμφωνα με τα σενάρια εκπομπών αερίων του θερμοκηπίου, τα οποία καθορίστηκαν από την πέμπτη έκθεση της Διακυβερνητικής Επιτροπής για την Κλιματική Αλλαγή (IPCC, 2014), καθώς και η προσομοίωση της αντίστοιχης ανάπτυξης ανεμογενών κυμάτων. Ο τελικός στόχος είναι η εκτίμηση της μεταβολής των κυματικών συνθηκών και του μεγέθους της μετεωρολογικής παλίρροιας λόγω του φαινομένου της Κ.Α. στον Κορινθιακό Κόλπο.

2 Η ΠΕΡΙΟΧΗ ΜΕΛΕΤΗΣ

Ο Κορινθιακός αποτελεί μια κλειστή και πολύ βαθιά (μέγιστο βάθος ≈ 900 m) θαλάσσια λεκάνη μεταξύ Στερεάς Ελλάδας και Πελοποννήσου, η οποία οριοθετείται από τον ισθμό της Κορίνθου στα ανατολικά και από το στενό Ρίου – Αντιρρίου στα δυτικά. Το συνολικό μήκος της ακτογραμμής της περιοχής μελέτης είναι περίπου 200 Km. Στην περιοχή μελέτης απορρέουν μικρά κυρίως υδατορρεύματα χωρίς δυνατότητα αξιόλογης στερεομεταφοράς, αλλά και σημαντικότεροι ποταμοί και χείμαρροι.

Στις παράκτιες περιοχές του Κορινθιακού Κόλπου όπου αναπτύσσεται έντονη ανθρωπογενής δραστηριότητα τις τελευταίες δεκαετίες έχουν κατασκευασθεί σειρά έργων προστασίας των ακτών από διάβρωση αλλά και λιμενικές υποδομές (αλιευτικά καταφύγια, μαρίνες). Τα παράκτια έργα προστασίας περιλαμβάνουν κυρίως προβόλους κάθετους στην ακτή, η πλειονότητα των οποίων κατασκευάσθηκε άνευ μελετών, και έργα θωράκισης, η πλειονότητα των οποίων δεν αποτελεί συστηματική θωράκιση με ογκολίθους αλλά με ακανόνιστη λιθορριπή. Σε αρκετές περιπτώσεις προβόλων έχει γίνει και τεχνητή επίχωση στα φατνώματα μεταξύ των προβόλων. Τέλος, έχουν κατασκευασθεί δύο αποσπασμένοι κυματοθραύστες στο Βέλο και ένας στο Ξυλόκαστρο.

3 ΜΕΘΟΔΟΛΟΓΙΑ

3.1 Εφαρμογή Μοντέλου RegCM4.6

Το περιοχικό κλιματικό μοντέλο RegCM4.6 (Giorgi et al. 2016) αποτέλεσε εργαλείο για τον υπολογισμό της ταχύτητας και της διεύθυνσης του ανέμου σε ύψος 10m από την ΜΣΘ, για τα έτη 2017 και 2055. Ο λόγος που επιλέχθηκε να γίνει προσομοίωση και του σύγχρονου κλίματος (έτος 2017) είναι η σύγκριση των αποτελεσμάτων της προσομοίωσης με πραγματικά δεδομένα από μετρήσεις της ΕΜΥ και άρα η αξιολόγηση του μοντέλου.

Το πρώτο βήμα για την εκτέλεση μιας προσομοίωσης περιλαμβάνει τον ορισμό του διαστήματος του τομέα και του πλέγματος, καθώς και την παρεμβολή των δεδομένων χρήσης γης και ανύψωσης στο πλέγμα του μοντέλου. Η ανάλυση πλέγματος επιλέχθηκε να είναι 20 km ενώ η ευρύτερη περιοχή που προσομοιώθηκε καλύπτει τον ελληνικό χώρο από το νότιο άκρο της Πελοποννήσου μέχρι τη βόρειο άκρο της Θεσσαλίας.

Το δεύτερο βήμα περιλαμβάνει την δημιουργία των αρχείων που χρησιμοποιούνται ως αρχικές και οριακές συνθήκες κατά τη διάρκεια της προσομοίωσης. Τα παραπάνω σύνολα δεδομένων προκύπτουν από μοντέλα γενικής κυκλοφορίας (GSMs) τα οποία υποστηρίζει το περιφερειακό μοντέλο RegCM και αξιοποιούνται από αυτό μέσω της διαδικασίας της υποκλιμάκωσης της πληροφορίας (downscaling). Η παρούσα ερευνητική εργασία χρησιμοποίησε τα αποτελέσματα του μοντέλου γενικής κυκλοφορίας HadGEM (Hadley Centre Global Environment Model version 2).

Επίσης, επιλέχθηκε να πραγματοποιηθεί προσομοίωση του κλίματος για το έτος 2017 και για το έτος 2055 σύμφωνα με τα σενάρια εκπομπών αερίων του θερμοκηπίου RCP2.6, RCP4.5 και RCP8.5 (Representative Concentration Pathways – RCPs, IPCC, 2014). Με τον όρο σενάρια εκπομπών αερίων του θερμοκηπίου ορίζεται ο υπολογισμός των μελλοντικών κλιματικών αλλαγών με τη χρήση ενός κλιματικού μοντέλου, όπου δίνεται σε κάθε χρονικό βήμα η μελλοντική ανάπτυξη των εκπομπών αερίων του θερμοκηπίου. Σύμφωνα με το σενάριο RCP2.6, θεωρείται ότι θα παρουσιαστεί ύφεση των αερίων του θερμοκηπίου την δεκαετία 2010-2020, και στην συνέχεια θα υπάρξει σημαντική μείωση των συγκεκριμένων αερίων. Από την άλλη, η ύφεση για το RCP4.5 θεωρείται πως θα γίνει το 2040, για το RCP6 το 2060, ενώ στο RCP8.5 θεωρείται πως οι εκπομπές των αερίων του θερμοκηπίου θα συνεχίσουν να αυξάνονται καθ' όλη τη διάρκεια του 21ου αιώνα.

Τέλος, έγινε επεξεργασία των δεδομένων που προέκυψαν από το μοντέλο RegCM μέσω του λογισμικού CDO. Συγκεκριμένα, απομονώθηκαν τα σημεία του πλέγματος που βρίσκονται στην περιοχή ενδιαφέροντος και για αυτά υπολογίσθηκε το μέτρο της ταχύτητας και η διεύθυνση του ανέμου από τις δύο συνιστώσες της ταχύτητας. για τους τρεις χειμερινούς μήνες των ετών 2017 και 2055 (Ιανουάριο, Φεβρουάριο και Μάρτιο) και για τα τρία κλιματικά σενάρια.

3.2 Ανάλυση Μεροληψίας (Bias Correction)

Η διόρθωση του αποτελέσματος ενός μοντέλου με τέτοιο τρόπο ώστε τα αποτελέσματα του μοντέλου να είναι συναφή με τα πραγματικά δεδομένα ονομάζεται στατιστική διόρθωση σφάλματος πόλωσης ή διόρθωση σφάλματος μεροληψίας. Στην παρούσα εργασία ο συντελεστής διόρθωσης υπολογίζεται συγκρίνοντας τα δεδομένα προσομοίωσης για το έτος 2017 και για το τρίμηνο Ιανουαρίου-Φεβρουαρίου-Μαρτίου με τα πραγματικά ανεμολογικά δεδομένα που προέκυψαν από μετρήσεις του μετεωρολογικού σταθμού της ΕΜΥ στο Βέλο Κορινθίας για την περίοδο 1987-2001 και για το τρίμηνο Ιανουαρίου-Φεβρουαρίου-Μαρτίου σύμφωνα με την

$$Συντ.Διορ.Μερ. = \frac{x_{RMS_{OBS}}}{x_{RMS_{SIM}}} \tag{1}$$

όπου $x_{RMS_{OBS}}$ η μέση τετραγωνική ρίζα (RMS) των πραγματικών δεδομένων ταχύτητας ανέμου και $x_{RMS_{SIM}}$ η τιμή RMS των αποτελεσμάτων προσομοίωσης ταχύτητας ανέμου και

$$x_{RMS} = \sqrt{\frac{1}{n}\sum_{i=1}^{n} {x_i}^2} \qquad (2)$$

όπου x_i η τιμή του μέτρου της ταχύτητας ανέμου ανά χρονικό βήμα (3h).

Στην Εικόνα 1 παρουσιάζονται οι συναρτήσεις πυκνότητας πιθανότητας (PDF) του μέτρου της ταχύτητας του ανέμου πριν και μετά την εφαρμογή των συντελεστών διόρθωσης για τα πραγματικά δεδομένα της ΕΜΥ (Σταθμός Βέλου Κορινθίας), και για τα τρία σενάρια κλιματικής αλλαγής για το έτος 2017. Αφού υπολογιστεί ο συντελεστής διόρθωσης, χρησιμοποιείται για να γίνει η διόρθωση και για τις τιμές προσομοίωσης για το έτος 2055. Στη συνέχεια η κατανομή Weibull προσαρμόσθηκε στα διορθωμένα δεδομένα του έτους 2055, για τον υπολογισμό της ταχύτητας ανέμου με περίοδο επαναφοράς, Τ=50 έτη.

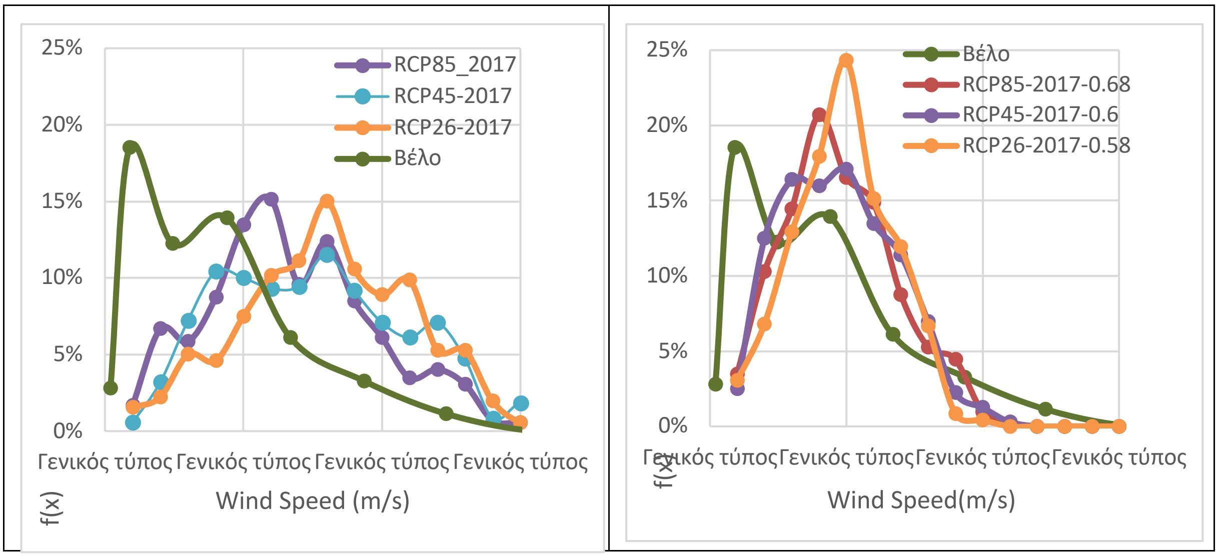

Εικόνα 1: a) PDF του μέτρου της ταχύτητας του ανέμου πριν την εφαρμογή των συντελεστών διόρθωσης b) PDF του μέτρου της ταχύτητας του ανέμου μετά την εφαρμογή των συντελεστών διόρθωσης.

3.3 Προσομοίωση Κυμάτων και Ρευμάτων στον Κορινθιακό Κόλπο

Με βάση τόσο ετήσια αλλά και ακραία γεγονότα, έγινε εισαγωγή των ανεμολογικών δεδομένων (ένταση και διεύθυνση) στο μοντέλο MIKE21 SW FM (DHI 2017), το οποίο είναι κατάλληλο για την προσομοίωση της γένεσης και του μετασχηματισμού κυμάτων, και στη συνέχεια στο μοντέλο MIKE21 Flow Model FM (DHI 2017), για την προσομοίωση της κίνησης των ρευμάτων στον Κορινθιακό και την ανύψωση της ελεύθερης επιφάνειας. Τα δεδομένα εισόδου ταχύτητας ανέμου βασίσθηκαν στις χρονοσειρές που προέκυψαν από το περιοχικό μοντέλο RegCM, στις οποίες πραγματοποιήθηκε κατάλληλη επεξεργασία όπως περιγράφηκε στην προηγούμενη παράγραφο.

Η θαλάσσια περιοχή που προσομοιώθηκε οριοθετείται στα δυτικά από το στενό Ρίου-Αντιρρίου, και στα ανατολικά από τον Ισθμό της Κορίνθου. Το υπολογιστικό πλέγμα αποτελείται από 336650 τριγωνικά στοιχεία (unstructured mesh), εμβαδού 450 - 11250 m^2. Τα κελιά μικρού εμβαδού κατανέμονται κοντά στην ακτογραμμή και σταδιακά το μέγεθος των κελιών μεγαλώνει προς τη μέγιστη τιμή του εμβαδού στα μεγάλα βάθη. Τα βυθομετρικά δεδομένα προήλθαν από βάση δεδομένων του προγράμματος MIKE C-MAP.

4 ΑΠΟΤΕΛΕΣΜΑΤΑ

4.1 Αποτελέσματα Προσομοίωσης Πεδίου Ανέμων

Σύμφωνα με τα δεδομένα της ΕΜΥ από το σταθμό του Βέλου Κορινθίας οι επικρατέστερες διευθύνσεις ανέμου είναι η Ανατολική και η Βορειοανατολική. Ανάλογα συμπεράσματα προκύπτουν και από τις προσομοιώσεις. Με βάση τις παραπάνω παρατηρήσεις, οι διευθύνσεις των ανέμων οι οποίες δόθηκαν στη συνέχεια ως δεδομένα εισόδου στο κυματικό και στο υδροδυναμικό μοντέλο είναι η Ανατολική και η Βορειοανατολική. Στον Πίνακα 1 έχουν καταγραφεί οι μέγιστες ταχύτητες αυτών των διευθύνσεων οι οποίες εμφανίζονται με συχνότητα μεγαλύτερη από 1% στην περίοδο του τριμήνου Ιανουάριος-Φεβρουάριος-Μάρτιος. Οι μεγαλύτερες ετήσιες ταχύτητες προκύπτουν σε όλα τα σενάρια για τον ανατολικό άνεμο, ενώ οι μέγιστες ταχύτητες εντοπίζονται για το σενάριο RCP8.5 και για το έτος 2055. Αντίθετα, με τις ετήσιες ταχύτητες, όπως φαίνεται στον Πίνακα 2 οι ακραίες τιμές ταχυτήτων είναι μέγιστες για τον ανατολικό άνεμο στο σενάριο RCP8.5 και για τον βορειοανατολικό άνεμο στο RCP4.5.

Πίνακας 1 Ταχύτητες οι οποίες εμφανίζονται με συχνότητα μεγαλύτερη από 1% σύμφωνα με τα τρία κλιματικά σενάρια για τα έτη προσομοίωσης 2017 και 2055.

Σενάρια	Έτος	2017		2055	
	Διεύθυνση Ανέμου	Α	ΒΑ	Α	ΒΑ
RCP2.6	Ταχύτητα (m/s)	7-8	6-7	8-9	5-6
	Συχνότητα Εμφάνισης (%)	5.9	1.9	1.1	2.1
RCP4.5	Ταχύτητα (m/s)	8-9	7-8	8-9	6-7
	Συχνότητα Εμφάνισης (%)	1.4	2.4	2.4	2.2
RCP8.5	Ταχύτητα (m/s)	8-9	6-7	9-10	9-10
	Συχνότητα Εμφάνισης (%)	2.6	1.4	1.1	4.7

Πίνακας 2 Τιμές του μέτρου της ταχύτητας ανέμου για περίοδο επαναφοράς T=50 έτη ανάλογα με τη διεύθυνση του ανέμου και για τα τρία κλιματικά σενάρια.

Σενάρια	Διεύθυνση Ανέμου	
	Α	ΒΑ
RCP2.6	15.34	16.50
RCP4.5	15.71	21.01
RCP8.5	18.03	18.95

4.2 Αποτελέσματα Προσομοίωσης Κυματικού Κλίματος

Σύμφωνα με τα αποτελέσματα του σεναρίου RCP8.5, η μέγιστη ετήσια ταχύτητα των ανέμων το έτος 2055 μπορεί να αυξηθεί έως και 50% σε σχέση με τα σημερινά δεδομένα συνεπώς η προσομοίωση του μελλοντικού κυματικού κλίματος έγινε με βάση το σενάριο αυτό. Οι παράκτιες περιοχές του Δήμου Αιγιαλείας είναι αυτές που πλήττονται κατά κύριο λόγο από τους έντονους κυματισμούς λόγω Ανατολικού ανέμου. Αντίθετα, οι κυματισμοί λόγω Βορειοανατολικού ανέμου πλήττουν όλες τις παράκτιες περιοχές της Πελοποννήσου από το Δήμο Αιγιαλείας και προς τα ανατολικά. Το ύψος κύματος στις συνθήκες του ετήσιου κυματικού κλίματος δεν ξεπερνάει τα 1.4 m για τον Ανατολικό άνεμο και τα 0.85 m για τον Βορειοανατολικό άνεμο. Τα παραπάνω, ακόμα και στις περιοχές που εμφανίζεται η εντονότερη κυματική δράση, φανερώνουν μια περιοχή που υπό φυσιολογικές κυματικές συνθήκες δεν κινδυνεύει από έντονες μορφολογικές αλλαγές (διάβρωση/ πρόσχωση).

Στην περίπτωση των ακραίων ανεμολογικών συνθηκών το μέγιστο ύψος κύματος υπερβαίνει τα 3.25 m λόγω πνοής Ανατολικού ανέμου και τα 3 m λόγω πνοής Βορειοανατολικού ανέμου. Κοντά στις ακτές το ύψος κύματος μειώνεται αρκετά και προσεγγίζει το 1 m και για τις δύο περιπτώσεις. Συνεπώς, όσον αναφορά την μελέτη των ακραίων γεγονότων παρατηρείται μια σημαντική αύξηση του ύψους κύματος σε σχέση με τα ετήσια γεγονότα. Οπότε η εμφάνιση ακραίων ανεμολογικών γεγονότων προκαλεί έντονους κυματισμούς καταιγίδας και κατ' επέκταση είναι πιθανό να μεταβάλει της συνθήκες ισορροπίας που έχουν διαμορφωθεί στην ακτή.

4.3 Αποτελέσματα Προσομοίωσης Υδροδυναμικού Πεδίου

Για την προσομοίωση της υδροδυναμικής κυκλοφορίας στον Κορινθιακό Κόλπο χρησιμοποιήθηκαν τα δεδομένα του σεναρίου RCP8.5, καθώς οι κλιματικές συνθήκες που διαμορφώνονται προκαλούν τις εντονότερες ανεμολογικά φαινόμενα σε σχέση με την παρούσα κατάσταση. Η ανεμογενής κυκλοφορία στον Κορινθιακό Κόλπο, όπως προκύπτει από τις προσομοιώσεις, έχει στοιχεία που παρατηρούνται στις λίμνες με έντονα παράκτια ρεύματα που ακολουθούν τη διεύθυνση του ανέμου. Η μέγιστη ταχύτητα παράκτιου ρεύματος για τα ετήσιες συνθήκες ανέμου προσεγγίζει τα 0.40 m/s για άνεμο Ανατολικής διεύθυνσης και τα 0.30 m/s για άνεμο Βορειοανατολικής διεύθυνσης. Η δράση του ανέμου δημιούργει επίσης κλίση της ελεύθερης επιφάνειας (wind setup) κατά τη διεύθυνσή του. Υπό τη δράση Ανατολικού ανέμου έντασης 11 m/s παρατηρείται αύξηση της μέσης στάθμης θάλασσας της τάξης των 0.015 m, ενώ υπό τη δράση Βορειοανατολικού ανέμου έντασης 10 m/s παρατηρείται αύξηση της μέσης στάθμης θάλασσας της τάξης των 0.003 m. Οι τιμές αυτές είναι πολύ μικρές ώστε να προκαλέσουν πλημμύρες και καταστροφές στις παράκτιες περιοχές.

Αντίστοιχα, για τα ακραία ανεμολογικά γεγονότα η μέγιστη ταχύτητα παράκτιου ρεύματος προσεγγίζει τα 0.50 m/s για άνεμο Ανατολικής διεύθυνσης και τα 0.40 m/s για άνεμο Βορειοανατολικής διεύθυνσης. Η μέση στάθμη θάλασσας αυξάνεται από τα ανατολικά προς τα δυτικά με μέγιστη διαφορά στάθμης 0.040m τόσο υπό τη δράση Ανατολικού ανέμου έντασης 11 m/s όσο και υπό τη δράση Βορειοανατολικού ανέμου έντασης 10 m/s.

5 ΣΥΜΠΕΡΑΣΜΑΤΑ

Καταλήγοντας, παρατηρείται ότι η ύφεση των αερίων του θερμοκηπίου την δεκαετία 2010-2020 με σημαντική μείωσή τους στη συνέχεια (σενάριο RCP2.6) μειώνει μελλοντικά την ταχύτητα του ανέμου και άρα την επίδραση των θαλάσσιων κυμάτων και ρευμάτων στην ακτή. Η ύφεση των αερίων του θερμοκηπίου το 2040 (σενάριο RCP4.5) δεν θα προλάβει να επιδράσει με κάποιο τρόπο στις ανεμολογικές συνθήκες του έτους 2055, οπότε το κυματικό κλίμα και η υδροδυναμική κατάσταση του Κορινθιακού δεν αναμένεται να μεταβληθούν σε σχέση με τις σημερινές συνθήκες. Από την άλλη, στην περίπτωση που οι εκπομπές των αερίων του θερμοκηπίου θα συνεχίσουν να αυξάνουν καθ' όλη τη διάρκεια του 21ου αιώνα (σενάριο RCP8.5), η ταχύτητα των ανέμων στον Κορινθιακό Κόλπο θα αυξηθεί σημαντικά.

Τέλος, προτείνεται η περεταίρω διερεύνηση της επίδρασης της κλιματικής αλλαγής στις ανεμολογικές και κυματικές συνθήκες του Κορινθιακού Κόλπου με αξιοποίηση δεδομένων από διαφορετικά μοντέλων γενικής κυκλοφορίας (GCM) και αξιολόγηση της συμπεριφοράς τους, χρήση της μεθόδου quantile mapping ως μέθοδο ανάλυσης μεροληψίας (bias correction) για την διόρθωση των σφαλμάτων που προκύπτουν από το περιοχικό κλιματικό μοντέλο, εκτίμηση κυματικού κλίματος υπό τον συνδυασμό δράσης διαφόρων διευθύνσεων ανέμου ανάλογα με τη συχνότητα εμφάνισής τους ανά έτος και σύγκριση χωρικής κατανομής ύψους κύματος του 2055 με μεταγενέστερες περιόδους.

Βιβλιογραφικές Αναφορές

DHI (2017) MIKE21 Spectral Wave Module Scientific Documentation, Denmark: MIKE by DHI.

DHI (2017) MIKE 21 & MIKE 3 FLOW MODEL FM Hydrodynamic and Transport Module Scientific Documentation, Denmark: MIKE by DHI.

Giorgi F Solmon F Giuliani G (2016) Regional Climate Model RegCM User's Guide Version 4.6, Trieste, Italy

IPCC (2007) Climate Change 2007: Synthesis Report. Contribution of Working Groups I, II and III to the Fourth Assessment, Geneva, Switzerland, 104pp.: IPCC.

IPCC (2014) Climate Change 2014: Synthesis Report. Contribution of Working Groups I, II and III to the Fifth Assessment Report of the, Geneva, Switzerland, 151 pp: IPCC.

Ζαχαριάδου,- Ζ (2013) Διπλωματική Εργασία: Κλιματική Αλλαγή και Διαχείριση Παράκτιων Τεχνικών Έργων, Θεσσαλονίκη: ΑΠΘ.

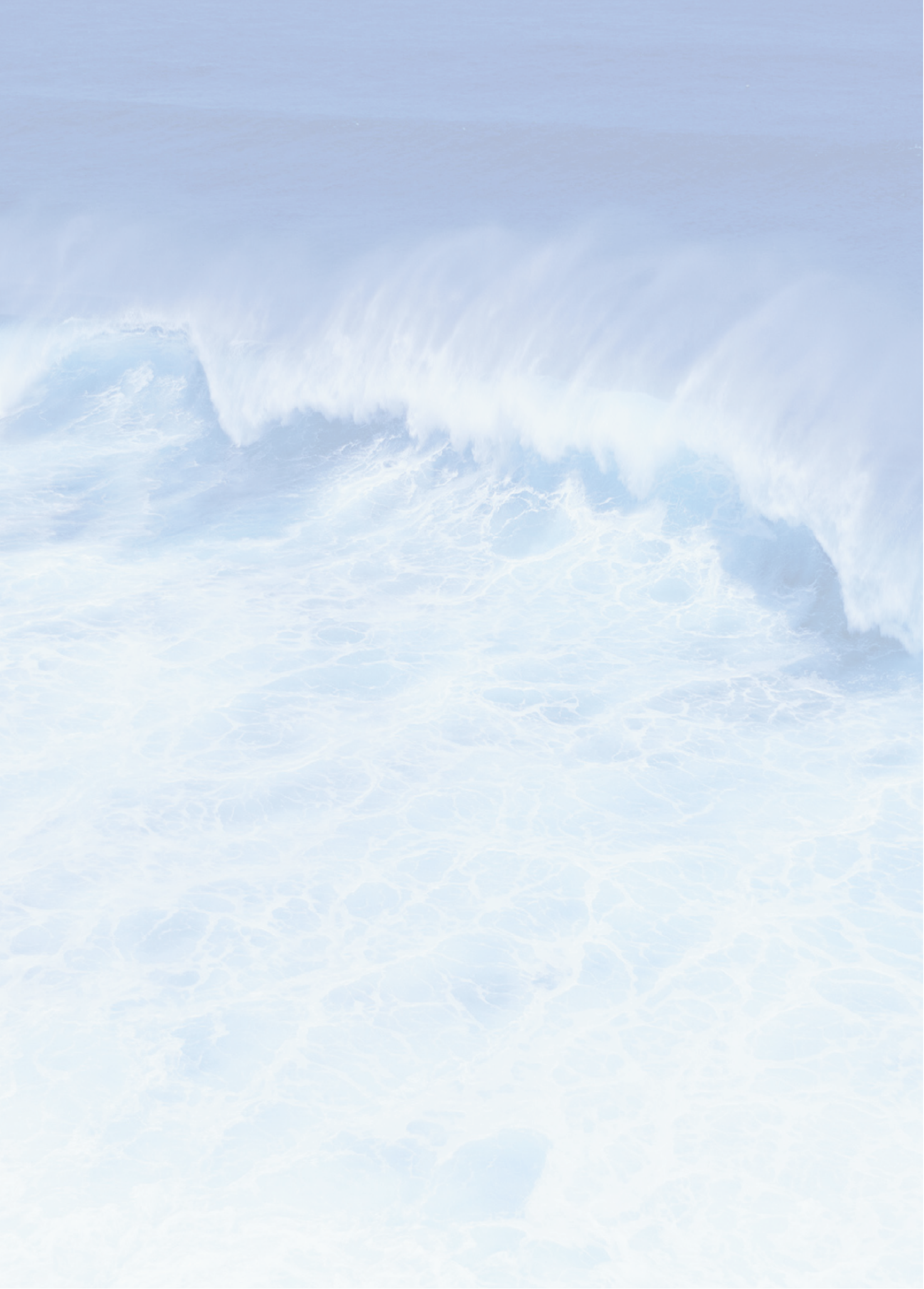

Climate change adaptation strategies in developing countries - An exemplary coastal protection project in Beira, Mozambique

Dr. H. Spekker*, H. Krebs

Inros Lackner SE, Linzer Str. 3, D-28359 Bremen / Germany
*Corresponding author: heiko.spekker@inros-lackner.de

Abstract

Beira is an important port city on the coast of Mozambique, with a population of approximately half a million people. The mostly informal settlements are characterised by high population density, inadequate infrastructure and a high poverty rate, which also makes them particularly vulnerable to extreme weather. Large parts of the city centre are just above sea level, and since the Indian Ocean in this area has a very large tidal range of up to 7 m, reliable coastal protection is of great importance. Beira is considered to be the city most threatened by climate change in Mozambique and one of the cities most threatened in Africa. It is predicted that the sea level in this region will rise and that rainfall and dry periods will increase. The situation will get even worse going forward. The inhabitants of informal settlements with their businesses are particularly at risk, as are other parts of the city centre as well. In 2019, two extreme weather events (storm Desmond and cyclone Idai) have led to catastrophic flooding and storm damages in Mozambique and Beira.

Keywords Climate change, Coastal protection, Tidal outlet, Nature-based solution, Mozambique.

1 CLIMATE CHANGE ADAPTATION MEASURES

The Chiveve tidal river, which runs through the city for a distance of approximately 5 km, was neglected in the past, and became increasingly silted up, to the point that it no longer served as a drainage channel for the surrounding area. Rubbish was disposed of on the wetlands, and the standing water promoted the spreading of diseases such as malaria and cholera. During very high tides or storm surges in the adjacent ocean, combined with heavy rainfall, the Chiveve regularly overflowed its banks and flooded much of its catchment area – particularly the informal settlements along its banks (Fig. 1).

Figure 1 Flooded areas in the informal settlement Goto during the rainy season

A new flood barrier (Fig. 2), designed by Inros Lackner and financed by the German KfW development bank on behalf of the German Federal Ministry for Economic Cooperation and Development (BMZ), is protecting the port city on Mozambique’s Indian Ocean coast, and improving the city’s drainage since 2017.

Figure 2 Aerial photograph of the Chiveve River mouth including the flood barrier

The barrier´s gates allow to control the water level upstream. The area’s drainage system now functions far more effectively due to the construction of a retention basin and a precise control of the gates. The flooding situation along the Chiveve River could be significantly improved. The barrier’s effectiveness in this regard was put to the test at the end of February 2017, when approximately 225 mm of rain fell during a 24-hour period – a level of rainfall that, on average, is only expected once every ten years. No significant flooding occurred in the project area. Also after cyclone IDAI and after storm Desmond in January 2019, when approximately 355 mm of rain fell during a 24-hour period, no extreme water levels were measured upstream of the tidal gate.

Inros Lackner in association with CES Consulting Engineers was contracted to provide planning and design services for all stages, from the initial feasibility study to the supervision of construction on site. The project, which was executed by a Chinese contractor, was completed on time and within budget. During the construction phase, both national and international media reported on the climate adaptation project. The site supervision team was honoured to regularly welcome government officials, ambassadors and other delegations to the site.

Figure 3 Construction of the drainage channel upstream of the tidal outlet

2 NATURE-BASED SOLUTIONS

The project included a comprehensive plan for the reestablishment of the original river course and nature-based erosion protection solutions along its embankments. It also included dredging of sludge within the fishing port downstream, resettlement measures, and the planting of young mangroves along the river banks including a nearby coastal area (Fig. 4).

Figure 4 Reforestation of mangrove forests in Nhangau

A local NGO is carrying out extensive reforestation measures in order to compensate the cutting of mangroves due to the construction works. The mangrove trees were cut into regular wood logs and used by a practical training centre for the manufacture of school furniture. An Info Point near to the construction site provides broad information of the construction works to the public.

3 GREEN URBAN INFRASTRUCTURE FOR BEIRA

A second phase, financed by KfW development bank and World Bank Group, involves the creation of a green landscape park in the river catchment area from 2018 to 2021. The green belt in the middle of the city centre is expected to protect the course of the river, which is lined with mangroves, from progressing urbanisation. It will be a recreational area for the population, including restaurants, exhibition centre, amphitheatre, botanical garden, sports facilities and children´s playgrounds. Over 7000 trees will be planted.

The green infrastructure is supported by the project, through a grant from the Pilot Program for Climate Resilience, which aims to transform the Chiveve River margin areas into a green urban park that offers ecosystem services (biodiversity, drainage, urban cooling and flood mitigation), as well as economic and recreational opportunities to Beira citizens.

Figure 5 Planned landscape development along the Chiveve River

In order to encourage people to use and therefore value the park and river system, passive and active recreational activities, art installations and activation nodes have been located along the river length. These nodes respond to the surrounding urban context and the existing social patterns and needs, providing exciting programming for the park.

References

Spekker, H, Heskamp, J. (2017): Flood protection for the City of Beira, Bautechnik 94 (2017), issue 12, vol. 94, DOI: 10.1002 / bate.201710102.

Beach erosion hazard under climate variability and change – The case of Saint Lucia (Eastern Caribbean)

I.N. Monioudi[1*], A. Nikolaou[1], R. Assariotis[2], M.I. Vousdoukas[3,1], A.F. Velegrakis[1]

[1]University of the Aegean, Department of Marine Sciences, University Hill, Mytilene, Greece
[2]UNCTAD, Policy and Legislation Section, Division on Technology and Logistics, Geneva, Switzerland
[3]European Commission, Joint European Research Centre (JRC), Via Enrico Fermi 2749, I-21027, Ispra, Italy
[*]Corresponding author: imonioudi@marine.aegean.gr

Abstract

This contribution presents an assessment of beach erosion hazard and risk in a Caribbean Small Island Developing State (SIDS): Saint Lucia. The geo-spatial characteristics and other attributes of all ('dry') beaches of Saint Lucia were recorded from readily available satellite imagery. This information was then used in conjunction with projections of Extreme Sea Levels (*ESLs*) and corresponding waves under different climatic scenarios which forced cross-shore morphodynamic model ensembles to obtain estimates of beach erosion along the Saint Lucian coast. *ESLs* were projected to increase considerably (by up to 60% in 2100) from their baseline (2000) levels. Severe storm erosion is projected from as early as 2050 and under a moderate emission scenario (RCP4.5); the 100-year extreme sea level event (ESL_{100}) may overwhelm up to 67% of the 91 Saint Lucian beaches. It was also found that the connectivity of the major transportation assets to the major tourist destinations of the island is under increased risk by the large density of landslides.

Keywords Beach erosion, Island beaches, Extreme sea levels, Climate Change impacts

1 INTRODUCTION

Small Island Developing States (SIDS) face significant challenges from Climate Variability and Change (CV & C), due to their limited physical size, small economies, and the high concentration of population, infrastructure, and services at the coast. Tourism is a key component of SIDS economies and is based on the "3S" model (Sea, Sand and Sun). A most critical component of 3S tourism is the availability of beaches that are environmentally and aesthetically sound and retain adequate carrying capacity (e.g., McArthur 2015; Huamantinco Cisneros et al. 2016). Beach erosion due to e.g. sea level rise might reduce significantly the carrying capacity and the quality of the beaches as environments of leisure and consequently the attractiveness of the country to tourism and travel, resulting to significant international travel expenditure loss.

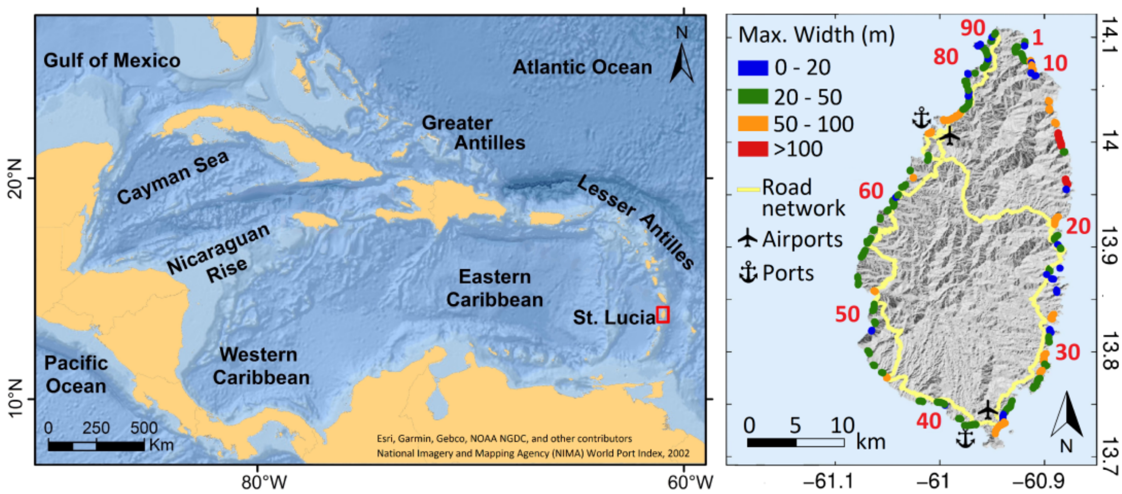

Figure 1 Saint Lucia: transport network and beaches with their maximum widths recorded in this study. Digital elevation model data from SRTM DTM and bathymetric data from GEBCO_2014 Grid were used

Also transport is a key enabler of tourism and plays a vital role in moving tourists from the island gateways to the island residences and on to various other attractions. The location, capacity, efficiency and connectivity of road transport can, therefore, play an important role in the mobility/connectivity within the island. The present contribution presents an approach for the assessment of beach erosion at a regional (island) scale under future *ESLs* and its application at the touristic island of Saint Lucia (Eastern Caribbean) (Figure 1). Also the risk of connectivity disruptions along the main road network of Saint Lucia due to potential landslides under extreme precipitation (hurricanes) was assessed.

2 METHODOLOGY

2.1 Beach characteristics/database

The geo-spatial characteristics of all (91 were identified) the ('dry') pocket beaches of St. Lucia have been recorded, on the basis of the images and other related optical information available in the Google Earth Pro application. In this study, 'dry' beaches were defined as the low-lying coastal sedimentary bodies bounded on their landward side by either natural boundaries (vegetated dunes and/or cliffs) or permanent artificial structures (e.g. coastal embankments, seawalls, roads, and buildings) and on their seaward side by the shoreline, i.e. the median line of the foaming swash zone shown on the imagery. Regarding the lateral extent of individual beaches, these were delimited by natural barriers, such as rock promontories. In addition other relevant information was recorded and codified, including: the presence of (a) natural features (e.g. river mouths, vegetation) and (b) artificial features such as coastal works and the density of the backshore infrastructure/assets (as a percentage of beach length).

2.2 Extreme sea levels and waves

ESL (i.e. the sum of the *SLR*, the maximum astronomical tide and the episodic level rise due to storm surges and wave set ups) and wave projections for the 21st century under the IPCC RCP4.5 and RCP8.5 scenarios were obtained from the dataset presented by the EC Joint Research Centre-JRC (Vousdoukas et al. 2018). The DFLOW-FM model has been used to assess *SLR*-induced changes in the tidal elevations from their baseline (2000) values estimated using the FES2014 model. Storm surge levels (*SSLs*) and waves (1980-2019) along the coast of the island were hindcasted through simulations forced by the ERA-INTERIM atmospheric conditions, whereas offshore significant wave heights (H_s), periods (T) and directions through the WAVEWATCH III model. Future *SSLs* and waves were projected by a 6-member GCM ensemble from the CMIP5 database (Vousdoukas et al. 2018). Finally, wave set-ups (η_s) were combined with *SSLs* in order to generate the episodic η_{CE} components. The simulations provided time series of the *ESLs* components with a 25 km grid resolution along the coastline. Non-stationary extreme value analysis was used to obtain extreme values for 9 return periods (the one in 1-, 5-, 10-, 20-, 50-, 100- and 200-, 500- and 1000-year events). The final dataset combines all *ESLs* components and their uncertainties in a probabilistic fashion through Monte Carlo simulations. Bivariate copula statistics (e.g., Li et al. 2018) were used to match the total water levels (and corresponding episodic η_{CE}) with the most likely corresponding wave parameters (significant wave height (H_s), period (T) and wave direction) to force the cross-shore morphodynamic models.

2.3 Beach erosion projections

Two ensembles of cross-shore (1-D) morphodynamic models were used: a 'long-term' ensemble consisting of the analytical models *Bruun, Dean* and *Edelman* and a 'short-term' ensemble comprising the numerical *SBEACH, Leont'yev, XBEACH* and *Boussinesq* models; the former is used to assess beach retreat/erosion under *SLR*, whereas the latter retreat due to temporary *SLR* (i.e. episodic storm-induced). With regard to *ESLs* (i.e. storm-induced η_{CE} superimposed on *SLRs*), the long-term and short-term ensembles were used consecutively (see also Monioudi et al. 2017). Given the spatial and temporal scales of the application, the input seabed slope and sediment data could not be based on observations. The models were set up using linear beach profiles (Monioudi et al. 2017) with various bed slopes (1/10, 1/15, 1/20, 1/25 and 1/30) and median sediment sizes (d_{50} of 0.2, 0.33, 0.50, 0.80, 1, 2 and 5 mm). Beach erosion/retreat was assessed for the 1-10, 1-50 and 1-100 year *ESLs* projected for the years 2030, 2050 and 2100 under the IPCC RCP4.5 (moderate) and RCP8.5 (business as usual) scenarios. Due to the different conditions used in the model set ups, each model produced a range of beach erosion projections. The means of the lowest and highest projections from all models in the ensemble were calculated, combined and compared to the recorded beach maximum widths (see Sect. 2.1) to project the minimum (most conservative) and maximum beach erosion, respectively under different climatic scenarios, date years and *ESL* return periods.

2.4 Estimation of connectivity disruptions due to potential landslides

Climate changes affect the stability of natural and engineered slopes and have consequences on landslides, but it is not clear the type, extent, magnitude and direction of the changes in the stability conditions, and on the location, abundance, activity and frequency of landslides in response to the projected climate changes. Since it is difficult to get landslide projections, information of landslides occurrence during past events is used for the estimation of the airport connectivity. The estimation of the number of potential landslides along the road network of Saint Lucia was achieved through (i) digitization of the major road network using the Google Earth Application and (ii) the landslide density per kilometre recorded during the Hurricane Tomas (Van Westen 2016).

3 RESULTS

3.1 Beach characteristics

Most Saint Lucian beaches are narrow: 26% of the recorded maximum 'dry' beach widths were found less than 20m and 81% less than 50m, with only 2% having maximum widths exceeding 100m. Regarding the sediment texture, the majority of the beaches have been classified as sandy beaches (76 beaches, 84% of the total); Mixed texture (sandy gravels) was allocated to 2 beaches, whereas for the remainder of the beaches there was no information available (14%). 32% of the beaches were found to be associated with active river mouths and 34% were found to directly front coastal infrastructure/assets (without any 'set-back' of the construction line). Finally, only 19% of the beaches were observed to host coastal technical works, with jetties appearing as the most dominant.

3.2 Extreme sea levels

ESLs are projected to rise in the course of the century. For example, under the RCP4.5 scenario, the ESL_{100} along the Saint Lucian coastline is projected as 1.85 and 2.21 m higher than the baseline mean sea level (*MSL*) in 2050 and 2100, respectively, and 0.26 and 0.62 m higher than the baseline ESL_{100}. *ESLs* will be increasingly controlled by the emission scenario. Regarding the contributions of the different *ESL* components and their temporal evolution (Figure 2, Table 1), it appears that although the episodic η_{CE} is the primary contributor, its dominance will decrease in the future, as it will change little compared with the accelerating *SLR*. Tidal levels will change little over the years.

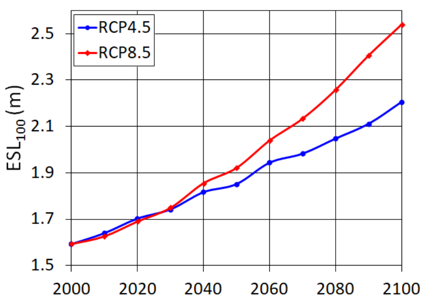

Figure 2 Time evolution of ESL_{100} under RCP4.5 and RCP8.5

Table 1 ESL_{100} and its components along the Saint Lucian coastline for different dates (2000-baseline, 2030, 2050 and 2100) and under the RCP4.5 and RCP8.5 scenarios. Key: *SLR*, mean sea level rise relative to the baseline *MSL*; η_{tide}, max.tidal level; η_{CE}, storm sea level component

	Baseline	RCP 4.5			RCP 8.5		
	2000	2030	2050	2100	2030	2050	2100
SLR (m)	0	0.14	0.26	0.57	0.16	0.32	0.90
η_{tide} *(m)*	0.17	0.16	0.15	0.17	0.16	0.15	0.17
η_{CE} *(m)*	1.43	1.44	1.44	1.46	1.43	1.45	1.46
ESL_{100} *(m)*	1.59	1.74	1.85	2.21	1.75	1.92	2.54

3.3 Beach erosion

ESL_{100} in 2050 and 2100 will result in storm beach erosion of up to about 62 and 73 m, respectively under the RCP4.5 scenario. Under the RCP8.5 scenario, erosion will be slightly greater in (64 m) 2050, but the differences between the two scenarios will increase (84 m) in 2100. Substantial impacts are projected as early as 2050, even under the RCP4.5. In 2050, and according to the most conservative projections, about 42% of all beaches are projected to lose at least 50% of their current maximum widths and 21% to be completely eroded under the (RCP4.5) 100-year *ESL* (ESL_{100}) (Figure 3). In terms of asset exposure, at least 16% of beaches presently fronting assets are projected to be overwhelmed during the event. In 2100, impacts could be devastating. Under the RCP4.5 ESL_{100}, 24–80% of all beaches will be completely (at least temporarily) eroded (23–97% of the beaches fronting assets) under the low and high projections of the model ensembles, respectively. Erosion due to the RCP8.5 ESL_{100} represents a catastrophic scenario, since up to 92% of all Saint Lucian beaches will be completely eroded, from which 97% are presently fronting assets. These frontline backshore assets will sustain large damages even in the case of a partial (or total) post-storm beach recovery as they are located firmly within the beach erosion-recovery envelop.

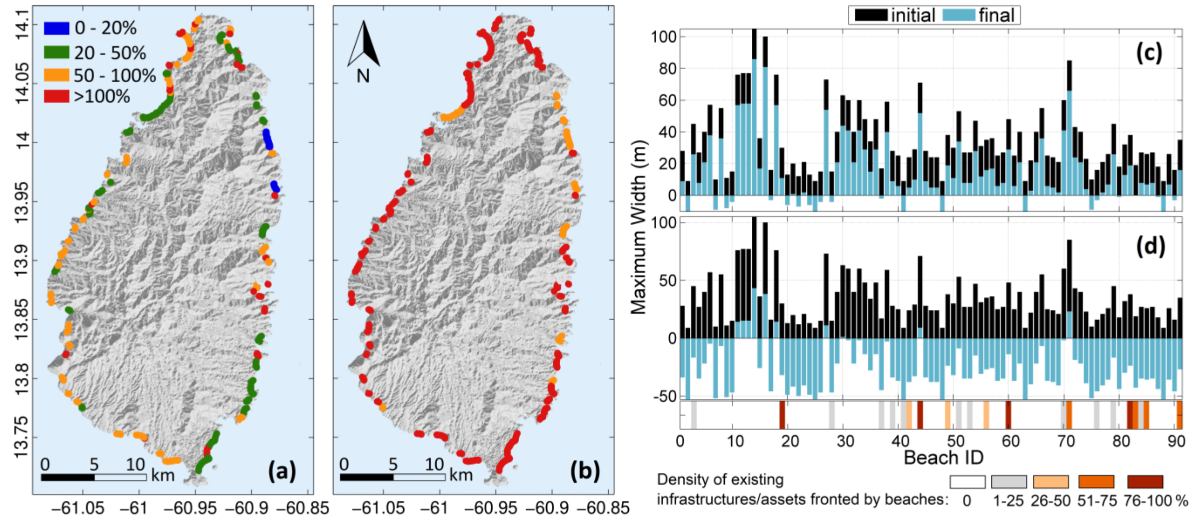

Figure 3 Projections of (a) minimum and (b) maximum beach retreat under a ESL_{100} (for the year 2050 and RCP4.5), showing beaches projected to retreat by distances equal to different percentages of their initial maximum widths *(BMWs)*. The current (initial) *BMWs* (black bars) are compared with those resulting from (c) the minimum and (d) maximum projected beach erosion (blue bars); negative values indicate total beach erosion. The recorded density of the frontline backshore assets (as a percentage of the beach length) is also shown

3.4 Estimation of airport connectivity (redundancy)

An estimation of connectivity impacts on the basis of the number of potential landslides (Figure 4) has been carried along the connecting road network between the 2 international airports (George Charles International Airport–GCIA and Hewanorra International Airport–HIA) and the 30 tourist beaches identified along the island coastline (Figure 4).

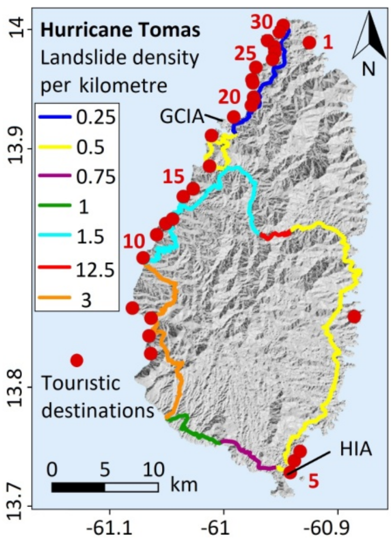

Touristic destinations	From HIA	From GCIA	Touristic destinations	From HIA	From GCIA
1	45.9	2.8	16	40.6	3.3
2	9.5	33.5	17	42.2	1.4
3	0.4	42.6	18	43.0	0.0
4	0.4	43.0	19	43.5	0.5
5	0.9	44.3	20	43.8	0.8
6	46.6	83.9	21	43.9	0.8
7	53.2	77.4	22	44.2	1.1
8	60.2	70.4	23	44.2	1.2
9	65.9	64.7	24	44.3	1.3
10	98.0	38.3	25	44.9	1.8
11	111.3	25.0	26	45.4	2.4
12	114.6	21.6	27	45.6	2.5
13	116.7	19.6	28	45.7	2.6
14	124.4	11.9	29	45.9	2.8
15	126.5	9.8	30	46.2	3.1

Figure 4 Landslide densities per kilometre of road (Post Hurricane Tomas) and the numbers of landslides along the road network connecting the airports HIA and GCIA to 30 touristic destinations

It was found that during such an event and in the absence of major technical works to armour the cliffs against road affecting landslides, access to major touristic destinations from HIA is generally at much greater risk than that from George Charles IA; along the main road from HIA, landslide densities were found to be up to 1.75/km (average density 0.75/km).

4 DISCUSSION AND CONCLUSIONS

CV & C impacts on the capital/product of tourism are related to the potential reductions in the beach carrying capacity due to coastal erosion (e.g., Scott et al. 2012). Application of the beach retreat prediction methodology showed that the beaches in Saint Lucia are vulnerable to *ESL*. Under increasing beach erosion/retreat, the long-term recreational value of the Saint Lucia beaches as well as the value of associated assets may fall considerably (e.g., Gopalakrishnan et al. 2011). Against this background, it appears that plans to respond effectively to the projected beach erosion risk should be urgently drawn up with different adaptation options analysed. Options based on the ecosystem approach should be considered first in order to protect both beaches and backshore ecosystems and infrastructure/assets (e.g., Peduzzi et al. 2013), although "hard" works might, in some cases, be still deemed necessary. However, the significance of beaches as critical economic resources and the low effectiveness of hard coastal works (e.g., breakwaters) to protect beaches from *SLR* indicate that beach nourishment schemes will also be required, at least for the most economically important beaches.

Finally, it appears that the road network connecting the major gateways of international tourism and the major tourist resorts is under an increased risk of landslides, especially during and following extreme precipitation (hurricanes). It was found that during such events, access to major touristic destinations from HIA is generally at much greater risk than that from GCIA. Technical works to armour the cliffs against road affecting landslides should be urgently considered.

References

Gopalakrishnan S, Smith MD, Slott JM, Brad Murray A (2011) The value of disappearing beaches: A hedonic pricing model with endogenous beach width. J. Environ. Econ. Manag. 61:97–310. https://doi.org/10.1016/j.jeem.2010.09.003

Huamantinco Cisneros MA, Revollo Sarmiento NV, Delrieux CA, Piccolo MC, Perillo GME (2016) Beach carrying capacity assessment through image processing tools for coastal management. Ocean & Coastal Management 130:138-147. http://dx.doi.org/10.1016/j.ocecoaman.2016.06.010

Li F, Zhou J, Liu C (2018) Statistical modelling of extreme storms using copulas: A comparison study. Coast. Eng. 142:52–61. https://doi.org/10.1016/j.coastaleng.2018.09.007

McArthur S (2015) Why Carrying Capacity Should be a Last Resort (2015). In: Singh TVir (ed.) Challenges in Tourism Research, Channel View Publications, p 288-302.

Monioudi IN, Velegrakis AF, Chatzipavlis AE, Rigos A, Karambas T, Vousdoukas MI, Hasiotis T, Koukourouvli N, Peduzzi P, Manoutsoglou E, Poulos SE, Collins MB (2017) Assessment of island beach erosion due to sea level rise: the case of the Aegean archipelago (Eastern Mediterranean). Nat Hazards Earth Syst Sci 17: 449–466. https://doi.org/10.5194/nhess-17-449-2017

Peduzzi P, Velegrakis AF, Estrella M, Chatenoux B (2013) Integrating the role of ecosystems in disaster risk and vulnerability assessments: Lessons from the Risk and Vulnerability Assessment Methodology Development Project (RiVAMP) in Negril Jamaica. In: Renaud FG et al. (eds) The role of Ecosystems in Disaster Risk Reduction, United Nations University Press (ISBN 978-9280812213), p 109-139.

Scott D, Simpson MC, Sim R (2012) The vulnerability of Caribbean coastal tourism to scenarios of climate change related sea level rise. Journal of Sustainable Tourism 20(6): 883-898. https://doi.org/10.1080/09669582.2012.699063

Van Westen CJ (2016) National Scale Landslide Susceptibility Assessment for Saint Lucia. CHARIM Caribbean Handbook on Risk Information Management, World Bank GFDRR, ACP- EU Natural Disaster Risk Reduction Program. http://www.charim.net/sites/default/files/handbook/maps/SAINT_LUCIA/SLULandslideReport.pdf

Vousdoukas MI, Mentaschi L, Voukouvalas E, Verlaan M, Jevrejeva S, Jackson LP, Feyen L (2018) Global probabilistic projections of extreme sea levels show intensification of coastal flood hazard. Nat Commun vol. 9:2360. https://doi.org/10.1038/s41467-018-04692-w

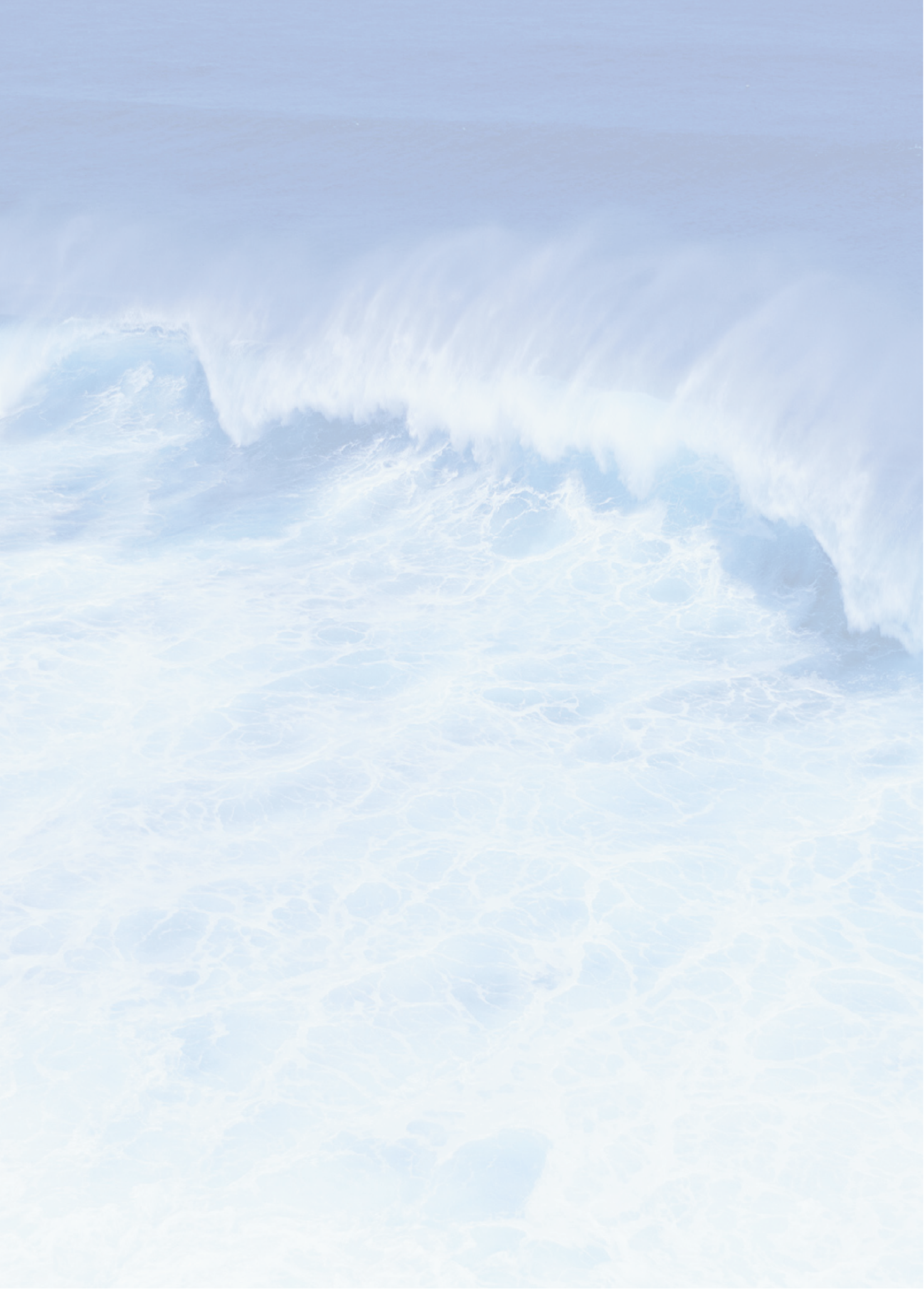

Protection of coastal monuments against climatic change under designing restrictions

G. Alexandrakıs[1*], D. Rompogıanakıs[2], E. Papadakıs[2], N. Kampanıs[1] S. Lırıtzakıs[3], C. Lıtınakı[3], E. Tsıplostefanakıs[3], S. Perogıannakı[3] and G. Fragkomanolakı[3]

[1]Coastal & Marine Research Lab, Foundation for Research & Technology-Hellas, Greece
[2]Neptune Coastal engineering Technical Consultants, Greece
[3]Port of Heraklion, Greece
*Corresponding author: alexandrakis@iacm.forth.gr

Abstract

In this work the combination of risk assessment analysis related to increasing sea level and storm frequency, wave numerical modelling, breakwater design and economic sustainability is presented. As a case study, the Venetian Coastal Fortress of the city of Heraklion is considered. Climatic modelling results indicate that for the coastal area of Heraklion the wind speed and directions are expected to change in the near and far future, with an increase in wind speeds but also an increase in the frequency of the wind directions that effect the monuments the most. Based on the results, mitigation actions were proposed that include, increasing the submerged armouring of the Venetian fortress and the use of natural based solutions for low slope areas in order to reduce wave energy, run up and overtopping, so that the monument can be made accessible for longer periods of time.

Keywords Wave overtopping, Breakwaters, storms, Heraklion

2 *INTRODUCTION*

Built heritage is a cultural asset inherited through generations which defines the origin and identity of a place (ICOMOS, 2002). The present concern is to preserve important structures and sites that promote identity and continuity of place, without compromising on development that is essential for the present times. Evolution of surrounding locations and natural aging of the historical structures is inevitable but it is essential to check both for sustained development. UNESCO (1972) defined that built Cultural Heritage comprises Architectural works which are of outstanding universal value. It was found that the built heritage across the globe is increasingly threatened with defects being caused not only by the natural causes of decay like gradual weathering and bio-chemical factors, but also by the variations in climatic, social and economic conditions. Climate change is a substantial and inevitable threat to the built heritage of our coasts and the way of life which co-exist with these environments, and the overall wellbeing. The impacts of climatic change present serious consequences on heritage structures and socio-economic activity that is directly or indirectly associated with it, including tourism (Kelly and Stack, 2009). Study by Intergovernmental Panel on Climate Change (IPCC), links vulnerability with climatic change, and point out that the vulnerability of a region depends to a great extent on its wealth, and that poverty limits adaptive capabilities (IPCC, 2000). Extreme weather and rising sea levels are more likely to cause catastrophic damage and destruction to coastal cultural heritage sites. Sea level rise (SLR) in view of climate change poses a serious threat to coastal areas and therefore, much research effort has focused on this aspect of coastal hazard (Church and White 2011; Hinkel et al. 2014; Hogarth 2014; Hoggart et al. 2014; Jevrejeva et al. 2014; Losada et al. 2013; Tol 2009). Extreme events, however, determine an additional hazard component. Some studies report an increased intensity and frequency of extreme water levels along several coastal regions in the world (Izaguirre et al. 2013; Ullmann and Monbaliu 2010; Wang et al. 2014; Weisse et al. 2014). Sea Level Rise and increased storm events can damage structures that were not designed to withstand prolonged structural pressure, erosion, and immersion. Risks affecting coastal cultural heritage may stem from exposure to one or more hazards and it is important to facilitate a holistic understanding of factors driving them. Wave energy and overtopping of coastal structures represents a potential hazard for people, property and infrastructure. Especially when the coastal structure is a monument or landmark, mitigation measures and monitoring are needed. Moreover, the anticipated increase in extreme events due to climatic change make protection and prevention action even more necessary. Additionally, restrictions in fund availability and landscape preservation for coastal monuments, make the designing of such interventions more demanding. Wave overtopping has always been of prime concern for coastal structures constructed to defend against flooding.

3 *CASE STUDY*

Heraklion is the largest urban centre in Crete, the capital of the region; it represents the most important place for the cultural, social and economic development of Crete. The Sea Fortress of “Koules”, located in the port of Heraklion, constitutes a characteristic type of the Venetian military architecture. Similar fortifications can be found in other locations in the Mediterranean basin). In fact, an important sector of CH in Greece and Europe is located on coastal areas throughout the Mediterranean (cities, ports, lighthouses, fortresses and other monuments). These monuments face hazard risks due to climate change (sea level rising, increasing intensity of extreme weather phenomena), which can be combined with other air and land associated hazards, increased salinity accelerating corrosion and deterioration of materials and structures, etc. The immediate contact of Koules with the sea makes the fortress vulnerable to salty northern winds, which are often very severe, reaching 9, 10 or even 11 units in the Beaufort scale. Especially during the winter season high waves are often literally covering the monument (Figure 1).

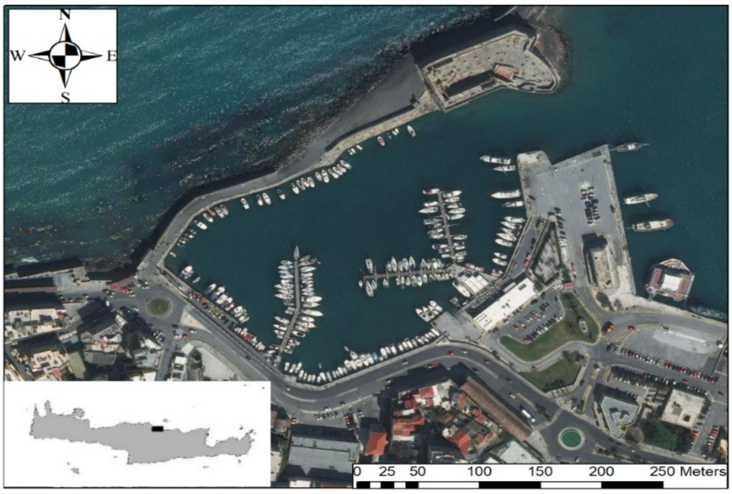

Figure 1 Study area

4 METHODOLOGY

The meteorological data statistical analysis focuses on two different time-scales (long and short-term analysis) were used. The data from the long-term analysis are evaluated on the base of the results from the EURO-CORDEX project. For the two future periods (near future: 2036 – 2065, far future: 2071 - 2100) are used (Alexandrakis et al 2019) as input data to the wave model analysis software. In this way, the significant wave height and period can be estimated for the coastal front of Heraklion and the impact on Koules monument can be addressed for the near and far future. For the calculation of the wave climate off the area, wave characteristics were estimated by JONSWAP model and in order to study the distribution of wave energy along the coast in the area, wave refraction diagrams were constructed using numerical models. Wave overtopping estimations basis were made using the formula (1) for rubble mound structures such as breakwaters and rock slopes

$$\frac{q}{\sqrt{gH_{m0}^3}} = aexp\left(-\frac{bR_c}{H_{m0}}\right) \tag{1}$$

It is an exponential function with the dimensionless overtopping discharge $q/(gH^3_{m0})^{½}$ and the relative crest freeboard R_c/H_{m0}.

Damage to armour layers was characterized by counting the number of displaced units or by measuring the eroded surface profile of the armoured slope by land and seafloor survey which included sediment samples and Starfish 450F Side Scan Sonar images. For armouring material estimations the Hudson (1961) methodology was used.

5 RESULTS

Based on the data from the long-term analysis are evaluated using the results from the EURO-CORDEX project that provides regional climate projections for Europe at 12.5km resolution. The provided data for the two future periods (near future: 2036 – 2065, far future: 2071 - 2100) are used to extract the near and far future wind time-series data to introduce to the wave model analysis software. This way the significant wave height and period can be estimated for the coastal front of Heraklion and the impact on Koules monument can be addressed for the near and far future. For the Heraklion coastal area, there is a wind speed shift to higher values over the near and far future distributions. Table 4 shows that the prevailing wind direction remains the NW (315deg.) throughout the two forecasting periods (near and far future periods) with the mean wind speed increasing by 0.15m/s in the near future and by 0.24m/s for the far future with respect to the reference period. The secondary wind direction is the Western direction (270deg).

Table 4 Occurrence (%) of Wind Direction for the Reference Period and the Near and Far Future

%	45°	90°	135°	180°	225°	270°	315°	360°
Ref.	0,49	0,24	0,37	2,53	8,33	36,39	46,10	5,55
Near	0,50	0,26	0,30	1,85	6,77	34,75	49,07	6,50
Far	0,54	0,26	0,38	1,68	5,18	33,77	51,16	7,03

4.1 Wave propagation

From the analysis of the refraction diagrams, it appears that the waves affecting the wider area are those originating from N, NE, NW and E. West origins waves arrive at the shoreline after refraction and diffraction, causing greatly weakening of the wave energy in the nearshore. The breaking depth (d_b) and the breaking wave height (H_b) in the coastal zone were determined. From the calculation of the maximum breaking depth for the maximum expected wave characteristics, the width of surf zone was determined as the area enclosed between the maximum breaking depth and the coastline (Table 5). The maximum expected wave height at break in the studied area is derived from NW waves and is 8.15m and waves breaking is expected to start at a depth of 9.70m (Table 2).

Table 2 Wave characteristics

		U_a(m/sec)	H_s(m)	T_s (sec)	h_c(m)	L_o(m)	H_b(m)	d_b(m)
N	Mean	21,27	4,09	8,69	7,77	117,81	4,53	5,24
	Max	33,91	6,80	10,28	12,45	164,84	7,27	8,72
NE	Mean	18.00	2.64	4.69	1.73	76,92	3,18	3,75
	Max	33.91	4.98	8.37	8.88	109,24	5,22	6,39
NW	Mean	20.62	4.6	9.36	14.6	136,62	5,12	5,90
	Max	33.91	7,57	11.03	13.97	189,76	8,15	9,70
E	Mean	21,26	3.15	7.22	5.86	81,26	3,41	4,04
	Max	33.91	5.03	8.42	8.97	110,58	5,27	6,45
W	Mean	19.94	0.81	3.01	1.34	20,06	1,33	1,77
	Max	33.91	1.34	3.59	2.11	14,13	0,81	1,04

key: U_a wind speed, T_p wave period, H_s significant wave height h_c closure depth; L_o wave length; H_b breaking wave heightand d_b breaking wave depth.

4.2 Armouring Design

To study the distribution of wave energy along the coast in the area, wave refraction diagrams were constructed using numerical models. For each wave direction affecting the coastal zone, refraction diagrams for waves with higher wavelengths were constructed, as well as the usual peak values for the area were calculated on a weighted average basis for the incidence. The waves originating from the north and northeast and the maximum intensity waves approach the coastline almost in parallel, with an average wave height of between 4.5m and 5m. For normal northern origin waves, the wave height is in the range of 3m - 3.5m. Near the coastline, the wave height is smaller, up to approximately 2.5m, due to shallow bathymetry. This is because the breaking zone begins at a distance about 500m for the north waves, and about 450m for the Northeast waves. Waves coming from northwest are approaching the coastline after refraction at the Cape Panagia. The average wave height of normal waves is 2-2.5m, while for normal maximum observed waves is between 2.5m and 3m. The breaking zone is even wider, and about 600m from the coast. The eastern origin waves approach the coastline with average wave height of ranging between 1.5m and 2.5m, while for the corresponding average maximum waves observed between 3m and 3.5m. For the waves coming from the west, the wave height appears to be in the range of 0.5-1m for normal waves, and 1-2m for the maximum.

The aim of this work is to estimate the problems caused by the wave impact in the area of the Koules fortress and to propose a solution for the degradation of the monument. The results have shown that the main impacts are from the N, NE, E and NW origin waves, which influence the area and impact mechanical stresses to the breakwater and have significant overtopping events. The problem of the degradation of the breakwater armour in the area of the Venetian Fortress of Koules is proposed to be addressed by strengthening the existing shielding of the area to limit the wave run-up. The proposed solution involves the completion of the existing armour along its entire length in the area of the Venetian Fortress of Koules, aiming to reduce the wave energy impacting the walls (through induced wave breakage) at greater distances compared to current impacts. The materials are composed of natural boulders in the brim weighting 150 Kg. each, while in the reef section of artificial boulders weighing 4 tn. each. The future constructions are environmentally compatible, but also comply with the monument's requirements, so that the new works will harmonize with the existing historical constructions. The extent of the project is shown in Figure 14 with an indicative section of armour reinforcement. Moreover, for the safety of the public and passers-by, a small concrete vertical wall with a seating area will be built, to limit sea water from high energy events to reach the breakwater deck.

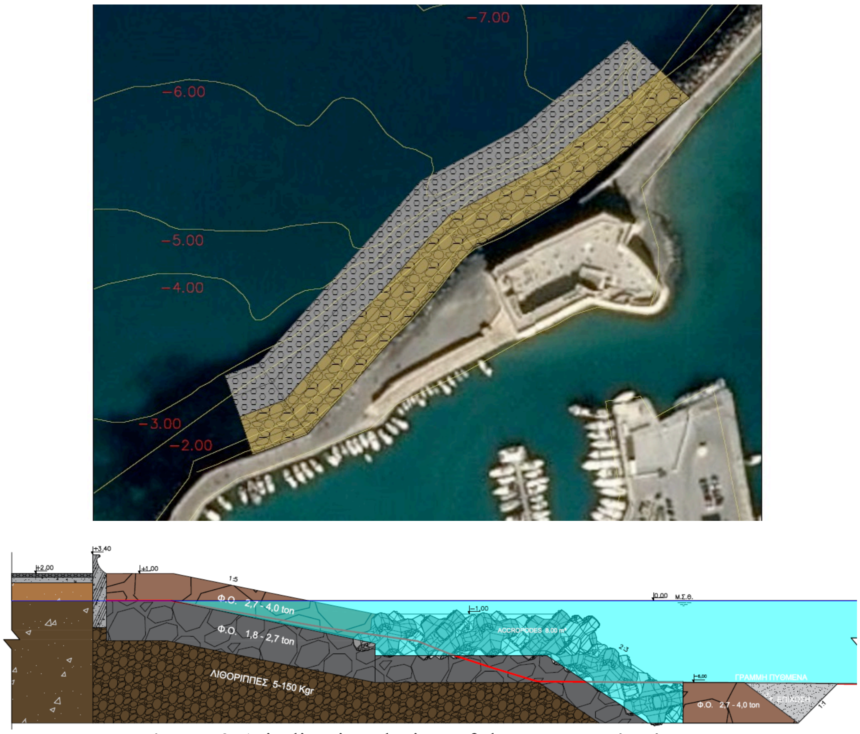

Figure 2 A indicative design of the proposed solution

Moreover, salts and crusts accumulation due to sea proximity, are proposed to be periodically monitored to control and check the stone erosion process. Moreover, seasonal monitoring of wind and wave effects and the observed structural cracks on the Venetian Fortress of Koules might be either related to vertical dead loads, or to scouring of foundations on the sea due to sea waves. At present, periodic analysis of satellite data aiming at understanding the stability of the scouring process is recommended as a solution for preventive conservation of the Fortress. With the use of the correlation of displacement data and wave height for the area of the breakwater it can be seen that large displacements occur in periods after strong wave events. Thus, the correlation analyses capabilities, supported by the wave sensor data, will help the interested party to better investigate the displacements in the Koules breakwater. Moreover, due to the changes in frequency and directions of wind and waves in the area due to climate change, the displacements of the breakwater and also the salt stray are expected to increase.

6 CONCLUSIONS

The aim of this work is to estimate the problems caused by the wave impact in the area of the Koules fortress and to propose a solution for the degradation of the monument. A comprehensive understanding of CC effects will build a basis for taking proactive rather than reactive measures and reduce the anticipated risks in the future, in an innovative paradigm for conservation. The correlation of displacement data and wave height helps to better investigate the displacements in the Koules breakwater. The results have shown that the main impacts are from the N, NE, E and NW origin waves, which influence the area and impact mechanical stresses to the breakwater and have significant overtopping events. Increasing underwater armouring of the monument will have no influence in visibility, an 80% reduce of wave spray and a 90% reduce of wave overtopping.

Acknowledgments

This work was supported by the HELLAS CH «Synergy ELI - LASERLAB Europe, HiPER & IPERION-CH.gr» (Secretariat for Research & Technology, 5 NSRF 2014-2020 Grant No 002735)

References

Alexandrakis G, Kozyrakis GV, Kampanis N (2019) Interventions on Coastal Monuments Against Climatic Change. In: Moropoulou A., Korres M., Georgopoulos A., Spyrakos C., Mouzakis C. (eds)

Transdisciplinary Multispectral Modeling and Cooperation for the Preservation of Cultural Heritage. TMM_CH 2018. Communications in Computer and Information Science, vol 961. Springer, Cham.
Hinkel J, Lincke D, Vafeidis AT, Perrette M, Nicholls RJ, Tol RSJ, Marzeion B, Fettweis X, Ionescu C, Levermann A (2014) Coastal flood damage and adaptation costs under 21st century sea-level rise. Proceedings of the National Academy of Sciences 111, 3292-3297.
Hogarth P (2014) Preliminary analysis of acceleration of sea level rise through the twentieth century using extended tide gauge data sets (August 2014). Journal of Geophysical Research: Oceans 119, 7645-7659.
Hoggart SPG, Hanley ME, Parker DJ, Simmonds DJ, Bilton DT, Filipova Marinova M, Franklin EL, Kotsev I, Penning-Rowsell EC, Rundle SD, Trifonova E, Vergiev S, White AC, Thompson RC (2014) The consequences of doing nothing: The effects of seawater flooding on coastal zones. Coastal Eng. 87, 169-182.
Hudson. R.Y., "Laboratory investigation of rubble-mound breakwaters." A.S.C.E. Waterways & Harbours Div. September 1959.
ICOMOS (2002) ICOMOS, International Cultural Tourism Charter. Principles and Guidelines for Managing Tourism.
IPCC (2000) IPCC special report on Emissions Scenarios., 2000, Intergovernmental Panel on Climate Change (IPCC).
Izaguirre C, Méndez FJ, Espejo A, Losada IJ, Reguero BG (2013) Extreme wave climate changes in Central-South America. Clim Change 119: 277–290.
Jevrejeva, S., Moore, J.C., Grinsted, A., Matthews, A.P., Spada, G. (2014) Trends and acceleration in global and regional sea levels since 1807. Global Planet. Change 113, 11-22.
Losada, I.J., Reguero, B.G., Méndez, F.J., Castanedo, S., Abascal, A.J., Mínguez, R. (2013) Long-term changes in sea-level components in Latin America and the Caribbean. Global Planet. Change 104, 34-50.
Tol RSJ (2009) Economics of Sea Level Rise. In: H.S. Editors-in-Chief: John, K.T. Karl and A.T. Steve (Editors), Encyclopedia of Ocean Sciences (Second Edition). Academic Press, Oxford, pp. 197-200.
Ullmann A, Monbaliu J (2010) Changes in atmospheric circulation over the North Atlantic and sea-surge variations along the Belgian coast during the twentieth century. Int J Climatol 30:558–568.
Wang XL, Feng Y, Swail VR (2014) Changes in global ocean wave heights as projected using multimodel CMIP5 simulations. Geophys Res Lett 41:1026–1034.
Weisse R, Bellafiore D, Menéndez M, Méndez F, Nicholls RJ, Umgiesser G, Willems P (2014) Changing extreme sea levels along European coasts. Coastal Eng 87: 4–14.

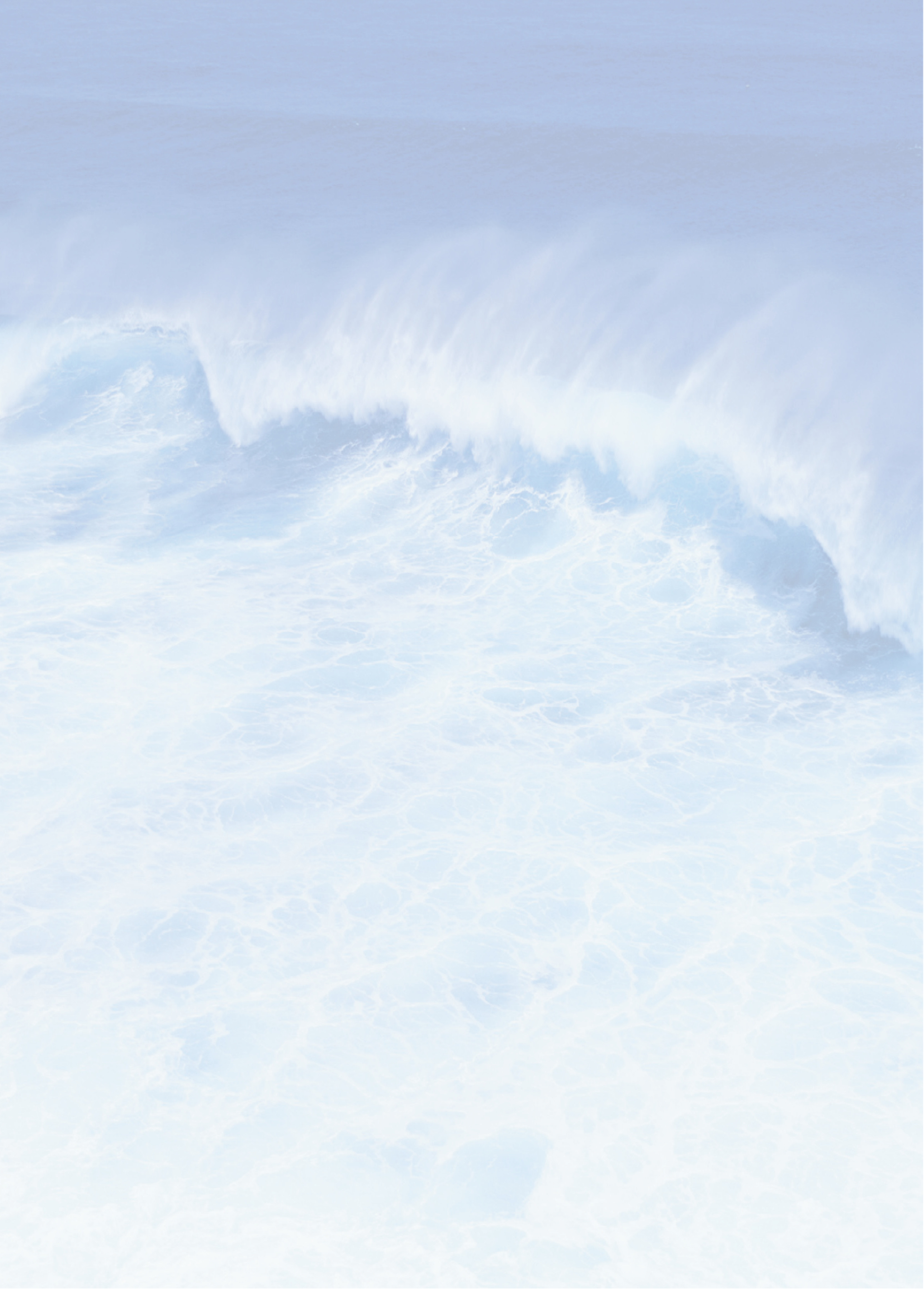

Master planning for the development or conversion of Port Areas: Two examples from the North of Germany

H.G. Krebs*, H. Spekker

Inros Lackner SE, Linzer Str. 3 D-28359 Bremen /Germany
*Corresponding author: hauke.krebs@inros-lackner.de

Abstract

Port areas are subject to constant change. In addition to further development for port-related activities, combined with the creation of new quays and industrial areas, conversion into an urban development area can also be a possible adaptation process. The paper will describe two different examples and approaches in Bremen and Emden. In these two northern German port cities, old harbour basins will be or have been backfilled and used for different purposes. The example of Jarssum Basin in Emden is intended to illustrate planning approaches for the further development of the port and its adaptation to the changed requirements of port users. The focus here is on the presentation of the consultant's approaches within the framework of the master planning and the corresponding difficulties in taking the requirements of the port users into account. Using the example of the city of Bremen, the conversion of an abandoned port area in a larger urban context will be explained. In particular, the approaches of the administration for the solution of the framework planning are explained and individual special problems and their solution are worked out.

Keywords Port Development, Conversion, Master Planning, Spatial Planning Überseeinsel, Jarssumer Hafen

1 JARSSUM BASIN / SEAPORT OF EMDEN

1.1 The Seaport of Emden

The port of Emden lies in the extreme northwest of Germany at the mouth of the Ems into the North Sea. It is the westernmost seaport on the coast of Germany. It currently has a transhipment volume of approx. 6 million tonnes. The main products are motor vehicles, forestry products and, increasingly, components for offshore wind turbines. For motor vehicles, the port is the third largest in Europe. The port is operated by the port company "Niedersachsen Ports". RoRo facilities in the outer port are generally used for the transhipment of motor vehicles. The inland port can be reached via two locks (Figure 1), i.e. the inner harbour basins of the seaport can be used for a total length of approx. 7 km without tidal influence.

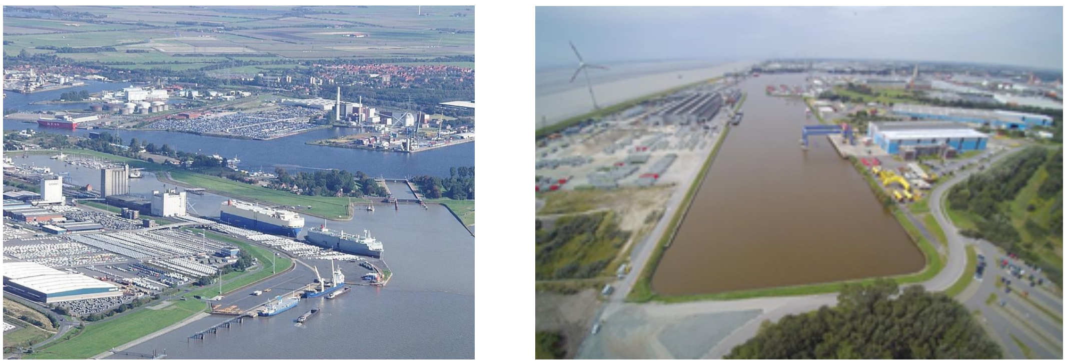

Figure 1 Sea Port of Emden: a) Outer Port and Lock, b) Inner Port: Jarssum Basin

1.2 The Jarssum Basin

As in many ports, Emden also lacks moorings that are deep enough for seagoing vessels in combination with developable open spaces. Therefore, a harbour basin was identified which appears suitable for redesign and development. It is an approximately 1,100 m x 350 m basin in the southeast of the Emden inland port, the so-called Jarssum basin (Figure 1).

Due to the strong sedimentation in the port of Emden, the water depth in the Jarssum basin is only less than 4 m with a target depth of 5.00 m. The water level in the port basin is +1.10 mCD. The quay facilities adjacent to the west have water depths of more than 10 m and sometimes up to 12.50 m.

In the area of the Jarssum basin, various manufacturing industries are located, all of which also transship via the adjacent quay facilities and are dependent on these. The port users concerned include a bulk handling company, a general cargo shipper and two companies loading large and heavy components onto ships for the construction of wind turbines (Figure 2).

Figure 2 Overview Port of Emden and Jarssum Basin (© Google, edited IL)

1.3 The general Idea and the Constraints

The basic idea and therefore the starting point of the planning was quite simple: the harbour basin was closed with a new sheet pile quay and the areas behind it were filled with suitable soil. In reality, however, this is not a greenfield project; rather, the abovementioned residents are considerably affected by the backfilling of the harbour basin.

- A manufacturer of components for offshore wind power operates its own crane system and has to transfer very large and heavy components directly from its production plant to a sea-going pontoon.
- The manufacturer of concrete components for the towers of wind power plants receives its raw materials (aggregates, cement, etc.) by inland waterway vessels and ships its ready products (concrete segments for wind towers) via inland vessel.
- All its internal logistics are geared to this transport chain
- A building materials trade requires the adjacent quay for its self-discharging ships: large quantities bulk goods (in particular stones as building materials) are handled here.

Further indirect obstacles arose in the course of the progressing planning:

- Difficult subsoil conditions. As the harbour is located in a historical river loop, the existing knowledge from previous construction projects can only be used to a limited extent and new, very costly subsoil investigations are necessary. The presence of explosive ordnance, which must first be detected, makes this even more difficult.
- Considerable landings in the area in front of the new (planned) quay. Here are considerable amounts of material with poor structural suitability.
- Little knowledge of the structural substance (cross-sections, design depths, etc.) of the adjacent structures

All listed obstacles could be minimized by very detailed research with the landlord and the neighbours, as well as in many meetings and discussions, in detail formulated inquiries and own researches and archives.

1.4 Port Users Requirements and phased Development

Several scenarios for the implementation of the project were developed from the very detailed requirement catalogues of the residents / users. The key point was always the phased development, in which the various users had to change their logistics chains step by step. In order to increase acceptance, an attempt was made at the same time to create improvements for the respective situation of the residents. Two alternatives were developed (Figure 3): Alternative 1 with a continuous new East Quay and Alternative 2 with a remaining small basin southeast.

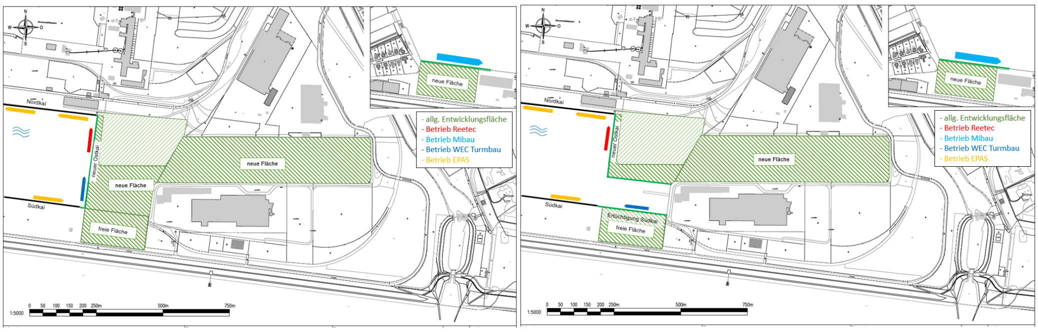

Figure 3 Basic Development Alternatives for Jarssum Basin: a) Alternative 1; b) Alternative 2b

The phased development then proceeds differently in both alterations, but is always based on the fundamental requirement to restrict users as little as possible. Since the measure is associated with very high investment costs and changes to the requirements can also occur over the implementation period, an attempt was made during the phased development to make the first steps as identical as possible for both alternatives: this means that it is possible to react to changed requirements at a later point in time.

1.5 Phased Backfilling of Basin

For the phased backfilling of the harbour basin two questions have to be solved: where does suitable material come from and how do I delimit the construction phases against each other?
Suitable material can basically be obtained from dredging measures in the Ems fairway. But there are also large quantities of soft silt in the harbour basin of the port of Emden that one would like to remove. Here, considerations are currently being made to fill this material, which is actually not suitable for construction purposes, into geosynthetic hoses. These then drain the soft silt and can then be used as boundaries for the respective construction phase (Figure . A decision in favour of a preferred solution currently depends on the knowledge of the subsoil.

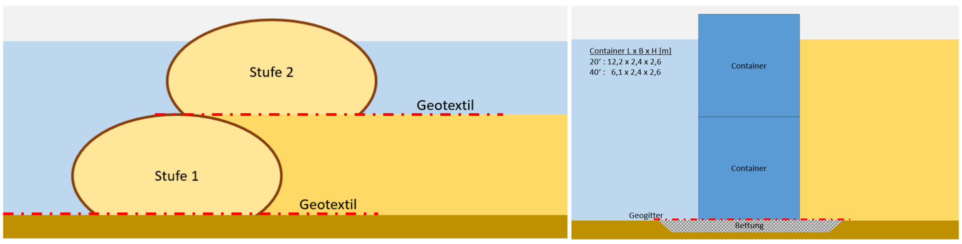

Figure 4 Alternatives for Reclamation Enclosure: a) Geotubes; b) filled Containers

1.6 Relocation of Bulk handling

The relocation of the bulk berth from the eastern south quay to the western south quay is a central component of the redesign. The bank wall must be reinforced or a dolphin berth built in order to allow self-discharging ships (Figure 5) to handle the cargo. A new bank wall was designed taking into account the unloading logistics and the maximisation of the storage areas (Figure 5).

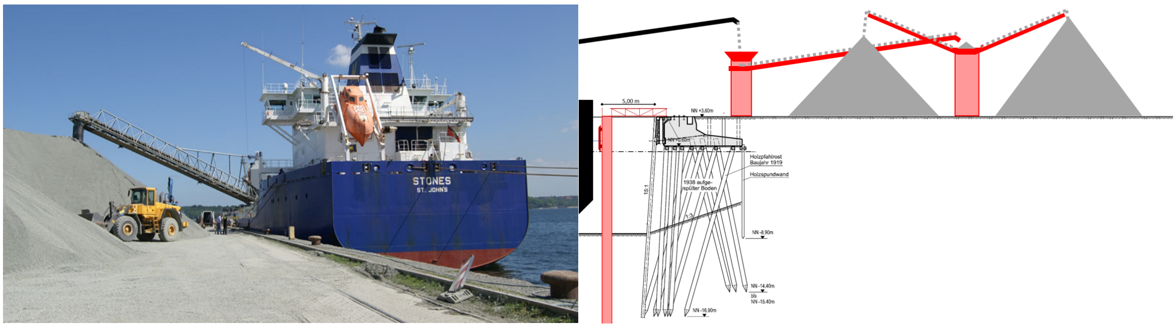

Figure 5 Bulk Handling: a) Current Situation; b) New Quay with Conveyor Belt System

1.7 Replacement Berths for Inland Vessels

Due to the fact that waiting berths for inland vessels were arranged in the Jarssum Basin, it became necessary to find replacement berths. In close consultation with the harbour captain, suitable nautical locations were identified and then concepts for these berths were designed according to the captains' wishes and requirements. Among other things, it is important that the accessibility on land is guaranteed. In this way, the inland vessels can put the private cars on land, make purchases and supply their ships.

2 ÜBERSEEHAFEN / PORT OF BREMEN

2.1 Background of Überseehafen (Overseas Port)

In the area of the so-called Überseehafen (Overseas Port) in Bremen, a new district of about 300 ha has been under construction for almost 20 years as a result of the abandonment of port use. The backfilling of a harbour basin initially created new open spaces on which living space and commercial use were created in the Überseestadt (Overseas City). The migration of some manufacturing companies and logistics companies has now freed up further space at the Überseeinsel (Overseas Island) for urban development. In this context, a number of questions have to be answered: adaptation of traffic development, protection of contaminated sites, and creation of a new flood protection system. But also the remaining port typical industries cause conflicts with the intended use to which answers have to be found.

2.2 Überseeinsel (Overseas Island)

The Overseas Island is a small part of the so-called Overseas City. In fact, it is a peninsula formed by a harbour basin in the north and the Weser in the south. On the overseas island there is a cereal factory, a shipyard, a rice mill and several logistics companies. The abandonment and sale of the cereal factory now opens up development opportunities on an area of around 41 hectares. The old factory site as part of the overseas island was purchased by a private investor who has agreed with the City of Bremen in a so-called "Urban Development Agreement" to combine the planning of the development on its 15 ha site with a large-scale development of the entire peninsula

2.3 Urban Framework Plan

The core of the project is the urban framework plan (Figure 7), in which the course for the future developments of the residential quarters, the traffic development, the open space planning, the energy concept and the mobility concept are presented. Restrictions such as ownership, contaminated sites, flood protection requirements, existing buildings and many other framework conditions are already taken into account. The benchmark for a framework plan is 1:2000.

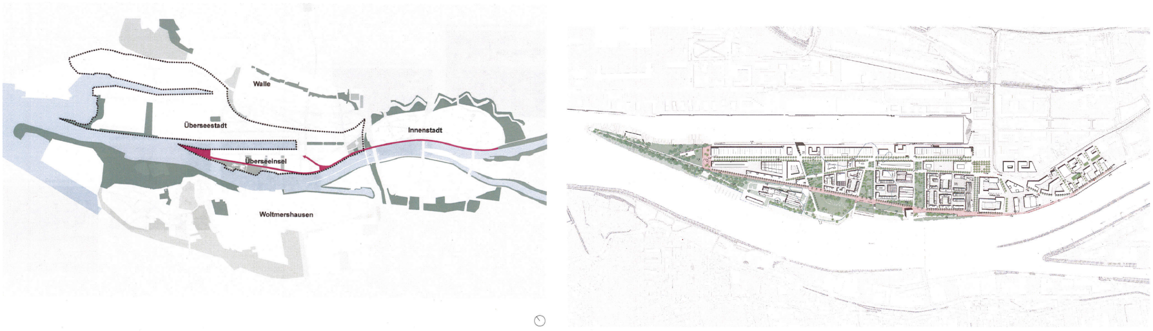

Figure 7 Überseeinsel: Context (©SMAQ); b) Open Space Planning (©MML)

2.4 New Living Quarters and Re-Use of existing Structures

On the site of the former cereal factory, a completely new district with buildings for services and apartments for families, students and old people will be built in the next 4 years. The investor consistently pursues alternative concepts; e.g. he does not want to allow individual traffic in the district, the energy supply is to be obtained entirely from wind and solar energy, etc.
The use of existing buildings is also planned. The intention is to turn a former silo into a hotel (Figure 8). An old warehouse will be converted into an alternative and eco-friendly shopping centre.

Figure 8 Überseeinsel: Living Quarter (©SMAQ); b) Visualisation Silo (©DMAA)

2.5 Flood Protection

The overseas island development area is largely at risk of flooding. For this reason, technical flood protection measures are planned. A so-called area protection is favoured, which consists of an externally circulating flood protection system. The latest findings of the IPCC were taken into account when determining the level of protection. In addition to a level of protection to be established at short notice, a second increase was also determined. All flood protection structures are to be planned in such a way that a later increase is technically possible without any problems (Figure 9).

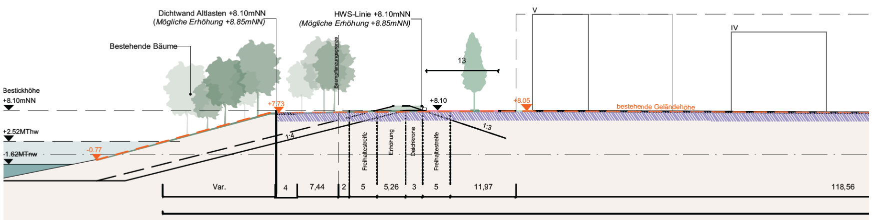

Figure 9 Überseeinsel: Example Cross Section of Flood Protection (© MML)

3 CONCLUSION

The development of port areas can take very different paths. If the development of a port facility is aimed at the consistent expansion of the port-related economy, then a large number of constructive engineering questions have to be dealt with in the planning. In the course of the conversion of port facilities and areas into urban living spaces - a task that is required in many river and port cities today - completely new tasks (unusual for port planners and coastal engineers) have to be handled.

SESSION 8 COASTAL ENGINEERING APPLICATIONS

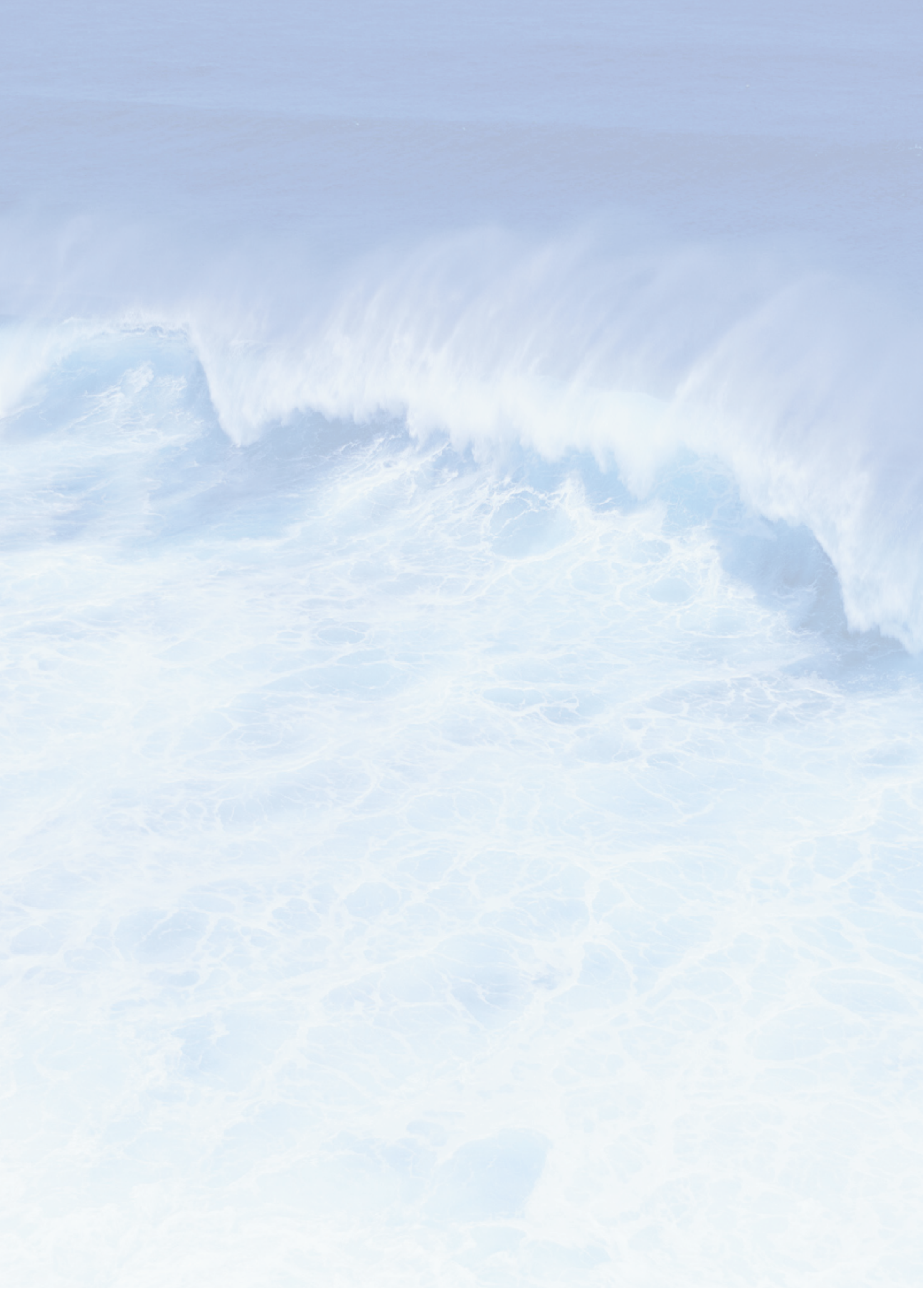

Anthropogenic impacts on the geomorphological regime of Preveza straits (Amvrakikos Gulf)

N. Georgiou[1*], E. Fakiris[1], D. Christodoulou[1], X. Dimas[1], C. Koutsikopoulos[2], G. Papatheodorou[1]
[1]Laboratory of Marine Geology and Physical Oceanography, University of Patras, 26 504, Greece
[2]Department of Biology, University of Patras, Rio, Patras,26 504, Greece
[*]Corresponding author: ngeorgiou@upatras.gr

Abstract

Amvrakikos Gulf is a hypoxic ecosystem prone to both physical and anthropogenic pressure. However, it is experiencing a series of anthropogenic interventions on- and off-shore, at the Preveza straits, where the oxygenation mechanism of the Gulf is taking place. Dredging, marine structures and other interventions, added further stress to the ecosystem thus resulting in the alteration of the hydrodynamic circulation, the geomorphological regime of the straits and the physicochemical properties of the Gulf. Intensive erosion deep scours are developed along the base of marine structures and at minimum cross sections. Hence, queries regarding the exploitation of the Gulf, the risk assessment and the sufficiency of regulations arise.

Keywords Scour holes, dredging - marine structures, ADCP - hydrodynamic circulation, Preveza straits - Amvrakikos.

1 INTRODUCTION

Amvrakikos Gulf is considered a one of a kind fjord-like, semi-enclosed Gulf (Ferentinos et al., 2010; Kountoura & Zacharias, 2014). It is a National Park surrounding large wetlands, located in the north-western Greece. Even though the Gulf is widely protected (Natura 2000, Ramsar Convention), degradation of the ecosystem's health has been observed during the last 20-30 years (Ferentinos et al., 2010; Naeher et al., 2012), leading to the development of a hypoxic-anoxic stagnant zone. The permanent vertical stratification of the water column, due to the two main rivers Louros and Aracthos, reduces vertical mixing, thus rendering the intruding Ionian Sea water masses the major oxygen provider (Kountoura & Zacharias, 2014). Connection between the Gulf and the Ionian Sea happens only through a narrow passage at the western part of the Gulf, the straits of Preveza, at a minimum cross section of 5.500 m^2 and a sill depth ranging from 10-12m depth (current survey). Preveza straits play a vital role in the viability of the Gulf since it simultaneously receives and releases almost the total amount of sea and brackish water respectively that exists in the Gulf. The brackish mass which outflows south towards the Ionian Sea, covers on average the upper 10m of the water column, while the sea water inflows to Amvrakikos Gulf below the brackish mass, occupying the rest of the water column. Maximum inflow and outflow velocities developed at the straits reach up to 125 cm/s, mainly close to the seafloor and/or at the surface of the water column (current survey, Figure 3iii). Preveza straits is a highly dynamic area which has been modified by a series of man-made constructions that started in late 30's and then in 70's and late 90's, in order to fit the needs of society. The shoreline was modified by the construction of the Preveza harbour which

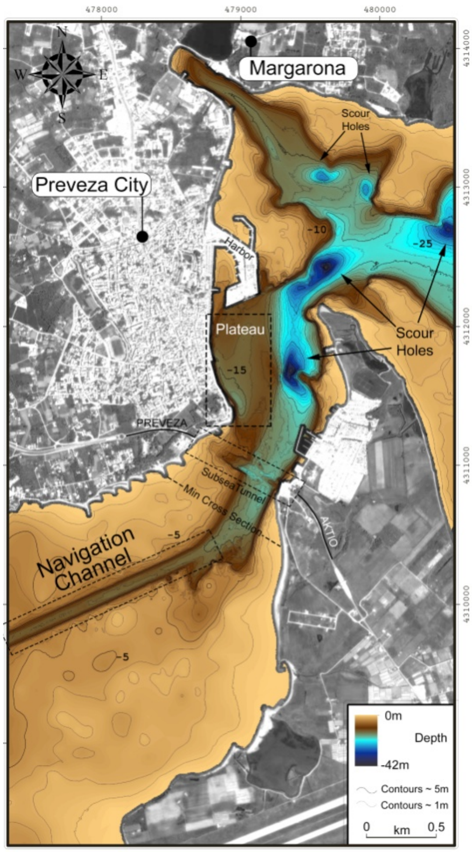

Figure 1 Bathymetric map of Preveza straits (multibeam data 2016)

reduced the minimum width of the straits to 450m. Moreover, an underwater tunnel of 910m length, that connects Aktio city with Preveza city, was constructed at 2002, while a navigation channel was dredged at the area of the sill. Additionally, the seafloor south of the harbour of Preveza was dredged, creating a bathymetric plateau of 14m average depth.

Human intervention, such as dredging or marine structures, altered the onshore & offshore geomorphology of the straits along with the hydrodynamic circulation mechanism. As observed by the geophysical data presented in the current study, these interventions provoked extensive erosion all along the submarine landscape and especially at the limits of the marine structures where intense scouring processes take place. Recently, great amounts of money have been expended in order to restore marine structures damaged by scouring (Summer, 2008). Viability of the constructions is highly questionable, thus the condition of the seafloor and the substrate of the area merits further investigation. In this study, data collected by using advanced geophysical equipment regarding the bathymetric and acoustic characteristics of the seabed as well as acoustic properties of the substrate, will be presented. Furthermore, properties of the water column such as current velocities and direction were acoustically mapped. The purpose of this paper is to present the impacts and risks provoked by human interventions at Preveza straits.

2 METHODOLOGY

During 2016 in the context of the EEA grants project: "Identification, consequences and management of the anoxic zone of Amvrakikos Gulf (NW Greece)", the seabed and the water column of the straits of Preveza were mapped in detail, using advanced geophysical equipment. A sub bottom profiler (SBP) (Geopulse Chirp) was used in order to map the substrate, an ELAC Nautik Seabeam 1185 multi-beam echo-sounder (MBES) and a dual frequency (100 & 400 kHz) side scan sonar (SSS) (Edgetech 4200) were used to map the bathymetry and morphology of the seabed, respectively. An ADCP (Acoustic Doppler Current Profiler-Teledyne Workhorse) was used for the velocity-direction-turbidity of the water column (hydrodynamics). In situ Troll 9500 multiparametric probe was used to measure temperature, salinity, DO (Diluted Oxygen) and turbidity. Finally, a tide gauge was installed at the main harbor of Preveza as well.

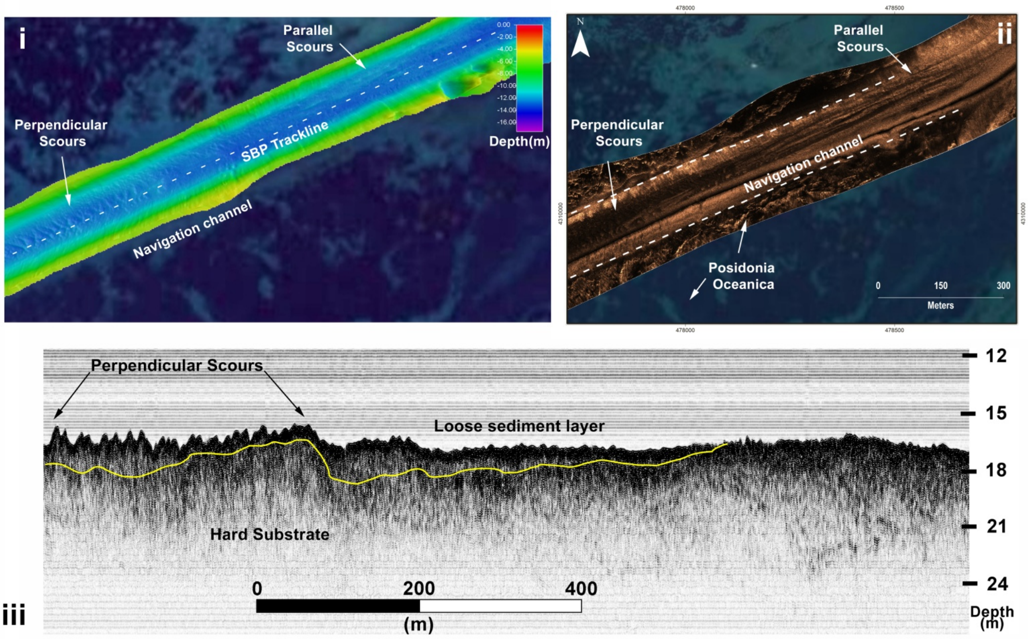

Figure 2i MBES map of the dredged navigation channel, 2ii. Acoustic backscatter and morphology of the seafloor, 2iii. Seismic profile of the substrate along the navigation channel.

3 RESULTS

The primary intervention was the dredging of the navigation channel at the entrance of the Gulf (Figure 1), where a dense P. oceanica field is apparent. The depth before all the dredging phases, based on the bathymetric map of the British navy (1830, provided by the Actia Nicopolis Foundation) and the Hellenic Navy Hydrographic Service maps (HNHS) was at -4m. At present, it has an average depth starting from 10-12m minimum depth, width of 100m and length of at least 2km (Figure 2i, ii). The seabed of the channel is characterized by medium to high backscatter intensity while higher intensities represent major erosion effect. Sinuous, asymmetrical scours, perpendicular to the channel suggest a NE flow direction. These scours are succeeded by linear scours of higher backscatter intensity which may have been formed by the bottom current activity or by the dredging itself. The scours' direction agrees with the current flow, as measured by the ADCP. The average velocity of the bottom currents inside the navigation channel is 60 cm/s. The seismic profiles showed the existence of hard substrate, with the presence of an overlying acoustically transparent thin layer of sediment. The penetration of the SBP at this area is limited due to the presence of sand on the seabed and by the dredging activity (Figure 2iii). The surrounding area is covered by an extended P. oceanica field with a maximum depth of -4m.

Further to the north the channel widens, deepens and trends more to the east where maximum depth of -16m is observed. This is the part of the entrance where the 5.500 m^2 minimum cross-sectional area is located (Figure 1). The channel is disrupted by the presence of the subsea tunnel that connects the city of Preveza with Aktio, since 2002 (Figure 3i).

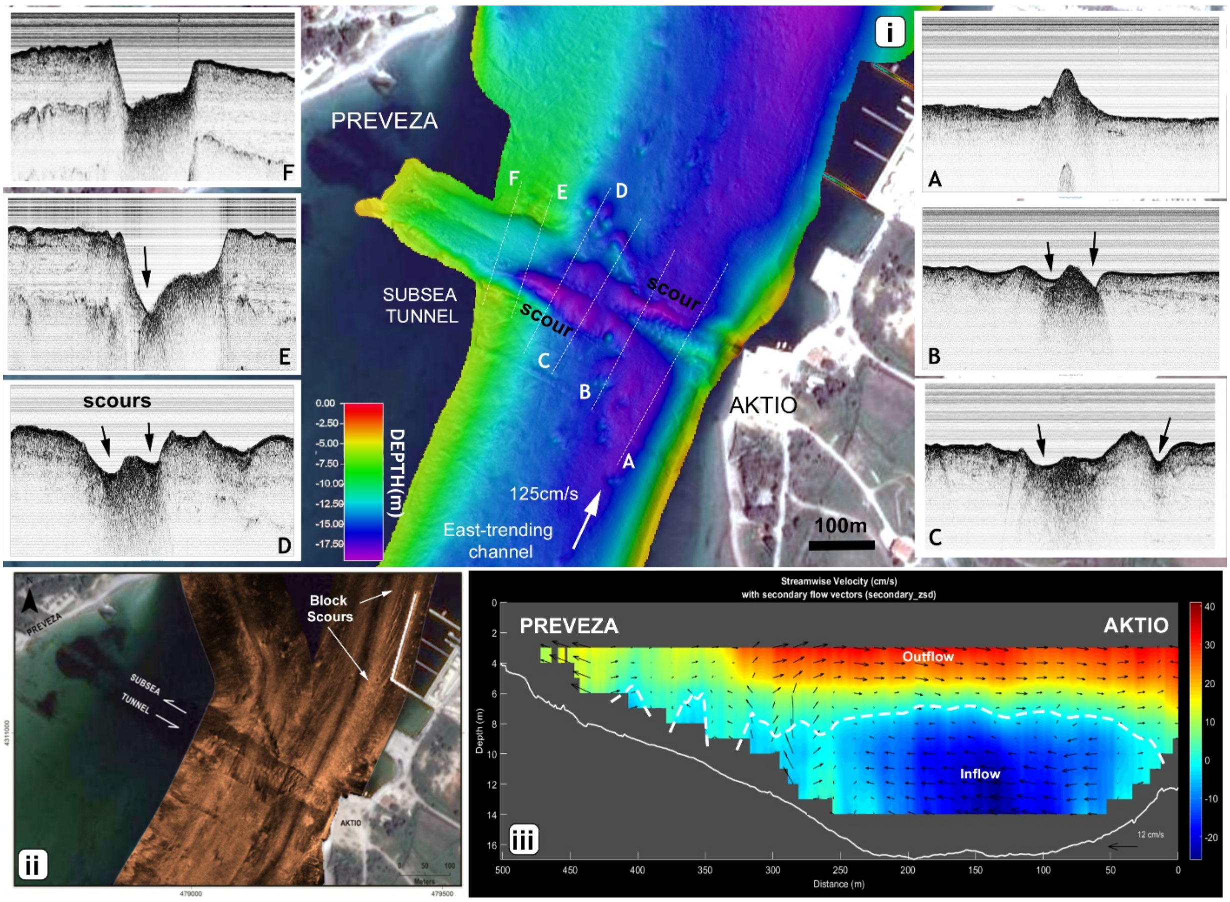

Figure 3i MBES bathymetric map of the subsea tunnel (Preveza-Aktio), 3i.(a,b,c,d,e,f): seismic profiles perpendicular to the tunnel showing the erosion at both sides of the structure, 3ii. Acoustic backscatter of the seafloor, 3iii. Hydrodynamic circulation along the whole extent of the tunnel. Colors represent the primary velocities (in cm/s): blue to light blue (negative values) serve as the inflow of the seawater into the Gulf and green to red colors (positive values) is the brackish mass outflowing to the Ionian Sea. Black arrows: secondary flows of the currents, Dashed white line: interface between the inflow and outflow.

The submarine landscape is widely affected by the dredging activities during its construction, especially at the Preveza landing. Along both sides of the tunnel, erosional scours of 8m maximum height and 50m width, appear (Figure 3i. B, C, D, E). Close to the coast of Aktio the subsea tunnel is outcropping from the sea bottom about 6m (Figure 3i.A) and appears to be heavily grazed by the bottom current activity which reaches its maximum velocity of 125cm/s, as observed by the ADCP cross section along the subsea tunnel (Figure 3iii). The bottom inflowing mass shows that the primary currents move towards the NNE while secondary flows (black arrows, Figure 3iii) advance along the subsea tunnel, resulting in the creation of the scours. Due to the heavy erosion the seabed presents high backscatter intensity, all along this part of the channel. Erosion is also noticeable close to the floating docks which are anchored to the seabed with cemented blocks. The cemented blocks (height: 0.5m, width 5m) create scours of 30-50m length and at least 5m width (Figure 3ii). Areas of medium to low backscatter intensity are present especially close to the Preveza landing where the erosion effect is diminished, and part of the tunnel landing is buried under the sediments.

The central part of the straits is highly affected by a series of technical constructions (Figure 4). A bathymetric barrier separates the central part of the straits, into the west bathymetric plateau and the east erosional channel. The bathymetric plateau was originally dredged for operational purposes and currently has maximum depth of -17m. It is exposed to erosion, based on the erosional features revealed on the bathymetric plateau and the toe of waterfront of Preveza city (Figure 4ii). Linear scour of 2,5m height and 20m width was also observed along the toe of Preveza's harbor. As witnessed by the ADCP, the erosion along the harbor and waterfront were created by the outflowing brackish water which flows parallel to the coastline (Lin et al., 2015). The brackish mass heads south to the Ionian Sea and develops an average speed of 60cm/s, with bursts of 125cm/s.

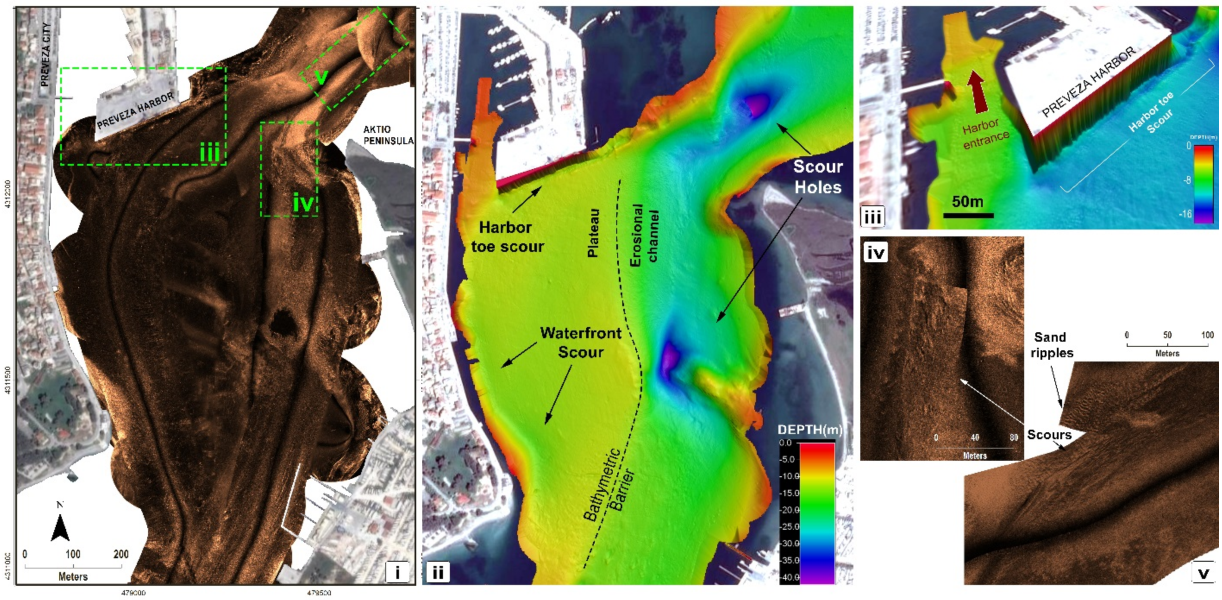

Figure 4i Acoustic backscatter map of the seafloor at Preveza straits, 4ii. Bathymetric map, 4iii.3d bathymetry of Preveza's harbor, showing the scour formed along the toe of the harbor, 4iv-v. Typical erosion features between the Preveza harbor and Aktio peninsula (see 4i for the exact location).

The eastern part of the straits is severely eroded by the sea water bottom inflow that has created three successive deep scour holes which tend to merge. The depth is -42m on average, while the dimensions are ranging from 400-450m length, 160-300m width and inclination range from 10-20 degrees. Based on the acoustic data, these deep scour holes geometry is mainly controlled by the morphology of the hard substrate, while they are formed where the cross-sectional area is diminished and current velocity is increased (Stigebrandt, 2012). Moreover, these scour holes form where the bottom currents meet an obstacle. Turbulence created by the obstacle, increases the load regionally and overcomes the seabed's threshold, resulting in the scour formation (Briaud et al., 1999; Zuylen, 2015). The substrate of the central part of the straits is characterized by the presence of two seismic units (Figure 5). The top unit (Unit A), which is mainly eroded, consists of successive, parallel, semi-continuous reflectors that represent a loose sedimentary unit. The bottom unit (Unit B) consists of a single discontinuous, abnormal, partly enhanced reflector which depicts the acoustic bedrock of the area and delimits the growth in extent, of the scour holes.

4 DISCUSSION & CONCLUSIONS

Erosion effect at the seafloor of the straits initially began when the sea level exceeded the bathymetric barrier of the sill (-4m) and the sea water entered the Gulf. The most decisive of the interventions that altered the geomorphology and hydrodynamics of the straits was the dredging of the navigation channel. The sill's deepening allowed greater amounts of sea water to enter the Gulf, hence greater current velocities were developed. Consequence of the dredging was the intensification of the erosion regime, which provoked the expansion and grazing of the pre-existing scour holes. Similar but less deep scour holes were observed in the Rhine Meuse delta, due to heterogeneous substrate formations (Huismans, Velzen, Mahoney, Hoffmans, & Wiersma, 2013) and at the toe of a breakwater built in the Mailiao harbor, provoked by wave induced current velocity of 100cm/s (Lin et al., 2015). Construction of the Preveza harbor diminished the cross-sectional area by 350m, although it didn't directly affect the hydrodynamic circulation, since it was originally built on a shallow bathymetric plateau. However, a significant scour is created at the harbor's toe, as well as along the Preveza waterfront. The subsea tunnel constructed perpendicular to the bottom inflow, is exposed to major hydrodynamic forces especially at the eastern side (Aktio) and as a result, significant scours are formed along both sides of the tunnel. These scours function as a load effect on the infrastructure and endanger the viability of the construction. Marine structures (Preveza harbor, tunnel) added further pressure and complexity to the hydrodynamic system, forcing thus the water mass to erode the seafloor. An issue that arises from the present study is the influence of human interventions on dynamic ecosystems. It should be noted that any human intervention planned to be implemented in so sensitive ecosystems should be thoroughly examined first through a detailed geophysical and physicochemical survey. Either wise crucial repercussions for the viability of the marine structures as well as ecosystem health and human lives, emerges. Questions regarding the condition of the marine structures and the current erosion degree remain.

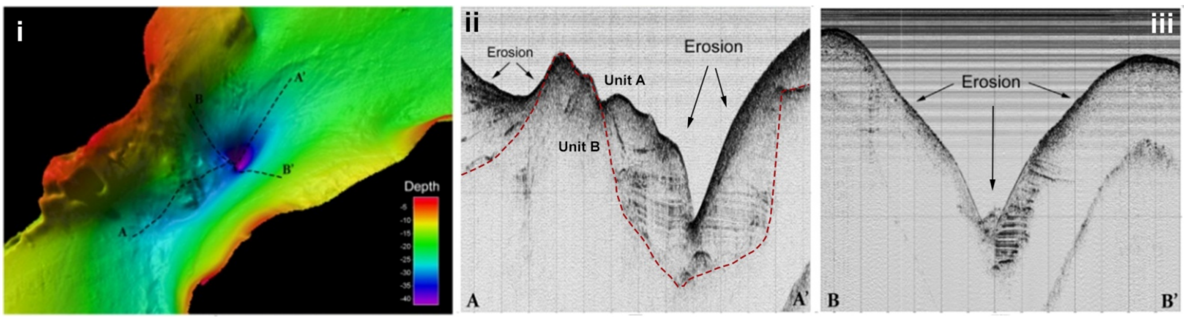

Figure 5i Typical 3d bathymetric image of the deep scour holes. AA', BB' sections are seismic profiles shown in figs 5ii & 5iii respectively, showing the interrupted stratigraphy by the intense erosion. Unit A: eroded loose sediment unit and Unit B: hard substrate.

References

Briaud, J.L., Ting, F., Chen, H.C., Gudavalli, R., Perugu, S., Wei, G. (1999) SRICOS: prediction of scour rate in cohesive soils at bridge piers. Journal of Geotechnical and Geoenvironmental Engineering, 125 (4), pp. 237-246.

Ferentinos, G., Papatheodorou, G., Geraga, M., Iatrou, M., Fakiris, E., Christodoulou, D., … Koutsikopoulos, C. (2010) Fjord water circulation patterns and dysoxic/anoxic conditions in a Mediterranean semi-enclosed embayment in the Amvrakikos Gulf, Greece. Estuarine, Coastal and Shelf Science, 88(4), 473–481. https://doi.org/10.1016/j.ecss.2010.05.006.

Huismans, Y., Velzen, G. Van, Mahoney, T. S. D. O., Hoffmans, G. J. C. M., & Wiersma, A. P. (2013) Scour hole development in river beds with mixed sand-clay-peat stratigraphy.

Kountoura, K., & Zacharias, I. (2014) Annual hypoxia dynamics in a semi-enclosed Mediterranean Gulf. Journal of Marine Systems, 139, 320–331. https://doi.org/10.1016/j.jmarsys.2014.07.007.

Lin, I., Tseng, I., Lee, C., & Chen, G. (2015) Seabed scour around a breakwater a case study in mailiao harbor, 23(6), 846–854.https://doi.org/10.6119/JMST-015-0610-1.

Naeher, S., Geraga, M., Papatheodorou, G., Ferentinos, G., Kaberi, H., & Schubert, C. J. (2012) Environmental variations in a semi-enclosed embayment (Amvrakikos Gulf, Greece) - Reconstructions based on benthic foraminifera abundance and lipid biomarker pattern. Biogeosciences, 9(12), 5081–5094. https://doi.org/10.5194/bg-9-5081-2012.

Stigebrandt, A. (2012) Hydrodynamics and Circulation of Fjords. In L. Bengtsson, R. W. Herschy, & R. W. Fairbridge (Eds.), Encyclopedia of Lakes and Reservoirs (pp. 327–344). Dordrecht: Springer Netherlands. https://doi.org/10.1007/978-1-4020-4410-6_247.

Summer, B. M. (2008) Coastal and offshore scour / erosion issues – recent advances, 85–94.

Van Zuylen, J.A (2015) (http://resolver.tudelft.nl/uuid:0f5d8709-9450-420b-99ec-fa9a44346309).

Μελέτη προστασίας και ανάπλασης της ακτής στον Άγιο Τύχωνα Λεμεσού. Βελτιστοποίηση διατάξεων έργων με μαθηματική προσομοίωση & πρώτα αποτελέσματα απόκρισης της ακτής μετά την κατασκευή των έργων

Χ.Δ. Σολομωνίδης[1*], Α.Δ. Τουμαζής[2], Α.Μ. Μπουτάτης[1], Μ.Κ. Χονδρός[3], Ε.Ν. Κυπραίου[1]

[1]Ρογκάν & Συνεργάτες, Βαλέττα 9, Τ.Κ. 15771 Αθήνα, Ελλάδα
[2]Διον. Τουμαζής & Συνεργάτες, Ρωμανού 4, Τ.Κ. 1070 Λευκωσία, Κύπρος
[3]Εργαστήριο Λιμενικών Έργων, ΕΜΠ, Τ.Κ. 15773 Αθήνα, Ελλάδα
[*]Υπεύθυνος επικοινωνίας: csolomonidis@roganassoc.gr

Περίληψη

Η παρούσα εργασία, αφορά στην προστασία και ανάπλαση του ανατολικού παράκτιου μετώπου της κοινότητας Αγίου Τύχωνα, της επαρχίας Λεμεσού, στις νότιες ακτές της Νήσου Κύπρου. Η περιοχή αυτή προσβάλλεται από σφοδρούς κυματισμούς του Νότιου-Νοτιοδυτικού Τομέα οι οποίοι έχουν προκαλέσει διάβρωση σε ορισμένα τμήματα του παράκτιου μετώπου. Αντικείμενο της παρούσας εργασίας είναι η διερεύνηση με μαθηματικά ομοιώματα της κυματικής διαταραχής, της παράκτιας υδροδυναμικής κυκλοφορίας και των τάσεων παράκτιας στερεομεταφοράς (μεταφοράς ιζήματος) στην υπό μελέτη ακτή αλλά και στις παρακείμενες ακτές. Στόχος της μελέτης είναι η ακτομηχανική διερεύνηση εναλλακτικών λύσεων έργων προστασίας της ακτής, η βελτιστοποίηση της διάταξης και της γεωμετρίας των παραπάνω εναλλακτικών διατάξεων και η ελαχιστοποίηση των επιπτώσεων στις παρακείμενες ακτές εκατέρωθεν της περιοχής μελέτης. Η βέλτιστη διάταξη προέκυψε μετά από σύγκριση των αποτελεσμάτων των μαθηματικών μοντέλων για κάθε ένα από τα εναλλακτικά σενάρια, συμπεριλαμβανομένου αυτού της υφιστάμενης κατάστασης. Τέλος, παρουσιάζεται η απόκριση της ακτής έμπροσθεν του ξενοδοχείου Halcyon μετά την κατασκευή των προτεινόμενων έργων, η οποία έχει ολοκληρωθεί.

Λέξεις κλειδιά Μαθηματική προσομοίωση, κυματοθραύστες, απόκριση ακτής.

1 ΕΙΣΑΓΩΓΗ

Το παραλιακό μέτωπο Λεμεσού από το ομώνυμο λιμάνι μέχρι την Μονή είναι σχεδόν εξολοκλήρου τεχνητό, αποτελούμενο από λιμενικά έργα, θωρακίσεις/ επιχώσεις, αποσπασμένους κυματοθραύστες, προβόλους, αποβάθρες. Ενώ αρχικά το παραλιακό μέτωπο της πόλης ήταν υποβαθμισμένο τα τελευταία χρόνια αποτελεί πόλο έλξης τόσον ντόπιων όσο και ξένων επισκεπτών.

Τα μελετητικά γραφεία Ρογκάν & Συνεργάτες Α.Ε. και Διονύσιος Τουμαζής και Συνεργάτες εκπόνησαν την μελέτη προστασίας και ανάπλασης του ανατολικού παράκτιου μετώπου της κοινότητας Αγίου Τύχωνα

Στα πλαίσια επίτευξης των στόχων/της μελέτης, καταστρώθηκαν και διερευνήθηκαν διεξοδικά τρία (3) εναλλακτικά σενάρια τα οποία περιλαμβάνουν διαφορετικές διατάξεις και τύπους έργων. Την ακτομηχανική διερεύνηση ακολούθησε η Μελέτη Εκτίμησης των Επιπτώσεων στο Περιβάλλον (ΜΕΕΠ) κατά την οποία εξετάστηκαν οι επιπτώσεις των εναλλακτικών σεναρίων έργων στο περιβάλλον τόσο κατά τη διάρκεια κατασκευής όσο και κατά τη διάρκεια λειτουργίας τους. Η τελικώς επιλεγείσα λύση αφορά την κατασκευή τεσσάρων (4) αποσπασμένων παράλληλων κυματοθραυστών.

2 ΠΕΡΙΓΡΑΦΗ ΤΗΣ ΠΕΡΙΟΧΗΣ ΜΕΛΕΤΗΣ ΚΑΙ ΠΡΟΒΛΗΜΑΤΑ ΠΑΡΑΚΤΙΑΣ ΖΩΝΗΣ ΠΡΙΝ ΤΗΝ ΚΑΤΑΣΚΕΥΗ ΤΩΝ ΕΡΓΩΝ

Η υπό μελέτη περιοχή βρίσκεται στις νότιες ακτές της νήσου Κύπρου, ανατολικά της Λεμεσού στην περιοχή Αγίου Τύχωνα, νότια του Πύργου. Η γενική κατεύθυνση της ακτογραμμής είναι από Α προς Δ. Όπως φαίνεται στην Εικόνα 1, ανατολικά οριοθετείται από την Μαρίνα του Αγ. Ραφαήλ, και δυτικά από την περιοχή του αρχαίου Λιμένα Αμαθούντας. Το συνολικό μήκος της εξεταζόμενης ακτής είναι περίπου 2.5 χλμ. Το ίζημα της περιοχής είναι γενικά λεπτόκοκκο, ενώ σε κάποιες περιοχές εμφανίζεται χονδρόκκοκη άμμος και κροκάλες. Ανατολικά της περιοχής μελέτης υφίστανται δυο ύφαλοι αναβαθμοί, ανατολικότερα αυτών υπάρχουν έξαλοι πρόβολοι προστασίας της ακτής. Στο ανατολικό πέρας της παρακείμενης ακτής, στην περιοχή της μαρίνας φιλοξενίας σκαφών αναψυχής του Αγίου Ραφαήλ, υπάρχει μεγάλη απόθεση ιζήματος εκατέρωθεν της μαρίνας, ιδίως όμως δυτικά αυτής. Η συγκεκριμένη εξέλιξη της ακτογραμμής υποδεικνύει ότι υπάρχει σημαντική στερεομεταφορά κατά μήκος της ακτής με κατεύθυνση από Δύση προς Ανατολή. Όπως φαίνεται στην Εικόνα 2, στο μεγαλύτερο μήκος της παραλίας το εύρος και η ποιότητα αυτής έχουν υποβαθμιστεί. Επιπλέον, σε ορισμένες περιοχές έχουν παρατηρηθεί διαβρωτικές τάσεις οι οποίες εξαρτώνται άμεσα και από την γωνία προσπτώσεως των εισερχόμενων κυματισμών. Τοπικά η διάβρωση προσεγγίζει μέχρι και τα 8m. Συνεπώς, η επίτευξη κυματικής ηρεμίας στην παραλία είναι βαρύνουσας σημασίας αφενός για να είναι προσιτή στους λουόμενους το μεγαλύτερο διάστημα του χρόνου και αφετέρου να προστατεύεται η ακτή από τη διάβρωση.

(a) (b)

Εικόνα 1 (a) Η περιοχή μελέτης (Πηγή: Google Earth), (b) Η αμμώδης ακτή στο ανατολικό τμήμα της περιοχής μελέτης, υφίσταται σημαντική διάβρωση

Εικόνα 2 Εξέλιξη της ακτογραμμής από το 1963 έως το 2008. Με χρώμα ροζ παρουσιάζονται οι περιοχές διάβρωσης ενώ με γαλάζιο οι περιοχές απόθεσης (Τμήμα Κτηματολογίου και Χωρομετρίας 2016)

2.1 Κυματικό Κλίμα στα Ανοιχτά της Περιοχής Μελέτης

Το κυματικό κλίμα της περιοχής μελέτης βασίστηκε στα κυματικά δεδομένα κοντά στην παράκτια περιοχή μελέτης (παρατηρήσεις κυματικών χαρακτηριστικών στην ισοβαθή των -20μ στην περιοχή της Μονής Μαρίνας), που παρουσιάζονται στην τεχνική έκθεση με τίτλο «Coastal Zone Management for Cyprus: Nearshore Wave Climate Analysis by Xenia Loizidou and John Dekker» (Delft Hydraulics, 1994).

Οι κυματισμοί Νότιου-Νοτιοδυτικού Τομέα (210^{o}N), είναι οι συχνότεροι και ισχυρότεροι ενώ η παραλία, στο σύνολό της, είναι εκτεθειμένη στους σφοδρούς προσπίπτοντες κυματισμούς Νότιας (180^{o}N) κατευθύνσεως αλλά και σε άλλες κατευθύνσεις (120^{o}N, 150^{o}N, 240^{o}N). Στον Πίνακα 1 παρουσιάζονται τα κυματικά δεδομένα εισόδου στα μαθηματικά μοντέλα.

Πίνακας 1 Κυματικές συνθήκες εισόδου στα μαθηματικά μοντέλα.

Dir (^{o}N)	0.75-1.75			1.75-2.75			2.75-3.75			3.75-4.75		
	H_s	T_p	f	H_s	T_p	f	H_s	T_p	f	H_s	T_p	f
120	1.25	5.03	3.5	2.25	6.75	0.26						
150	1.25	5.03	1.95	2.25	6.75	0.16						
180	1.25	5.03	2.4	2.25	6.75	0.38	3.25	8.11	0.04	4.25	9.28	0.01
210	1.25	5.03	5.03	2.25	6.75	0.37	3.25	8.11	0.01	4.25	9.28	0.01
240	1.25	5.03	2.24	2.25	6.75	0.02						

Σύνολο:	15.12	1.19	0.05	0.02

3 ΜΑΘΗΜΑΤΙΚΗ ΠΡΟΣΟΜΟΙΩΣΗ ΚΥΜΑΤΙΚΩΝ ΚΑΙ ΥΔΡΟΔΥΝΑΜΙΚΩΝ ΣΥΝΘΗΚΩΝ

3.1 Βυθομετρικό Υπόβαθρο

Για τη διερεύνηση των διεργασιών στην παράκτια ζώνη έγινε αρχικά η κατασκευή ενός δομημένου, ορθογωνικού αριθμητικού καννάβου, που να αντιπροσωπεύει τη βαθυμετρία της περιοχής μελέτης. Τα δεδομένα βυθομετρικής αποτύπωσης λήφθηκαν από το Τμήμα Κτηματολογίου και Χωρομετρίας της Κυπριακής Δημοκρατίας σε ψηφιακή μορφή. Το βυθομετρικό υπόβαθρο της ευρύτερης περιοχής της παραλίας καλύπτει μια περιοχή 2 x 3,4 km, και έχει χωρικό βήμα Δx = Δy = 2,5m τόσο για τη βαθυμετρία του σεναρίου μηδενικής λύσης, όσο και για τη βαθυμετρία κάθε εναλλακτικής λύσης η οποία συμπεριλαμβάνει και τα αντίστοιχα έργα.

3.2 Μοντέλο Μετασχηματισμού Κυμάτων

Για την μεταφορά του κυματικού κλίματος στην παράκτια ζώνη χρησιμοποιήθηκε το μοντέλο MIKE 21 PMS (D.H.I. 2017),. Το μοντέλο περιγράφει την διάδοση των κυματισμών στις παράκτιες περιοχές, λαμβάνοντας υπόψη τα φαινόμενα της διαθλάσεως, περιθλάσεως και της ρηχώσεως λόγω μεταβολής της βαθυμετρίας, και την απώλεια ενέργειας, λόγω τριβής βυθού και θραύσεως των κυματισμών.

3.3 Υδροδυναμικό Μοντέλο

Για κάθε κυματικό πεδίο, προσδιορίστηκε με την χρήση δισδιάστατου υδροδυναμικού μοντέλου MIKE 21 HD (D.H.I. 2017) που αναπτύχθηκε από το Danish Hydraulic Institute, το ανυσματικό πεδίο ταχυτήτων των κυματογενών ρευμάτων. Το μοντέλο υπολογίζει την κυματογενή κυκλοφορία την οφειλόμενη τόσο στην θραύση των κυματισμών όσο και σε τυχόν υπάρχοντα ρεύματα, στη δράση του ανέμου.

3.4 Μοντέλο Στερεομεταφοράς

Στη βάση της κυματογενούς κυκλοφορίας που υπολογίσθηκε στο προηγούμενο βήμα, θα προσδιορισθεί με το μαθηματικό μοντέλο MIKE 21 ST (D.H.I. 2017), που αναπτύχθηκε από το Danish Hydraulic Institute (D.H.I.), ο ρυθμός στερεομεταφοράς, αλλά και ο αρχικός ρυθμός διαβρώσεως ή εναποθέσεως ιζήματος, σε κάθε σημείο του δισδιάστατου κανάβου της περιοχής ενδιαφέροντος. Επίσης υπολογίζεται ο ρυθμός μεταβολής της βαθυμετρίας.

4 ΠΕΡΙΓΡΑΦΗ ΕΝΑΛΛΑΚΤΙΚΩΝ ΛΥΣΕΩΝ/ ΣΕΝΑΡΙΩΝ

Κατά τη διάρκεια εκπόνησης της παρούσας μελέτης -πέραν του σεναρίου μηδενικής λύσης (DN)- προσομοιώθηκαν συνολικά οχτώ (8) εναλλακτικά σενάρια τα οποία περιλάμβαναν διαφορετικές διατάξεις και τύπους έργων (προβόλους, συστήματα αποσπασμένων κ/θ, τεχνητή αναπλήρωση ακτής). Τα τρία επικρατέστερα, εξετάστηκαν διεξοδικότερα και περιγράφονται και παρουσιάζονται στην παρούσα εργασία.

<u>Εναλλακτική διάταξη έργων «W1»:</u> Στην διάταξη αυτή εξετάζονται: Τρείς (3) αποσπασμένοι κ/θ με μήκος στην ίσαλο 125μ, μήκος ανοίγματος μεταξύ τους 50μ και υψόμετρο στέψης +0.50μ. Η απόστασή τους από την υφιστάμενη ακτογραμμή είναι ίση με 175μ. Τεχνητή αναπλήρωση ακτής σε πλάτος περίπου 20μ και μήκος περίπου 400μ και ανακατασκευή υφιστάμενου δυτικού προβόλου μήκους 40μ.

<u>Εναλακτική διάταξη έργων «W2»:</u> Στην διάταξη αυτή εξετάζονται: Τρείς (3) αποσπασμένοι ύφαλοι κυματοθραύστες με τα χαρακτηριστικά που περιγράφονται και στην εναλλακτική W1. Τεχνητή αναπλήρωση ακτής πλάτους περίπου 20μ και μήκους περίπου 400μ και ανακατασκευή υφιστάμενου δυτικού προβόλου μήκους 40μ.

<u>Εναλλακτική διάταξη έργων «W3»</u>: Στην διάταξη αυτή εξετάζονται: Τέσσερις (4) αποσπασμένοι έξαλοι κ/θ με μήκος στην ίσαλο 105μ, μήκος ανοίγματος μεταξύ τους 45μ και υψόμετρο στέψης +0.50μ. Η απόστασή τους από την υφιστάμενη ακτογραμμή είναι ίση με 130μ. Τεχνητή αναπλήρωση ακτής πλάτους περίπου 10μ και μήκους περίπου 400μ.

5 ΑΠΟΤΕΛΕΣΜΑΤΑ ΠΡΟΣΟΜΟΙΩΣΕΩΝ ΚΑΙ ΤΕΛΙΚΩΣ ΕΠΙΛΕΓΕΙΣΑ ΛΥΣΗ

Από την Ανάλυση της Υφιστάμενης Καταστάσεως διαπιστώθηκε ότι:

- Η παραλία προσβάλλεται από σφοδρούς κυματισμούς του Νότιου – Νοτιοδυτικού Τομέα, οι οποίοι προκαλούν έντονη κυματική διαταραχή σε όλη την περιοχή μελέτης.
- Στην περιοχή των υφάλων ερειπίων του αρχαίου λιμένα Αμαθούντας δημιουργούνται έντονα κυματογενή ρεύματα, κυρίως από τους κυματισμούς νοτιοδυτικής κατευθύνσεως. Αντίστοιχα, το μεγαλύτερο δυναμικό στερεομεταφοράς προκύπτει από την κυματογενή κυκλοφορία που προκαλούν οι Νοτιοδυτικοί κυματισμοί.
- Διαπιστώνονται εναλλασσόμενες τάσεις για διάβρωση και απόθεση στο μεγαλύτερο μέρος της ακτής. Επικρατέστερες είναι οι τάσεις για διάβρωση στο ανατολικότερο τμήμα της ακτής έως και 350μ δυτικά αυτού.

Από την Διερεύνηση Εναλλακτικών Διατάξεων Έργων διαπιστώθηκε ότι:

- Οι διατάξεις οι οποίες προσφέρουν σε μεγαλύτερο βαθμό κυματική ηρεμία για τους κυρίαρχους κυματισμούς είναι οι W1 και W3 δηλαδή οι διατάξεις εξάλων κυματοθραυστών.
- Στην σκιά των κυματοθραυστών επιτυγχάνεται ενίσχυση των τάσεων για απόθεση ιζήματος πίσω από τον άξονα καθενός και για διάβρωση στην περιοχή των διακένων. Συνεπώς όσο μικρότερα είναι τα διάκενα, τόσο μικρότερες οι τάσεις για διάβρωση.
- Οι έξαλοι κυματοθραύστες είναι αποτελεσματικότεροι στην επίτευξη τάσεων αποθέσεως.
- Οι υφιστάμενοι πρόβολοι δυτικά των προτεινομένων κυματοθραυστών καθώς και οι υφιστάμενοι ύφαλοι αναβαθμοί στο ανατολικό τμήμα της περιοχής μελέτης περιορίζουν στο ελάχιστο δυνατό την επιρροή των κυματοθραυστών στις παρακείμενες ακτές.
- Η εναλλακτική διάταξη W3 επιτυγχάνει τις ισχυρότερες τάσεις αποθέσεως άμμου (ή/ και διατηρήσεως φερτής άμμου) στην παραλία ενδιαφέροντος.
- Ενδεικτικά στην Εικόνα 3 παρουσιάζονται τα αποτελέσματα του μοντέλου όσο αφορά τη μέση ετήσια δυνητική μεταβολή στάθμης πυθμένα για όλες τις εναλλακτικές διατάξεις.

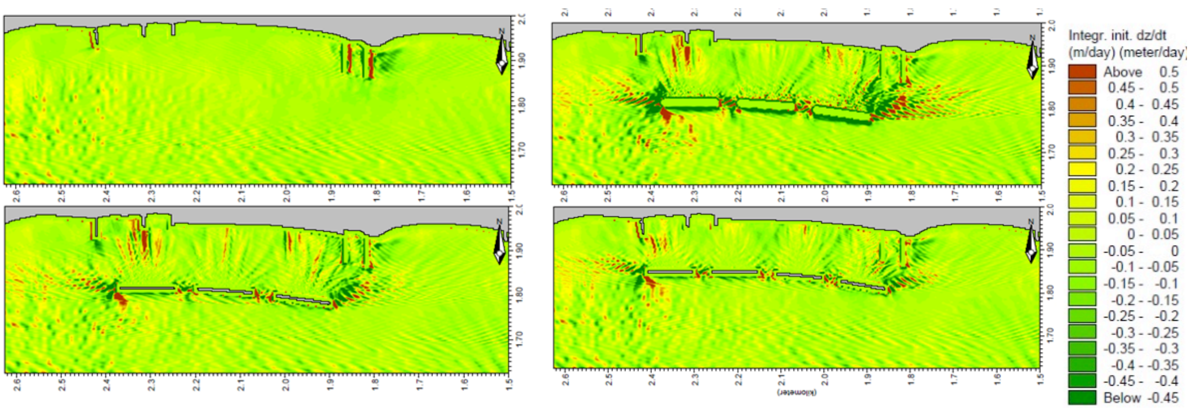

Εικόνα 3 Σύγκριση μέσης ετήσιας δυνητικής μεταβολής στάθμης πυθμένα για τις εναλλακτικές DN (πάνω αριστερά), W1(κάτω αριστερά), W2 (πάνω δεξιά) και W3 (κάτω δεξιά)

6 ΣΥΜΠΕΡΑΣΜΑΤΑ ΑΚΤΟΜΗΧΑΝΙΚΗΣ ΔΙΕΡΕΥΝΗΣΗΣ

Διαπιστώνεται ότι όλες οι εξετασθείσες διατάξεις επιτυγχάνουν σε κάποιο βαθμό την ισχυροποίηση των τάσεων αποθέσεως της άμμου στην παραλία μεταξύ αλλά η πλέον επιτυχής διάταξη θεωρείται η εναλλακτική διάταξη W3. Παράλληλα, όπως προέκυψε από την ΜΕΕΠ, η τελική πρόταση που διαμορφώθηκε που μεγιστοποιεί τις θετικές επιπτώσεις στο περιβάλλον ελαχιστοποιώντας τις δυνητικές αρνητικές επιπτώσεις

7 ΕΠΙΔΡΑΣΗ ΤΩΝ ΕΡΓΩΝ ΣΤΗΝ ΜΟΡΦΟΛΟΓΙΑ ΤΗΣ ΑΚΤΗΣ ΜΕΤΑ ΤΗΝ ΚΑΤΑΣΚΕΥΗ ΤΟΥΣ

Η κατασκευή των έργων ξεκίνησε τον Μάρτιο 2018 και ολοκληρώθηκε τον Οκτώβριο 2018.

Η κατασκευή τεσσάρων αποσπασμένων κυματοθραυστών έγινε από φυσικά πετρώματα όπως φαίνεται στην Εικόνα 4, σε θέσεις που δεν υπάρχουν Λιβάδια Ποσειδωνίων ούτε αρχαιότητες. Οι κυματοθραύστες είναι χαμηλής στέψης, +0.5m ΜΣΘ, έχουν μήκος 105m και διάκενο 45m και βρίσκονται σε απόσταση περίπου 130m από την ακτογραμμή, σε βάθος περίπου 3m .

Οι κυματοθραύστες βελτίωσαν σημαντικά την κατάσταση της ακτής στον Άγιο Τύχωνα Λεμεσού καθώς προστατεύουν την παραλία από την κυματική ενέργεια που προσπίπτει στο χερσαίο χώρο και ισχυροποιούν τις τάσεις αποθέσεως άμμου στην παραλία, όπως φαίνεται στην Εικόνα 4.

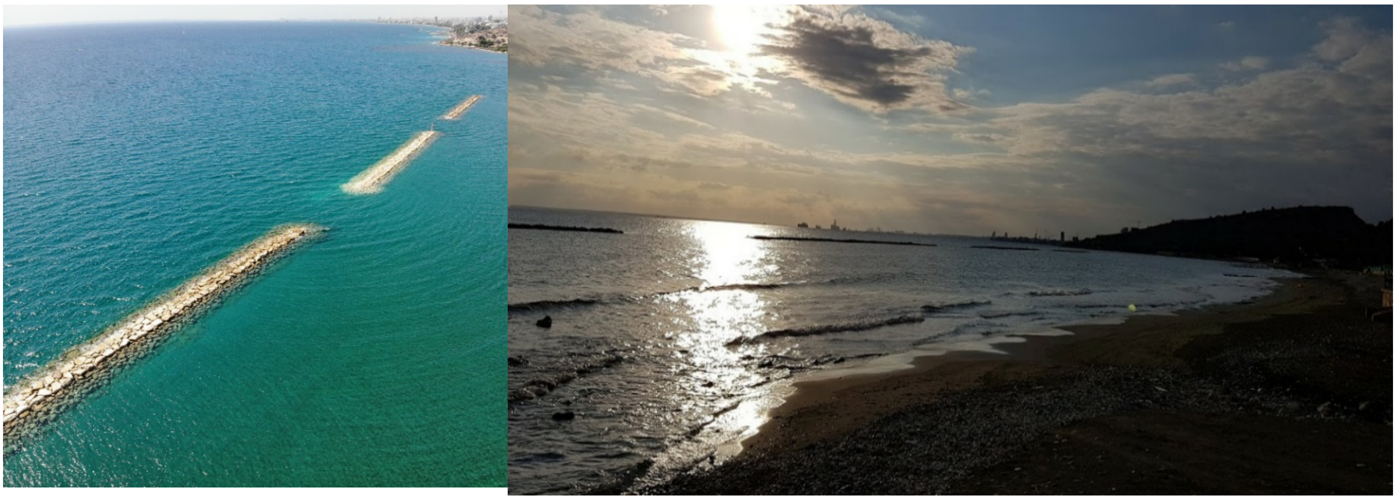

Εικόνα 4 a)Αεροφωτογραφία με τους τρεις από τους τέσσερεις αποσπασμένους κυματοθραύστες που κατασκευάστηκαν για την προστασία της ακτής του ξενοδοχείου Halcyon b)Απόκριση της ακτής μετά την κατασκευή των έργων. Παρατηρείται διευρυμένο πλάτος παραλίας.

Βιβλιογραφικές Αναφορές

Delft Hydraulics, (1994): Coastal Zone Management for Cyprus: Nearshore Wave Climate Analysis by Xenia Loizidou and John Dekker

DHI, (2017): MIKE 21 PMS, HD & ST User Manuals, (v.2017), DHI Water & Environment.

Κυπριακή Δημοκρατία, Τμήμα Κτηματολογίου και Χωρομετρίας, (2016) https://eservices.dls.moi.gov.cy/#/national/geoportalmapviewer

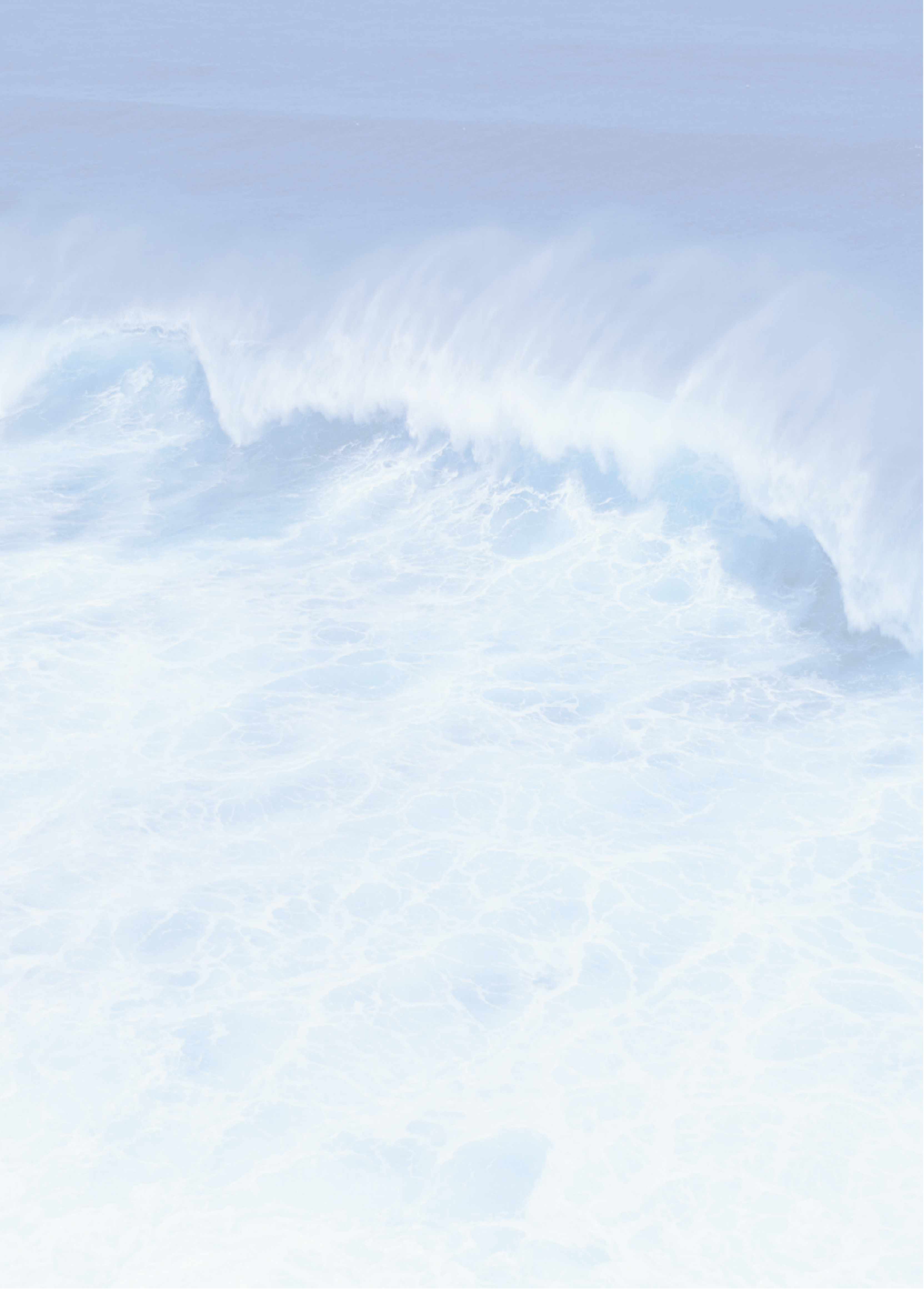

Sea bed evolution in the vicinity of longitudinal submerged discontinuous breakwaters - "Acripelagos"

V. Afentoulis[1*], N. Chini[2], P. Bardey[1], C. Raffourt[1],

[1]ACRI-IN, 260 Route du Pin Montard - BP 234 - F-06904 Sophia-Antipolis Cedex, France
[2]ACRI-IN Brest, Bâtiment Le Grand Large, Quai de la Douane, 29200 Brest, France
[*]Corresponding author: vasileios.afentoulis@acri-in.fr

Abstract

The influence of shore parallel defence structures on sediment transport patterns is numerically investigated, along the coastal zone of Cannes in France. Extreme and long-duration storm events have become more frequent over the last years and they have significantly affected the coastal environment of this densely urbanised area. A landward retreat of the coastline has been observed, which is associated with the presence of high-energy wave-induced currents and coastal defences located on the upper part of the beach. XBeach and Swan, two state-of-the-art numerical models, are coupled in order to transport inshore offshore wave characteristics and evaluate the sediment transport mechanisms in shallow waters. This study enlightens a novel approach for the design of sea structures, providing significant insights into flow-seabed interactions.

Keywords Coastal structures, Breakwater, Numerical simulation, Morphodynamics, XBeach, Swan.

1 INTRODUCTION

The performance of longitudinal submerged discontinuous breakwaters has been investigated as a possible shoreline erosion prevention device, in the coastal region of Cannes in France. This area is particularly vulnerable to coastline retreat due to extreme meteorological conditions that prevailed in recent years. Storm events associated with high energetic waves and intense littoral currents occur frequently in this zone, causing a significant sediment loss. Moreover, coastal defences and vertical-wall structures, located on the upper part of the beach, intensify wave reflection and increase local scour and general reduction in the sea bed levels. The present study explores the overall influence of shore parallel innovative discontinuous double breakwaters on the morphological response of the sea bottom, relying on numerical approaches. The breakwater system is used in combination with mechanical placement of coarse sand sediment (beach nourishment) in order to advance the shoreline and increase the total volume of sand in the littoral system.

Significant efforts have been made in the last decades to investigate hydrodynamics and morphodynamic conditions around low-crested structures (Postacchini et al. 2016) (Kramer et al. 2005) (Losada et al. 2005) (Van Rijn 2011). Submerged breakwaters are widely perceived to be efficient of providing beach protection, avoiding a loss of beach amenity or aesthetic considerations often associated with groins and revetment walls (Ranasinghe and Turner 2006). However, modified hydrodynamics are generated around these submerged structures, as sea level set-up increases, and associated induced pressure gradients generate seaward rip currents through the gaps between contiguous breakwaters (Calabrese et al. 2008) (Vicinanza et al. 2009) (Brocchini et al. 2004). These currents play an important role in coastal erosion as they are associated with rip embayments (i.e. megacusps) that expose the shoreline to high erosion rates during extreme storm events (Thornton et al. 2007) (Michallet et al. 2013). This study suggests an innovative breakwater design solution in order to overcome the adverse impacts of submerged structures. The proposed geometry concerns a low-crested structure composed of two parallel rouble mound breakwaters along the coastline with asymmetric openings (channels). The main function of this optimized configuration is to channelize wave-induced flux offshore so as to limit the sea level set-up in the protected area. Figure 1 depicts the geometry of these structures, located at a depth of about 4m in the coastal zone of Cannes. Furthermore, this structure is characterized by a significant reduced total material volume due to the presence of openings, thus providing a cost-effective solution. For this system a patent is pending under the name "Acripelagos".

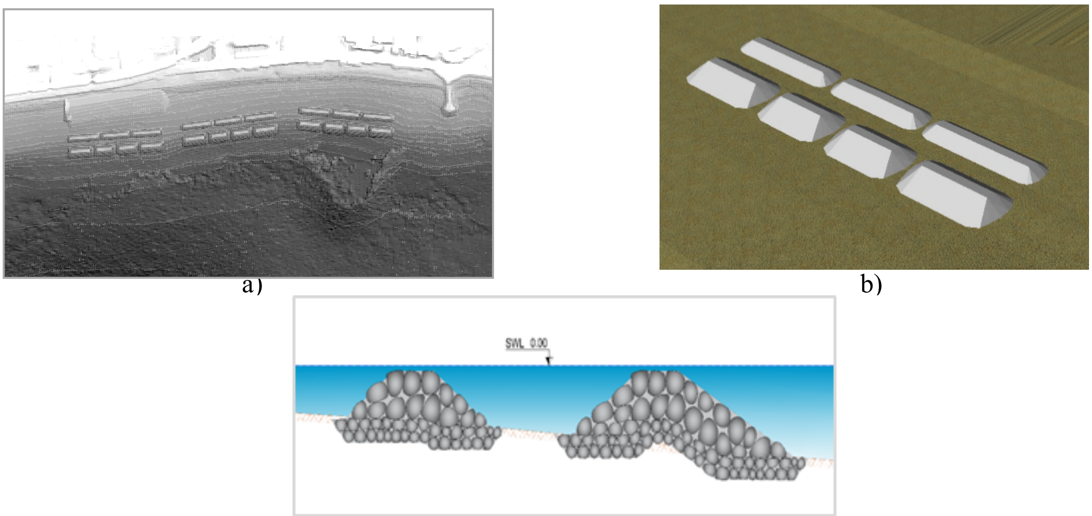

Figure 1 a) Illustration of shore parallel discontinuous submerged breakwaters, b) Details of the breakwater form in 3D, c) Cross-section of the double submerged breakwater.

2 METHODOLOGY

The prevailing offshore wave conditions and tide characteristics are analysed in order to determine the input data for the numerical simulation of hydrodynamic and morphodynamic processes. XBeach and Swan, two state-of-the-art numerical models, are coupled in order to transport inshore offshore wave characteristics and evaluate the sediment transport mechanisms in shallow waters. Simulating Waves Nearshore (SWAN) is a third-generation wind-wave model (Booij et al., 1999), which has been utilized for hindcasting surface gravity waves (Rogers et al., 2003) and forecasting future conditions (Rogers et al., 2007) (Mao et al. 2016). This numerical model is based on the spectral action balance equation (Gelci and Cazale, 1953). SWAN evaluates coastal processes, such as the propagation and decay of waves, taking into account current-induced and depth-induced refraction and frequency shifts, wind input, whitecapping dissipation, bottom friction, depth-induced wave breaking, and nonlinear wave-wave interactions (Booij et al., 1999). A triangulated flexible mesh generated on the wet part of the case study area is used to simulate the wave propagation with SWAN model (Figure 2b). This mesh contains 17,056 nodes and 33,400 elements and it is locally refined in the shallow water areas. The wave directions are distributed into 36 bins with a constant bandwidth of 108, and frequencies are discretized over 32 bins with a logarithmic scale over the range of 0.0512–1 Hz. Wave breaking is introduced through the formula of Battjes and Janssen (1978), and the breaker index (γ) is considered equal to 0,73. Bottom friction is taken into account through the formulation of Hasselmann et al. (1973) and a constant coefficient of 0.067 m^2s^{-3} is used. The initial wave conditions applied on the offshore boundary of the numerical model are extracted from provided data concerning wave height, period and direction time series at the reference point shown in Figure 2. Computed wave height distribution and wave-relative streamlines during a storm event are evident in Figure 2a.

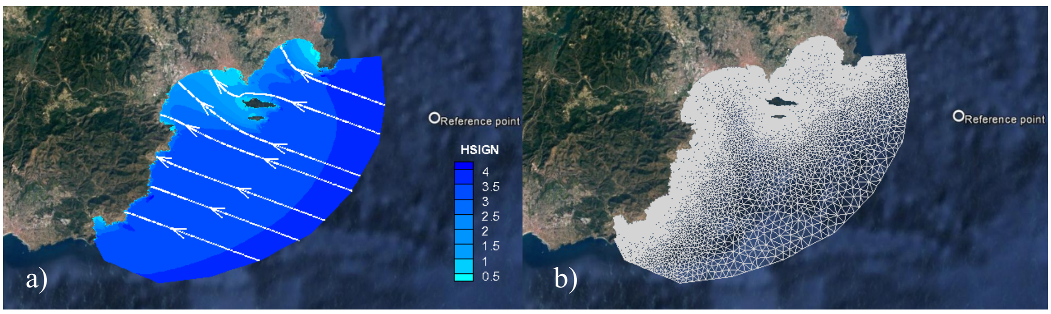

Figure 2 a) Map of computed significant wave height and wave-relative streamlines, b) Triangulated flexible mesh of SWAN model.

The SWAN simulation corresponds to a total duration of 1 year, as non-stationary runs with time steps of 24 hours are used in order to provide wave conditions for XBeach model and predict beach morphological response. XBeach solves the time-dependent short-wave action balance, roller energy equations, non-linear shallow water equations of mass and momentum, sediment transport and bed update (Roelvink et al. 2009; Smit et al. 2010; Bolle et al. 2011). The frequency domain is reduced to a single representative peak frequency, assuming a narrow-banded incident spectrum. Radiation stresses are calculated through the wave action balance and roller energy equations. Wave-induced mass fluxes and return flows in shallow water are calculated through the Generalized Lagrangian Mean formulation described in Andrews and McIntyre (1978). Sediment transport rates are calculated using an advection-diffusion equation (Galappatti and Vreugdenhil 1985). XBeach has been widely used for the evaluation of morphodynamic conditions in coastal zones (Vousdoukas et al. 2012) (Afentoulis et al. 2017). The computational grid is constructed with a variable spatial step which decreases progressively shoreward (dx=10 m offshore and dx= 1 m nearshore). The bathymetry extends 1 km and 0.5 km in alongshore and crosshore direction respectively. Figure 3 shows the bottom elevation and irregular computational grid. XBeach simulations are carried out in 2D surf beat mode and in 1D non-hydrostatic mode. Sediment properties represent a uniform sand porosity of 0.4 and a grain size (D_{50}) of 0.8 mm. The grain size (D_{50}) of the coarse sediments used for beach nourishment is considered 2 mm. A constant Chezy number of 32 $m^{0.5}s^{-1}$ is applied to estimate bed resistance.

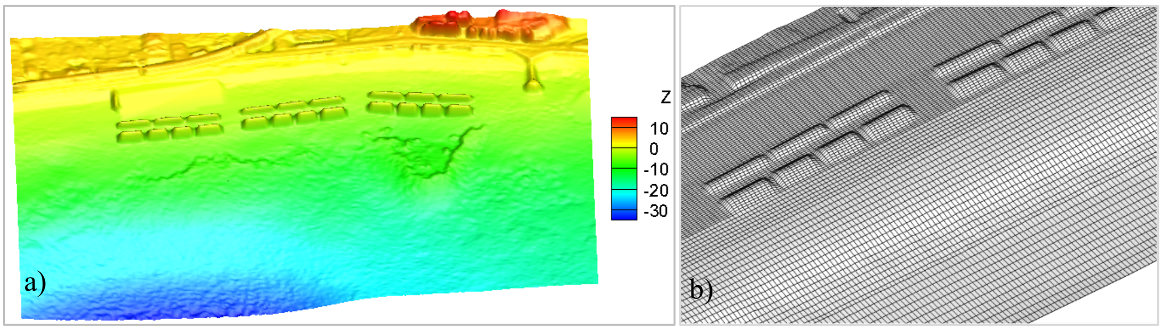

Figure 3 a) Bottom elevation of the coastal area in Cannes, b) Irregular computational grid of XBeach model.

3 RESULTS AND DISCUSSION

The complex physical processes in the nearshore area are particularly assessed in order to estimate the final coast shape 1 year after the installation of the breakwater system. The combined action of waves and currents, as well as groundwater flows are evaluated with XBeach model. Figure 5a depicts the maximum wave height distribution during a severe storm (Initial conditions: Hmo = 2 m and Tp = 9 s), superimposed with isobath lines. the wave amplitude decreases notably in the area between the shore and the structures (H_{max} = 0.6 m), as detached breakwaters provide shelter from the wave action. Outside of this area the wave height value varies from 2 to 3.5 m. Figure 5b demonstrates the sea bed evolution after 1 year, superimposed with isobath lines. The most striking result to emerge from the graph is that an accretion of 1.5 m is generated in the wave sheltered zones. However, erosive zones are identified in the gaps between the breakwaters and in the non-protected foreshore areas. Changes in seabed morphology are negligible for a water depth greater than 6 m. In order to investigate the effects of swash and groundwater dynamics, XBeach model is utilized in 1D non-hydrostatic mode. For this scope, a representative crosshore profile is chosen with a constant spatial step (dx) of 1 m (Figure 5). After the beach nourishment the seabed in the shoreface consists mainly of coarse sand with a mass median diameter (D_{50}) equal to 2 mm while the layer thickness of nourishment sand is about 1.5 m. The final sea bed geometry of the selected profile, as it is derived from the one-dimensional simulation of morphodynamic processes over a year, is illustrated in Figure 6. The simulation concerns two scenarios: A) seabed evolution under the presence of the breakwater system with initial beach nourishment (Figure 5a), B) seabed evolution without coastal structures with initial beach nourishment (Figure 5b). The obtained numerical results revealed that the proposed structures, offer satisfactory protection to the coastal area, since an overall retention of the nourished sediments is observed, whilst in the case of an equivalent unprotected beach an offshore sediment movement is generated. However, slight erosion is presented near the seaward toe of the structure.

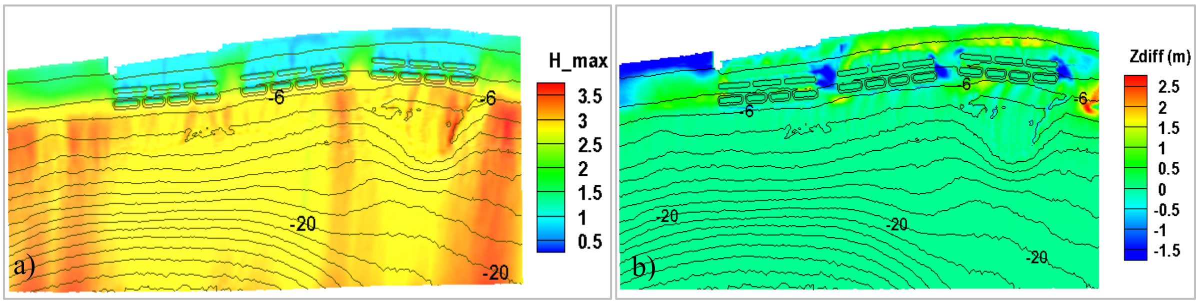

Figure 4 a) Map of computed maximum wave height during a storm event (superimposed with isobath lines), b) Morphological sea bed changes 1 year after the installation of the breakwater system (superimposed with initial isobath lines).

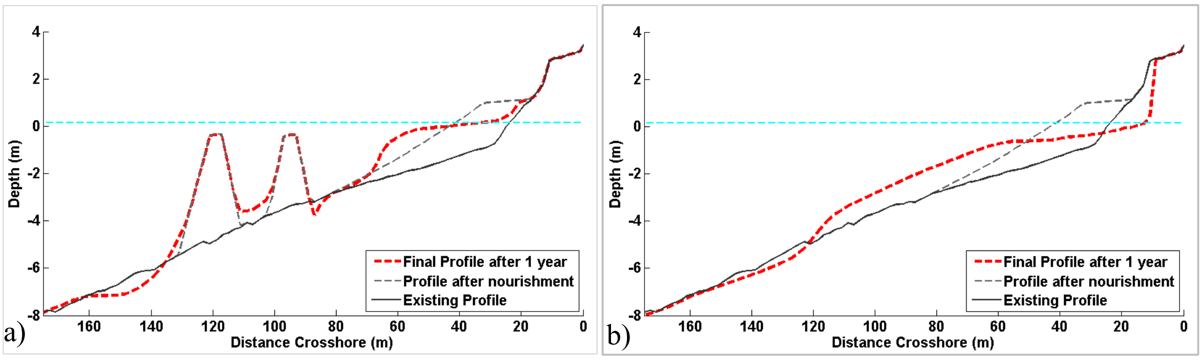

Figure 5 a) 1D sea bed evolution one year after the installation of the breakwater system, with initial beach nourishment, b) 1D sea bed evolution after one year after, with initial beach nourishment and without coastal defence structures.

This study enlightens a novel approach for the design of sea structures, providing significant insights into flow-seabed interactions. The submerged discontinuous breakwaters offer a consistent environmentally friendly solution to deal with beach erosion phenomenon, contributing to the long-term stability of the coast. After an initial beach nourishment, it shown that the sediments are retained in the beach system, as the wave climate is modified in the protected area due to the presence of the structures. However, erosive zones are generated in the offshore toe of the structure and in the gap between contiguous breakwaters. Furthermore, the proposed configuration is characterized by a significant reduced volume comparing to traditional hard protection works, providing a cost-effective solution. A dedicated study is underway to evaluate the fluid–seabed-structure system in an interactive mode, in order to optimize the form and performance of the discontinuous submerged breakwaters.

References

Afentoulis V, Eleftheria K, Eleni S, Moschos E, Lykou A, Makropoulos C, Tsoukala V (2017) Coastal Processes Assessment Under Extreme Storm Events Using Numerical Modelling Approaches. Environmental Processes, 4(3), 731-747.

Andrews DG, McIntyre M (1978) An exact theory of nonlinear waves on a lagrangian-mean flow. J Fluid Mech 89(04):609–646.

Battjes J A, Janssen JPFM (1978). Energy loss and set-up due to breaking of random waves. Coastal Engineering, pp. 569–588, Am. Soc. Civ. Eng., N. Y.

Bolle A, Mercelis P, Roelvink D, Haerens P, Trouw K (2011) Application and validation of XBeach for three different field sites. Coast Eng Proc 1(32):40.

Booij, N., R. C. Ris, and L. H. Holthuijsen (1999) A third-generation wave model for coastal regions: 1. Model description and validation, J. Geophys. Res., 104(C4), 7649–7666.

Brocchini M, Kennedy AB; Soldini L, Mancinelli A (2004) Topographically-controlled, breaking wave-induced macrovortices. Part 1. Widely separated breakwaters. Journal of Fluid Mechanics, 507, 289–307.
Calabrese M, Vicinanza D, Buccino M (2008) 2D wave set up behind submerged breakwaters. Ocean Engineering, 35(10), 1015– 1028.
Galappatti G, Vreugdenhil C (1985) A depth-integrated model for suspended sediment transport. J Hydraul Res 23(4):359–377.
Gelci R, and H. Cazale (1953) Une théorie énergétique de la houle appliquée au Maroc, C. R. Soc. Sci. Nat. Phys. Maroc., 4, 64–66.
Hasselmann K, Barnett TP, Bouws E, Carlson H, Cartwright DE, Enke K, Meerburg A (1973) Measurements of wind-wave growth and swell decay during the Joint North Sea Wave Project (JONSWAP). Ergänzungsheft 8-12.
Kramer M; Zanuttigh B, Van der Meer JW, Vidal C, Gironella FX (2005) Laboratory experiments on low-crested breakwaters. Coastal Engineering, 52(10–11), 867–885.
Losada IJ, Lara JL, Christensen ED, Garcia N (2005) Modelling of velocity and turbulence fields around and within lowcrested rubble-mound breakwaters. Coastal Engineering, 52(10– 11), 887–913.
Mao M, Van Der Westhuysen A J, Xia M, Schwab D J, Chawla A (2016) Modeling wind waves from deep to shallow waters in Lake Michigan using unstructured SWAN. Journal of Geophysical Research: Oceans, 121(6), 3836-3865.
Michallet H, Castelle B, Barthélemy E, Berni C, Bonneton P (2013) Physical modeling of three-dimensional intermediate beach morphodynamics. Journal of Geophysical Research: Earth Surface, 118(2), 1045-1059.
Postacchini M, Russo A, Carniel S, Brocchini M (2016) Assessing the hydro-morphodynamic response of a beach protected by detached, impermeable, submerged breakwaters: a numerical approach. Journal of Coastal Research, 32(3), 590-602.
Ranasinghe R, Turner IL (2006) Shoreline response to submerged structures: a review. Coastal Engineering,53(1), 65-79.
Roelvink D, Reniers A, Dongeren AV, de Vries JT, McCall R, Lescinski J (2009) Modelling storm impacts on beaches, dunes and barrier islands. Coast Eng 56(11–12):1133–1152.
Rogers WE, Hwang PA, Wang DW (2003). Investigation of wave growth and decay in the SWAN model: Three regional-scale applications. J. Phys. Oceanogr., 33(2), 366–389.
Rogers WE, Kaihatu JM,Hsu L, Jensen RE, Dykes JD, Holland KT (2007) Forecasting and hindcasting waves with the SWAN model in the Southern California Bight. Coastal Eng., 54(1), 1–15.
Smit P, Stelling G, Roelvink D, Thiel de Vries JV, McCall R, Dongeren AV, Zwinkels C, Jacobs R (2010) Xbeach: non-hydrostatic model. Report, Delft University of Technology and Deltares, Delft, The Netherlands
Thornton EB, MacMahan J, Sallenger AHJr (2007) Rip currents, mega-cusps, and eroding dunes, Mar. Geol., 240, 151–167.
Van Rijn LC (2011) Coastal erosion and control. Ocean & Coastal Management, 54(12), 867-887.
Vicinanza D, Caceres I, Buccino M, Gironella X, Calabrese M (2009) Wave disturbance behind low crested structures: Diffraction and overtopping effects. Coastal Engineering, 56(11), 1173–1185.
Vousdoukas MI, Ferreira Ó, Almeida LP, Pacheco A (2012) Toward reliable storm-hazard forecasts: XBeach calibration and its potential application in an operational early-warning system. Ocean Dynamics, 62(7), 1001-1015.

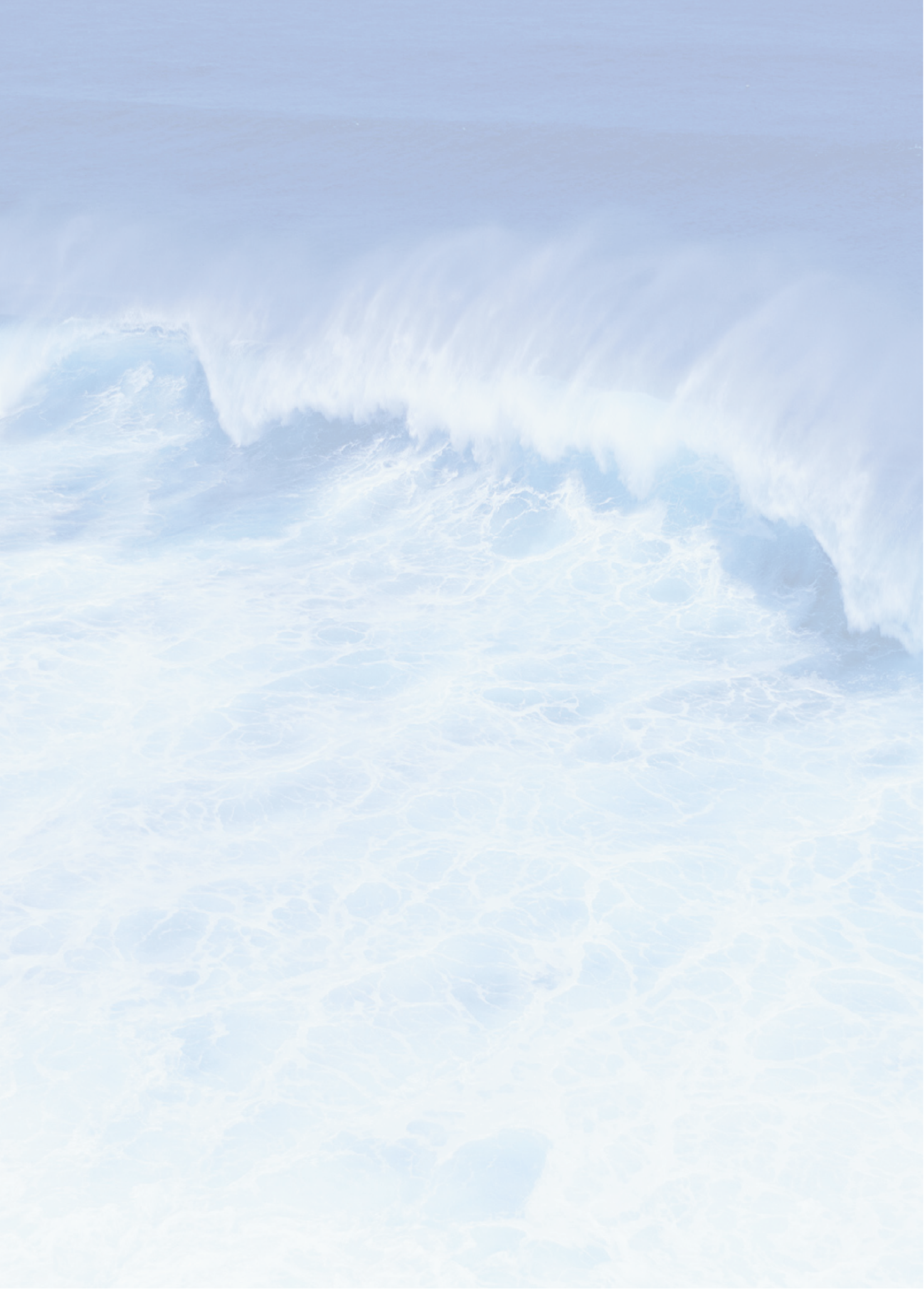

Integrated coastal management including detached breakwater system and artificial nourishment

S. Kousoulos[1], I. G. Koutsourelakis[2], N. Panagopoulos[2*] H. Tsekos[1]

[1]ADK Consulting Engineers
[2]TRITON Consulting Engineers
[*]Corresponding author: triton@tritonsa.gr

Abstract

The aim of the current paper is the presentation of the design process for the selection of the interventions required for the coastal management at a coastal zone of approximately 5.0 kms in length. The under study area is situated at the northwestern coast of the Messenian bay and part of it is occupied by the coastal town of Petalidi. The coast is subjected to strong wave events originating from the greater southerly sector. The coastline morphology is greatly variable taking into account its significant length, the geology and the effect of seasonal streams that outflow in it. The knowledge of all these complex coastal processes was succeeded through elaborate studies that provided input concerning all the critical factors, namely the geology, the surficial sediments, the sediment input from streams and the wave climate. The optimization of the critical interventions was carried out through mathematical modeling, both 1D and 2D, by implementing the MIKE21 software suite. The latter arguably consists the most popular and widely tested commercial software package that enables the modeling all the critical marine processes which influence coastal morphology. The alternative intervention options that were checked include the majority of the possible works combinations, all coupled with beach nourishment. These interventions aim to protect the exposed public and private property, the minimization of the environmental impact and the maintenance costs.

Keywords Petalidi, Breakwaters, Nourishment, Beach

1 LOCAL CONDITIONS

The Petalidi coastal area is subjected to strong wave and storm events from the greater southerly sector, i.e. the SW, S and SE sectors. Owing to its length, significant differentiations occur between its various sub-sections in terms of topography, geology, hydrology and wave climate. Moreover, the central part of the under study coastline is occupied by the small town of Petalidi, where the local infrastructure extends down to the waterline. Especially there, the continuous coastal erosion has exposed the infrastructure to direct wave impact. All these factors have a strong influence on the local conditions and have been thoroughly analyzed prior to the selection of the required actions.

2 FIELD STUDIES

Extensive field studies and measurement works were required in order to accurately document the local conditions and the factors that influence the sediment transport regime in the coastal area. These field works are listed here below:

2.1 Topographic survey

The topographic/bathymetric survey was conducted in September of 2018 and covered an area of approx.150.000 m^2. The bathymetry surveyed reached a depth of approximately -10 m thus practically covering all the littoral zone.

2.2 Geological Survey

The geological survey apart from the understudy coastal zone extended to all landforms along the catchment area of the three major water streams outflowing in the study area (ref to **Figure 9**). The study area has been divided to the following sub-sections:

- Section A-B: From the southern border of the study area to the Petalidi promontory
- Section B-C:|From the Petalidi promontory to the northern end of the Petalidi Village
- Section C-D: From the northern end of the Petalidi Village to the end of the study area (near the mouth of Karyas stream)

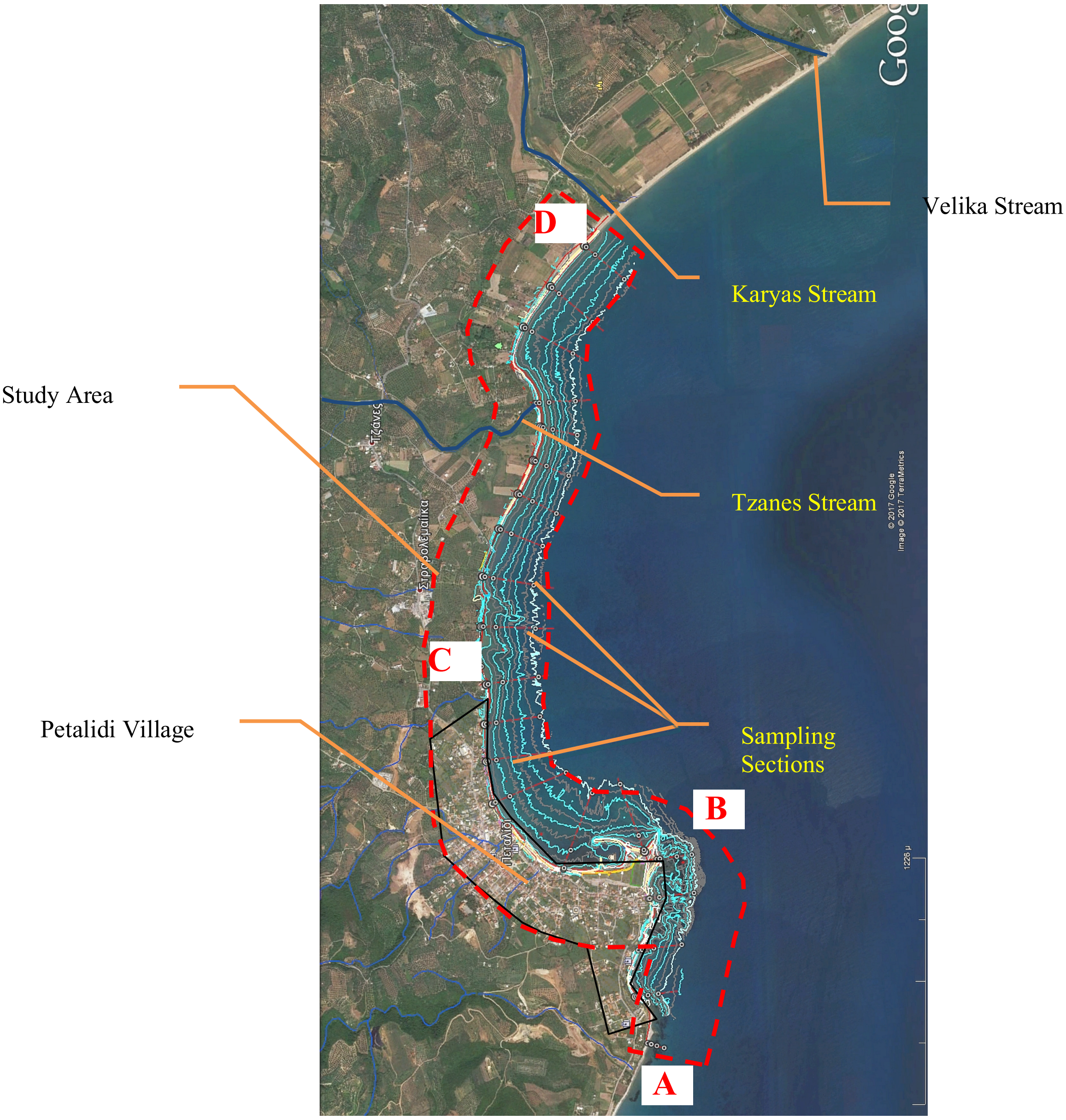

Figure 9 Under Study Area with main geological, hydrological features along with sampling locations

2.3 Seabed sampling Campaign

The sampling campaign included more than 100 samples in sections spaced along 250 m intervals. Each section covers the entire shoreface profile from the dry part of the beach down to a depth of -5.0 m. The sampling sections are depicted in **Figure 9** with red lines.

3. DATA ANALYSIS AND MODELING

3.1 MetOcean and Wave Climate Analysis Study

The extensive dataset collected from the field studies is coupled with data concerning the wind and wave climate in the area. The latter was selected from the available wind recording stations of the HNMS (Kalamata and Methoni stations) and the offshore hindcast database of ECMWF which includes both wind and wave data covering a period of 37 years. A regional scale model was created covering the entire Messenian gulf as depicted in **Figure 10**

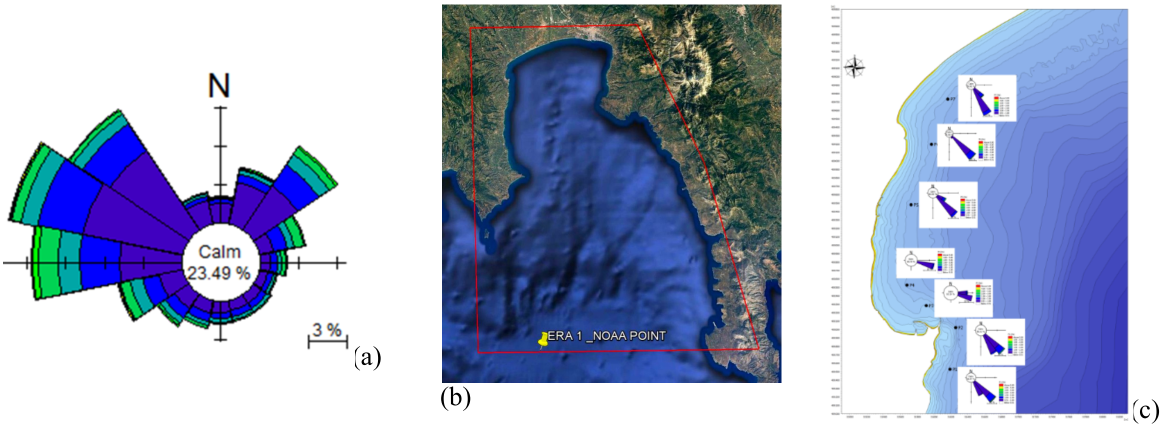

Figure 10 *Offshore Wave data (a) with the extent of the modeled area(b) and the local wave climate (c)*

3.2 Hydrological Analysis

The hydrological study carried out for the three major water streams outflowing in the coastal area resulted in the following sediment fluxes.

Table 5 Sediment rates for the three major streams of the understudy area

Stream	2015	2000	1985
Velika	14.400 m^3	15.118 m^3	15.119 m^3
Karyas	7.004 m^3	7.220 m^3	7.215 m^3
Tzanes	7.981 m^3	7.981 m^3	7.982 m^3

3.3 Analysis of the historical evolution of the coastline and extraction of the Coastal Vulnerability Index (CVI)

The conducted CVI analysis took into account the following parameters

- Geomorphology(GEO)
- Historical coastal modification rate(ERO)
- Coastal zone slope (CS)
- Rated of sea level rise due to climate change (RSLR)
- Yearly average wave height (significant) (H)
- Average tidal range (T)

The resulting CVI analysis outputs are depicted in the following **Figure 11**.

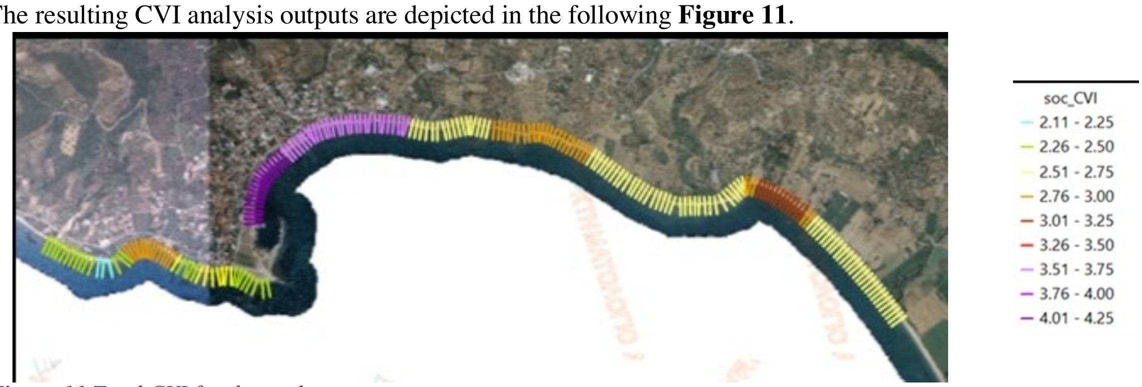

Figure 11 *Total CVI for the study area*

Based on the CVI analysis, the priority areas for coastal protection interventions are as listed below

1. In front of the village or Petalidi
2. Coastal zone in front of Petalidi camping
3. Eros Beach Coastline
4. Central coastal area (between the existing small groynes

3.4 Sediment Transport Analysis

The sediment transport analysis was carried out in two stages. In the first stage the selection of the appropriate works is carried out while in the second stage the optimization of the works proposed in the initial stage in carried out. For both stages, the baseline conditions and the conditions with the addition of the foreseen interventions were simulated.

3.4.1 Selection of Appropriate Interventions

All modeling carried out for the critical priority areas by taking into account the shoreline evolution for 5, 10 and 15 years. The effect of storm events was also introduced in the simulations with the storm of 12/12/2008. The alternative options evaluated in this stage mainly considered detached breakwaters, either as a system or single ones, depending on the examined sub-section and groynes. All these were coupled with artificial nourishment for the creation of a dry beach width of 15.0 m.

The results for the Petalidi area considering either 6 detached breakwaters, approx. 65 to 80 m in length and a gap of 45 m, or four (4) T-shaped groynes with a length of 55 to 80 m at 150 m to 180 m intervals. The results of shoreline evolution for these two alternatives, are depicted in the following **Figure 12**.

Figure 12 Envelope of shoreline evolution for (a) detached breakwaters and (b) T-shaped groynes for the Petalidi area

Based on the above analysis the solution with detached breakwaters, was found preferable and was further optimized in the second stage analysis.

Concerning the second most critical area, namely the "Petalidi Camping" Area, owing to the coastal orientation, the alternatives of one detached breakwater (length of 110 m) and two detached (80 m length with a 35 m gap) were examined. Both solutions were coupled with beach nourishment using appropriately graded sediment. The results of the analysis are depicted here below in

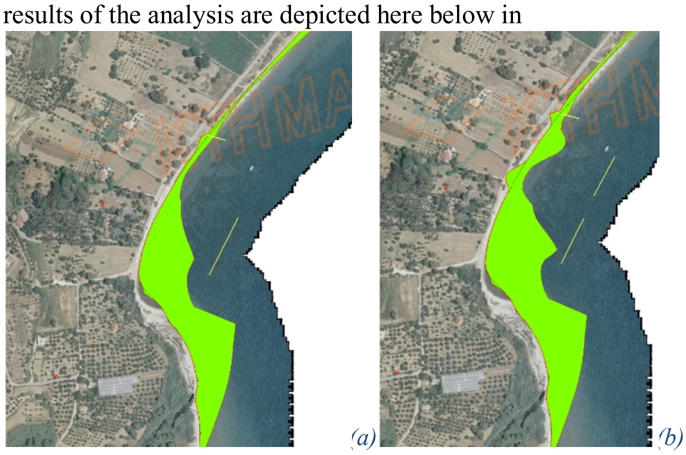

Figure 13 Envelope of shoreline evolution for (a) single detached breakwaters and (b) double detached breakwaters for the "Petalidi Camping" area

Due to the ambiguous outputs both solutions were introduced in the detailed optimization modeling.

3.4.2 Optimization of the proposed works and interventions.

The second stage optimization analysis incorporated all relevant wave, hydrodynamic and sediment transport processes with increased accuracy using the MIKE21 modeling suite.

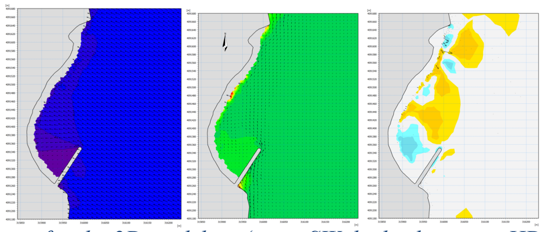

__Figure 14__ Presentation of three stages for the 2D modeling (wave-SW, hydrodynamics-HD, sediment transport-ST)

The Petalidi area breakwater system was further optimized by lowering the crest to +1.20 m. For the camping area the proposed intervention is a single 130 m long breakwater while for the “Eros Beach” coast an artificial headland is proposed to be constructed in order to take advantage of the natural bathymetry there.

4 CONCLUSIONS

The recorded shoreline erosion, especially in the Petalidi town frontage, can be attributed to geological and human related interventions. The alternative solutions that have been investigated include detached breakwaters, groynes and artificial headlands. All the above combinations of interventions have been coupled with artificial nourishment of the eroded coastlines with appropriately graded sediment. The acceptance criteria are mainly the protection of the threatened public and private property and the blending of the proposed works with the natural environment. Moreover the proposed interventions offer the collateral gain of enabling the upgrading of the understudy beaches for recreational activities, a status that has been lost due to the increased erosion. In view of that, the safety of the visitors and swimmers has been also taken into account as an additional acceptance criterion for the proposed works.

References

US Army Corps of Engineers (2006), Coastal Engineering Manual (CEM).

Kamphuis, JW (2000) Introduction to coastal engineering and management. Advanced series on Ocean Engineering. Vol. 16, World Scientific.

Johnson HK, Appendini CM, Soldati M, Elfrink B, Sørensen P (2001) Numerical modelling of morphological changes due to shoreface nourishment. Proc. 4th Conference on Coastal Dynamics. ASCE, pp. 878-887.

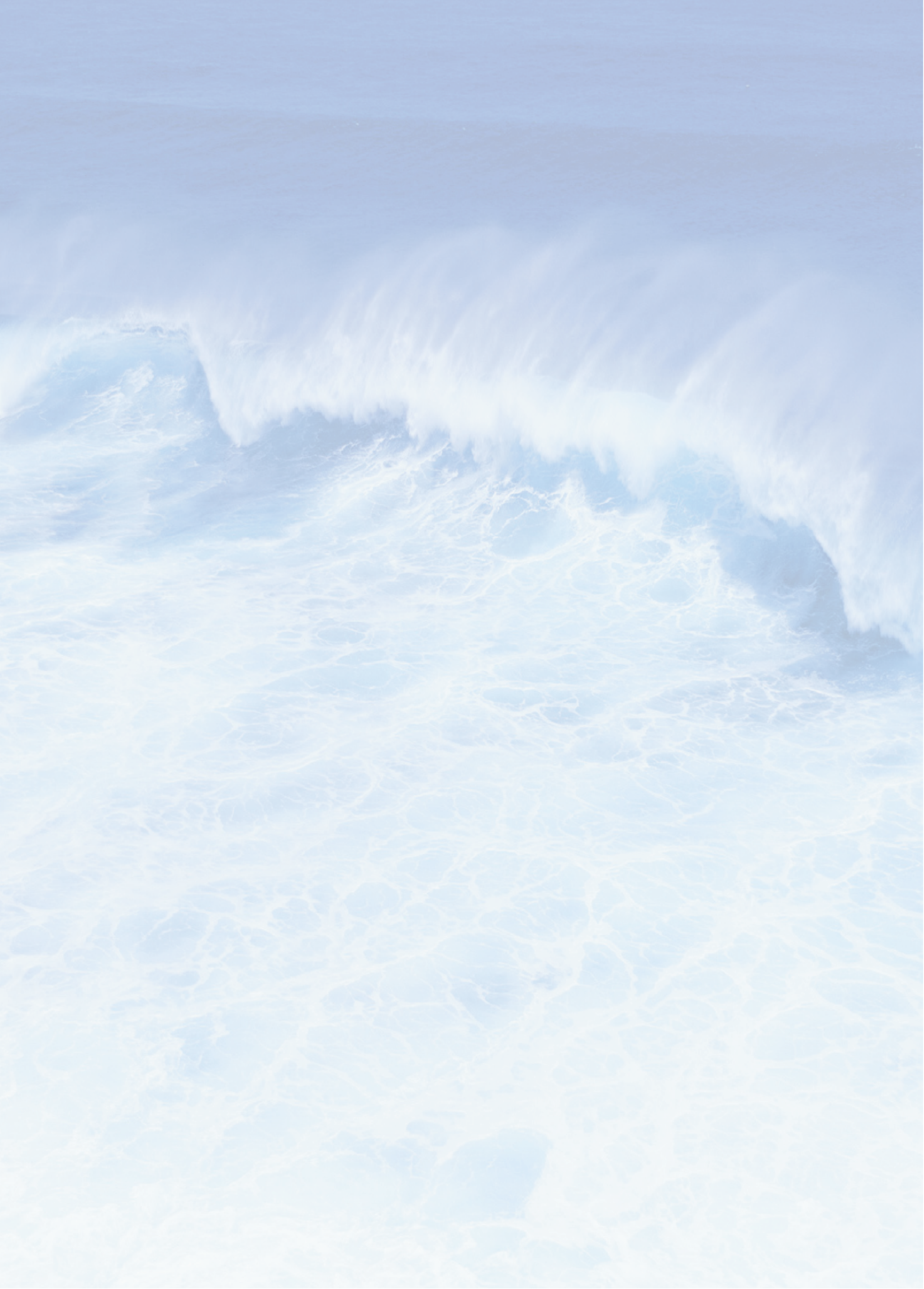

Proposed measures for the restoration of the coastal area under erosion in the Bay of Platis Gialos – Sifnos Isl. (Greece)

A. G. Petropoulos [1]*, N. Evelpidou[1], V. Kapsimalis[2] and Ch. L. Anagnostou [2]

[1] Faculty of Geology and Geoenvironment, National and Kapodistrian University of Athens, Panepistimiopolis, 15784 Athens, Greece
[2]Institute of Oceanography, Hellenic Centre for Marine Research, 46.7 km Athens-Sounio Avenue, Mavro Lithari, 19013 Anavyssos, Greece
*Corresponding author: alexpetrop@geol.uoa.gr

Abstract

A large percentage of the coastline in Greece, with strong tourist, economic and natural interest, are Pocket Beaches. In the present study, the processes of coastal erosion, existing on Platis Gialos beach, are described and examined due to: (i) limited rivers stereotransfer, (ii) the construction of a protective wall along the coastline, and (iii) the construction of a fishing shelter. In particular, are being analyzed the geological and sedimentological composition of the background, the geometrical characteristics, the morphological peculiarities, the orientation towards the prevailing oceanographic conditions and the coastline development in two seasonal periods (winter/summer), focusing on the existing morphodynamic condition of the coast. The methodology followed in the study included: (i) long-term geomorphological evolution of the coastal zone through the analysis of satellite images, in order to estimate the intensity of coastal erosion, (ii) data of the numerical recomposition of the wind and wave conditions of the study area, (iii) topographic sections at the surface and the subsea of the coastal zone, through D-GPS, perpendicular to the coastline, (iv) collection of surface land and marine sediments, and (v) analytical recording and mapping of the summer and winter shorelines via the D-GPS. Taking into account the results and identifying the morphodynamic environment of Platis Gialos beach, a "soft" invasive method is proposed on the beach, such as artificially beach nourishment, in order to restore disturbed balance and achieve its protection from the erosion.

Keywords Coastal Erosion, Man-made Structures, Morphodynamic Condition, Beach Nourishment.

1 INTRODUCTION – SCOPE OF THE WORK

The coast of Platis Gialos at Sifnos Isl. has been under erosion and permanent coastal retreat for several years. The first signs of erosion began when human prevented the sediments transport from the rivers to the coast, as it built all the river beds, also, the construction of a protective wall for the waves, parallel/vertical and close to the coastline, leads to the aggravation of the erosion phenomenon. Finally, the construction that highlighted the magnitude of the problem in the study area was the fishing shelter. The eroded area at the central and west part of the coast reached at 20 m in contrast with the northeast part of the beach where there is a deposition of 25 m (Fig. 1). The purpose of this work is to study the morphodynamic processes and the sediment transport in the bay, and to propose restoration measures for the coast, following "soft" shore techniques.

Figure 1 Platis Gialos coast, before (left-2003) and after (right-2016) the construction of the fishing shelter (source: GoogleEarth)

2 DESCRIPTION OF THE STUDY AREA

Coast of Platis Gialos is defined as a pocket beach with a total length of 750 m and a bay width of 1000 m, also the length from the entrance of the bay until the coast is 1000 m. It is bounding by headlands which block any sediment exchange with the neighboring parts of the coast; making them an autonomous and independent ecosystem. It is located at the South part of Sifnos Island, at central the Cyclades with a SE orientation (Fig. 2). From the geographical position and the orientation of the coast, it appears that the most common waves that affect the area of interest are coming from the S, SE address. The Southern coastal expanse of the study area extends to the coasts of North Crete forming the significant length of 165 km, in contrast to the Southeastern coastal expanse that reaches Sikinos Isl. and Folegandros Isl. and are equal to 45 km. At the same time, the Kitriani Isl. protects the coast from waves of the Southwestern orientation and diminishes the energy of the Southern direction due to the diffraction that exists in it. We had visited the area in two different seasonal periods of 2018 (winter/summer) recording the geomorphological processes at the study area.

2.1 Geological Setting

The morphology of the area in Platis Gialos is flat near the beach and hilly inward. The geology of the island contains metamorphic rocks. Specifically, from the oldest to the younger they come across the following (NAMA Development S.A. 2003): Dolomites marbles, laminations of Gneiss schist in marbles, Micro-Macrocrystallic Marbles, Gneiss, Schists with glaucophane, Glaucophanitic schists, Glaucophane, Quaternary deposits are also observed.

From a tectonic point of view, fault lines with direction N-S, SSW-**NNE** and E-W are observed. However, Sifnos Isl. is ranked as the lowest grade of seismic hazard (http://www.oasp.gr/).
The potential feeders of the coast with fertilizer materials necessary for the formation of an alluvial beach are three main torrents, with small basins, which flow into the bay (Fig.2).

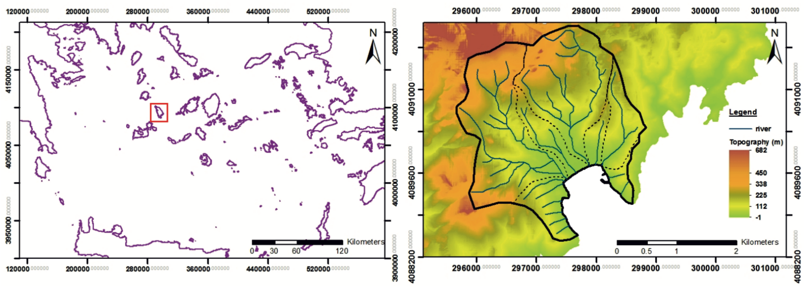

Figure 2 The left image place Sifnos Isl. in Greece. The right image depicts the morphology of the study area, the main drainage basin, the subasins, and the hydrographic network.

2.2 Meteorological Setting

The climate of Sifnos is characterized as semi-dry with warm winter and with cool summer which characterized by strong winds and droughts. The island, according to the Western Cyclades is one of the driest areas of Greece.

Average temperatures peak during July and August at 27.5 C and 27.3 C respectively, with a minimum of January and February at 8.3 C and 7.8 C (Weather station of Milos Isl. 1989-1997). Rainfall tends to have extreme behavior, being few but fierce. The average annual precipitation height for Milos is 379.5 mm. The driest month is July (0.0mm) and rainier December (82.7mm) (Weather station of Milos Isl. 1989-1997). The annual winds are classified as small and medium to high intensity, i.e. on the Beaufort scale 1-7. And their usual values of speed, for the period 1995-2004, are in the order of 3 -5 Beaufort. As to the distribution of the wind directions and intensity, more frequent (~22%) is the northern, followed by northwest (~12%) and southwest (~12%) (Soukisian et al. 2007) (Fig. 3). As well to the wave conditions, the most common wave spread directions with a ~27% incidence are derived from the directions N and NW. The average value of significant wave height in the 1995-2004 period is 0.5 – 1.5 m. The highest values appear mainly from the sections (0^o, 225^o) with a wave height of 2.5 – 3 m (Soukisian et al. 2007).

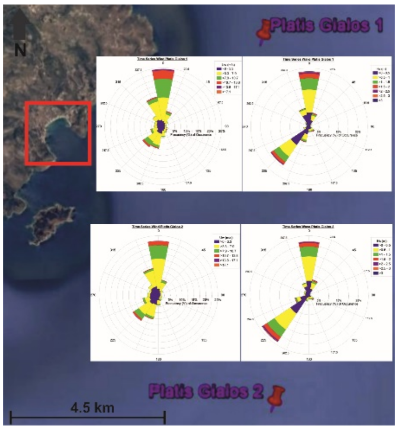

Figure 3 The wind and wave conditions of the study area from two different spots of the open sea area

3 METHODOLOGY

For the beach survey was used, i) D-GPS (Spectra Precision SP80 GNSS Receiver) for carrying out the topography of the area by 26 descriptive shore-sections profiles, vertical to the coastline, every 20 m, which extended from the man-made constructions to the depth of ~1.5 m. ii) in situ sediment sampling in the subaerial and subaquatic coastal area. Laboratory analyses were followed by the methods of dry granulometry, in order to categorize the samples, in different types on the basis of Folk & Ward (1957) method by the use of the GRATISTAT (v.8) software. iii) use of the application Digital Shoreline Analysis System (DSAS) in the software ArcMap 10.3 (Thieler et al. 2009), to quantitate the long-term shoreline displacements. At each transect, the rate of displacement was measured. This was carried out by comparing satellite imagery (Google Earth) for the periods 5/2003, 7/2003, 1/2008, 9/2011, 9/2012, 7/2013, 5/2016 and the imprint of the coastline (4/2018, 12/2018) with a D-GPS.

Marine survey was completed using, i) side-scan single beam eco-sounder (StarFish 450), to determine the seabed morphological features of the bay, the imaging data were collected with the functional emission frequencies of 450 kHz. ii) bathymetric eco-sonar (Lowrance LCX-15MT) at the frequencies of 200 kHz, to collect the bathymetric data. iii) data of the numerical recomposition of the wind and wave conditions of the study area from two different spots of the open sea area (Fig. 4). The wind and wave data are results of numerical analysis of wind and wave conditions refer to the period of 10 years, 1995-2004 (Soukisian et al. 2007).

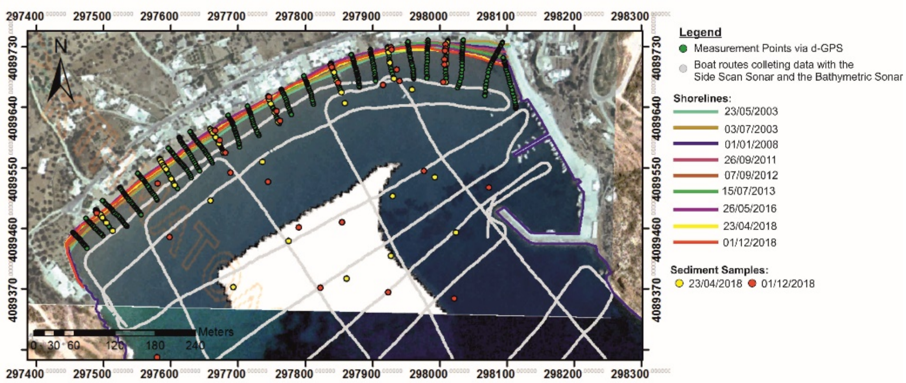

Figure 4. Display of the field work and the collection of data from the study area.

4 RESULTS AND DISCUSSION

Of the total of 92 sediment samples of subaerial and subaquatic coastal area, was characterized as Sand (125 – 250 μm) and as Slightly Gravelly Sand to Gravelly Sand (125 – 500 μm) at summer and winter period respectively, while marine sediments where characterized as Slightly Gravelly Sand (63

– 250 μm) at both summer and winter (Fig. 5). Bay presents relatively gentle slopes and shallow depths (with the maximum measured depth, -48 m), with small variations between winter and summer profile, which are intensifying until the depth of -2 m (Fig. 6). The side-scan single beam leads to substrate component mapping, separating them to sand-clay/hard substrate/beachrock/fluvial deposits.

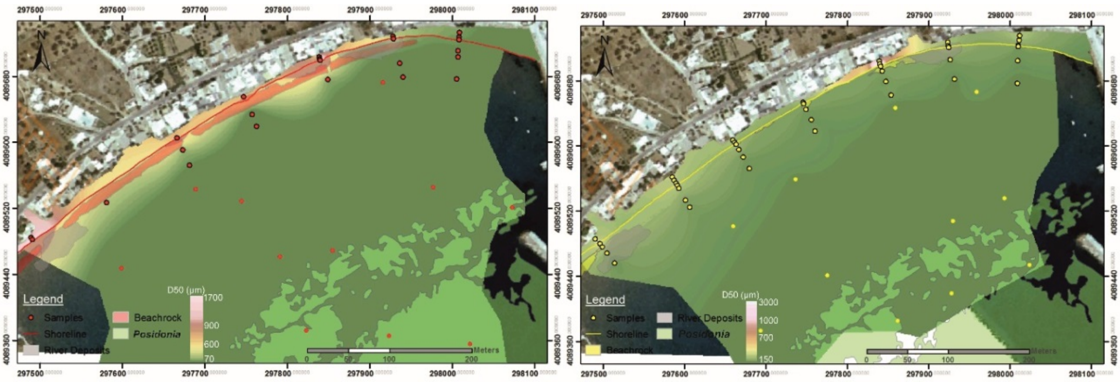

Figure 5 D50 distribution at the study area for the winter (left) and the summer (right) period.

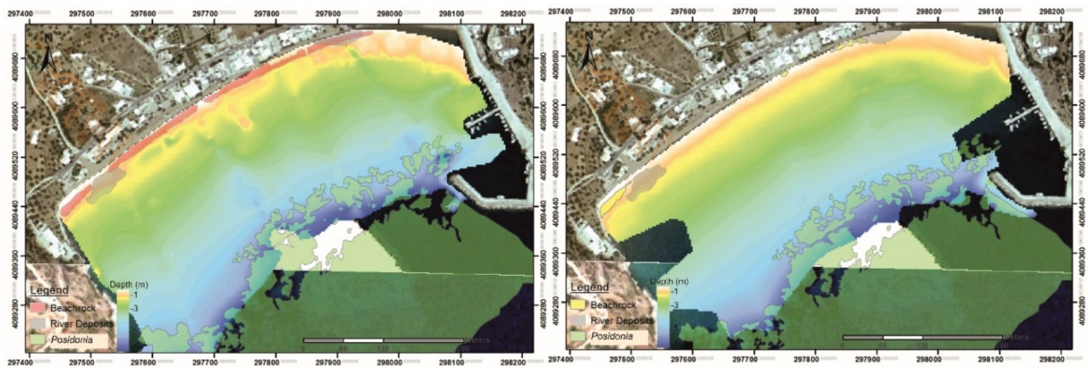

Figure 6 The bathymetry till the depths of 10 m at the winder (left) and at the summer (right) period.

To determine the coast profile difference between the two seasonal periods, topographic sections were made along the coast for each season, which are equidistant to one another 100 m. The topographic profile sections for the two different periods display the amount of the sediments that varies depending on the season (Fig. 7). Almost all of the topographic sections present a trend where the summer profile overlaps the winder profile in total. Only the western topographic profile (section 7) seems that at the winter the subaerial sediment is in greater quantity than the summer. Also at the 6 first winter sections from the west to east the beachrock reveal from 10 to 15 m in the topographic section, testifying the existence of coastal erosion. Beachrock also reveals at the summer profiles but to a lesser extent.

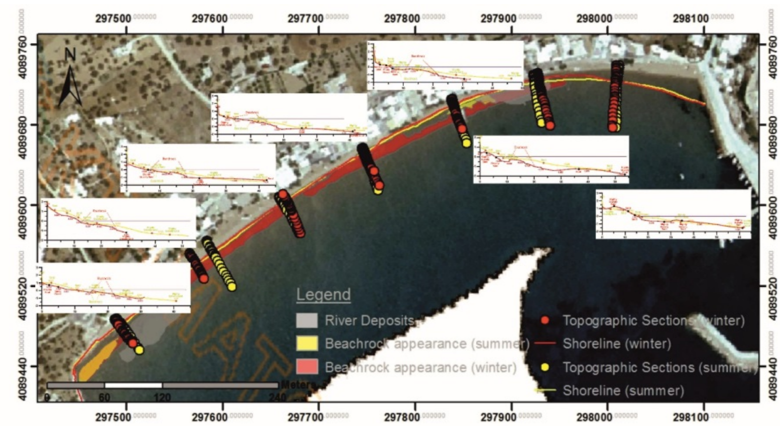

Figure 7 Comparative topographical sections between winter (red) and summer (yellow) period.

Taking account the results of the application Digital Shoreline Analysis System (DSAS) from 2003 until 2016, the western and central part of it are under erosion the last 10 years and especially due to the construction of the fishing shelter and the anthropogenic intervention in the natural mechanism of sediment supply from the torrents, the values of the erosion reaches the 16 m. However, at the eastern part and near the fishing shelter, the coastal deposition reaches the 26 m (Fig. 8).

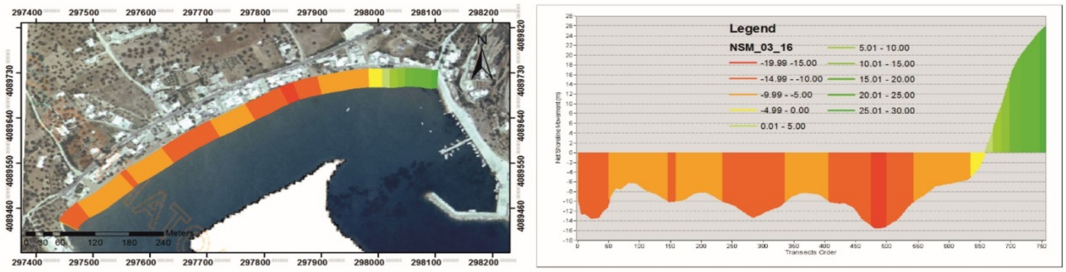

Figure 8 The picture displays the size of coastal erosion and coastal deposition at the coast of Platis Gialos from 2003 to 2016 using the add-on application Digital Shoreline Analysis System (DSAS) in the software ArcMap 10.3 (Thieler et al. 2009)

5 CONCLUSIONS

The coastal area of the Platys Gialos bay is eroded due to: a) anthropogenic intervention in the natural mechanism of sediment supply from the torrents and b) due to the construction of the fishing shelter, as well the existence of the protective wall parallel to the coastline and vertical to the coast in few meters from the coastline, exacerbate the phenomenon. In order to protect the area, we propose to use methods environmentally and economically acceptable. Applying “hard techniques” (e.g. breakwaters) will charge the area with a high cost and will relegate the quality of the environment. Also, the categorized of the marine sediments proved that sand extraction from the marine area and placing at the shore has not the proper size to withstand the coastal erosion. Taking the above into account, we conclude that the proper method is the “soft” interference like beach nourishment, but with a size of sediments, two-three categories (0.5 - 4 mm) above the existing one. Also, the sediments that have to be used must be proper not only in size but and environmentally. The material should be researched in terms of quality (relevant petrographic composition with the existing offshore materials of the beach), so as not to cause further ecological disruptions. Finally must quantifying the required loan materials for the artificial nourishment of the coast.

Further Investigations

The placement of i) a weather station, a wave / current measuring instrument, at the Bay, for at least one full seasonal year, ii) a mathematical simulation applications with real weather/wave/current data and iii) the installation of a continuous "video recording" station on the coast, will provide a better insight and a more comprehensive view of the morphodynamic situation of the Platis Gialos Bay.

Acknowledgements

Special thanks to Prof. Seraphim Poulos for the disposal of scientific equipment. Also, i would like to thanks General Secretariat for Research and Technology (GSRT) and the Hellenic Foundation for Research and Innovation (HFRI) for financial support.

References

Folk, R.L. and Ward, W.C. (1957) Brazos River bar: a study in the significance of grain size parameters, Journal of Sedimentary Petrology, vol. 27, pp. 3-26.

NAMA Development S.A. (2003) "Landfill of Sifnos Island: Technical Report".

Soukissian, T.H., Hatzinaki, M., Korres, G., Papadopoulos, A., Kallos, G., Anadranistakis, E., 2007, “Wind and Wave Atlas of the Hellenic Seas”, Hellenic Centre for Marine Research Publ., 300 pp., ISBN-987 960 86651 9-4

Thieler, E.R., Himmelstoss, E.A., Zichichi, J.L. and Ergul, A. (2009) Digital Shoreline Analysis System(DSAS), Version 4.0 — An ArcGIS Extension for Calculating Shoreline Change: U.S. Geological Survey Open-File Report 2008–127.

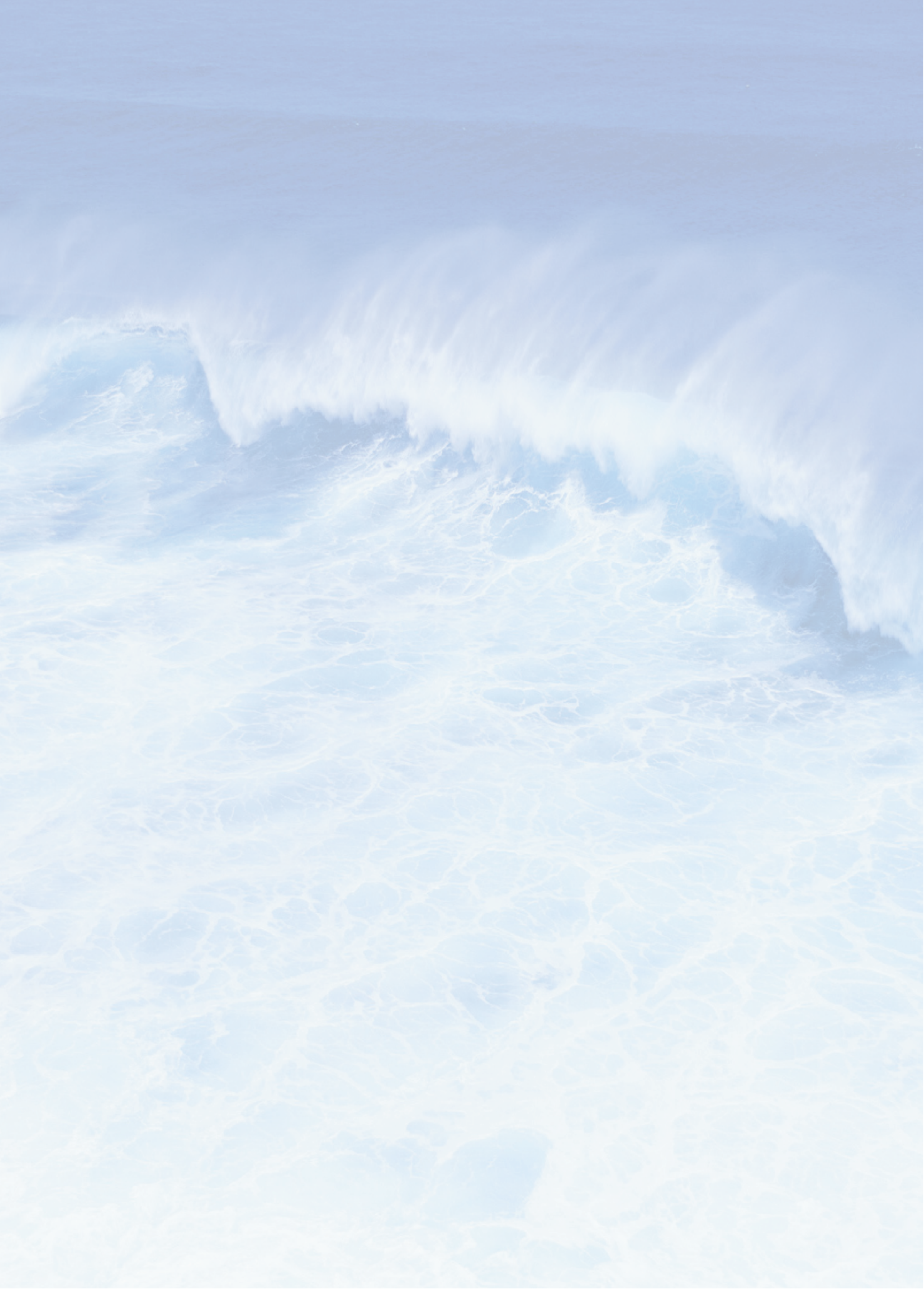

Ακτομηχανική και αρχιτεκτονική μελέτη διαμόρφωσης αλιευτικού καταφυγίου στην εκβολή του ποταμού Λιοπετρίου, Κύπρου

Σ.Μ. Γουλουμής[1*], Β. Ιερείδης[2], Α. Χρίστου[3], Χ. Χατζηγιάγκου[4]

[1]Πολιτικός μηχ. Ε.Μ.Π., Λιμενολόγος-ακτομηχανικός, Αθήνα, Ζωγράφου, Τ.Κ.157 72, Ελλάδα
[2]Αρχιτέκτων μηχ., Υπεύθυνος Συμβούλων Μελετητών, ΙΜΑ ΑΡΧΙΤΕΚΤΟΝΙΚΗ, 1010 Λευκωσία, Κύπρος
[3]Πολιτικός μηχανικός, Πάφος , Κύπρος
[4]Αγρονόμος Τοπογράφος Μηχανικός Α.Π.Θ., 2049 , Στρόβολος – Λευκωσία, Κύπρος
[*]Υπεύθυνος επικοινωνίας: spirosgls@gmail.com

Περίληψη

Η Κυπριακή Δημοκρατία ανέθεσε μελέτες για την διαμόρφωση του Αλιευτικού Καταφυγίου στην εκβολή του Ποταμού Λιοπετρίου, στην νότια ακτή της Κύπρου. Η κοίτη του ποταμού έχει καταληφθεί από τα πρόχειρα παραπήγματα των αλιέων στις όχθες και εντός του ποταμού, εδραζόμενα σε εκατοντάδες πασσάλους κάθε είδους. Η αρχιτεκτονική μελέτη που εκπονήθηκε, προβλέπει την αφαίρεση όλων των υφιστάμενων άναρχων κατασκευών και την διαμόρφωση νέων καλαίσθητων ξύλινων προβλητών επί μεταλλικών πασσάλων για την προσόρμιση των σκαφών και την εξυπηρέτηση των αλιέων. Εκπονήθηκε μελέτη διερεύνησης της κυματικής επίδρασης στις νέες κατασκευές και στα λειτουργικά χαρακτηριστικά του καταφυγίου, σε σχέση με την υδροδυναμική λειτουργία. Προέκυψε ότι η θαλάσσια παλίρροια, που είναι σχετικά έντονη στην ανατολική Μεσόγειο θάλασσα, επηρεάζει συνεχώς και με εναλλασσόμενο τρόπο την κοίτη και τη εκβολή του Ποταμού, καθώς η αυξομείωση της στάθμης του νερού μεταβάλει συνεχώς την ταχύτητα και την κατεύθυνση της ροής του. Η φυσική διαμόρφωση μεγάλης αβαθούς περιοχής στην εκβολή του ποταμού, περιορίζει σημαντικά την μετάδοση των κυμάτων στα ανάντη, καθιστώντας περιττά τα έργα προστασίας για την εισχώρηση των κυμάτων, όπως οι κυματοθραύστες. Η προστασία της κοίτης του ποταμού με συρματοκιβώτια και λιθορριπές που επιλέχθηκε, θα είναι αποτελεσματική και, καθώς θα ενσωματωθεί στα πρανή, θα συνάδει με το φυσικό περιβάλλον.

Λέξεις κλειδιά Καταφύγιο, Ποταμός, Παλίρροια, Συρματοκιβώτια.

1 ΓΕΝΙΚΑ

Το Τμήμα Πολεοδομίας και Οικήσεως (ΤΠΟ) σε συνεργασία με το Τμήμα Αλιείας και Θαλασσίων Ερευνών (ΤΑΘΕ) της Κυπριακής Δημοκρατίας, διεξάγει μελέτη για την Διαμόρφωση του Αλιευτικού Καταφυγίου και του Ποταμού στο Λιοπέτρι, κοινότητα της επαρχίας Αμμοχώστου. Στα πλαίσια αυτά ανατέθηκε Παροχή Υπηρεσιών Πολιτικού Μηχανικού για την εκπόνηση Ακτομηχανικής Μελέτης. Ο Ποταμός Λιοπετρίου εκβάλλει στην νότια ακτή της Κύπρου, ανατολικά της Λάρνακας. Στη δυτική όχθη της εκβολής και στις όχθες της κοίτης έχουν προσορμίσει πολλά αλιευτικά σκάφη (ΕΙΚΟΝΑ 1).

1.1 Διαχρονική εξέλιξη του Ποταμού Λιοπετρίου

Σύμφωνα με μαρτυρίες, κατά τον 18ο αιώνα ο Ποταμός χρησιμοποιούταν σαν λιμενική εγκατάσταση για την μεταφορά εμπορευμάτων και λατομικών προϊόντων προς Λίβανο, Συρία, Αίγυπτο. Στα νεότερα χρόνια, πολλά αλιευτικά σκάφη είχαν βρει καταφύγιο στις όχθες του και σήμερα είναι καταγεγραμμένα 132 σκάφη αλιευτικά ή αναψυχής (στοιχεία έτους 2015 του Τμήματος Αλιείας και Θαλασσίων Ερευνών). Το μήκος της κοίτης του ποταμού είναι 630 περίπου μέτρα με πλάτος από 15-40 μέτρα, ενώ το πλάτος της εκβολής στην θάλασσα φθάνει τα 110 μ.

Όπως φαίνεται σε ορθοφωτοχάρτες των ετών 1963, 1993 και 2014, το 1963 οι όχθες του ποταμού ήταν δασωμένες σε μεγάλο μήκος, χωρίς οδούς πρόσβασης και με πολύ μικρές και λίγες κατασκευές στις όχθες. Αντίθετα, 30 χρόνια μετά το 1993, έχει γίνει σημαντική αποψίλωση και έχουν διανοιχθεί πολλές οδοί στις όχθες του ποταμού, ο οποίος έχει παράλληλα διευρυνθεί. Οι όχθες είναι πλέον διάστικτες από διάφορες κατασκευές. Παρόμοια, το 2014 έχει αυξηθεί ο αριθμός των κατασκευών, παρόχθιων και εντός του ποταμού, ο οποίος έχει διευρυνθεί ακόμη περισσότερο, πιθανώς και λόγω διάβρωσης των όχθων. Επίσης, έχει ανεγερθεί φάρος επί μικρού μόλου στο δυτικό άκρο της εκβολής.

Εικόνα 1 Φωτογραφία κοίτης και εκβολής Ποταμού από νότια.

Οι λιγοστές βροχοπτώσεις κατά τη διάρκεια των τελευταίων δεκαετιών, είχαν ως αποτέλεσμα τη σημαντική μείωση της φυσικής τροφοδοσίας του υδροφορέα και αντίστοιχη μείωση της παροχής του ποταμού.

2 ΑΡΧΙΤΕΚΤΟΝΙΚΗ ΠΡΟΣΕΓΓΙΣΗ ΑΝΑΠΛΑΣΗΣ ΚΑΤΑΦΥΓΙΟΥ

Μετά από Διεθνή Αρχιτεκτονικό Διαγωνισμό δύο φάσεων, η ομάδα που πήρε το πρώτο βραβείο (αρχιτέκτονες Βασίλης Ιερείδης, Αιμίλιος Μιχαήλ, Αλέξανδρος Ζώμας, Ελένη Μητάκου, Αλεξία Ραίση, Παρασκευή Φανού, Δημήτρης Χατζόπουλος) επέλεξε μεταξύ άλλων και τον σχεδιασμό των εγκαταστάσεων που προβλέπεται να κατασκευασθούν στις όχθες του ποταμού για την εξυπηρέτηση των αλιέων με ασφαλείς θέσεις παραβολής των σκαφών, μικρά οικήματα και αποθηκευτικούς χώρους. Θεωρήθηκε απαραίτητο να διαφυλαχθούν ο ιδιαίτερος χαρακτήρας και η λειτουργία του αλιευτικού καταφυγίου με κατασκευές που θα εντάσσονται αρμονικά στο περιβάλλον. Έτσι, προτάθηκε σε αντικατάσταση όλων των παραπηγμάτων να κατασκευασθούν ξύλινοι προβλήτες και αποθήκες επί μεταλλικών πασάλων, αποφεύγοντας την διατάραξη της ροής του ποταμού.

3 ΦΥΣΙΚΕΣ ΣΥΝΘΗΚΕΣ

3.1 Κυματικό κλίμα στην εκβολή του ποταμού

Από διερεύνηση των διατιθέμενων στοιχείων βρέθηκαν κυματικά στοιχεία εικοσαετούς διάρκειας παρατηρήσεων που αφορούν στην περιοχή Δεκέλεια στα δυτικά και στην Αγία Νάπα στα ανατολικά της περιοχής μελέτης (X. Loizidou and J. Dekker, 1994). Τα υψηλότερα χαρακτηριστικά ύψη κύματος Hs παρατηρήθηκαν στην περιοχή της Αγίας Νάπας και προέρχονταν από νοτιοδυτικές διευθύνσεις με ύψη Hs = 4.25m έως 4.75m, από νότιες διευθύνσεις με ύψη Hs = 3.25m έως 3.75m και από νοτιοανατολικές διευθύνσεις με ύψη Hs = 2.25m έως 2.75m.

Τα κύματα που εισχωρούν στην εκβολή του ποταμού προέρχονται από ανατολικές-νοτιοανατολικές διευθύνσεις από τομέα πελάγους 105^o - 135^o ως προς τον βορρά, με μέγιστο χαρακτηριστικό ύψος κύματος Hs = 2.25m και εισέρχονται στην εκβολή υπό γωνία 120^o-110^o=10^o.

Λόγω της ύπαρξης του μόλου όπου υπάρχει ο φάρος στην εκβολή του Ποταμού, τα κύματα από νοτιοανατολικές διευθύνσεις από τομέα πελάγους 135^o - 165^o ως προς τον βορρά, με μέγιστο χαρακτηριστικό ύψος κύματος Hs = 2.75m, εισχωρούν στην εκβολή του μετά από περίθλαση και διάθλαση, εισερχόμενα υπό γωνία 150^o-110^o=40^o.

Τα κύματα από νότιες διευθύνσεις από τομέα πελάγους 165^o - 195^o ως προς τον βορρά με μέγιστο χαρακτηριστικό ύψος κύματος Hs = 3.75m, εισχωρούν στην εκβολή του ποταμού μετά από ισχυρή περίθλαση και διάθλαση και εισέρχονται στην εκβολή υπό γωνία 180º-110º=70º.

3.2 Παλίρροια

Στην ανατολική Μεσόγειο θάλασσα καταγράφεται παλιρροιακό φαινόμενο το οποίο επηρεάζει και το νησί της Κύπρου. Οι παλιρροιογράφοι που έχουν τοποθετηθεί και λειτουργούν σε κάποιες λιμενικές εγκαταστάσεις δίνουν αξιόπιστες καταγραφές. Η διακύμανση της παλίρροιας στο λιμένα Λάρνακας παρουσιάζει μέγιστο εύρος 0,42 μ. Πρόσφατα όμως καταγράφηκε ακραίο παλιρροιακό φαινόμενο στην υπό κατασκευή μαρίνα της Αγίας Νάπα, σε απόσταση 4 χλμ. ανατολικά του Ποταμού.

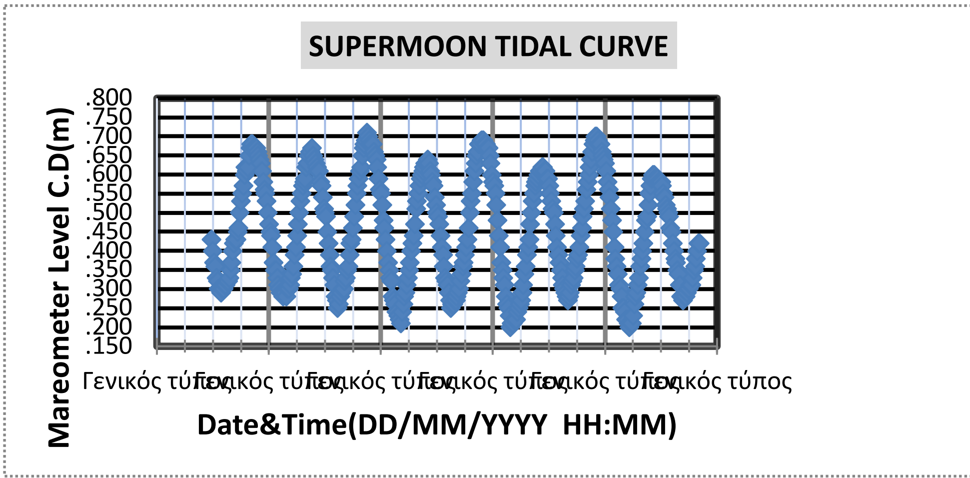

Σχήμα 1 Επεισόδιο μέγιστης παλίρροιας με εύρος 51cm, που μετρήθηκε από την εταιρία P.I.S. UNDERWATER & LAND SURVEYINGSERVICES L.T.D. στην Αγία Νάπα, Νοέμ. 2016

Στο Σχήμα 1 παρουσιάζεται η διακύμανση της παλίρροιας στην μαρίνα της Αγίας Νάπα μεταξύ 14 και 15 Νοεμβρίου 2016, όπου κατά την πανσέληνο σημειώθηκε μέγιστη διακύμανση της μέσης στάθμης της θαλάσσιας επιφάνειας με εύρος 51 εκατοστά.

Πρέπει να σημειωθεί ότι η θαλάσσια παλίρροια η οποία έχει συνεχή διακύμανση μεγάλου εύρους, επηρεάζει συνεχώς και με εναλλασσόμενο τρόπο τον Ποταμό καθώς αυξομειώνει την στάθμη του νερού στην κοίτη του και επομένως την κατεύθυνση της ροής του.

3.3 Μετρήσεις ροής του ποταμού

Για την καλύτερη τεκμηρίωση της ροής του ποταμού, διενεργήθηκαν μετρήσεις της ροής του νερού σε 14 θέσεις επί των όχθεων. Για την μέτρηση της ταχύτητας και κατεύθυνσης της ροής του νερού του ποταμού, χρησιμοποιήθηκε εξοπλισμός νέας τεχνολογίας, που χρησιμοποιεί τεχνολογία μέτρησης της ταχύτητας των αιωρούμενων σωματιδίων του νερού, με τη μέθοδο Doppler (Acoustic Doppler Velocimeter). Η ροή που μετρήθηκε είχε μικρές ταχύτητες από 1 μέχρι και 9 cm/s. Οι τιμές κοντά στην εκβολή έδειξαν ροή από την θάλασσα προς το ποτάμι λόγω παλίρροιας και εισχώρηση του θαλασσινού νερού στην κοίτη του ποταμού, ενώ οι μετρήσεις στα βόρεια της κοίτης έδειξαν ήπια ποτάμια ροή που πρέπει να προέρχεται από υπόγεια ύδατα.

3.4 Βυθομετρία και χαρακτηριστικά της εκβολής του ποταμού

Στην παρακάτω ΕΙΚΟΝΑ 2 παρουσιάζεται η ευρύτερη εκβολή του ποταμού στην θάλασσα και φαίνεται η εκσκαφή που έχει προκαλέσει η ροή του στον θαλάσσιο πυθμένα, σχηματίζοντας υποθαλάσσια κοίτη, επιβεβαιώνοντας τη συνεχή ροή του ποταμού λόγω της απορροής του υετού (η οποία γίνεται επιφανειακά και υπόγεια) και λόγω της συνεχούς παλίρροιας και άμπωτης, καθιστώντας απαγορευτική την κατασκευή «σκληρών» έργων στην ευρύτερη κοίτη του ποταμού, αφού θα εμπόδιζαν την ροή.

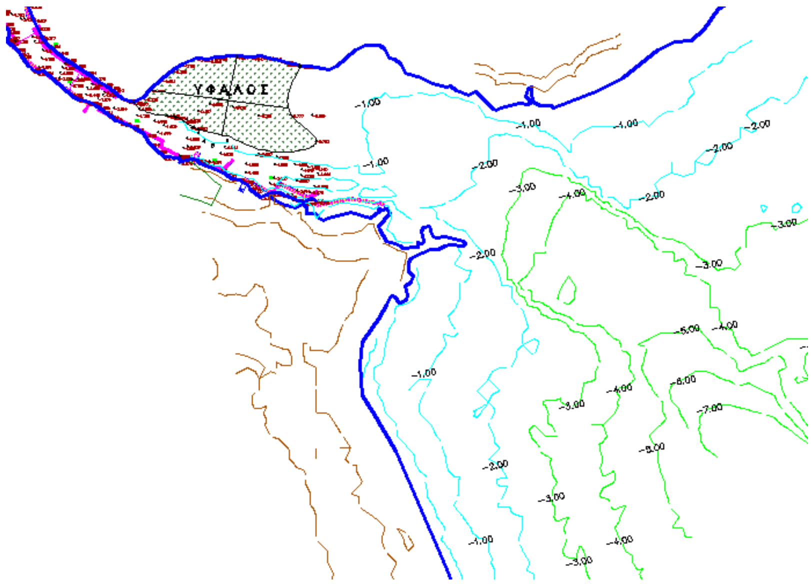

Εικόνα 2 Βυθομετρία εκβολής Ποταμού Λιοπετρίου και θέση ύφαλου.

Ο αμμώδης ύφαλος στην εκβολή σε στάθμη -0,70μ. μέχρι -0,40μ. (ο οποίος είναι καλυμμένος με φύκια που του προσδίδουν σταθερότητα), έχει διαστάσεις περίπου 120 μέτρα μήκος και πλάτος 70 μέτρα και λειτουργεί ως ύφαλος κυματοθραύστης (submerged breakwater) απομειώνοντας σημαντικά το ύψος και την ισχύ των προσπιπτόντων κυμάτων (όπως φαίνεται στην Εικόνα 2), τα μεγαλύτερα των οποίων υπολογίζεται ότι έχουν μήκος κύματος μικρότερο των διαστάσεων του υφάλου.

4 ΥΠΟΛΟΓΙΣΜΟΣ ΔΙΑΔΟΣΗΣ ΚΥΜΑΤΙΣΜΩΝ

Εξετάσθηκε η διάδοση των μεγαλύτερων κυμάτων με περίοδο επαναφοράς 20 ετών για μετάδοση από νοτιοδυτικές, νότιες και νοτιοανατολικές διευθύνσεις που εισέρχονται στην εκβολή του Ποταμού Λιοπετρίου. Λήφθηκαν υπόψη τα χαρακτηριστικά της περιοχής εκβολής του ποταμού, τα χαρακτηριστικά μορφολογίας πυθμένα, κλίσεις παράκτιου πυθμένα, η βυθομετρία της λιμενολεκάνης και της ευρύτερης περιοχής εκβολής του ποταμού, η μορφολογία στις όχθες του ποταμού και των παράκτιων πρανών και υπολογίσθηκαν η διασπορά της κυματικής ενέργειας από τα φαινόμενα ρήχωσης και περίθλασης.

Ο καθηγητής Αθανάσιος Α. Δήμας, διευθυντής του Εργαστηρίου Υδραυλικής Μηχανικής του Τμήματος Πολιτικών Μηχανικών Πανεπιστημίου Πατρών, εκπόνησε την αριθμητική προσομοίωση

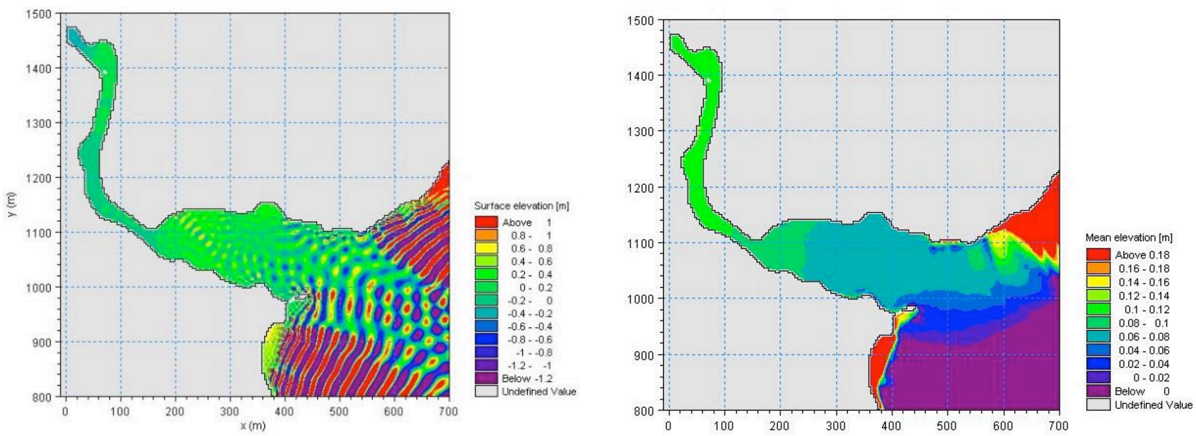

Εικόνα 3 Κατανομή κυματογενούς ανύψωσης ελεύθερης επιφάνειας στις εκβολές του ποταμού όπου φαίνεται η θραύση του κύματος και set-up. Παρατηρείται η αυξημένη ανύψωση της στάθμης του νερού στο βορειοδυτικό άκρο της κοίτης λόγω εγκλωβισμού του κύματος σε περιορισμένο χώρο.

διάδοσης των κυμάτων με στόχο τη διερεύνηση της κυματικής διείσδυσης εντός του Ποταμού Λιοπετρίου. Επίσης, έγινε υπολογισμός ανύψωσης της θαλάσσιας επιφάνειας λόγω του κυματισμού (setup) καθώς και η ταχύτητα του παράλιου κυματογενούς θαλάσσιου ρεύματος. Όπως φαίνεται στις προσομοιώσεις (Εικόνα 3), επιβεβαιώνεται ότι τα μεγαλύτερα κύματα που φθάνουν στην εκβολή του ποταμού υφίστανται ισχυρή ρήχωση με αποτέλεσμα να μην μεταδίδονται στα ανάντη.

Εικόνα 4 Δορυφορική φωτογραφία διάδοσης κυμάτων από ΝΔ διευθύνσεις στην εκβολή του Ποταμού.

5 ΑΞΙΟΛΟΓΗΣΗ ΥΦΙΣΤΑΜΕΝΗΣ ΚΑΤΑΣΤΑΣΗΣ ΠΟΤΑΜΟΥ ΚΑΙ ΕΡΓΑ ΠΡΟΣΤΑΣΙΑΣ

Οι πολλές εκατοντάδες πάσσαλοι (700-900 πάσσαλοι !!!) κάθε είδους και μεγέθους που έχουν χρησιμοποιηθεί τα τελευταία σαράντα και περισσότερα χρόνια για την στήριξη των 119 πρόχειρων εξεδρών για την εξυπηρέτηση των αλιέων, λειτουργούν πλέον σαν ένα είδος «βαθιάς εξυγίανσης» των όχθεων του ποταμού, βελτιώνοντας σαφώς τα γεωτεχνικά χαρακτηριστικά του υποβάθρου, σταθεροποιώντας το έδαφος των όχθεων. Η ύπαρξή τους επί δεκαετίες, καθιστά πολύ δύσκολη την αφαίρεσή τους η οποία καθίσταται απαγορευτική, γιατί θα μπορούσε να προκαλέσει την ακούσια ανασκαφή των όχθεων της κοίτης σε μεγάλο βάθος, επιφέροντας μεγάλες βλάβες και μόνιμη αλλοίωση της μορφής και λειτουργίας του ποταμού. Για την αφαίρεση των πασσάλων για λόγους ασφάλειας και καλαισθησίας θα πρέπει να χρησιμοποιηθούν μή καταστροφικές μέθοδοι. Συστήνεται η χρήση συρματοκοπής για την αποκοπή των τμημάτων των πασσάλων που εξέχουν από τον πυθμένα του ποταμού. Όσοι πάσσαλοι δεν ενοχλούν, θα παραμείνουν με κατάλληλη σήμανση ασφαλείας.

Καθώς η ανύψωση της στάθμης της θάλασσας λόγω παλίρροιας αλλά και set-up έχει επίδραση στα πρανή της κοίτης του ποταμού ρευστοποιώντας τα μαλακά εδάφη, ενώ δεν υπάρχει δόκιμος τρόπος αποτροπής της, είναι απαραίτητη η προστασία των πρανών της κοίτης του ποταμού για την αποφυγή της διάβρωσής τους. Για την καλύτερη περιβαλλοντική προσαρμογή των επεμβάσεων, επιλέχθηκε να γίνει τοποθέτηση συρματοκιβωτίων βαρέως τύπου, πληρωμένων με λίθους κατάλληλου μεγέθους για την προστασία των πρανών. Τα συρματοκιβώτια θα βυθισθούν τελικά στο μαλακό έδαφος και ακόμα και όταν τα σύρματα διαβρωθούν, οι λίθοι θα ενσωματωθούν στα πρανή προσφέροντας προστασία. Στα τμήματα της κοίτης με πιο σταθερό έδαφος, είναι αρκετή η προστασία με κατάλληλη λιθορριπή. Το συνολικό αποτέλεσμα των επεμβάσεων αναμένεται να αναβαθμίσει τον Ποταμό Λιοπετρίου αναδεικνύοντας το φυσικό περιβάλλον, προσφέροντας παράλληλα καλές εγκαταστάσεις στους αλιείς.

Βιβλιογραφική Αναφορά

X. Loizidou, J. Dekker (1994) Nearshore wave climate analysis for Cyprus. published by Coastal Unit, Public Works Department, Nicosia, p 300.

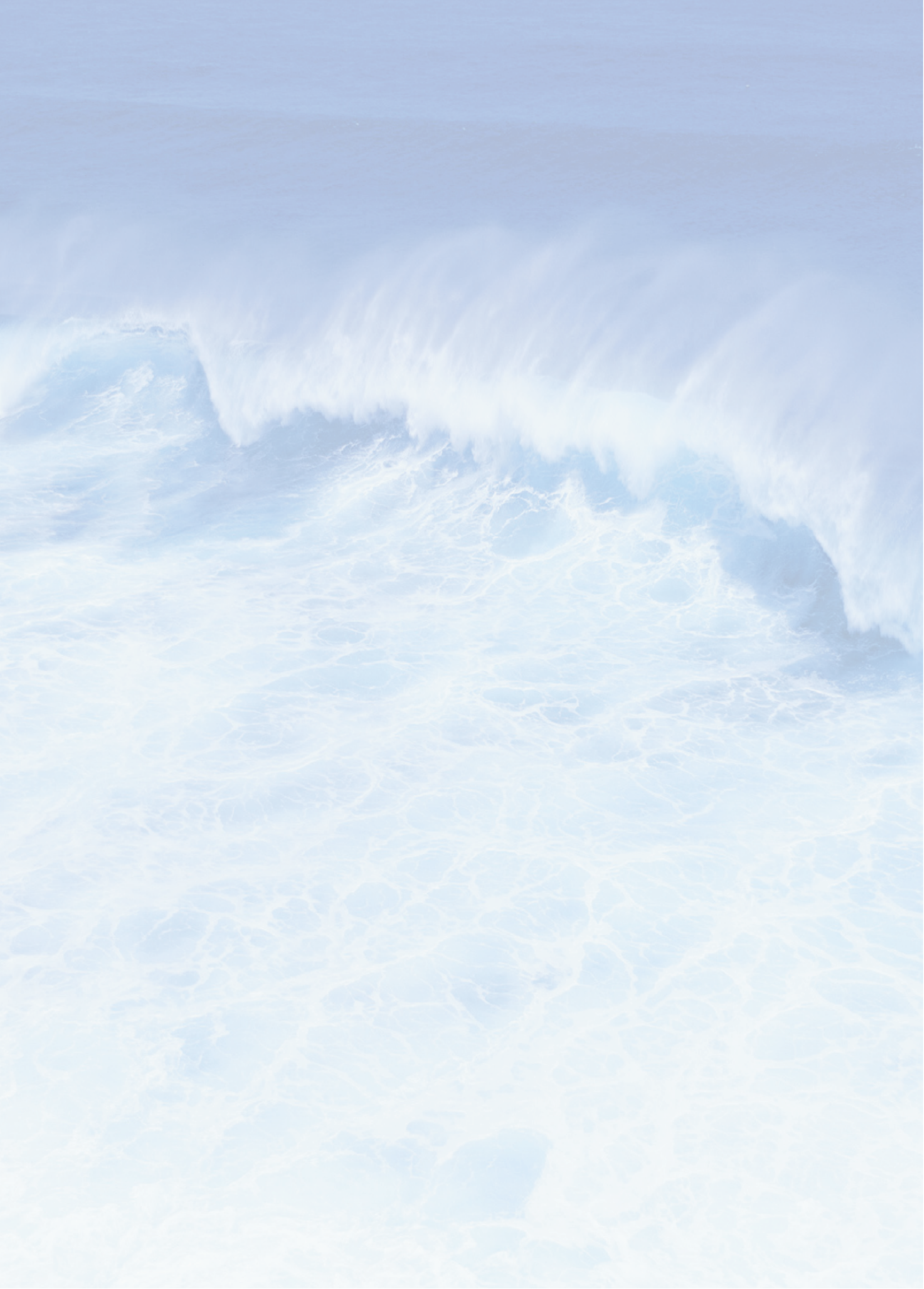

SESSION 9 WAVE HYDRODYNAMICS

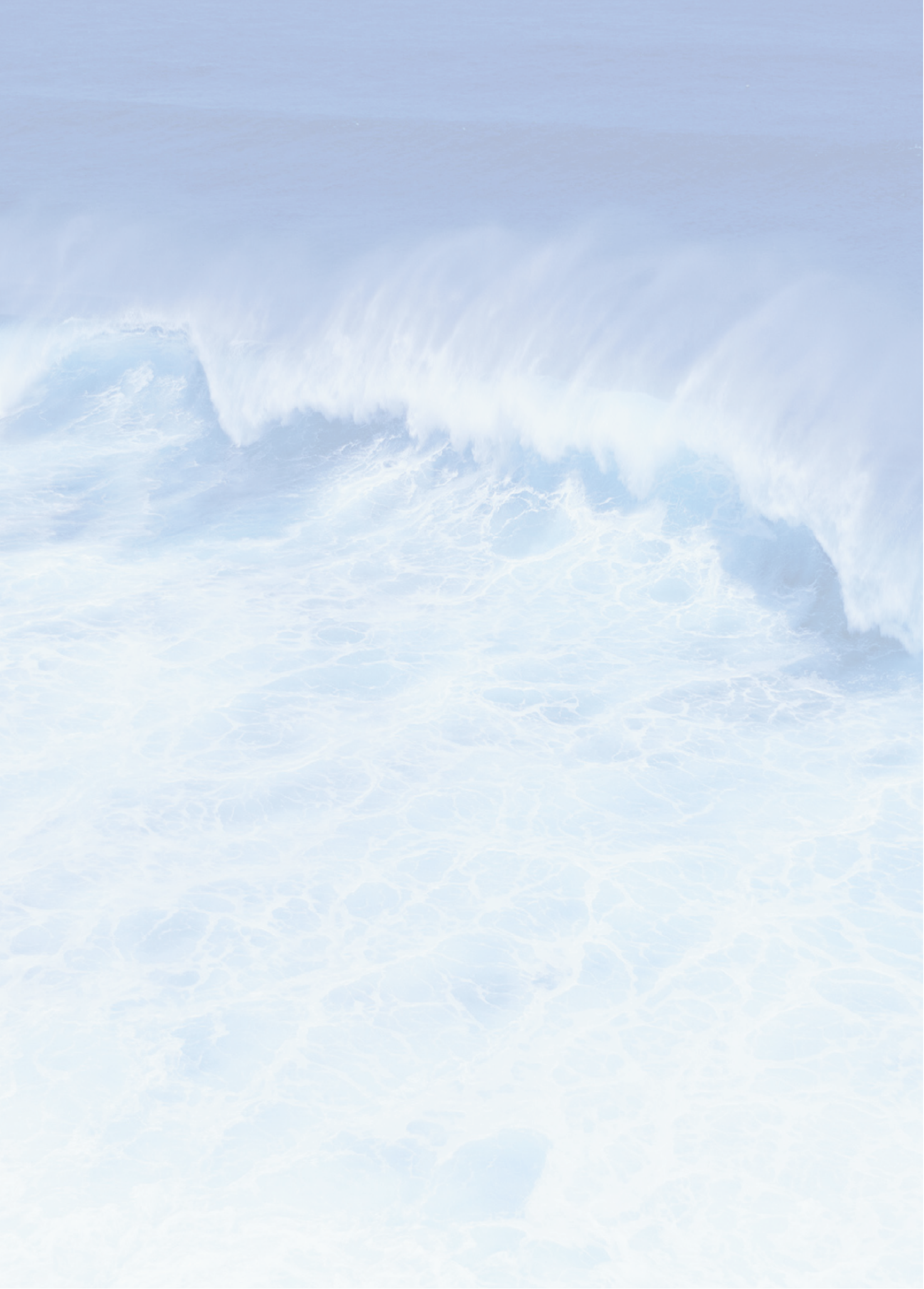

Advanced numerical models for simulation of nearshore processes

M.K. Chondros[1*], A.S. Metallinos[1], Th.V. Karambas[1,2], C.D. Memos[1,3], A.G. Papadimitriou[1]

[1]Scientia Maris, Agias Elenis 10, Zografos, 15772, Greece
[2]Department of Civil Engineering, Aristotle University of Thessaloniki, Thessaloniki 54124, Greece
[3]School of Civil Engineering, National Technical University of Athens, Zografos 15780, Greece
[*]Corresponding author: michondros@gmail.com

Abstract

Two advanced numerical models are presented in this paper, developed by Scientia Maris, to meet real-life challenges by simulating nearshore wave processes. The first one, Maris-HMS, is a nonlinear hyperbolic mild slope model and the second one Maris-PMS, is a nonlinear parabolic mild slope model. Both models are capable of simulating the transformation of complex regular and irregular wave fields in coastal areas with varying bathymetries. The developed numerical models showed a satisfactory agreement with laboratory measurements and in most cases performed equivalently or better than other widely known commercial models.

Keywords Mild-slope equations, Numerical models, Coastal processes, Nonlinear amplitude dispersion.

1 INTRODUCTION

Simulation of nearshore wave propagation is of paramount importance in port and coastal engineering projects. During the past few decades, numerous researchers have contributed to the development of numerical models capable of simulating complex physical phenomena. Among a plethora of different equations and methodologies the so-called "mild-slope" models, based on the mild-slope equation (Berkhoff, 1972), have been widely used since they offer ease in implementation and relatively quick simulation times in conjunction with satisfactory accuracy for engineering applications. A significant number of models have been developed, based on this equation, for simulating nearshore processes including shoaling, refraction, diffraction, reflection, bottom friction and depth-induced wave breaking. The original mild-slope equation was derived as an inseparable elliptical partial differential equation with complex variables. Directly solving this equation is a prohibitively time consuming process, especially when considering large numerical domains. Therefore various approximations have been proposed. In the present work, two advanced mild-slope models are presented, as developed by Scientia Maris to incorporate nonlinear effects which are of utmost importance in the nearshore. The first one, Maris-HMS, is a nonlinear hyperbolic mild slope model, while the second one Maris-PMS is a nonlinear parabolic-type mild slope model. Both models are capable of simulating the transformation of complex wave fields, in coastal areas with varying bathymetries in a reasonable computational time. The model results are compared with the experimental measurements of Berkhoff et al. (1982), showing thus their ability to accurate predict the wave field. The developed numerical models are also compared against widely known commercial models, achieving an overall equivalent or better performance.

2 THEORETICAL BACKGROUND AND VERIFICATION OF PROPOSED MODELS

2.1 Maris-PMS, a Parabolic-type Mild Slope model

The first model, Maris-PMS hereafter, is based on the work of Kirby and Dalrymple (1983) that derived a parabolic equation, in the form of a cubic Schrödinger differential equation, governing the complex amplitude A of the fundamental frequency component of a Stokes wave. Kirby (1986) presented the following nonlinear parabolic equation based on minimax principles in order to allow for large angle propagation:

$$C_g A_x + i(\bar{k} - a_0 k) C_g A + \frac{1}{2}(C_g)_x A + \frac{i}{\omega}\left(\alpha_1 - b_1 \frac{\bar{k}}{k}\right)(CC_g A_y)_y - \frac{b_1}{\omega k}(CC_g A_y)_{yx} + \frac{b_1}{\omega}\left(\frac{k_x}{k^2} + \frac{(C_g)_x}{2kC_g}\right)(CC_g A_y)_y + \frac{i\omega k^2}{2} D|A|^2 A + \frac{w}{2} A = 0 \quad (1)$$

where the parameter D is given by $D = \frac{(\cosh 4kh + 8 - 2\tanh^2 kh)}{8\sinh^4 kh}$, A is a complex amplitude related to the water surface displacement by $\eta = Ae^{-i(kx-\omega t)}$, x is the principal direction of propagation, k local wave number, ω wave angular frequency, h water depth, $\bar{k}$ is a reference wave number, taken as the average wave number along the y axis, C phase speed, C_g group velocity, w is a dissipation factor and finally a_0, α_1 and b_1 coefficients used for the minimax approximation depending on the range of angles to be considered. The local wave number, k, is related to the angular frequency of the waves, ω, and the water depth, h, by the linear dispersion relation $\omega^2 = gk\tanh(kh)$.

In order to include the nonlinear wave propagation effects, Kirby and Dalrymple (1986), instead of using the linear dispersion relation, proposed the following approximate nonlinear dispersion relation:

$$\omega^2 = gk\big(1 + f_1(kh)\varepsilon^2 D\tanh(kh + f_2(kh)\varepsilon)\big) \quad (2)$$

where $f_1(kh) = \tanh^5(kh)$, $f_2(kh) = [kh/\sinh kh]^4$, $\varepsilon = k|A|$.

Alternatively, an analytical approach is proposed in the present paper in order to incorporate exact nonlinearity at any depth, as initially proposed by Chondros and Memos (2014). This is achieved by calculating the local Ursell parameter, $\mathrm{Ur} = \mathrm{HL}^2/\mathrm{h}^3$, (H denotes wave height and L wave length) and the wave steepness, $\mathrm{s} = \mathrm{H}/\mathrm{L}$, in all grid cells of the domain. Given the above parameters and taking advantage of the regions of validity of analytical wave theories as proposed by Hedges (1995), one can calculate the exact nonlinear amplitude dispersion relation in accordance to any of Stokes second or fifth order, Cnoidal or Solitary theories as follows:

Table 1 Regions of wave theories validity and respective dispersion relation

Regions of wave theories validity			Dispersion relation
$\boldsymbol{s < 0.04}$	$Ur < 40$	Stokes 1st	$\omega^2 = gk\tanh(kh)$
$\mathbf{s > 0.04}$	$Ur < 40$	Stokes higher	$\omega^2 = gk(1 + \varepsilon^2 D)\tanh(kh)$
$\mathbf{s > 0.00}$	$40 < \mathrm{Ur} < 4000$	Cnoidal	$\omega^2 = gk^2\mathrm{h}\big(1 + H/mh(2 - m - 3E/K)\big)$, where K, E are the complete elliptic functions of the first and second kind, respectively. The parameter $\boldsymbol{m}$ is the modulus of the elliptic functions. Alternatively, the modified Cnoidal equation is used herein: $\omega^2 = gk^2\mathrm{h}(1 + f(m)H/h)$, Bell et al. (2004) assumed a value of 0.4 for $f(m)$
$\mathbf{s > 0.00}$	$\mathrm{Ur} > 4000$	Solitary	$\omega^2 = gk^2h(1 + H/h)$
The above regions are limited by wave breaking limits in deep and shallow waters			

In order to investigate the performance of the model based on the analytical approach against the approximate equation of Kirby and Dalrymple (1986) we include here a comparison in the experiment described by Berkhoff et al. (1982). The bathymetry in this experiment consisted of an elliptic shoal resting on a 1:50 plane sloping seabed, as shown in Figure 1. The entire slope was turned at an angle of 20$^{\mathrm{o}}$ with respect to the wave paddles. The incident monochromatic wave height was *H*=0.0464 m with period *T*=1.0 sec. The normalized wave heights in sections S4-S7 are given in Figure 2 for both approaches along with the experimental measurements.

As it can be seen, the model with the analytical approach of calculating the nonlinear amplitude dispersion relation behaves very well and captures correctly the wave focusing along sections S4, S5, S6 and S7. An almost equivalent performance is observed with the model incorporating the approximate Eq. 2. Through the aforementioned analytical approach the exact nonlinear phase and group velocities and the wave numbers can be calculated in each grid cell in respect to the most appropriate nonlinear theory, automatically calculated by the model. Nevertheless, we should mention that wave properties do not vary smoothly across the division between Stokes and Cnoidal waves and for larger amplitudes the series solution does not converge.

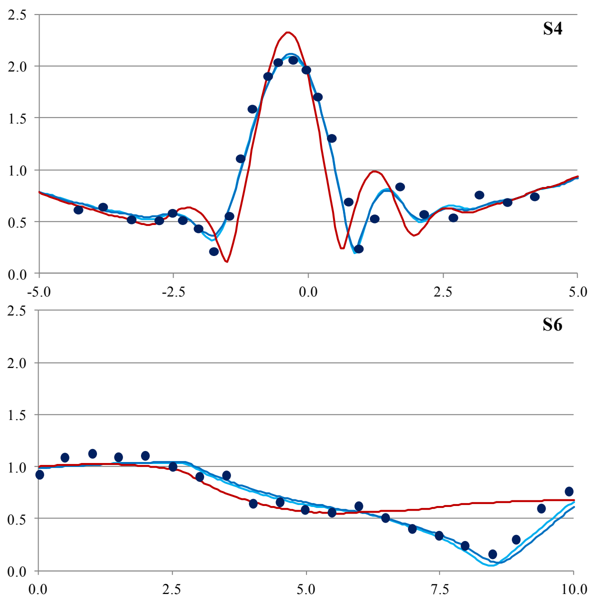

Figure 1 Normalized wave heights along sections S4-S7, Berkhoff et al.'s (1982) experiment (dots); Maris-PMS with the analytical approach (light blue) and with the approximate Eq. 2 (blue); MIKE21 PMS (red)

2.2 Maris-HMS, a Hyperbolic-type Mild Slope model

In addition to the aforementioned parabolic approximation of the mild-slope equation, numerous models have been developed based on the elliptical and hyperbolic types of this equation. Copeland (1985) proposed, as an approximation to the original elliptical equation, a set of three coupled first-order hyperbolic equations, and solved these equations with the use of time-stepping techniques. Karambas et al. (2010, 2013) further developed this model to include energy dissipation due to wave breaking and bottom friction, deriving thus a model capable of simulating all the main wave transformation phenomena including wave reflection in harbors and coastal areas in the vicinity of ports with varying bathymetries. The basic continuity and momentum equations are written as:

$$\eta_t + \frac{c}{c_g}\nabla\frac{c_g}{c}\boldsymbol{Q_w} = 0 \tag{3}$$

$$\boldsymbol{U_{w,t}} + \frac{c^2}{d}\nabla\eta = v_h\nabla^2\boldsymbol{U_w} \tag{4}$$

where η is the surface elevation, $\mathbf{U_w} \equiv (U_w, V_w)$ is the mean velocity vector, ∇ is the horizontal gradient operator, d is the depth, $\mathbf{Q_w} = \mathbf{U_w}\mathrm{h_w} = (\mathrm{Q_w}, \mathrm{P_w})$, $\mathrm{h_w}$ is the total depth ($h_w = \mathrm{d} + \eta$), and v_h is an horizontal eddy viscosity coefficient copying with wave breaking and wave reflection.

As mentioned above, this model does not take into account nonlinear wave propagation effects which are of paramount importance in the nearshore zone. Hence, we develop a model herein, Maris-HMS, based on the above equations to incorporate nonlinearity. This can be achieved by adopting one of the following two proposed methods:

Firstly, the linear version of the model, meaning that phase and group velocities and wave numbers are calculated via the linear dispersion relation, are applied to simulate the wave propagation and calculate initial estimates of wave heights all over the numerical domain. As soon as a linear steady state has been reached the nonlinear dispersion relation is implemented. The new, nonlinear phase and group velocities and the wave numbers can now be calculated in each grid cell. The simulation continues with the new values of the above quantities and this process is repeated in a constant time interval equals to the wave period, until a second steady state is reached. On the one hand the first method incorporates the nonlinear effects accurately (as it will be shown below), while on the other hand requires nearly the double simulation time to achieve a “nonlinear” steady state. Although the increased simulation time remains reasonable for engineering applications, we further propose an alternative way to minimize the required simulation time and produce a fast, yet accurate, numerical model. The parabolic mild-slope model, presented in the previous chapter, is implemented to calculate the spatial distribution of wave height in the numerical domain, taking into account the nonlinear effects. This model requires zero simulation time and is capable of calculating the nonlinear phase velocities in each cell of the grid. These velocities are then fed into the hyperbolic mild-slope model replacing the calculation based on the linear dispersion relation. By adopting this latter method, the “one-way coupling” of parabolic and hyperbolic mild slope models can predict accurately the wave characteristics in the coastal zone with low computational cost and fast simulation times.

The above two methods are implemented to simulate the experiment of Berkhoff as presented above. It can be seen (Figure 2) that both of them converge very well to the experimental data. A deviation is observed in the middle of Section 1. This deviation was observed for all the models implemented in the present paper. Their results are close to each other, proving that the second method of introducing the nonlinearity, without requiring additional simulation time, can be applied. Furthermore the results of the linear version of the model are depicted in the same figure. In Sections 1 and 2 the improvement is not significant since the nonlinear effects do not contribute yet. In Sections 5 and 6 the results of the nonlinear model are significantly better than those of linear model, proving the importance of the improvement, achieved in this paper, to capture correctly the wave focusing downstream of the shoal by simulating the combined shoaling, diffraction and refraction effects.

The advanced nonlinear mild-slope models developed herein, Maris-PMS and Maris-HMS, are compared (see Figures 2 and 3) to the benchmark experiment of Berkhoff and against similar models: MIKE21 PMS (DHI, 2007a), MIKE21 EMS (DHI, 2007b), ARTEMIS (Aelbrecht et al., 1997) and CGWAVE (Panchang and Xu, 1995). ARTEMIS takes into account nonlinear effects due to rapidly varying topography; MIKE21 EMS is a linear model, while CGWAVE simulates wave propagation taking into account the nonlinear amplitude dispersion. MIKE21 EMS depicts a significant deviation from experimental data, especially in Section 5. ARTEMIS behaved relatively well, while Maris-HMS and CGWAVE gave the most satisfactory results due to incorporation of nonlinear amplitude dispersion relation. Applications of the proposed models Maris-PMS and Maris-HMS can be found in the companion paper of Metallinos et al. (2019).

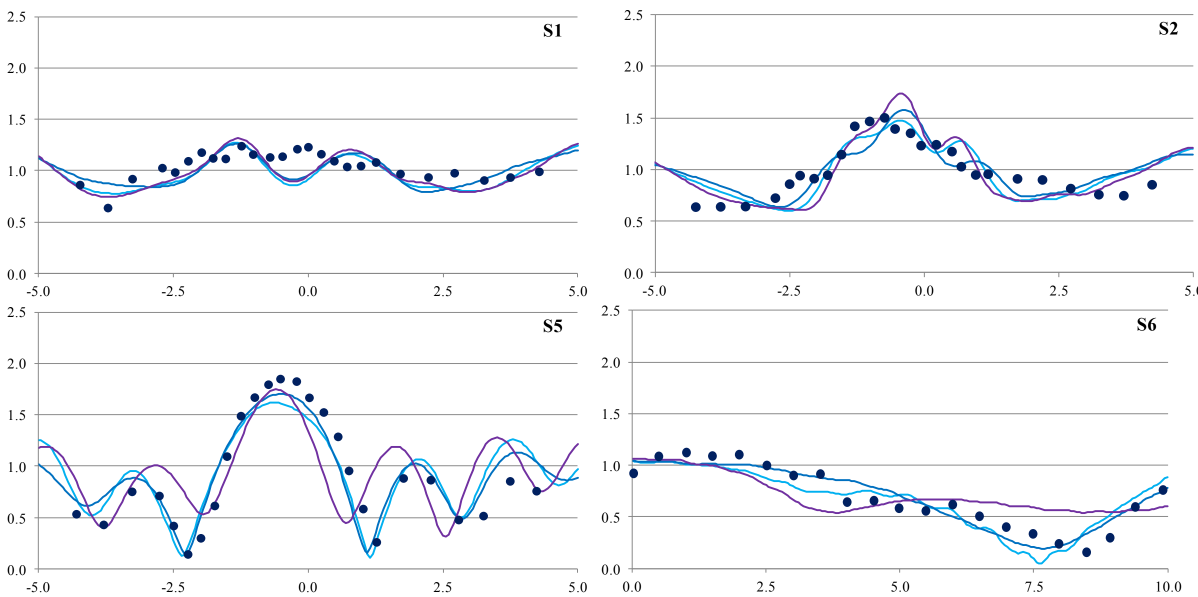

Figure 2 Normalized wave heights along sections S1, S2, S5 and S6, Berkhoff et al.'s (1982) experiment (dots); Maris-HMS linear version (purple), nonlinear version with the first (blue) and second method (light blue)

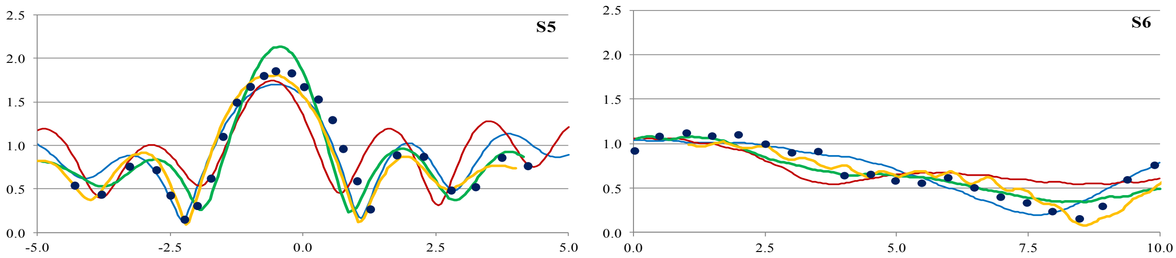

Figure 3 Normalized wave heights along sections S5 and S6, Berkhoff et al.'s (1982) experiment (dots); Maris-HMS (blue line); MIKE21 EMS (red line); ARTEMIS (green line); CGWAVE (yellow line)

3 CONCLUSIONS

In conclusion, Maris-PMS and Maris-HMS model results are close to the experimental data in the cases examined. These models showed better or equivalent performance against widely known commercial models. Both models are capable of simulating the transformation of complex regular and irregular wave fields in coastal areas with varying bathymetries.

References

Aelbrecht D., Sauvaget, P. and Lang, P. (1997) ARTEMIS Software. EDF Report HE-42/97/038/A.

Bell, P.S.,Williams, J.J., Clark, S., Morris, B.D., Vila-Concejo, A., (2004). Nested radar systems for remote coastal observations. Journal of Coastal Research Special Issue 39, 1.

Berkhoff, J.C.W., (1972). Computation of combined refraction-diffraction. Proc. 13th Int. Conf. Coastal Engineering, Vancouver.

Berkhoff, J.C.W., Booij, N., Radder, A.C., (1982). Verification of numerical wave propagation models for simple harmonic linear water waves. Coastal Engineering, 6, 255–279.

Chondros, M.K. and Memos, C.D. (2014). A 2DH Nonlinear Boussinesq Wave Model of Improved Dispersion, Shoaling, and Wave Generation Characteristics, Coastal Engineering, Vol.91, pp. 99-122

Copeland, GJM (1985): A Practical Alternative to the Mild-Slope Equation. Coastal Engineering, 9, 125-149.

DHI, 2017a. MIKE21 Parabolic Mild-Slope module: Scientific doc. Danish Hydraulic Institute.

DHI, 2017b. MIKE21 Elliptic Mild-Slope module: Scientific doc. Danish Hydraulic Institute.

Hedges, T.S., (1995). Regions of validity of analytical wave theories. Water, Maritime and Energy Journal. Proceedings of the Institution of Civil Engineers. 112, 111–114.

Karambas, T., Christopoulos, S. and Avgeris, I. (2010). HARBOUR_L: Integrated mathematical model for the design of harbor works. In Proc. 5th Pan-Hellenic Conference of Harbour Works, Athens, Greece.

Karambas Th., E. Koutandos, N. Kampanis, (2013). Numerical simulation of wave induced morphology evolution. Maritime Engineering Journal, 166 (3), 113 –124.

Kirby, J.T., (1986). Rational approximations in the parabolic equation method for water waves, Coastal Engineering, 10, 355-378.

Kirby, J.T. and Dalrymple, R.A., (1983). A parabolic equation for the combined refraction- diffraction of Stokes waves by mildly varying topography. Journal of Fluid Mechanics, 136: 453-466.

Kirby, J.T. and Dalrymple, R.A., (1986). An approximate model for nonlinear dispersion in monochromatic wave propagation models. Coastal Engineering, 9, 545–561.

Metallinos, A.S, Chondros, M.K, Karambas, Th., Memos, C.D Papadimitriou, A. (2019). "Advanced Numerical Models for Wave Dısturbance Simulation in Port Basins", 1st International Scientific Conference on Design and Management of Harbor, Coastal and Offshore Works. Athens, Greece, 8 to 11 May.

Panchang, V. G. and Xu, B. (1995). CGWAVE: A Coastal Wave Transformation Model for Arbitrary Domains, Tech. Report, Dept. of Civil and Environmental Engineering, University of Maine, Oct. 1995.

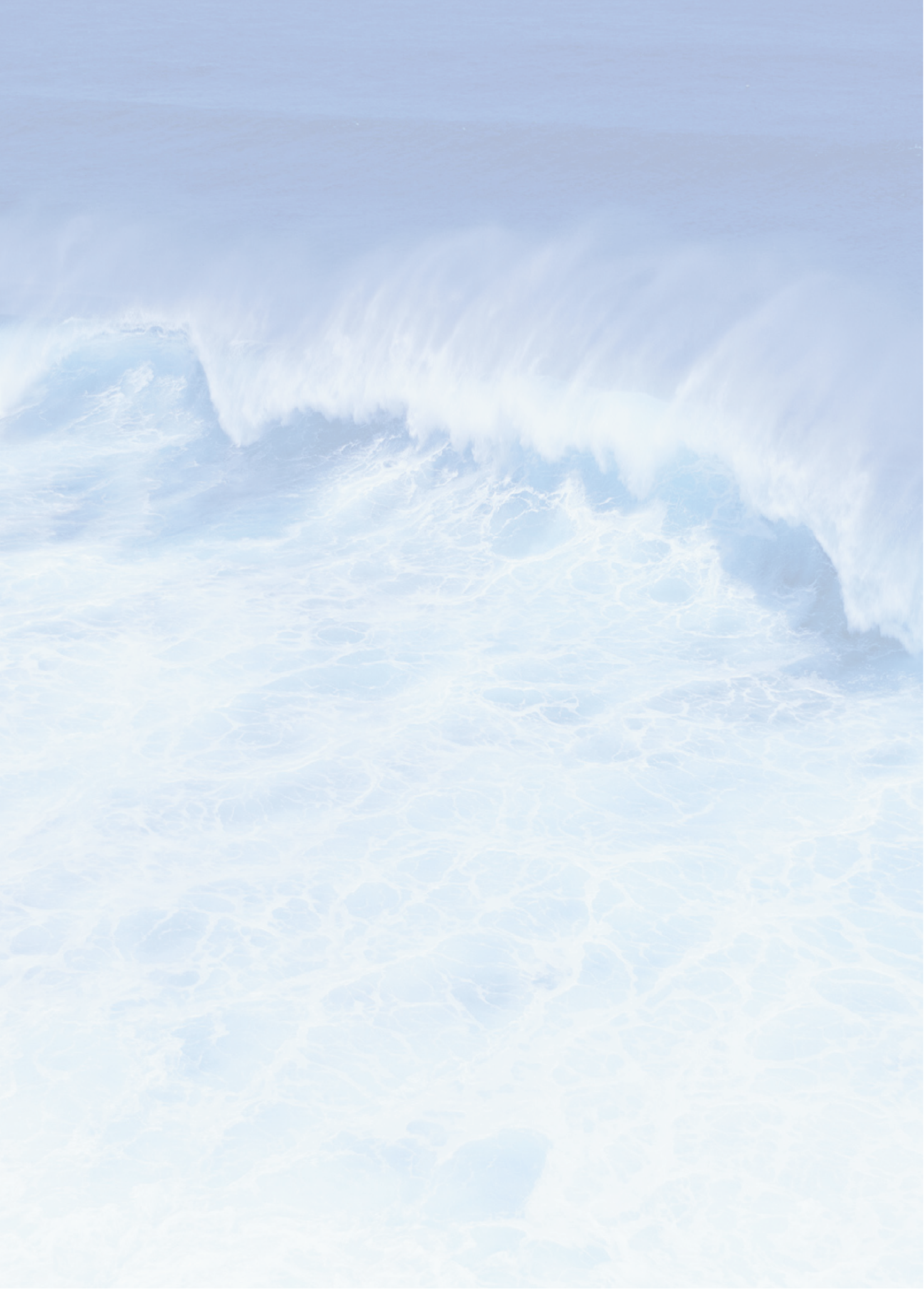

Adapting OpenFOAM® CFD numerical model, to the simulation of significant coastal zone wave processes in full three dimensional (3D) applications

I.G. Kazakis*, Th.V. Karambas

Department of Civil Engineering, Aristotle University of Thessaloniki, Thessaloniki, 54124, Greece
*Corresponding author: kazakisi@civil.auth.gr

Abstract

Protection and restoration of coasts and sandy beaches is related to the construction of coastal structures, including various types of breakwaters. Wave diffraction in the lee of such structures along with wave breaking and related hydrodynamic phenomena, produces strong wave induced currents, resulting to the appearance of morphodynamic processes. Sediment transport leads to the accretion /erosion of coastal areas, with direct effects on the morphological formation of the coastal zone with economic and social impacts. This study focuses on the efficiency and applicability of OpenFOAM®, open-source CFD numerical model in the assessment of hydrodynamic processes of coastal zone through the investigation of diffraction and wave induced current phenomena behind a detached breakwater. The numerical scheme is suitably framed by initial conditions of wave propagation and absorption in a full three-dimensional (3D) application, and its results are compared against analytical solution and experimental data concerning the wave height and current velocity.

Keywords OpenFOAM®, 3D Simulation, Wave Diffraction, Wave Induced Current.

1 INTRODUCTION

The main purpose of present work is to validate OpenFOAM® as a simulation tool of significant physical wave processes in coastal zone in full three dimensional (3D) applications. The considerable amount of freedom that is being gained by approaching such problems using free surface modeling in the context of Reynolds averaged Navier – Stokes equations, sets OpenFOAM® in an advantageous position among the community of numerical modeling tools. The majority of existing numerical models for simulate surface water waves, generally limited to Boussinesq – type models both in the surf and in swash zone, (Karambas and Koutitas 2002, Karambas and Samaras 2017). All the above methods have depth integrated approach and are limited essentially in two dimensional applications. Instead, three dimensional characteristics of wave phenomena in surf zone, such as the prediction of undertow and its depth variation, poses as necessity the existence of full three dimensional numerical models. The ability of generation and absorption of free surface water waves providing by toolboxes waves2Foam (Jacobsen et al. 2012), and IHFoam (Higuera et al. 2013a) expands the applicability of the numerical Model, setting up new standards and opportunities in coastal engineering applications. There are several works on the validity of the numerical model, mainly comparing two-dimensional (2D) application with experimental data, (Chen et al. 2014) , or three-dimensional (3D) application emphasized in wave height measurements, (Higuera et al. 2013b). According to the authors knowledge there is not an extended work until now in three dimensional (3D) validation applications of coastal zone and specifically in surf zone hydrodynamics processes using OpenFOAM®. In that way the purpose of this work focuses on the adaption of OpenFOAM® numerical model with the contribution of waves2Foam toolbox and a selected turbulence closure model (Devolder et al. 2018), for simulating surf zone hydrodynamic phenomena in full three dimensional (3D) approach.

2 GOVERNING EQUATIONS

The solver, *interFoam*, part of OpenFOAM®, solves Navier Stokes equations for two incompressible, isothermal immiscible fluids in three dimensions in combination with Volume of fluid Method (VoF) according to Finite Volume Method (FvM).The set of governing equations is given below (see Table 1 for symbols).

Continuity equation:

$$\frac{\partial u}{\partial x}+\frac{\partial w}{\partial y}+\frac{\partial w}{\partial z}=0 \tag{1}$$

Momentum equations in three dimensions x,y.z respectively:

$$\frac{\partial \rho u}{\partial t}+\left(u\frac{\partial \rho u}{\partial x}+v\frac{\partial \rho u}{\partial y}+w\frac{\partial \rho u}{\partial z}\right)=-\frac{\partial p}{\partial x}+\mu_{eff}\left(\frac{\partial^2 u}{\partial x^2}+\frac{\partial^2 u}{\partial y^2}+\frac{\partial^2 u}{\partial z^2}\right)+\sigma\kappa\frac{\partial \alpha}{\partial x} \tag{2}$$

$$\frac{\partial \rho v}{\partial t}+\left(u\frac{\partial \rho v}{\partial x}+v\frac{\partial \rho v}{\partial y}+w\frac{\partial \rho v}{\partial z}\right)=-\frac{\partial p}{\partial y}+\mu_{eff}\left(\frac{\partial^2 v}{\partial x^2}+\frac{\partial^2 v}{\partial y^2}+\frac{\partial^2 v}{\partial z^2}\right)+\sigma\kappa\frac{\partial \alpha}{\partial y} \tag{3}$$

$$\frac{\partial \rho w}{\partial t}+\left(u\frac{\partial \rho w}{\partial x}+v\frac{\partial \rho w}{\partial y}+w\frac{\partial \rho w}{\partial z}\right)=-\frac{\partial p}{\partial z}+\mu_{eff}\left(\frac{\partial^2 w}{\partial x^2}+\frac{\partial^2 w}{\partial y^2}+\frac{\partial^2 w}{\partial z^2}\right)+\rho g_z+\sigma\kappa\frac{\partial \alpha}{\partial z} \tag{4}$$

Equation of interface – VoF Method:

Volume of fluid method is provided by OpenFoam for tracking free surface position. Using this method, every free surface computational cell is divided in two parts, one which represents the air volume and the other which represents water volume. The calculation of the water-air fraction in every cell is possible with the help of the scalar quantity α, with value fluctuating between 0 and 1. When the cell is full of water, α is equal to 1 and when the cell is full of air, α is equal to 0, while it takes intermediate values (between 0 and 1) when the cell contains both water and air. The "α" value is calculated with the following equation for every free surface computational cell:

$$\frac{\partial a}{\partial t}+\frac{\partial u_i a}{\partial x_i}+\frac{\partial u_{c,i} a(1-a)}{\partial x_i}=0 \tag{5}$$

According to VoF Method equations of density and Dynamic Viscosity are obtained:

$$\rho = \alpha\rho_{water}+(1-a)\rho_{air} \tag{6}$$

$$\mu_{eff} = \alpha\mu_{water}+(1-a)\mu_{air}+\rho v_t \tag{7}$$

Table 1. Equation's quantities

Symbol	Name	Unit
$\boldsymbol{\rho}$	Density	$kg \cdot m^{-3}$
t	Time	*[s]*
P	Pressure	*Pa*
$\boldsymbol{g}$	Gravitational acceleration	$m \cdot s^{-2}$
$\boldsymbol{\mu}$	Dynamic Viscosity	$kg \cdot m^{-1} \cdot s^{-1}$
v_t	Turbulent Viscosity	$m^2 \cdot s^{-1}$
u, v, w	Velocity components at *x,y,z* Directions	$m \cdot s^{-1}$
σ	Surface tension	*N/m*
κ	Curvature	m^{-1}

2.1 Turbulence Modeling

After extended research and validations among available turbulence numerical models and according to useful results of (Brown et al. 2016) and (Larsen & Fuhrman 2018), wave energy loss due to the over production of turbulence was observed, resulted to underestimations in the measured wave height and the velocities of wave induced current. Thus, numerical scheme was coupled with buoyancy modified k – ω SST turbulence model (Devolder et al. 2018). Buoyancy modified k – ω SST turbulence model differs from the original k – ω SST model as provided in OpenFOAM®, as the density is explicitly included in the turbulence transport equations and a buoyancy term is added to the turbulent kinetic energy (TKE) equation.

The buoyancy modified k – ω SST model is defined as:

$$\frac{\partial \rho k}{\partial t} + \frac{\partial \rho k u_i}{\partial x_i} - \frac{\partial}{\partial x_i}\left[\rho(\nu + \sigma_k \nu_t)\frac{\partial k}{\partial x_i}\right] = \rho P_k + G_b - \rho \beta^* \omega k \tag{8}$$

$$\frac{\partial \rho \omega}{\partial t} + \frac{\partial \rho \omega u_i}{\partial x_i} - \frac{\partial}{\partial x_i}\left[\rho(\nu + \sigma_\omega \nu_t)\frac{\partial \omega}{\partial x_i}\right] = \frac{\gamma}{\nu_t}\rho G - \rho \beta \omega^2 + 2(1 - F_1)\rho \frac{\sigma_{\omega 2}}{\omega}\frac{\partial k}{\partial x_i}\frac{\partial \omega}{\partial x_i} \tag{9}$$

The buoyancy term G_b is defined as:

$$G_b = -\frac{\nu_t}{\sigma_t}\frac{\partial \rho}{\partial x_i} g_i \tag{10}$$

Buoyancy term contributes to the suppressing of turbulence level at free water surface especially in zone where the governing direction of the density gradient is vertical, i.e. the zone near the free surface where non – breaking waves are propagating and consequently the turbulent viscosity ν_t, tends to zero. As a result, in case of non-breaking waves the model switches to a laminar regime near the free surface, preventing excessive wave damping (Devolder et al. 2018). As opposite, in the surf zone a fully turbulent solution is obtained where the density gradient consists of an important horizontal component. At the breaking point this condition is obtained when shoaling waves are reaching their limiting wave height (Devolder et al. 2018).

3 RESULTS

3.1 Wave Diffraction Comparison against "Wiegel" analytical solution

In order to investigate water wave diffraction properly in OpenFOAM® environment, a hypothetic 3D wave basin was created, length of 18 m, width of 12m and constant depth of 0.8 m, (see Table 2). A simulation of total time 60 s was carried out. A breakwater approximately in the middle of the tank is used as an obstacle to regular incident wave condition of Stoke's first wave theory with wave height H_0 = 0.15 m, period T = 1.2 s, and wavelength L_0 = 2.12 m. In order to avoid wave reflections, relaxation zones were used, included in waves2Foam toolbox (Jacobsen et al. 2012). The zones are applied alongside the wave basin and in front of wave breaker (Figure 1a).

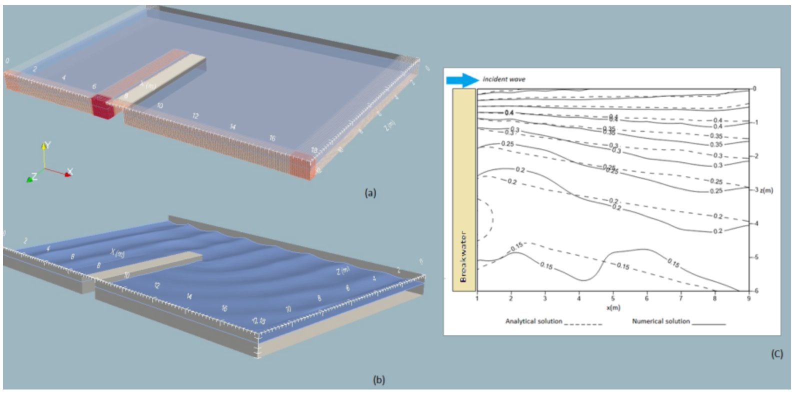

Figure 1 a) 3D Wave Basin layout with relaxation zones, b) wave diffraction at last time step, (Paraview® visualization) c) Comparison of numerical values of numerical diffraction coefficient against analytical solution

Initial conditions, for wave, pressure and velocity were used in the incident open boundary of the computational domain. Adjustable time step was selected with minimum value of 0.001 s and maximum value of 0.01 s to keep Courant number, $C_0 = c\,{}^{\Delta t}/_{\Delta x} \leq 0.25$.

The resulted numerical solution was compared against analytical data of Penny and Price (1944) work, found in "Wiegel" diffraction table. The comparison achieved by measurements of wave height in the lee of breakwater. The diffraction coefficient, $k_d = {}^{H}/_{H_0}$ as a result of the analytical solution was compared with numerical measurements (Figure 1c). A good agreement is observed between numerical and analytical values demonstrating the effectiveness of discretization values of time and space.

Table 2 Dimensions and characteristics of numerical simulations

Length	Width	Height
18 m	12 m	1 m

Discretization			
dx (m)	dz (m)	dy (m)	dt (s)
0.04	0.04	0.02	0.001
450 grid points at x direction	300 grid points at z direction	50 grid points at y direction	
Total number of grid points : 6.750.000			
Number of grid points per wave length : 53			
Number of grid points at maximum water depth: 40			
Total simulated time : 60 s			

3.2 Wave induced Eddy Current behind semi-infinite Breakwater

The simulation of wave induced eddy current behind a detached breakwater obtained by the reproduction of Mory & Hamm (1997) experiment (Figure 2). The sea bed consisted of three parts. A 4.4 m length zone of constant depth h = 0.33 m close to the wave generator, an underwater plane beach with slope 1 in 50 and an emerged plane beach with slope at 1 in 20 (Table 3).

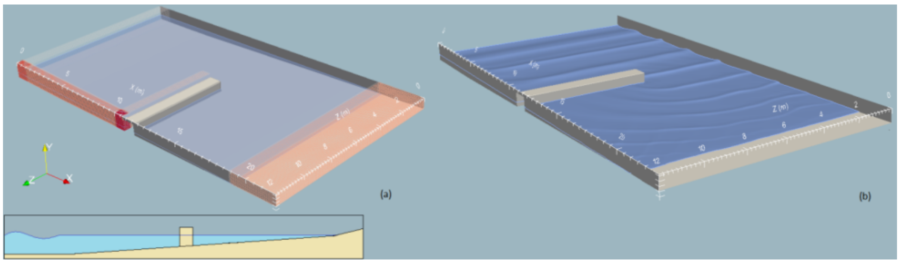

Figure 2 a) 3D Wave Basin layout with relaxation zones, b) Numerical Simulation at last time step, (Paraview® visualization).

Regular incident wave conditions (H_0 = 0.075 m, period T = 1.69 s, and wavelength L_0 = 2.804 m) was considered, using first – order Cnoidal theory as intended for swallower water rather than class of Stokes theories.

Table 3 Dimensions and characteristics of numerical simulations

Length	Width	Height
21.8 m	12 m	0.528 m

Discretization			
dx (m)	dz (m)	dy (m)	dt (s)
0.04	0.04	0.00825	0.001
545 grid points at x direction	300 grid points at z direction	64 grid points at y direction	
Total number of grid points : 10.464.000			
Number of grid points per wave length: 70			
Number of grid points at maximum water depth: 40			
Total simulated time : 120 s			

Initial conditions for wave, pressure and velocity were used the incident boundary of the computational domain, together with the initial values for k, ω, v_t. An adjustable time step was selected with minimum value of 0.001 s and maximum value of 0.01 s to keep Courant number, C_0 =

$c\,{}^{\Delta t}/_{\Delta x} \leq 0.25$. The comparison of time averaged velocities measurements in mean water depth against experimental values are present in Figure 3. Eddy pattern measured behind the breakwater is observed, producing a strong jet – like flow of up to 0.25 m/s similar to the experimental results. A characteristic feature is the wide eddy in the center, with almost quiescent fluid. The good consistency between numerical and experimental values that is obtained, demonstrates the effectiveness of coupling numerical model, with k – ω SST buoyancy modified turbulence model.

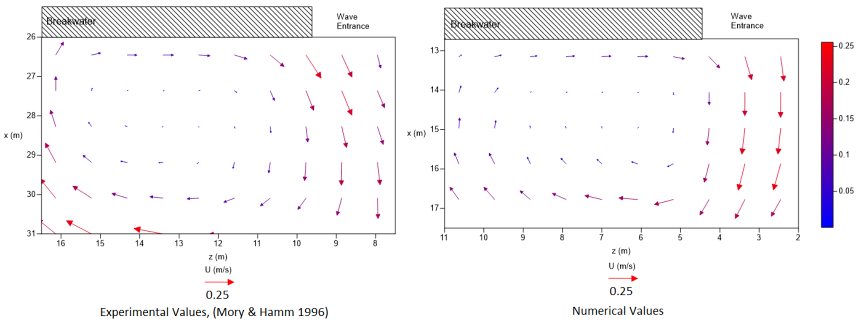

Figure 3 Time averaged horizontal velocities at mean water depth behind the breakwater: Comparison of numerical values against experimental results

References

Larsen BE, Fuhrman DR (2018) On the over-production of turbulence beneath surface waves in Reynolds-averaged Navier–Stokes models. Journal of Fluid Mechanics 853:419–460. doi: 10.1017/jfm.2018.577

Karambas T, Samaras A (2017) An Integrated Numerical Model for the Design of Coastal Protection Structures. Journal of Marine Science and Engineering 5:50 doi: 10.3390/jmse5040050

Karambas ThV, Koutitas C (2002) Surf and Swash Zone Morphology Evolution Induced by Nonlinear Waves. Journal of Waterway, Port, Coastal, and Ocean Engineering 128:102–113. doi: 10.1061/(ASCE)0733-950X(2002)128:3(102)

Mory M, Hamm L (1997) Wave height, setup and currents around a detached breakwater submitted to regular or random wave forcing. Coastal Engineering 31:77–96. doi: 10.1016/S0378-3839(96)00053-1

Devolder B, Troch P, Rauwoens P (2018) Performance of a buoyancy-modified k-ω and k-ω SST turbulence model for simulating wave breaking under regular waves using OpenFOAM ®. Coastal Engineering 138:49–65. doi: 10.1016/j.coastaleng.2018.04.011

Brown SA, Greaves DM, Magar V, Conley DC (2016) Evaluation of turbulence closure models under spilling and plunging breakers in the surf zone. Coastal Engineering, 114, pp.177–193. doi: 10.1016/j.coastaleng.2016.04.002

Higuera P, Lara JL, Losada IJ, (2013b) Simulating coastal engineering processes with OpenFOAM®. Coastal Engineering 71:119–134. doi: 10.1016/j.coastaleng.2012.06.002

Higuera P, Lara JL, Losada IJ (2013a) Realistic wave generation and active wave absorption for Navier-Stokes models. Application to OpenFOAM®. Coastal Engineering 71:102–118. doi: 10.1016/j.coastaleng.2012.07.002

Jacobsen N, Fuhrman D, Fredsøe J (2012) A wave generation toolbox for the open-source CFD library OpenFOAM. Internation Journal of Numerical Methods in Fluidsthods in Fluids 70:1073–1088. doi: 10.1002/fld.2726

Chen LF, Zang J, Hillis AJ, Morgan GCJ, Plummer AR (2014) Numerical investigation of wave – structure interaction using OpenFOAM. Ocean Engineering 88:91–109. doi:10.1016/j.oceaneng.2014.06.003

Acknowledgments

This research was founded by General Secretariat for Research and Technology (GSRT) and Hellenic Foundation for Research and Innovation (HFRI).

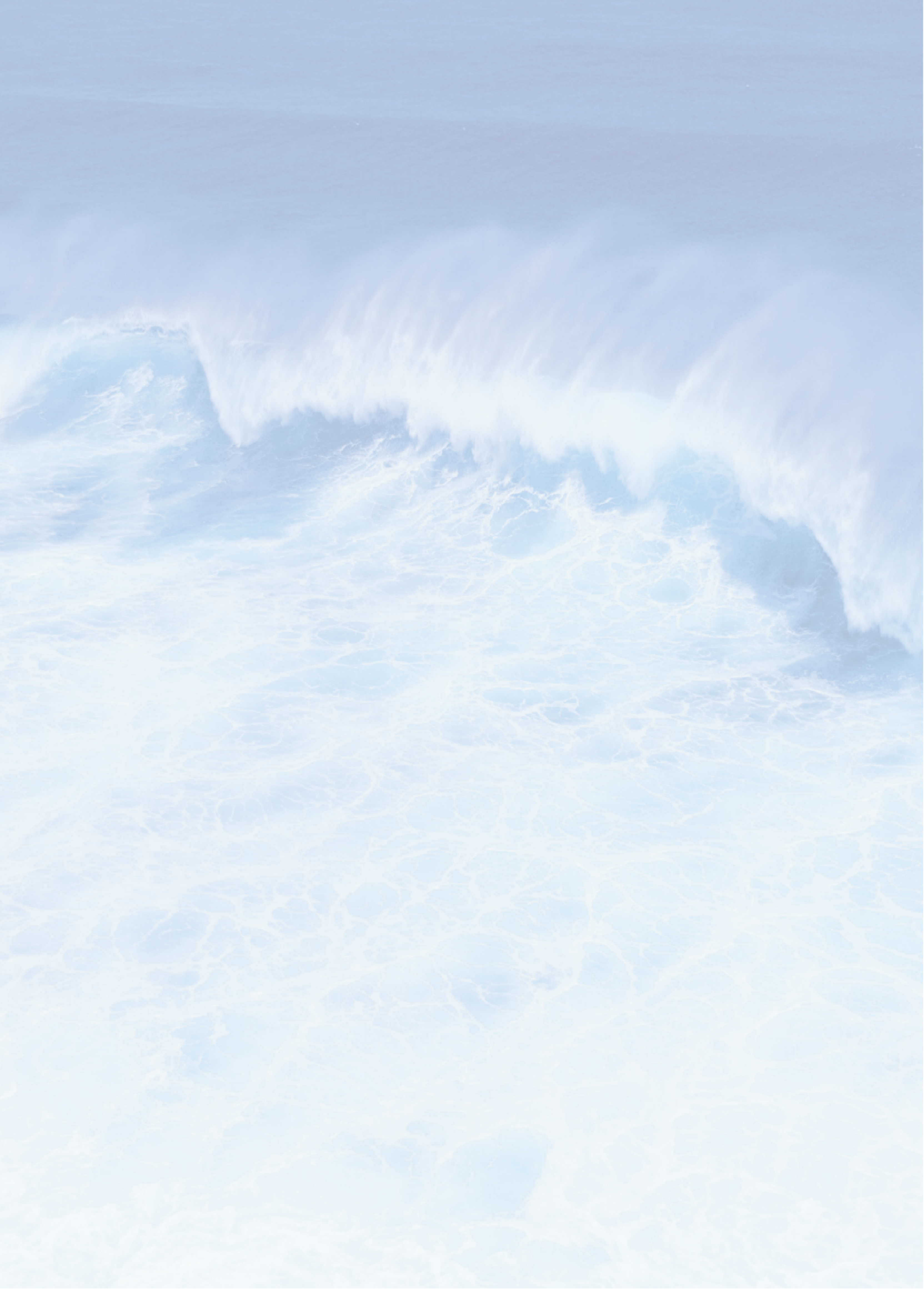

Nonlinear changes and energy dissipation in random water waves in finite water depths

I. Karmpadakis*, C. Swan, M. Christou

Department of l Civil Engineering and Environmental Engineering, Imperial College London, SW7 2BU, UK
*Corresponding author: i.karmpadakis14@imperial.ac.uk

Abstract

The present study investigates the influence of nonlinear wave-wave interactions and wave breaking on random water waves. More specifically, this is addressed by examining the short-term distributions of crest heights arising in intermediate water depths. These represent a key input parameter in a wide range of engineering applications. As such, their accurate prediction is of great importance for the effective design and safety of marine structures and vessels.The results presented herein are based upon the analysis of a vast database of field measurements, recorded by wave radars in the North Sea. These are supplemented by an extensive laboratory investigation of directionally spread sea-states. Strict quality control procedures were applied to the field measurements and a thorough validation process was adopted for the experimental investigation. The latter involved establishing good agreement between results obtained in facilities with very different operational characteristics. Most importantly, close agreement was obtained between laboratory and field data arising in similar sea-state conditions.With respect to the distribution of crest heights, the existing statistical models are assessed using both field and experimental measurements. This analysis has provided conclusive evidence of significant departures from the widely applied distributions in engineering design. These arise both as amplifications beyond the models' predictions in sufficiently steep sea-states and reductions in those cases with significant wave breaking. The outcomes of this study have significant implications regarding both the occurrence of wave-in-deck loading and the calculation of the forces exerted on marine structures. In this sense, they should be taken into consideration during the design of new structures or the reliability assessment of existing structures.

Keywords Nonlinear waves, Wave breaking, Crest heights, Wave statistics.

1 INTRODUCTION

The survivability of most marine structures is critically dependent upon the underlying distribution of crest heights during storm conditions. These are typically used to infer representative water particle kinematics, calculate wave loading and predict the occurrence of extensive wave-overtopping or wave-in-deck loading.

Currently applied design practice suggests that target sea-states with a specific return period are obtained using either hindcast meteorological models or *in-situ* measurements. Based on the metocean characteristics of these sea-states, the short-term distribution of crest heights can be estimated. While various statistical models have been proposed in the literature, the two most commonly applied are the Rayleigh (Longuet-Higgins, 1952) and Forristall (Forristall, 2000) distributions. The functional form of these models is given by:

$$Q(\eta > \eta_c) = \exp\left[-\frac{1}{a}\left(\frac{\eta_c}{H_s}\right)^{\beta}\right], \tag{1}$$

where Q is the probability of exceedance of the crest height (η_c), H_s is the significant wave height and a and β are the scale and shape parameters of the distributions. The latter two parameters have fixed values for the Rayleigh model $\left(a = \frac{1}{8}, \beta = 2\right)$ but vary as a function of the mean sea-state steepness, S_1, and the Ursell number, Ur, for the Forristall model; their exact description being provided in (Forristall, 2000). In principle, the Rayleigh distribution is based on the assumption that a sea-state can be accurately described using linear random wave theory (with a relatively narrow spectral bandwidth). As such, it has been found to underpredict the largest waves in the ocean. In contrast, the Forristall model can accurately capture nonlinear changes in crest heights arising at a second-order of wave steepness; the model being primarily based on a large set of numerical simulations using second-order random wave theory. Moreover, the Forristall model includes two versions; the first addresses unidirectional sea-states and the second addresses directionally spread sea-states.

While the second-order model (Forristall distribution) has been extensively validated and is presently recommended practice (D.N.V., 2010), recent findings suggest that noteworthy discrepancies between the model predictions and real seas can potentially arise. Considering unidirectional deep-water waves, (Onorato *et al.*, 2006) have shown that higher-order nonlinear interactions can lead to significant amplifications of the largest crest heights. These amplifications were shown to rapidly reduce for short-crested sea-states (Onorato *et al.*, 2009). However, (Latheef and Swan, 2013) have argued that despite these reductions, the nonlinear amplifications remain significant for realistic sea-states. Accumulated evidence from field measurements act to support this view (Bitner-Gregersen and Magnusson, 2004; Gibson, Christou and Feld, 2014).

In shallower water depths the description of the free water surface becomes progressively more challenging due to stronger nonlinear interactions and the occurrence of wave breaking. To this end, the present study examines the relevance of the two aforementioned physical mechanisms with respect to the statistical distribution of crest heights.

2 METHODS

The present study utilises two complementary datasets to identify the importance of higher than second-order nonlinear interactions and the effects of wave breaking. The first dataset relates to field measurements recorded using wave radars mounted on the side of offshore oil and gas platforms. A photograph of such a wave radar is illustrated in Figure 1(a). In total, data recorded in 10 locations in the North Sea were analysed, with water depths ranging between $8\text{ m} < d < 40\text{ m}$. For the purposes of this paper, the crest heights arising at the shallowest and deepest location are considered. To extract these crest heights the raw time-histories were quality controlled following a strict methodology outlined by (Christou and Ewans, 2011). Once erroneous measurements were removed, the continuous surface elevation measurements were divided into 20-minute long sea-states. Finally, a database with zero-crossing and spectral quantities was formed for each sea-state and platform. This allows for measurements with similar sea-state characteristics (e.g. H_s, T_p, d) to be grouped together and derive statistically significant results.

a)

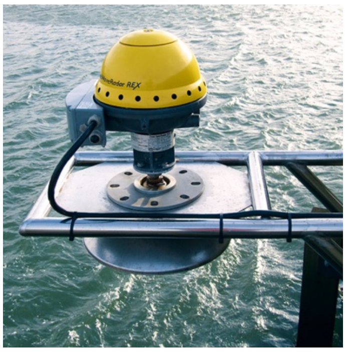

b)

Figure 1 Photographs of a) a wave radar mounted on an offshore platform and b) the directional wave basin at Imperial College London

The second dataset relates to experimental measurements. The majority of these measurements were performed in the directional wave basin at Imperial College London (shown in Figure 1(b)). Supplementary experiments were carried out in the shallow water wave basin at Queen's University Belfast. These two facilities have very different operational and geometric characteristics (such as wave-maker type, absorbing beach configuration and dimensions). As such, the use of two facilities serves the purpose of cross-validating our experimental results as well as extending the range of sea-states under investigation.

All experimental test cases presented herein were generated using a JONSWAP spectral shape (Hasselmann *et al.*, 1973) with a peak enhancement factor $\gamma = 2.5$ and a wrapped normal directional spreading function with a standard deviation of $\sigma_\theta = 10^{o}$. These were chosen to represent realistic storm conditions in intermediate water depths (Jonathan and Taylor, 1997). To investigate the effect of sea-state steepness on the crest height distributions, sea-states with varying significant wave height, H_s, but constant peak period, T_p, were simulated. For each test case, 20 seeds with random initial phases (($\psi_i \in [0,2\pi)$) were generated; each one having a duration of 1024 s. Adopting a scaling of 1:100 each random seed relates to a sea-state of approximately 3 hours at full scale. The time-histories of each random simulation were then analysed in a similar manner as the field measurements and an experimental database was formed. The results relating to all random simulations for each sea-state were collected and re-ordered to derive probability distributions extending to very small probabilities of exceedance ($Q \approx 10^{-4}$). In this respect, each simulation is treated as a sub-sample of a larger population defined by the sea-state characteristics (H_s, T_p, σ_θ). In adopting this approach, rare events arising in realistic sea-states can be generated experimentally. These are generally difficult to encounter in the field due to the limited number of available wave records and the inherent variability of incident conditions.

In Figure 2(a), close agreement is demonstrated between normalised crest heights and wave heights arising in the two experimental facilities. These results relate to a sea-state with effective water depth, $k_p d = 1$, and sea-state steepness $S_p = 0.03$; where the latter is defined as $S_p = \frac{2\pi H_s}{g T_p^2}$. The agreement observed in Figure 2(a) demonstrates that the experimental results presented herein are facility independent. Most importantly, similarly good agreement can be found in comparing experimental and field results with similar sea-state characteristics. This is demonstrated in Figure 2(b) for sea-states with $k_p d \approx 1.5$ and $\frac{H_s}{d} = 0.13$. Taken together these comparisons provide confidence in the experimental method and demonstrate the ability to accurately simulate conditions encountered in the open ocean. More comparisons of this type alongside a detailed presentation of the experimental apparatus and analysis methodology can be found in (Karmpadakis, 2018).

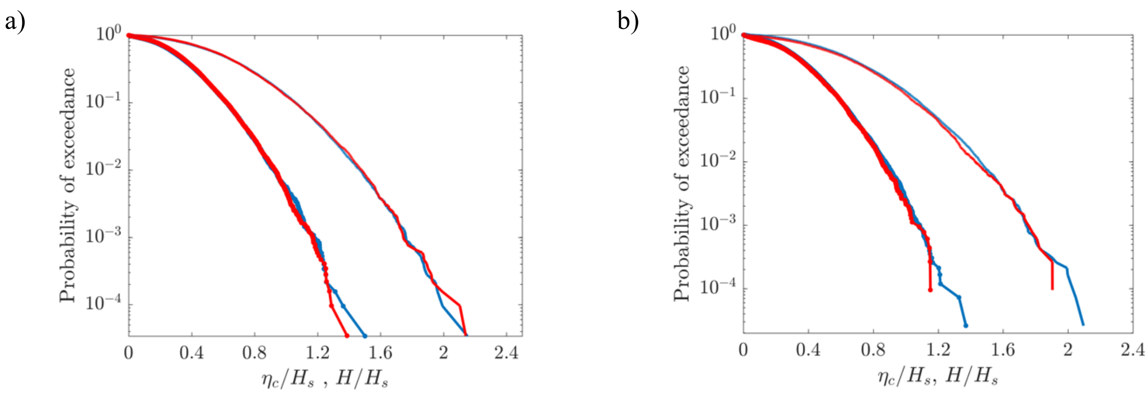

Figure 2 Normalised crest height, η_c/H_s, and wave height, H/H_s, distributions comparing a) results from the wave basins at Imperial College London (blue) and Queen's University Belfast (red) and b) field measurements (blue) and experimental results (red)

3 RESULTS

While field measurements are very instructive in the sense that they provide an accurate representation of realistic wave conditions, typically the amount of available data are limited. This means that the observed statistics are accompanied with relatively large confidence intervals. Moreover, extreme storms are not frequently encountered in the available datasets. To this end, we have used the field measurements to identify the occurrence of the processes of interest in the ocean and the experimental measurements to extend these findings to rare events and sea-states.

Considering field measurements, Figures 3(a) and 3(b) show crest height distributions recorded at water depths of $d = 45$ m and $d = 8$ m, respectively. In both cases, the measured data are compared to the predictions of the Rayleigh and Forristall distributions. Figure 3(a) shows that the largest crest heights ($Q < 10^{-2}$) are underpredicted by both the linear and second-order models. In fact, the amplifications beyond the Forristall model lie outside the confidence intervals; the latter being calculated as in (Tayfun and Fedele, 2007). This suggests that nonlinear interactions arising at third-order and above contribute in the formation of the largest waves. In contrast, Figure 3(b) shows that the largest crest heights fall below the Forristall line and tend towards the Rayleigh distribution. This is attributed to the dissipative effects of wave breaking. More specifically, wave breaking acts to reduce the crest elevation of the largest waves and, subsequently, lead to a drop in the tail of the distribution. Simultaneously an increase in the crest elevation of smaller waves ($Q > 10^{-2}$) can be observed. This is a common attribute of sea-states in which extensive wave breaking is observed and partly represents the redistribution of "broken" waves towards larger probabilities of exceedance. The sea-states in both figures are characterised by a mean peak period of $T_p = 13$ s, but Figure 3(a) corresponds to $\frac{H_s}{d} \approx 0.2$ while Figure 3(b) to $\frac{H_s}{d} =\approx 0.4$. As such, the effects of depth induced wave breaking are much more pronounced in the latter case.

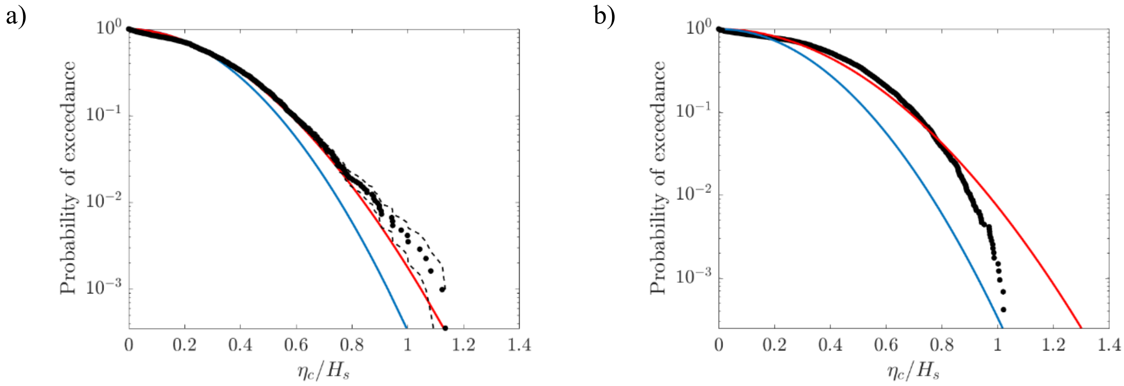

Figure 3 Normalised crest height distributions, η_c/H_s, compared to the predictions of the Forristall distribution (red) and the Rayleigh distribution (blue). Sub-plot (a) relates to sea-states with $d = 40$ m and $\frac{H_s}{d} \approx 0.4$, while sub-plot (b) to sea-states with $d = 8$ m and $\frac{H_s}{d} \approx 0.2$; both with $T_p = 13$ s

In using the experimental measurements to extend these findings, Figure 4(a) presents results normalised by the predictions of second-order theory. Adopting this normalisation, the deviations under investigation become clearly apparent. More specifically, sea-states with the same effective water depth, $k_p d = 1.5$, but varying steepness, $0.02 \leq S_p \leq 0.06$, are shown in different colours. The same behaviour as described above can be observed. For $S_p < 0.04$ amplifications above second-order can be observed for the largest crest heights. These reach a maximum of 10% for $Q \approx 10^{-3}$. Once the sea-state steepness is further increased ($S_p > 0.04$), the tails of the distributions are shown to reduce. Combining the deviations at $Q = 10^{-3}$ for all experimental results and expressing them in the parameter space defined by the mean sea-state steepness, S_1, and the Ursell number, Ur, an overview of the discrepancies can be obtained. This is shown in Figure 4(b). The contour plot presented therein summarizes the results discussed earlier and provides guidance regarding the expected behaviour of the largest crest heights in a wide variety of incident conditions.

4 CONCLUDING REMARKS

Taken together the results presented herein demonstrate the effects of the competing mechanisms of nonlinear amplifications and wave breaking in intermediate water depths. The good agreement between experimental and field measurements allows the use of the former to infer the behaviour of sea-states that have not been encountered in the field. More importantly, these results show that higher than second-order effects can arise in directionally spread sea-states in these water depths; a result that has only been shown using idealised wave groups so far (Toffoli *et al.*, 2013).

a) b)

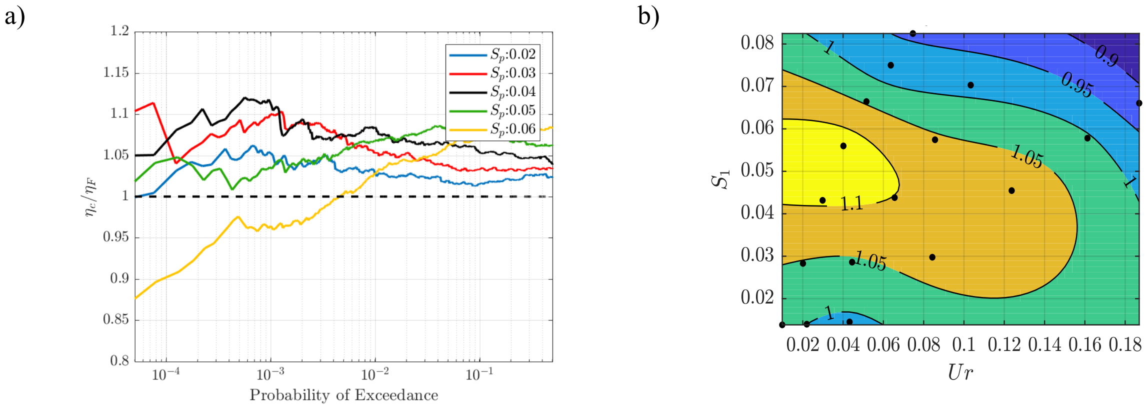

Figure 4 (a) Crest heights normalised by the predictions of second-order theory considering sea-states with $k_p d = 1.5$ and varying steepnesses. (b) Contour of deviations at $Q = 10^{-3}$ for all experimental cases.

References

Bitner-Gregersen, E. M. and Magnusson, A. K. (2004) 'Extreme events in field data and in a second order wave model', *Rogue Waves*, pp. 1–16. Available at: http://www.ifremer.fr/web-com/stw2004/rwtemp/fullpapers/bitner-gregersen.pdf.

Christou, M. and Ewans, K. (2011) 'Examining a Comprehensive Dataset Containing Thousands of Freak Wave Events: Part 1— Description of the Data and Quality Control Procedure', *Structures, Safety and Reliability*, 2(February), pp. 827–837. doi: 10.1115/OMAE2011-50169.

D.N.V. (2010) *DNV-RP-C205 Environmental Conditions and Environmental Loads*, *Det Norske Veritas*.

Forristall, G. Z. (2000) 'Wave Crest Distributions: Observations and Second-Order Theory', *Journal of Physical Oceanography*, 30(8), pp. 1931–1943. doi: 10.1175/1520-0485(2000)030<1931:WCDOAS>2.0.CO;2.

Gibson, R., Christou, M. and Feld, G. (2014) 'The statistics of wave height and crest elevation during the December 2012 storm in the North Sea', *Ocean Dynamics*, 64(9), pp. 1305–1317. doi: 10.1007/s10236-014-0750-5.

Hasselmann, K. *et al.* (1973) 'Measurements of Wind-Wave Growth and Swell Decay during the Joint North Sea Wave Project (JONSWAP)', *Ergnzungsheft zur Deutschen Hydrographischen Zeitschrift Reihe*, A(8)(12), p. p.95.

Jonathan, P., Taylor, P. H. (1997) 'On Irregular, Nonlinear Waves in a Spread Sea', *Journal of Offshore Mechanics and Arctic Engineering*, 119(1), p. 37. doi: 10.1115/1.2829043.

Karmpadakis, I. (2018) *Wave Statistics in Intermediate and Shallow Water Depths*. Imperial College London.

Latheef, M., Swan, C. (2013) 'A laboratory study of wave crest statistics and the role of directional spreading', *Proceedings of the Royal Society A: Mathematical, Physical and Engineering Sciences*, 469(2152), pp. 20120696–20120696. doi: 10.1098/rspa.2012.0696.

Longuet-Higgins, M. S. (1952) 'On the Statistical Distribution Of Sea Waves', *Journal of Marine Research*, 11(3), pp. 245–266.

Onorato, M. *et al.* (2006) 'Extreme waves, modulational instability and second order theory: wave flume experiments on irregular waves', *European Journal of Mechanics, B/Fluids*, 25(5), pp. 586–601. doi: 10.1016/j.euromechflu.2006.01.002.

Onorato, M. *et al.* (2009) 'Statistical properties of mechanically generated surface gravity waves: A laboratory experiment in a three-dimensional wave basin', *Journal of Fluid Mechanics*. Cambridge University Press, 627, pp. 235–257. doi: 10.1017/S002211200900603X.

Tayfun, M. A. and Fedele, F. (2007) 'Wave-height distributions and nonlinear effects', *Ocean Engineering*, 34(11–12), pp. 1631–1649. doi: 10.1016/j.oceaneng.2006.11.006.

Toffoli, A. *et al.* (2013) 'Experimental evidence of the modulation of a plane wave to oblique perturbations and generation of rogue waves in finite water depth', *Physics of Fluids*, 25(9). doi: 10.1063/1.4821810.

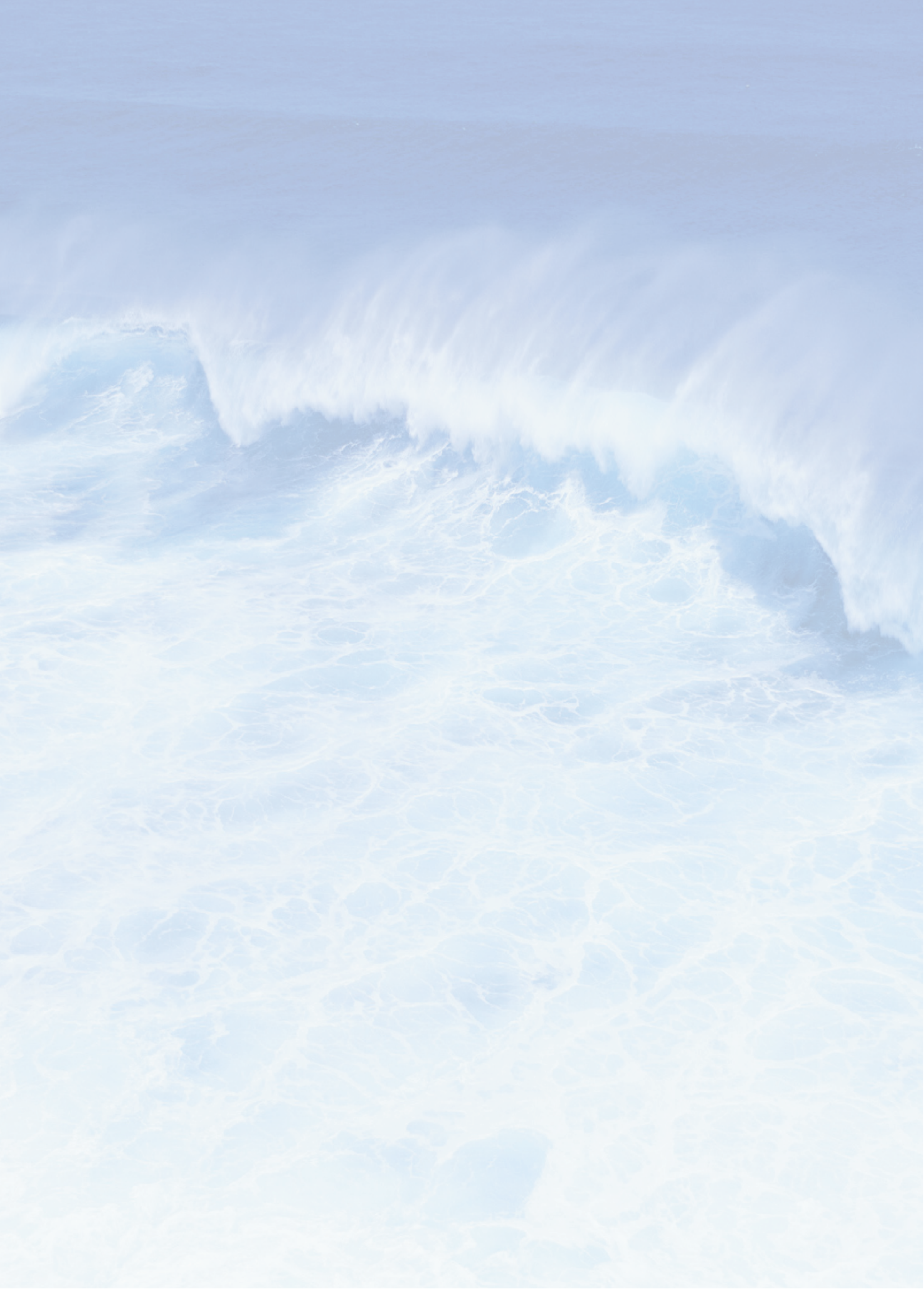

Prediction of extreme wind-generated waves offshore the Piraeus Port using a numerical model of wave growth in the SW Aegean Sea

M. Sklia, A.A. Dimas*

Department of Civil Engineering, University of Patras, Patras 26500, Greece
*Corresponding author: adimas@upatras.gr

Abstract

The objectives are the computation of extreme wave heights developing offshore the Piraeus Port based on a numerical model of wave growth in the SW Aegean Sea, and the correlation of these values to the return period of extreme winds. The numerical software MIKE21 was used for the solution of the wave action conservation equation using the fully spectral formulation. Instationary simulations were performed to obtain the wave growth results as a function of wind duration. The computational domain includes the basin of the SW Aegean Sea, while the grid resolution was selected so that results were grid independent. Several wind scenarios were examined, which included five wind directions in the SE to SW sector, and three wind speeds: 8, 9, and 10B (Beaufort scale). The results indicated that the SSE winds generated the waves with the highest heights offshore the Piraeus Port for all wind speeds. The analysis of wind data from the Hellenic National Meteorological Service station in Milos Island indicated that the wind with a 100-year return period in the SW Aegean Sea has a strength of 9B. For the corresponding SSE wind of 9B, fetch-limited conditions are established after 8hrs, and the resulting significant wave height offshore the Piraeus Port is equal to 7.3 m.

Keywords Piraeus Port, Wind-generated waves, Wave action, Return period.

1 INTRODUCTION

In recent years, the investigation of high waves in the Aegean Sea Basin has been modeled both in large and regional scale models (Galiatsatou et al. 2015). The objective of the present work is the prediction of wave parameters, i.e. height and period, offshore the Port of Piraeus under extreme wind conditions. Such parameters may be used as design values for all harbor and marine works planned for the development of the Piraeus Port. The prediction is based on the use of a sophisticated numerical model of wind-induced spectral wave growth (DHI 2017) in the SW Aegean Sea. The results include the high wave climate offshore the Port of Piraeus along with its correlation to the return period of extreme winds.s impact.

2 METHODOLOGY

2.1 Formulation

The software, which was used to perform the simulations in the present study, was MIKE 21 SW (DHI 2017), a third-generation spectral wind-wave model, which can simulate growth, decay and transformation of wind generated waves in offshore and coastal areas.

In the present application, the Fully Spectral Formulation was used as wave growth was of importance. Under this formulation, the dynamics of the waves are described by the wave action conservation equation

$$\frac{\partial N}{\partial t} + \nabla \cdot \left(\vec{C}\, N \right) = \frac{S}{\sigma} \tag{1}$$

where $N(\vec{s}, t, \sigma, \theta) = E / \sigma$ is the wave action density, $\vec{s}(x, y)$ is the Cartesian coordinate vector, t is time, σ is the wave angular frequency, θ is the wave direction, E is the wave energy density, $\vec{C} = (C_x, C_y, C_\sigma, C_\theta)$ is the propagation velocity of a wave group in the four dimentional space, and S is the energy balance source term. Energy balance is modeled as a superimposition of various physical phenomena

$$S = S_{in} + S_{nl} + S_{ds} + S_{bed} + S_{surf} \tag{2}$$

where S_{in} models the energy generated by the wind, S_{nl} models the wave energy tranfer due to nonlinear wave- wave interaction, S_{ds} models the dissipation related to white capping, S_{bed} models the dissipation due to bed friction, and S_{surf} models the dissipation related to depth-induced breaking. The significant parameters in the wind input term are the friction velocity and the sea rougness, assuming a logarithic profile for the wind flow. Here, the coupled model in Komen et al. (1994) was used. Regarding energy transfer, it is known that nonlinear energy transfer between different components of a directional-frequency spectrum is critical for the spatial and temporal evolution of a wave field. Quadruplet wave interaction formulation was chosen here following the discrete interaction approximation in Hasselmann and Hasselmann (1985) for the parametrization of S_{nl}. The model, which was used here to incorporate wave dissipation due to the white capping effect along with a combination of wind-sea and swell, was the one introduced in Bildot et al. (2007). In the present application, bed friction was ignored, as well as water level variations.

The governing equation was solved using the cell-centered finite volume method. The spatial discretization was based on an unstructured triangular mesh approach, while the integration in time is performed through a fractional step approach with the application of a multi-sequence explicit Euler scheme. A spectral discretisation is also applied using logarithmic distribution of frequencies and provinding the model with a range of frequences expected to occur in the domain.

2.2 Implementation

The area of interest in this study was the region offshore the Piraeus Port, and the main objective was to simulate wind-induced wave growth from winds in the SE to the SW sector. Hence, the computational domain was the SW sector of the Aegean Sea, and the corresponding bathymetry is shown in Figure 1 as constructed by data obtained from the database MIKE C-MAP (DHI 2014). The computational mesh comprised 1.7×10^6 triangular cells with average edge length of 300 m and smallest allowable angle of 26 deg (Figure 2). Concerning time intergration, instationary simulations were performed where the time-step was calculated dynamically during the simulation. A typical average time-step of the simulations was 25 sec.

For the nonlinear energy transfer, the quadruplet wave interaction in the spectral wave module was chosen. For the effect of white capping, the constant parameter option was chosen with disipation coefficients C_{ds} = 2.1 and δ = 0.6, while the mean angular frequency and mean wave number were computed with exponents $p_\sigma = p_k = 1$, as proposed in Bidlot et al. (2007).

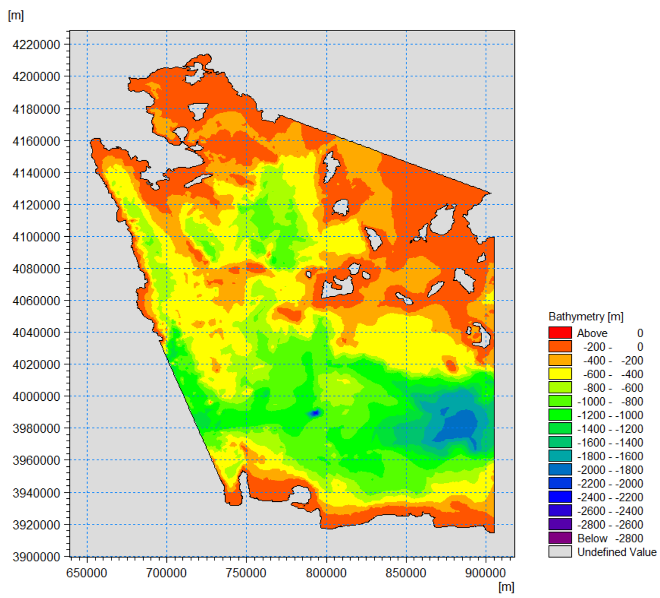

Figure 1 The bathymetry of the computational domain in the SW Aegean Sea

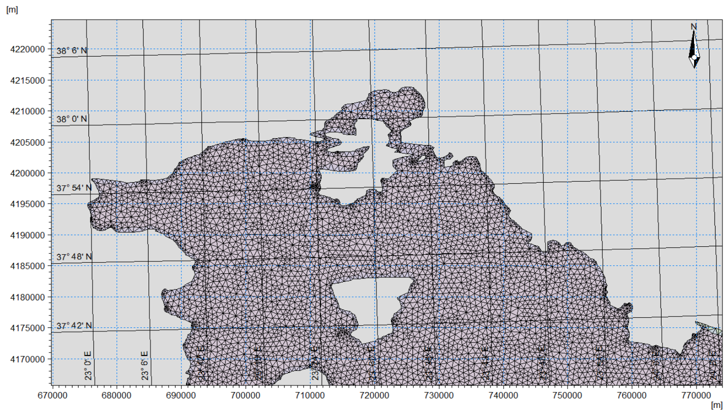

Figure 2 Detail of the unstructured computational mesh in the area offshore of Piraeus Port

Simulations were performed for winds of three (3) strengths (8B, 9B, and 10B), and each originated from five (5) directions (SE, SSE, S, SSW, and SW), for a total of 15 cases. For each case, the maximum wind speed of the corresponding Beaufort scale range was applied as a constant over the computational domain, while a directional range of ±30 deg about the mean wind direction was considered.

3 RESULTS

3.1 Wave Distribution

A total of 15 combinations of wind speed and direction were examined in order to identify the possible cases that will correspond to the high wave climate offshore the port of Piraeus under strong winds with stable characteristics. Typical results for SE and S winds at the maximum wind speed of 10B are presented in Figure 3. For the SE wind, high waves are mainly directed towards the Argolida Gulf, and are less potent in the Saronicos Gulf south of the Aegina Island. The S wind seems to generate a stronger wave penetration in the Saronicos Gulf, which results into high waves offshore the port of Piraeus. Waves generated by the SW wind, not shown here due to space limitation, are restrained due to the presence of the Argolis Peninsula, resulting again to less potent waves offshore the Port of Piraeus. Consequently, waves generated by SE, SSE and S winds are the most intense waves in the area of interest. Typical wave height and direction results in the Saronicos Gulf region offshore the Piraeus Port, for wind strength of 10B, are shown in Figure 4. Similar results for wind strength of 9B are shown in Figure 5. It is aparent that the SSE winds result in the highest waves offshore the Piraeus Port as these waves have a clear fetch from the northern coastline of Crete.

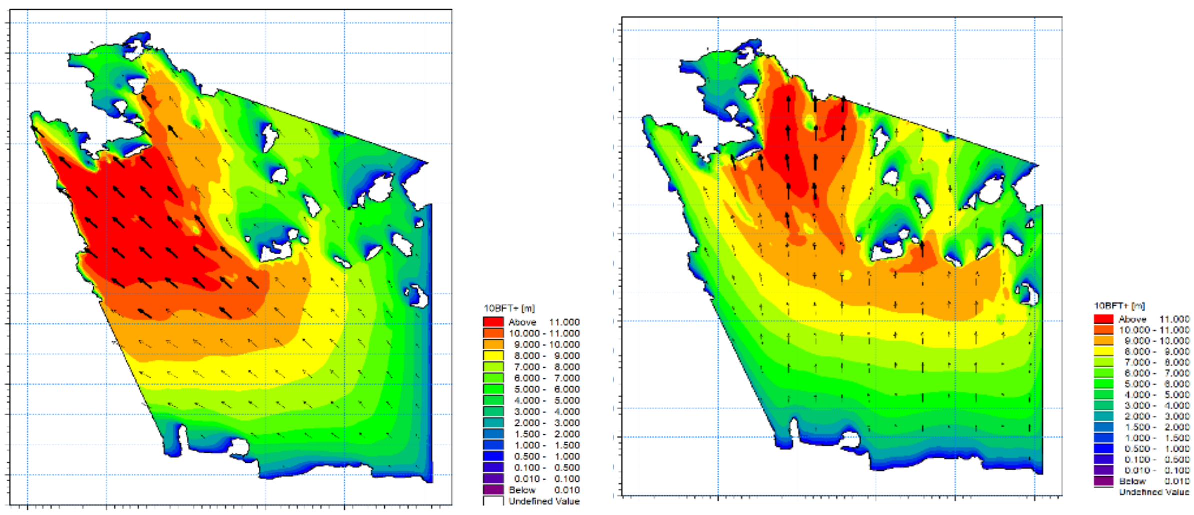

Figure 3 Significant wave height and wave direction induced by SE (left) and S (right) winds of 10B for fetch-limited conditions

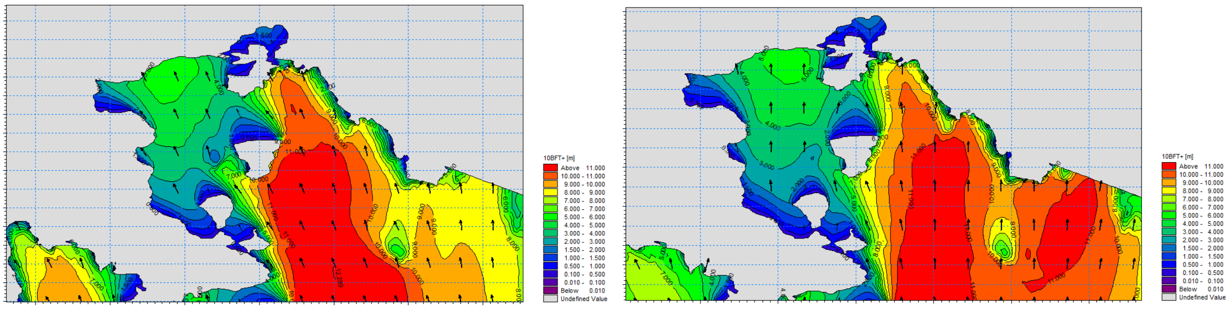

Figure 4 Significant wave height and wave direction induced by SSE (left) and S (right) winds of 10B for fetch-limited conditions in the area offshore of Piraeus Port

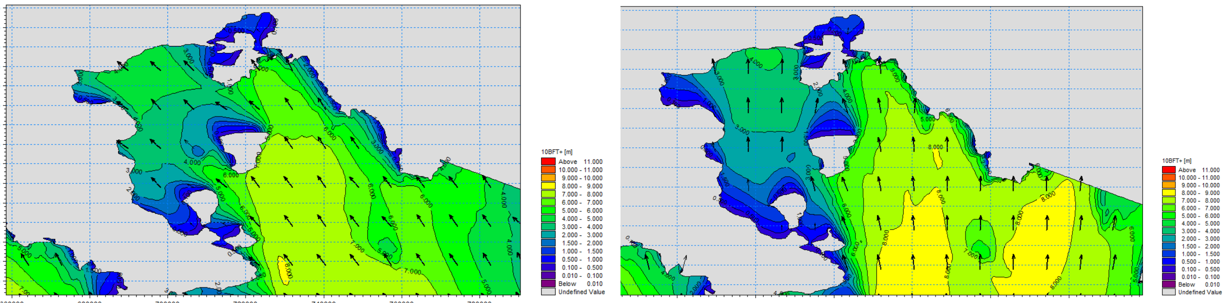

Figure 5 Significant wave height and wave direction induced by SSE (left) and S (right) winds of 9B for fetch-limited conditions in the area offshore of Piraeus Port

3.2 Return Period of Extreme Winds

In order to obtain the appropriate return period of high waves offshore the Piraeus Port, a study was undertaken to compute the return period of extreme winds in the SW Aegean Sea. Wind data were acquired by the database of the Hellenic National Meteorological Service (hnms.gr) for the decade 1995-2004. Specifically, the wind speed measurements, U_{164}, taken every three hours at the Meteorological Station of Milos (altitude 164m) were used as representative of the wind climate in the SW Aegean Sea. These data were initially processed in order to obtain the wind speed at the reference altitude of 10m above sea level using the empirical formula

$$U_{10} = U_{164}\left(10/164\right)^{1/7} \tag{3}$$

The methodology used here to compute the return period of extreme winds was the one proposed in USACE Coastal Engineering Manual (CEM 2002) referring to long-term statistics. Specifically, the method is based on the assumption that extreme winds follow the Fisher-Tippett I (FT-I) distribution function using the maximum monthly wind speeds (Gringorten 1963). The use of the FT-I distribution to calculate the maximum wind speed with return period T_r results into the formula

$$U_r = \bar{U}_m + 0.78\sigma_m\left[\ln\left(12T_r\right) - 0.577\right] \tag{4}$$

where U_r is the wind speed with r-year return period, $\bar{U}_m$ is the mean value of the maximum monthly wind speeds and σ_m is the standard deviation of the maximum monthly wind speeds.

The methodology requires the use of 3-year datasets at minimum; in the present study data from 10 consecutive years (1995-2004) were used. From this dataset, only the maximum monthly winds with direction in the sector 135-225 deg (SE to SW) were used to compute the mean and the standard deviation values. While processing the dataset, a repeatable pattern of significantly low wind speeds from the southern directions was observed from June to August. This pattern coincides with the existence of the strong Etesian Winds during the same season in the Aegean Sea. Therefore, the wind speeds from June to August were excluded from the analysis. The final results for the mean speed and the standard deviation were $\bar{U}_m = 8.95$ m/s and $\sigma_m = 2.83$ m/s, respectively.

Then, using Eq. (4) for several values of the return period, T_r, up to 100 years, the corresponding wind speeds were computed and shown in Figure 6. Note that the 100-year wind speed was found to be 23.3 m/s, i.e. wind of 9B. Hence, the simulations with wind strength of 9B (Figure 5) are the ones related to the wave climate with 100-year return period offshore the Piraeus Port. Specifically for the SSE winds, which result into the highest waves in this region, the development of wave height with wind duration is presented in Figure 7 at a specific location offshore the Piraeus Port. It is observed that after 8hrs, fetch-limited conditions are established and the resulting significant wave height is equal to 7.3 m.

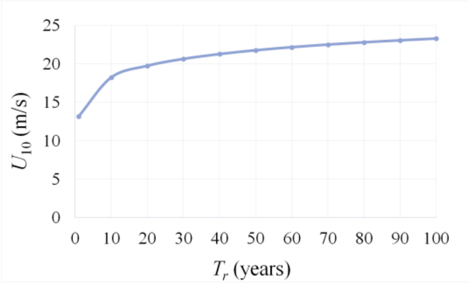

Figure 6 Correlation of wind speed to return period for the SW Aegean Sea based on data from the Hellenic National Meteorological Service station in Mylos Island

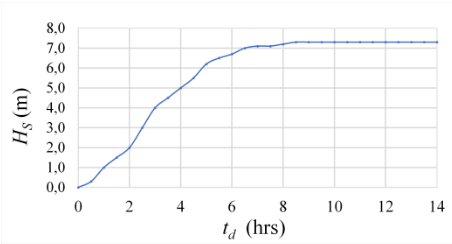

Figure 7 Variation of significant wave height with respect to wind duration at the location offshore the Piraeus Port with coordinates (x,y) = (730000,4195000) in the Greek Grid (Figure 2) for SSE winds of 9B

4 CONCLUSION

In the present work, the wind-induced wave growth in the SW Aegean Sea basin was studied in order to obtain design values of high waves offshore the Piraeus Port. It was found that the SSE wind has the potential to generate the highest waves offshore the Piraeus Port, and its strength with 100-year return period is 9B. For fetch-limited conditions, a significant wave height of 7.3 m is developed.

Aknowledgements

This work was performed using an educational license for MIKE 21 by DHI Water and Environment.

References

Bidlot J, Janssen P, Abdalla S (2007) A revised formulation of ocean wave dissipation and its model impact. Technical Report Memorandum 509, ECMWF, Reading, U.K.
DHI (2014) MIKE C_MAP, User Guide. DHI, Denmark.
DHI (2017) MIKE 21 Spectral Waves FM, User Guide. DHI, Denmark.
Galiatsatou P, Anagnostopoulou C, Prinos P (2015) Modelling nonstationary extreme wave heights in the present and the future climate of the Greek Seas. Proc. 3rd IMA Int. Conf. on Flood Risk.
Gringorten I (1963) A Plotting Rule for Extreme Probability Paper. J. Geoph. Res. 68(3): 813-814.
Hasselmann S, Hasselmann, K (1985) Computation and parameterizations of nonlinear energy transfer in a gravity-wave spectrum, Part 2: Parameterisations of nonlinear energy transfer for applications in wave models. J. Phys. Oceanog. 15: 1378-1391.
Komen GJ, Cavaleri L, Doneland M, Hasselmann K, Hasselmann S, Janssen PAEM (1994) Dynamics and modelling of ocean waves. Cambridge University Press, UK.
USACE (2002): Coastal Engineering Manual: Chap.8, Hydrodynamic Analysis and Design Conditions. USACE, USA.

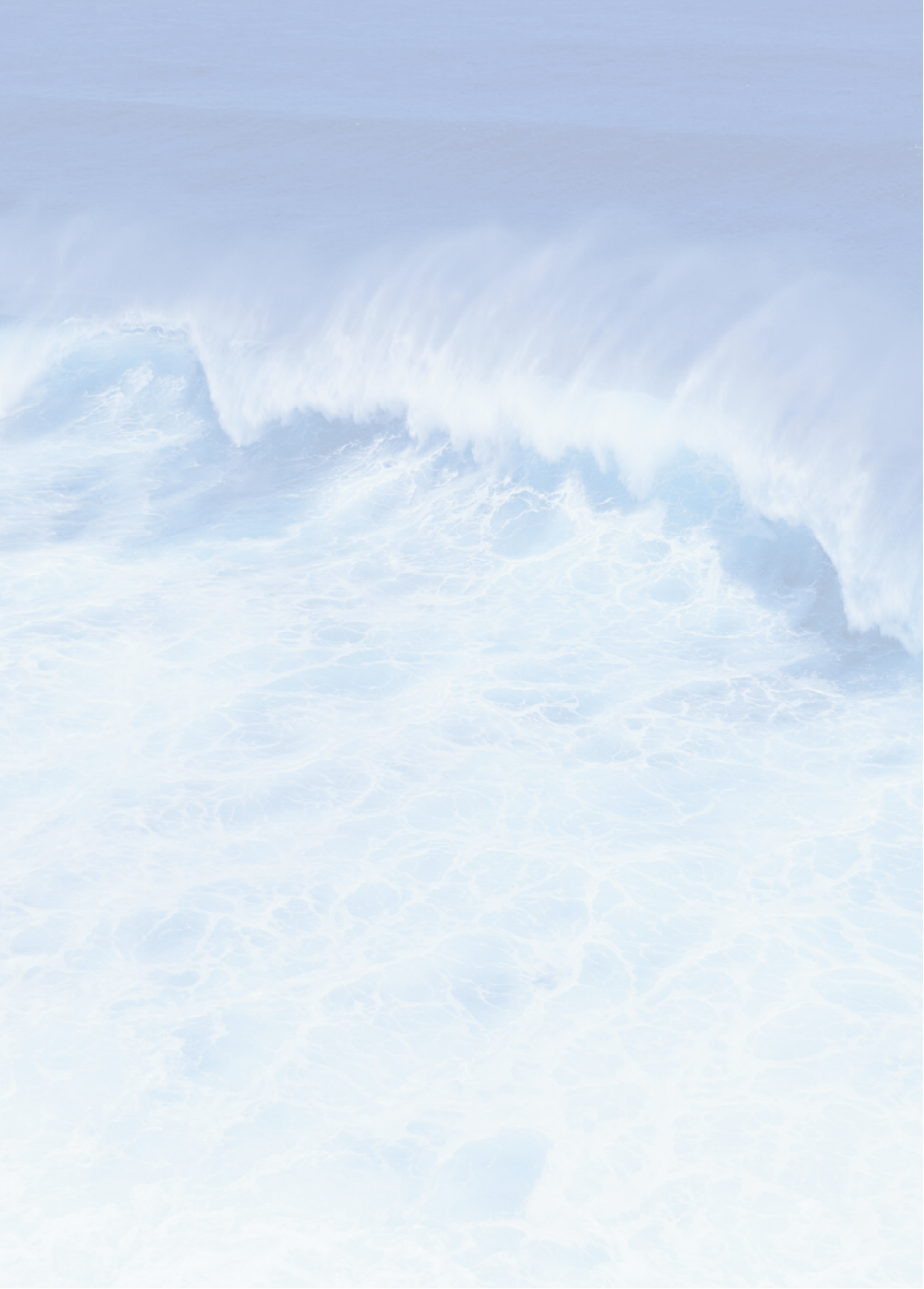

Numerical simulation of ship-borne waves using a 2DH post-Boussinesq model

A.G. Samaras*, Th.V. Karambas

Laboratory of Maritime Engineering and Maritime Works, Department of Civil Engineering, Aristotle University of Thessaloniki, University Campus, 54 124, Thessaloniki, Greece
*Corresponding author: asamaras@civil.auth.gr

Abstract

This work presents results on the simulation of the generation and propagation of ship-borne waves, using an advanced nonlinear dispersive wave model based on higher order Boussinesq-type equations. The model includes a single frequency dispersion term, expressed through convolution integrals; it is adapted to represent ship-borne waves by adopting the approach for wave generation by a moving local pressure disturbance, achieved through adding a respective pressure term in its governing equations. The model is tested against: (a) the analytical solution for the calculation of the angles of ship wakes presented in the pioneering work of Havelock in 1908; (b) laboratory experiments of waves produced by a high-speed ship in a channel; and (c) numerical experiments presented by other researchers. Results compare well to data from all the aforementioned studies, confirming the model's capabilities and highlighting its accuracy in the representation of ship-born waves.

Keywords Ship-borne waves, Numerical modelling, Post-Boussinesq model, Model validation.

1 INTRODUCTION

Ship-borne waves have been of interest to researchers and engineers for more than the last century and have been studied systematically through mathematical analysis, field observations, laboratory experiments and numerical modelling. Thompson (1887) is considered to have set the bases for this field, his lecture "On Ship Waves" being the first documented scientific approach on the phenomenon. Havelock (1908) followed, presenting the mathematical framework for describing the angles of ship wakes. After these first pioneering works, many researchers have contributed to the study of waves generated by ships travelling in various flow regimes. In the context of this version of this work, one may indicatively refer to: the analytical works of Huang et al. (1982) and Wu (1987); the experimental investigations of Landweber and Thews (1935), Johnson (1957), Lee et al. (1989) and Gourlay (2001); the observational works of Velegrakis et al. (2007) and Torvsik et al. (2009); and the recent modelling works of David et al. (2017) and Shi et al. (2018) using Boussinesq-type models.

In Section 2 of this paper, the 2DH post-Boussinesq model of Karambas and Memos (2009) and its adaptation for the representation of ship-borne waves are briefly presented, followed, in Section 3, by the validation of the model through comparison with the analytical solution of Havelock (1908) and the laboratory experiments of Gourlay (2001). Model applications for flow regimes beyond the range tested by Gourlay (2001) are indicatively discussed as well, closing with the conclusions drawn from this work.

2 THE 2DH POST-BOUSSINESQ MODEL

This work is based on the 2DH post-Boussinesq model of Karambas and Memos (2009), which is adapted to represent ship-borne waves for the purposes of this study. Essential model aspects regarding the model's governing equations, its aforementioned adaptation and the scheme used for the numerical solution are briefly presented in the following sections.

2.1 Model equations

The model's momentum equations are extracted adopting a methodology based on the Fourier transform, leading to equations similar to the respective ones for long waves, incorporating a single additional frequency dispersion term. The latter is expressed through convolution integrals, which are estimated using appropriate impulse functions. Momentum equations are expressed as:

$$\frac{\partial U}{\partial t}+U\frac{\partial U}{\partial x}+V\frac{\partial U}{\partial y}+g\frac{\partial \zeta}{\partial x}=-\int_{\infty}^{\infty}\int_{-\infty}^{\infty}\left(\frac{\partial \zeta}{\partial x}(x-\xi_1,x-\xi_2,t)-\frac{\partial \zeta}{\partial x}\right)K(\xi_1,\xi_2)\,d\xi_1 d\xi_2 \quad (1)$$

$$\frac{\partial V}{\partial t}+U\frac{\partial V}{\partial x}+V\frac{\partial V}{\partial y}+g\frac{\partial \zeta}{\partial y}=-\int_{-\infty}^{\infty}\int_{-\infty}^{\infty}\left(\frac{\partial \zeta}{\partial y}(x-\xi_1,x-\xi_2,t)-\frac{\partial \zeta}{\partial y}\right)K(\xi_1,\xi_2)\,d\xi_1 d\xi_2 \quad (2)$$

where U, V are the depth-averaged velocity components along the x- and y- directions, respectively, ζ is the surface elevation and g the gravitational acceleration. In Eqs. 1-2 the kernel $K(x,y)$ is given by:

$$K(x,y)=\frac{g}{2\pi d^2}\left[\frac{1}{r/d}-\sum_{n=1}^{\infty}\frac{(-1)^{n-1}}{\sqrt{n^2+(r/d)^2/4}}\right] \quad (3)$$

where d is the water depth and $r^2 = x^2+y^2$. The model is wavenumber free and as far as the linear dispersion relation is concerned, the approach is exact (i.e. the model poses no restriction on the water depth).

2.2 Wave generation by ship-borne waves

The model is adapted to represent ship borne waves by adopting the approach for wave generation by a moving local pressure disturbance, achieved through adding a pressure term (i.e. ψ_S) in its governing equations. Following the rationale of David et al. (2017), the aforementioned term for an elongated ship-like pressure distribution is expressed as (Bayraktar and Beji 2013):

$$\left(\psi_S\right)_{i,j}=D_p\left[1-c_L\left(x_i/L_p\right)^4\right]\left[1-c_B\left(y_j/B_p\right)^2\right]e^{-a\left(y_j/B_p\right)^2} \quad (4)$$

where D_p, L_p, B_p are the draft, length and breadth (measured from the longitudinal center axis) of the pressure, respectively, with $D_p = 10^5 D_s$ (D_s being the corresponding ship draft), and a, c_L, c_B are form parameters set to 16, 2 and 16, respectively, resulting in a slender body. The terms $(\psi_S/\rho)_x$ and $(\psi_S/\rho)_y$ are accordingly added to the right-hand sides of Eqs. 1 and 2. It is noted that the approach of Shi et al. (2018) for the pressure disturbance was also tested in the model, yielding similar results.

2.3 Numerical scheme

The numerical solution is accomplished by a widely used simple and well documented explicit 2nd order finite difference scheme, centered in space and forward in time, on a staggered grid, conserving mass and energy for non-breaking waves in a satisfactory manner. The discrete continuity equation is centered in the level points and the momentum equations in the flux points.

3 MODEL APPLICATIONS & DISCUSSION

3.1 Analytical solution of Havelock (1908)

Havelock (1908) presented the mathematical framework for describing the angles of ship wakes (i.e. wedge angles), following the work of Thomson (1887). Havelock's work for a point impulse moving on water of finite depth resulted in an analytical solution describing the above angle as a function of the depth-based Froude number F_d, that is the ratio of the speed of the moving impulse (i.e. ship speed in our case) to wave celerity in shallow water. The comparison of wedge angle results obtained from model runs and the analytical solution of Havelock (1908) is presented in Figure 1; the close agreement observed in it confirms that the model represents well wedge angles for both subcritical and supercritical regimes.

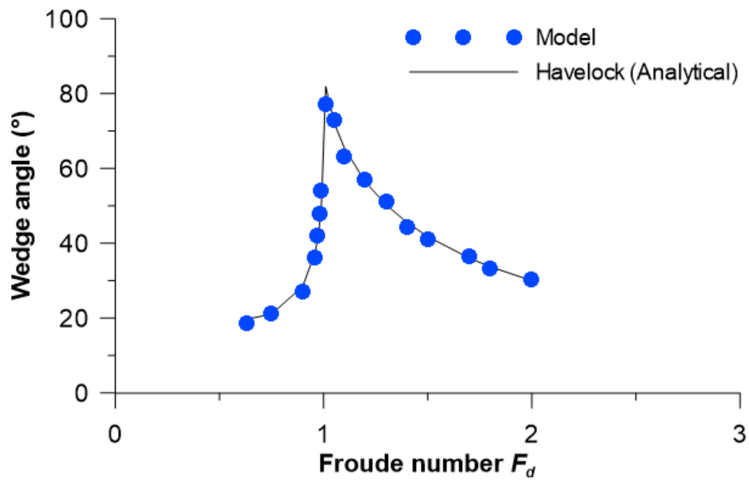

Figure 1 Comparison of wedge angle results obtained from model runs and Havelock's analytical solution.

3.2 Experimental data of Gourlay (2001)

Gourlay (2001) carried out a series of laboratory experiments at the Australian Maritime College of the University of Tasmania, in order to investigate the various flow regimes accompanying a ship travelling in a channel at supercritical speeds. The experimental setup in the 60.0 m long, 3.5 m wide towing tank of the facility, included the use of a 1.6 m long monohull vessel, with both length to beam and beam to draught ratios equal to 4. Two different water depths – corresponding to depth to draught ratios of 1.14 and 2.05 – were used, and tests were run for gradually incrementing vessel speeds corresponding to F_d = 1.05 and upwards. Regarding the ship-generated waveforms for the depth to draught ratio of 1.14 examined in this work, Gourlay (2001) found that the smooth solitons for lower F_d numbers first began to break at F_d = 1.12, and remained broken as F_d increased. For $1.12 < F_d < 1.35$ a gradual transition from broken solitons to almost-pure bores was observed, with steady supercritical flow commencing for $F_d > 1.48$.

Figure 2 presents the comparison between model results and experimental data of the scaled free surface height as a function of time, for F_d = 1.15. Results and data refer to the location of the first wave probe in the experimental setup described above, located at (x,y) = (34.375 m, 0.72 m) of the channel. The model agrees well with measurements, capturing both the breaking solitons ahead of the moving ship and the disturbance after the ship's bow passing the probe (at approximately $t \approx 22.5$ s according to Gourlay 2001), performing better than the model of Shi et al. (2018) in this aspect.

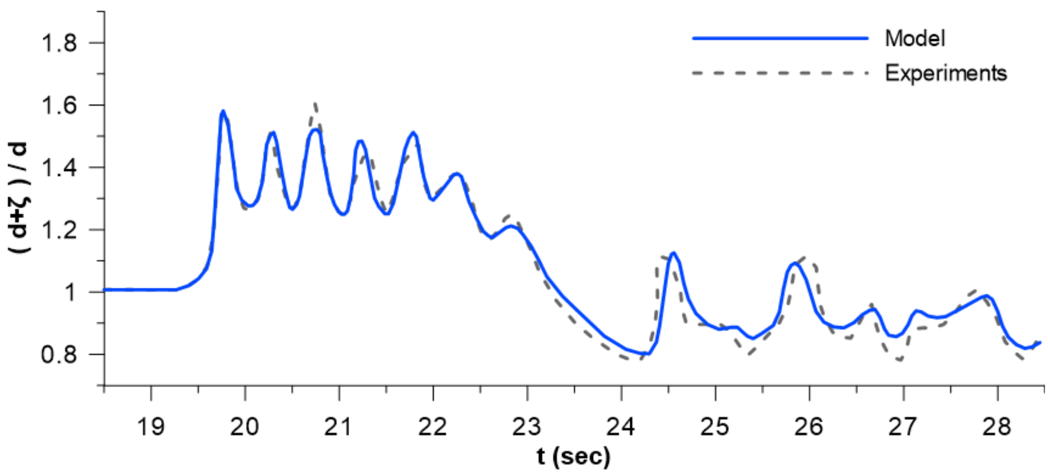

Figure 2 Comparison between model results and the experiments of Gourlay (2001) of scaled free surface height as a function of time, for F_d = 1.15.

Figure 3 presents the comparison between model results and experimental data of the scaled mean wave oscillation amplitude as a function of the Froude number. The figure illustrates the transition from solitons to a pure bore as F_d increases (that was also mentioned in the previous), and eventually to a practically flat shelf of water for $F_d > 1.4$. Model results are in good agreement with measurements for Froude numbers up to $F_d = 1.3$, while for $1.3 < F_d < 1.4$ the model appears to underestimate mean wave oscillation.

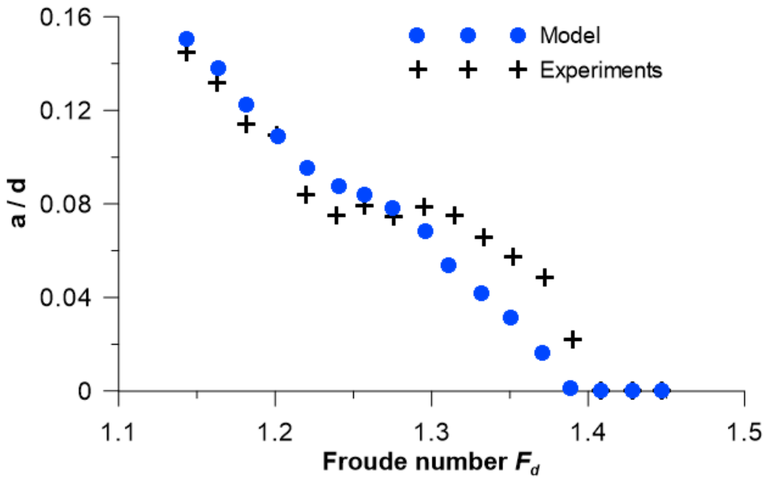

Figure 3 Comparison between model results and the experiments of Gourlay (2001) of scaled mean wave oscillation amplitude as a function the Froude number.

Model runs were also performed for various setups and Froude numbers, beyond the range tested by Gourlay (2001), following the rationale of the numerical experiments presented by Shi et al. (2018). Figure 4 indicatively presents results of an exemplary run (using the same experimental setup) for a Froude number equal to 0.80, its intended purpose being mainly to demonstrate the wave pattern in the channel behind the moving vessel, with the ship wake and the nonlinear reflection effects from the channel walls clearly identifiable.

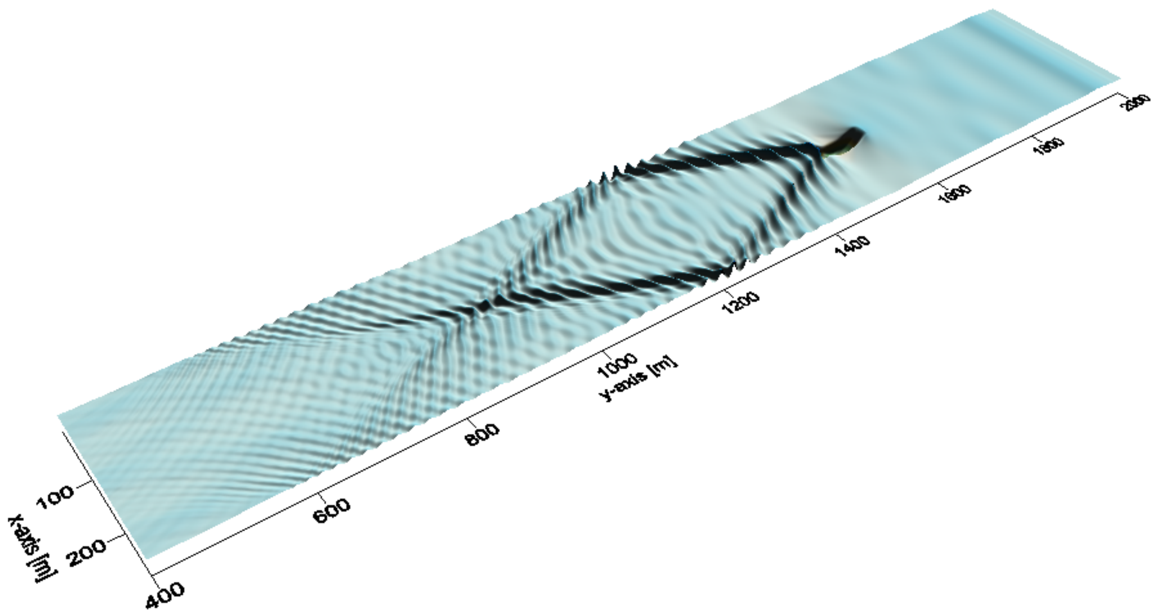

Figure 4 Computed nonlinear waves generated by a ship travelling in a channel (experimental setup of Gourlay 2001) for $F_d = 0.8$.

4 CONCLUSIONS

This works presents an advanced nonlinear dispersive wave model based on higher order Boussinesq-type equations and its implementation for the simulation of ship-borne waves. Model results are in good agreement with: (a) the analytical solution of Havelock (1908), for the description of wedge angles in sub-/super-critical regimes; and (b) the experimental data of Gourlay (2001), for the waves produced by a high-speed ship in a channel, progressing from smooth solitons to broken solitons, pure bores and supercritical flow with the increase in Froude number values. Indicative results are also presented for Froude numbers beyond the range tested by Gourlay (2001), their full presentation and detailed analysis being the subject of a future extended version of this work. All in all, the validation presented in the previous confirms the model's capabilities and accuracy, setting the basis for future work by the authors on the same path.

References

Bayraktar Ersan D, Beji S (2013) Numerical simulation of waves generated by a moving pressure field. Ocean Eng 59:231-239 doi:10.1016/j.oceaneng.2012.12.025.

David CG, Roeber V, Goseberg N, Schlurmann T (2017) Generation and propagation of ship-borne waves - Solutions from a Boussinesq-type model. Coast Eng 127:170-187 doi:10.1016/j.coastaleng.2017.07.001.

Gourlay TP (2001) The supercritical bore produced by a high-speed ship in a channel. J Fluid Mech 434:399-409 doi:10.1017/s002211200100372x.

Havelock TH (1908) The propagation of groups of waves in dispersive media, with application to waves on water produced by a travelling disturbance. Proc R Soc Lond A Math Phys Sci 81:398-430 doi:10.1098/rspa.1908.0097.

Huang DB, Sibul OJ, Webster WC, Wehausen JV, Wu D-M, Wu TY (1982) Ships moving in the transcritical range. Paper presented at the conference on cehaviour of ships in restricted waters, Varna, Bulgaria.

Johnson JW (1957) Ship waves in navigation channels. Paper presented at the 6th conference on coastal engineering, Gainesville, Florida.

Karambas TV, Memos CD (2009) Boussinesq model for weakly nonlinear fully dispersive water waves. J Waterw Port C - ASCE 135:187-199 doi:10.1061/(asce)0733-950x(2009)135:5(187).

Landweber L, Thews JG (1935) The influence of shallow water on the resistance of a cruiser model. U.S. Experimental Model Basin, Navy Yard, Washington, D.C.

Lee S-J, Yates GT, Wu TY (1989) Experiments and analyses of upstream-advancing solitary waves generated by moving disturbances. J Fluid Mech 199:569-593 doi:10.1017/s0022112089000492.

Shi F, Malej M, Smith JM, Kirby JT (2018) Breaking of ship bores in a Boussinesq-type ship-wake model. Coast Eng 132:1-12 doi:10.1016/j.coastaleng.2017.11.002.

Thomson W (1887) On Ship Waves. Proc Inst Mech Eng 38:409-434 doi:10.1243/pime_proc_1887_038_028_02.

Torsvik T, Didenkulova I, Soomere T, Parnell KE (2009) Variability in spatial patterns of long nonlinear waves from fast ferries in Tallinn Bay. Nonlin Processes Geophys 16:351-363 doi:10.5194/npg-16-351-2009.

Velegrakis AF, Vousdoukas MI, Vagenas AM, Karambas T, Dimou K, Zarkadas T (2007) Field observations of waves generated by passing ships: A note. Coast Eng 54:369-375 doi:10.1016/j.coastaleng.2006.11.001.

Wu TY-T (1987) Generation of upstream advancing solitons by moving disturbances. J Fluid Mech 184:75-99 doi:10.1017/s0022112087002817.

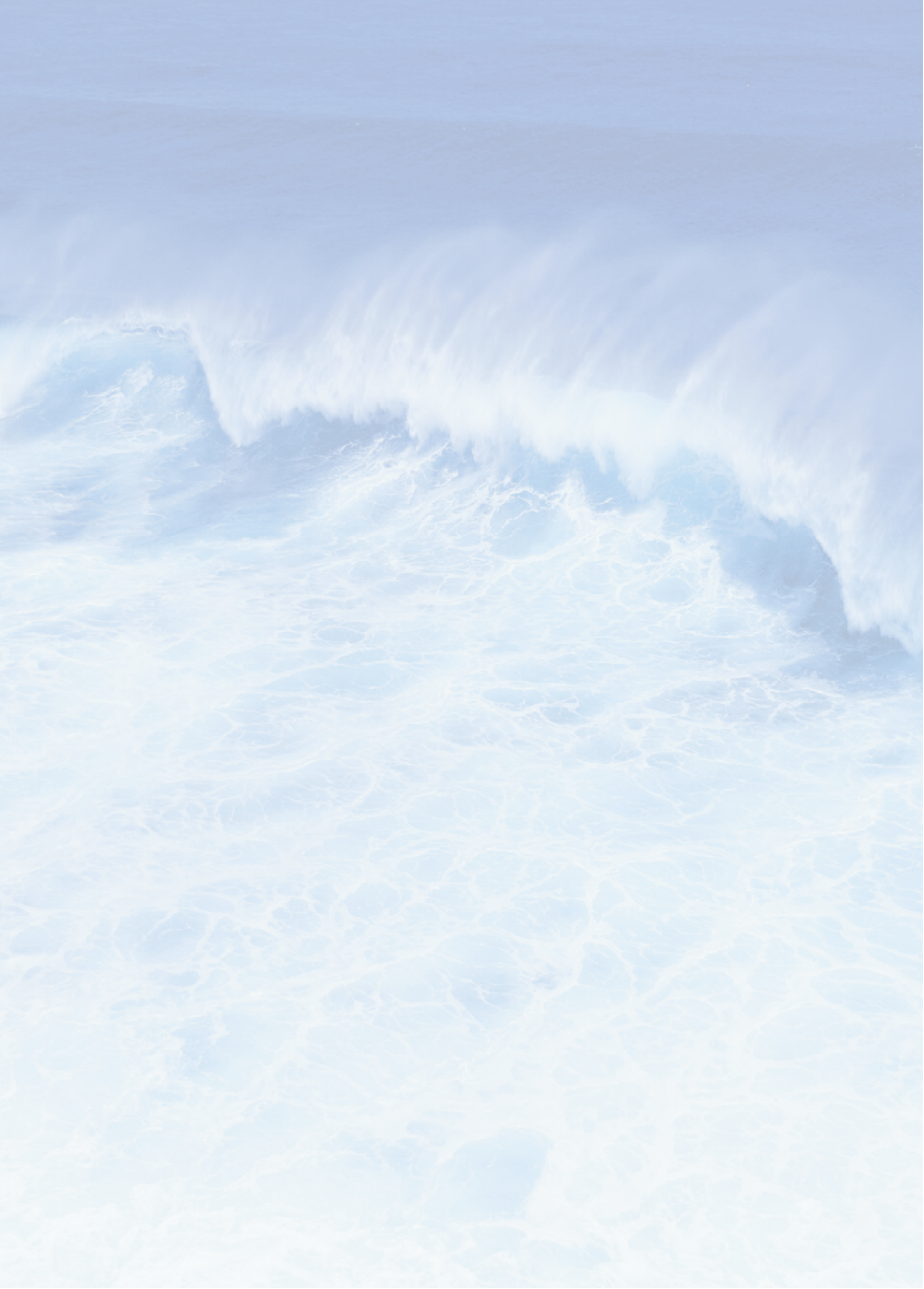

An efficient Navier-Stokes based numerical wave-tank for complex wave hydrodynamics

C. Frantzis[1*], D.G.E. Grigoriadis[2]

[1]PhD Student
[2]Assistant Professor
Computational Sciences Laboratory, UCY-CompSci, Department of Mechanical & Manufacturing Engineering,
University of Cyprus, 75 Kallipoleos, Nicosia, 1678, Cyprus
[*]Corresponding author: cfrant02@ucy.ac.cy

Abstract

The numerical study of wave hydrodynamic phenomena can be performed using different tools and methods depending on the complexity of each case. Simpler methods can provide fast estimates, but they fail to provide accurate solutions for challenging problems which involve highly non-linear phenomena. The most accurate method is the solution of the Navier-Stokes (NS) equations that describe the incompressible flow of two immiscible fluids (water and air). When solving the full set of NS, one can accurately capture phenomena such as wave breaking and/or fluid structure interactions. However, in this case, the computational resources required for the solution of the NS equations could be prohibitively large, due to the variable coefficient pressure Poisson equation that must be solved. In this study, the development of a new, efficient three-dimensional (3D) NS-based numerical wave tank (NWT) is presented. The method of Frantzis and Grigoriadis (2019) is adopted, where a constant coefficient Poisson equation is solved for the pressure difference, allowing the use of fast direct solvers (FDS). The presence of submerged obstacles was taken into account using the IB method and the free-surface was captured with a level-set (LS) method. A relaxation method was used for the wave generation and absorption. The developed two-fluid NWT is validated against standard test cases, experimental measurements for spilling breaking wave and the 3D interaction between a vertical abutment and a solitary wave. When compared against conventional NWTs of research or open-source codes, the developed NWT accelerated the execution time by a factor of 30.

Keywords Computational efficiency, Two-fluid approach, Conservative level-set, Fast direct solvers.

1 INTRODUCTION

The detailed study of highly non-linear wave hydrodynamic phenomena can be accurately achieved by the solution of the full set of the Navier-Stokes (NS) equations. The evolution of computers, along with the high fidelity and accuracy provided by this approach, allows nowadays researchers to use such an expensive computational fluid dynamics (CFD) method. However, even today, detailed three-dimensional (3D) NS simulations on practical applications may be impossible, due to enormous requirements in computational resources. Therefore, the development of efficient numerical methods is crucial to enable detailed parametric studies of more demanding flow cases.

The widely used fractional step method, which is used for the time advancement of the velocity and pressure fields, requires the solution of a Poisson equation for the pressure which is the most computational intensive procedure of the simulation. Thus, for the reduction of the total computational cost, a significant reduction of the Poisson solution must be achieved.

In single fluid problems, the matrix of coefficients of this Poisson equation only depends on the numerical grid. On the other hand, when a two-fluid solution is attempted, the motion of the interface leads to a Poisson equation with a matrix of variable coefficients in space and time due to the local dependencies on the density field. This characteristic excludes the use of conventional direct solvers (e.g. LU-based), because the inversion of a large matrix would be required at every time-step, leading to an enormous computational cost. As a consequence, so far, the most popular choice for the solution of the pressure field was iterative solvers, that do not require the inversion of the matrix but the coefficients in the matrix can be updated at every time-step.

Recently, Dodd and Ferrante (2014) proposed a transformation for the pressure Poisson equation leading to constant coefficient matrix. Later on, Frantzis and Grigoriadis (2019) developed a constant coefficient Poisson formulation that is also suitable for the use of the Immersed Boundary (IB) to describe solid obstacles within the domain. Eliminating the need of inverting the matrix at every time step is an important advantage of these formulations, because they enable the use of direct solvers and especially the fast direct solvers (FDS). The latter ones can give the solution one to two orders of magnitude faster compared to iterative solvers, and have significantly reduced RAM requirements.

In this study, the formulation of Frantzis and Grigoriadis (2019) is adopted to develop an efficient numerical wave-tank which uses (i) a FDS for the solution of the Poisson equation, (ii) the IB method to describe solid obstacles of arbitrary geometry within the domain, (iii) the Level-set method to track the two-fluids interface, and (iv) the relaxation method for the wave generation and absorption. The developed NWT was tested validated against standard test cases (i.e. propagating waves and standing wave) and against experimental measurements for spilling breaking waves and the 3D interaction between a vertical abutments and a solitary wave. Moreover, the performance of the developed NWT was compared against the conventional approach of using an iterative solver to solve the variable coefficient Poisson.

2 MATHEMATICAL DESCRIPTION & NUMERICAL METHODS

2.1 Governing Equations

The incompressible flow of two viscous and immiscible fluids, without surface tension effects, is described by the spatial averaged Navier-Stokes equations, which in their non-dimensional form read,

$$\nabla \cdot \vec{u} = 0 \tag{1}$$

$$\frac{\partial \vec{u}}{\partial t} = -\vec{u} \cdot \nabla \cdot \vec{u} + \frac{1}{\rho Re} \nabla \cdot [(\mu + Re \cdot \mu_t)(\nabla \vec{u} + (\nabla \cdot \vec{u})^T)] - \frac{\nabla \mathrm{P}}{\rho} + \frac{\vec{a}}{Fr} \tag{2}$$

where $\vec{u}$, P, ρ, μ and μ_t are the non-dimensional velocity, pressure, density, dynamic viscosity and dynamic turbulent viscosity fields, respectively. All these variables evolve in space and time. $\vec{a}$ is the unit vector of the gravity acceleration and Re and Fr are the non-dimensional Reynolds and Froude numbers, respectively. These are given by, $\mathrm{Re} = U_o L_o \rho_o / \mu_0$ and $\mathrm{Fr} = {U_o}^2/(g L_o)$. U_o, L_o, ρ_o and μ_o are the characteristic velocity, length, density and dynamic viscosity scales.

The value of μ_t can be defined by any turbulence model available in the literate. In the current study, the Large Eddy Simulation (LES) approach is employed and the simple Smagorinsky model is selected to represent the unresolved scales of motion. The turbulent viscosity $\mu_t$is defined as $\mu_t = \rho(C_s \Delta)^2 |\bar{S}|$, where $\Delta = (\Delta x \Delta y \Delta z)^{1/3}$ is the filter length scale, $|\bar{S}| = \left(2\bar{S}_{ij}\bar{S}_{ij}\right)^{1/2}$ is the modulus of the strain tensor and C_s is a Smagorinsky constant set equal to 0.2.

2.2 Numerical Methods

2.2.1 Interface Capturing and Fluid Properties

The position of the interface at each time instant is captured by the conservative level-set method (Sussman et al. 1998), where the scalar variable φ, that describes the minimum signed distance from the interface, is introduced. Therefore, solving an advection equation for this variable, using the known velocity field, the position of the interface at the new time instant is calculated.

$$\frac{\partial \varphi}{\partial t} + \nabla \cdot (\vec{u}\varphi) = 0 \tag{3}$$

Additionally, the so called re-initialisation equation is solved after the advection equation in order to ensure that φ is maintained as the minimum signed distance from the interface. The discontinuous nature of the density and viscosity fields at the interface may introduce numerical instabilities. Therefore, an artificial thickness of the interface is introduced and the density and viscosity fields are calculated using the smoothed Heaviside function $H(\varphi)$, which takes the value of unity in one fluid and zero in the other. Close to the interface $H(\varphi) = 0.25\left(\varphi/_{\varepsilon} + 1/_{\pi}\sin\left(\pi\varphi/_{\varepsilon}\right)\right)$, where ε is a constant that defines the half thickness of the interface. Here, $\varepsilon = 2min(\Delta x_{min}, \Delta y_{min}, \Delta z_{min})$.

2.2.2 Constant Coefficient Poisson Equation

Following the steps of the well-known fractional step method, the Poisson equation for the pressure that arises reads,

$$\nabla \cdot \left(\frac{\nabla P^{n+1}}{\rho^{n+1}}\right) = \nabla \cdot \vec{u}^* \tag{4}$$

where $\vec{u}^*$ is the provisional velocity field. After implementing the pressure splitting scheme of Dodd and Ferrante (2014) and the extension/modifications of Frantzis and Grigoriadis (2019), a constant coefficient Poisson for the pressure difference must be solved, instead,

$$\nabla^2 \delta P^{n+1} = \frac{\rho_o}{\Delta t}\nabla \cdot \vec{u}^* + \nabla \cdot \left[\left(1 - \frac{\rho_o}{\rho^{n+1}}\right)\nabla \hat{P}\right] - \nabla^2 P^n \tag{5}$$

where $\hat{P}$ is an approximation of P^{n+1}, given by the extrapolation $\hat{P} = 2P^n - P^{n-1}$.

2.2.3 Numerical Implementation and discretisation schemes

The equations presented above are discretised and solved on a Cartesian staggered grid arrangement, using finite differences. Solid obstacles within the domain are taken into account using the IB method and the required modifications proposed by Frantzis and Grigoriadis (2019). Eq. 5 is solved using a FISHPAK-based FDS. The time-step Δt is dynamically controlled by the CFL restriction criterion. Detailed description of the current implementation is presented in Frantzis and Grigoriadis (2019). It is noted that the QUICK 3rd-order upwind scheme was used for the descretisation of the convective term of Eq. 2. The wave generation is performed with the relaxation method, using theoretical expressions for the free-surface elevation and the velocity field in the water. The wave absorption is also performed with the relaxation method.

3 VALIDATION RESULTS

The developed NWT was firstly tested for propagating Stokes waves of 2nd-order to examine its temporal convergence and accuracy due to the additional temporal error of the pressure splitting scheme (extrapolation error of $\hat{P}$). Waves of height $H = 0.1d$ and length $\lambda = 4d$ were simulated for different CFL values. The vertical resolution was $\Delta z/d = 0.0125$ and the aspect ratio of the cells was set to $AS = 2$. It was found that the CFL value should be set equal to 0.025 to eliminate the temporal error associated with the pressure splitting scheme. In a conventional NWT, where the variable coefficient Poisson is solved and there is no pressure splitting temporal error, the CFL value is usually set equal to 0.1. Thus, the developed NWT requires 4 times smaller time-step in order to perform accurately. However, even with this time step reduction, the proposed NWT is still computationally more efficient compared to the conventional approaches, as it is demonstrated in section 4.

3.1 Spilling Breaking Wave

In this paragraph, the proposed NWT is validated against the experimental data of Ting and Kirby (1996) for a spilling breaking wave. The Figures 1-3 demonstrate the comparison of the present numerical results and their experimental data, showing the capability of the proposed NWT to accurately simulate demanding cases with high non-linear phenomena such as the wave breaking.

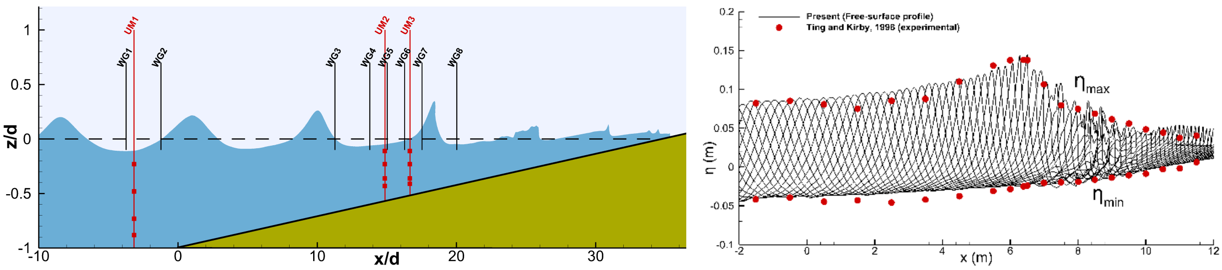

Figure 1 (left): schematic diagram of the spilling breaker case with locations of free-surface elevation sensors (WG) and velocity sensors (UM) (Left), (right): Free-surface envelope of the present numerical results (black solid lines) and η_{min} and η_{max} of the experimental measurements (red circles) (Right)

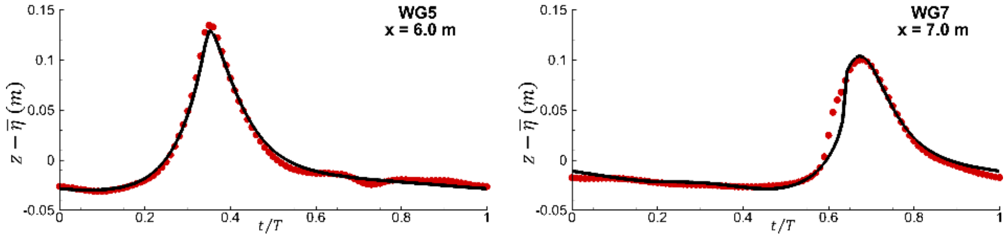

Figure 2 Comparison of the present NWT against experimental measurements for the phase-averaged values of the free-surface elevation z with respect to the mean free-surface elevation $\bar{\eta}$, before wave breaking (left) and after (right). (Lines and colors similar to Figure 1 (right))

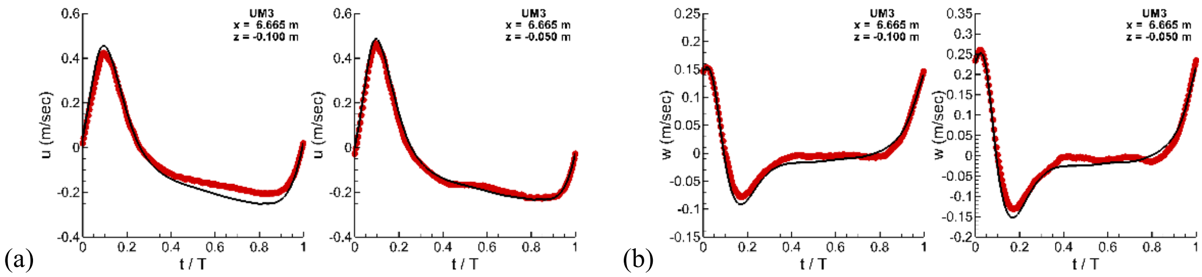

Figure 3 Comparison of the present NWT against experimental measurements for the phase averaged horizontal velocity u (a) and vertical velocity w (b) at a location after the breaking, for $z_1 = -0.1m$ (left) and $z_2 = -0.05$ (right) with respect to the still water level. (Lines and colors similar to Figure 1 (right))

3.2 3D Interaction between a Solitary Wave and a Vertical Abutment

The proposed NWT was also validated against the experimental data of Lara et al. (2012), for the case of the 3D interaction between a solitary wave and a vertical abutment. The schematic diagram of the top view of the NWT along with the locations of the wave-gauges is presented in Figure 4. More details on the geometrical and wave parameters of the case can be found in (Lara et al. 2012).

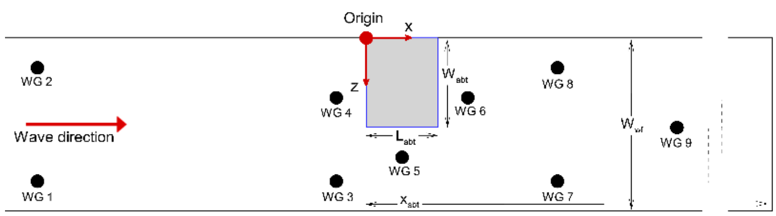

Figure 4 Schematic diagram (top view) of the NWT and the location of the elevation sensors (WG) in the vicinity of the abutment

A uniform grid was used in all directions with $(Nx, Ny, Nz) = (2600,100,64)$. The simulation of 100 time units lasted 35 hours on a single server equipped with $64Gbytes$ of RAM and two Intel(R)

Xeon(R) E5-2680 CPU units of 14 cores each, synchronised at $2.4GHz$. The good agreement of the present numerical results against the experimental data is shown in Figure 5.

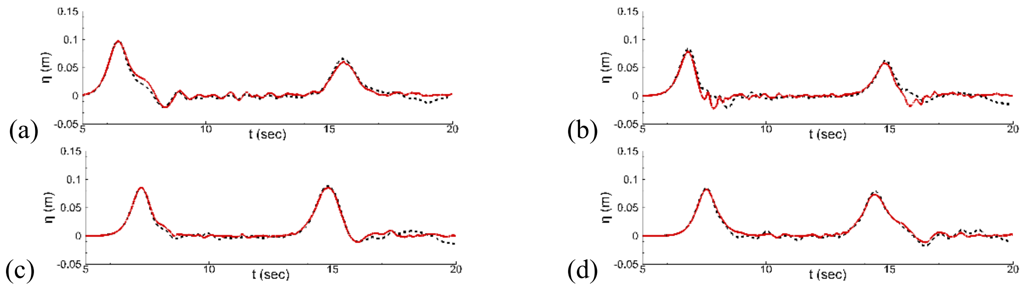

Figure 5 Free surface elevation at locations (a) WG1, (b) WG5, (c) WG8, (d) WG9. Red solid lines refer to the present numerical results and black dashed lines to the experimental measurements of Lara et al. (2012)

4 COMPUTATIONAL PERFORMANCE

In order to address the performance of the proposed NWT against conventional ones, the Poisson was solved with the two approaches, (i) solving Eq. 4 with an iterative solver, using $CFL = 0.1$ and (ii) solving Eq. 5 with a FDS, using $CFL = 0.025$. Propagating waves were simulated in a 3D domain of different resolution. The grid size and the performance results of the two approaches are summarised in Table 1, using the server described in the previous paragraph.

Table 1 Computational performance of the developed NWT. Wall clock time for the Poisson solution only, using BiCGStab or FDS. % of the FDS solution to the full solver and speed-up for 4 times more time steps.

Grid Cells	Poisson solution only			Full NS solver	
(Nx, Ny, Nz)	BiCGStab (sec)	FDS (sec)	Speed-up	FDS (%)	Final Speed-up ($RF = 4$)
(1200,24,38)	1.82	7.81×10^{-3}	243.5	10.36	6.4
(2400,48,76)	31.11	8.89×10^{-2}	350.0	14.92	12.9
(2400,96,76)	86.47	2.08×10^{-1}	415.5	15.69	16.1
(4800,96,152)	560.70	1.08	517.9	24.47	31.0
(4800,192,304)	2121.39	5.68	373.3	31.65	29.0

For smaller problems, where the reduction of the cost is not crucial, the proposed NWT may perform about 6 times faster. For larger problems though, the simulations is accelerated up to 30 times.

5 CONCLUSIONS

The method adopted in the present study to develop a new NWT can accurately simulate flows with irregular solid boundaries, using the IB method. When a FDS is employed, the solution is achieved 1-2 orders of magnitude faster, depending on the size of the problem. Thus, more demanding flow cases and high-fidelity simulations can be performed easier. Moreover, the use of FDS require significantly less RAM resources, allowing the use of smaller computers and also GPU computing.

References

Dodd M S, Ferrante A (2014) A fast pressure-correction method for incompressible two-fluid flows. Journal of Computational Physics 273:416-434.

Frantzis C, Grigoriadis DGE (2019) An efficient method for two-fluid incompressible flows appropriate for the immersed boundary method. Journal of Computational Physics, 376:28-53.

Lara J L, del Jesus M, Losada IJ (2012) Three-dimensional interaction of waves and porous coastal structures: Part II: Experimental validation. Coastal Engineering 64:26-46.

Sussman, M., Fatemi, E., Smereka, P., Osher, S., (1998) An improved level set method for incompressible two-phase flows. Computers & Fluids 27 (5):663-680. Ting, F. C., & Kirby, J. T., (1996) Dynamics of surf-zone turbulence in a spilling breaker. Coastal Engineering 27 (3-4):131-160.

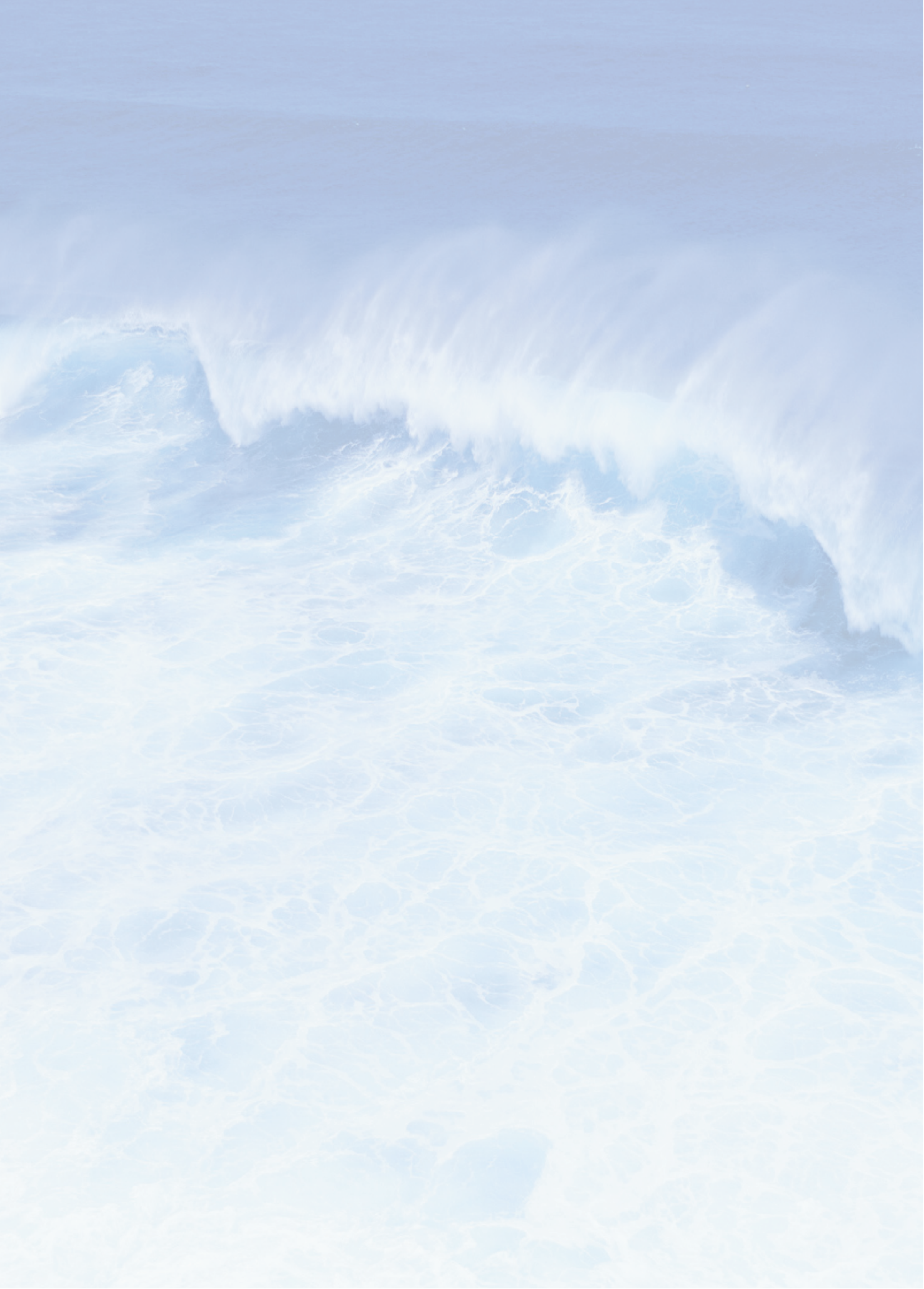

A three-dimensional approach for a spheroid water entry problem

D. Th.Tsaousis[*], K.I. Chatjigeorgiou, I. E. Anastasiou

School of Naval Architecture and Marine Engineering, National Technical University of Athens, 9 Heroon Polytechniou Ave., Zografos Campus, 15773, Athens, Greece
[*]Corresponding author: thtsaousis@naval.ntua.gr

Abstract

The purpose of this study is to investigate the water entry problem of a spheroid. Our approach relies on the results concerning a sphere penetrating violently the undisturbed free surface of a volume of liquid. The volume of the liquid is assumed to be infinite in 3D. The developed method solves the governing mixed boundary value problem using integral representations for the velocity potential. We use linear potential theory and both cartesian and polar coordinates. The semi-axes of the spheroid, (A, B, B) approach the radius R of a sphere. Since the section of the sphere with the water is a circle of time varying radius $b(t)$, as the penetration evolves, we assume that the analogous section of the spheroid with the free surface of the liquid, is almost an ellipse. We express the ellipse, in polar coordinates, assuming a slight deformation of the circle, by importing the small eccentricity of the ellipse. There are two corresponding theories, i.e. von Karman's and Wagner's. We provide a solution for the 3D Wagner problem.

Keywords Water entry, Spheroid, Wagner 3D, Slamming.

1 INTRODUCTION

Slamming in marine hydrodynamics is a severe phenomenon that is encountered in several forms, such as steep wave impact, breaking wave impact and sudden water entry. Wave impact leads to huge hydrodynamic loading. It is a phenomenon of great interest for naval architects and marine engineers, because it is involved in important applications, such as the slamming of the bow of ships -especially for containers-, sloshing in tanks etc. There have been several studies reported in the literature that concerned water entry problems of bodies of different geometries, varying from blunt structures such as a sphere, to sharper, like a wedge. However, most of these studies tackle the hydrodynamic problem in 2D. There are two theories which allow the calculation of the wetted surface of the entering body, based on the von Karman and the Wagner models. The Wagner theory assumes a deformation of the initially calm free surface of the water, due to the slamming phenomenon, which leads to over-estimation of the actual wetted surface of the body and unavoidably to higher impact loads. This is in contrast to the von Karman's approach according to which the free surface remains completely undisturbed, after the body has penetrated the free surface.

The main task of the present study is to develop a 3D solution method for a spheroid water entry problem. A fundamental assumption is made, that is the geometry of the spheroid is very close to that of a sphere. So, we are allowed to assume that the section between the body and the free surface of the water is an ellipse, approached as a slightly deformed circle. This approach is valid if the eccentricity of the ellipse is small enough, in order avoid violating the Laplace equation.

The problem is formulated as a mixed boundary value set, because of the simultaneous existence of Dirichlet and Neumann conditions. The solution relies on determining the contact line between the body and the water. The contact line is in fact the separation boundary, separating the wetted part of the body from the rest volume of the liquid. The Neumann condition holds on the wetted part of the body, and the Dirichlet condition holds beyond it.

2 FORMULATION OF THE PROBLEM

2.1 The mixed-type hydrodynamic boundary value problem

A schematic representation of the problem under consideration is shown in "Figure 1". The volume of the liquid is infinite in all three dimensions. At the beginning of the time $t = 0$, the spheroid is in touch with the initially undisturbed surface of the water and as the phenomenon evolves, the body penetrates the liquid, by constant velocity V. At a specific time instant, the width $r_0(t)$, corresponds to the intersection point, between the body and the liquid, as given by the von Karman theory. The width $r_1(t)$ implies the contact line calculated by the Wagner theory. Due to the small time approximation (Chatjigeorgiou et al 2016), we are allowed to assume that the width $r_1(t)$ is situated on $z = 0$. This is equivalent to assume the projection of the spheroid's portion, determined by $z = \eta(x, y, t)$, onto the undisturbed free surface.

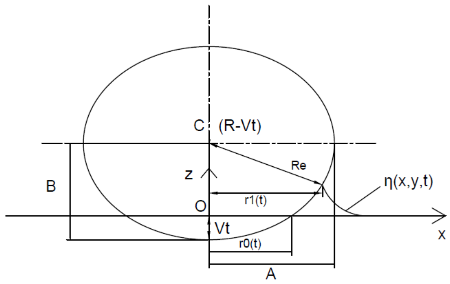

Figure 1 von Karman $r_0(t)$ and Wagner $r_1(t)$ approaches. Definition of parameters of the penetrating body

To this end, we write the width $r_1(t) = \sqrt{R_1^2 - 2R_1 c\cos(\theta) + c^2}$, where $R_1(t) = b(t) \cdot (1 + \varepsilon f(\theta))$, $b(t)$ is the time varying radius of the circle – cross section between the sphere and the free surface- at the same time instance, c is the semi-focal distance, ε is the elliptic eccentricity of the von Karman section of the spheroid and is assumed that $\varepsilon = \varepsilon(t) \ll 1$. Finally, $f(\theta)$ is a function of the angle, $\in [0,2\pi]$. Here we take $f(\theta) = \cos(\theta)$ (Disibuyuk et al 2017). The equation for $R_1(t)$ describes the shape of an ellipse, in polar coordinates, with the origin at the focus of the ellipse. The liquid is assumed inviscid, incompressible and the flow is irrotational. The hydrodynamic boundary value problem is composed by the following set of equations [using both polar (r, θ, z) and Cartesian (x, y, z) coordinates] (Korobkin and Scolan, 2006; Scolan and Korobkin , 2001)

$$\nabla^2\phi = 0, \qquad r \geq 0, \qquad 0 \leq \theta \leq 2\pi, \qquad z \leq 0 \tag{1}$$

$$\phi = 0, \qquad r \geq r_1, \qquad 0 \leq \theta \leq 2\pi, \qquad z = 0 \tag{2}$$

$$\frac{\partial\phi}{\partial z} = -V, \qquad 0 \leq r < r_1, \qquad 0 \leq \theta \leq 2\pi, \qquad z = 0 \tag{3}$$

$$\phi \to 0, \qquad x^2 + y^2 + z^2 \to \infty \tag{4}$$

$$\frac{\partial\eta}{\partial t} = \frac{\partial\phi}{\partial z}, \qquad r > r_1, \qquad 0 \leq \theta \leq 2\pi, \qquad z = 0 \tag{5}$$

$$\eta = Vt + B - \sqrt{{R_e}^2 - {r_1}^2} \tag{6}$$

Equation (1) is the Laplace equation, eq. (2) is the Dirichlet dynamic boundary condition on the free surface, beyond the instantaneous contact line, eq. (3) is the Neumann condition on the wetted area of the spheroid at every time instant, eq. (4) is the far-field condition which means that every disturbance generated by the entering of the body should vanish away from the solid. Finally, eq. (5) is the kinematical condition of the free surface and eq. (6) is the so-called Wagner condition, which gives the deformation of the free surface of the water and is calculated simply by geometry. Clearly, the associated boundary value problem is of mixed type, since Dirichlet and Neumann conditions, eqs. (2) and (3) respectively, hold on different portions of the water free surface.

2.2 The integral equation approach for the solution

A possible solution of the Laplace equation, expressed initially in Cartesian coordinates is

$$\phi = \int_{-\pi}^{\pi}\int_{0}^{\infty} \xi(u,t)e^{uz}e^{iu(x\cos a + y\sin a)}duda \tag{7}$$

Next, we employ the degenerate form of the Gegenbauer's addition theorem (Abramowitz and Stegun 1970; p.363) and using polar coordinates, after some mathematical manipulations, the above expression for the velocity potential is reduced to

$$\phi = 2\pi \int_{0}^{\infty} \xi(u)e^{uz}J_0(ur)du \tag{8}$$

Subsequently we try to satisfy both the Dirichlet and the Neumann conditions, by forming a system which has to be solved in terms of the unknown function $\xi(u)$. The dual integral equations are

$$\int_{0}^{\infty} u\xi(u)J_0(ur)du = -\frac{V}{2\pi}, \qquad 0 \le r < r_1 \tag{9}$$

$$\int_{0}^{\infty} \xi(u)J_0(ur)du = 0, \qquad r_1 < r \tag{10}$$

Eqs. (9) and (10) form a boundary value problem of mixed type. According to the classical book of Sneddon (1966; p.84) the unknown function $\xi(u)$ becomes

$$\xi(u) = -\frac{V}{2\pi}\frac{2}{\pi}\frac{\sin(ur_1) - ur_1\cos(ur_1)}{u^2} \tag{11}$$

Substituting eq. (11) into eqs. (9) and (10), the integrals formed are convergent. To prove this allegation, we provide "Figure 2".

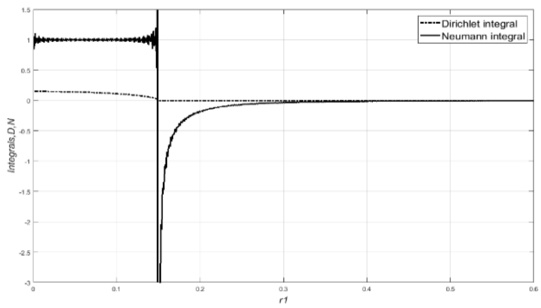

Figure 2 Infinite integrals of the Neumann and Dirichlet boundary conditions, $r_1 = 0.15$,

Introducing eq. (11) into eq. (8) and normalizing the intervals where eqs. (9) and (10) hold, letting $r/b = \rho$ and $ur_1 = v$, the velocity potential becomes

$$\phi = -r_1 V \frac{2}{\pi} \int_0^{\infty} \frac{\sin v - v \cos v}{v^2} e^{vz/r_1} J_0(v\rho) dv \tag{12}$$

The velocity obtained from the above equation at $z = 0$ is

$$\frac{\partial \phi}{\partial z} = -V \frac{2}{\pi} \int_0^{\infty} \frac{\sin v}{v} J_0(v\rho) dv + V \frac{2}{\pi} \int_0^{\infty} \cos v \; J_0(v\rho) dv \tag{13}$$

The infinite integrals of eq (13) can be calculated analytically (Gradshteyn and Ryzhik 2007) and numerically as well.
From eq. (5) we next integrate eq. (13) against time, so we get

$$\eta = -Vt + \frac{2}{\pi} V \int_0^{t} \frac{r_1(\tau)}{\sqrt{r^2 - {r_1}^2(\tau)}} d\tau, \qquad r \geq r_1 \tag{14}$$

Combining eqs. (6) and (14) for $r = r_1(t)$ yields

$$2Vt - \frac{2}{\pi} V \int_0^{t} \frac{r_1(\tau)}{\sqrt{r_1(t)^2 - {r_1}^2(\tau)}} d\tau = -B + \sqrt{{R_e}^2 - r_1(t)^2} \tag{15}$$

which is an integral equation with a single unknown the time varying radius R_e.

2.3 Hydrodynamic loading

The instantaneous vertical force can be calculated using, the linear term only, Bernoulli's equation. The hydrodynamic load is given by

$$F_z = -\rho \int_S \frac{\partial \phi}{\partial t} n_z dS = -\rho \int_0^{2\pi} \int_0^{r_1} \frac{\partial \phi}{\partial t} n_z r dr d\theta, \qquad z = 0 \tag{16}$$

Finally the hydrodynamic load is obtained by

$$F_z = \rho V \frac{2}{3\pi} \int_0^{2\pi} \frac{\partial (r_1^3(t,\theta))}{\partial t} d\theta \tag{17}$$

The integral of eq. (17) is calculated numerically.

3 RESULTS

The results provided are in terms of the width and the hydrodynamic force acting on the spheroid against time. All the aforementioned results are shown in a normalized form. The width is normalized by R_e, the force by $\rho R_e^2 V^2$ and finally time is normalized as Vt/R_e.

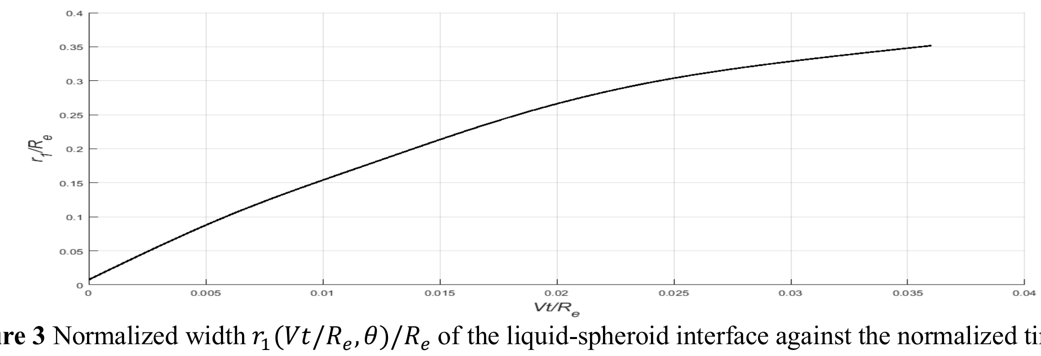

Figure 3 Normalized width $r_1(Vt/R_e, \theta)/R_e$ of the liquid-spheroid interface against the normalized time, at $\theta = 0°$

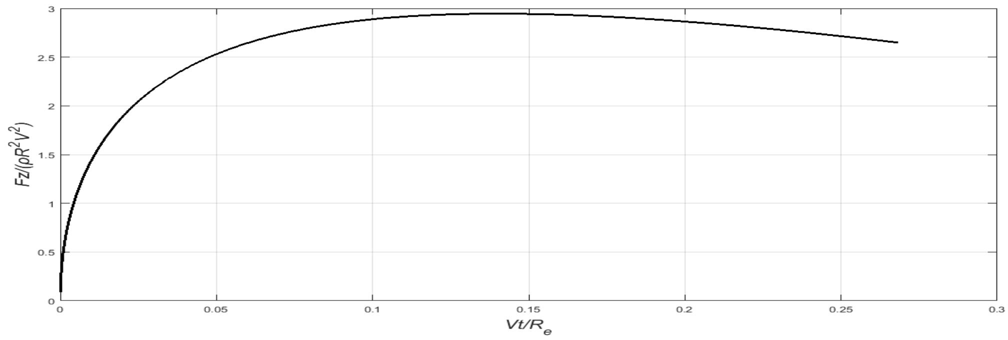

Figure 4 Normalized vertical force on the spheroid during water entry

The vertical force obtains a maximum at $Vt/R_e \approx 0.13$ and gradually is reduced.

4 CONCLUSIONS

The present study tackled the problem of the 3D Wagner water entry problem of a spheroid. The analysis was based on the corresponding problem of a sphere. The fundamental assumption was that the section of the penetrating body with the water is an ellipse of small eccentricity. We expressed the ellipse, in polar coordinates, as a slightly deformed circle of a specific radius at the same time instant. The wetted surface was calculated, as well as the hydrodynamic loading, which was found to be a little greater than that of the sphere's.

References

Sneddon IN (1966) Mixed Boundary Value Problems in Potential Theory, North-Holland Publishing Company, Amsterdam.

Scolan Y-M, Korobkin AA (2001) Three-dimensional theory of water impact. Part 1. Inverse Wagner problem, Journal of Fluid Mechanics 440, 293-326.

Gradshteyn IS, Ryzhik IM (2007) Table of Integrals, Series and Products (7th edition), Elsevier Academic Press, London.

Korobkin A, Scolan Y-M. (2006) Three-dimensional theory of water impact. Part 2. Linearized Wagner problem, Journal of Fluid Mechanics 549, 343-373.

Abramowitz M, Stegun IA (1970) Handbook of Mathematical Functions, Dover Publications Inc., New York.

Chatjigeorgiou IK, Korobkin AA, Cooker MJ (2016) Three-dimensional steep wave impact on a vertical cylinder, Journal of Hydrodynamics, 28(4):523-533

Chatjigeorgiou IK, Cooker MJ Korobkin AA (2016) Three-dimensional water impact at normal incidence to a blunt structure, Proc. R. Soc. A 472: 20150849

Disibuyuk NB Korobkin AA, Yilmaz O (2017) Linear wave interaction with a vertical cylinder of arbitrary cross section: an asymptotic approach, Journal of Waterway, Port, Coastal Ocean Eng., 143(5): 04017028

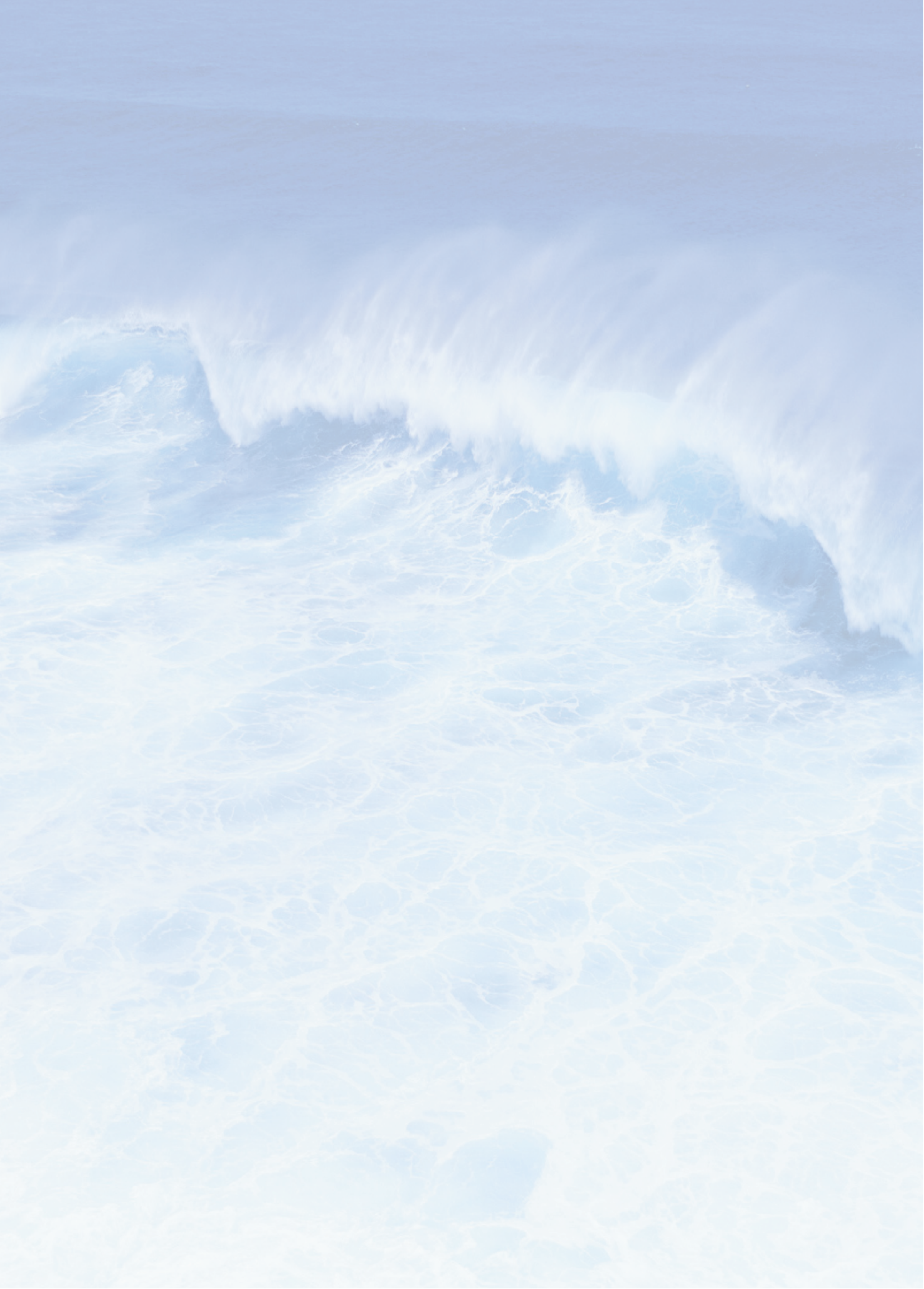

Simulation of a series of breakwaters with a series of elliptical cylinders

E. Charisi[1,2*], V. Katsardi[1], I.K. Chatjigeorgiou[3]

[1]Civil Engineering Department, University of Thessaly, Volos, Greece
[2]Department of Civil and Environmental Engineering, Imperial College London, UK
[3]School of Naval Architecture and Marine Engineering, National Technical University of Athens, Greece
[*]Corresponding author: effrosyni.charisi18@imperial.ac.uk

Abstract

The present paper examines a series of detached breakwaters, forming vertical walls, parallel to the coastline and bottom-founded to the seabed. The induced hydrodynamic interactions are investigated by simulating the series of breakwaters with an array of elliptical cylinders subjected to regular waves. The interaction phenomena were approached using the Mathieu functions addition theorem which converts elliptical harmonics from one elliptic coordinate system to a remote elliptic coordinate system. The breakwaters were considered as non-porous, impermeable solids. The paper investigates the geometry configuration of the cylinders and, in particular, how various geometrical parameters affect the hydrodynamic loading (forces and moments) and the free-surface elevations upstream, downstream and on the elliptical cylinders. These parameters are the slenderness of the elliptical cylinders and the distance between the centres of two consecutive bodies. Moreover, two different arrays of breakwaters were considered consisted of three and five breakwaters. Further, two cases of water depth were investigated, corresponding to shallow water and intermediate water depth conditions. Finally, two different angles of the incident wave heading were examined. It was found that the developed analytical methodology is a robust, accurate and efficient tool for the optimization of configurations such as series of detached breakwaters.

Keywords Detached breakwaters, Elliptical cylinders, Mathieu functions, Hydrodynamics.

1 INTRODUCTION

It is the purpose of this paper to study the hydrodynamic interaction of propagating regular waves with breakwaters simulated with elliptical cylinders. Indeed, this is a problem that plays a crucial role to coastal engineering challenges, such as the interaction of waves with coastal protection structures like detached breakwaters that are used for coastal protection associated with beach erosion due to wave action. An analytical approach to the problem is presented allowing the derivation of expressions for hydrodynamic properties, as the velocity potential and the hydrodynamic loading at the area of influence of the structure. The aforementioned magnitudes are considered critical for the design of coastal structures subjected to waves.

The development of an analytical solution methodology for the water wave diffraction problem by arrays of elliptical cylinders is possible due to the existence of separable solutions of the Laplace equation in elliptic coordinates. Multiple body arrays subjected to the action of propagating waves, induce diffraction phenomena of the incoming waves, leading to rather complex variations of the hydrodynamic loading, which are depicted as peaks in surge and sway forces, as well as large free-surface elevations between the cylinders and also on the wetted surfaces of the bodies. The complications in hydrodynamic loading are caused mainly because When additional parameters are implemented into the problem, such as the number, geometry, slenderness of the bodies in conjunction with the water depth.

Chatjigeorgiou and Mavrakos (2010) were the first to achieve an analytical solution regarding the hydrodynamic interactions by arrays of elliptical cylinders. In order to accomplish that, the so-called addition theorem for Mathieu functions was employed. The respective results for the induced forces were presented initially only for a pair of cylinders. Subsequently, Chatjigeorgiou (2011) presented an analytical solution for groups of multiple elliptical and circular cylinders.

2 THE HYDRODYNAMIC PROBLEM

In the present research, two different arrays of detached breakwaters were investigated; one consisting of three breakwaters, and one consisting of five. Each breakwater was simulated with an elliptical cylinder. All the cylinders are bottom founded in water of depth d and are subjected to monochromatic waves of radial frequency ω and amplitude $H/2$, which are propagating with an angle β to the positive x-direction. The semi-major and semi-minor axes are denoted by a and b, respectively. Elliptic cylindrical coordinates(u, v, z) were employed, where $u = constant$ and $v = constant$. The z-axis is fixed at the sea-bed facing vertically upwards. The transformation from elliptic cylindrical coordinates to cartesian coordinates is $x = c\, cosh\, u\ cos\, v$ and $y = c\, sinh\, u\, sin\, v$, where $c = (\alpha^2 - b^2)^{1/2} = \alpha\varepsilon$ with ε the elliptic eccentricity, obtained by the expression $\varepsilon^2 = 1 - (b/a)^2$.

The fluid is considered to be incompressible, inviscid and the flow is irrotational; therefore, these assumptions allow the use of linear potential theory. The fluid's motion in three dimensions can be described by the velocity potential $\Phi(x, y, z, t)$, which can be expressed as below

$$\Phi(x, y, z, t) = Re\{\phi(x, y, z)e^{-i\omega t}\}, \tag{1}$$

where Re is the real part of the components in the brackets and t denotes the time. As known, the spatial velocity potential $\Phi(x, y, z)$ must satisfy the Laplace equation in every part of the fluid and the linearized boundary condition on the free surface as well as the kinematic boundary condition on the bottom must be satisfied. The coordinate system (x, y, z) was fixed on the bottom, while the vertical axis z was facing upwards. The total velocity potential must satisfy the Neumann boundary condition on the wetted surface of all the bodies of the array. Regarding the linear hydrodynamic problem, it can be assumed that the total velocity potential consists of two components; the first denotes the contribution if the incident wave (ϕ_I), while the second denotes the total wave diffraction effect (ϕ_D). Consequently, it is clear that the diffraction potential must satisfy the proper radiation condition for outgoing waves at infinity, known as the Sommerfeld condition,

$$\lim_{r\to\infty} r^{1/2}\left(\frac{\partial}{\partial r} - ik_0\right)\phi_D = 0, \tag{2}$$

where $r = \sqrt{x^2 + y^2}$ and k_0 is the wavenumber given by the dispersion equation.

Regarding an array of multiple bodies, it is rather convenient to express both of the wave potentials related to the hydrodynamic problem in coordinates that have as a reference point every body that constitutes the array. If (x_k, y_k, z) are the cartesian coordinates of a random point of the field with respect to the coordinate system of body k, then the incident wave potential has the following format

$$\phi_I = -i\frac{gH}{\omega 2}\frac{Z_0(z)}{Z_0(h)}\Lambda_k e^{ik_0(x_k cos\alpha + y_k sin\alpha)} \tag{3}$$

where $Z_o(z) = {N_o}^{-1/2}\cosh(k_o z)$, $N_o = \frac{1}{2}\left[1 + \frac{\sinh(k_o h)}{2k_o h}\right]$ and $\Lambda_k = e^{ik_o(X_k\cos\alpha + Y_k\sin\alpha)}$.

Further, the incident wave potential can be expressed in terms of the local elliptic coordinate system of the arbitrarily chosen body k (u_k, v_k, z) and the transformed Mathieu functions and Modified Mathieu functions to even and odd periodic and radial Mathieu functions respectively (Meixner and Schäfke, 1954):

$$\phi_I = -2i\frac{gH}{\omega 2}\frac{Z_0(z)}{Z_0(h)}\left[\sum_{m=0}^{\infty} i^m Mc_m^{(j)}(u_k; q_k)ce_m(v_k; q_k)ce_m(a; q_k) + \sum_{m=1}^{\infty} i^m Ms_m^{(1)}(u_k; q_k)se_m(v_k; q_k)se_m(a, q_k)\right] \tag{4}$$

where $q_k = (k_0\alpha_k/2)^2$ is the Mathieu parameter, $ce_m(v_k; q_k)$ and $se_m(v_k; q_k)$ are the even and odd periodic Mathieu functions, $Mc_m^{(j)}$ and $Ms_m^{(1)}$ are the even and odd radial Mathieu functions respectively, and (j) denotes the kind of radial Mathieu functions.

The zero velocity condition on the wetted surface of the body k imposes that the total diffraction potential due to the scattering of waves by all bodies of the array must be expressed with respect to the local elliptic coordinate system of the body k. The total diffraction potential around the k^{th} should consists of the diffraction potentials due to the wave scattering resulting from all the bodies of the array; therefore, it can be deduced that $\varphi_D = \sum_{k=1}^{N} \varphi_D{}^{(k)}$, with N being the number of bodies in the array. The total scattered wave field around the body k, because of the contribution of all the bodies in the array is presented below

$$\frac{1}{h}\varphi_D = -i\omega\frac{H}{2}Z_o(z)\sum_{m=0}^{\infty} i^m A_m{}^{(k)} Kc_m{}^{(k)} Mc_m{}^{(3)}(u_k;q_k)ce_m(v_k;q_k)$$
$$-i\omega\frac{H}{2}Z_o(z)\sum_{m=1}^{\infty} i^m B_m{}^{(k)} Ks_m{}^{(k)} Ms_m{}^{(3)}(u_k;q_k)se_m(v_k;q_k)$$
$$-i\omega\frac{H}{2}Z_o(z)\sum_{j\neq k}^{N}\sum_{m=0}^{\infty} i^m A_m{}^{(j)} Kc_m{}^{(j)} Mc_m{}^{(3)}(u_j;q_j)ce_m(v_j;q_j)$$
$$-i\omega\frac{H}{2}Z_o(z)\sum_{j\neq k}^{N}\sum_{m=1}^{\infty} i^m B_m{}^{(j)} Ks_m{}^{(j)} Ms_m{}^{(3)}(u_j;q_j)se_m(v_j;q_j) \tag{5}$$

The total diffraction potential must be expressed with respect to the local elliptic coordinate system of body k, in the same way that was done for the incident wave potential. For this purpose, the products of Mathieu functions in the last two terms of the right-hand side of Eq. 5, expressed with respect to the local elliptic coordinate systems (u_j, v_j, z), must be expressed with respect to the local elliptic coordinate system of body k. In order to accomplish that, the addition theorem for Mathieu functions was employed (Meixner and Schäfke 1954; Særmark 1959). After extensive mathematical manipulations, the summation of $\varphi_I + \varphi_D$ yields the total velocity potential, as presented at the expression below

$$\frac{1}{h}\varphi(u_k, v_k, z) = -i\omega\frac{H}{2}Z_0(z)\left\{\sum_{m=0}^{\infty} i^m \tilde{A}_m{}^{(k)} ce_m(v_k;q_k)\left[Kc_m^{(k)}Mc_m^{(3)}(u_k;q_k) - Mc_m^{(1)}(u_k;q_k)\right]\right.$$
$$\left.+\sum_{m=1}^{\infty} i^m \tilde{B}_m{}^{(k)} se_m(v_k;q_k)\left[Ks_m^{(k)}Ms_m^{(3)}(u_k;q_k) - Ms_m^{(1)}(u_k;q_k)\right]\right\} \tag{6}$$

Further, the linear hydrodynamic loading can be obtained by integrating the hydrodynamic pressure on the wetted surface of each body in the array. By using only the linear term of the Bernoulli equation, the hydrodynamic loading in the x and y-axis (surge and sway forces) can be given by the relations

$$F_x^{(k)} = -i\omega\rho b_k \int_0^h \int_0^{2\pi} \varphi\,(u_{k0}, v_k, z)\cos v_k dv_k dz \tag{7}$$

$$F_y^{(k)} = -i\omega\rho a_k \int_0^h \int_0^{2\pi} \varphi\,(u_{k0}, v_k, z)\sin v_k\, dv_k dz \tag{8}$$

In addition, the water elevation in every point of the free surface in the field, can be obtained by

$$\eta(u_{k0}, v_k, h) = \frac{i\omega}{g}\varphi(u_{k0}, v_k, h) \tag{9}$$

3 RESULTS AND DISCUSSION

Two different arrays were selected; one consisting of three elliptical cylinders and the other consisting of five elliptical cylinders. In every case, all the elliptical cylinders have the same dimensions, meaning that $\alpha_1 = \alpha_2 = \alpha_3 = \alpha_4 = \alpha_5 = \alpha$ and $b_1 = b_2 = b_3 = b_4 = b_5 = b$. The variable $2D$ denotes the distance between the centres of two consecutive cylinders. Three cases were investigated for $2D$ equal to $2.5a$, $3a$ and $3.5a$. As it is obvious, all the distances are normalized with respect to the semi-major axis a. Moreover, two cases for the angle of the incident wave β were considered; the first forming an angle of 90° with the x-axis, while the second one forming an angle of

45°. Finally, two cases regarding the water depth were examined, for shallow and intermediate water depth. An indicative configuration of elliptical cylinders is demonstrated in Figure 1

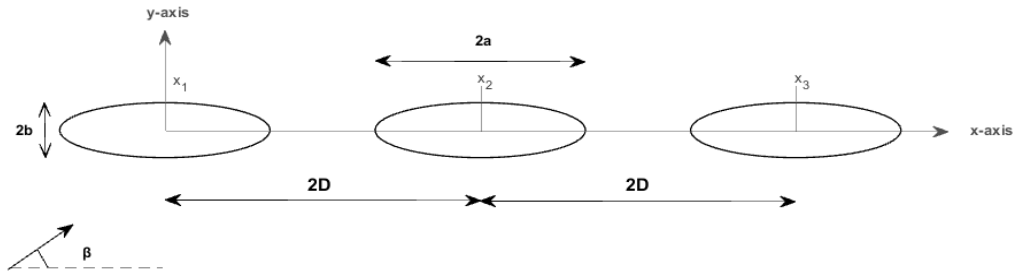

Figure 1 Indicative elliptical cylinders configuration

For every case, the maximum forces in the y-axis were calculated, in addition to the respective frequencies where maxima occur. Further, for the aforementioned frequencies, the free surface elevation of the water was estimated at the area of influence of the breakwater (Figure 2). In the shallow water case, it was found that the optimal distance between the centres of two consecutive breakwaters (2D) is equal to three times the semi-major axis a. However, for the intermediate water depth case this was somewhat larger (3.5 times the axis a).

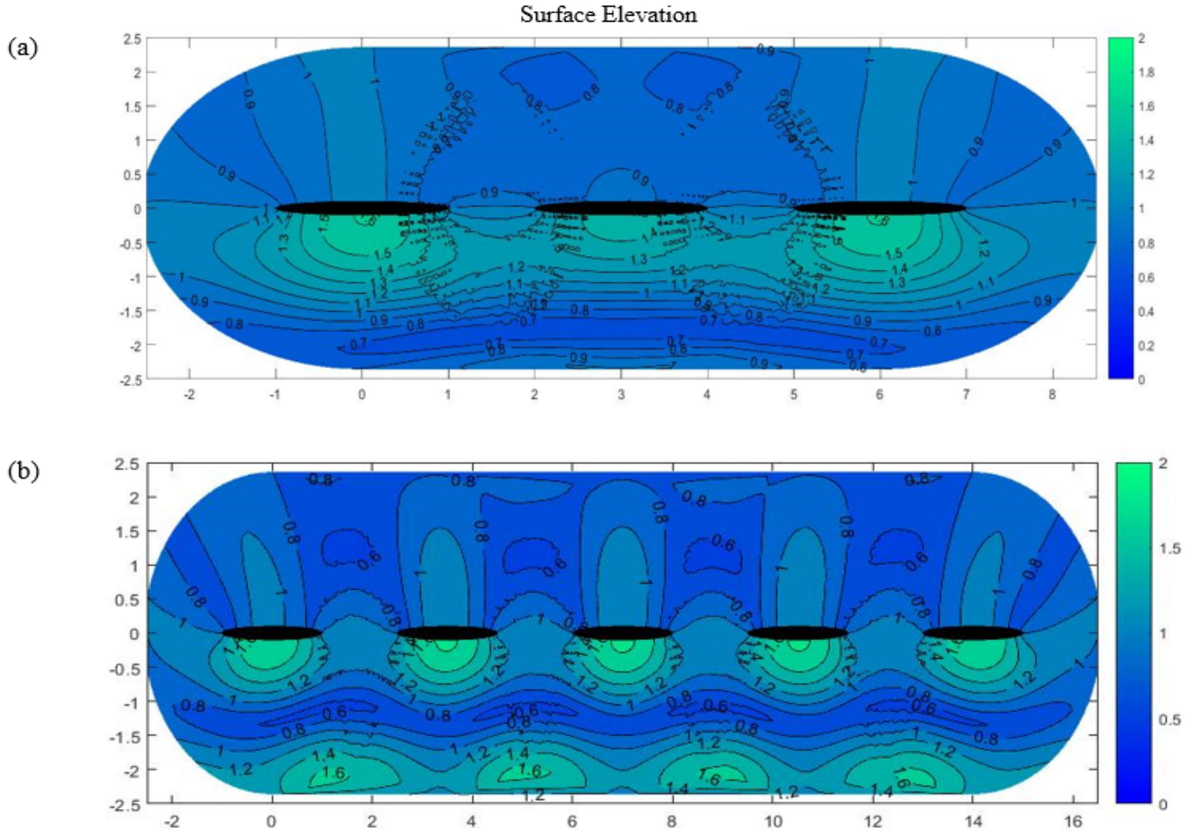

Figure 2 Schematic representation of the free surface elevations at the area of influence of the breakwaters for (a) an array of 3 elliptical cylinders, and (b) for an array of 5 elliptical cylinders

Regarding the geometry of the elliptical cylinders, it can be deduced that, as the slenderness of the bodies increase, the maximum water surface elevation downstream reduces. Moreover, the surface elevation also decreases for deeper water conditions. Overall, for shallow water depth it was deduced that an array with 3 elliptical cylinders is the optimal solution. On the contrary, for intermediate water depth, an array of 5 elliptical cylinders appears to be the most efficient (Figure 3).

(a) (b)

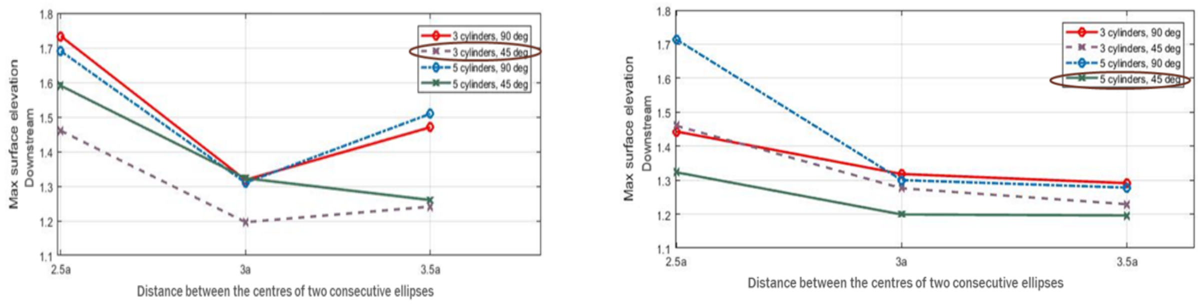

Figure 3 Comparative results for (a) shallow waters and (b) intermediate water depth

4 CONCLUSIONS

An analytical approach for the hydrodynamic loading of plane breakwaters simulated with elliptical cylinders was employed. For this purpose, linear potential theory was applied, taken into account two different components for the incident and total diffraction wave potential. In order to consider the Laplace equation in elliptic coordinates, the velocity potentials were expressed in terms of Mathieu functions. Finally, the addition theorem for Mathieu functions was employed to express the total diffraction potential due to the scattering effect of waves in interaction with all the bodies, with respect to the local elliptic coordinate system of an individual body. The numerical results proved the contribution of the elliptical breakwaters in reducing the free surface elevation downstream. This fact could play a crucial role in coastal engineering and coastal protection challenges.

References

Chatjigeorgiou, IK (2011). "Three dimensional wave scattering by arrays of elliptical and circular cylinders," Ocean Engineering, 38, 1480-1494.

Chatjigeorgiou, IK, and Katsardi, SA (2018). "Hydrodynamics and near trapping effects in arrays of multiple elliptical cylinders in waves", Ocean Engineering, 157, 121-139.

Chatjigeorgiou, IK, Mavrakos, SA (2010). "An analytical approach for the solution of the hydrodynamic diffraction by arrays of elliptical cylinders", Applied Ocean Research, 32, 242–251.

Katsardi, V, Grammenos, T, Katifeoglou, S, Mavrakos, SA and Chatjigeorgiou, IK. (2016). Hydrodynamic Loading and Wave Run-up on "Elliptical" Breakwaters. Proceedings of the Twenty-sixth (2016) International Ocean and Polar Engineering Conference, ISBN 978-1-880653-88-3.

Meixner, J, and Schäfke, FW (1954). Mathieusche funktionen und sphäroidfunktionen. Berlin: Springer.

Særmark, KA (1959). "A note on addition theorems for Mathieu functions", Zeitschrift für angewandte Mathematik und Physik, 10, 426-428.

Schäfke, F.W., 1953. Das additionstheorem der Mathieuschen funktionen. Mathematische Zeitschrift 58, 436–447.

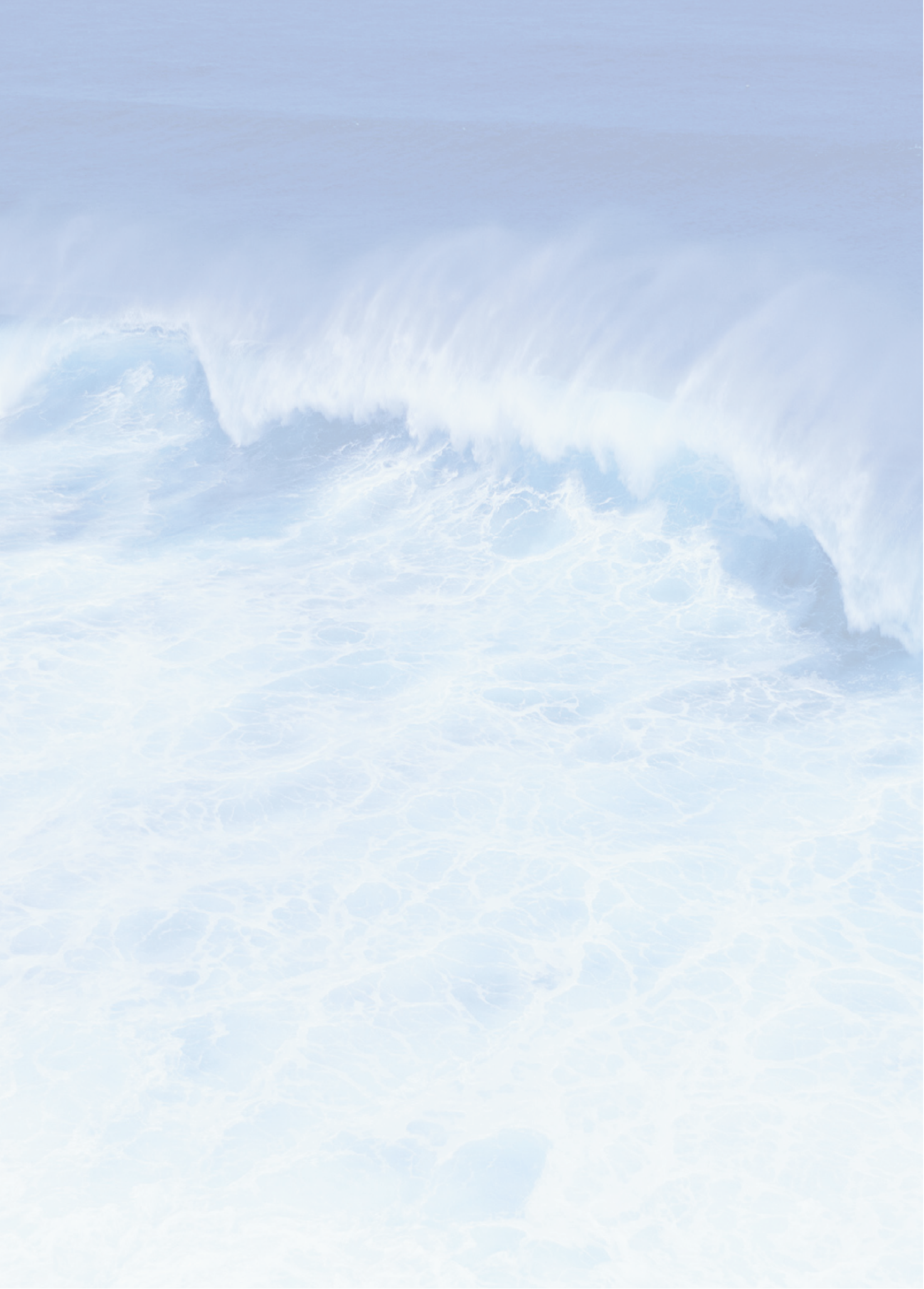

Marine corrosion of steel with aerobic and anaerobic biofilms under changeable nutrient concentration conditions

D.S. Sophianopoulos[*], V.S. Pantaz[1], M.I. Ntin[1]

[1]Department of Civil Engineering, University of Thessaly, Volos, Magnisia, 38334, Greece
[*]Corresponding author: dimsof@civ.uth.gr

Abstract

A diffusional model of marine corrosion wear for steel structures is developed and presented in this work, based on the assumption that long-term corrosion depends on both aerobic and anaerobic bacterial activity, associated with to nutrient changes. This activity of bacteria biofilms is quantitatively evaluated and verified, based on observed data of hydraulic structures of Far East of Russia. It is shown that any short-term increases of nutrients and anthropological pollutants concentrations may significantly accelerate a corrosion rate. Results reveal that the influence of anaerobic biofilms on the corrosion rate acceleration of immersed steel structures is underestimated.

Keywords Steel, Modelling Studies, Microbiological Corrosion.

1 INTRODUCTION

Results of numerous researches suggest that the marine corrosion of steel is strongly connected to the vital activity of bacteria. As previously indicated (Melchers 2014, Bekker et al. 2011), the long-term corrosion process develops differently than that of earlier stages. On the early stage, corrosion is controlled by an inflow of dissolved oxygen, while the activity of anaerobic bacteria under corrosion products layer controls the corrosion on later stages.

Usually, hydraulic structures with metal elements have lifetimes much longer than 2-3 years; consequently, the vital activity of anaerobic bacteria determines the long-term corrosion prediction. First, it is necessary to define factors, which have a predominant influence on the growth of bacteria. It has been shown (Melchers 2014), that temperature and nutrients transfer are the most significant factors. Among groups of nutrients for different species of bacteria, one may include dissolved oxygen, inorganic nitrogen (which is represented by nitrates, nitrites and ammonium). Inorganic phosphorus and dissolved sulfates are other groups of bacteria nutrients. It is possible to assume that the activity of bacteria is controlled by that nutrient group, which possesses the greatest deficit.

The problem of water pollution by urban and industrial sewage is the reason of the growth of concentration of inorganic nitrogen and phosphorus in seawater. Hence, the corrosion rate for steel hydraulic structures grows accordingly and depends on zone location (Melchers, 2013). For a long-term prediction, it is necessary to create a model, which takes in account physical and biological factors of marine corrosion in immersed zone.

Such a diffusional model is developed in the present work, assuming that long-term corrosion depends on both aerobic and anaerobic bacterial activity, which is connected with nutrient changes. Based on recorded data of steel sheet pile walls in ports of Far Eastern Russia and quantifying the activity of aerobic as well anaerobic bacteria biofilms, it is shown that any short-term increases of nutrients and anthropological pollutants concentrations significantly accelerate the corrosion process.

2 PRELIMINARY DATA ELABORATION FOR CORROSION RATE PREDICTION

Before the actual short presentation and validation of the model proposed herein (which was based on data available from steel sheet piling walls in Ports of the southern part of Far Eastern Russia, namely, Golden Horn Bay, Diomede Bay, and Nakhoda Bay), these data were used for the evaluation and prediction of corrosion rate, via the linear approximate model, presented recently (Melchers 2014).

Defining the lifetime of each structure as t_e, the observed average corrosion rate as $c_p(t_e) = O$, the predicted values of corrosion rate $C(t_p)$ was evaluated for both unpolluted and polluted water conditions, assigned the abbreviations P and P_1 respectively. Thereafter, the ratios O/P, O/P_1 and P/P_1 were determined and statistically manipulated, in terms of Box-Plot ratios. Such an indicative typical plot is depicted in Figure 1.

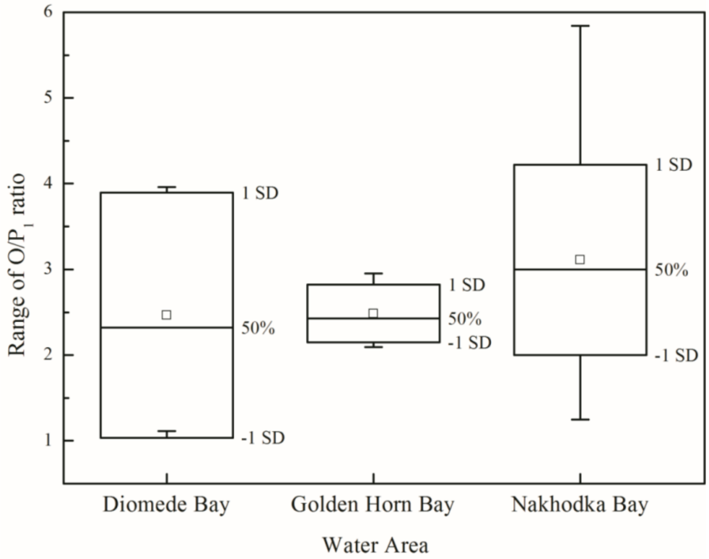

Figure 1 Box Plot - Rate of O/P_1 ratio

It was found that for the unpolluted condition case the recorded corrosion rates significantly exceed the predicted ones, since the O/P ratio varies from 1.5 to 7. If pollution is accounted for in the linearized model, the corresponding ratio O/P1 lies between the values of 1.3 to 6, revealing the same discrepancy. Moreover, predicted rates for polluted and unpolluted conditions (P/P1) have a difference not greater than 1.2-1.8 times. These findings are attributed, to a certain extent, to the omission of one or more significant factors in the simulation.

3 PROPOSED DIFFUSION MODEL OF NUTRUENTS WITH AEROBIC AND ANAEROBIC BIOFILMS

It is assumed that marine corrosion of later stages (more than 2-3 years) is primarily dominated by vital activity of bacteria. This activity, obviously, depends on the availability of nutrients, on their diffusion and on the intensity of their consumption by aerobic and anaerobic bacteria. The activity of anaerobic bacteria is the most interesting area for research, because, as assumed, the intensity of corrosion is fully defined by the aforementioned activity on the interface between steel substrate and the anaerobic bacteria biofilm. The scheme of the model is illustrated in Figure 2.

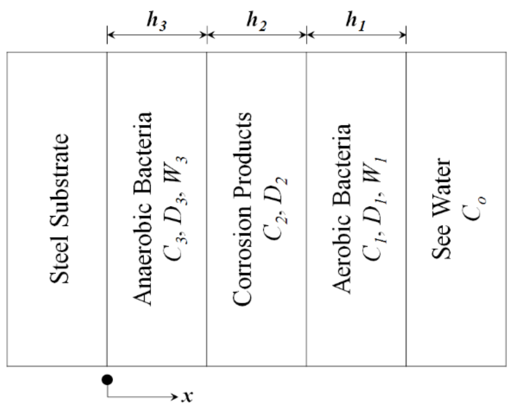

Figure 2 Schematic of the proposed diffusive corrosion model with biofilms

More specifically, there are three layers between the steel substrate and sea water, namely: (1) aerobic bacteria layer in contact with sea water, (2) corrosion products layer, and (3) anaerobic bacteria layer between the steel substrate and corrosion products layer. It is also assumed that nutrients concentration in sea water is constant.

The 1st layer is characterized by three parameters; the diffusion coefficient D_1, the concentration of nutrients C_1 in the layer and the intensity of nutrients consumption therein, W_1. As supposed, the limitative factor of aerobic biofilm growth is dissolved oxygen concentration. According to the model described by Chernov and Kharchenko (2003), for accepted concentration of dissolved oxygen (7.8 mg/L), the thickness of the aerobic biofilm is equal to h_1=35.1*10-6 m. All oxygen is consumed by the layer in given conditions. The existence of anaerobic layer directly under the aerobic one is possible, but this factor is neglected for simplicity. This simplification is justified though, since any bacteria waste products are more easily transferred to water than through corrosion products to deeper layers via diffusion. Moreover, the surface biofilm is exposed to numerous influences, may be damaged, peeled etc., and hence it cannot grow thick.

The 2nd layer of thickness h_2 consists of corrosion products. It is assumed that it is the barrier for nutrients transfer to the 3rd (anaerobic bacteria) layer, and is related with the concentration coefficient C_2 and the diffusion coefficient D_2. The latter is taken equal to 0.8*10-12 m^2/s, a value experimentally obtained for the oxygen diffusion coefficient through corrosion product layer (Dillman et al. 2007).

The 3rd layer fully consists of anaerobic bacteria, because all oxygen has been already consumed by the 1st layer of aerobic bacteria. The activity of anaerobic layer is characterized by its thickness h_3, which depends on the quantity of nutrients transfer and the rate of consumption by bacteria; this layer controls corrosion rate on later stages. It is necessary to determine the dependence of h_3 on incoming nutrients, because this will allow the evaluation of the volume of active bacteria and, consequently, the determination of the volumes of their waste products, which are the main cause of corrosion. For this layer, C_3 is the concentration of nutrients, W_3 is the consumption rate of nutrients, while D_3 is the diffusion coefficient. The flowchart of the proposed model is given in Figure 3; its mathematical formulation is omitted, due to the limited allowable space of the manuscript.

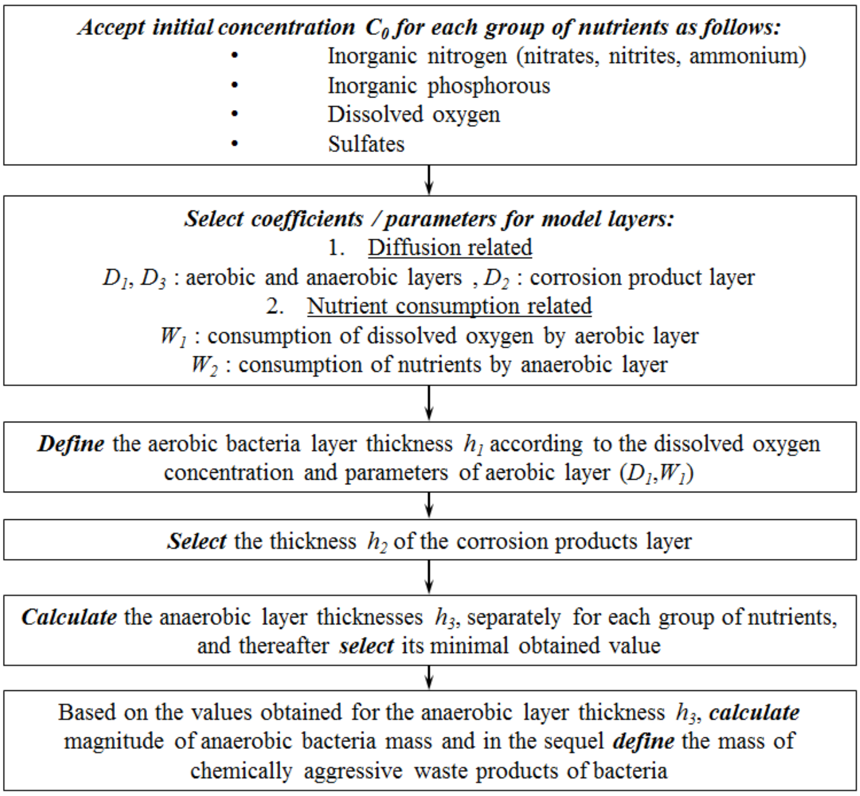

Figure 3 Flowchart of the proposed model

4 NUMERICAL RESULTS AND DISCUSSION

Numerical results were obtained for a range of values of the anaerobic layer h_3. In doing this, the inorganic nitrogen concentration C_0 was chosen to lie between 0.000001 and 0.002 kg/m^3, while the corrosion product thickness h_2 ranged from 0.1 to 15 mm.

Moreover, the values of the rest of parameters involved for the determination of h_3 were adopted from existing relevant literature. More specifically, coefficients of inorganic consumption for aerobic and anaerobic bacteria were assumed equal to W_1=W_3=0.022 kg/m^{3}s (Stewart 2003), while the diffusion coefficients were chosen equal to D_1=D_3=0.176 m^2/s and D_2=0.8*10-12 m^2/s (Dillmann et al. 2007, Lewandowski et al. 1991). Finally, for fixed dissolved oxygen concentration of 7.8 mg/L, the selected value of the aerobic layer thickness h_1 was 35.1*10^{-6} m (Chernov and Kharchenko 2003).

It was found that It was found that h_3 varied from 0.0162 to 1.75 mm. Its distribution as a surface plot of the form $h_3 = f(C_0, h_2)$ is depicted in Figure 4. while contour plots of this surface for the selected variation of values of h_2 and C_0 are shown in Figure 5.

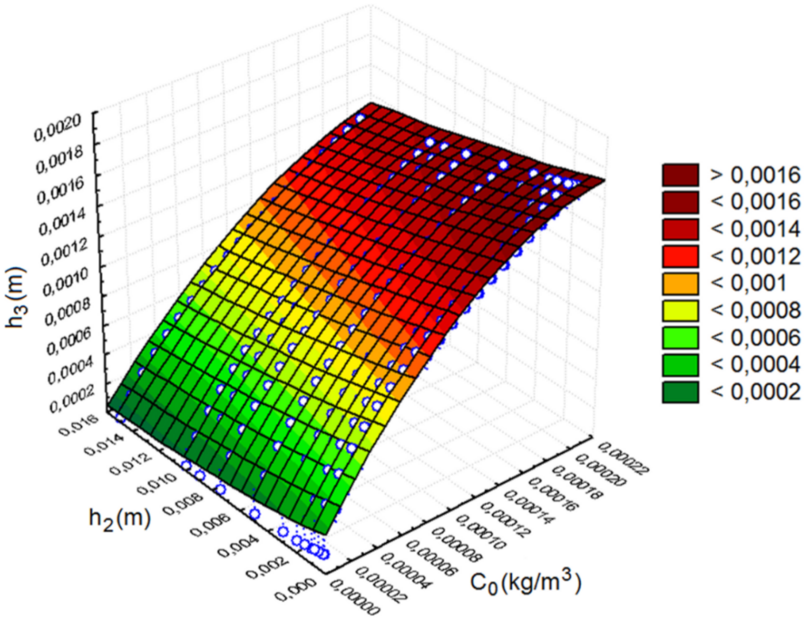

Figure 4 Surface plot of h_3 as a function of C_0 and h_2

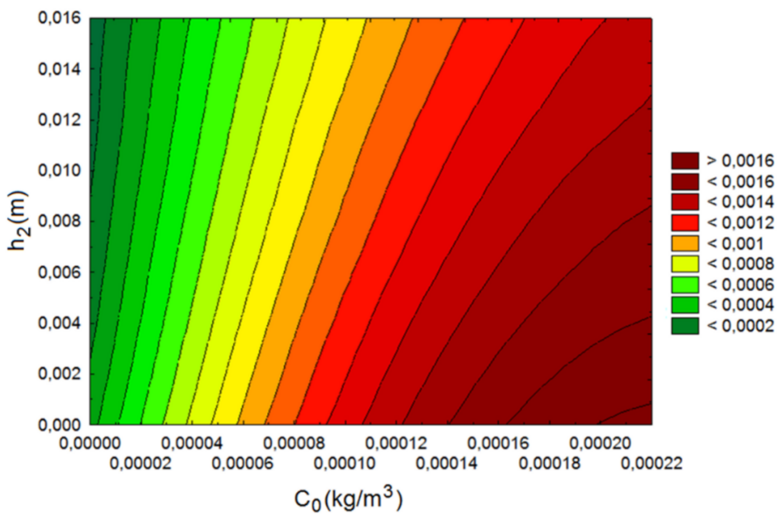

Figure 5 Contour plots of h_3 for the chosen variations of C_0 and h_2

Evidently, nutrients concentrations increase is the most important factor for anaerobic layer growth, while the corresponding one of corrosion products layer has an inhibitory effect on anaerobic layer growth, been although a factor weaker than the factor of nutrients concentration changes, as it can be perceived in Figure 5.

Additionally, it can be seen that the anaerobic layer thickness is significantly larger than the aerobic layer one, a finding confirming the important role of this specific layer in the whole corrosion process. It should be noted that accepting equal diffusion coefficients for different bacteria layers may be well accepted for the foregoing approach, since molecular sizes of the nutrients engaged do not differ to a noticeable amount. Beyond the above comments, the observed corrosion rates were larger than the predicted ones; hence, it can be concluded that short-term nutrient concentration changes accelerate the corrosion process. The duration of the valid influence of these factors is unknown at the present stage, but it surely exceeds a year time period. Finally, the present modeling stage allows for the rough estimation of bacterial layer activity and waste product prediction. Perhaps it will be necessary for the improvement of the model to postulate the accounting of the qualitative and quantitative evaluation of waste products, like for instance hydrogen sulfide as well as the estimation of the effect of bacteria metabolism. On any event, the philosophy of the proposed model is not expected to transform significantly with the addition of the above.

5 CONCLUSIONS

The most important conclusions that can be drawn from this investigation are:

The main factor which controls the anaerobic bacteria layer growth is nutrients concentration is sea water. Increases of concentration might increase anaerobic layer thickness. This thickness may reach 0.1-1.17 mm for observed conditions.

A growth of corrosion products thickness reduces anaerobic bacteria activity by reduction of nutrient transfer. Nevertheless, the influence of corrosion products is less significant than influence of nutrient concentration growth. Consequently, random short-term and periodical concentration increases may seriously accelerate corrosion in comparison with predicted corrosion rate based on average annual concentrations.

A model of nutrients transfer through corrosion products, aerobic and anaerobic layers, has been developed, concerning steel marine structures. Based on intensity of nutrients consumption by bacteria, there is an opportunity of quantitative estimation of the growth limiting factor (a nutrient which provides minimal value of thickness h_3). Based on anaerobic layer thickness, it is possible to evaluate waste products rate and corrosion rate.

References

Bekker AT, Kovalenko RG, Luybimov VS, Kim LV (2001) Steel constructions corrosion wear processes modeling of sea hydraulic engineering structures. Paper presented at the International Offshore and Polar Engineering Conference, Maui, Hawaii, USA.

Chernov BB, Kharchenko UV (2003) Model of concentration changes in the biofilm on an inert support. Electronic Journal Investigated in Russia: 2304–2310.

Dillmann P, Beranger G, Piccardo P, Matthiessen H (2007), Corrosion of Metallic Heritage Artefacts: Investigation, Conservation and Prediction of Long-term Behaviour. Woodhead Publishing, Cambridge.

Lewandowski Z, Walser G, Characklis WG (1991) Reaction kinetics in biofilms. Biotechnology and Bioengineering 38(1): 887–882.

Melchers RE (2013) Influence of dissolved inorganic nitrogen on accelerated low water corrosion of marine steel piling. Corrosion 69(1): 95–103.

Melchers RE, Long-term immersion corrosion of steels in seawaters with elevated nutrient concentration. Corrosion Science 81: 110–116.

Stewart PS (2003) Diffusion in biofilms. Journal of Bacteriology 185(5): 1485–1491.

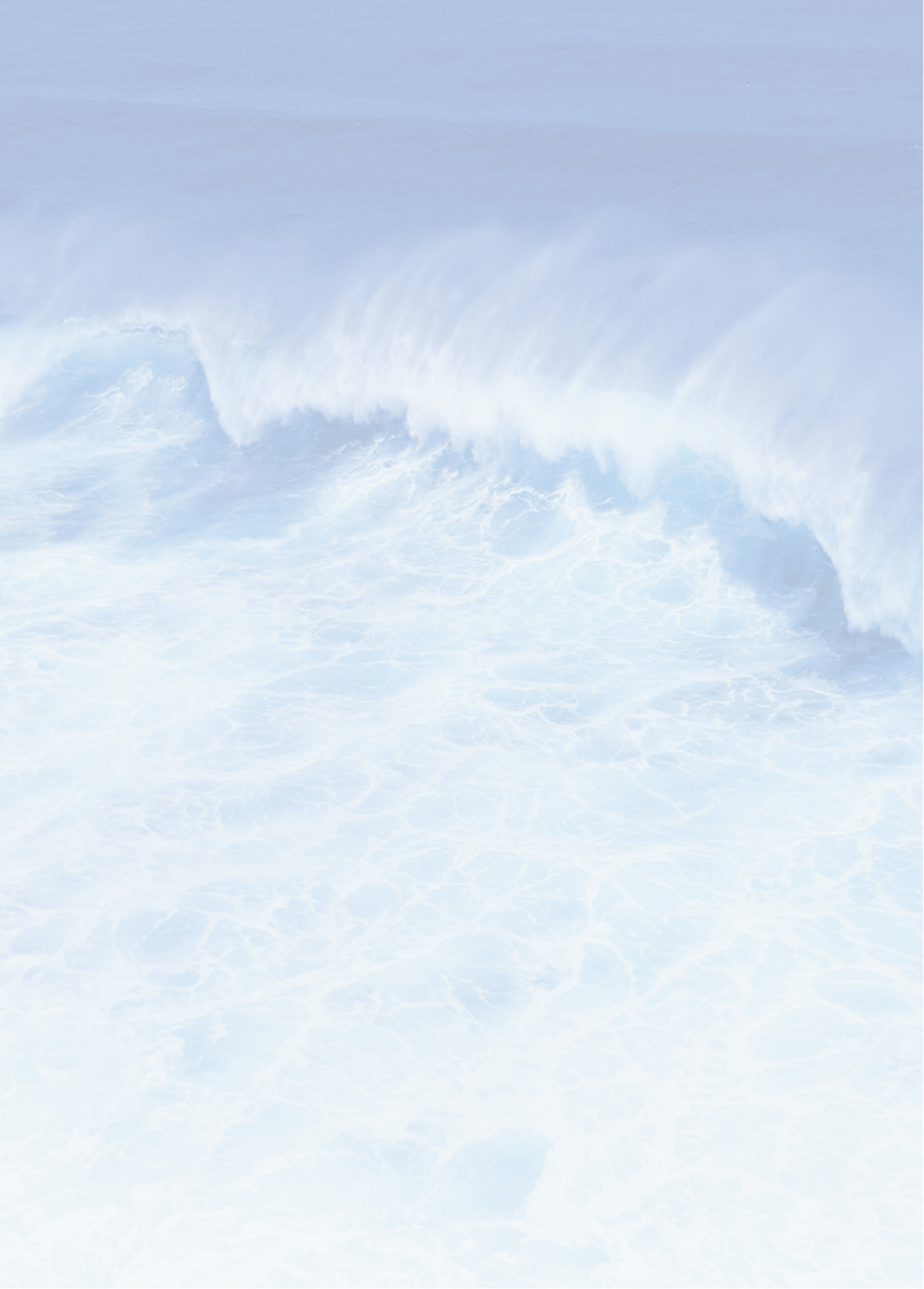

Modeling the "Agia Zoni II" oil spill released in 2017 in the Saronikos Gulf

P.E. Makatounis*, L. Tsiatsiou, A. Stamou

Laboratory of Applied Hydraulics, School of Civil Engineering, NTUA, Athens, 15780, Greece
*Corresponding author: panmakat@mail.ntua.gr

Abstract

On the 10th of September 2017 the sinking of the oil tanker "Agia Zoni II" caused an oil spill in Saronikos Gulf. To simulate the behaviour of this oil slick, we employed the 2D mathematical model GNOME that was developed by the NOAA Institute. GNOME requires the input of wind and sea current data during the oil pollution incident, which we collected from various sources. We observed very large differences between these data; thus, we developed various scenarios of input data combinations and performed calculations for all of them. Calculations showed that predicted GNOME splots are generally in good agreement with satellite images; practically, on the 18th of September 2017, about 64 % of the amount of oil released in the sea reached the shoreline, while the remaining (33 %) was dispersed or evaporated. Generally, GNOME simulates satisfactorily the behaviour of the oil slick taking into account the lack of oil spill data and the large variability of the available wind and sea current data.

Keywords Oil slick, Mathematical models, Simulation, GNOME, Saronikos Gulf

1 INTRODUCTION

According to the International Tanker Owners Pollution Federation (ITOPF), two large oil spills and four medium spills from tankers were recorded in 2017. The first large spill occurred in June when the tanker Rama 2 sank in the Indian Ocean with over 5,000 metric tons of oil on board. The second incident involved the oil tanker "Agia Zoni II" that sank on the 10th of September 2017 while at anchorage west of the port of Piraeus, Greece. The vessel was loaded with 2,362 metric tons of heavy fuel oil and 370 metric tons of marine gas oil. An unconfirmed quantity of the oil spilled into the sea causing pollution damage to the east coast of Salamina Island and coastal areas in the vicinity of the Port of Piraeus and Athens (https://www.iopcfunds.org/agia-zoni-ii-claimants/). The Salamina Port Authority and a private company assigned for decontamination operations; on the 11th of September they laid out two floating dams in areas along the Cynosura Bay and Salinas Bay of Selini, as well as between the Naval Proximity School and the Zea Marina, while private divers tried to seal the vents of the sunken tanker. Tank trucks were used to remove oil (https://insurancemarinenews.com/insurance-marine-news/marine-accident-round-13th-september-2017-2/).

Oil spills normally spread out and move on the sea surface with wind and current while undergoing a number of chemical, physical and biological changes due of processes that are collectively termed weathering; these include spreading, evaporation, dispersion, emulsification, dissolution, oxidation, sedimentation and sinking, and biodegradation. We may simulate weathering processes and forecast the fate of oil once spilled via an oil spill model (OSM); moreover, based on these simulations we can estimate subsequent risk (Papadonikolaki et al. 2014). There are various models in the literature that apply a number of different approaches; these range from simple oil spill trajectory to sophisticated 3D models that describe the movement and the distribution of the oil properties (https://www.itopf.org/). In the present work, we simulate the behaviour of the oil slick incident of the tanker "Agia Zoni II" in Saronikos Gulf using the OSM GNOME (NOAA 2002). To run the model, we need to input into GNOME the oil characteristics (i.e. the type and quantity of oil spilled), along with key environmental input data, which include wind velocity and direction, sea currents, air and sea temperatures. Usually, accuracy and availability of this data can often be an issue; this was indeed true in the present study.

2 MATERIALS AND METHODS

2.1 The GNOME model

The General NOAA Operational Modeling Environment (GNOME), which was developed by the National Oceanic and Atmospheric Administration (NOAA) Institute simulates the weathering processes of oil spills that are within continuous flow fields. GNOME requires input of sea currents, derived by hydrodynamic models, and wind characteristics, calculated by wind models. In GNOME, we need to define the "windage factor" that reflects the surface water movement and the "turbulent diffusion coefficient" that represents turbulent mixing. Typically, the windage factor is around 3% of the wind speed; usually, it is less than 6% of the wind speed.

2.2 *Description of the incident*

The tanker "Agia Zoni II" sailed on September 9th, 2017 at 10:00 from Aspopyrgos refineries loaded with 2,362 metric tons (t) fuel oil, 370 t marine gas oil, 15 t of additional marine fuel oil coal, 300 L of lubricants and 200-300 L of chemicals. On 10th of September 2017, at 01:45 the ship sank southwest of Atalanti Island, near to Salamina Island and the oil leakage occurred. The result of the leak was the widespread pollution of the Salamina marine and coastal area. According to the Ministry of Merchant Marine, the amount of oil that leaked was equal to 137 t. On Monday 11th of September 2017 oil pollution had been extended to 1.5 km. The next day according to the decontamination company, the ship was sealed and the oil leak had ended. The pollution had reached Piraeus. On 13th of September 2017 the pollution was extended to the areas of Vari and Voula. Until Friday 15th September 2017 the anti-pollution actions were continuously operating with floating and terrestrial means, both at the point of sinking and the perimeter of the wreck. In this area, the oil spill has been restricted. The next day in the coastal zone from Glyfada to the passenger port of Piraeus, individual and small-sized zones of shine were observed.

2.3 *Input data, scenarios and characteristics of calculations*

We obtained and processed wind and sea current data from the atmospheric models SKIRON and POSEIDON (Kallos et al. 1997 and Papadopoulos et al. 2002) and the POSEIDON sea circulation model, respectively. Also, we used wind data from weather forecasting websites (www.timeanddate.de, www.wunderground.com), the National Meteorological Service and the National Observatory of Athens. We observed very large differences in these data and the subsequent calculations. Thus, we developed a large number of scenarios (combinations) of input data and performed calculations for all of them following the deterministic calculation methodology that was applied by Makatounis et al (2017) in the Gulf of Patras. We used relatively large maximum values of "windage factor" that ranged from 1% to 6%, based on local observations (Lehr 2001) and wind persistence value equal to 15 minutes (NOAA 2012). The calculation characteristics are summarized in Table 1.

Table 1 Characteristics of the computations

Parameter	Value	Unit	Parameter	Value	Unit
Computational time	192	h	Release amount	137	t
Time step of computations	0.01	h	Half-life time	14.4	h
Release duration	2	days	Diffusion coefficient	50,000	cm^2s^{-1}
Release amount	137	t	Particle number	1,000	-

3 RESULTS AND DISCUSSION

3.1 *Calculated oil slick movement vs. satellite images*

In Figure 1 we compare the calculated oil slick Les with satellite images (WWF 2017) for one of the most realistic scenarios.

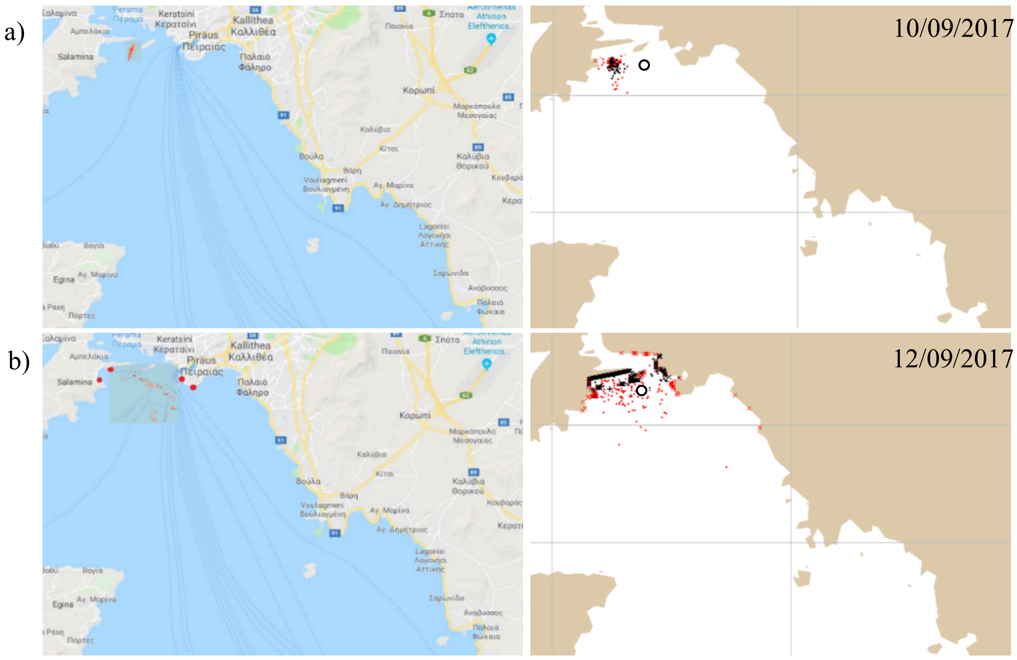

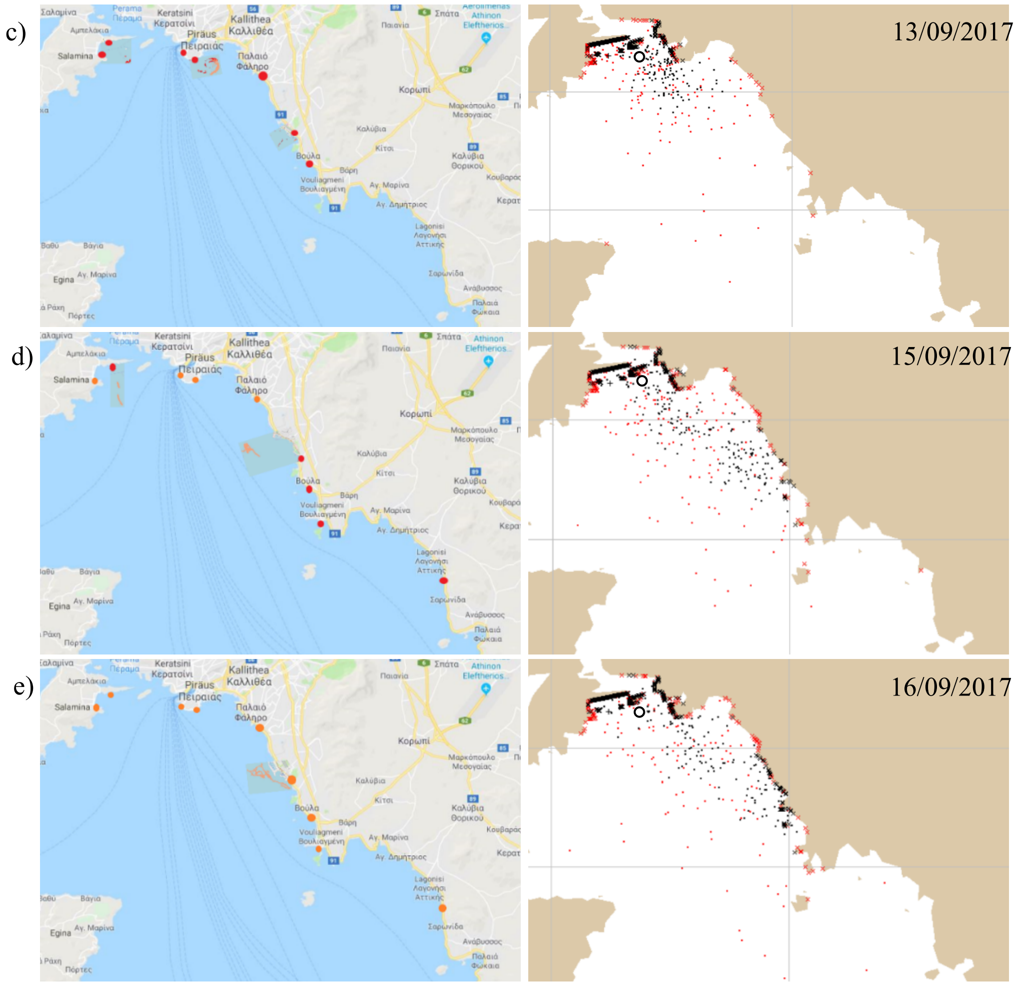

Figure 1 Comparison of calculated oil slick Les (right) with satellite images (left) (source: WWF 2017)

Figure 1 depicts that GNOME splots are generally in satisfactory agreement with satellite images. More specifically, on the release day (10th September) calculated oil spill splots (see Figure 1a) were directed from the location of the incident (shown with a black circle) towards the Cape of Cynosura to the Selini Bay, being driven by the prevailing E winds. In the early hours of the 2nd day (11th September), prevailing NE winds moved the oil splots towards the eastern coastline of Salamina Island; until the afternoon of the 2nd day the oil slick had affected the entire eastern coastline of the island. On the 3rd day (12th September), Figure 1b shows that the oil spill has been extended towards NE (prevailing winds were mostly SW) covering a large area, from Salamina Island until Piraeus (Piraiki); predicted oil splots in Figure 1b show a very good agreement with the observed locations that were affected by the oil slick (noted by red small circles in the satellite images). However, the predicted oil spill slows a somehow slower movement that the real incident. This slower movement is more evident on the 4th day (13th September); Figure 1c shows that prevailing NW winds in the morning "pushed" initially towards the predicted oil slick towards SE, close to the coastline of the Saronikos Gulf, but without reaching it. However, in the afternoon of the 4th day, SW winds starts to drive the oil splots towards the coastline and more particularly to the coastal regions of Paleo Faliro, Glyfada and Voula, where major pollution problems were observed. Oil pollution in these areas continued to occur in the 5th day (14th September), while on the 6th and 7th day (15th and 16th September), when prevailing winds were mainly NW and SW, satellite images (Figure 1d and 1e, respectively) show that the oil spill remains in the coastal area NW of Voula. However, they also show that the coasts of Vouliagmeni and Lagonissi were polluted by the oil spill. Calculated oil splots reached the coastal area of Vouliagmeni; however, they did not reach the coast of Lagonissi.

3.2 Calculated oil mass balance

The calculated variation of the oil mass balance with time (MacKay and Matsugu 1973) is shown in Figure 2.

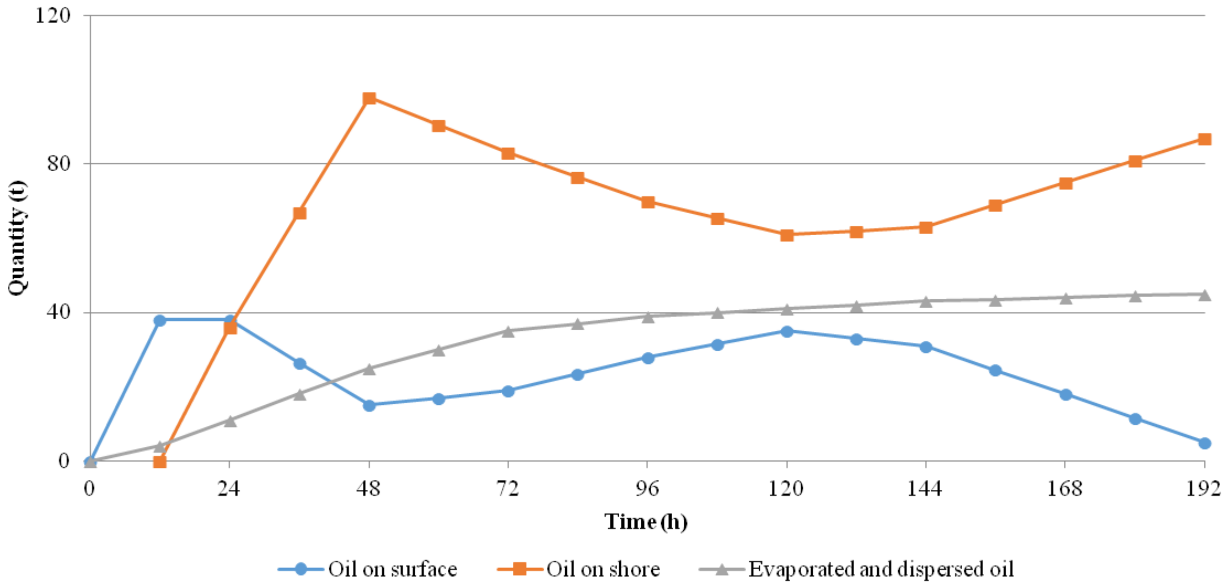

Figure 2 Calculated variation of the oil mass balance with time

Figure 2 shows that the quantity of oil on surface increases until it reaches a maximum value equal to about 38 t at t=20-24 hours; then it decreases to about 15 t at t=48 h, increases again until a new (lower) local maximum value equal to 35 t (at t= 120 h) and finally (after t=120 h) starts to decrease continuously to practically negligible values at t=192 h due to the increase of oil quantities that reached the shoreline and being evaporated/dispersed. This latter quantities show a continuous increase from the beginning of the incident with rates that are higher in the first 3 days, while later the rates decrease significantly; at t=192 h the quantity of oil evaporated/dispersed is equal to 45 t. Figure 2 depicts that the oil spill arrives at the coast almost 12 hours after the incident. The amount of oil on shore increases continuously until it reaches a maximum value equal to 98 t at t=48 h; then, it decreases due to refloating (i.e. it is "transformed" to oil on surface) until reaching a minimum value equal to 61 t at t=120 h and finally it starts increasing to a local maximum value equal to 87 t at t=192 h, i.e. the end of calculations. In other words, we observe that on the 18th of September 2017, about 64 % of the amount of oil released in the sea reached the shoreline, while the remaining (33 %) was dispersed/evaporated.

4 CONCLUSIONS

To simulate the behaviour of this oil slick, we employed GNOME using as input wind and sea current data during the incident that we collected from various sources. We observed very large differences between these data; thus, we developed various scenarios of input data combinations and performed calculations for all of them. Calculations showed that predicted GNOME splots are generally in good agreement with satellite images; practically, on the 18th of September 2017, about 64 % of the amount of oil released in the sea reached the shoreline, while the remaining (33 %) was dispersed or evaporated. Generally, GNOME simulates satisfactorily the behaviour of the oil slick taking into account the lack of oil spill data and the large variability of the available wind and sea current data.

Acknowledgements
For the provision of wind data, the authors thank Dr. K. Lagouvardos, Research Director of the Institute for Environmental Research and Sustainable Development of the National Observatory of Athens and the National Meteorological Service (Mrs. K. Kontochristou).

References

IOPC FUNDS (2017) Agia Zoni II

Kallos G, Nickovic S, Papadopoulos A, Jovic D, Kakaliagou O, Misirlis N, Boukas L, Mimikou N, Sakellaridis G, Papageorgiou J, Anadranistakis E, Manousakis M (1997) The regional weather forecasting system SKIRON. Paper presented at the International Symposium on Regional Weather Prediction on Parallel Computer Environment, University of Athens, Athens

Lehr WJ (2001) Review of modeling procedures for oil spill weathering behavior, in: Brebbia CA (ed) Oil spill modeling and processes, WIT Press, Southampton, p 51-90

MacKay D and Matsugu RS (1973) Evaporation rates of liquid hydrocarbon spills on land and water. Can J Chem Eng 51: 434-439

Makatounis PE, Skancke J, Florou E, Stamou A, Brandvik PJ (2017) Management of oil spill contamination in the Gulf of Patras caused by an accidental subsea blowout. Environ Pollut 231: 578-588

NOAA, Office of Response and Administration (2002) GNOME User's Manual

NOAA, Office of Response and Restoration (2012) General NOAA Operational Modeling Environment (GNOME) Technical Documentation. Washington

Papadonikolaki GS, Altan YC, Stamou AI, Otay EN, Christodoulou GC, Copty NK, Tsoukala VK, Telli-Karakoc F, Papadopoulos A (2014) Risk assessment of oil spill accidents. Glob NEST J 16: 743-752

Papadopoulos A, Katsafados P, Kallos G, Nickovic S (2002) The weather forecasting system for Poseidon - an overview. J Atmos Ocean Sci 8: 219-237

WWF Greece (2017) Oil pollution in Saronikos. Athens

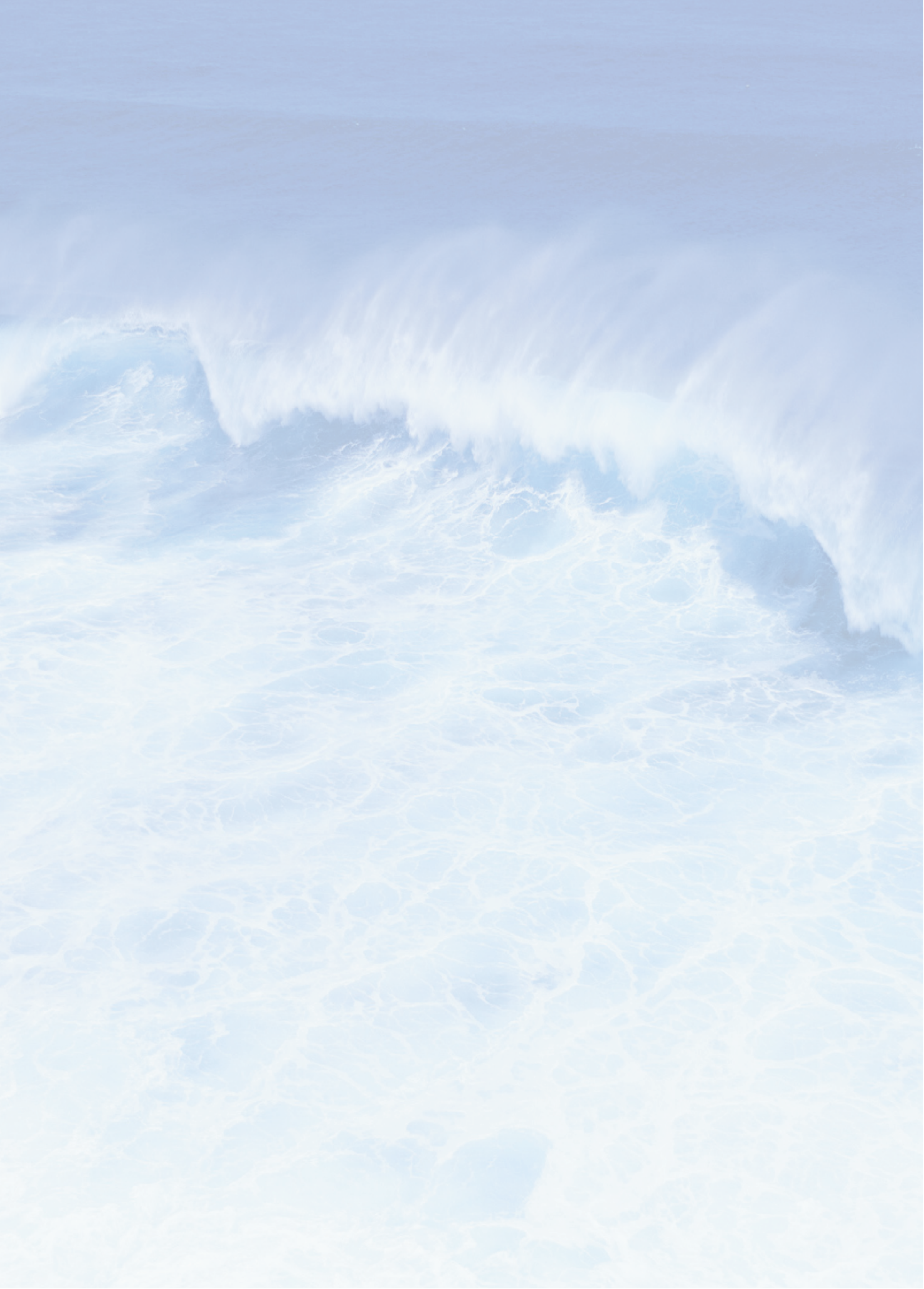

Geomorphology modification and its impact to coastal ecosystems

I.Zacharias[1*], A.Gianni[2]

[1]Department of Civil Engineering, University of Patras
[2]Department of Environmental & Natural Resources Management, University of Patras
*Corresponding author: izachari@upatras.gr

Abstract

Although there are many studies referred to impacts on water body anoxia caused by nutrients management and changes in meteorological or hydrological regimes, there is lack of information about the impacts on water column anoxia resulted by morphological modifications. This study aims to address these issues by examining the Aitoliko lagoon. Human-induced morphological changes in the Messolonghi–Aitoliko lagoonal system during the last decades constitute a natural scale experiment and an excellent opportunity to record and understand the relationship between morphological modifications and changes in water column hydrography and anoxia, in such environments. Anoxia constitutes an important environmental problem, affecting coastal systems around the world. The physicochemical alterations on the water column of anoxic basins, caused by morphological modifications, were studied. Deepening on the connecting sill between the permanent anoxic Aitoliko lagoon and Messolonghi lagoon was accomplished on May 2006. Seasonal variations of parameters like temperature, salinity and dissolved oxygen along the lagoon's water column were recorded and studied in a net of 14 stations, after sill's dredging. Wind speed and wind direction time series were used to estimate the wind's contribution to the hydrographical changes. The water fluxes between the two environments increased, due to the sill's cross section increase. Salty water inflow into Aitoliko lagoon was recorded during the sampling period and was correlated with monimolimnion oxygenation throughout winter months. The meteorological conditions that prevailed during the sampling period could not create strong water inflows into the Aitoliko lagoon, and consequently it was not the reason for the recorded alterations in the lagoon's water body anoxia.

Keywords Aitoliko lagoon, Anoxia, Morphology, Oxygenation

1 INTRODUCTION

Anoxic environments have been of scientific interest since the early '30s (Skei, 1983). Nowadays, permanent or seasonal anoxic coastal basins, fjords and lakes constitute natural laboratories for oceanographers, chemists and biologists. Anoxia constitutes an important environmental problem. Bottom water anoxia/hypoxia for longer or shorter periods can be a natural phenomenon caused by vertical water stratification (Yao and Millero, 1995). However, it is usually human activities that result in the strengthening of stratification or in high loads of nutrients and organic matter into water bodies with poor circulation (Diaz, 2001). In marine systems with extremely limited water exchange and excessive anthropogenic input of nutrients and organic matter (e.g. Baltic, Black and Caspian Seas), bottom water has become permanently hypoxic/anoxic. The ecological consequences rapidly become perceptible (Eden et al., 2003).

In transitional and coastal water bodies, morphology, nutrients load and salt/fresh water budget control anoxic conditions. Morphology is the dominant factor responsible for permanent stratification of fjords, semi-enclosed seas and continental deep depressions. Shallow and narrow sills are accountable for bottom water stagnation and anoxia. Black Sea (Glazer et al., 2006) and Cariaco Basin (Astor et al., 2003) are some characteristic examples of morphology-induced anoxia, while Adriatic Sea (Justi ́c et al., 1993) and Danish coasts (Josefson and Hansen, 2004) are nutrient-induced anoxic environments.

In anoxic layers, hydrogen sulfide is producing through the reduction of sulfates, $NH4^{+}$ is enhancing and $PO4^{-3}$ (over oxic conditions) is released from organic matter degradation. $PO4^{-3}$ is also released from sediments, reducing the N to P ratio and supporting the algal blooms. Thus, more organic matter is produced to fuel anoxia. All these processes are bacterially catalyzed and are more intense after spring surface photosynthesis when elevated rates of detritus materials reaching the anoxic layer. Anoxia preconditions may be disturbed, affecting the characteristics of the anoxic environment in certain ways. Nutrients management (Boesch, 2006) leads to the increase of dissolved oxygen concentrations mainly in seasonal stratified/anoxic environments such as NW continental shelf of Black Sea and numerous of estuaries in England (Jones, 2006).

Short term meteorological changes as storms and/or events of prolonged intensive winds have catastrophic results related to the advection of anoxic water to the surface, total anoxia and massive deaths (Luther et al., 2004). Long-term meteorological changes (e.g. climate changes) deplete oceanic oxygen by increasing stratification and warming as well as by causing large changes in rainfall patterns, enhancing discharges of fresh water and agricultural nutrients to coastal ecosystems. Conversely, when climate becomes stormier and stratification decreases because of increased mixing, the risk of oxygen depletion declines (Diaz and Rosenberg, 2008).

Although there are many studies referred to impacts on water body anoxia caused by nutrients management and changes in meteorological or hydrological regimes, there is lack of information about the impacts on water column anoxia resulted by morphological modifications. This study aims to address these issues by examining the Aitoliko lagoon. Human-induced morphological changes in the Messolonghi–Aitoliko lagoonal system during the last decades constitute a natural scale experiment and an excellent opportunity to record and understand the relationship between morphological modifications and changes in water column hydrography and anoxia, in such environments.

The main objective of this study is to investigate and correlate geomorphological changes in anoxic basins with physicochemical alterations in their water column. Deep water renewal and the consequently monimolimnion oxygenation, in meromictic systems, are the questions to be answered. Aitoliko lagoon constitutes the case study, as it is a semi-enclosed anoxic basin on which recent human-induced morphological changes have implicated in increased water exchange with its source basin (Messolonghi lagoon). Seasonal variations of parameters like temperature, salinity, and dissolved oxygen along Aitoliko lagoon water column were recorded and studied. It was attempted to associate the wind speed and direction, during the study period, with the recorded monimolimnion oxygenation, after 55 years of recorded anoxia (Chalkias, 2006).

2 DISCUSSION

The permanent stratified Aitoliko lagoon constitutes an environment where anoxia is controlled predominantly by its morphology (large depth, small length), the morphology of Messolonghi lagoon (source basin) and the narrow and sallow sill. Salt/fresh water budget and nutrient load play supplementary roles. Aitoliko lagoon behaves like a typical anoxic basin such as many fjord type basins (e.g. Framvaren Fjord). Thus, human induced morphological changes in the Messolonghi–Aitoliko lagoonal system constitute a natural scale experiment and an excellent opportunity to record and understand the relationship between morphological modifications and changes on water column hydrography and anoxia, in such environments. Past studies report a permanent stratified anoxic environment on which the depth of anoxic-oxic interface decreases through the time, from 18 m in 1951 to 4 m in 2006. This reflects the progressive limitation between the source (Messolonghi) and sink (Aitoliko) lagoons throughout these years. In the present study Aitoliko lagoon monimolimnion oxygenation during the winter months (January and February 2007), is reported for the first time.

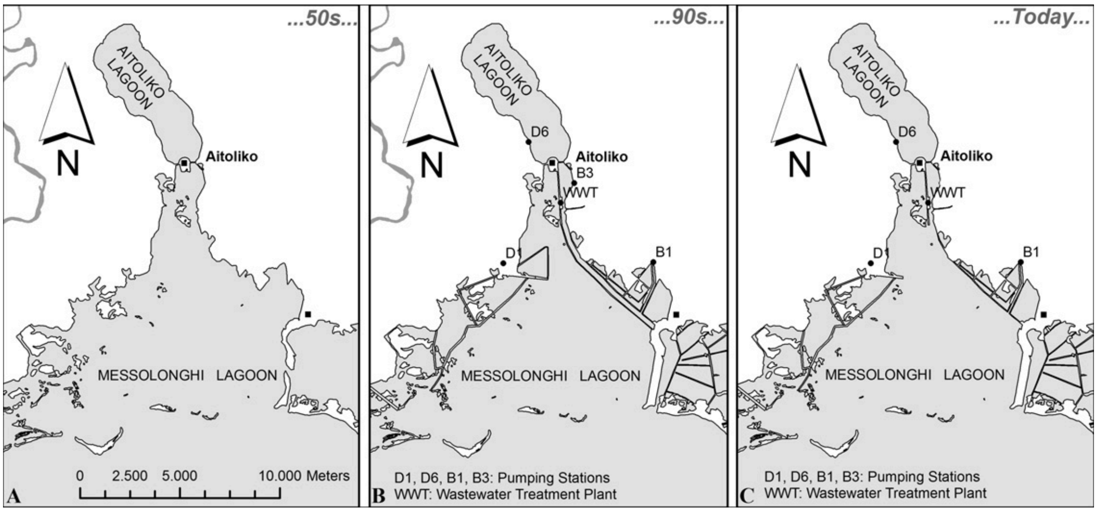

Figure 1 Morphology of Messolonghi–Aitoliko lagoonal system through the time. The black straight lines represent human made banks in Messolonghi lagoon.

Winter lagoon's oxygenation is ascribed to the salty water inflows from the adjacent Messolonghi lagoon. A bottom density current, at the southern part of Aitoliko lagoon was recorded from June until October 2006. This water mass entrained surrounding water and it was vertically expanded. When the water in the dense bottom current achieved the same density as the surrounding water, it was interleaved into the interior of Aitoliko lagoon promoting efficient vertical mixing within the basin. Vertical density instabilities in Aitoliko lagoon were recorded, demonstrating the mixing in its water column. Mixing processes, including breaking of interfacial waves during entrainment are related to the degree of density stratification.

From June to October 2006, salinity of the above-mentioned water mass in Aitoliko water column increased. This resulted from the salinity increase in the source basin (Messolonghi lagoon), which was caused from meteorological conditions and fresh/salt water budget. Density increase of the inflow water in combination with the weakness of density stratification in Aitoliko's water column after the autumn thermal overturn resulted in the depression of the saltier water mass at greater depths. That marks the mixing depth increase and it is probably the key to answer lagoon's bottom water oxygenation during winter time.

However, the question to be answered has to do with the reason behind the inflow of the saltier water into Aitoliko lagoon that led to the bottom water oxygenation. In shallow systems, tidal currents may induce the appropriate turbulent energy to promote vertical mixing. In the deep Aitoliko lagoon the prevailing tidal amplitudes are not capable to renew the bottom water. Intensive and prolonged southern winds can enforce denser water from Messolonghi to inflow Aitoliko lagoon and cause mixing of the water column. Furthermore, under strong and prolonged southern winds, water level will be raised in the downwind direction, inducing the pycnocline rise at the near-sill-area, thus allowing the better exchange of monimolimnion. North and northeasterly winds can cause an outflow of surface water, leading to a lowered sea level in the lagoon. When the wind decreases, water will enter the lagoon again due to the pressure difference caused by low sea level in the lagoon. The water that enters the lagoon is probably surface water mixed with saline Messolonghi water, meaning that it will be denser than the surface water and sink below that, ventilating the hypolimnion.

For these reasons wind contribution to lagoon's monimolimnion ventilation had to be investigated in this study. Throughout the sampling period strong winds (10–12 m/s) were always associated with northeast directions, while southern winds were always weak (up to 6 m/s). Focusing on the ventilation period (January and February 2007), wind speed and wind direction time series showed weak winds with variable direction and strong northern winds just before the samplings.
Nevertheless, there are some reasons that we cannot ascribe Aitoliko lagoon bottom water ventilation in the strong northern winds. First of all, even though northeasterly winds were prevailed during

December 2006, the monimolimnion of Aitoliko lagoon was anoxic. Neither the strong northern–northeasterly winds during spring 2007 result in bottom water ventilation. Besides, during January 2007, when for first time, the bottom water of Aitoliko lagoon is presented to be oxygenated; weak southern winds were prevailed in Aitoliko lagoon. Only, in February 2007, high dissolved oxygen concentrations in the monimolimnion of Aitoliko lagoon are combined with strong northeasterly winds.

Finally, in winter time, salinity values in Messolonghi lagoon is not higher than 36, at the southern part. The water that outflows Aitoliko lagoon during northern and northeasterly winds is mixing with the Messolonghi lagoon and inflows again in Aitoliko lagoon when wind decreases and pressure differences permit it. The mixing of the brackish surface water of Aitoliko lagoon with the Messolonghi water, with salinity values lower than 36, does not produce water, dense enough to dive in Aitoliko lagoon hypolimnion ventilating it. Conclusively, meteorological conditions prevailed in study area cannot alter water body anoxia, through vertical mixing, which means that wind was not the reason for the monimolimnion oxygenation.

Sill's dredging increased the channel's maximum depth in 3 m and the total cross-sectional area about 30%. Consequently, water fluxes between Aitoliko and Messolonghi lagoons increased at about 30%. These morphological modifications allowed salty water from the source basin to flow in Aitoliko lagoon. Physicochemical characteristics of this water depend on meteorological conditions and fresh/salt water budget in Messolonghi lagoon, and therefore, present seasonal variability. In late autumn months the inflow water presents its maximum salinity value. Increased density results to the depression of this layer in the water column of Aitoliko lagoon. At the same time (late autumn) lagoon's water column presents its minimum stability, after autumn thermal overturn. Moreover, dissolved oxygen saturation rates in surface layers increase as gradually temperature decreases during this period. The combination of low energy of Aitoliko water column with the increased salinity/density of the inflow water and the higher oxygen concentrations in the surface waters facilitated interfacial mixing processes and monimolimnion ventilation during winter months.

3 CONCLUSIONS

Morphological changes in coastal anoxic environments are particularly rare. Such changes affect directly the water exchange in lagoons and, consequently, the physicochemical balance on their water column. Morphological changes in the Aitoliko–Messolonghi lagoonal system affected Aitoliko's hydrography and water column anoxia twice during the last decades: in the, 90s when extensive human interference led to a wide anoxic layer from 4 m down to lagoon's bottom, and once recently when monimolimnion oxygenation resulted from the sill's deepening. In conclusion, the limited deepening of a sill can create a mild increase of water flow into an anoxic lagoon. This inflow of oxygenated saltier water from the source basin results in a weak mixing of the water column. Such small-scale mixing can introduce oxygen into the halocline waters, without destroying the stratification. Such morphology modification can lower the anoxic-oxic interface and not destroy the anoxic character of the lagoon. Reducing the connection between an anoxic coastal basin and its source basin water column, anoxia is amplified, while when morphological modifications facilitate water exchanges through these basins bottom water oxygenation can occur. Ventilation depth is dependent on the physicochemical characteristics of the source basin. Morphological modifications, when they are possible, could constitute a natural way of anoxic environment restoration.

References

Boesch DF (2006) Scientific requirements for ecosystem-based management in the restoration of Chesapeake bay and Coastal Louisiana. Ecol. Eng. 26, 6–26.

Chalkias G (2006) Methodology development for the determination of heavy metals in coastal environments. In: Atomic Absorption Spectroscopy. Application to Lake Trichonis and Aitoliko Lagoon. University of Ioannina (in Greek).

Diaz RJ (2001) Overview of hypoxia around the World. J. Environ. Qual. 30, 275–281.

Diaz RJ, Rosenberg R (2008) Spreading dead zones and consequences for marine ecosystems. Science 321, 926–929.

Eden N, Katz T, Angel DL (2003) Dynamic response of a mud snail Nassarius sinusigerus to changes in sediment biogeochemistry. Mar. Ecol. Progr. Ser. 263, 139–147.
Glazer BT, Luther III, GW, Konovalov SK, Friederich GE, Trouwborst RE,Romanov AS (2006) Spatial and temporal variability of the Black Sea suboxic zone. Deep Sea Res. II 53, 756–1768.
Jones PD (2006) Water quality and fisheries in the Mersey estuary, England: a historical perspective. Mar. Pollut. Bull. 53, 144–154.
Justic D, Rabalais NN, Turner RE, Wiseman WJ (1993) Seasonal coupling between riverbone nutrients, net productivity and hypoxia. Mar. Pollut. Bull. 26, 184–189.
Luther III GW, Ma S, Trouwborst R, Grazer B, Blickley M, Scarborough R, Mensinger M, (2004) The role of anoxia, H2S, storm events in fish kills of deadend canals of Delaware Inland Bays. Estuaries 27, 551–560.
Yao, W., Millero FJ (1995) The chemistry of the anoxic waters in the Framvaren Fjord, Norway. Aquat. Geochem. 1, 53–88.

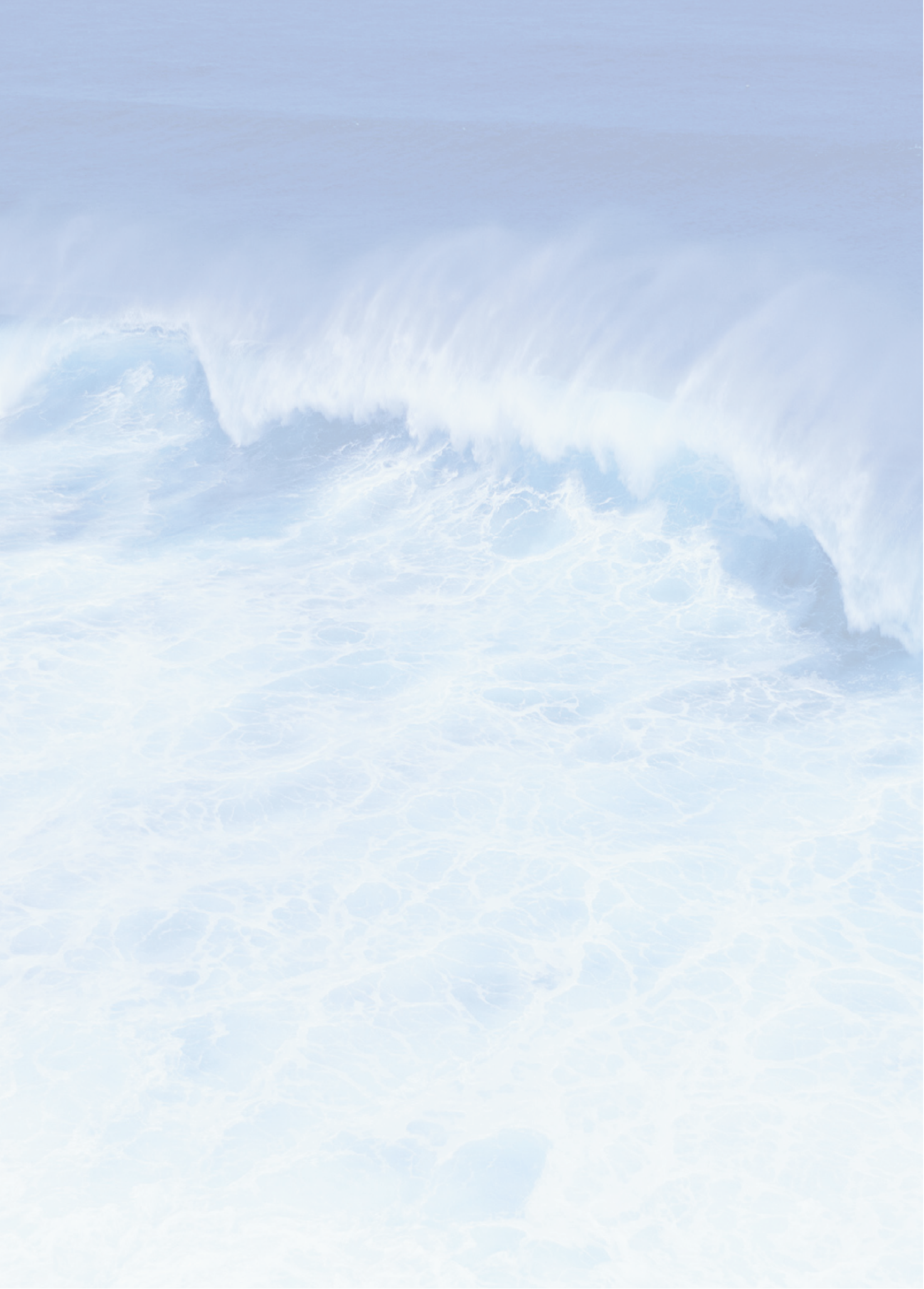

Improving the water renewal of restricted lagoons. Application to pappas lagoon (Western Greece)

N. Th. Fourniotis[1,2 *], G.M. Horsch[1], G.A. Leftheriotis[1]

[1]Department of Civil Engineering, University of Patras, University Campus, 265 00 Patras, Greece
[2]Department of Civil Engineering, Technological Educational Institute of Western Greece, Megalou Alexandrou 1, 263 34 Patras, Greece
[*]Corresponding author: nfou@upatras.gr

Abstract

A series of numerical experiments have been conducted concerning the water exchange of a restricted lagoon with the adjacent water body that is influenced by the tide. A method is proposed that applies to restricted lagoons with at least two inlets, subjected to the same tidal forcing. It consists of altering either the amplitude or the phase of the tide in one of the inlets. It is shown in the paper that this will result in an alteration of the function of the lagoon, from a lagoon periodically exchanging water equal to a tidal prism within each tidal cycle with the adjacent water body, to a flow through system, substantially improving the flushing rate of the lagoon. The method is confirmed by application to the Pappas lagoon, in Western Greece, for which the alteration of the characteristics of the tide at one (the northern) inlet, is implemented numerically, resulting to a differential forcing, which renews the lagoons waters substantially

Keywords Lagoon, MIKE 3 FM (HD, TR), Tidal hydrodynamics, Tidal inlet.

1 INTRODUCTION

In recent years many lagoon ecosystems have been affected by natural and mostly anthropogenic influences, leading to alterations in the physical, chemical, and biochemical parameters of these complex ecosystems, which in turn may directly affect fish production and ecosystem dynamics (Corzi and Ardizzone 1985, Chauvet 1988). The concentration of the corresponding substances in lagoon ecosystems is generally dependent on hydrodynamic circulation and water renewal time or the ability of the ecosystem to achieve a significant flushing rate, which are the crucial factors for decisions with regard to lagoon restoration design and management actions, aiming at the improvement of environmental conditions and fishery exploitation.

Among the physical parameters that affect the water quality of coastal lagoons, renewal of water has long been identified as a key parameter and has been made the basis of the early classification by Kjerfve (1986) in choked, restricted, and leaky systems according to the degree of water exchanged with the adjacent coastal ocean (i.e. the open sea). More recently, the water renewal time has been proposed as the basis for the classification of lagoons (Andréfouët et al. 2001). As a result of the importance of water renewal in lagoons, the creation of new artificial tidal inlets has been proposed and applied as a solution in several instances (see e.g., Aubrey et al. 1993). In a recent work, Fourniotis et al. (2018) demonstrated that the amount of water exchanged in each tidal cycle is not the basic parameter to determine the flushing time, since the differential arrival of the tidal signal at the inlets of a lagoon substantially determines the water renewal of the water body. More specifically, it is shown that the development of differential amplitude and/or a phase lag and thus a generation of a pressure gradient along the body of a lagoon causes to this lagoon to function as a flow-through system, with a contaminant short time of water renewal.

This contention is confirmed by numerically creating a difference in amplitude and/or a phase lag between the northern tidal inlet or the Papas lagoon and the other two inlets, which in actual reality receive identical signals. This results in the development of a periodic pressure gradient along the body of the Papas lagoon. This mechanism is found to be the key factor that causes the lagoon to function as a flow-through system, resulting in a much shorter water renewal time, in comparison to the original system, in which no substantial pressure gradient is generated between tidal inlets under the effect of the actual tidal forcing.

2 MATERIALS AND METHODS

2.1 The Study Area

The Papas Lagoon is embedded within the northwestern coast of the Peloponnese, adjacent to the Gulf of Patras. The lagoon is of elongated shape, with its main axis along the NW–SE direction. It is 5 km long, 1 km wide on average, and covers an area of about 6.2 km^2 (Papatheodorou et al. 2012). It is a deep water body, with a mean depth of 1.8 m and a maximum depth of 5 m. It is connected to the Gulf of Patras with three stable tidal inlets, the length and width of which lie within 160–260 m and 25–50 m, respectively. During the winter, it is supplied with fresh water by a small draining stream discharging into the lagoon's southeastern part, which borders cultivated land (Krasakopoulou and Pagou 2011). The lagoon is subject to extensive fish exploitation and aquaculture. It is naturally eutrophic, with no anthropogenic influences on the waterfront. Within the last 35 years, nine dystrophic crises have been reported, followed by mass fish mortality and benthic fauna; these occurred during the summer months of the years 1979, 1984, 1987, 1996, 1997 (NCMR 2000), 2004, 2010, and 2012 (Cladas et al. 2016). The dystrophic crises have been related to the decomposition of large beds of macro algae (Krasakopoulou and Pagou 2011). The lagoon is protected by the Ramsar Convention. The proper management of the lagoon, which is of primary importance to local fishermen, includes plans for dredging operations, creation of inlets, or other infrastructure works in the area, with the aim of improving the hydrodynamic circulation and water renewal of this ecosystem.

2.2 The Hydrodynamic Code and the Advection–Diffusion Code

The simulations presented herein have been performed using the commercially available CFD (Computational Fluid Dynamics) code MIKE21 and MIKE3 Flow Model FM (where FM stands for flexible mesh). The MIKE3 Flow Model FM has been used for three-dimensional flow simulations. It is a modeling system developed by the Danish Hydraulic Institute (DHI), based on a finite volume and an unstructured mesh approach. The details of the codes can be found in DHI (2018a, b, c), and the specific choices selected in the runs described below can be found Fourniotis et al. (2018)

2.3 Computational Domain and Grid

Due to a lack of free surface time series measurements at the entrance of the tidal inlets of the Papas lagoons, which would have been adequate data as boundary conditions for flow simulations, the only alternative is the computation of such data. The only locations that are suitable for boundaries of numerical simulations and where, at the same time, the harmonic constituents of the tide are available, are both ends of the Gulf of Patras, one of which (OB1) is close to the tidal inlets of the Papas lagoon (Achilleopoulos 1990). It would have been numerically inefficient to perform fully three-dimensional simulations in a domain comprising of an area as large and deep as the Gulf of Patras (135 m maximum depth) together with the lagoonal system, which includes extensive areas with depth less than 1 m. Thus, it was decided to resort to two-dimensional, depth-averaged simulations in a domain similar to the one used by Horsch and Fourniotis (2017) covering the entire area of the Gulf of Patras to extract boundary conditions for the three-dimensional simulations in the Papas lagoon. Such two-dimensional simulations are adequate, in terms of tidal propagation, even in summer conditions when thermal stratification is set in the Gulf.

The numerical domain for the three-dimensional simulations covers the entire Papas lagoon system and a small part of coastal waters in front of the tidal inlets of the lagoon. Specifically, a truncated computational domain was formed covering the entire lagoon and the adjacent open waters of the southwestern part of Gulf of Patras, consisting of three zones in the horizontal (Figure 1).

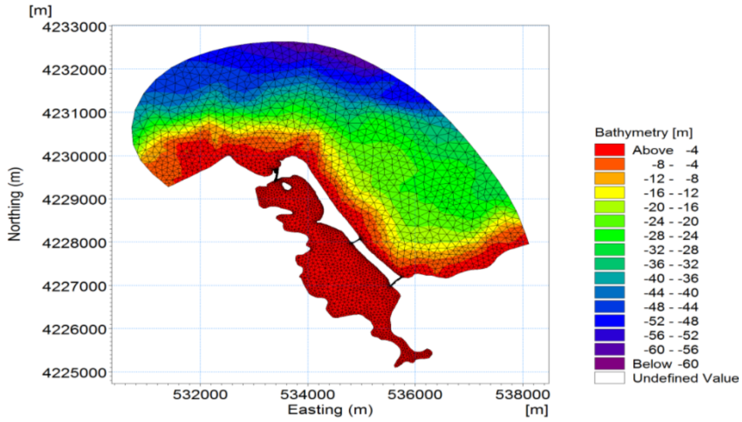

Figure 15 Numerical domain for the wider area of the Papas lagoon, covering part of the Gulf of Patras.

2.4 Boundary and Initial Conditions

In all cases considered herein, the coastline has been defined as an impermeable, zero normal velocity boundary, while the bottom is a no-slip (via wall functions), impermeable boundary. Concerning the Papas lagoon, tidal elevation time series that resulted from the two-dimensional simulations of the Gulf of Patras were used as open boundary conditions in the simulations that follow. The bottom roughness was set equal to 0.01 m and care was taken to ensure that the geometry of the bottom cell was compatible with the requirement of fully rough flow, assuming the minimum flow depth to be 0.4 m. Furthermore, initial conditions were needed in all two regions: (a) the opening (OB1) at the northeastern part of the Gulf and, (b) the Papas lagoon. Mean temperature and salinity profiles were imposed as initial conditions throughout the Gulf basin. The required profiles for the Gulf of Patras were taken as in Fourniotis and Horsch (2015). It should be noted that, the simulations were performed considering barotropic flow, even for the summer months when the Gulf's waters (outside the Papas lagoon) were found to be stratified (Papailiou 1982). This seems justified because in the shallow waters of the Gulf, within the domain chosen, previous simulations show that the stratification is destroyed and the waters become nearly isothermal and these waters are of constant salinity. Further, according to measurements of Cladas et al. (2013), stratification does not seem to be important in the lagoon during the summer months. Therefore, the flow, both into the lagoon, in the tidal channels and in the near vicinity outside it, can be taken as homogeneous.

2.5 The Tracer

In this section we present the method we applied to numerically estimate the residence time of the Papas lagoonal ecosystem. Various transport time scales have been used in the literature to quantify the renewal of waters in natural systems (e.g., Monsen et al. 2002). The present work has been stimulated by research in coastal lagoons that suffer from recurring dystrophic crises, the inception of which has been observed to occur locally before spreading to the entire lagoon (Cladas et al. 2016). Therefore, it is desirable to aim at calculating a time scale characterizing the local transport rate rather than an integral time scale characterizing the overall renewal of the entire lagoon. For the Papas lagoon, the latter has been carefully calculated in the form of flushing time by Krasakopoulou and Pagou (2011) who based their calculations on water quality measurements in the lagoon. We note that even though they call their time scale a residence time, we have referred to it as a flushing time since herein we use the definition of Monsen et al (2002) for flushing time as an integral scale, and retain the local character they give to the term residence time.

More precisely, for the purposes of the calculation, we define as residence time the time needed for the concentration of a conservative, passive tracer to fall to 1/e (~37%) of its initial value (see for example Stamou et al 2012, Ranjbar and Zaker 2018). By defining the initial concentration of the conservative numerical tracer to be equal to 1 inside and 0 outside the lagoon, we are thus able to calculate the residence time at each point inside the lagoon by following the evolution of the concentration of the tracer as determined by the advection–diffusion equation. This information should be useful in the analysis of the very complex problem of the inception of the recurring dystrophic crises that plague especially the Papas lagoon. We note, however, that the *e*-folding value is a mere convention and that in different applications the use of different cutoffs may be required. This is especially true for research concerning the causes of the dystrophic crises, a topic not well understood at this time.

3 RESULTS AND DISCUSSION

In this section our attention is confined to purely tidal flow, ignoring wind-induced effects, since this is the most severe situation that arises, in terms of water renewal, in the lagoon. In order to enhance the lagoon hydrodynamics subsequently increasing the flushing rate of the system, we numerically forced one of its tidal inlets with a modified tidal signal, *i.e.*, by altering the amplitude or the phase of the tide entering the inlet of the lagoon. Our aim is to generate a differential tidal forcing at least between two inlets of the lagoon, resulting in the development of differential amplitude and/or a phase lag and therefore a pressure gradient along the basin. Under the above described modified forcing the lagoon functions as a flow-through system, with a concomitant short time of water renewal. This analysis was tested by performing simulations in which we forced the northern tidal inlet of the lagoon by applying a tidal signal having (a) half the actual tidal range, (b) a short phase lag compared to the original, while maintaining the original unaltered forcing at the other two inlets. The result was, anticipating below, that the residence time for this numerically modified Papas lagoon decreased to 10 days, as compared to the more than 40 days when the original tidal forcing is allowed to occur, where all the three inlets are exposed to the same tidal signal (Figure 2).

Comparing the original unaltered system to the modified one, it is apparent that, in the former, the mechanism of water renewal results from the mere introduction of a volume of water equal to the tidal prism at the first half of the tidal cycle, recirculation and mixing of that volume within the lagoon, and subsequent exit of an almost equal amount in the second half of the tidal cycle. In contrast, in the latter case, i.e. the numerically modified lagoon, the water introduced at the middle inlet at the first half of the tidal cycle moves northwards and exits from the northern tidal inlet and a smaller amount of water enters from the northern inlet at the second part of the cycle. This process substantially improves flushing time.

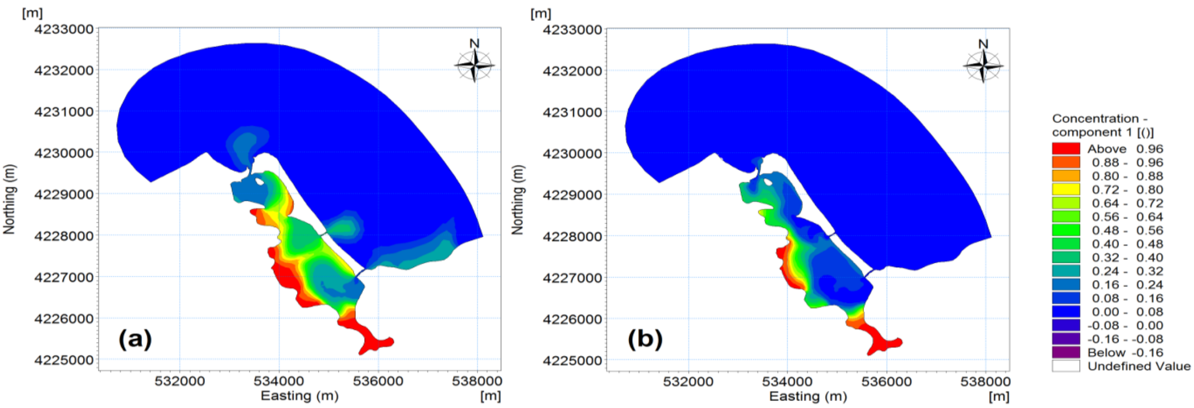

Figure 16 Concentration levels after 10 days of simulation for the original (a) and the modified (b) tidal forcing.

Given that unlike in the modified case, in the original case high concentration of a numerical tracer, uniformly distributed within the lagoon at the initiation of the simulation, was found later between the two eastern inlets, if one could achieve the above described alteration in the hydraulic exchange process of the lagoon, one might expect to avoid the dystrophic crisis which was actually observed and measured by Cladas et al. (2016) to develop between the two eastern inlets.

4 CONCLUSIONS

Restricted lagoons suffer from long residence times, which result because of the limited tidal hydraulic exchange between the lagoon and the adjacent open waters. The present study documented, however, that this state is not solely a result of the geometry of the lagoon, but also of the hydrodynamic function of these water bodies. More specifically, it is shown that if the tidal forcing applied at different tidal inlets of the lagoon generates a pressure gradient along the basin, the results may be the creation of a flow-through system, which flushes the lagoon waters considerably more efficiently than the slow process of tidal prism exchange and mixing in successive tidal cycles. This contention is confirmed for the numerically modified case of Papas lagoon. It is concluded that this advantage, in terms of flushing rate, should be taken into account whenever possible when deciding the location and geometry an additional tidal inlet, created in a lagoon in order to enhance its flushing rate.

References

Achilleopoulos P (1990) Tides in Gulfs and Straits of Western Greece. Ph.D. Thesis, University of Patras, Patras, Greece.

Andréfouët S, Pagés J, Tartinville B (2001) Water renewal time for classification of atoll lagoons in the Tuamotu Archipelago (French Polynesia). Coral Reef, 20, 399-408.

Aubrey DG, Giese GS (1993) Formation and Evolution of Multiple Tidal Inlets; American Geophysical Union: Washington, DC, USA.

Chauvet C (1988) Manuel Sur I Amenagement Des Peches Dans Les Lagunes Cotieres La Bordigue Mediterraneenne Fao Document Technique Sur Les Peches 290; Food and Agriculture Organization of the United Nations (FAO): Rome, Italy, p. 77.

Cladas Y, Papantoniou G, Bekiari V, Fragkopoulou N (2016) Dystrophic crisis event in Papas Lagoon, Araxos Cape, Western Greece in the summer 2012. Mediterr. Mar. Sci, 17, 32–38.

Cladas Y, Papantoniou G, Ketsilis V, Fragopoulou N (2013) Dystrophic crisis event Papas Lagoon (Araxos Achaia). 15th Panhellenic Ichthyologists' Conference, Aquatic Ecosystems: Uses, Impact and Management, Thessaloniki, Greece, pp. 10-13.

Corsi F, Ardizzone GD (1985) Some environmental conditions affecting yellow eels catchability. Oebalia, 11, 561-571.

DHI (2018a) MIKE 21 FLOW MODEL FM, Hydrodynamic Module-User Guide. DHI Software. pp. 132.

DHI (2018b) MIKE 3 FLOW MODEL FM, Hydrodynamic Module-User Guide. DHI Software. pp. 138.

DHI (2018c) MIKE 3 FLOW MODEL FM, Transport Module-User Guide. DHI Software. pp. 46.

Fourniotis NT, Horsch GM, Leftheriotis GA (2018) On the Hydrodynamic Geometry of Flow-Through versus Restricted Lagoons, Water, 10(3), 237.

Fourniotis NT, Horsch GM (2015) Baroclinic circulation in the Gulf of Patras (Greece). Ocean Eng, 104, 238-248.

Horsch GM, Fourniotis NT (2017) Wintertime Tidal Hydrodynamics in the Gulf of Patras, Greece. J. Coastal Res., 33, 1305-1314.

Kjerfve B (1986) Comparative oceanography of coastal lagoons. In Estuarine Variability; Kennedy, V.S., Ed.; Academic Press: New York, NY, USA, pp. 63-81.

Krasakopoulou E, Pagou K (2011) Seasonal steady-state budgets of nutrients and stoichiometric calculations in an Eastern Mediterranean lagoon (Papas Lagoon-Greece). Mediterr. Mar. Sci, 12, 21-41.

Monsen N, Cloern J, Lucas L, Monismith S (2002) A comment on the use of flushing time, residence time and age as transport time scales. Limnol. Oceanogr, 47, 1545-1553.

National Centre for Marine Research (2000) Monitoring of the Papas Lagoon (Cape Araxos/Achaia) Ecosystem-Management and Protection Proposal; Final Technical Report; Pagou, K., Ed.; NCMR: Athens, Greece; p. 190.

Papailiou DD (1982) Oceanographical Study in Patras Gulf Waters for Pollution Management; University of Patras, Department of Mechanical Engineering: Patras, Greece, Volume 2, p. 161. (In Greek)

Papatheodorou G, Avramidis P,Fakiris E, Christodoulou D, Kontopoulos N (2012) Bed diversity in the shallow water environment of Pappas Lagoon in Greece. Int. J. Sediment Res, 27, 1-17.

Ranjbar MH, Zaker HN (2018) Numerical modeling of general circulation, thermohaline structure, and residence time in Gorgan Bay, Iran. Ocean Dyn, 68, 35-46.

Stamou AI, Loverdou L, Matsoukis C, Albanis T, Gkesouli A (2012) Modeling renewal times in Amvrakikos gulf, Greece. Global NEST J, 14, 386-392.

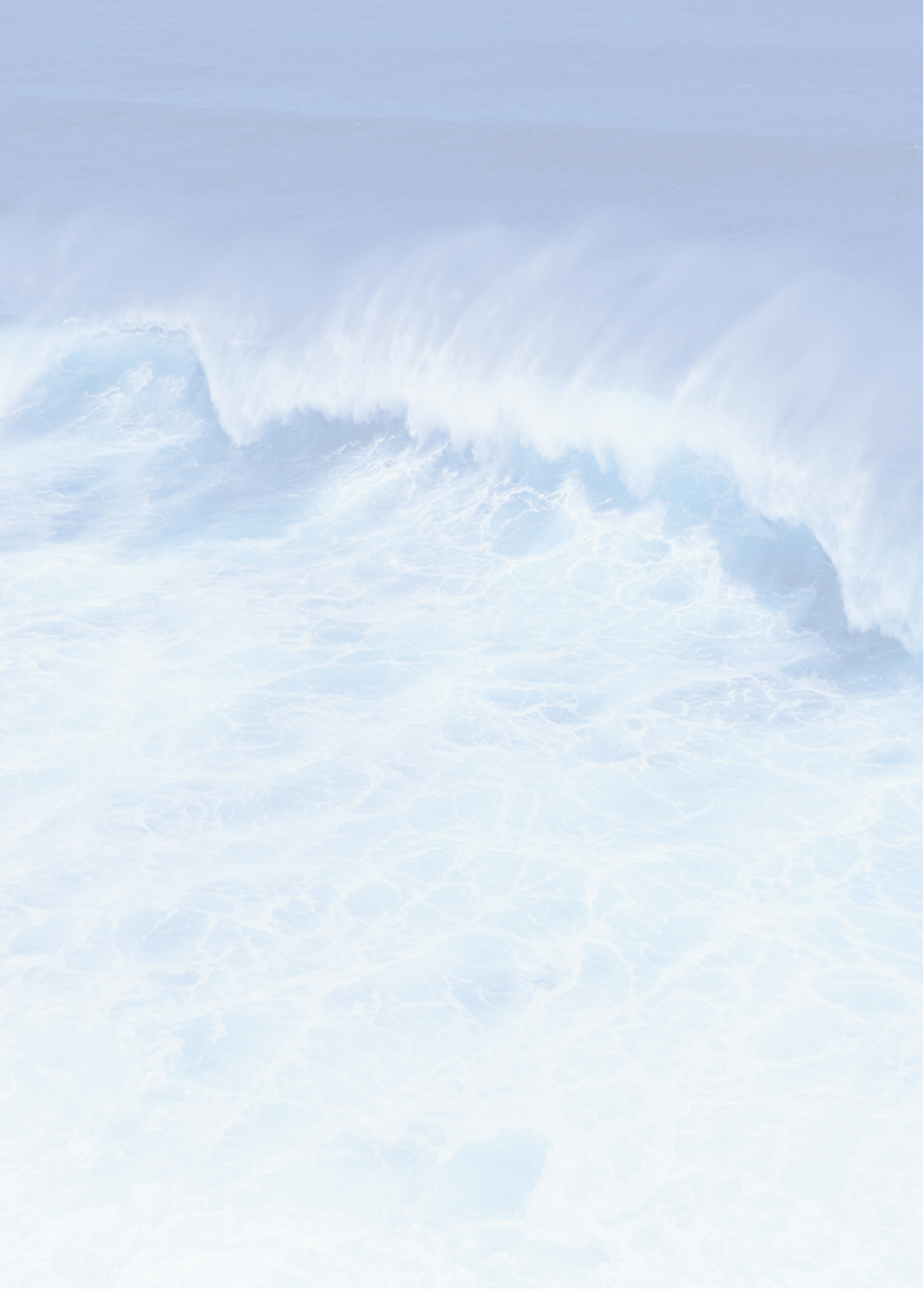

Προβλήματα και Προοπτικές στην συλλογή και διαχείριση αποβλήτων πλοίου και καταλοίπων φορτίου στην Ελλάδα

Θ. Γιαντσή*

Εργαστήριο Λιμενικών Έργων ΕΜΠ, Ηρώων Πολυτεχνείου 5, Ζωγράφου, 15780, Ελλάς
*Υπεύθυνος επικοινωνίας: dgiantsi@central.ntua.gr

Περίληψη

Στην παρούσα εργασία γίνεται μια σύντομη αναφορά στο Διεθνές, Ευρωπαϊκό και Ελληνικό Θεσμικό Πλαίσιο για την συλλογή και διαχείριση των απόβλητων και κατάλοιπων πλοίων όπως ισχύει σήμερα καθώς και στα κύρια προβλήματα που παρατηρήθηκαν κατά την εφαρμογή του. Σήμερα τόσο το Ευρωπαϊκό όσο και το Εθνικό Θεσμικό Πλαίσιο είναι υπό αναθεώρηση, ενώ το Διεθνές Δίκαιο συνεχώς τροποποιείται. Έχει δημοσιευθεί πρόταση τροποποίησης της ισχύουσας Ευρωπαϊκής Οδηγίας η οποία επιφέρει σημαντικές αλλαγές στην ισχύουσα κατάσταση. Επίσης γίνεται σύντομή περιγραφή της υφιστάμενης κατάστασης στην Ελλάδα, μιας χώρα με πολλούς μικρούς λιμένες, με πολλούς φορείς διαχείρισης λιμένων και στα σύνορα της Ευρωπαϊκής Ένωσης. Επισημαίνονται τα ιδιαίτερα προβλήματα που υπάρχουν στον Ελληνική αγορά της λιμενικής αυτής υπηρεσίας. Από τις επερχόμενες αλλαγές στο θεσμικό πλαίσιο διαφαίνονται επίσης θετικές προοπτικές για την ανάπτυξη του κλάδου, ενώ παρουσιάζονται προτάσεις για την βελτιστοποίηση των αλλαγών προς όφελος τόσο των χρηστών όσο και των παρόχων των υπηρεσιών και φυσικά του περιβάλλοντος.

Λέξεις κλειδιά Απόβλητα πλοίου, Κατάλοιπα φορτίου, Εγκαταστάσεις Παραλαβής αποβλήτων, Σχέδιο Παραλαβής και Διαχείρισης, Αποβλήτων

1 ΕΙΣΑΓΩΓΗ

Στον τομέα των διεθνών συμφωνιών, οι συμβάσεις συνιστούν έγγραφα υπογεγραμμένα από κράτη μέλη διεθνών οργανισμών και στη συνέχεια εφαρμόζονται από τα κράτη μέλη με την ενσωμάτωσή τους από τα εθνικά θεσμικά πλαίσια. Στην περίπτωση της Ευρωπαϊκής Ένωσης (ΕΕ), απαιτείται ένα πρόσθετο βήμα, το οποίο περιλαμβάνει την έγκριση της συμφωνίας από το Θεσμικό Πλάισιο της ΕΕ. Στην Ελλάδα, ως κράτος-μέλος της ΕΕ, τα ιεραρχικά βήματα υλοποίησης περιλαμβάνουν: τη Διεθνή Σύμβαση, τις νομικές πράξεις της ΕΕ (όπως Κανονισμός, Οδηγία ή Απόφαση) και τέλος τις εθνικές νομικές πράξεις ως Νόμος ή Προεδρικό Διάταγμα ή (Κοινή) Απόφαση ή συνδυασμό των ανωτέρω. Στην περίπτωση της νομοθεσίας περί αποβλήτων πλοίων, η διαδικασία είναι πιο περίπλοκη λόγω του γεγονότος ότι η διαχείριση των αποβλήτων επί των πλοίων υπόκειται στις συμβάσεις του Διεθνούς Ναυτιλιακού Οργανισμού (IMO) μέχρι την παράκτια παράδοσή τους, όπου άλλες συμβάσεις ή νομοθετικές πράξεις τίθενται σε ισχύ.

2 ΘΕΣΜΙΚΑ ΠΛΑΙΣΙΑ

2.1 Διεθνές δίκαιο

Για την προστασία του θαλάσσιου περιβάλλοντος και την πρόληψη της ρύπανσης από τα πλοία εγκρίθηκε και τέθηκε σε ισχύ από τον Διεθνή Ναυτιλιακό Οργανισμό (IMO 2017) η Διεθνής Σύμβαση MARPOL 73/78 . Σύμφωνα με τη Σύμβαση, οι ροές αποβλήτων που παράγονται στα πλοία εν πλω και κατά τη διάρκεια των εργασιών φορτίου πρέπει να υποβάλλονται σε επεξεργασία είτε επί του σκάφους είτε μέσω παράδοσης στην ξηρά. Η αρχική έκδοση της σύμβασης MARPOL 73/78 έχει τροποποιηθεί πολλές φορές, ενώ σχεδιάζονται και είναι προγραμματισμένες νέες τροποποιήσεις.

Κατά την Σύμβαση MARPOL 73/78 οι κανονισμοί και οι οδηγίες για τη διαχείριση των αποβλήτων και των υπολειμμάτων χωρίζονται σε έξι παραρτήματα τα ακόλουθα: Σε παρένθεση δίνονται οι ημερομηνίες που τέθηκαν σε ισχύ.

- Παράρτημα Ι: Πετρελαιοειδή Απόβλητα (02/10/1983)
- Παράρτημα ΙΙ: Επιβλαβείς χύδην ουσίες (01/07/1992)

- Παράρτημα III: Επιβλαβείς ουσίες σε συσκευασμένη μορφή (27/09/2003)
- Παράρτημα IV: Λύματα (31/12/1988)
- Παράρτημα V: Στερεά Απόβλητα (31/12/1988)
- Παράρτημα VI: Ουσίες αέριας ρύπανσης –Έλεγχος αερίων εκπομπών (19/05/2005)

Όσον αφορά το Παράρτημα III για την παράδοση των συσκευασμένων επιβλαβών ουσιών καθ ύλην αρμόδιος είναι ο πλοίαρχος του πλοίου και έχει το δικαίωμα να παραδώσει τα απόβλητα αυτά όπου ίδιος επιθυμεί.

Επίσης Σημειώνεται ότι το Παραρτημα V Στερεά απόβλητα χωρίζεται σε 9 υποκατηγορίες. α) πλαστικά, β) απορρίμματα τροφίμων, γ) οικιακά απόβλητα (π.χ. προϊόντα από χαρτί, κουρέλια, γυαλί, μέταλλα, μπουκάλια, κλπ.), δ) μαγειρικά ελαία, ε) Στάχτες αποτεφρωτήρων, στ) Λειτουργικά απόβλητα, ζ) Κατάλοιπα φορτίου, η) Σφάγια ζώων, i) Αλιευτικά εργαλεία.

Επιπλέον από 1-1-2018 τέθηκε εν μέρει σε ισχύ ο Κώδικας για τα Διεθνή Θαλάσσια Επικίνδυνα Εμπορεύματα, -International Maritime Dangerous Goods (IMDG) Code. (IMO 2006)-. Ο Κώδικας αυτός διαχωρίζει τα επικίνδυνα σε 9 κλάσεις τις ακόλουθες: Κλάση 1 – Εκρηκτικά, Κλάση 2 – Αέρια, Κλάση 3 - Εύφλεκτα υγρά, Κλάση 4 - Εύφλεκτα στερεά και άλλες εύφλεκτες ουσίες, Κλάση 5 - Οξειδωτικές ουσίες και οργανικά υπεροξείδια, Κλάση 6 - Τοξικές και μολυσματικές ουσίες, Κλάση 7 - Ραδιενεργό υλικό, Κλάση 8 - Διαβρωτικές ουσίες και Κλάση 9 - Διάφορες επικίνδυνες ουσίες και αντικείμενα.

Για την ασφαλή παράδοση στην ξηρά των αποβλήτων πλοίου απαιτείται η ύπαρξη ενός Σχεδίου Παραλαβής και Διαχείρισης αυτών ανά λιμένα καθώς και οι αναγκαίες εγκαταστάσεις παραλαβής των αποβλήτων. Για την διευκόλυνση των Κρατών Μελών στην ενσωμάτωση της MARPOL 73/78 στους Εθνικά τους Δίκαια, δημοσιεύθηκε η Εγκύκλιος του Διεθνούς Ναυτιλιακού Οργανισμού MEPC.1/Circ.834. (IMO 2014)

Αναφέρεται επίσης η προσφάτως τεθείσα σε ισχύ Σύμβαση (BWM) (IMO 2004) για την Διαχείριση του Έρματος και των ιζημάτων των πλοίων, η οποία εγκρίθηκε στις 13 Φεβρουαρίου 2004 και τέθηκε σε ισχύ στις 8 Σεπτεμβρίου 2017.

2.2 Ευρωπαϊκό δίκαιο

Οι υποχρεώσεις των κρατών μελών για τα απόβλητα και τα υπολείμματα από τα πλοία είναι: α) η αποτελεσματική παράδοση τους στην ξηρά, β) η επεξεργασία τους και γ) η τελική διάθεσή τους. Στην Ευρωπαϊκή Ένωση, η επεξεργασία και η τελική διάθεση των αποβλήτων διέπονται από τις πολιτικές της ΕΕ για την προστασία του περιβάλλοντος και είναι το κύριο θέμα της οδηγίας 2008/98 /ΕΚ, όπως τροποποιήθηκε από την οδηγία (ΕΕ) 2018/851. Η κατάταξη των αποβλήτων γίνεται σε 20 βασικές κατηγορίες και υπάρχει επιπλέον διαχωρισμός βάση των εξαψήφιων κωδικών ΕΚΑ. Όπως φαίνεται η κατηγοριοποίηση είναι πολύ πιο λεπτομερής από ότι επιβάλει η MARPOL73/78. Η αποτελεσματική παράδοση στην ξηρά αποτελεί αντικείμενο της οδηγίας 2000/59/ΕΕ (OJEC, L 332 / 28.12.2000), σχετικά με τις λιμενικές εγκαταστάσεις παραλαβής αποβλήτων πλοίων και υπολειμμάτων φορτίου.

Η Ανακοίνωση της Επιτροπής (2016 / C 115/05) με τίτλο «Κατευθυντήριες γραμμές για την ερμηνεία της Οδηγίας 2000/59/ΕΚ.»,(OJEC 2000) εκδόθηκε για την ενσωμάτωση της εγκυκλίου MEPC.1/Circ.834 του IMO στις Εθνικές Νομοθεσίες.

Η Οδηγία 2000/59 / ΕΕ αναφέρεται αποκλειστικά στα παραρτήματα I, IV και V των αποβλήτων πλοίου και καταλοίπων φορτίου κατά MARPOL 73/78 και αφορά *«α) όλα τα πλοία, συμπεριλαμβανομένων των αλιευτικών σκαφών και των σκαφών αναψυχής, ανεξάρτητα από τη σημαία τους, στο λιμένα κράτους μέλους, εξαιρουμένου κάθε πολεμικού πλοίου, βοηθητικού πολεμικού ναυτικού ή άλλου πλοίου που ανήκει ή διοικείται από ένα κράτος και χρησιμοποιείται, προς το παρόν, μόνο για κυβερνητική μη εμπορική υπηρεσία και β) όλους τους λιμένες των κρατών μελών που επισκέπτονται κανονικά τα πλοία που εμπίπτουν στο πεδίο εφαρμογής του στοιχείου α).»*

Η υποχρέωση για την εκπόνηση σχεδίου Παραλαβής και Διαχείρισης αποβλήτων (ΣΠΔ) περιλαμβάνεται στην Οδηγία. Σύμφωνα με την Οδηγία, τα εν λόγω σχέδια αναθεωρούνται τουλάχιστον ανά τριετία.

Η ECORYS (2017), εκπόνησε μελέτη για την ΕΕ, η οποία αξιολογεί τον αντίκτυπο και τις προκλήσεις της εφαρμογής της οδηγίας 2000/59 / ΕΕ. Διαπιστώθηκαν δύο κύρια προβλήματα, συγκεκριμένα: α) Η απόρριψη σημαντικού τμήματος των αποβλήτων στη θάλασσα και β) ο διοικητικός φόρτος.

Πρόσφατα επίσης τέθηκε σε ισχύ ο κανονισμός (ΕΕ) 2017/352 (OJEC 2017) για τη θέσπιση πλαισίου παροχής λιμενικών υπηρεσιών και κοινούς κανόνες για τη χρηματοοικονομική διαφάνεια των λιμένων. Οι διατάξεις του κανονισμού επηρεάζουν τις υπηρεσίες συλλογής αποβλήτων πλοίων και καταλοίπων φορτίου απελευθερώνοντας σημαντικά την συγκεκριμένη αγορά στους λιμένες που ανήκουν στο Διευρωπαϊκό Δίκτυο Μεταφορών όπως έχει ορισθεί στον Κανονισμό 1315/2013 ΕΕ/ (OJEC 2013)

Τον Ιανουάριο του 2018 δημοσιεύθηκε η πρόταση οδηγίας σχετικά με τις λιμενικές εγκαταστάσεις παραλαβής αποβλήτων από πλοία που θα καταργεί την οδηγία 2000/59 / ΕΚ και θα τροποποιεί τη οδηγίας 2009/16 / ΕΚ και την οδηγία 2010/65 / ΕΕ. Τέλος, η Επιτροπή Μεταφορών και Τουρισμού του Ευρωπαϊκού Κοινοβουλίου ενέκρινε τον περασμένο Ιούνιο και Οκτώβριο τροπολογίες στην προαναφερόμενη πρόταση.

2.3 Εθνικό δίκαιο

Στην Ελλάδα, η ενσωμάτωση της Σύμβασης MARPOL73/78 και της Οδηγίας 2000/59 / ΕΕ έγινε με την Κοινή Υπουργική Απόφαση (ΚΥΑ) 8111.1 /41/2009 ΦΕΚ (Β412), όπως ισχύει σήμερα και βρίσκεται υπό αναθεώρηση αναμένοντας την νέα οδηγία, μη έχοντας ενσωματώσει την Απόφαση της Επιτροπής. Στην Ελλάδα τα απόβλητα των πλοίων διαχωρίζονται σε υγρά και στερεά. Για την εφαρμογή της ΚΥΑ το ΥΝΑΝΠ έχει εκδώσει διευκρινιστικές εγκυκλίους.

Υπόχρεοι στο να διαθέτουν εγκαταστάσεις παραλαβής αποβλήτων και καταλοίπων πλοίων είναι οι λιμένες Διεθνούς ενδιαφέροντες, εθνικής σημασίας και Μείζονος Ενδιαφέροντος σύμφωνα με τις ΚΥΑ 8111.1 /41/2009 Παράρτημα ΙΙΙ και ΚΥΑ 8315.2/02/07 ΦΕΚ(Β202). Επίσης υπόχρεοι είναι οι Τουριστικοί και οι Ιδιωτικοί λιμένες.

Για την εναρμόνιση της ελληνικής νομοθεσίας με τον Κανονισμό 352/2017 ΕΕ, όσον αφορά την συγκεκριμένη υπηρεσία, ψηφίσθηκε το άρθρο 105 του Νόμου 4504/2017 (ΦΕΚ., 184 Α/29.11.2017) με το οποίο απελευθερώνεται η συγκεκριμένη αγορά. Τα προβλήματα που προέκυψαν καθιστούν δύσκολη έως αδύνατη την εφαρμογή του ενώ ήδη έχουν εμφανισθεί τροποποιήσεις του άρθρου. Μέχρι το 2017 η επιλογή αναδόχου παρόχου της συγκεκριμένης υπηρεσίας γινόταν μέσω μειοδοτικού διαγωνισμού για 2 κατηγορίες αποβλήτων (υγρά και στερεά). Σήμερα σύμφωνα με τον Ν.4504/2017, τα 25 λιμάνια που είναι ενταγμένα στο Διευρωπαϊκό Δίκτυο Μεταφορών είναι υποχρεωμένα να διατηρούν μητρώο εγκεκριμένων Παρόχων ώστε να υπάρχει η δυνατότητα επιλογής από τους χρήστες.

3 ΑΝΑΜΕΝΟΜΕΝΕΣ ΑΛΛΑΓΕΣ ΣΤΗΝ ΝΕΑ ΟΔΗΓΙΑ

Η πρόταση για την νέα οδηγία, όσον αφορά τις λιμενικές εγκαταστάσεις παραλαβής των αποβλήτων πλοίων και των καταλοίπων φορτίου, προκρίθηκε να βρίσκεται πιο κοντά στις κατευθυντήριες γραμμές της MARPOL 73/78. Οι σημαντικότερες αλλαγές που διαφαίνονται και που είναι αντικείμενο προς συζήτηση; είναι οι παρακάτω:

- Στην νέα οδηγία θα περιλαμβάνεται η παραλαβή αποβλήτων πλοίου και καταλοίπων φορτίου των Παραρτημάτων I, II, IV, V και VI της MARPOL 73/78. (Τα Παραρτήματα II και VI δεν συμπεριλαμβανόταν στην Οδηγία 2000/59 / ΕΕ.
- Αλλαγές στους ορισμούς – όρους, και στην μορφή (φόρμα) των Παραρτημάτων της Οδηγίας ώστε να είναι σε συμφωνία με τον ΙΜΟ και μείωση του διοικητικού φόρτου
- Επιβάλλεται η ύπαρξη εγκαταστάσεων παραλαβής αποβλήτων σε όλους τους λιμένες και όχι σε ορισμένους όπως ίσχυε μέχρι σήμερα και ήταν στην διακριτική ευχέρεια του κράτους μέλους
- Αλλαγές στις επιθεωρήσεις
- Τα τέλη αντικαθίστανται από συστήματα ανάκτησης του κόστους
- Ενσωματώνεται η Σύμβαση για την Διαχείριση του Έρματος του ΙΜΟ σύμφωνα με απόφαση της Επιτροπής Μεταφορών και Τουρισμού του Ευρωκοινοβουλίου

- Δίνεται ιδιαίτερη έμφαση στην μείωση της ρίψης απορριμμάτων στην θάλασσα

Τέλος σημειώνεται ότι τα απόβλητα ναυπηγείων δεν θα συμπεριλαμβάνονται στην νέα οδηγία.

4 Η ΕΛΛΗΝΙΚΗ ΑΓΟΡΑ

4.1 Ζήτηση

Σήμερα στην Ελλάδα υπάρχουν περισσότερες από χίλιες λιμενικές εγκαταστάσεις εκ των οποίων περίπου οι 900 διαθέτουν φορέα διαχείρισης, ενώ περισσότερες από 250 είναι «ορφανές» . Υπόχρεες στην παροχή της συγκεκριμένης υπηρεσίας και στην σύνταξη Σχεδίου Παραλαβής και Διαχείρισης Αποβλήτων πλοίου και καταλοίπων φορτίου, (το οποίο δύναται να είναι και περιφερειακό συμπεριλαμβάνοντας περισσότερες λιμενικές εγκαταστάσεις,) είναι οι 57 λιμένες Διεθνούς Ενδιαφέροντος, Εθνικής σημασίας και Μείζονος Ενδιαφέροντος σημασίας , περίπου 50 Τουριστικοί λιμένες και περίπου 60 ιδιωτικές εγκαταστάσεις – Τερματικά, συνολικά 167 λιμενικές εγκαταστάσεις στο σύνολο των 1060.

Βάσει στοιχείων του Υπουργείου Ναυτιλίας και Νησιωτικής Πολιτικής (ΥΝΑΝΠ), (Γιαντσή, 2018) στο Υπουργείο , το οποίο είναι υπεύθυνο για την αδειοδότησή τους ήταν κατατεθειμένα 108 Σχέδια, εκ των οποίων περισσότερα από τα μισά ήταν υπό αναθεώρηση, αφού αυτό απαιτείται κάθε τρία (3) έτη. Σημειώνεται ότι υπάρχουν υπόχρεες λιμενικές εγκαταστάσεις υπό κρατική διαχείριση οι οποίες δεν διαθέτουν Σχέδιο Παραλαβής και Διαχείρισης αποβλήτων πλοίων.

4.2 Προσφορά

Όπως έχει ήδη αναφερθεί η παραλαβή των αποβλήτων των πλοίων χωρίζεται σε στερεά και υγρά.

Στην κατηγορία των στερεών σήμερα δραστηριοποιούνται βασικά 4 εταιρείες, οι οποίες έχουν την απαιτούμενη εμπειρία. Στερεά απόβλητα πλοίων παραλαμβάνουν επίσης σε ορισμένες νήσους και Δημοτικές υπηρεσίες. Εκ των τεσσάρων εταιριών η μια είναι δεσπόζουσα κατέχοντας μερίδιο αγοράς μεγαλύτερο του 50%. Γενικά υπάρχει μονοπωλιακή τάση δραστηριοποίησης των εταιρειών ανά περιοχή. Όσον αφορά την κατηγορία των υγρών αποβλήτων πλοίου και καταλοίπων φορτίου εμφανίζονται να δραστηριοποιούνται 6 εταιρίες. Μέχρι πρότινος στον τομέα δραστηριοποιούνταν 4 εταιρείες. Μετά το άνοιγμα της αγοράς εμφανίσθηκαν ακόμη 2 εταιρείες, με πολύ μικρό μερίδιο. Μια εταιρία δεσπόζουσα στην Βόρειο Ελλάδα εμφανίζεται να παρέχει και τις δύο υπηρεσίες (στερεά και υγρά). Σημειώνεται ότι δεν παρουσιάζονται στοιχεία για τους Τουριστικούς και ιδιωτικούς λιμένες. Και στα υγρά υπάρχει δεσπόζουσα εταιρία με εγκαταστάσεις επεξεργασίας των πετρελαϊκών αποβλήτων.

5 ΠΡΟΒΛΗΜΑΤΑ ΣΤΗΝ ΕΛΛΗΝΙΚΗ ΑΓΟΡΑ

Στην συνέχεια παρουσιάζονται και σχολιάζονται βασικά προβλήματα της ελληνικής αγοράς και πιθανά προβλήματα που θα προκύψουν από την Νέα Οδηγία:

- Πολλές λιμενικές εγκαταστάσεις, εκ των οποίων οι περισσότερες είναι νησιωτικές, με αποτέλεσμα οι πάροχοι που δραστηριοποιούνται σε αυτές να αντιμετωπίζουν ιδιαίτερα προβλήματα διαχείρισης, επεξεργασίας και τελικής διάθεσης, καθόσον για την περαιτέρω διαδικασία απαιτείται η μεταφορά των αποβλήτων. Σήμερα υπόχρεες στην συλλογή αποβλήτων πλοίων είναι 167 λιμενικές εγκαταστάσεις. Το πρόβλημα θα εξογκωθεί όταν προστεθεί το σύνολο των λιμενικών εγκαταστάσεων. Οι περισσότεροι φορείς διαχείρισης στα μικρά λιμάνια ανήκουν στην Τοπική Αυτοδιοίκηση (Δημοτικά Λιμενικά Ταμεία) και είναι το λιγότερο υποστελεχωμένοι.
- Υπάρχει ολιγοπώλιο στην αγορά. Ακόμη και στην περίπτωση που απελευθερωθεί η υπηρεσία οι εν δυνάμει πάροχοι με σχετική εμπειρία είναι λίγοι. Εξάλλου λόγω της νησιωτικότητας οι παρεχόμενες υπηρεσίες είναι ακριβές με κίνδυνο Υποχρέωσης παροχής δημόσιας υπηρεσίας.
- Τα Σχέδια Παραλαβής και Διαχείρισης (ΣΠΔ) αποβλήτων συντάσσονται χωρίς προδιαγραφές, διαρκούν μόνο 3 έτη και στην συνέχεια χρήζουν αναθεώρησης. Στην περίπτωση που υποχρεωθούν όλες οι λιμενικές εγκαταστάσεις να συντάξουν ΣΠΔ ο διοικητικός φόρτος στο ΥΝΑΝΠ αναμένεται τεράστιος.
- Η μη διαλογή των απορριμμάτων. Τα στερεά απόβλητα δεν παραδίδονται διαχωρισμένα κατά

κατηγορίες όπως επιθυμούν οι εταιρείες αλλά για λόγους ευκολίας παραδίδονται όλα μαζί με συνέπεια αυξημένες χρεώσεις, προβλήματα διαλογής κλπ

- Οι εξαιρέσεις που υπάρχουν δεν επαρκούν. Ιδιαίτερα προβλήματα απαντώνται στα νησιά με αυξημένη κίνηση κρουαζιέρας και ειδικότερα στην περίπτωση που τα πλοία έχουν λιμάνι τελικού απόπλου Ευρωπαϊκής Ένωσης τα συγκεκριμένα νησιά, οπότε τα πλοία είναι υποχρεωμένα να παραδώσουν το σύνολο των αποβλήτων τους.
- Το νέο αναμενόμενο θεσμικό πλαίσιο, τόσο Ευρωπαϊκό όσο και Εθνικό, το οποίο ακόμη δεν έχει διαμορφωθεί, αναμένεται να διευρύνει το αντικείμενο και θα επιφέρει αλλαγές και στον τρόπο εκτίμησης των χρεώσεων των υπηρεσιών. Η μη σύνδεση του μέχρι τώρα με τις κατευθύνσεις του IMO δημιουργεί προβλήματα.

6 ΠΡΟΟΠΤΙΚΕΣ ΣΤΗΝ ΕΛΛΗΝΙΚΗ ΑΓΟΡΑ

Παρά τα υπάρχοντα και διαφαινόμενα προβλήματα με το νέο θεσμικό πλαίσιο δημιουργούνται πολλά υποσχόμενες προοπτικές σε συνδυασμό με την περαιτέρω βελτίωση του Θεσμικού Πλαισίου όπως:

- Η απελευθέρωση της αγοράς θα επιφέρει την αύξηση του ανταγωνισμού, είσοδο νέων εταιρειών στην αγορά , καλύτερες τιμές και υπηρεσίες, νέους χρήστες.
- Οι αναμενόμενοι αυστηρότεροι κανόνες θα βελτιώσουν την προστασία του περιβάλλοντος και θα ελαχιστοποιήσουν τις απορρίψεις αποβλήτων στον θαλάσσιο αποδέκτη.
- Ο διαχωρισμός των στερεών σε υποκατηγορίες θα αυξήσει την ανακύκλωση και τους δείκτες αυτής. Η εφαρμογή και στους αλιευτικούς λιμένες θα μειώσει τόσο το οργανικό όσο και το ανόργανο φορτίο που απορρίπτεται στην θάλασσα.
- Έρευνα, Ανάπτυξη, Καινοτομία, νέες θέσεις εργασίας κ.λπ. Στα πλαίσια αυτά θα πρέπει να αναπτυχθούν μέθοδοι για την επεξεργασία των αποβλήτων εν πλώ, να κατασκευασθούν νέες εγκαταστάσεις στην ξηρά για την υποδοχή των αποβλήτων, μεταξύ αυτών εγκαταστάσεις και για την επεξεργασία του έρματος.

7 ΣΥΜΠΕΡΑΣΜΑΤΑ

Η αγορά της συλλογής και διαχείρισης αποβλήτων πλοίων και καταλοίπων φορτίου είναι μια δυναμική αγορά με πολλές ευκαιρίες ανάπτυξης στην χώρα μας εφόσον επιλυθούν σημαντικά θεσμικά προβλήματα. Προβλήματα έχουν εμφανιστεί όχι μόνον στην Ελληνική αγορά, η οποία λόγω ιδιαιτεροτήτων εμφανίζεται πιο προβληματική και λιγότερο ανταγωνιστική σε ορισμένες περιπτώσεις. Θα πρέπει να δοθούν τα εργαλεία ώστε να επιλυθούν τα δομικά προβλήματα και να αναπτυχθούν ευκαιρίες για την ανάπτυξη του κλάδου και την προστασία του περιβάλλοντος.

Βιβλιογραφικές Αναφορές

ECORYS (2017) 'Supporting Study for an Impact Assessment for the Revision of Directive 2000/59/EC on Port Reception Facilities', Final Report, European Commission.

Giantsi Th., Tsioupli S., Flegkas K., Koufos P. and Angelopoulos J., 2018, "Collection and Handling of Ship Waste and Cargo Residues in Greece: Present and Future", Book of Proceedings, International Conference Protection and Restoration of the Environment XIV, Thessaloniki, 3-6 July 2018.

IMO (2004) BWM: International Convention for the Control and Management of Ship's Ballast Water and Sediments.

IMO (2006), IMDG.1: International Maritime Dangerous Goods Code (Volume 1).

IMO (2014) MEPC/834 "Consolidated Guidance for Port Reception Facility Providers and Users"

IMO (2017) MARPOL Consolidated Edition 2017.

Official Journal of the European Communities (OJEC) (2000) 'Directive 2000/59/EU on Port Reception Facilities (PRF) for ship-generated waste and cargo residues'.

OJEC (2016) 'Commission Notice (2016/C 115/05) Guidelines for the interpretation of Directive 2000/59/EC on port reception facilities for ship generated waste and cargo residues'.

OJEC (2017) 'Regulation (EU) 2017/352 of the European Parliament and of the Council of 15 February 2017 establishing a framework for the provision of port services and common rules on the financial transparency of ports.

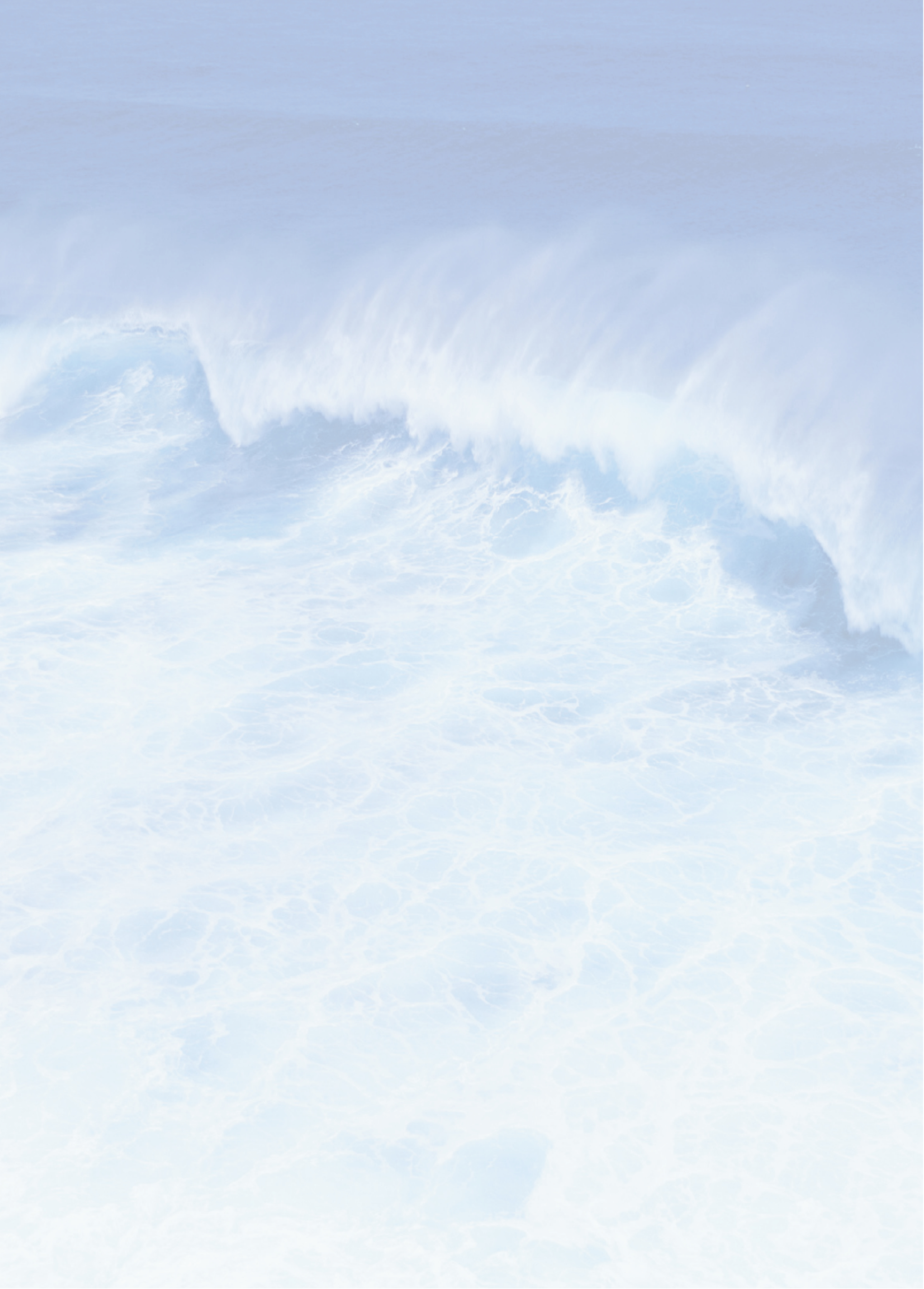

SPECIAL SESSION IV - SUSTAINABLE PORTS

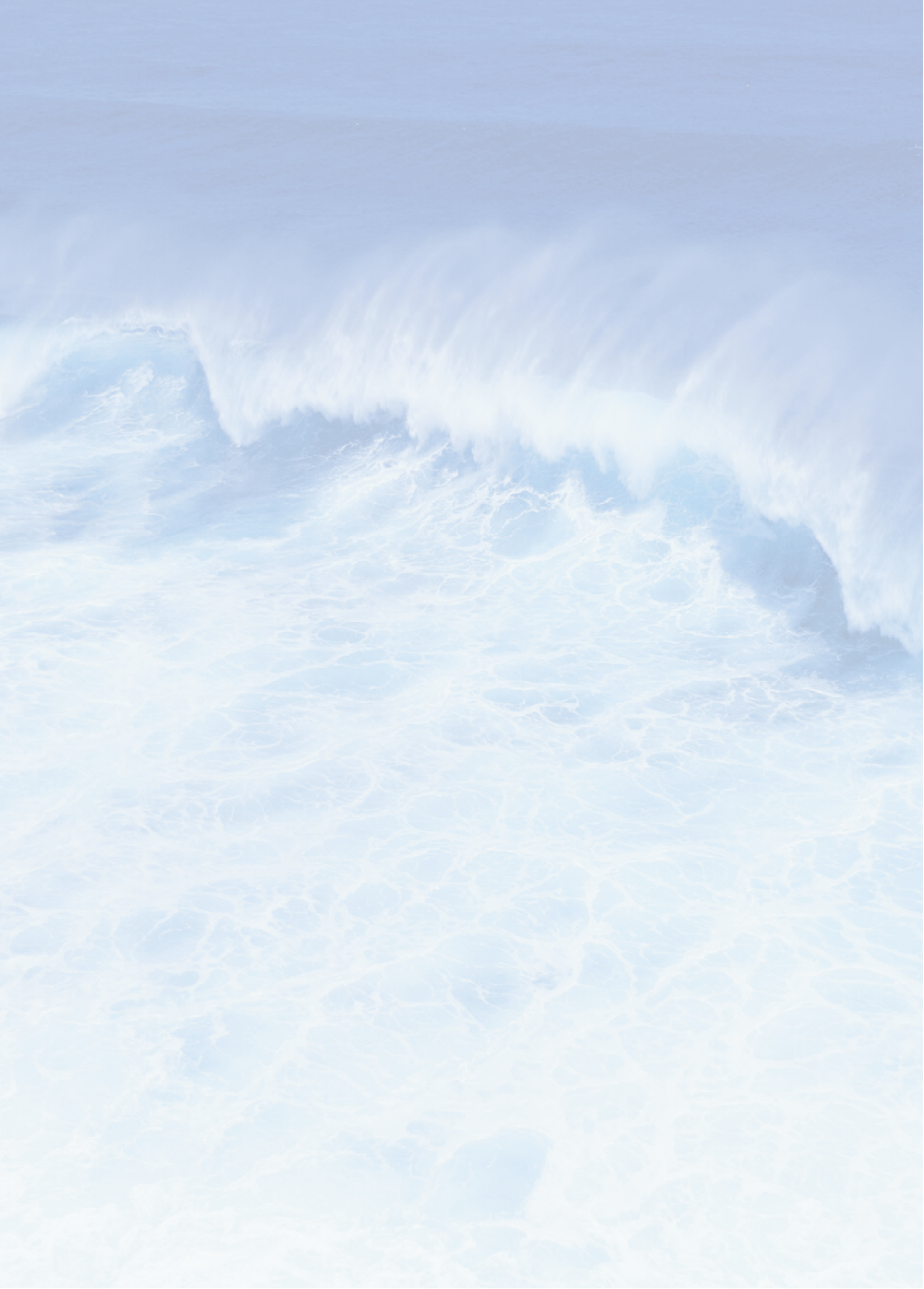

Environmentally friendly breakwater design

D. Carevic[*], D. Bujak, G. Loncar

Faculty of Civil Engineering University of Zagreb, Kaciceva 26, 10000 Zagreb, Croatia
[*]Corresponding author: dalibor.carevic@grad.hr

Abstract

Breakwaters are structures which separate a port basin from surrounding sea water and this way disable natural water renewal. The seas with small tidal ranges are especially endangered by possibility of algal blooms occurrences or generally low water quality. The coastal countries which relay on summer tourism have interest to improve water quality in a city harbors and marinas. This article gives some specific structural measures (breakwater types) for better water renewal in closed basins forced by natural generators: wind, waves and tidal oscillations.

Keywords Flushing culverts, Permeable breakwaters, Pontoon breakwaters, Port water renewal, Transmission coefficient.

1 INTRODUCTION

Water in marinas must be visually clean (no oil, litter, sewage wastes or other traces of pollution). In order to comply with a high environmental standard, it is very important that such ports itself and the water around it are visually clean. Natural phenomena such as algal blooms can look like pollution, without that being really. These requirements are prescribed in a Blue flag's marina criteria manual as a condition for the Blue flag mark awarding. The Blue flag is a popular tourist mark in the world today, which is becoming tourist orientation when choosing a destination. It is today recognizable model of ecological education and public awareness, when it comes to sea and coastline concerns, especially for the beaches and marinas. Blue Flag Intellectual Property and International Leader of this program is the Foundation for Environmental Education - FEE, founded by the Council of Europe in 1981. This criterion is not only applicable for marinas but also for city communal ports or any small enclosed water bodies in city centers.

Ports in seas with a larger tidal range rely on the process of water renewal where significant volume of water in port is changed in one tidal cycle. In the seas with small tidal range (as the Mediterranean Sea, Baltic, Caribbean sea, Black sea, etc.) the water in ports suffer from stagnation and lower water quality (Gómez et al. 2017). Especially are endangered smaller water areas distant from port's entrance where tidal circulation does not have influence. One undesirable example is shown at Figure 17.

Measures which could be used for improvement of the water circulation in ports are generally separated in passive and active measures (Carevic et al. 2019). The passive measures include design of the coastal structures such as the layout geometry of the port, the width and position of the port entrance, the sea depth within the port, the slope of the sea bottom and the use of breakwater structures which improve water circulation. Regarding active circulation improvement measures, pumps and aerators are rarely used because of the costs of operation and maintenance.

This article gives some specific structural measures (breakwater types) which application can improve the renewal of seawater in closed basins forced by natural generators: wind, waves and tidal oscillations. All these natural generators make water mass into the movement and improve water exchange between outer and inner water body. Depending on the intensity of the each of specific natural generators at some location they contribute in a different extent to the overall volume exchange (Bartolic et al. 2018). The problems with low water quality are often expressed during the warm summer periods when is expected the largest pressure of tourism activities. In summertime the expected intensity of winds and waves is moderate to low thus the main generator are tidal oscillations. But some contribution gives wind through the mixing of the water body in the port and waves by pushing some volume of water through the flushing culverts if they are properly designed.
One of the important conclusions in the paper Carevic et al. 2019, is that overall water exchange in port is strongly dependent on ratio A_e/A_o (A_e-cross section of port entrance, A_o- cross section of openings in breakwater body). It means that for the larger cross section area of the openings in the breakwater body, the overall quality of seawater in port is better. This is especially valid when dominant generator of circulation is wind. From the opposite side a problem related to the enlargement of the openings in the breakwater body is the excessive penetration of wave energy during winter storms which makes questionable the functionality of port. This article

gives some specific breakwater types which might be used with aim for having better water quality in the port basins and their limitations of applicability.

Figure 17 Example of low water quality in the city port Zenta (Split, Croatia)

2 BREAKWATER TYPES

Selection of a breakwater type for some specific location depends on many factors such as foundation soil condition, wave climate, tidal range, type and purpose of the port, water depth, etc. As it is written in the chapter before, for better seawater conditions, the very important is to have larger number of openings in the breakwater body properly positioned. Hereafter the selection of the breakwater types is presented which are suitable for application at locations where water quality in the port is important.

The selection of the breakwater types has been conducted in relation to project deep-water wave heights. Exposed locations (Hs>1,4m, fetch>10km) require massive rubble mound or vertical type breakwaters which could resist to strong wave attacks. In such situations it is recommendable to use flushing culverts as it is presented at Figure 18a. The cross section areas of the flushing culverts should be selected in a such way that functionality of port in the vicinity of flushing culverts is preserved. Transmission coefficients of flushing culverts depends on the type of the flushing culvert. Recommendable types are: circular, rectangular and channel type presented in **Figure 19**. Equations for calculation of the transmission coefficients are given in papers Carevic et al. 2018, 2019 for circular cross section and Tsoukala and Moutzouris 2009 for rectangular cross section. The channel type has still not well enough investigated but due to similarity with submerged breakwater it is possible to use equations for transmission coefficients in the case of such structures (D'Angremond et al 1996).

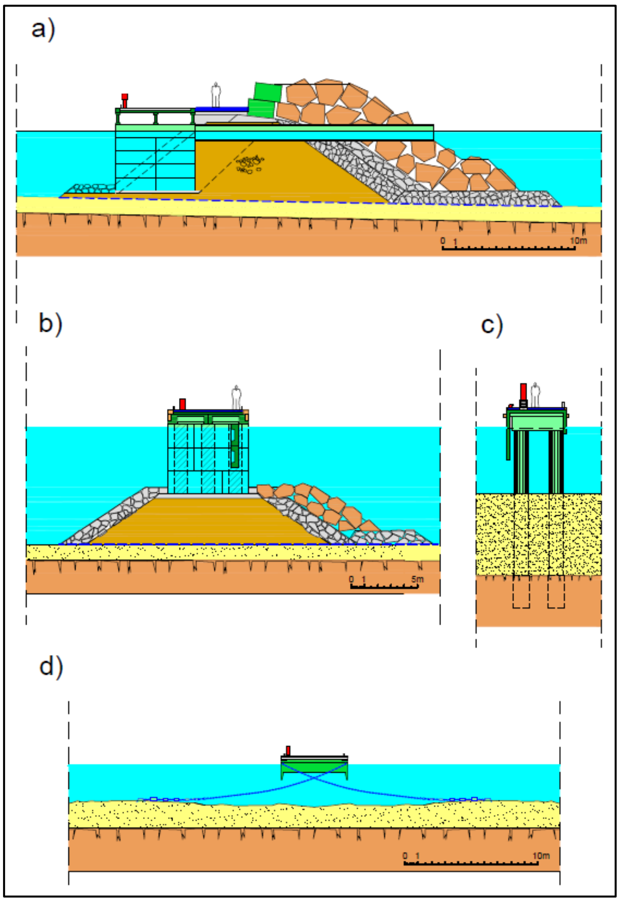

Figure 18 Breakwater cross sections with enabled water circulation

At moderately exposed locations (Hs≤1,2-1,4m, fetch≤5-10km) it is possible to apply permeable breakwaters with immersed concrete curtain. The application of these structures depends on conditions of the foundation soil so it is possible to use structures founded on piles (Figure 18c) or underwater embankment (Figure 18b). These structures could be used in total length of the breakwater or only at one restricted section where smaller wave heights usually occur. A structural problem with breakwater founded on embankment is that it has small weight thus it cannot bear larger horizontal wave forces and problem in the case of the pile founded breakwater is that it became very expensive for depths larger than 10-12m. Transmission below a thin rigid curtain is explained in paper Wiegel 1960 for regular waves.

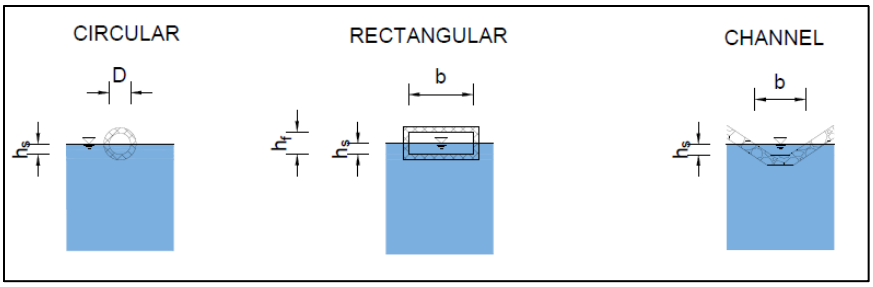

Figure 19 Flushing culverts cross sections

Well protected locations (Hs≤1,1m, fetch≤5km) enable application of pontoon breakwater (Figure 17d) which requires the lowest financial investment and give the best water circulation between closed and surrounding sea. Transmission below pontoon breakwaters is well researched and usually given by manufacturer or it can be found in PIANC (1997). The application of pontoon breakwaters gives a large number of possibilities at the end of a period of exploitation. It is possible to recycle or reuse such breakwater under the relatively low costs.

General conclusion can be given that water renewal in small ports, especially in seas with microtidal range (0,5-1,0m), should have openings in their breakwaters to improve sea exchange with outer water body. In this paper are given three characteristic examples at Figure 20. Each example corresponds to the specific level of port's indentation in the surrounding land. The port indentation can be classified in three categories: open, semi-open and closed type. Due to low level of water exchange in closed type bays the cross section of openings in the breakwater bodies should be the largest. Such bays have low water quality and in such conditions, ports suffer from low water quality either. From the other side it is expectable that in deeply indented bay the wave heights are not significant, so it is possible to predict larger cross section areas of openings without distribution of port functionality or use pontoon breakwaters. In the case of open type, it is expectable that surrounding sea have a good water quality so this way the inner sea of the port has a source of the seawater with a better quality.

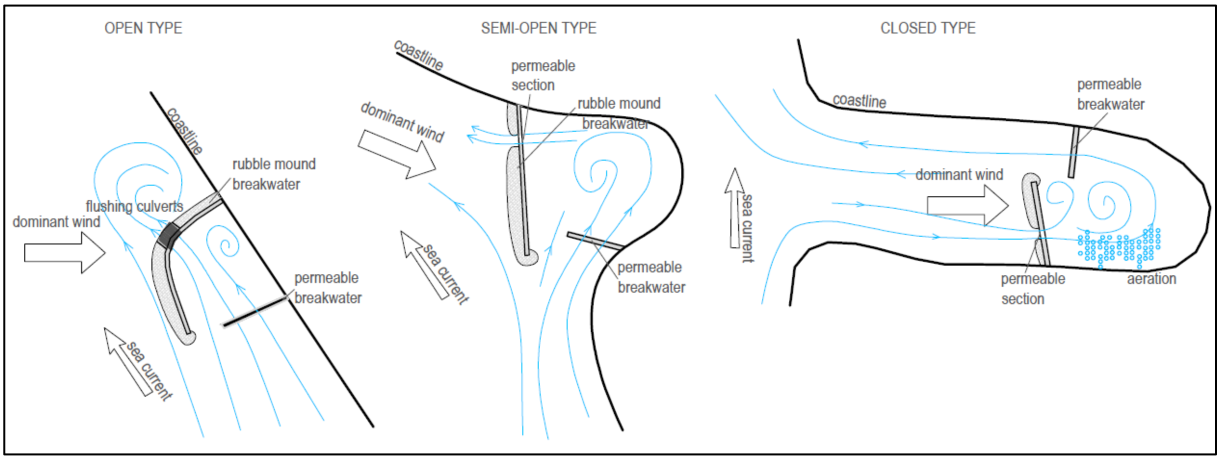

Figure 20 Examples of the breakwater openings construction for ports in microtidal seas

According to the paper Carevic et al. 2019 it was concluded that the ratio A_o/A_e =0.02 to 0.04 secure volume that circulates through the openings of 1-2% of the volume which passes through the entrance of the port which seems as a very small influence to the overall water exchange in the port's water body. But the main strength of such openings is that they, if properly designed, improve water quality in the, so called, "dead zones"; smaller water bodies dislocated from port's entrance. Such dead zones suffer from a low water quality and often give negative impression of the port surroundings.

3 CONCLUSION

Ports which require good seawater quality, such as marinas and small craft harbors, which rely on tourism and endeavor to attract tourists should have acceptable environmental conditions. One of the most hardly achieved is good water quality in the port's basin. This paper gives review of structural measures which could be applied for new ports or existing ones. The application of the presented structural measures depends on the several natural factors which differ from location to location (wind, tidal range, waves). Thus, the proper design of good water circulation requires application of in situ measurements and numerical modeling of water circulation.

The knowledge of the water circulation in ports is still rising and knew researches should be directed to the development of the automatic system of weirs which could control inflow-outflow through the openings.

References

Carevic D, Bujak D, Loncar G, Bartolic I (2019) Use of culverts for improving exchange of seawater in ports. Gradevinar 71, 197-207. DOI: https://doi.org/10.14256/JCE.2527.2018.

Gómez AG, Ondiviela B., Fernández M. and Juanes JA (2017) Atlas of susceptibility to pollution in marinas. Application to the Spanish coast, Mar. Pollut. Bull., vol. 114, no. 1, pp. 239–246.

PIANC (1997) Special Report of the International Comission for Sport and Pleasure Navigation; Supplement to Bulletin No 93, Review of selected standards for floating dock designs.

Wiegel R (1960) Transmission of waves past a rigid vertical thin barrier. J. of the Waterways and harbors division, ASCE, Vol 86, No. WW1, pp1-12.

Carevic D, Mostečak H, Bujak D, and Lončar G (2018): Influence of water-level variations on wave transmission through flushing culverts positioned in a breakwater body, J. Waterw. port Coast. Ocean Eng., vol. 144, no. 5.

Tsoukala VK and Moutzouris, CI (2009) Wave transmission in harbors through flushing culverts, Ocean Eng., vol. 36, no. 6–7, pp. 434–445.

Bartolic I., Loncar G., Bujak D, Carevic D. (2018): The Flow Generator Relations for Water Renewal through the Flushing Culverts in Marinas, Water, vol. 10, no. 7, p. 936, 2018.

Blue flag marina criteria and explanatory notes (2018). In: Blue Flag's Criteria. Foundation for Environmental Education – FEE. Available via https://www.blueflag.global/criteria. (Acessed 15 Apr 2019).

D'Angremond K, der Meer V, and de Jong R, "Wave transmision at low-crested structures," in Proc. ICCE, 1996, pp. 3305–3318.

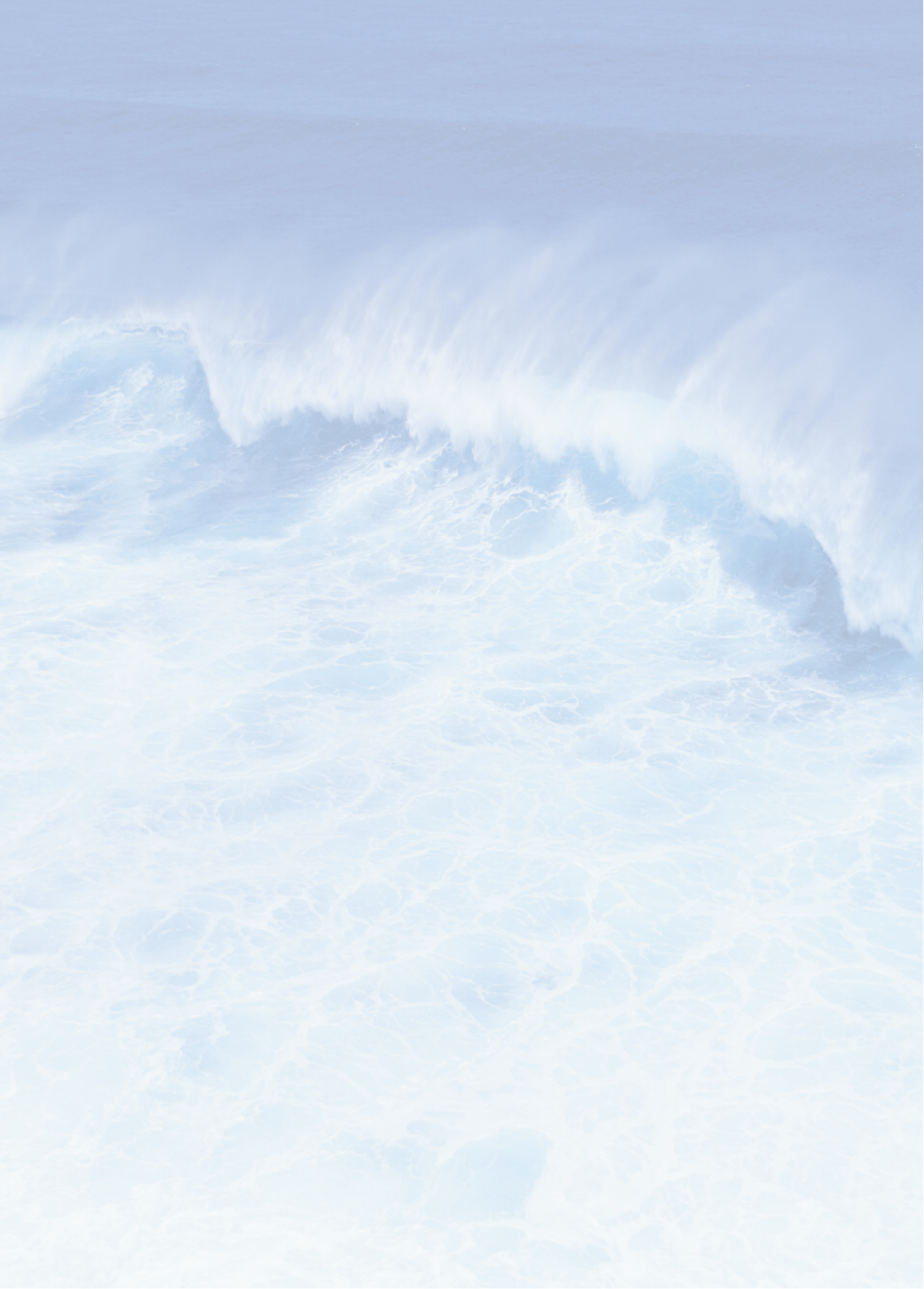

Evaluating the prospect of nearly zero energy ports

N. Sifakis, O. Mavroudis, Th. Tsoutsos*

Renewable and Sustainable Energy Systems Lab, School of Environmental Engineering, Technical University of Crete, Chania, Greece

*Corresponding author: Theocharis.tsoutsos@enveng.tuc.gr

Abstract

Ports are situated in susceptible areas to climate change impacts and operate as central hubs in the transport of raw materials and cargo, and are characterized by high–energy demand and supply activities. The growth of the trade activities and the continuous technological advances on the global market are forcing ports to find new ways to be competitive and to evaluate all the possible actions and means for their optimization and greenification. The overall idea and research interest related to the development of sustainable port infrastructure is totally connected to the essential requirements of the diminishing of the harmful environmental impacts without putting in risk the economic growth within ports. The main objective of this paper is to investigate, analyse and evaluate, through the proposed methodology, various energy data of Rethymno's port. Through the anticipated methodology, a step-by-step process is going to be utilized in order to initially analyse, via statistical methods, and evaluate the available data. The outcomes of the preliminary analysis are going to be used in order to implement the port's model into a specific software and create another brand-new hypothetic model.

Keywords Nearly Zero Energy Ports; Energy Efficiency; Renewable Energy Sources; Energy Saving into ports

1 INTRODUCTION

Within the strategy for competitive, sustainable and secure energy, the European Commission (EC) defined the energy priorities till 2050 and set the priority actions to tackle the challenges of saving energy, accomplishing a market with competitive prices and secure supplies, to address climate change and EU strongly encourages the environmental performance of services and products. (European Commision 2018). Ports are gratified to obey even stricter monitoring and social necessities regarding environmental protection (Acciaro, Ghiara and Cusano 2014).

Environmental aspects also should be converted to a competitive benefit in the future in order to appeal to probable transaction allies and possible stockholders. As such, port authorities should design arrangements to become nearly Zero Energy Ports (nZEP) in the long-term. While this topic is vital, the current research work needs to be expanded and to be further investigated. In cases of ports planning or certain suburb design, where preliminary planning decisions must be taken, some fixed parameters and their relationship with the microclimate are essential to be taken into consideration.(Tsitoura et al. 2016)

On the other hand, both sea vessels and means of transport used nearby, are a major source of pollution. Ports globally are responsible for significant social costs resulting from Greenhouse Gas (GHG) emissions due to the operation of their heavy services. As a result, many port executives have started the implementation of solutions in order to reduce transport costs and possible dilemmas; such actions include both internal measures such as formulating a number of financial incentives and infrastructural facilities to reduce GHG emissions by ships and transport vehicles, as well as initiatives aimed at the modal shift.

Due to the rising awareness on sustainable port development, progressively more knowledge and experience are mandatory in order to decrease the effect of port activities on climate change, as well as the impact of port infrastructures on the natural habitats (ecosystems) and national markets. It is estimated that 20% of the world's power consumption is related to artificial lighting and 1.3% to outdoor lighting. In addition, ports' crucial energy demand is related to lighting energy demand and after thorough research and with the aid of the port's personnel, it was found out that almost 75% of port's energy consumption was related to lighting. For this reason, the energy efficiency of the lighting fixtures and energy management would lessen radically the corresponding energy consumption.

There is significant potential for sustainable technology solutions into ports. Only in Greece, there are 128 ports, of which, 4 are International, 10 are National and the rest 114 are local ports and this enhances the prospect of nZEP in Greece as it is a naval-related country. In order to enhance more the prospect of nZEP, it is indicative that there are more than 3,000 ports in Europe and more than 7,500 ports, worldwide. The port environmental priorities globally, annually are shown for the period 1996 to 2018 are presented in Table 6. (Ecoports, Portopia 2018)

Table 6 Top 10 environmental priorities of European ports during 1996-2018

a/a	1996	2004	2009	2013	2018
1	Port Development (water)	Garbage / Port waste	Noise	Air quality	Air quality
2	Water quality	Dredging operations	Air quality	Garbage / Port waste	Energy consumption
3	Dredging disposal	Dredging disposal	Garbage / Port waste	Energy consumption	Noise
4	Dredging operations	Dust	Dredging operations	Noise	Relationship with local community
5	Dust	Noise	Dredging disposal	Ship waste	Ship waste
6	Port development (land)	Air quality	Relationship with local community	Relationship with local community	Port development (land)
7	Contaminated land	Hazardous cargo	Energy consumption	Dredging operations	Climate change
8	Habitat loss / degradation	Bunkering	Dust	Dust	Water quality
9	Traffic volume	Port development (land)	Port development (water)	Port development (land)	Dredging operations
10	Industrial effluent	Ship discharge (bilge)	Port development (land)	Water quality	Garbage / Port waste

The main goal of this study is the inquiry of all the viable solutions for an nZEP development in Rethymno. Both current and future needs and perspectives are taken into account in order to properly set up and design a nearly Energy Zero Port. Various crucial factors concerning the economic aspect (reducing the operating cost of the harbour), environmental conditions (reducing pollutants coming from GHG emissions of the port and the old town around it) as well as achieving social acceptance and safety, were taken into consideration. This took place in order to ensure that the suggestions will be tangible, sustainable and have a positive impact on the surroundings of the port.

2 METHODOLOGY

Firstly, a thorough literature research and data acquisition was done in order to "create" a solid database; only high-end databases were utilized in order to obtain the reviewed papers such as ScienceDirect, Nature, Google Scholar, and CiteCeerx; as major keywords used "energy ports", "green ports", "ports sustainability", "port's development", "sustainable port infrastructures". By using the available data a line diagram was created demonstrating the trend over the last 2 decades (**Figure 21**). The trend line of the selected papers is almost 1.5 times higher than this of Web of Science which indicates that more and more scientists/researchers and governments across the world due to nZEP and sustainability policies.

As a next step, Rethymno's port was selected as a case study because it is a small to medium port as the majority of ports in Greece and, more importantly, because the research team was able to gather the required information and data from the port's personnel and the responsible authorities. Unfortunately, there was only one smart meter installed on the port facilities and as a result, hourly data was available for only the 1/3 of the total energy consumption. The rest of the energy consumption was available on monthly tables regarding the other 2/3, which were helpful as well.

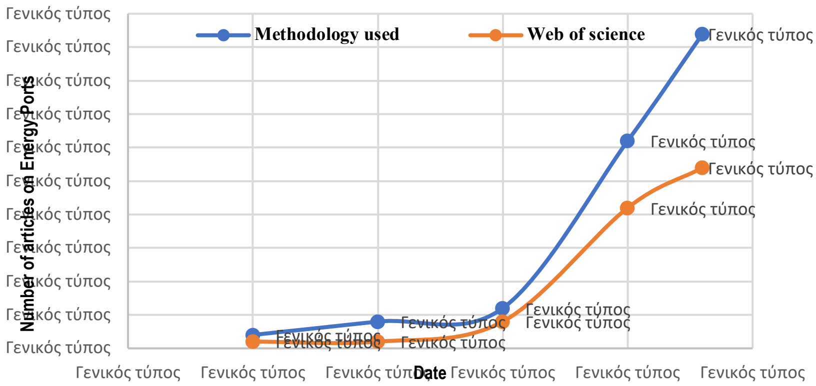

Figure 21 The trend around research regarding energy and sustainability in ports

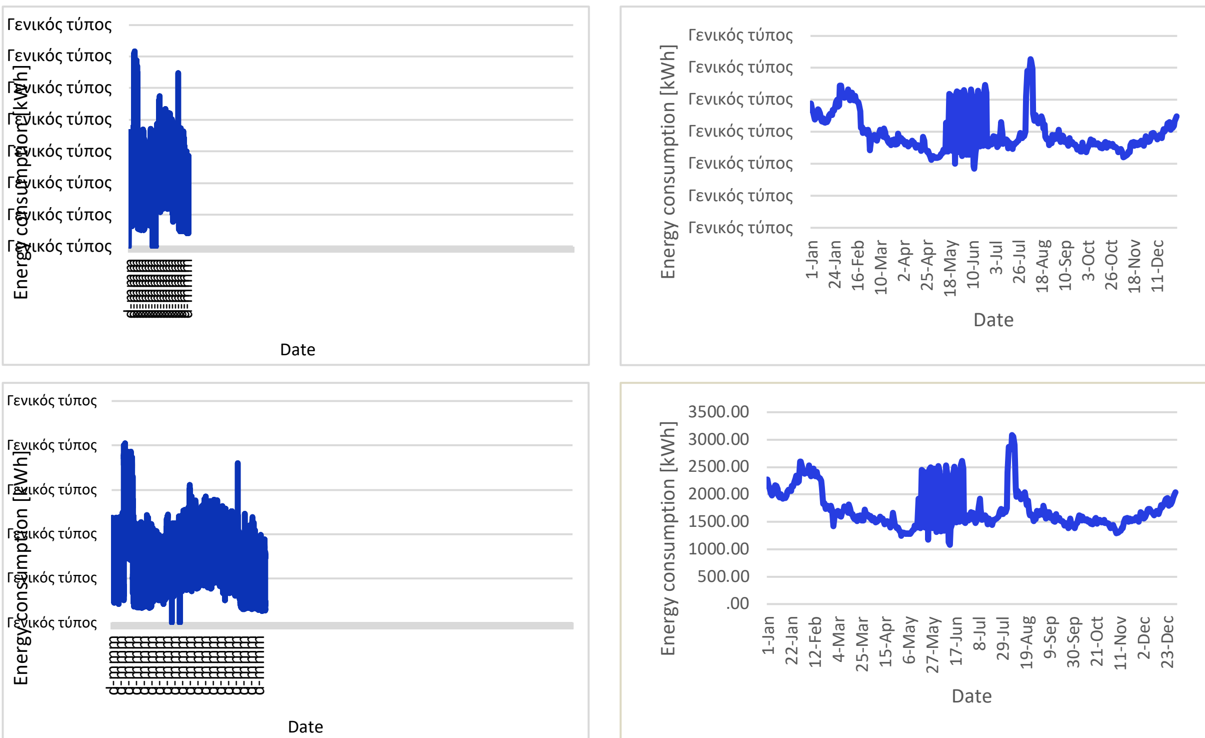

Figure 22 a) Hourly energy consumption of port's marina b) Daily energy consumption of port's marina c) Total hourly energy consumption of port d) Total daily energy consumption of port

The first step was the statistical analysis and create a time series diagram of the hourly energy consumption data of the port's marina. (Fig. 2a) Based on the diagram, it was decided to create a time series on daily basis (Fig.2b). Then, using some approximate methods to factor into the energy consumption the other 2/3 of the energy consumption, two new time series were designed depicting the average hourly and daily total energy consumption of the port infrastructure. (Fig. 2c, 2d respectively). Energy consumption of port is extremely high if someone takes into consideration its activities and the operations that take place there. So, immediate actions have to be taken into consideration in order to fix the current state and improve its ecological footprint and sustainability.

Special emphasis was given to lightning upgrades and implementation of Photovoltaic Systems. To accomplish this intention, resolutions and implementations were examined so as to be in compliance with the features and structures of the old harbour. This was achieved both by researching the existing bibliography and cooperating with the municipality and harbour personnel, who provided all the required data and information.

3 RESULTS

3.1 Lighting equipment

The first thing to do was to replace the old-fashioned equipment with a new one. The most appropriate lamps are LED ones, as their efficiency today is 135 lm/W while on 2020, it is estimated to reach more than 200lm/W and their lifespan is more than 50,000h. The current lightning equipment was selected to be replaced by LED with the same lumen and being complied with the most recent EU legislation regarding lighting in port areas (Standard, European Norme Europeenne Norm 2007), and the specs of the two equipment are presented in **Error! Reference source not found.**

Table 7 Lighting equipment specs before and after the replacement

Location	Type		Lumen	Lumen/W		Power [W]		Pcs	Total consumed energy* [MWh]	
a/a	Before	After		Before	After	Before	After		Before	After
Marina	Na	LED	14000	50	120	300	120	66	86.7	34.7
Venizelou St.	HQI	LED	4500	25	120	250	40	169	185.1	29.6
Marina (Dock)	Hg	LED	8000	55	120	150	70	30	19.7	9.2
Venetian part	Hg	LED	8000	55	120	150	70	51	33.5	15.6
Pedestrian St.	Bollard	LED	3500	30	120	110	30	122	58.8	16.0
Palm lightning	Nar. Beam	LED	3500	50	120	90	30	396	156.1	52.0
Total									**551.9**	**157.2**

*For the calculation of the consumed energy, 12 operation hours per day for 365 days were considered

Only by replacing the old-fashioned energy demanding lighting equipment with LED ones, the energy savings are almost 383MWh/year which can be translated to 57.402€/year (average energy cost of 0.15euros/kWh was taken into consideration) and 258tn CO_{2eq}/year (The CO_{2eq} factor for Crete equals to 0.67377kg $_{CO2/k}$Wh) and a payback period of 2.0 years.

3.2 Implementation of PV Systems

In order to cover the energy needs of the whole port by using "green energy", it was decided that the most appropriate technology was this of the PV systems as they are noiseless and the impact on the environment is relatively low and the technical and potential problems that may occur, are not great if everything is set up following the instructions.

Table 8 Proposed PV technologies specs and their simulation results

Location	Type	Installed Power[kW]	kWh/kWp	Perform. ratio	Energy [MWh/year]
Administration building	Si-Mono	74.4	1,428.6	80.2	106.3
Venetian part building	Si-Mono	79.8	1,440.4	80.9	114.9
Proposed carport	Si-Mono	99.6	1,498.5	84.1	149.3
Total		**249**			**366.8**

At this case, it is of high importance to avoid disturbance of the residents, as the port facilities are inside the residential area and the proposed structures are not too big to disturb the visibility of the area, they may go unnoticed, at all. Fulfilling this purpose, only 3 areas of the ports were selected in order to place the PV panels on them, (a) the Administration building, (b) the Venetian Port building and (c) a new (is proposed to be constructed as a part of the PV system) carport in the Marina's area of the port where a simple parking will be enhanced and two Electric Vehicles (EV) chargers will be installed as well. The specs of the systems, as well as some results of their simulation using helioscope software, are presented into **Error! Reference source not found.**. In the third proposed construction, the E V charging energy will come from RES, enhancing their ecological footprint and will promote also the city with the creation of a "charging station network using RES" (Virtual Net Metering and green energy offset).

3.3 Achieving the goal of converting the port to nZEP

The initial port consumption was 638.5MWh/ year, after replacing the old lighting equipment with LED ones, the port consumption decreased to 255.8MWh/year and after the implementation of the EV chargers, the final port energy consumption increased to 366.5MWh/year. On the other hand, the PV systems that are proposed to be installed will produce 366.8MWh/year (covering the full amount of energy consumed) and will cost a great amount of money [for the PV systems, all the required costs are calculated (Grid-connection, installation, supply of systems)] as an initial investment and using the appropriate economical equations, the payback period (for the payback period, the appropriate economical equation was utilized) of the whole investment is 4.60 years. Last but not least, the energy cost of the port will be diminished and only the taxes of the invoice will have to be paid and an additional 245tn CO_{2eq}/year will be avoided (totally 505tn CO_{2eq}/year will be avoided).

4 CONCLUSIONS AND RECOMMENDATIONS FOR FURTHER RESEARCH

The case study of Rethymno port proved that there is high potential into converting ports, especially medium ones, to nZEP, as their energy consumption is mainly caused by old-fashioned technologies and techniques. In this specific case, it was investigated that almost the 3/4 of the total energy consumption was due to the lighting of the port which was decreased to less than the 45% of the total energy consumption in the final proposed case.

The energy savings are important due to both the energy costs diminishing and the avoided CO_{2eq}, which enhances both the elimination of GHG and the decarbonization of ports. The question is, what point will energy savings reach if smart energy management systems (EMS) and techniques are adopted and as a result, the required installed power of the PV systems will be decreased, as well.

Last but not least, the most useful recommendations for further research are:

- The examination of implementing EMS and smart techniques, such as automation into the port
- The examination of implementing other types of RES technologies
- The replacement of all old-fashioned technologies in every port's service, with new-generation ones

ACKNOWLEDGEMENTS

We would like to thank the Onassis Foundation for funding this specific research work through the "Scholarships for Hellenes" and the Rethymno port's personnel and authorities for their precious aid.

References

Acciaro M, Ghiara H and Cusano M I (2014) 'Energy management in seaports: A new role for port authorities', *Energy Policy*. Elsevier, 71, pp. 4–12. doi: 10.1016/j.enpol.2014.04.013.

Ecoports, Portopia E (2018) 'Top 10 environmental priorities of European ports for 2018'.

European Commision (2018) *Directive (EU) 2018/844 of the European parliament and of the council*, *Official Journal of the European Union*. doi: 10.1007/3-540-47891-4_10.

Standard European Norme Europeenne Norm E (2007) *En 12464-2 European Standarf for lighting of work places - Part 2: Outdoor work places*.

Tsitoura M, Michailidou M, Tsoutsos T (2016) 'Achieving sustainability through the management of microclimate parameters in Mediterranean urban environments during summer', *Sustainable Cities and Society*. Elsevier B.V., 26, pp. 48–64. doi: 10.1016/j.scs.2016.05.006.

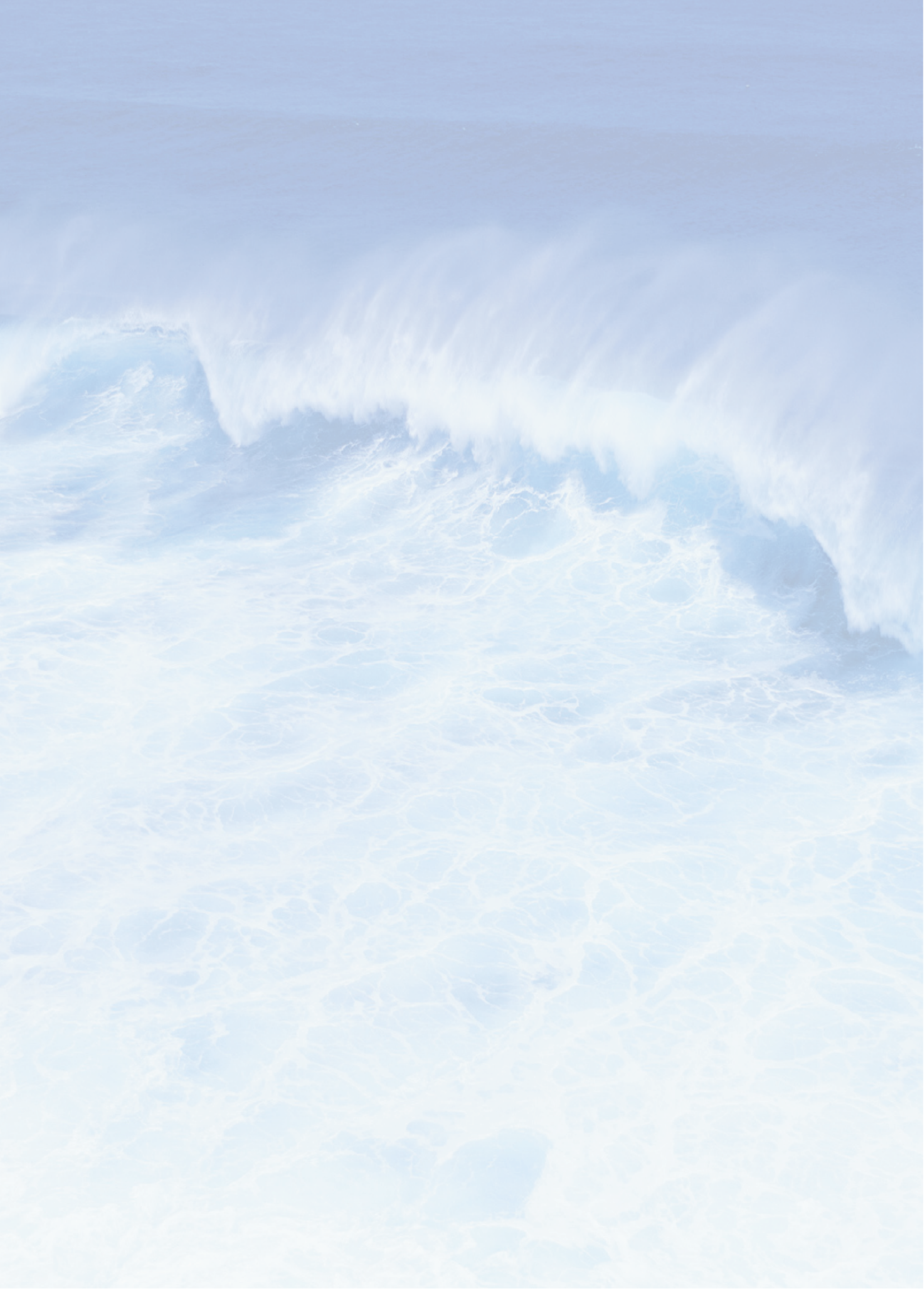

Prospects of carbon capture and utilisation technologies in industrial complexes near Greek ports

M. Kasidoni[1*], N. Stylogiannis[1], M. Loizidou[1]

[1]School of Chemical Engineering, National Technical University of Athens, Athens, 9 Heroon Polytechniou st, Zografou Campus, 157 80, Greece
[*]Corresponding author: mariakasidoni@hotmail.com

Abstract

Over the last decade, strategies and technologies have been developed for diminishing climate risk and damage due to the increased levels of the Greenhouse Gas Emissions released to the atmosphere. Carbon Dioxide Removal geoengineering technologies contribute towards carbon sequestration, but they can also be considered as a pathway to new industrial opportunities along with the creation of high value products. Advocating for tailor-made CCU regional solutions may reduce the economic uncertainty of the various non-commercial CCU technologies. To this end, a methodology was designed compiling selected assessment approaches in order to identify CCU potential in Greece, while using suitable metrics to back up the winning solution. The main outcome of this assessment indicates that industrial complexes with vicinity to ports are suitable for the development of concrete curing CCU technologies.

Keywords Carbon capture and utilisation, Region prioritisation, Cost analysis, Concrete curing.

1 INTRODUCTION

Over the last decade, a powerful portfolio of strategies has been developed for diminishing climate risk and damage due to the increased levels of the Greenhouse Gas Emissions released to the atmosphere. Amongst the various Carbon Dioxide Removal geoengineering technologies available, the adoption of CCU technologies seem to provide twofold benefits. Not only can such technologies contribute towards carbon sequestration, but they can also be considered as a pathway to new industrial opportunities along with the creation of high value products. CCU stands for the capture of increased Carbon Dioxide (CO_2) atmospheric concentrations and its subsequent use in various industrial processes either as a carbon molecule carrier, or as a product with commercial value. Due to this inherent potential, CCU has been characterised as a promising technology, but with a relatively small existing market for CO_2 utilisation.

More specifically, although a number of promising CCU technologies are under development, most of them have not been commercialized yet. In most cases, the main problems identified are relevant to conversion efficiencies, costs, developing markets and social acceptance. Considering the aforementioned, it is of utmost importance to provide evidence of their potential contribution to the global competitiveness of the European industry so as to overcome the obstacles of inefficient solutions leading to increased carbon costs (SAM 2018). As a result, solutions of high Technology Readiness Level (TRL) that circulate or remove CO_2 at competitive costs shall be proved valuable for the near future.

However, since there is no silver bullet for this issue, one of the many important drivers for the CCU market deployment is the enhancement of future CO_2 markets. To this end, by identifying CO_2 point sources, mapping and region prioritization of focus areas can be detected for further aligning utilization opportunities based on the strong demand for products derived from CO_2. In this context, another important aspect is the identification of possible buyers, in order to increase the potential market opportunities for CCU deployment in a specific area. Inevitably, efficient and flexible transport of CO_2 is also of crucial importance. Considering the abovementioned, industrial complexes near ports offer additional opportunities for the development of a more stable CCU system chain.

To this end, advocating for tailor-made CCU regional solutions was the stimulus for this study. In particular, this study shall present a methodology for assessing and matching the CO_2 availability and utilisation potential within the Greek territory. As a result, industrial complexes near Greek ports are considered to bear important characteristics, such as (i) greater potential for deploying well established CO_2 capture technologies, as well as (ii) more opportunities for possible CO_2 buyers. In this framework, valuation models shall be used in order to provide the most suitable CCU solution for an industrial complex near a Greek port.

2 METHODOLOGY FOR IDENTIFYING CCU POTENTIAL IN GREECE

A methodology has been designed compiling selected assessment approaches in order to identify CCU potential in Greece, while using suitable metrics to back up the winning solution. The methodological approach is consisted of two distinct parts. At first, an assessment was conducted focusing on region prioritization in terms of identifying areas in Greece suitable for CCU development. Following, valuation models were used in order to estimate the value of the operating assets and the value of equity for the proposed projects based on the initial assessment findings.

More specifically, an assessment focusing on identifying areas in Greece with potential of CCU development took place. The methodology used was relevant to region prioritization assessments conducted for locating areas of CCU interest within the EU Member States (EU MS) (Patricio et al. 2017,). In this framework, the potential availability of CO_2 as a resource was compared to the potential demand for CCU within the Greek territory. With reference to the quantities of CO_2 emissions recorded for Greece, several databases were identified. Nevertheless, since the focus of this study is the identification of CCU business opportunities, official data that companies are obligated to record under the Regulation No 166/2006 of the European Parliament and of the Council were used. The data were depicted on a map, thus locating complexes with carbon intensive companies. Following, a rough estimation for the potential demand of CCU took place. The main limitation with reference to this quantification is detected in the emerging character of all CO_2 capture and CCU technologies. Therefore, an initial assumption in regards to the technology readiness was necessary so as to proceed with the valuation models. In this framework, a TRL higher than seven (7) was accepted. After identifying the main CCU processes that are almost ready-to-market, the relevant production sectors were quantified. As a result, the areas of specific interest with carbon intensive companies were ranked based on the available workforce allocated.

Following, a preliminary screening based on the economic cost of the most dominant CCU technologies for Greece was conducted. To this end, parameters, such as the existing infrastructure that could be easily retrofitted, as well as capital and transportation costs were estimated based on existing scientific literature. In this framework, the most highly ranked CCU technology was used for a project proposal that would be further valuated in order to provide an insight on creating new business structures to innovative markets (Schiavi and Behr 2018).

In particular, one valuation model was used in order to measure what the CO_2 value chain project can return to its stakeholders after meeting reinvestment needs (Zimmermann et al. 2018). This parameter determines the value of the project according to the cash flow left after meeting all financial obligations, including debt payments, and after covering capital expenditure and working capital needs. In this framework, the net income is converted to cash flow by subtracting out the CO_2 project's reinvestment needs. More specifically, the capital expenditures are subtracted from net income since they represent capital outflows. In this context, depreciation/amortization is added back as non-cash charges. Therefore, the difference between capital expenditures and depreciation is a function of the growth characteristics of the project.

Following, in regards to the assumptions of this valuation model, this project is considered of high growth thus having high net capital expenditures, since it is expected that it will monopolize the regional market. High growth projects in industries with high working capital requirements (retail of CO_2 developed products) have large increases in working capital respectively. Therefore, only the changes in net working capital are considered. In addition, the level of debt on the overall cash flow of the project is highlighted. Depending on the nature of the project (developing a new market), the debt repayment may be fully or partially financed by the issue of new debt, which is cash inflow as this is the case for environmental projects with replicable potential for regions of the European Union. Allowing for the cash flow effects of net capital expenditures of net capital expenditures, changes in working capital, and net changes in debt on equity investors, the cash flows left over these changes as the Free Cash Flow to equity (FCFE) are defined. Overall, the use of an FCFE model leads to two

main outcomes considering its underlying principle that the FCFE will be paid out to the stakeholders, namely: (i) there will be no future cash build in the project, since the cash that is available after debt payments and reinvestment needs is paid out to stockholders each period, and (ii) growth in FCFE originates from operating assets. In this framework, growth is estimated via the equity reinvestment rate and the non-cash Return on Equity (ROE).
In addition, the project was also valued by discounting the cumulative cash flows to all claimholders by the Weighted Average Cost of Capital. Under this model, the optimal financing mix of the project is the one that maximizes project value. The Free Cash Flow to Firm (FCFF) is the sum of all cash flows to all claimholders, including stockholders, bondholders, and preferred stockholders. Discounting the FCFF at the cost of capital will yield the value of the operating assets of the project, adding the value of the non-operating assets to arrive the project value. Nevertheless, there are two conditions that have to be met in using this model. First, the growth rate has to be less or equal to the growth rate of the economy in case the cost of capital is at nominal terms, or to the real growth for the case that the cost of capital is real cost of capital. Second the characteristics of the project have to be consistent with the assumptions of stable growth. In this case, the reinvestment rate has to be consistent with the stable growth rate, for example by deriving reinvestment from the stable growth rate. If reinvestment rate is estimated from net capital expenditures and change in net working capital, then the net capital expenditures should be similar to those other firms in the industry, while the change in working capital should not be negative because it creates cash inflow that it is dangerous to assume this in perpetuity. The cost of capital should also be reflective of a stable growth firm.
It has to be noted that the outcomes of each part of the assessment were closely interrelated, since each result depends strongly on the assumptions of the former part of the assessment. To this end, particular emphasis was placed on the structure of strong and realistic assumptions that would only be used in order to have the most realistic outcome when using the valuation models. Each one of the assumptions, as well as the outcomes of each part of the assessment were then crosschecked considering scientific literature. Finally, the main outcome was characterized considering the environmental benefit, social acceptance, as well as regulatory and business feasibility.

3 RESULTS

Following the methodology, the outcome of each part shall be provided. More specifically, in regards to the focus area that was identified based on the first part of the assessment, industrial complexes with vicinity to ports were found to bear the highest CCU potential. This was not an unexpected outcome since industries have always been competing for maritime space due to the less available space inland, as well as because of the higher inland transportation costs of bulky products (UN 2009) and more recently for less-bulky products. Especially for Greece, industry development with proximity to ports has always been of high importance considering its long coastline. As a result, higher CO_2 concentrations were allocated proportionally.
In addition, the main CCU options available for Greece were also identified. However, concrete curing was considered to have the highest potential for Greek ports based on the infrastructure available. More specifically, the literature review conducted focusing on the capital and transportation costs of such investments highlighted that concrete curing not only holds relatively lower costs, but also has mid-term development compared to the rest CCU investments. In this framework, two (2) valuation models were used in order to determine Present Value of the Project in terms of: (i) the investment strategy where high leverage is used to increase the potential of returns by investing to this project (use of the FCFF instead of the FCFE approach) and/or (ii) the growth assumptions of the project and the relationship between capital spending and depreciation. For both models, one optimistic and one conservative scenario were applied.
More specifically, a start-up for concrete curing project was proposed to be assessed, since innovative products are to be launched in a conservative-in-nature (i.e. mature) industry, such as the cement industry (Mott MacDonald 2010). In this framework, literature review for identifying CO_2 quantities captured in concrete blocks was conducted and the capture target of CO_2 was allocated deliberately over a five-year period, in order to compensate with the necessary adoption for developing a new business line of CO_2 cement products. As a result, two (2) types of newly developed products were considered with 7% and 24% CO_2 capture, respectively. In the same context, initial investment for

CO_2 capture and concrete curing retrofitting an existing cement plant was based on cost estimations and comparative assessments conducted on carbonation cost as a mean of carbon sequestration, respectively (Zhang et al. 2017). In this context, the relevant fixed and variable expenses for capital expenditure were estimated as a one-off price per ton. Complementary to the initial investment, operational expenses both for CO_2 capture and concrete curing were considered based on the CO_2 uptake of newly developed cement products. Last but not least, carbon allowances for carbon credits, as well as carbon offsets were also considered within the valuation models. Based on the abovementioned, earnings generated throughout the ordinary business course of products portfolio with 7% and 24% CO_2 uptake without considering capital expenditures and financing costs were accounted to have positive within 5-7 years.

In addition, it has to be noted that since the newly developed products are transferred from ports, several benefits are also encountered. The scope of promoting maritime transportation is threefold, focusing on using port services as a mean to foster differentiation strategies, minimizing the transportation costs, and promoting carbonated products safely. Ports have standardized the cargo transshipment resulting in significantly reduced costs. At the same time, they offer a number of services such as reliability, quality of service, high sailing frequency, competitive rates, information technology, and professional management.

Following, amongst the various benefits of investing in CCU concrete curing technologies in industrial complexes near ports is the fact that carbonated masonry blocks can be treated as other conventional products during their transport. Based on the abovementioned and the Michael Porter's Generic Differentiation Strategy Model framework, it is highlighted that low price is supported by using the port's services and the new products are valuable and unique for its buyers. The procedure is innovative in terms of the region and allows cement producers to gain competitive advantage, quality and responsiveness to customer needs. In this framework, costs are essential for developing a new market (product–based) but are not the primary strategic target. Moreover, differentiators allow cement producers to build further on brand loyalty directly with the end-customers. Consequently, the number of end-customers seeking environmentally-friendly products and less sensitive in price increases. To conclude, these products shall turn out to be very difficult to imitate because competitors are outside the scope of cement production, must also invest substantial resources to both match the capabilities of the differentiator, as well as have to break the customer loyalty.

4 CONCLUSIONS

The economic uncertainty of various non-commercial CCU technologies that is consistent to weak industry competitiveness thus contributing towards the use of inefficient climate mitigation solutions, can be reduced by advocating tailor-made CCU regional solutions. In this framework, a methodology was designed based on selected assessment approaches in order to identify CCU potential in Greece. The methodology resulted in high potential of concrete curing for industrial complexes near Greek ports. In this framework, a start-up for concrete curing project was valuated considering new products in a mature industry supply chain. The principle outcome refers to a feasible investment in terms of economics because of the revenues and low transportation costs, as well as to low societal risks due to the product responsiveness to customer needs. Finally, further research in terms of conversion approaches, as well as economic feasibility of emerging CCU technologies shall provide an insight the applicability of CO_2 mitigation technologies.

5 ACKNOWLEDGEMENTS

This research was supported by funding from the National Technical University of Athens under the Special Account for Research Grants.

References

Mott MacDonald (2010) Global Technology Roadmap for CCS in Industry, Sectoral Assessment: Cement. Mott MacDonald, United Kingdom.

Patricio J, Angelis-Dimakis A, Casillo-Castillo A, Kalmykova Y, Rosado L (2017): Region prioritization for the development of carbon capture and utilization technologies, Journal of CO_2 Utilization, vol. 17, pp. 50-5.

SAM Scientific Advice Mechanism European Commission (2018) Novel carbon capture and utilisation technologies. European Union, Brussels.

Schiavi GS, Behr A, (2018) Emerging technologies and new business models: a review on disruptive business models. Innovation & Management Review, 15:338-355, doi.org: 10.1108/INMR-03-2018-0013.

UN United Nations Economic and Social Commission for Asia and the Pacific (2009) Impact of trade facilitation on export competitiveness: A regional perspective. United Nations, New York.

Zhang D, Ghouleh Z, Shao Y (2017): Review on carbonation curing of cement-based materials, Journal of CO_2Utilization.

Zimmermann A, Müller LJ, Marxen A, Armstrong K, Buchner G, Wunderlich J, Kätelhön A, Bachmann M, Sternberg A, Michailos S, Naims H, Styring P, Schomäcker R, Bardow A (2018): Techno-Economic Assessment & Life Cycle Assessment Guidelines for CO_2 Utilization. CO_2Chem Media and Publishing Ltd doi: 10.3998/2027.42/145436, 21:119-131, doi: 10.1016/j.jcou.2017.07.003.

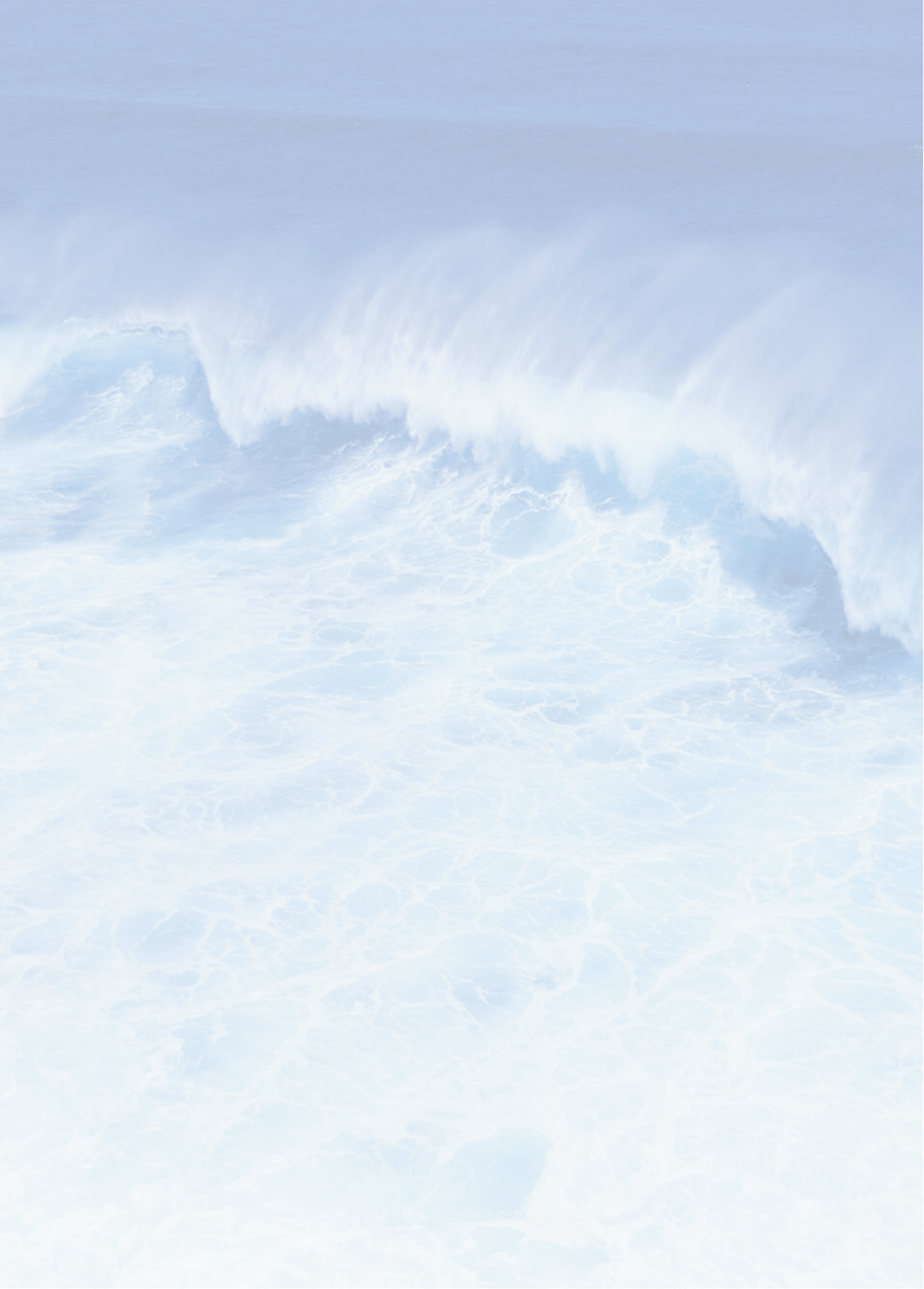

Η επίτευξη της βιώσιμης ανάπτυξης των τουριστικών λιμένων, με τη χρήση μοντέλων περιβαλλοντικής διαχείρισης

Σ.Μ. Μανώλογλου*, Β.Σ.Τσελέντης

Τμήμα Ναυτιλιακών σπουδών Πανεπιστημίου Πειραιώς, Πειραιάς, 185 34, Ελλάδα
*Υπεύθυνος επικοινωνίας: manologloy@yahoo.gr

Περίληψη

Με την πάροδο του χρόνου, τα λιμάνια εξελίχθηκαν από απλούς σταθμούς φορτοεκφόρτωσης, σε μεγάλα διαμετακομιστικά κέντρα, αυξάνοντας κατακόρυφα την χωρητικότητά τους μέσω περίπλοκων και πολυδάπανων έργων. Στο ίδιο πλαίσιο κινήθηκαν και οι τουριστικοί λιμένες όπου συγκεντρώνονται πολλά σκάφη αναψυχής στις νησιωτικές περιοχές, επιβαρύνοντας με διάφορους τρόπους την παράκτια ζώνη. Η ανάπτυξη αυτή των λιμανιών απαιτεί πολύπλοκη και πολύπλευρη διοίκηση σύμφωνα με τα πρότυπα της διοίκησης ολικής ποιότητας και της βιώσιμης ανάπτυξης, σε συνδυασμό με την περιβαλλοντική διοίκηση. Επιπρόσθετα, τα έργα υποδομής και ανωδομής προϋποθέτουν την εκπόνηση ειδικών μελετών περιβαλλοντικών επιπτώσεων όπου θα πιστοποιούνται όλες οι διαδικασίες των έργων. Ειδικά για την Ευρωπαϊκή Ένωση, ο λιμενικός τομέας συνιστά τομέα αυξημένου ενδιαφέροντος, αφού διακινεί το 90% των εμπορικών συναλλαγών της Ένωσης με τρίτες χώρες και περίπου το 35% της ενδοκοινοτικής κυκλοφορίας, καθώς και 200 εκατομμύρια επιβάτες ετησίως. Η ζήτηση για μεταφορικές υπηρεσίες αυξάνεται κάθε χρόνο από το 1970, κατά 2, 3% για τα αγαθά και κατά 3, 1% για επιβάτες· Φαίνεται λοιπόν ότι η αυξητική αυτή τάση θα συνεχιστεί και στο μέλλον, με την ανάπτυξη του λιμενικού τομέα να θεωρείται δεδομένη. Καθίσταται επομένως ευρέως αποδεκτό ότι περιβαλλοντικό management των λιμένων, δηλαδή η οργάνωση των λιμενικών δραστηριοτήτων με στόχο τη διασφάλιση της περιβαλλοντικής προστασίας και της αειφόρου ανάπτυξης, αποτελεί ένα σημαντικό και ολοένα αυξανόμενο μέρος του λιμενικού management και της ποιοτικής διασφάλισης των προσφερόμενων λιμενικών υπηρεσιών.

Λέξεις κλειδιά Παράκτια ζώνη, Τουριστικός λιμένας, Λιμενικό μάνατζμεντ, Περιβαλλοντική πιστοποίηση.

1 ΕΡΓΑΛΕΙΑ ΕΛΕΓΧΟΥ ΠΕΡΙΒΑΛΛΟΝΤΙΚΗΣ ΠΡΟΣΤΑΣΙΑΣ

Σήμερα είναι γεγονός ότι ο λιμενικός τομέας και η κοινωνία γενικότερα αποδέχεται την περιβαλλοντική προστασία ως επιστημονική, νομική και ηθική αναγκαιότητα και ότι η πρόκληση πλέον βρίσκεται στο να αναπτυχθούν διοικητικές και οργανωτικές δομές για την αποτελεσματικότερη εφαρμογή των λιμενικών περιβαλλοντικών πολιτικών. Μία επιτυχημένη περιβαλλοντική διαχείριση των λιμενικών δραστηριοτήτων απαιτεί να είναι σε θέση οι υπεύθυνοι για τη λήψη αποφάσεων, αφενός να μπορούν να εκτιμήσουν και να καταλάβουν το εύρος των περιβαλλοντικών θεμάτων και των επιπτώσεων τους και αφετέρου να μπορούν ταυτόχρονα να αναπτύξουν και να εφαρμόσουν δράσεις και πολιτικές οι οποίες να διασφαλίζουν την περιβαλλοντική προστασία (Επιτροπή των Ευρωπαϊκών Κοινοτήτων, 2017). Η βέλτιστη περιβαλλοντική διαχείριση λιμενικών δραστηριοτήτων απαιτεί να γνωρίζουν οι υπεύθυνοι τα εργαλεία ελέγχου για περιβαλλοντική προστασία. Αυτά περιλαμβάνουν: Κανονισμούς, Οδηγίες, Κώδικες πρακτικής, Περιβαλλοντικούς περιορισμούς, Περιβαλλοντική ποιότητα αλλά και οικονομικά μέτρα και ενδεχόμενες ποινές μη-συμμόρφωσης. (Dalley R. & Deeming, K, 1994)

2 ΣΥΣΤΗΜΑΤΑ ΠΕΡΙΒΑΛΛΟΝΤΙΚΗΣ ΔΙΑΧΕΙΡΙΣΗΣ

Τα λιμάνια αποτελούν σύνθετα και δυναμικά περιβάλλοντα, των οποίων τα χαρακτηριστικά και οι ιδιομορφίες εξαρτώνται άμεσα από το μέγεθος, την τοποθεσία, τους υδρογραφικούς παράγοντες, τη σχέση τους με τη βιομηχανία, τον αστικό χώρο και την εμπορική λειτουργία τους. Επιπλέον, κατά τη διεξαγωγή των λιμενικών εργασιών, εμπλέκονται και πολλοί παράμετροι, κυρίως νομικής, οικονομικής, εμπορικής, τεχνικής, και οργανωτικής φύσεως, οι οποίοι συνυπολογίζονται στις αποφάσεις των φορέων διαχείρισης. (Wooldridge C.F. and

Couper A.D 1995).Οι λιμενικές δραστηριότητες μπορεί να επιδράσουν ποικιλόμορφα σε συγκεκριμένα τμήματα του χερσαίου, θαλάσσιου και αέριου περιβάλλοντος. Όμως, αυτές οι επιδράσεις στην περίπτωση των λιμανιών, δεν είναι εύκολο να εντοπιστούν και να εκτιμηθούν, αφού αφορούν ένα δυναμικό και πολύπλοκο σύστημα, το οποίο αποτελείται από την ξηρά, τη θάλασσα και την ατμόσφαιρα. (Τσελέντης 2006). Ο προσδιορισμός της ποιότητας του περιβάλλοντος σε περιοχές που υφίστανται ανθρωπογενείς επεμβάσεις είναι δύσκολος και συχνά οδηγεί σε λανθασμένα συμπεράσματα αν δεν διεξάγονται μακροπρόθεσμες μελέτες, οι οποίες συμπεριλαμβάνουν και καταμετρούν μια σειρά παραμέτρων, που αποτελούν αποδεδειγμένα αντιπροσωπευτικούς δείκτες των φυσικών βιογεωχημικών διεργασιών.

2.1 Το σχέδιο της Ευρωπαϊκής Επιτροπής "Eco-Management and Audit Scheme"

Το σχέδιο της Ευρωπαϊκής Επιτροπής είναι ένα πρότυπο συστημάτων περιβαλλοντικής διαχείρισης που εξασφαλίζει και αποδεικνύει την συμμόρφωση των εταιριών με την περιβαλλοντική πολιτική, καθώς και με τους περιβαλλοντικούς στόχους που έχουν τεθεί, συμπεριλαμβανόμενης της ισχύουσας νομοθεσίας. Μέσω του προτύπου δεν θέτονται συγκεκριμένοι περιβαλλοντικοί ή επιχειρησιακοί στόχοι αλλά βοηθάει τους οργανισμούς να εφαρμόσουν περιβαλλοντική πολιτική και να ανταποκρίνονται στις νομοθετικές απαιτήσεις, παρέχοντας γενικά πρότυπα. Το ΄΄Eco-Management and Audit Scheme΄΄ καθορίζει τα στοιχεία που πρέπει να εξεταστούν, προκειμένου να δημιουργηθεί ένα αποτελεσματικό σύστημα περιβαλλοντικής διαχείρισης. Τα κυριότερα σημεία συνοψίζονται στην προκαταρκτική Έρευνα, την Περιβαλλοντική Πολιτική, την Οργάνωση και το Προσωπικό, στην κατάστρωση Διαχειριστικού Προγράμματος αλλά και την Τεκμηρίωση με Έγγραφα και Περιβαλλοντικούς Έλεγχους. (Wooldridge C.F, Tselentis B.S., Whitehead D 1998).

2.2 Ο Ευρωπαϊκός Οργανισμός Λιμένων - European Sea Ports Organization (ESPO)

Ο Οργανισμός Ευρωπαϊκών Λιμένων (ESPO), ο πρώτος ανεξάρτητος οργανισμός λιμένων κρατών-μελών της Ευρωπαϊκής Ένωσης, αποτελεί το φορέα σημαντικών πρωτοβουλιών σχετικά με την προστασία του περιβάλλοντος στα λιμάνια. Μέχρι την ίδρυση του ESPO το Μάρτιο του 1993, τα διάφορα ζητήματα του λιμενικού κλάδου αντιμετωπίζονταν με την από κοινού εργασία των αντιπροσώπων των λιμανιών με την Ευρωπαϊκή επιτροπή, χωρίς να υπάρχει το πλεονέκτημα ενός οργανισμού δημιουργημένου και οργανωμένου από τα ίδια τα μέλη του. Ο ESPO επιτρέπει την υιοθέτηση πολιτικών και στρατηγικών των οποίων ο σχεδιασμός βασίζεται στην καθημερινή εμπειρία, επομένως στην γνώση των προβλημάτων από τους άμεσα ενδιαφερόμενους. Η έκδοση ενός Κώδικα Πρακτικής (Code of Practice) και διάφορα άλλα ερευνητικά προγράμματα έχουν συμβάλει και εξακολουθούν να συμβάλλουν τόσο στην ανάπτυξη περιβαλλοντικής πολιτικής, όσο και στην αποτελεσματική εφαρμογή των διαφόρων μεθόδων. Συγκεκριμένα, η σύνταξη του Κώδικα Πρακτικής αποτέλεσε κύριο μέλημα του ESPO και πραγματοποιήθηκε αμέσως μετά από την ίδρυση του οργανισμού. Εκδόθηκε το Δεκέμβριο του 1994 και συνδυάζει γενικές συστάσεις για τη διαχείριση με συγκεκριμένους στόχους, αντικείμενα και τομείς δραστηριότητας, όπως παρακολούθηση περιβαλλοντικών παραμέτρων, βυθοκορήσεις, λιμενικό σχεδιασμό και ανάπτυξη, σχέδια δράσης σε περιπτώσεις έκτακτης ανάγκης. (www.ESPO.com). Ο Κώδικας έπρεπε να λάβει υπόψη τη σημαντική ποικιλία που επικρατεί στο λιμενικό κλάδο, αφού κάθε λιμάνι αντιμετωπίζει διαφοροποιημένα περιβαλλοντικά προβλήματα, ανάλογα με τη θέση του, το μέγεθός του, το είδος των λειτουργιών του, τις εθνικές και τοπικές συνθήκες.

2.3 Σύστημα περιβαλλοντικού ελέγχου λιμένα - Port Environmental Review System (PERS)

Πρόκειται για ένα σύστημα περιβαλλοντικής πιστοποίησης που αναπτύχθηκε από τα ίδια τα λιμάνια και έχει εδραιώσει τη φήμη του ως το μόνο περιβαλλοντικό πρότυπο διοίκησης στον τομέα τη λιμενικής βιομηχανίας. Το σύστημα δεν συνεργάζεται απλώς με τις βασικές προϋποθέσεις των αναγνωρισμένων περιβαλλοντικών προτύπων (πχ. ISO 14001), αλλά λαμβάνει υπόψη του τα χαρακτηριστικά των λιμανιών δίνοντας τους παράλληλα σαφής στόχους. Τέλος, αξίζει να σημειωθεί πως η εφαρμογή του εποπτεύεται και από τους Lloyd's Register γεγονός που αποδεικνύει την σημαντικότητά του ως εργαλείο περιβαλλοντικής πιστοποίησης, ενώ τα πιστοποιητικά που εκδίδονται έχουν τυπική ισχύ δύο ετών.

3 ΤΑ ΠΡΟΤΥΠΑ ΠΕΡΙΒΑΛΛΟΝΤΙΚΗΣ ΠΙΣΤΟΠΟΙΗΣΗΣ ΤΩΝ ΤΟΥΡΙΣΤΙΚΩΝ ΛΙΜΕΝΩΝ

Με βάση τα στοιχεία της Ένωσης Μαρίνων Ελλάδος η Ελλάδα διαθέτει 22 οργανωμένες μαρίνες παρέχοντας 8.500 θέσεις ελλιμενισμού. Ακόμη, διαθέτει 55 χωροθετημένες μαρίνες και 80 τουριστικά καταφύγια, με τις συνολικές θέσεις ελλιμενισμού να ανέρχονται 14.400 θέσεις. Οι κυριότερες μαρίνες της Ελλάδος είναι της Βουλιαγμένης, της Ζέας, της Γλυφάδας, του Φλοίσβου, του Αλίμου, του Φαλήρου, του Άγιου Κοσμά, η Olympic marine κ.α . Όπως και στα εμπορικά και επιβατικά λιμάνια, έτσι και στα τουριστικά, κρίνεται επιβεβλημένη η ανάγκη χρήσης συστημάτων περιβαλλοντικής πιστοποίησης που θα συμβάλουν στην αποδοτικότερη και στην πιο φιλική προς το περιβάλλον λειτουργία των μαρίνων. (www.greek-marinas.gr)

3.1 Gold Anchor Award

Η ιδέα στην οποία βασίζονται οι αρχές της πιστοποίησης "gold anchor" είναι η πίστη ότι η βιομηχανία των μαρίνων χρειάζεται πελατοκεντρική εστίαση για τις λειτουργίες ων μαρίνων. Οι πελάτες των τουριστικών λιμένων προσδοκούν καλές υπηρεσίες, κατάλληλο εξοπλισμό, ασφάλεια και αξίες προστιθέμενης αξίας, ανεξάρτητα από τη διαπίστευσή της. Όπως συμβαίνει και με τον ξενοδοχειακό κλάδο, δεν είναι όλοι διατεθειμένοι να πληρώσουν έξτρα χρήματα για καλύτερες εγκαταστάσεις και ποιοτικές υπηρεσίες. Η πιστοποίηση "gold anchor" συνδέεται με τα ακόλουθα χαρακτηριστικά. Πρώτον οι πιστοποιημένες μαρίνες παρέχουν πολύ καλές υπηρεσίες προς τους χρήστες, δεύτερον οι υπηρεσίες αυτές είναι προστιθέμενης αξίας σε όλα τα στάδια της διαπίστευσης και τρίτον η πιστοποίηση (απόκτηση σημαίας) σημαίνει ότι οι μαρίνες-μέλη, έχουν επιτύχει τα αναγνωρισμένα πρότυπα που θέτει το πρότυπο "gold anchor". (www.goldanchors.com)

3.2 Πρότυπο περιβαλλοντικής πιστοποίησης ISO 14001

Το πρότυπο ISO 14001 ανήκει στην οικογένεια προτύπων ISO και παρέχει πρακτικά εργαλεία στους οργανισμούς και τις εταιρίες όλων των ειδών που θέλουν να διαχειρίζονται την ευθύνη τους απέναντι στο περιβάλλον. Το ISO 14001 του 2015 και τα υποστηρικτικά πρότυπα όπως το ISO 14006 του 2011, εστιάζουν στα περιβαλλοντικά συστήματα για να το πετύχουν. Το πρότυπο παρέχει όλα εκείνα τα αποτελεσματικά μέσα που πρέπει να ακολουθήσουν οι μαρίνες ώστε να επιτευχθούν οι περιβαλλοντικοί τους στόχοι. (Τσελέντης, 2006).Η απόκτηση λοιπόν του ISO 14001 πιστοποιεί πως όλες οι διαδικασίες και λειτουργίες των μαρίνων γίνονται με γνώμονα την περιβαλλοντική προστασία και την ποιοτική διαχείριση και λειτουργία.

4 ΣΥΜΠΕΡΑΣΜΑ

Η συνεχιζόμενη ανάπτυξη μεταφράζεται συνήθως σε αυξανόμενη κατανάλωση των φυσικών πόρων, και υψηλότερο κοινωνικό κόστος. Με δεδομένο πως οι δυνατότητες του περιβάλλοντος, σχετικά με την αφομοίωση αρνητικών εκροών είναι πεπερασμένες, ο κίνδυνος για διατάραξη της οικολογικής ισορροπίας είναι εμφανής και παρουσιάζεται ανάλογα αυξημένος με την ανάπτυξη του λιμενικού κλάδου. Η συμμόρφωση ενός λιμένα με τα πρότυπα της ορθής και υπεύθυνης περιβαλλοντικής πολιτικής καθιστά το λιμάνι φιλικότερο προς το χρήστη και την περιοχή στην οποία δραστηριοποιείται, αλλά και πιο ασφαλές και ποιοτικό για όλες τις δραστηριότητες που λαμβάνουν χώρα μέσα σε αυτό. Σε ότι αφορά την προστασία του περιβάλλοντος, οι περιβαλλοντικές πιστοποιήσεις θωρακίζουν το λιμάνι από τους κάθε λογής κινδύνους περιβαλλοντικής όχλησης. Προκειμένου επομένως να διασφαλιστεί η περιβαλλοντική απόδοση σε ένα λιμάνι και σε κάποιο επιθυμητό επίπεδο, είναι απαραίτητη η κατανόηση τόσο των δυνητικών περιβαλλοντικών συνεπειών και των πηγών τους, όσο και η δομή εργασίας εκείνη που προωθεί το επιθυμητό αποτέλεσμα. Οι πολιτικές και οι στρατηγικές πρέπει να είναι γνωστές και αποδεκτές από το σύνολο των εμπλεκομένων στο λιμάνι, ενώ η οργανωτική δομή πρέπει να είναι σε θέση να διαχειρίζεται τις όποιες προκλήσεις. Τα συστήματα περιβαλλοντικής διαχείρισης είναι εργαλεία που βοηθούν, παρέχοντας τα μέσα για τη διαχείριση της διαδικασίας εργασίας, όπως επίσης και την επικοινωνία της εταιρικής περιβαλλοντικής πολιτικής, των στόχων και της εξέλιξης του έργου.

Βιβλιογραφικές αναφορές

Dalley R, Deeming, K (1994) “Ports and the Environment”. CSM, The Official Journal of the RICS Vol. 3, Part 5.32

Wooldridge CF Tselentis BS, Whitehead D,(2008) "Environmental management of port operation – the ports sector's response to the European Dimension" in Maritime Engineering and Ports, pp.227-242. eds C.A. Brebbia and Sciutto. Wessex Institute of Technology Press, Southampton, UK, 1998.

Wooldridge CF and. Couper AD "Validity of Scientific Criteria for Environmental Auditing of Port and Harbour Operations", July 1995.

Επιτροπή των Ευρωπαϊκών Κοινοτήτων (2017) "Πράσινη Βίβλος σχετικά με τους θαλάσσιους λιμένες και τις ναυτιλιακές υποδομές”

Τσελέντης Β (2006) Διαχείριση θαλάσσιου περιβάλλοντος και ναυτιλία, Εκδόσεις Σταμούλη Α.Ε., Αθήνα

ESPO Bulletin

http://europa.eu.int/comm./energy_transport/etif/transport_goods_a/performance_by_mode_tkm

http://ec.europa.eu/environment/emas/index_en.html

www.greek-marinas.gr – Ένωση Μαρίνων Ελλάδος

www.gold-anchors.com – Ένωση ελέγχου και πιστοποίησης των λιμένων σκαφών αναψυχής (μαρίνων)

DMPCO 2019

Laboratory of Harbour Works, National Technical University of Athens
Iroon Polytechniou Str. 5, GR 15780, Athens, Greece
Phone: + 30 210 7722367, 210 7722374 | Fax: + 30 210 7722368
Email: registration@dmpco.gr | lhw@cental.ntua.gr
www.dmpco.gr